Radiation Grafted Membranes for Polymer Electrolyte Fuel Cells

Habilitationsschrift

zur Erlangung der *Venia Legendi*
für das Fach Phyikalische Chemie

eingereicht am

Laboratorium für Physikalischen Chemie
Departement Chemie und Angewandte Biowissenschaften
Eidgenössische Technische Hochschule, Zürich

vorgelegt von

Lorenz Gubler

geboren am 14. August 1971
von Grenchen, SO

Zürich, 2016

„[…] we must resign ourselves to the condition that a hydrogen-oxygen battery is a potent destructive machine for any hydrocarbon based chemical.”

- R.B. Hodgdon, J.R. Boyack, A.B. LaConti, *TIS Report 65DE 5*, General Electric Company, Lynn MA, USA, 1966

Acknowledgement

Table of Contents

Synopsis

Electrochemical energy conversion and storage technologies play a key role in future energy and mobility scenarios. Fuel cells offer the prospect of clean and efficient electricity generation for a variety of applications, such as stationary power systems and electric vehicles. The commercial competitiveness strongly depends on the performance, reliability, durability and cost of fuel cell systems. The development of cost-efficient ion-conducting membranes for the polymer electrolyte fuel cell (PEFC) with designed architecture and functional properties can contribute to bringing technology forward in this direction.

The modification of a pre-existing polymer film via radiation induced graft copolymerization ("radiation grafting") is a versatile and potentially low cost method to introduce desired properties into the material, such as ion conductivity. Compared to commonly used perfluoroalkylsulfonic acid (PFSA) membranes, such as Nafion®, in fuel cells, radiation grafted proton conducting membranes can be prepared using cheap base polymers and commercially available grafting monomers. The challenges herein are mainly associated with achieving concurrently performance and durability attributes competitive to those of PFSA membranes.

This work focuses on the polymer design aspects and understanding of chemical degradation phenomena of radiation grafted proton conducting membranes for fuel cells. A brief historical outline and extensive review of developments in radiation grafted membranes over the past decade aims at placing this study into the context of the technological state-of-the-art. The central topics of membrane development are the use of α-methylstyrene and nitrile comonomers as graft component to improve chemical stability. Moreover, polymer-bound antioxidants are introduced to this end. The study of membrane degradation mechanisms is based, on the one hand, on pulse radiolysis studies of oligomer model compounds to study mechanisms of radical induced polymer breakdown. On the other hand, single cell tests under accelerated degradation conditions combined with qualitative and quantitative membrane characterization techniques are invaluable tools to develop an understanding of membrane aging phenomena.

The studies presented here highlight that radiation grafted fuel cell membranes, if properly designed, can compare favorably with PFSA membranes in terms of performance and durability. Process development and scale-up of membrane fabrication are among the grand challenges of the future, which is beyond the scope of academic research and requires industrial involvement.

Introduction

1 A Historical Perspective

Fuel cells using an ion-exchange membrane as polymer electrolyte and separator were first described in the 1950s by Grubb from the General Electric (GE) Company [1]. A few years earlier, the preparation of free-standing ion exchange membranes had been reported for the first time [2]. This invention attracted considerable attention across the world and contributed to the succeeding development of the synthesis technology of ion exchange membranes. An ion-exchange polymer is characterized by the presence of ionic groups fixed to the polymer backbone and counterions that are mobile when the polymer is hydrated. The absence of a corrosive liquid electrolyte, selective charge transport, mechanical robustness, high conductivity, good barrier properties for reactant gases and electrons in polymer electrolytes based on an ion-exchange polymer were put forward as key advantages over a liquid electrolyte. A thin membrane electrolyte allows the preparation of fuel cells with high volumetric power density that can be operated at room temperature. For a fuel cell using H_2 and O_2 as reactant gases, the membrane conducts either H^+ or OH^- ions, thus constituting an acid or alkaline electrolyte [3].

1.1 Early Hydrocarbon Based Membranes

The progress in polymer electrolyte fuel cell (PEFC) performance and lifetime is closely associated with the development of ion conducting membranes used as polymer electrolyte [4]. The early ion-exchange materials used by Grubb and Niederach were synthesized by condensation of phenolsulfonic acid and formaldehyde [5]. These types of membrane were referred to as "homogeneous" membranes, since a single-phase material is obtained [6]. Yet these membranes were brittle and readily hydrolyzed in the fuel cell, releasing H_2SO_4. In further studies, commercially available "Amberplex C-1" (Rohm and Haas Company, now part of Dow Chemical Company) membranes, consisting of particles of sulfonated and cross-linked polystyrene embedded in a binder matrix, such as polyethylene, were used. A typical membrane thickness was 0.6 mm. These cation-exchange membranes had a conductivity in the proton form similar to that of 0.1 N sulfuric acid [7]. In analogy, anion exchange membranes, such as "Amberplex A-1" (Rohm and Haas Company), were used, in which the cross-linked polystyrene was chloromethylated and subsequently aminated with trimethylamine to introduce quaternary ammonium anion exchange sites. "Amberplex" membranes were so-called "heterogeneous" membranes, prepared by embedding colloidal ion-exchange particles in an inert polymeric binder [6]. However, the chemical and physical properties of these membranes were still poor, fuel cell lifetimes at 60°C did not exceed 200 h [5].

A first *succès d'estime* for the polymer electrolyte fuel cell (PEFC) was its implementation as power source in the Gemini space capsule of the NASA starting in 1962 [8]. The power output of these fuel cell systems was 1 kW. The fuel cells were developed by GE, using an ion-exchange membrane fabricated by the American Machine Foundry (AMF), referred to as "D" membrane. This ion-exchange membrane was prepared by the copolymerization of styrene and 1.25 % of the crosslinker divinylbenzene within the matrix of Aclar 22A, a copolymer of chlorotrifluoroethylene (CTFE) and vinylidenefluoride (VDF), followed by sulfonation [5, 9]. The term "grafting" was used in the context of the preparation of these membranes [5], yet experimental details were not provided. Presumably, the polymerization was carried out by swelling the fluorocarbon polymer in the monomer mixture, followed by the initiation of the polymerization reaction using a chemical initiator. In this case, grafting could occur by chain transfer from the initiator or the growing polystyrene chain to the fluorocarbon. The formation of chemically grafted polymers in solution had already been described by Smets and Claesen in 1952 [10]. It was also in the context of the PEFC development for space application that the incorporation of an antioxidant was mentioned for the first time, "to slow the rate of polystyrene breakdown" [11]. At an operating temperature of 40 to 60°C in the PEFC, these membranes had a useful lifetime of 500 to 1'000 h, which was sufficient for a space mission. Yet, lifetime strongly decreased at temperatures above 70 °C. It was also attempted to directly sulfonate PVDF with oleum. Ion conducting membranes were obtained, yet their oxidative stability was found to be lower compared to a commercial membrane at that time of the type mentioned above produced by AMF [12]. One issue of the PEFC was its lack of reliability, because the conductivity of the membrane depended on the water content, which led to variable power output. Therefore, in the subsequent space programs of NASA, such as the Apollo missions, alkaline fuel cells were used.

1.2 Fluorinated Membranes

Based on the notion that hydrocarbon polyelectrolytes undergo rapid decomposition, partially fluorinated materials started to be developed. One of the approaches chosen was the use of the sulfonated homopolymer of α,β,β-trifluorostyrene (TFS) ("S" membrane [5]), which showed enhanced chemical and thermal stability compared to the sulfonated polystyrene analog [13-15]. The use of poly(TFS sulfonic acid) membranes led to an increase in the lifetime of the fuel cell of a factor of five compared to poly(styrene sulfonic acid) (PSSA) membranes [14] (**Figure 0-1**). However, those membranes displayed poor mechanical properties. In addition, the sulfonation of poly(TFS) was found to be extremely difficult, which was attributed to the meta-directing influence of the perfluorinated polyalkyl chain, to which the aromatic units are attached [13]. Membranes with improved mechanical robustness were obtained by blending the fluorocarbon sulfonic acid polymer with poly(vinylidene fluoride) (PVDF) using triethyl phosphate as

plasticizer, which led to an extended lifetime of 5'000 h at 80°C [15]. Much later, a family of copolymers based on TFS and substituted TFS homopolymer membranes, referred to as BAM3G membranes, were developed by Ballard Power Systems (Burnaby, B.C., Canada) [16]. Membranes of this type showed a durability of 14'000 h at 80°C in the single cell [17].
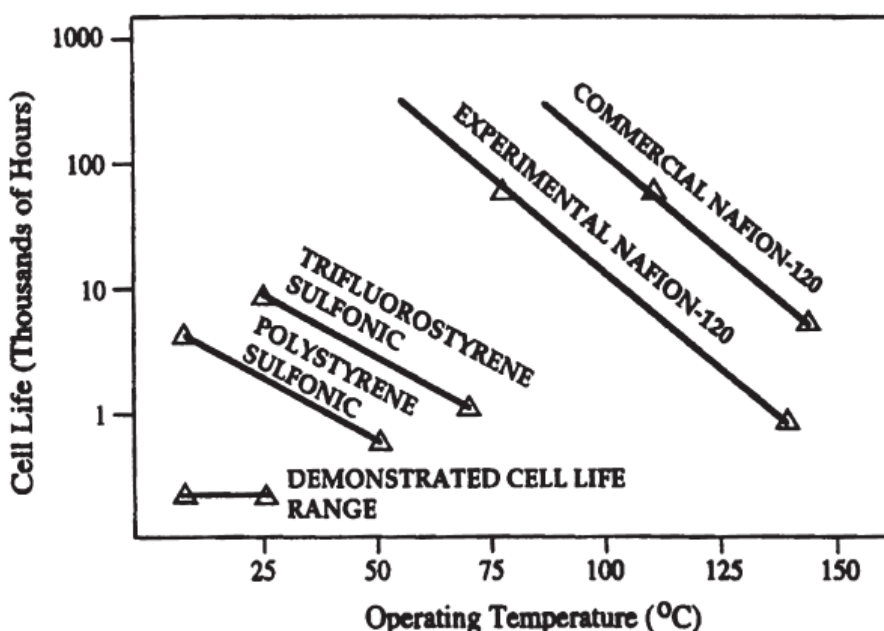
Figure 0-1. Lifetime of different types of proton exchange membrane in the fuel cell [14].

1.3 Perfluoroalkylsulfonic Acid (PFSA) Membranes

The invention of perfluoroalkylsulfonic acid (PFSA) membranes, such as Nafion® (E.I. Dupont de Nemours & Co.), in the 1960s had a profound impact on the development of the PEFC for the next 50 years. Still today (2015), PFSAs are predominantly used in PEFC systems that are commercially available or under development. PFSA ionomers are a copolymer of tetrafluoroethylene (TFE) and a sulfonyl fluoride vinyl ether monomer [18]. After film formation by extrusion, the sulfonyl fluoride is converted to the sulfonic acid via hydrolysis in alkaline solution [19]. Since around the early 2000s, PFSA membranes have been increasingly fabricated by solution-casting, which has advantages over the extrusion & hydrolysis process in terms of production rate and quality control [20]. The ratio of the two monomers determines the ion exchange capacity. Today, a number of PFSA membranes by various suppliers are available for use in fuel cells, such as DuPont (Nafion®), Asahi Glass (Flemion®), Asahi Kasei (Aciplex®), Solvay Solexis (Aquivion®), 3M and W.L. Gore & Associates. The membranes from the different suppliers differ in the composition of the comonomer (**Figure 0-2**). Nafion® is a representative of a long side chain (LSC) PFSA ionomer, whereas the membrane from 3M and Aquivion® are short

side chain (SSC) PFSA ionomers. The side chain in Aquivion® is particularly short, which leads to a better retention of crystallinity and thus mechanical integrity as the equivalent weight[1] is lowered well-below 1'000 g/mol to maximize conductivity [21].
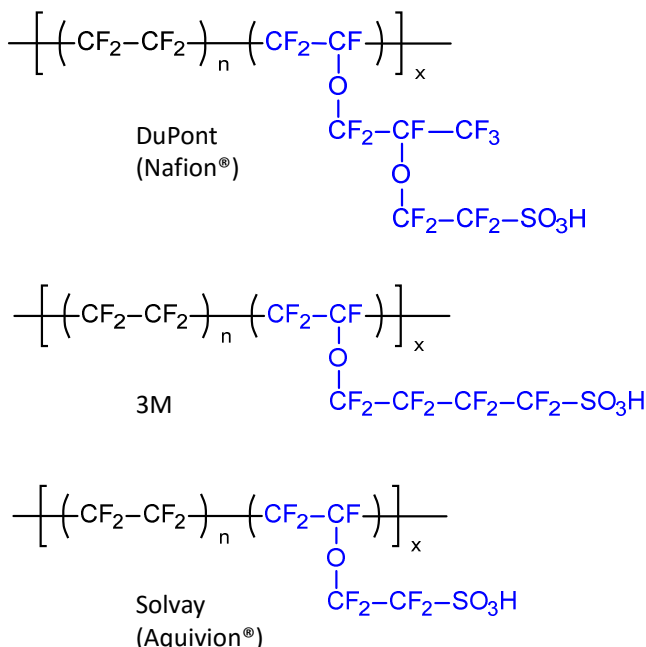
Figure 0-2.   Selection of perfluoroalkylsulfonic acid ionomer materials (supplier and trade name, if applicable) available as membranes.

DuPont originally developed PFSA membranes in the early 1960s for use in the chlor-alkali industry. Nafion® was invented in 1962 by W. Grot and first used in a chlor-alkali cell in 1964 [22-25]. The properties of PFSA ionomers are dominated by the strong difference in the chemical nature of the PTFE backbone and the polar and hydrophilic sulfonic acid groups. It was recognized early that Nafion® was well-suited for PEFCs. The first Nafion® based PEFC was tested in 1966 by GE for the NASA [26]. In 1966 and 1968 the NASA performed trials with fuel cells comprising early versions of Nafion® in the framework of a 30-day Biosatellite space mission program [5]. The perfluorinated nature imparts the membrane with high stability. Nafion® 120 membranes have shown lifetimes of 60'000 h at temperatures of 43 to 82 °C [5]. Since the first use of Nafion® in the PEFC, significant improvements have been made by DuPont and the other manufacturers regarding physical and chemical properties by improving the molecular weight and eliminating weak links in the polymer structure [5]. Also, mechanically reinforced membranes have been developed [27-29]. Despite the vastly improved stability

---

1   The equivalent weight (EW) is a measure for ionic site density, expressing the weight of the polymer per sulfonic acid site, which is typically used in relation with PFSA ionomers. Its reciprocal value is the ion exchange capacity (IEC), mostly expressed in mmol/g, which is the more typical property used in the context of partially fluorinated or hydrocarbon membranes.

compared to partially fluorinated or non-fluorinated membranes, the stability of PFSA membranes under harsh dynamic operating conditions, for instance in automotive fuel cell systems, involving rapid load changes, temperature fluctuations and excursions above 90°C, thousands of start-stop cycles, and hundreds of start-ups from below 0°C, is still a concern and slows the market introduction of PEFC power sources, alongside with high investment costs [30].

1.4 Early Radiation Grafted Membranes

Radiation-induced grafting is a process whereby a polymeric constituent is covalently attached ("grafted") to a pre-existing, activated polymer substrate. The activation is performed by exposing the base polymer to various sources of energy to introduce active sites: plasma treatment, ultraviolet-light, and high energy (ionizing) radiation, such as X-rays, gamma rays, electron beam, and swift heavy ions [31, 32]. Graft copolymers allow the combination of properties of two incompatible polymeric constituents. The key features of the radiation grafting technology, such as the influence of the nature of the base polymer, the type of radiation used, and the conditions of the grafting reaction, are reviewed in Chapter I.

Graft-copolymer membranes have been characterized as being more heterogeneous than "homogeneous" membranes and more homogeneous than "heterogeneous" ones, since base polymer and graft component occupy different microscopic regions, yet are more intricately linked to one another than in the macroscopically mixed, heterogenous membranes [6]. The preparation of graft copolymers through radiation induced polymerization of a monomer onto a trunk polymer was described for the first time in the early 1950s [33]. The first account of ion-exchange membranes prepared via radiation grafting was given by Behr et al. in 1956 [34]. Different base polymers, such as poly(methyl methacrylate) (PMMA) and polyethylene (PE), were exposed to vinyl monomers, e.g., styrene and acrylonitrile, and to gamma radiation from a ^{60}Co source, which led to the formation of bulk graft copolymers. In case of PE, graft copolymers were also formed when the base film was not pre-swollen in the monomer. However, when polytetrafluoroethylene (PTFE) was used as base polymer, only surface grafting was observed, indicating that the graft copolymerization did not take place in the bulk. Subsequently, in a more detailed study the key factors influencing the formation of the graft copolymer put forward were: i) temperature, ii) irradiation dose rate, iii) diffusion rate of monomer into the polymer, iv) variation of the solubility of monomer in the polymer as a function of the graft level [35]. Cation exchange membranes were prepared by grafting of styrene onto PE followed by sulfonation and, subsequently, characterized for ion exchange capacity, water uptake and conductivity. Also, anion exchange membranes were prepared, either by chloromethylation of the grafted polystyrene

followed by quaternization or amination, or by grafting vinylpyridine and subsequent quaternization.

Substantial early work on polymer functionalization by radiation induced grafting has been performed by Adolphe Chapiró in the late 1950s and 1960s [36]. He performed extensive investigations into the key parameters influencing the grafting reaction, such as the type of polymer substrate and kind of monomer used, irradiation conditions (atmosphere, radiation dose, dose rate), pre-grafting storage, monomer concentration in the grafting solution, reaction temperature, and the effect of solvents and additives. Initially, grafting was identified as a suitable method to effectively functionalize otherwise inert fluoropolymers films, e.g., PTFE [37]. PTFE does not swell in any known organic solvent or monomer, hence it is not possible to pre-swell the base film in a monomer solution and then initiate the grafting reaction by exposing the swollen polymer to ionizing radiation. Other base films, such as polyethylene (PE), do show some degree of swelling. For instance, PE takes up about 10 % by weight of styrene at room temperature [34]. Chapiró highlighted that bulk grafting of PTFE is possible under specific conditions, namely if the monomer is able to swell the partially grafted regions of the base polymer, which is the case for styrene [37]. Therefore, for the cases where the base polymer shows little or no swelling in the grafting solution consisting of grafting monomer, solvent and, possibly, other additives, grafting proceeds via the "front mechanism" [38-40], whereby grafting initially occurs at the surface of the base film. The grafted region swells in the grafting solution and further grafting proceeds by the gradual diffusion of the reaction mixture through the already-grafted layer (**Figure 0-3**). This "grafting front" moves into the bulk of the base film and eventually coalesces with the grafting front moving into the film from its other surface. The functionalization throughout the film thickness is essential for proton exchange membranes, because protons have to be transported from one side of the membrane to the other. Many of the base films used as substrate for radiation grafting with a view to the application of the obtained membrane as polymer electrolyte in an electrochemical application show limited swelling in many monomers and organic solvents, thus grafting necessarily has to follow the "front mechanism". The extent to which grafting fronts are established is governed by the ratio of the rate of polymerization and the rate of monomer diffusion into the base polymer. Radiation grafting for bulk functionalization of a polymer is therefore a complex reaction-diffusion mechanism [41-43], key parameters being rate of polymerization, monomer concentration and the extent of swelling of the base polymer and grafted polymer in the reaction mixture, film thickness, reaction temperature, dose rate and total dose in case of direct radiation grafting and pre-irradiation grafting, respectively.

1.5 Industrial Development Efforts

Commercially oriented work was initially directed towards the development of battery separators and dialysis membranes [44, 45]. The grafting of TFS into an inert fluorocarbon base polymer was first reported by D'Agostino et al. in a patent filed on December 1974 [46]. The target applications for those sulfonated membranes were chlor-alkali and fuel cells. Ellinghorst et al. described a range of radiation grafted polymers of different combinations of base material and grafting monomers for various separation applications [47]. Base polymers included: poly(vinyl fluoride) (PVF), poly(vinylidene fluoride) (PVDF), poly(ethylene-*alt*-tetrafluoroethylene) (ETFE), polypropylene (PP). Grafting monomers used were *N*-vinylpyrrolidone (NVP), vinyl acetate (VAc), styrene (S), acrylic acid (AAc), methacrylic acid (MAA), dimethylaminoethyl methacrylate (DMAEMA), 4-vinylpyridine (4VP), and *N*-vinyl imidazole (VIm).

Although there is a colossal number of publications on radiation graft polymerization, there are very few commercial applications, while some are under development. Membranes prepared by grafting of acrylic

Figure 0-3. Illustration of the grafting front mechanism [48].

acid (AAc) onto dense polyethylene (PE) have been used in Japan as separator materials in alkaline batteries since 1985 [49]. Similar materials are produced in Taiwan [50]. Also, nonwoven PE is used as a substrate for grafting (**Figure 0-4**). Polymers functionalized by radiation graft copolymerization have found notable application as adsorbent materials in a range of processes: gas adsorbents for acid and alkaline gases are synthesized by grafting of AAc, glycidyl methacrylate (GMA), and vinylbenzyl chloride (VBC) onto a nonwoven fabric. The GMA and VBC units lend themselves in versatile manner to post-functionalization, for instance by introducing sulfonic acid, phosphonic acid, amines, amidoxime or quaternary ammonium groups [51]. In the GDR and USSR, modified polyamide or polyethyleneterephtalate (PET) fabric, for instance to render it hydrophilic and anti-static, was prepared on pilot line reel-to-reel processes by grafting of acrylic acid and similar monomers [52]. Line speeds on the order of 10 m/min were achieved.

Figure 0-4.   Reel-to-reel process line for the preparation of functionalized non-woven fabric by pre-irradiation induced grafting [53].

Adsorbent materials with selective affinity for specific metal ions can be fabricated by radiation grafting [54]. Typical grafting monomers are acrylonitrile (AN), MAA and GMA, which are post-functionalized to introduce the corresponding metal-ion chelating group. Such adsorbents have been used in Japan to collect uranium from seawater as early as 1984. Another application is the removal of toxic metals from the environment, such as cadmium, antimony, scandium, or radioactive cesium (**Figure 0-5**).

In these adsorbent materials, bulk grafting of the polymer substrate is not required, since absorption takes place at the surface of the functionalized fabric. Hence, diffusion of the monomer into the base polymer is uncritical and the grafting reaction can be completed in a relatively short time. Other applications include the preparation of functional fabrics with anti-crease, anti-static, deodorant, antibacterial, fireproof, and cool-feeling behavior, and biomedical products (cell-culturing dish) [49, 52].

A growing interest in hydrogen technology in the 1970s led to the development of membrane electrolyte water electrolyzers [55]. Early developments were carried out at General Electric, USA, and Brown Boveri, Switzerland, using Nafion® as electrolyte membrane [56]. However, it was recognized that the application of Nafion® membranes is hampered in large scale units due to high costs of perfluoriated materials. Therefore, there was an interest in using more cost-effective, partially fluorinated membranes [4]. Whereas D'Agostino used simultaneous irradiation grafting

of TFS onto FEP [46, 57, 58], Momose et al. studied the pre-irradiation grafting of TFS onto various base films to obtain cation as well as anion exchange membranes [59-63]. In 1983, Xu et al. reported the pre-irradiation grafting of styrene and mixtures of styrene and DVB onto FEP films in vacuum or N_2 atmosphere, followed by sulfonation, to obtain cation exchange membranes, or chloromethylation and quaternization to obtain anion exchange membranes [64]. Commercially available radiation grafted membranes (RAYMION, from Chlorine Engineers Corp., Japan; PERMION 4010, from RAI Research Corp., USA) were evaluated in water electrolysis cells at a temperature of 80 °C [56]. RAYMION is based on an ETFE film, onto which trifluorostyrene (TFS) is grafted, whereas PERMION is based on PTFE, with styrene grafted chains. It was found that the stability of RAYMION is comparable to that of Nafion® 117 over 10'000 h, whereas PERMION 4010 showed rapid degradation, which was attributed to the poor oxidative stability of the polystyrene groups of PERMION 4010 compared to the fluorinated side chains of RAYMION [4, 65].

Figure 0-5. Batch-mode operated pilot-scale reactor for the manufacture of Cs-adsorptive fiber material [66].

1.6 Fuel Cell Development Takes Off

The late 1980s marked an important era in fuel cell development. Up to the early 1980s, thick Nafion membranes (e.g., Nafion® 120, thickness ~250 µm) and Pt-black electrodes with a loading of several mg/cm^2 of Pt were used as electrochemical components in PEFCs. Two main advancements in the technology took place in the late 1980s [26, 67]: i) the use PFSA membranes with lower thickness and lower equivalent weight (higher acid content), and ii) the development of catalyst layers using Pt supported on high surface area carbon in combination with an impregnation with soluble PFSA ionomer, which led to a reduction of Pt loading by an order of

magnitude. The seminal work at that time was performed at the Los Alamos National Laboratory (LANL). Around the same time, the company Ballard Power Systems (Burnaby, British Columbia, Canada) began to develop PEFC hardware and prototype stacks. From around 1990 onwards, research and development of PEFCs experienced a huge boost, with commercial applications becoming seemingly foreseeable, such as in electric vehicles or stationary combined heat and power (CHP) applications. In the 1990s, many of the developments were oriented towards improving power density of PEFC stacks, using the same approaches as those already taken in the early studies, namely further reducing catalyst loadings to sub-mg/cm^2 [68] and developing thin (20 μm), mechanically reinforced PFSA membranes [69]. Although satisfactory power densities for use of PEFCs as power source in electric vehicles have been achieved [70], there are, broadly speaking, following key challenges to be tackled for wide-scale introduction of PEFC technology, both for mobile and stationary applications: durability, reliability and cost of stack and system hardware [71].

Ballard Advanced Materials (BAM), a subsidiary of Ballard Power Systems, pioneered work on alternative, non-PFSA membrane materials, with a view of reducing cost [17]. The series of membranes developed named BAM1G, BAM2G, and BAM3G were based on sulfonated poly(phenylquinoxalene) (PPQ), poly(2,6-diphenyl-4-phenylene oxide), and polytrifluorostyrene. Furthermore, BAM developed the family of materials referred to as BAM® Grafted PEMs, for which trifluorostyrene (TFS) and -naphtalene were used as monomer [72-76]. ETFE as well as poly(ethylene-*co*-chlorotrifluoroethylene) (ECTFE) were used as base polymer. In contrast to the earlier efforts of D'Agostino and Momose [57, 60-62] in using TFS as monomer for radiation grafting, substituted TFS, such as *p*-methoxy-TFS or *p*-methyl-TFS, was used in the BAM® Grafted PEM, owing to the improved grafting kinetics compared to unsubstituted TFS. The durability of the BAM® Grafted PEM has not been reported in the open literature. The development of membrane materials at Ballard Power Systems was discontinued in 2008 as a result of a realignment of the business strategy.

2 Fuel Cells in the Context of Renewable Energy Scenarios

A sustainable energy chain does not only require the introduction of renewable sources of primary energy, but also calls for clean and efficient means of energy conversion and storage. Electrochemical technologies offer the prospect of modular, decentralized, flexible and custom-designed solutions for electricity generation and storage [77]. Fuel cell technology is anticipated to play a significant role in the distributed generation of electricity, with the possibility to co-use heat (combined heat and power), at various power levels. Whereas high-temperature fuel cells are more geared towards constant and base-load operation with power ratings typically above 100 kW, low-temperature fuel cells lend themselves to flexible power generation in decentralized installations or even individual homes, with power output ranging from a few 100 W to tens of kW [78]. In addition, there have been and are tremendous efforts to develop fuel cell powered electric vehicles, which offer the prospect of clean and efficient mobility [79]. Development programs for fuel cell cars and buses have been ongoing for more than 15 years, and the automotive industry is pursuing the technology and is committed to introduce fuel cell cars and buses into the marketplace in parallel to the establishment of a hydrogen refueling infrastructure [80]. At the present time, there are early market applications for fuel cells, including the PEFC, namely backup power for telecom installations, distributed power generation using by-product hydrogen, materials handling for battery replacement in industrial vehicles (forklifts, etc.), and powering of busses in government supported programs [81, 82]. Starting from 2015, Toyota has started selling its 'Mirai' fuel cell vehicle, yet at a relatively high price of around 60'000 USD and at a volume of only a few 100 cars per year [83]. The same applies to the Hyundai 'Tucson' fuel cell electric vehicle. In the context of stationary application, at the end of 2015 more than 120'000 residential micro-CHP units (ENE FARM) have been deployed in Japan, now becoming cost-competitive to existing technologies [84]. Nevertheless, it is important to push technology forward and continue research towards better and cheaper materials and components [30, 85].

Key challenges to market penetration are durability and cost [85]. Degradation phenomena are related to limitations in stability of the classes of materials used in the various types of fuel cell, in high temperature as well as low temperature ones. In addition, the operating conditions play a vital role in aging processes. While fuel cells can be operated for tens of thousands of hours under well-controlled and constant laboratory conditions [5, 27], under real-life conditions, in particular with automotive drive cycle profiles, the lifetime of fuel cells is limited to a few thousand hours [85]. The high cost of fuel cells compared to existing technologies for power generation are the result of, on the one hand, inherent materials costs, e.g. for interconnect components or noble metal catalyst materials, and, on the other hand, low production volumes, which does not justify

implementation of large-scale and low-cost process technologies. To drive forward technology development and industrialization, it is therefore essential to continue research on the fundamentals of materials and components, understand requirements from an application point of view, identify limitations of existing materials, introduce new materials or improve existing ones, and establish knowledge of structure-property-performance relationships.

2.1 *The Polymer Electrolyte Fuel Cell (PEFC)*

Fuel cells are electrochemical energy conversion devices that convert the chemical energy stored in a fuel, e.g., hydrogen, and an oxidant, in most cases oxygen from air, directly into electricity [86]. Among the various fuel cell types in existence or under development (**Figure 0-6**), those based on solid electrolytes are particularly attractive, since the handling of hot and corrosive liquid electrolytes, such as in the case of the alkaline fuel cell (AFC), phosphoric acid fuel cell (PAFC), or the molten carbonate fuel cell (MCFC), can be avoided. The solid oxide fuel cell (SOFC) is an all-solid-state device operating at a temperature of typically 700-1'000°C, which is suited for stationary power generation, whereby the high quality waste heat produced can be further used in
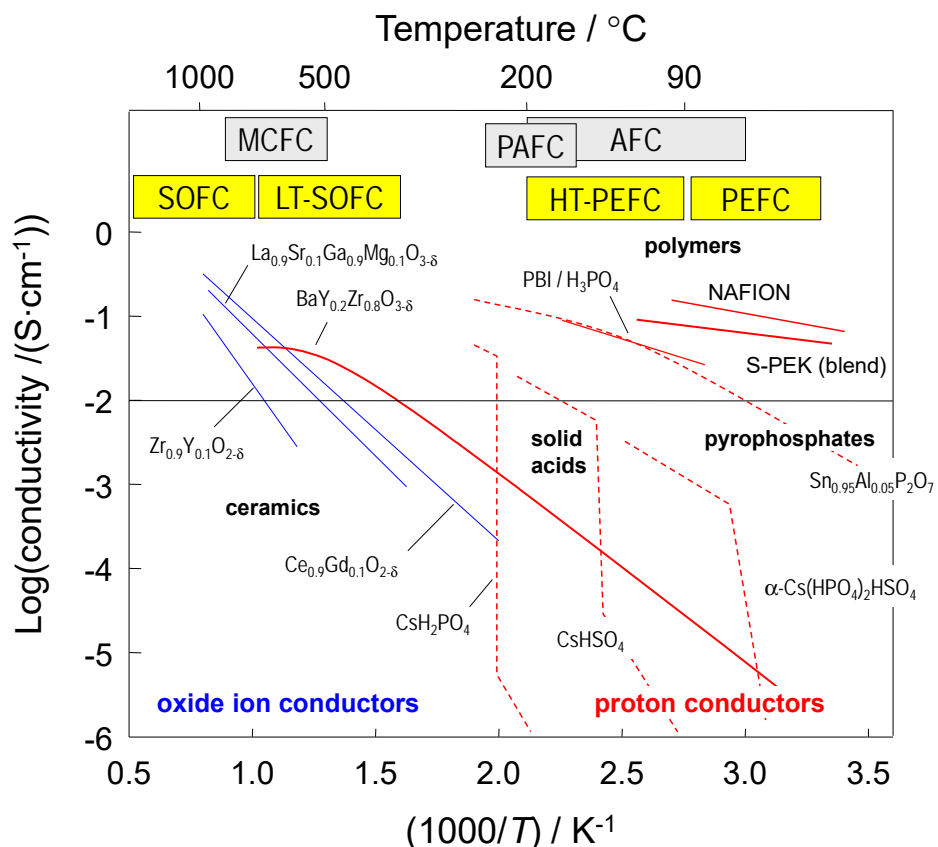
Figure 0-6.   Ionic conductivity as a function of temperature for selected classes of materials considered for the application in fuel cells. The temperature range of operation for fuel cells with liquid electrolyte (grey boxes) and solid electrolytes (yellow boxes) are indicated (cf. text for details). A minimum conductivity for fuel cell application of 0.01 S/cm is typically considered. (Overview based on figures by K.-D. Kreuer and T. Norby)

secondary processes. Low temperature (LT-)SOFCs are developed with a view to reducing cell material costs and high-temperature aging phenomena. The polymer electrolyte fuel cell (PEFC) uses a proton conducting membrane electrolyte and typically operates at temperatures of 60 to 100°C. It is therefore particularly interesting for applications with variable load profile and intermittent operation involving frequent startup and shutdown, such as vehicle propulsion, remote power sources, back-up power systems, and portable electricity generation [87-89]. A PEFC can be started-up in straightforward manner from room temperature and, with proper operating strategy, also from temperatures below 0°C.

Hydrogen is the ideal fuel for fuel cells, since it can be electrochemically oxidized at high rate and low overpotential [90]. However, the use of more readily available fuels or fuels that can be more easily stored, such as natural gas, liquid propane gas, or methanol, is highly desirable, given the fact that no wide-spread hydrogen infrastructure is available at the moment. Hence, natural gas is the fuel of choice for stationary applications. It can be directly converted to electricity in the SOFC via internal reforming. In the PEFC, the only fuel – other than H_2 – that can be electrocatalytically oxidized at practical rate and with reasonable efficiency is methanol. Such direct methanol fuel cells (DMFCs) are being developed for small portable applications as power packs for independent power supply, e.g., for camping or military applications [91]. Yet the lower power density and lower efficiency of the DMFC compared to the H_2 fueled PEFC and, in particular, the high noble metal catalyst requirement of around 5 g/kW [92] prevents the DMFC from being practical and commercially viable for many applications with large market potential, such as fuel cell electric vehicles [93]. The switch from an acid to an alkaline environment to reduce catalyst requirements holds some promise. In fact, the AFC was the first type of fuel cell that was developed to reach technical maturity in the late 1950s [26]. Although the first type of fuel cell that was used in space by the NASA was a PEFC (Gemini missions), it was later replaced by AFC modules in the Apollo and Space Shuttle missions (cf. also Section 1.1). Alkaline anion-exchange membrane (AEM) fuel cells have gained interest recently, because they offer the potential to combine the benefits of a solid polymer electrolyte (compact design of repetitive unit, no corrosive liquid) and an alkaline environment (use of non-noble metal catalysts). In the AEM fuel cell, OH⁻ anions are transported from the cathode to the anode and, consequently, the product water is generated at the anode. However, the power density and stability of the AEM are generally much inferior compared to the PEFC employing an acidic proton exchange membrane (PEM) [94], although progress is being made to replace the traditionally used quaternary ammonium head groups with other, more stable functional groups [95-97]. A general issue of an alkaline environment, however, is the carbonation of the electrolyte in the presence of CO_2, which precludes or at least aggravates the use of air as oxidant.

Fuel flexibility of the PEFC can be achieved by using reformed fuels [98]. A large variety of carbonaceous fuels, such as methanol, methane, ethanol, and higher fractions of hydrocarbons, can be reformed, typically in a catalytic process via steam reforming, partial oxidation or a combination thereof, to obtain a hydrogen-rich gas, which is subsequently fed to the fuel cell [99]. The reformate gas contains hydrogen, carbon dioxide and some level of carbon monoxide, as well as nitrogen if the reforming involves partial oxidation using air. In high temperature fuel cells, such as the MCFC and the SOFC, CO-rich gas mixtures can be directly electrochemically converted. Yet, CO poisons the Pt-catalyst of the PEFC by forming an almost complete adsorbate layer, thereby blocking the access of hydrogen [100]. To minimize anode overpotential losses at a temperature of 80°C, the CO concentration in the reformate gas has to be reduced down to ppm-level in a water-gas shift reactor with a subsequent preferential CO-oxidation cleanup step. This increased complexity of the reformer system hampers commercialization of PEFC systems operating on reformed fuel, e.g., natural gas fed combined heat and power (CHP) units. An increase in the operating temperature of the PEFC above 100°C is therefore highly desirable to relax the requirements of limiting CO content in the reformate fuel. The increase of the PEFC operating temperature beyond 100°C is associated with challenges, though. Since increasing the reactant gas pressure and the water vapor pressure to properly humidify the membrane are not desired from a system efficiency and complexity of the balance-of-plant point of view, the cell is expected to operate at reduced relative humidity of 50 % at 100°C or 25 % at 120°C [101]. Under these conditions, the water content of the ionomer decreases to the equivalent of a few molecules of water per sulfonic acid group, resulting in a considerable loss in proton conductivity [102]. The specifications defined by the US Department of Energy (DOE) state a conductivity requirement of 0.1 S/cm at a temperature of 120°C [103]. Current membrane technology, with PFSA materials showing the best performance, falls short by about a factor of 5 to 10, depending on the side chain structure and equivalent weight of the ionomer [101]. In addition, the softening of PFSA materials at temperatures of around 100°C represents a serious problem, which exacerbates mechanical degradation through viscolastic creep of the polymer and failure due to membrane rupture or MEA shorting [104]. Hence, this intermediate temperature (IT-) PEFC technology has not matured yet sufficiently to justify implementation in fuel cell systems for commercial use.

Fuel cells based on the use of phosphoric acid doped polymers as electrolyte represent an entirely different technology, which can operate without externally humidified reactant gases [105]. These high temperature (HT-) PEFCs, operating at temperatures between 160 and 180°C, have reached some degree of maturity and are currently being developed for commercial application by a number of industrial companies. The electrolyte is comprised of a mixture of an aromatic polymer with high thermal stability, most commonly polybenzimidazole (PBI) and derivatives thereof, and

phosphoric acid as proton transport medium [106]. The N-heterocycles of the polymer are able to form hydrogen bonds and thus provide binding sites for phosphoric acid. Although free phosphoric acid is also present in this polymer electrolyte, it can still be considered as a solid-state electrolyte, since the polymer membrane is a monolithic, gel-type material. The main target application for the HT-PEFC is stationary power generation with use of reformed fuels. Owing to the higher temperature compared to the low temperature (LT-) PEFC using hydrated sulfonic acid polymer electrolytes, the anode can tolerate CO at the percent level [107], which drastically simplifies the reformer unit by reducing the requirements for CO cleanup. Shortcomings of this technology, however, are the low activity of the cathode towards the oxygen reduction reaction (ORR), which is a consequence of the blockage of active platinum sites by anion (mainly $H_2PO_4^-$) adsorption [108]. Also, the transition of the temperature regime where water condensation may occur during startup and shutdown is problematic, since the presence of liquid water can lead to leaching out of the phosphoric acid from the membrane.

Among the various other materials proposed as solid state electrolyte for fuel cells, two classes of materials are worth mentioning, since they have reached some degree of maturity and undergone development to the cell level with demonstration of encouraging fuel cell performance. Solid acids are materials with chemistry and properties between those of a normal salt (such as Na_2SO_4) and an acid (such as H_2SO_4) [109]. They usually consist of oxyanions, such as SO_4^{2-}, that are linked together by hydrogen bonds. An example of a solid acid is $CsHSO_4$. These compounds show a "superprotonic phase transition", for $CsHSO_4$ it is at 141°C, which is associated with a jump in conductivity of several orders of magnitude [110]. In the superprotonic phase, the lattice structure loosens up with the oxo-anion acquiring a rotational degree of freedom, which facilitates the proton transfer between neighboring anions [109]. Also, the material becomes ductile above the transition temperature. A proof of principle solid acid fuel cell (SAFC) with $CsHSO_4$ electrolyte was demonstrated by Haile et al., attaining current densities of around 50 mA/cm^2 at an operating temperature of 160°C, albeit with a colossally high Pt catalyst loading of 18 mg/cm^2 [110]. Unfortunately, $CsHSO_4$ gradually reacts with H_2 to H_2S and Cs_2SO_4 [111]. Hence, efforts have been switched to CsH_2PO_4 [112]. Other problems are encountered here, such as the high protonic phase transition temperature of 228°C and the tendency to dehydrate according to $CsH_2PO_4 \rightarrow CsPO_3 + H_2O$. Fuel cell performance at 250°C using such CsH_2PO_4 electrolyte of 50 μm thickness with promising current density of 15 mA/cm^2 at a cell voltage of 0.6 V and a Pt loading of the electrodes of 4 mg/cm^2 has been demonstrated [111]. However, relatively stringent conditions, such as high pressure or humidified atmospheres, are required to maintain the "superprotonic" phase of CsH_2PO_4. At ambient atmosphere, decomposition occurs just a few degrees above the phase transition temperature [112].

Another class of anhydrous proton conductors can be found among metal pyrophosphates (MP_2O_7) [113]. Nagao et al. reported an anhydrous conductivity of around 0.1 S/cm for $Sn_{0.9}In_{0.1}P_2O_7$ at a temperature of 250°C [114]. The conduction mechanism in these materials appears to be based on the presence of electron holes, which react with water to yield mobile protons in the lattice [113, 115]. Composite membranes of $Sn_{0.9}In_{0.1}P_2O_7$ and an organic binder were prepared with a thickness of 60 μm and assembled together with carbon fiber based gas diffusion electrodes with Pt loading of 0.5 mg/cm^2 into single cells [114]. Interesting fuel cell performance was attained, whith current densities of 50 to 150 mA/cm^2 at a cell voltage of 0.6 V, using dry H_2 and air at temperatures between 100 and 200°C.
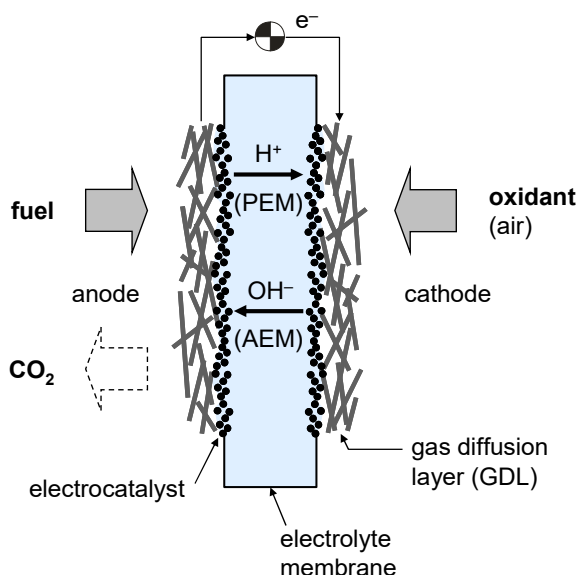
Figure 0-7. Schematic of the basic electrochemical unit of a polymer electrolyte fuel cell (PEFC), the membrane electrode assembly (MEA). The fuel is oxidized at the anode. If a carbonaceous fuel is used, CO_2 is released. Electrons are transferred from anode to cathode via an external circuit. At the cathode, oxygen is reduced. A proton conducting cation exchange membrane can be used as polymer electrolyte (water produced at the cathode) or an OH$^-$ conducting anion exchange membrane (water produced at the anode).

The membrane technology discussed in this work is focused on H$^+$ conducting membranes for low temperature fuel cells. The basic electrochemical element of the PEFC is the membrane electrode assembly (MEA), consisting of a polymer (ionomer) membrane sandwiched between two gas diffusion electrodes (**Figure 0-7**). The electrochemical reactions take place in the catalyst layer, which is about 10 μm thick and composed of a mixture of the noble metal catalyst and ionomer. The primary function of the membrane is that of an electrolyte (transport of H$^+$) and separator to prevent the passage of reactant gases and electrons. The required conductivity is on the order of 0.1 S/cm at the operating temperature of the cell. The membrane typically has a thickness of 25 to 50 μm in case of the H_2 fed PEFC, and 150 to 200 μm in case of the direct methanol fuel cell (DMFC) [116]. The ensemble of bulk properties that have to be taken into consideration and

carefully balanced for the development of a polymer material into a membrane electrolyte for fuel cell application is depicted in **Figure 0-8**, the importance of which will be briefly reviewed in the following sections. In addition to these bulk properties, surface properties are of importance in the context of the formation of a low impedance interface between membrane and electrodes upon MEA lamination and assembly [4]. Since the major share of research and development for low temperature fuel cells is devoted to the proton conducting PEFC[1], the focus of this work is on this type of fuel cell, the low-temperature type of which predominantly comprises a membrane with sulfonic acid type exchange sites.
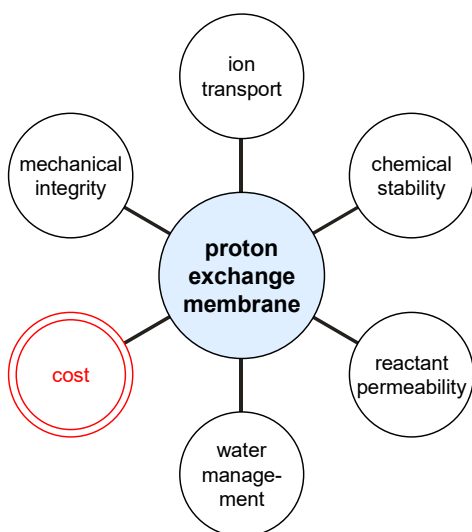
Figure 0-8. The development of ion conducting membranes for use as electrolyte in fuel cells is associated with a range of functional requirements as well as economic targets.

The conductivity of the ionomer is governed by the ionic site density, expressed in terms of equivalent weight ($g_{polymer}/mol_{H+}$) or its reciprocal value, the ion exchange capacity ($mmol_{H+}/g_{polymer}$), the water content of the membrane, which is commonly expressed as the number of water molecules per exchange site (hydration number, λ), and temperature [117-119]. Increasing the ion exchange capacity leads to an increase in water uptake and conductivity, yet excessive swelling of the membrane leads to the dilution of the exchange sites and, eventually, dissolution of the polymer. In view of applications targeted at temperatures of 90°C or higher, the conductivity of ionomers under reduced relative humidity conditions is a key property. There have been major efforts devoted to the development of proton conducting membranes for hot (100 – 120°C) and dry (25 – 50 % r.h.) conditions, yet so far the most promising materials are still perfluoroalkylsulfonic acid (PFSA) ionomers, in particular short-side chain versions with equivalent weight below 800 g/mol [104, 120].

---

[1] If not otherwise noted, the term "PEFC" will refer to the proton exchange membrane (PEM) fuel cell.

The durability of the membrane is governed by its capability of maintaining the function as electrolyte and separator over the necessary lifetime of the fuel cell. Generally, mechanical and chemical mechanisms of membrane degradation are distinguished (cf. Chapter IV) [103]. Chemical degradation is caused by the presence of reactive intermediates, such as the $HO^{\bullet}$ radical, which are believed to be created in the MEA as a result of the interaction of H_2 and O_2 on the surface of the Pt catalyst [121]. In addition, H_2O_2 is considered to be an important and potentially harmful intermediate, because its decomposition yields radical species [122]. The attack of the membrane polymer by radical species causes chain scission, loss of polymer constituents, and leads to a decrease in the molecular weight of the ionomer. In case of PFSA membranes, this leads to membrane thinning [103]. As a consequence, the reactant crossover increases and the material is weakened. The mechanical robustness of the membrane thus deteriorates, which increases the susceptibility to creeping and the probability for pinhole formation and puncturing of the membrane by imperfections in the electrode. During fuel cell operation, mechanical and chemical degradation almost exclusively occur at the same time, because both mechanical and chemical stress factors are present. Also, the two modes are not independent, but underlie synergistic effects [123]. The rate of mechanical-chemical degradation is exacerbated under dynamic operating conditions, when the water content of the iomomer keeps changing as a function of time, which leads to the build-up and relaxation of internal stresses in the membrane, which is clamped within the cell fixture and cannot freely expand and contract [124].

In the vast number of articles published on the development of ionomer membranes for fuel cells, the focus is too often on conductivity alone, and in many cases the importance of mechanical properties is not given sufficient attention. The tensile properties of ionomer membranes strongly depend on temperature and relative humidity [125]. Hydrated membranes show distinct viscoelastic behavior and are subject to creep induced degradation and failure [126]. Only polymers with adequate mechanical properties are suitable candidates for fuel cell application. Often, even though conductivity values might be attractive, candidate materials proposed in the literature suffer from excessive swelling and / or poor mechanical robustness, such that not even MEA preparation and cell assembly can be accomplished.

In addition to functionality, cost is a key attribute of a fuel cell component. The prospect of cost-effectiveness is an important driver for development of new materials and processes. Cost is also the main driver for the research and development on alternative membrane materials for fuel cells. In a crude approach to cost analysis, generally materials and processing costs can be distinguished. The development of novel membranes ought to encompass also the identification of options for processing at various production scales.

2.2 Polymer Chemistries and Membrane Classes

From a materials science and engineering point of view, the use of a polymer as electrolyte in a fuel cell is a clever choice, since polymer films can be made thin and flexible. Thin membranes yield better performance and water management properties. Flexibility is related to mechanical robustness and is a key feature to implement low-cost, large volume reel-to-reel processing technologies. This chapter is concerned with reviewing the type of materials that are being used or considered as polymer electrolyte in fuel cells (**Figure 0-9**). Given the large body of literature on this subject, the classes of materials discussed here are those that have reached a certain degree of maturity and undergone testing in a fuel cell configuration. Durability data obtained under fuel cell operating conditions are even scarcer, probably due to required robust testing infrastructure and the time-consuming and resource-intensive nature of the experiments.
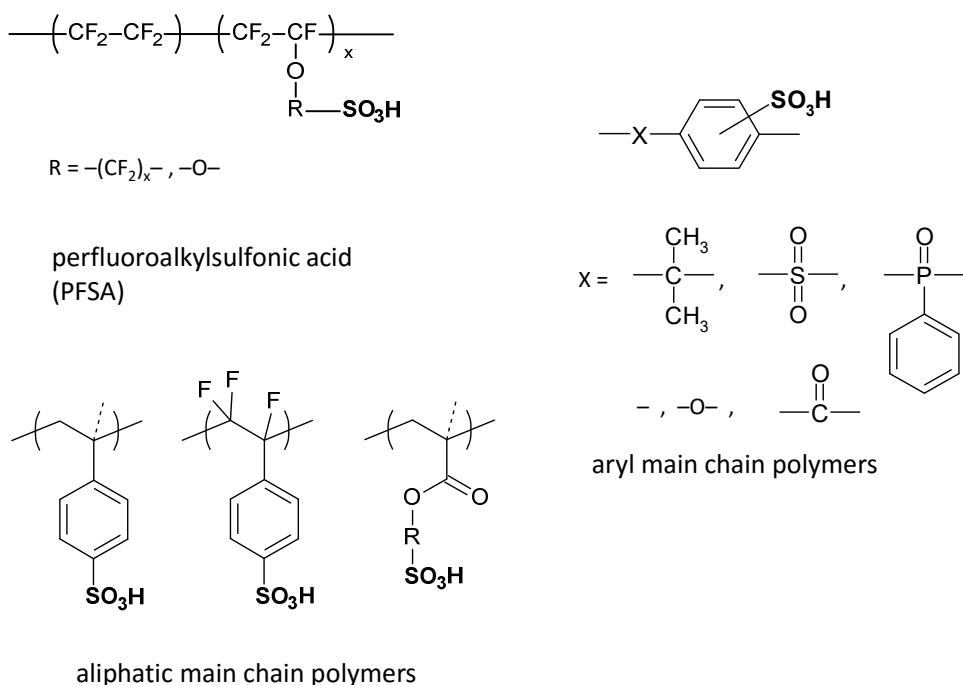
Figure 0-9. Candidate classes and representative types of proton exchange membranes for fuel cell application. The acid functionality is provided by sulfonic acid groups (adapted from [127]).

In general, electrolyte membranes are classified into acidic or basic types, yet the acidic proton exchange membrane (PEM) is most widely used owing to its superior conductivity and chemical stability. Generation of mobile protons is accomplished via the introduction of acid sites into the polymer, yielding an 'ionomer'. As it is desired to have an acid with high dissociation constant, sulfonic acid is predominantly used for this purpose. Substantial efforts are devoted by academia and industry to the development of new fuel cell membrane materials, driven either by the need for membranes with improved functionality (e.g., conductivity, robustness) or reduced cost [128].

Promising candidate materials are partially fluorinated or non-fluorinated ionomers containing aromatic units with attached –SO$_3$H groups, either in the main polymer chain, or attached to an aliphatic main chain (**Figure 0-9**).

PFSA membranes have found wide-spread use in fuel cells, including commercial applications [82]. This is because of the satisfactory functionality in terms of performance and durability as well as the proven technology and the potential ease of scaling up the production, owing to the experience in chlor-alkali technology. However, the high cost is a major shortcoming of PFSA ionomers. This is a result of the complex fluorine chemistry involved in the synthesis, including hazardous intermediates and processing steps with low yield [19, 129]. Therefore, there has been an ever-growing need of non-perfluorinated, more cost-efficient proton-conducting membranes.

From the vast literature on the topic of proton conducting membranes for fuel cell applications, the class of materials that is most widely studied is the family of polyaromatic membranes [130, 131]. These are polymers with aromatic units in the main chain, such as polysulfones or poly(ether ketones) and their many derivatives, which are typical representatives of polymers with high temperature stability. Most of the used polymers are pure hydrocarbon membranes. The sulfonic acid sites are commonly located on the aromatic units of the main chain. With this polymer architecture, a rather high ionic content of typically 1.8 mmol/g is required for a conductivity of 0.1 S/cm to match that of Nafion® with equivalent weight 1'100 g/mol [132]. This is believed to be a consequence of the limited flexibility of the stiff aromatic backbone and its weak hydrophobic nature, resulting in less favorable morphology of the phase-separated nano-structure [133]. The associated substantial swelling of the material can lead to dissolution, even at moderate temperatures below 80°C [130]. Attaching the sulfonic acid group to the backbone polymer via a short aliphatic side chain instead of directly was shown to yield improved conductivity at similar ion exchange capacity and water uptake, in particular at reduced relative humidity, which is an indication of a more favorable morphology [131]. An approach that has been adopted by a number of groups to promote phase separation is the use of block copolymer structures comprising hydrophilic and hydrophobic blocks [134-136]. For properly designed block copolymers, the proton conductivity at a given ionic content was shown to be one order of magnitude higher compared to a random copolymer [136]. Consequently, the fuel cell performance was substantially enhanced, in particular at reduced relative humidity [137]. There has been a number of reports on fuel cell performance and durability of polyaromatic membranes [138], most notably by M. Watanabe et al. from the University of Yamanashi with reports of lifetimes of several thousand hours at 80°C cell temperature [139, 140] (**Figure 0-10**). Although polyaromatic

membranes show inferior oxidative stability compared to PFSA membranes under *ex situ*, Fenton test conditions, their stability *in situ* in an accelerated stress test may exceed that of Nafion®, owing to the much lower rate of reactant crossover in these materials [141]. Fuel cell tests under dynamic operating conditions have not been reported for these membranes. Polyaromatic membranes usually exhibit a higher sensitivity to mechanical embrittlement or fatigue as a result of dynamic operation or relative humidity cycling compared to PFSA membranes, which is possibly related to swelling/shrinkage issues [103]. Microcrack formation is considered a predominant failure mechanism for these materials.
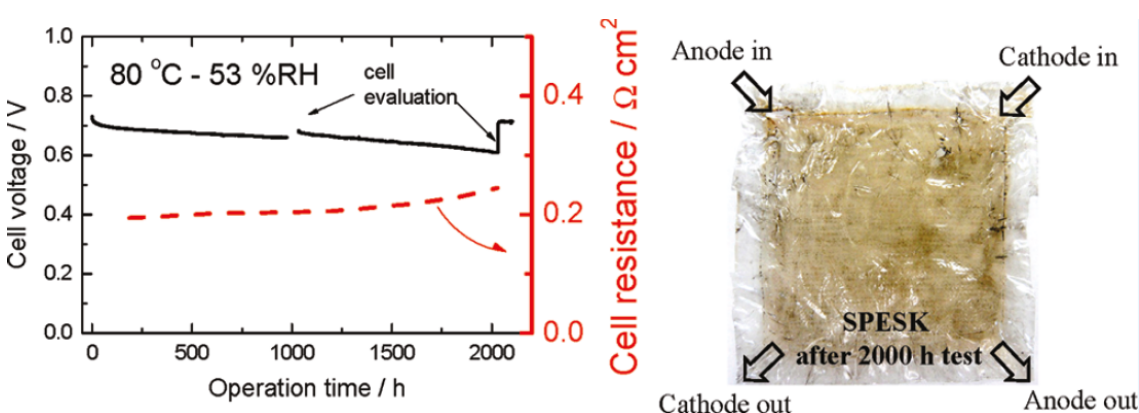
Figure 0-10. Left: history plot of a fuel cell test at a constant current density of 0.2 A/cm^2 employing a sulfonated multiblock poly(arylene ether sulfone ketone) (SPESK) membrane. Right: visual appearance of the membrane at the end of test. The loss in ion exchange capacity was around 6 % [140].

Polymer blends represent another approach to combine different polymer constituents with dissimilar functionalities. There are, however, relatively few groups working on this approach with the aim of designing a membrane compatible with the fuel cell environment. In the concept of the Arkema company, a polymer blend is formed from an inert and thermally stable fluoropolymer, poly(vinylidene fluoride) (PVDF), and an aliphatic polyelectrolyte [142]. The work seems to have been discontinued, the reasons for which are not known, yet from the published results one may speculate that the conductivity at reduced relative humidity might have been considered insufficient, whereas the accelerated aging tests for chemical and mechanical stability and comparison with cells comprising thin Nafion® membranes showed encouraging results [143]. A particular issue with polymer blends is that the phase-separated morphology obtained after preparation of the membrane is thermodynamically unstable. The lack of a "locked-in" microstructure can lead to the coalescence of polymer domains with the driving force of reducing the interfacial area between hydrophilic and hydrophobic phase, which eventually leads to a macro-phase separated structure.

Limited fuel cell experimental data are available for the various other polymer types that have been put forward. One type worth mentioning is that of (semi-)interpenetrating polymer networks (IPN) [144]. An approach adopted by Qiao et al. is the combination of polyvinyl alcohol (PVA) with poly(2-acrylamido-2-methyl-1-propanesulfonic acid) (PAMPSA). Those polymers can be co-casted from aqueous solution and post-crosslinked using bifunctional aldehydes [145, 146]. Performance evaluation in the DMFC has been reported, yet characterization in the H_2 fueled cell and *in situ* durability have not been reported in the literature.
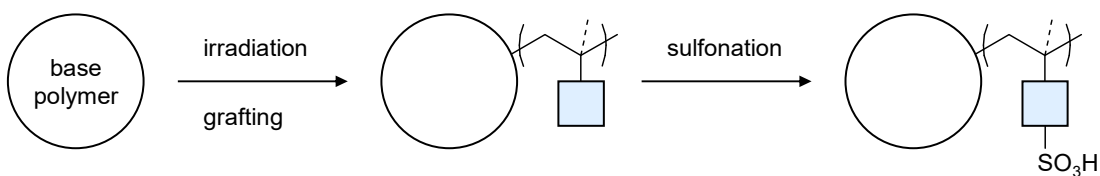
Figure 0-11.   Schematic representation of polymer functionalization by radiation grafting and sulfonation to obtain a proton conducting membrane, which can be used as polymer electrolyte in fuel cells.

The class of membranes that is at the focus of this work, radiation grafted membranes, has shown some promise as electrolyte membrane for fuel cells (**Figure 0-11**). Radiation grafting is a process whereby reactive sites are introduced into a pre-formed base polymer through exposure to UV-light, a plasma, or ionizing radiation, such as γ-rays or an electron beam, and contacting the activated film with monomer to initiate the growth of corresponding polymer chains ("grafts") onto the base polymer backbone [31, 32, 147]. Whereas activation using UV-light and plasma only allows the near-surface regions of the polymer to be modified, ionizing radiation can have sufficiently high penetration depth, depending on the energy of the radiation, to modify films with thicknesses of 0.1 mm or more. A key parameter in radiation grafting is the graft level or degree of grafting, also referred to as grafting yield, which is defined as the increase in weight of the sample upon grafting normalized to the initial weight of the base film (cf. Chapter II, Section 1.1). It was already recognized in the 1950s, when first publications on radiation grafted polymers appeared, that graft copolymers allow the combination of properties of two highly incompatible polymeric constituents. A brief historical review of radiation grafted and other membranes for fuel cell application is given in Section 1 of this chapter.

2.3 Beyond Fuel Cells

Electrochemical technologies offer the prospect of modular, decentralized, flexible and custom-designed solutions for energy conversion and storage. In addition, electromobility is expected to gradually grow over the coming decades, moving fuel cell as well as battery technology into the focus of attention. For the deployment of large numbers of fuel cell vehicles, a hydrogen infrastructure will have to be established, and the only economically viable technique to produce

hydrogen in a sustainable manner today is via water electrolysis using electricity from renewable sources.

Cost is a key attribute, and many of the electrochemical technologies have the downside of being too expensive today and therefore not economically viable. Furthermore, increasing power and / or energy density is essential. This calls for the development of high performance, durable and reliable materials and components. Polymer electrolyte membranes or separators are used in a range of different electrochemical devices beyond fuel cells (**Figure 0-12**), which are expected to be key technologies in future energy scenarios largely based on renewable primary energies.

Electrolysis

- water electrolysis for high purity H_2 production
- H_2 for fuel cell vehicles
- renewables: storage of excess electricity ("power-to-gas")

Flow batteries

- grid-scale storage of electricity
- decoupled energy and power rating

Lithium batteries

- consumer electronics
- electromobility
- load leveling, peak shaving

Figure 0-12.   Electrochemical devices comprising a polymer electrolyte or separator with future prospects in electrochemical energy storage and conversion applications in the context of renewable energy scenarios and electromobility. (Image sources: Giner Electrochemical Systems, Redflow Energy Storage Solutions, Clayton Power).

Alkaline water electrolysis, which uses a porous diaphragm and aqueous KOH solution as electrolyte, is an established industrial technology and has been used for over a century for industrial hydrogen production. Yet for "energy" applications, i.e., in the context of the grid-scale storage of electricity via power-to-gas and the production of "green" hydrogen for mobility (fuel cell vehicles) and industrial use, polymer electrolyte water electrolysis (PEWE) using a proton exchange membrane is the preferred technology. Whereas the alkaline electrolyzer is typically operated at current densities of a few hundred mA/cm^2, the PEWE operates at much higher current densities of 1-2 A/cm^2 [148], owing to the use of a thin polymer electrolyte (typically ~0.2 mm thick) and associated low ohmic resistance. The stack is therefore considerably smaller compared to an alkaline stack for a desired H_2 production rate. In addition, the PEWE technology lends itself to operation at high (differential) pressure, which reduces or eliminates the need for downstream

mechanical compression of the hydrogen and, possibly, oxygen product gases. Differential pressure operation can be attractive if H_2 is the desired commodity produced at high pressure, whereas the oxygen can be discharged at low pressure, which alleviates the requirements of the balance of plant components related to the handling of oxygen. Ongoing development is aimed at reducing ohmic resistance, e.g., by using thinner, reinforced membranes, to allow increase of the current density to 4 A/cm^2 or more. 3M recently demonstrated cell operation, using a 50 μm PFSA membrane with an equivalent weight of 825 g/mol, at 15 A/cm^2 at a voltage of 2.5 V [149]. However, such thin membranes lead to high rates of H_2 and O_2 crossover [150], which impairs the faradaic efficiency of the electrolysis, reduces the purity of the product gas, and may cause the formation of explosive gas mixtures.

Redox flow batteries are electrochemical devices for the grid-scale storage of electrical energy, in particular in the context of energy scenarios with a high share of fluctuating renewables (solar, wind) [151]. A redox flow battery consists of two external tanks filled with liquid electrolyte and a stack of cells that contain porous electrodes separated by an ion exchange membrane. The membrane avoids cross-mixing of redox-active species and allows the transport of background electrolyte ions. The all-vanadium redox flow battery (VRB) is the most advanced type [152]. VRBs use the same redox-active element on the negative and positive electrode, preventing irreversible cross-contamination of the electrolytes. The electrolyte membrane is a key cost driver in a VRB system and accounts for about half of the stack cost [153]. An ideal membrane for a redox flow battery should have low ohmic resistance, low permeability for redox-active species and water, and high chemical stability in the respective electrolyte solution. The currently widely used perfluorinated materials such as Nafion® have neither been designed for this application, nor are they cost-effective. The objective of ion exchange membrane development for redox flow cells is to maximize conductivity in the respective environment and prevent the passage of redox-active species. At the same time, owing to the high share of the membrane in the total system cost, the use of inherently more cost-efficient membrane materials is of great economic interest. Last but not least, new membrane materials should be of high mechanical and chemical robustness, since the lifetime of a redox flow battery is expected to be 10 years and more [154].

Lithium-ion batteries have found wide-spread application in consumer electronics, such as computer notebooks and mobile phones. There are substantial efforts in penetrating electric vehicle and grid-scale energy storage applications. The energy density of state-of-the-art lithium-ion batteries is limited by the lithium-ion chemistry [155]. Therefore, importance of post-lithium-ion batteries is growing, as the energy density demands will continue to grow. The lithium-sulfur (Li–S) battery is a promising technology, as its practical energy density is estimated to be a factor

of 2 to 3 higher compared to the Li-ion technology [156]. One of the challenges in using sulfur as positive electrode material is the solubility of the partially reduced lithium polysulfides (S_n^{2-}, n = 3-6) in the liquid non-aqueous electrolyte, and this leads to massive self-discharge and specific capacity loss during charge/discharge cycling due to detrimental "shuttling" of the polysulfides between the positive and negative electrode. A large research and development effort is taken to tackle this issue, for instance by electrode engineering or introducing polysulfide barrier properties into the separator [157].

Polymer membranes used as electrolyte or separator in electrochemical energy devices (**Figure 0-12**) need to provide transport pathways for specific ions, while the passage of unwanted species (e.g., reactants, products) is to be avoided. In addition, the electrolyte needs to be robust, durable and of low cost. The method of radiation grafting is a versatile method and lends itself to the preparation of functionalized polymer structures (films, fibers, non-wovens) for a range of different purposes. Research on radiation grafted membranes for electrochemical applications at PSI has already started to be diversified into new fields.

The use in electrolysis cells is perhaps straightforward, and the requirements are largely similar to the ones pertinent to fuel cell application. As outlined above, one important side-effect of electrolyzer operation, in particular at elevated pressures of, say, 20 bar or more, is the crossover of product gases (H_2, O_2). Therefore and for the reason of mechanical robustness, mostly thick PFSA membranes are used as electrolyte in PEWE cells today. This, however, limits the power density of the cell, whereas the use of thin membranes brings about problems of excessive gas crossover. It was shown in recent work at the PSI that a dedicated design of a proton exchange membrane based on radiation grafting can yield a favorable combination of resistance and gas crossover properties [158]. A grafted membrane using a base film of 25 µm with a final membrane thickness of around 40 µm in water swollen state was shown to have an area resistance similar to that of Nafion® 212 (60 µm thick) combined with a hydrogen crossover smaller than that of Nafion® 117 (200 µm) [159].

Ion-exchange membranes for the all-vanadium redox flow cell (VRB) are cation or anion exchange membranes. Although anion exchange membranes may be expected to provide better barrier properties for vanadium cations, they show notable crossover of vanadium, because the high ionic strength of the liquid electrolyte leads to breakdown of Donnan exclusion [160]. Furthermore, ohmic resistance is typically higher than in case of proton exchange membranes due to the lower mobility of transported ionic species [161]. In our recent work at PSI, we developed

an amphoteric ion exchange membrane for the VRB containing sulfonic acid protogenic groups and amidoxime motifs [162]. When exposed to VRB electrolyte containing 2 M sulfuric acid, the amidoxime moieties are protonated and thereby significantly reduce the uptake and crossover of vanadium species, while the conductivity of the membrane is not significantly impaired compared to when it is immersed in water. With this membrane, the coulombic and voltage efficiency of a vanadium redox flow cell was significantly enhanced compared to cells containing Nafion® 212 or Nafion® 117 membrane. Moreover, no capacity fading and was observed after 122 charge/discharge cycles, whereas in the case of Nafion® the cells showed considerable build-up of electrolyte imbalance and concomitant capacity fading already after 35 charge/discharge cycles [163].

A slightly different approach was chosen in the context of Li–S cells for improving the polysulfide barrier properties. Here, a porous polyethylene separator, similar to the one commonly used in lithium-ion batteries (Celgard), was asymmetrically functionalized by plasma activation and subsequent graft polymerization of styrene sulfonate onto the separator. The resulting separator containing poly(lithium styrene sulfonate) grafts located near one face of the separator was shown to exhibit improved barrier properties for polysulfides, resulting in improved coulombic cycling efficiency and discharge capacity of the Li–S cell [164, 165].

Last but not least, application of the radiation grafting technology is possible beyond the preparation of electrolyte materials. We have recently shown the use of the radiation grafting method to create gas diffusion layers (GDLs) with patterned wettability to improve the water management in PEFCs. The material was prepared by exposing the GDL, which contains a fluoropolymer as wet-proofing agent, to electron beam radiation in selected areas using a mask, followed by grafting of hydrophilic monomers onto these areas, which rendered them hydrophilic [166]. The resulting patterned GDL with hydrophilic and hydrophobic areas showed improved water management and superior fuel cell performance due to removal of the product water via the hydrophilic channels, while oxygen diffusion in the hydrophobic areas is less restricted compared to an unmodified GDL.

3 Motivation

Although the most widely used membrane type in commercial PEFC systems and demonstrators is of the perfluoroalkylsulfonic acid (PFSA) class, the development of alternative materials has been pursued extensively over the past ten to twenty years, the key drivers for which are the lowering of the cost, increase of the operating temperature, and improvement of the durability [167]. Reduction of membrane cost can be achieved by choosing cheaper starting materials and / or adopting cheaper process technologies for membrane fabrication. With respect to durability, PFSA membranes are considered to be among the most stable materials. Yet still, their durability is limited in the major high volume transport and stationary applications, and considerable efforts have been taken to improve their chemical and mechanical stability via reducing imperfections in the polymer [20], creating mechanically reinforced membranes [28, 69], and introducing additives for scavenging of radical intermediates [168, 169].

There is therefore a driving force for developing alternative membrane materials for fuel cells for several reasons: first of all, materials of inherently lower cost can reduce investment costs for fuel cell systems and thus accelerate market introduction of fuel cell technology. Furthermore, a versatile membrane chemistry allows the adaptation of its composition and architecture towards a specific target application or a specific fuel cell operating strategy. It is these assets that make radiation grafting an attractive technology. For instance, the content of ionic groups can be readily adjusted via the graft level. Independent of the ionic site density, the water uptake and swelling of the membrane can be controlled via the content of crosslinker introduced during grafting. In PFSA membranes, the increase in ionic content is always associated with an increase in water uptake until at some point the membrane becomes soluble in water. In addition, radiation grafting allows the introduction of additional functionalities, such as barrier comonomers to reduce reactant permeation through the membrane, or antioxidants to improve the chemical stability, as will be shown in the results chapters.

The focus of this thesis is on membranes for fuel cells, yet the concept of designing polymer electrolytes with specific transport properties via radiation grafting may well be extended to other electrochemical energy storage and conversion devices, such as electrolyzers, redox flow batteries or certain types of lithium batteries. The method of radiation grafting also lends itself in these cases to design membrane materials with functional properties adapted to the specific device to enhance performance, efficiency, lifetime or a combination thereof.

4 Structure of the Thesis

The *leitmotif* of this thesis is the elaboration of conceptual approaches in the framework of the development of radiation grafted membranes for fuel cells with the aim of improving performance and durability of the material and demonstrate competitiveness of the technology on the device level with commercially available benchmark PFSA membranes. An essential ingredient enabling the development of polymer functionalization strategies is to promote the understanding of factors limiting performance and durability of radiation grafted membranes. Degradation mechanisms, for example, are likely to be of a different nature compared to PFSA membranes, and understanding them allows appropriate measures to be taken to mitigate aging. In this context, the adoption and development of suitable accelerated test protocols is of vital importance to selectively study key degradation phenomena, increase sample throughput and shorten innovation cycles.

The thesis is structured into four main Chapters, preceded by the Introduction and followed by Conclusions & Prospects and References. The content of the work is based, on the one hand, on a number of book chapters, peer-reviewed publications and conference proceedings. These sources are listed at the beginning of each chapter. On the other hand, this thesis contains unpublished work, which is either supplementary material to one of the published sources, or based on completely independent studies.

Chapter I constitutes a review of radiation grafted membranes for fuel cells, in particular with a view to highlighting aspects that have so far received insufficient attention, in the author's opinion, in the literature. In addition to discussing the more fundamental aspects of the radiation induced modification and functionalization of polymeric materials, the developments over the past ten years are summarized, encompassing not only proton conducting membranes, but also anion exchange membranes for alkaline fuel cells and phosphoric acid doped membranes for high-temperature polymer electrolyte fuel cells. The content of Chapter I is largely similar to the review article published as *Adv. Energy Mater.* 4 (2014), 1300827.

Experimental methods of membrane synthesis and characterization techniques are reported in Chapter II. In particular, the unique aspects in connection with the studies reported here, and specific methods adapted to the needs of the work are discussed. The aim is to highlight conceptual approaches and experimental details in general terms, rather than providing a detailed recipe that enables repeating of the experiments. These can be found in the original journal articles associated with the respective study.

Chapter III deals with the concept of 'co-grafting', i.e. with the grafting of a combination of monomers onto the base polymer backbone, with the aim of achieving specific functionalities. In the present case, the aim is to improve the durability of the widely reported styrene based grafted membranes, which have intrinsic stability limitations. The concepts involve the incorporation of comonomers that improve the gas barrier properties of the membrane, i.e., nitrile comonomers, such as acrylonitrile (AN) and methacrylonitrile (MAN). In addition, the replacement of styrene by α-methylstyrene (AMS) suggests itself, which addresses the poor stability of the αC-H bond in polystyrene. Furthermore, the incorporation of an antioxidant is explored on the basis of a styrene grafted model membrane to tackle the problem of poor oxidative stability.

The study of the mechanisms of chemical degradation, which is a main challenge for alternative, non-perfluorinated membrane materials for fuel cells, is at the focus of Chapter IV. Here, the mechanisms of the formation of reactive intermediates, such as the hydroxyl radical (HO$^{\bullet}$), during fuel cell operation are reviewed in detail, as well as the experimental techniques to study the associated oxidative attack and chemical degradation. In one section, fundamental studies on the attack of HO$^{\bullet}$ on model compounds in aqueous solution representative of the grafted electrolyte component, such as an oligomer of poly(styrenesulfonic acid) (PSSA), using pulse radiolysis are reported. The method yields kinetic rate constants of polymer attack and relevant follow-up reactions and can serve as a basis for devising stabilization and antioxidant strategies. Furthermore, accelerated aging studies of radiation grafted membranes are discussed, which on the one hand highlights key differences to the behavior of PFSA membranes, and, on the other hand, shows the effect of stabilizing strategies, such as the incorporation of barrier comonomers. Moreover, the effect of relative humidity on the rate of membrane degradation is investigated, where fundamental differences between radiation grafted membranes and PFSA membranes become apparent. Last but not least, the importance of studying hydrolysis is highlighted.

The key findings and main lessons learned are elaborated in the Conclusions & Prospects section. Although key puzzle pieces for the development of radiation grafted membranes for fuel cells are presented in this thesis, the various challenges are by no means tackled exhaustively. Many aspects are beyond the scope of the work reported here, such as process related developments and scale-up, improvement of monomer utilization and materials throughput. In view of the variety of electrochemical energy conversion and storage devices relying on polymeric separators or electrolytes, future directions for research are highlighted, aimed at developing polymer electrolytes with tailored properties and prospects of cost-efficient fabrication, such as in electrolyzers, batteries and flow cells.

Chapter I

Polymer Design Aspects of
Radiation Grafted Membranes for Fuel Cells

Much of the work on radiation grafted membranes for fuel cells was started in the 1990s, which will be summarized in the following section. Aspects of graft copolymer design and membrane synthesis will be discussed with a focus on topics that have not been extensively covered in existing literature, yet which the author deems important and critical. Subsequently, a review of recent developments in the area, summarizing studies published roughly from 2005 onwards, will be given and the current status of development highlighted.

1 Review of Existing Literature

1.1 Interaction of Ionizing Radiation and Polymers

The development of proton conducting membranes for use as polymer electrolyte in fuel cells requires an in-depth understanding of the mechanisms of the interaction of ionizing radiation with polymeric materials, radical induced graft polymerization and implications of follow-up reactions. In addition, an understanding of the effects of the various processing steps during material synthesis on the properties of the final membrane has to be developed. The effects of radiation on polymeric materials are described in detail in numerous monographs and textbooks, cf. for instance references [170-172]. In the radiation processing of polymers, γ-radiation and accelerated electrons are the main types of ionizing radiation used [52]. Both types of radiation cause essentially the same microscopic events in the irradiated polymers, and the resulting transformations do not depend on the nature of radiation. However, electrons and photons have a different penetration depth. An important parameter describing the energy transfer to the substrate per unit length for a given type of radiation is the linear energy transfer (LET). The average LET of a 1 MeV electron or a ^{60}Co γ-ray in water is around 0.3 keV/μm. This low LET eventually leads to a homogeneous deposition of energy in the irradiated polymer. However, the situation is different in case of irradiation with α-particles ($^{4}He^{2+}$) or heavier ions. Due to the high LET of 100 keV/μm or more, a continuous, localized track of excitation and ionization events is created in the polymer. This results in the formation of a highly localized damage area with a cylindrical shape, called a latent track. By selective removal of the polymer in these areas through etching, so-called track-etched membranes can be prepared, which can be used for separation applications due to the uniform sizes of pores obtained with diameter tunable from the tens of nanometers to the micrometer scale [173]. In addition, grafting reactions can be performed in the latent tracks and thus locally functionalized polymers obtained [174, 175].

In the approaches discussed in this chapter, the goal is to modify polymer films uniformly. Therefore, the discussion will be focused on low LET radiation in subsequent paragraphs. Irradiating polymeric materials with γ-rays or high-energy electrons with energies above around 100 keV leads to a significant number of bond cleavage events and formation of free radicals. This is accompanied with or followed by a range of secondary processes, such as chain scission, crosslinking, gas evolution, formation of unsaturation, and cyclization. In air atmosphere, oxygen reacts with radicals, forming peroxyl radicals, which can further react to peroxides or hydroperoxides.

1.2 Grafting as a Technique for Polymer Functionalization

The use of irradiated polymers to initiate graft polymerization reactions was described in detail by Chapiró [36]. He distinguished between three different methods to prepare radiation grafted copolymers:

1. Simultaneous radiation grafting is the process whereby the base polymer is exposed to the monomer and radiation at the same time. Free radial sites are thus generated and the polymerization reaction is initiated. Since initiation also takes place by direct activation of the monomer, extensive homopolymerization can take place, which leads to a low utilization of the monomer.

2. Pre-irradiation of the base polymer in inert gas atmosphere or vacuum leads to the formation of radicals trapped in the polymer. The subsequent exposure of the irradiated film to the monomer initiates the grafting reaction. It is important to realize that radicals generated within the crystalline phase of a polymer can exhibit extreme lifetimes of months or even years at ambient temperature [176], yet monomer molecules cannot penetrate the crystallites to access such radicals. The lifetime of the radicals in the amorphous phase depends on the glass transition temperature, T_g , of the polymer: above the T_g, radicals readily recombine owing to the mobility of the polymer chains [177].

3. When pre-irradiation is carried out in air, the oxygen reacts with the created radicals to form peroxyl radicals and peroxides (**Table 1-1**). The decomposition of the peroxide upon heating the pre-irradiated polymer in the presence of monomer initiates the grafting reaction. Pre-irradiation grafting by this peroxide method is widely used due to the easy control of the process without the need to provide an inert atmosphere during irradiation and storage of the material. Also, the process of irradiation is thus decoupled from the subsequent grafting reaction and possible follow-up treatment. A drawback, however, is the higher irradiation dose required to generate a sufficient number of peroxides to obtain reasonable degrees of grafting, which can lead to excessive radiation damage of the polymeric material.

A simplified overview of the radiation chemistry, nature of the active site, and configuration of the formed grafts for the pre-irradiation methods outlined above is illustrated in **Figure 1-1**. In case of irradiation of the polymer in the absence of oxygen, either during simultaneous irradiation grafting or pre-irradiation grafting in inert atmosphere, radicals formed by bond scission constitute the active site. In case of pre-irradiation in the presence of air, radicals readily react to form (hydro)peroxides. Their decomposition upon heating of the activated film in the monomer solution yields again radicals, which initiate the polymerization reaction. The grafted chain is therefore thought to be attached to the base polymer via an oxygen link –O– [32]. Chapiró argued, however, that since oxygen addition to a perfluorinated polymeric radical is a reversible process, $P^\bullet + O_2 \rightleftharpoons POO^\bullet$, initiation of grafting may involve the carbon-centered radical $P^\bullet$ [178, 179]. Moreover, in hydrogen-containing polymers it is conceivable that the oxyl radical $-O^\bullet$ abstracts a hydrogen atom from a neighboring chain, whereby a carbon centered radical $P^\bullet$ is formed. A grafted chain initiated by $P^\bullet$ will be tethered to the base polymer chain by a C–C bond. However, according to the author's knowledge, no study has been published on the nature of the initiating center in air-irradiated polymers, probably because the low concentration of linking points of base polymer and grafted chain precludes experimental verification.

Table 1-1. Reactions in irradiated polymers in the presence of molecular oxygen upon formation of primary polymer chain radicals $P^\bullet$. Chain scission reactions are not considered [31, 32, 178, 180].

Formation of peroxides:	
$P^\bullet + O_2 \leftrightarrow POO^\bullet$	reversible addition of O_2, formation of peroxyl radicals
[a]$POO\bullet + PH \rightarrow POOH + P\bullet$	hydrogen abstraction from neighboring chain
$P\bullet + P\bullet \rightarrow P–P$	chain crosslinking
$POO\bullet + P\bullet \rightarrow POOP$	recombination, formation of peroxide
$2\ POO\bullet \rightarrow POOP + O_2$	disproportionation, formation of peroxide
Decomposition of peroxides:	
[a]$POOH \rightarrow PO\bullet + HO\bullet$	thermally induced decomposition of hydroperoxide
$POOP \rightarrow 2\ PO\bullet$	thermally induced decomposition of peroxide
[a]$2\ POOH \rightarrow PO\bullet + POO\bullet + H_2O$	bimolecular reaction at high [POOH]
[a]$POOH + Fe^{2+} \rightarrow PO\bullet + Fe^{3+} + OH^-$	metal ion catalyzed decomposition of hydroperoxide
$POOP + Fe^{2+} \rightarrow PO\bullet + PO^- + Fe^{3+}$	metal ion catalyzed decomposition of peroxide
$POO\bullet + Fe^{2+} \rightarrow PO\bullet + O^- + Fe^{3+}$	metal ion catalyzed decomposition of peroxyl radical
[a]$PO\bullet + PH \rightarrow POH + P\bullet$	hydrogen abstraction from neighboring chain
chain initiation:	
$PO\bullet + M \rightarrow POM\bullet$	initiation by oxyl radical
$P\bullet + M \rightarrow PM\bullet$	initiation by carbon centered radical

[a] only for polymers containing hydrogen

1) Simultaneous irradiation grafting

2) Pre-irradiation and storage of polymer under inert gas atmosphere

peroxide

3a) Pre-irradiation in air for perfluorinated polymer

irradiation

hydroperoxide

3b) Pre-irradiation in air for partially fluorinated or non-fluorinated polymer

irradiation

- abstract H
- chain initiation (homopolymerization)
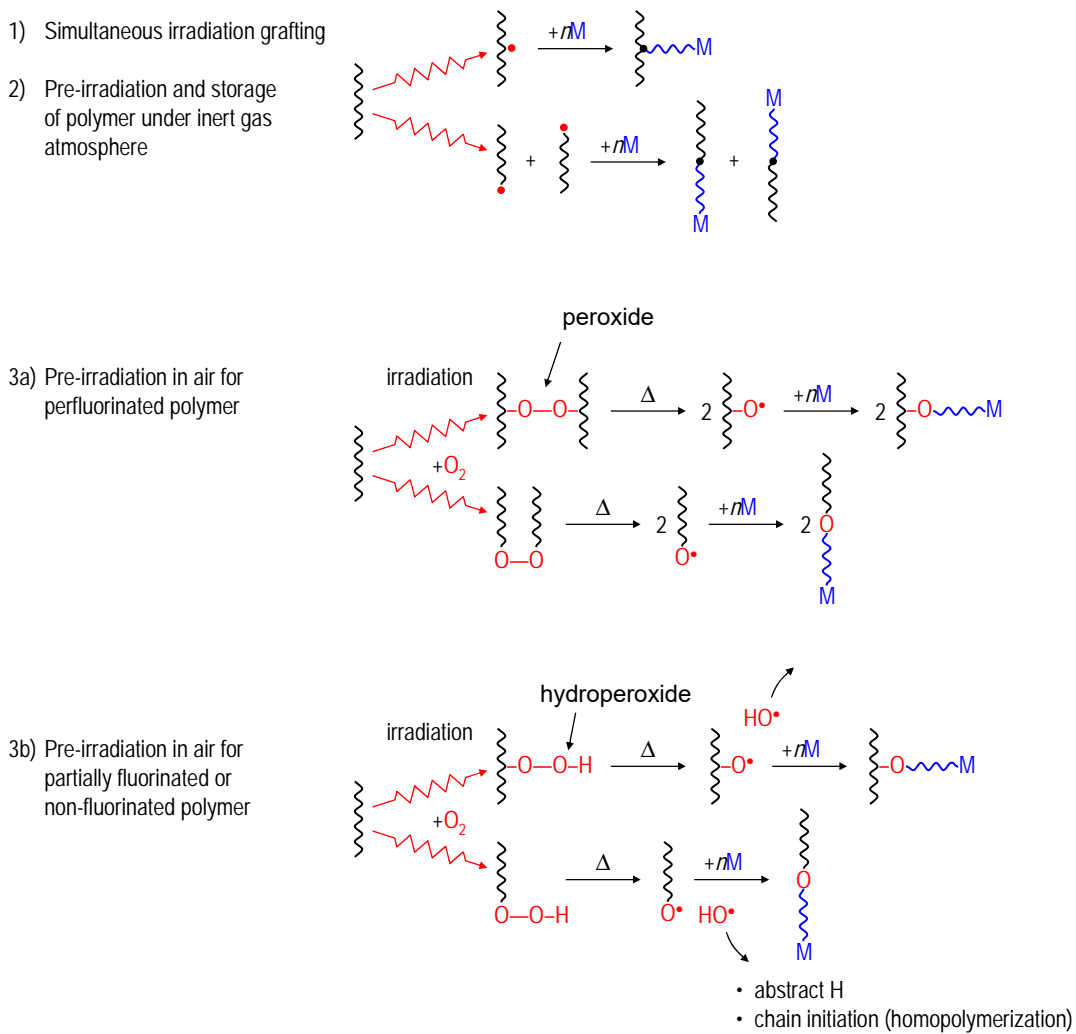
Figure 1-1. Simplified illustration of the various methods of radiation grafting, involving the formation of active sites through exposure to high-energy radiation, formation of (hydro)peroxides in case of pre-irradiation in air, and initiation of the graft copolymerization reaction. In case of chain scission upon irradiation, the active site is formed at the end of the chain fragments. Adapted from [181].

Monomer liquid   Squeezing roll

① ② ③ ④
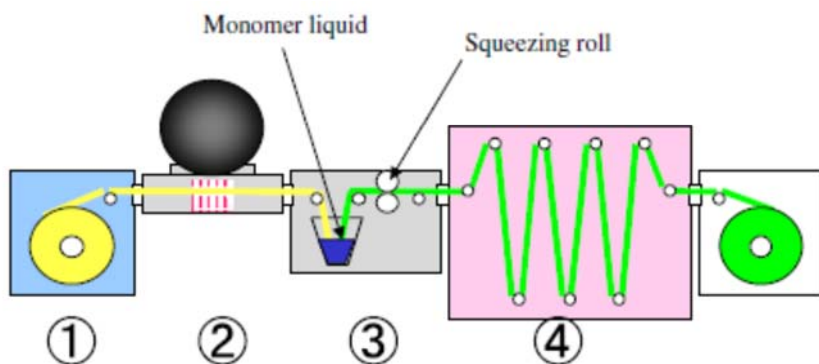
Figure 1-2. Schematic illustration of a continuous process for the preparation of pre-irradiation grafted polymers. (1) Base polymer unwinding and pre-treatment, (2) electron beam irradiation, (3) monomer impregnation zone, (4) reaction zone [53].

Whereas the peroxide method is practical for laboratory use, high-volume manufacture on an industrial scale requires the development of a reel-to-reel process. Of the various conceivable design concepts, the process illustrated in **Figure 1-2** consists of a separate irradiation section, followed by a monomer impregnation and grafting reaction zone. Additional chemical treatments, such as sulfonation, can be easily included in the process. In this setup, the base film can be irradiated in intert gas atmosphere and directly transferred to the reaction chamber without exposing the polymer to ambient air, thus avoiding peroxidation.

1.3 Influential Parameters

Owing to the versatility of the process of preparing radiation grafted copolymers, there is broad range of different parameters influencing the process and properties of the final material. First of all, the configuration of the base polymer is of decisive importance, i.e., whether it is a dense film, a porous substrate, or a fibrous material. This defines to what extent diffusion limitations will play a role in the grafting process. Porous substrates and fibers lend themselves to surface functionalization, which is exploited technically in the synthesis of membranes for separation technology [51] or modified fibers for the textile industry [49]. For the preparation of membranes for use as electrolyte and separator in electrochemical cells, one wishes, in most of the cases conceivable, to start out with a dense polymer film. Since it is necessary to transport the ions across the thickness of the film, the functionalization of the base film to introduce ionic conductivity needs to be carried out in the bulk the film, which can be associated with considerable diffusion limitations.

The influence of relevant grafting parameters has been described in great detail by Chapiró [36], but also in a number of monographs [52, 182-185] and, more recently, in review articles [31, 32, 147, 186]. Some important properties pertaining to the base polymer will be discussed in detail in Section 3 of this chapter. The processes resulting from exposing the base polymer to ionizing radiation do not only depend on the chemical nature of the polymer matrix, but also on product-specific parameters, such as molecular weight (distribution), extent of branching, crystallinity, degree of orientation, and presence of additives. In addition, dose rate, total dose, atmosphere and temperature influence the changes to the chemical and physical properties of the base polymer. The degree of grafting, i.e., the increase in weight after the grafting reaction with respect to the weight of the starting material, obtained under a particular set of conditions generally increases with the irradiation dose, as can be expected. A more efficient use of radicals is possible in simultaneous radiation grafting, whereas a sizeable fraction of radicals decays in pre-irradiated films before the grafting reaction takes place [186]. In case of simultaneous radiation grafting, irradiation dose is determined by the grafting time, for pre-irradiation grafting the two parameters

can be chosen independently. The rate with which active sites are formed in the base polymer is governed by the dose rate. Its value ranges from very low values below 1 kGy/h in case of γ-irradiation from a ^{60}Co source up to tens of kGy/s using e-beam irradiation facilities [49]. In the simultaneous grafting method, the dose rate determines the rate of initiation and grafting yield [36], whereas in the pre-irradiation method it defines the time of exposure to the radiation to accumulate a certain dose. If pre-irradiation is carried out at a temperature above the glass transition temperature, T_g, of the base polymer or the decomposition temperature of the peroxides, significant radical decay will occur and the yield of radicals to initiate polymerization will be low. The process parameters related to the grafting reaction, such as temperature, concentration of monomer in the grafting solution, type of solvent(s) and additives used, can have a large influence on the rate of grafting and the properties of the obtained graft copolymer or final polymer obtained after post-functionalization. The reader is referred to a number of book chapters and review articles for details in this respect [31, 36, 49, 147, 185, 186]. One key insight gained worth mentioning is that the use of non-solvent as a monomer diluent can lead to a significant improvement of the grafting rate, which was first described by Odian et al. at beginning of the 1960s for the grafting of styrene in the presence of methanol onto PE, PP, and PVC [187-189]. The effect was attributed to a reduced termination rate of the growing chains, caused by an insolubilization of the grafted chains (*Trommsdorff-Norrish* effect). Later, similar observations were made by other authors and explained in slightly different ways. In the context of the grafting of styrene and a crosslinker onto FEP base film, Rager found considerably enhanced grafting kinetics when moving from the previously used toluene solvent to polar solvents, in particular isopropanol [190]. Additions of water further increased the grafting rate.

In general, in the assessment of a particular combination base polymer, radiation type and dose, monomer(s), solvents, additives, and experimental conditions it is insufficient to merely take the overall degree of grafting as a figure of merit of the grafting process, there is a number of additional aspects that need to be considered. First of all, the grafting may be uniform across the area of the film, in case of which the inhomogeneities can often be spotted as patches with different visual appearance or wrinkling of the film. Secondly, the grafting may not be homogeneous over the thickness of the film. This is particularly the case for grafting reactions that proceeds according to a pronounced "front" mechanism [32, 48]. Moreover, if the reaction mixture contains more than one monomer, the distribution of monomer units in the film may change with depth [191, 192]. Furthermore, it is conceivable that films prepared under different conditions (irradiation dose, temperature, reaction mixture) yield graft copolymers with dissimilar graft chain length or chain length distribution, which may affect the nano-scale phase-separated morphology

of the polymer and, consequently, the macroscopic membrane properties, such as water uptake and conductivity [193, 194].

1.4 Radiation Grafted Membranes for Fuel Cells

Considering the synthesis of radiation grafted proton conducting membranes for application in fuel cells, a number of review articles have been published on the topic. *Nasef* and *Hegazy* [31] and *Gupta et al.* [186] describe comprehensively key aspects of membrane preparation, including radiation chemistry of polymers when exposed the ionizing radiation, influence of relevant grafting parameters, typical choice of base polymer films and grafting monomers, and influence of grafting conditions, such as irradiation dose, composition of the grafting solution, and temperature. Nasef and Hegazy describe various types of membranes for application in separation technology, water purification, energy conversion as well as biomedical technology [31]. Important properties relevant for fuel cell application are discussed by *Gupta et al.* [186]: mechanical properties, ion exchange capacity, water uptake, proton conductivity, as well as surface properties of the membrane. Also, preparation of membrane-electrode assemblies and cell testing in hydrogen and methanol fueled cells are highlighted. A literature review of articles reporting the characterization of radiation grafted membranes in the fuel cell is given by Gubler et al., including durability data whenever available, for H_2 and methanol fueled cell configurations [65]. Up to the time the article was published, the majority of membranes prepared by the various groups around the world, from academia as well as industry, were based on PVDF, ETFE, or FEP as base polymer, and styrene as grafting monomer. A notable exception was Ballard Power Systems (Burnaby, British Columbia, Canada), in the case of which α,β,β-triflorostyrene (TFS) and derivatives thereof were used as grafting monomers due to the expected higher chemical stability. Already in the studies carried out in the 1990s, it became obvious that for styrene based systems, crosslinking is an essential and necessary design feature to increase lifetime under fuel cell operating conditions to above 1'000 h. Under constant conditions, continuous operation over 4'000 h without notable loss in performance could be obtained [195], and over 1'000 h under dynamic operating conditions with varying load [196, 197]. In the past decade, the community has seen a number of synthetic approaches moving away from only styrene and crosslinked styrene based membranes. These concepts will be reviewed in Section 3 of this chapter.

The literature reviewed so far was focused on proton exchange membranes. Over the last decade, the interest in anion exchange membrane fuel cells has increased tremendously, because of the prospect of using non-noble metal catalysts. The preparation of anion exchange membranes via radiation grafting has been reported in detail by Varcoe et al. [94]. The chemistry of the membrane

is essentially based on ETFE as base film and grafted vinylbenzyl chloride (VBC), which is subsequently modified to obtain quaternary ammonium groups as fixed cationic charges. Although anion exchange membranes showed promising performance in the fuel cell, the general stability issues at temperatures above 60°C have so far prevented serious considerations of commercialization for fuel cell application [96].

1.5 Radiation Grafted Polymers in Commercial Applications

Despite the efforts put into the development of radiation grafted functional polymers over the past decades, commercial success has been limited to niche market applications [49]. The main commercial products are separators for alkaline batteries prepared by grafting of acrylic acid onto polyethylene (PE) film. Substantial efforts have been made in the development of adsorbent materials, especially in Japan, for air purification, collection of uranium from seawater, and removal of toxic metal ions from the environment. Furthermore, the range of commercial materials encompasses functional fabrics, and selected products for biomedical use, such as cell-culturing dishes. A number of radiation grafted products, e.g., permanent-press clothes or antibacterial tissues, were commercialized but then discontinued, or the process was taken to pilot plant level but then failed to commercialize, because alternative technologies turned out to be more economic [49]. Some of these were still based on a grafting approach, yet the activation of the substrate was carried out chemically, by UV or plasma treatment. In the context of the fuel cell, there have been attempts of product and process development on the pilot scale [198, 199], yet the developments were discontinued, albeit not necessarily or entirely due to technical reasons. The reasons may be sought in the complexity of the requirements for fuel cell application. The material needs to be developed to meet a range of different, even opposing specifications. It has been shown repeatedly that only a membrane with well-balanced properties can provide performance as well as durability, in particular under dynamic operating conditions [197]. The lack of understanding of the complex interplay of factors affecting membrane properties and performance may have aggravated development of the membrane for commercial purposes.

2 Base Film Requirements

In all the synthetic approaches adopted in the context of the development of radiation grafted membranes for fuel cells, the base polymer chosen has always been a commodity product of technical quality. These polymer films are manufactured with specifications related to their target applications, such as chemical industry or weather-proof architectural components. Their properties are not tailored to using them as substrate for the preparation of radiation grafted membranes. In general terms, the requirements for the base polymer are:

i) Irradiation needs to yield active sites that can initiate the graft polymerization reaction.

ii) The material should be hydrophobic to promote hydrophilic-hydrophobic phase separation in the final ion-exchange membrane.

iii) It must allow the diffusion of the grafting monomer(s) into the polymer.

iv) The base film has to be thermally stable and mechanically robust, with appropriate fracture toughness, also upon irradiation.

v) The polymer needs to be chemically stable against the chemicals used during the synthesis of the membrane and the environment encountered in the fuel cell.

The objective of this section is to identify the key requirements for a polymer to be used as base film for the preparation of a proton conducting membrane using the radiation grafting technique.

2.1 Radiation Chemistry

The purpose of exposing the base polymer to ionizing radiation is to create "active sites" that can initiate a polymerization reaction when the film is brought into contact with monomer. The active sites may be, as outlined above, trapped radicals ($R^\bullet$), in case the polymer is irradiated and kept in an inert atmosphere until the grafting reaction is started. Also, cationic or anionic sites may be created, yet it is unlikely that grafting occurs via an ionic mechanism due to the required high purity of the reaction medium. The cleavage of bonds as a result of irradiation, be it electron or photon radiation, leads to a number of additional effects. The main chemical changes in the polymer induced by ionizing radiation are i) scission of the main chain, ii) formation of crosslinks, iii) release of volatile products, iv) creation of unsaturation, i.e., double bonds, and v) cyclization [200, 201]. In the presence of oxygen, peroxyl radicals and, eventually, (hydro)peroxides (POOP', POOH) are formed, which decompose upon heating to yield active radicals during the grafting process. An overview of the processes occurring in a range of representative polymers upon irradiation is given in **Table 1-2**, expressed as radiation chemical yield (G-value) [170]. The selected polymers are intended to highlight key properties of respective material classes. PTFE is

a representative of a perfluorinated material, PE is the corresponding polyolefin, and PVDF is a partially fluorinated fluoropolymer. The effect of the presence of aromatic units is seen in PS (pendant aromatic unit) and PET (aromatic unit in the main chain).

The event that is of primary interest is the yield for the formation of radical species $G(R^\bullet)$, which is commonly measured by electron paramagnetic resonance (EPR) / electron spin resonance (ESR) spectroscopy. It is interesting to note that from a radiation chemistry point of view PVDF shows similarities to PE, yet from a chemical stability point of view, it is behaves more like PTFE. Radiation chemistry data for other fluoropolymers, such as PFA, FEP and ETFE, could not be collated in comprehensive manner, owing to the limited number of studies reported on this subject. Another very fundamental categorization of polymers can be made based on whether the structure contains aromatic units or not. The presence of aromatic units imparts the polymer with intrinsic resistance to radiation induced chemical changes, in **Table 1-2** shown in the example of polyethyleneterephtalate (PET) and polystyrene (PS). Aromatic groups absorb excitation energy, but their excited states undergo efficient decay to the ground state, with a low yield for bond cleavage and hence for radical formation [202]. This phenomenon may be termed "bullet-proof vest" or "sponge" effect [52], owing to the effective dissipation of deposited energy. The polymers with the highest stability against radiation induced damage are, therefore, polymers with aromatic units in the main chain and few or no aliphatic hydrogen atoms at all, such as polyimides, poly(ether ketones) (PEEK), polysulfones, etc [202]. Owing to the low radical yield, these materials do not lend themselves for radiation grafting. Nevertheless, PEEK has been reported recently to serve as base polymer for radiation grafting of a styrene derivative [203]. PET is a polymer with aromatic as well as aliphatic units in the chain. The use of PET films, fabric and threads as substrate for grafting of various hydrophilic monomers, such as acrylic acid and acrylamide has been reported, with the aim of improving electrostatic or fire-resistant properties or dyeability [184]. In the same context, polyamide has been used as substrate, using the pre-irradiation technique in air due to the high yield for the formation of peroxides, $G(-OOH) = 3.7$. In very general terms, polymers are classified into the crosslinking (Structure 1) and scission (Structure 2) type [172].
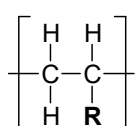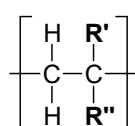
Structure 1   Structure 2

Table 1-2. Response of various polymers upon irradiation with ionizing radiation, expressed as radical chemical yield G, which indicates the number of events of a given kind per 100 eV of absorbed dose. $G(R^\bullet)$: formation of radicals, $G(X)$: crosslinking events, $G(S)$: chain scission events, $G(gas)$: evolution of gas. If not otherwise noted: room temperature values. inert gas conditions or vacuum.

Polymer	$G(R^\bullet)$		$G(X)$		$G(S)$		$G(gas)$	
PTFE	0.14–0.40	[204-206]	0.1–0.3	[207]	1–4 [a]	[204, 208]	0.02–0.3 [b]	[52, 208, 209]
PVDF	3.3	[210]	0.65–1.0	[211-213]	0.3–0.64	[211-213]	1.7 [c]	[209]
PE	2.8–3.3 [d]	[200, 214]	1-3	[202, 215, 216]	0.2-0.9	[202, 216]	2.8-3.9 [e]	[52, 202, 217]
PS	0.1	[200]	0.02-0.05	[172, 216]	0.01-0.02	[172, 216]	0.02-0.07 [e]	[52, 172, 209]
PET	0.02-0.03	[184]	0.08-0.14	[172, 216]	0.07-0.17	[172, 216]	0.016 [f]	[172]
PA6[e]	0.05	[184]	0.4-0.7	[172, 184, 216]	0.6-0.7	[172, 216]	1.1	[209]

[a]   mainly CO, CO_2 and CF_2O [52]; in air: 4.5 [208], ~20 [204]

[b]   CO, CO_2, CF_2O [52]

[c]   mostly HF [218]

[d]   various types of PE, temperature: 77 K

[e]   high yield of peroxides: $G(-OOH) = 3.7$ [184]

[f] H_2

For example, vinyl polymers with a methyl substituent at the α-position (R'=CH$_3$), e.g., polymethacrylates, polymethacrylamides, or poly-α-methylstyrene, always display a higher ratio of scission to crosslinking events upon irradiation compared to the corresponding polymers of Structure 1 (polyacrylates, polyacrylamides, polystyrene). Therefore, polymers with a quaternary carbon belong to the scission type. It has been argued that the steric repulsion of the two substituents (R', R'') cause a strain in the backbone, resulting in a weakening of the carbon-carbon bond [36]. Wall found that polymers with a low heat of polymerization are prone to chain scisison, whereas polymers with a high heat of polymerization tend to crosslink [219].

The polyolefins, i.e. polyethelyene (PE) and polypropylene[1] (PP), have been widely used in the form of fibers and non-woven substrate for the preparation of ion exchange resins and adsorbents [51]. They exhibit favorable radiation chemistry, since they belong to the crosslinking type polymers, not the degrading type [52]. Also, peroxidation readily occurs, making them amenable to pre-irradiation in air [220].

Fluoropolymers are characterized by their excellent chemical and thermal resistance, low dielectric constant, and low surface energy. They have therefore found application in chemical industry and as weatherproof materials [221]. Also, fluoropolymers are used in the semiconductor industry, because they are available at high purity [218]. Fluoropolymers have been widely used as base film material for the preparation of graft copolymers [31], in particular with a view to synthesizing ion conducting membranes for fuel cells [65, 222], owing to their partially crystalline structure and high melting point, resistance to an aggressive chemical environment, and hydrophobic nature. Fluoropolymers exhibit a somewhat different radiation chemistry compared to their hydrocarbon analogues. Owing to the strong C-F bond, fluorine atom transfer is highly unlikely, in contrast to the case of polyolefins, where hydrogen atom transfer is an important process in the radiation chemistry [52] and thermal and oxidative aging of the material [223]. Therefore, carbon radicals in fluoropolymers do not tend to undergo disproportionation reactions [218]. Consequently, release of F$_2$ gas upon irradiation is unlikely.

Table 1-3. Bond dissociation energies in fluoropolymers [224].

Bond	ΔH_{BDE} (kJ/mol)
C-C	$370-420$
C-H	$430-450$
C-F	$480-520$

---

[1] Exlusively isotactic PP, since atactic PP is a soft, rubbery, amorphous polymer with little use.

Attempts have been made to explain the radiation chemistry of the different fluoropolymers by taking into consideration the various bond dissociation energies (**Table 1-3**). In perfluoropolymers, the C-F bond is much stronger than the C-C bond, hence main chain scission is very likely to occur. In partially fluorinated or pure hydrocarbon polymers, one would also expect C-C bonds to be broken rather than C-H bonds. However, a considerable number of broken C-C bonds recombine again as a result of the structural immobility of the chain ("cage effect"), resulting in the overall predominant cleavage of C-H bonds [52]. For the family of fluoropolymers considered here, the following "pecking order" has been identified [172]:

Trends for **crosslinking**:

PVF > PVDF > ETFE > FEP > PFA > PTFE

Trends for **degradation**:

PTFE > PFA ≈ FEP > ETFE > PVDF > PVF

The ranking of polymers according to their susceptibility to degradation via chain scission is almost the opposite to the order for their tendency to crosslink under the influence of ionizing radiation. Considering the composition of the polymers, it turns out that a higher hydrogen / lower fluorine content favors crosslinking, whereas a higher fluorine / lower hydrogen content favors chain scission. In hydrogen-rich polymers, hydrogen is likely to split off, resulting in a high yield for recombination of chains to form H- or Y-type crosslinks, whereas in hydrogen-poor polymers, main chain scission is more prevalent, because C-F bond splitting is less likely compared to C-H bond splitting. Yet, in analogy to the classification of non-fluorinated vinyl polymers discussed above based on the presence or absence of quaternary carbon, similar arguments may be put forward in the context of fluoropolymers. Owing to the larger van der Waals radius of the fluorine atom compared to that of the the hydrogen atom, the presence of fluorine atoms leads to steric hindrance effects on the chain. Therefore, as a general trend, the more fluorine the polymer contains, the more it is prone to undergo scission reactions upon irradiation. The correlation is not strict, though, in particular if copolymers, such as poly(VDF-co-HFP) or ethylene chlorotrifluoroethylene (ECTFE), are taken into consideration [213]. Furthermore, considerable differences may exist between nominally identical polymers from different sources, owing to differences in, e.g., crystallinity, exact composition, and presence of additives, for instance "prorads", which promote crosslinking reactions. Following the general categorization, it is not surprising that the perfluorinated polymers, PTFE, PFA, and FEP, display the highest susceptibility to chain degradation. The much more inferior stability of PTFE against ionizing radation compared to FEP and PFA is associated with its high crystallinity (**Table 1-4**). The

radicals formed in PTFE upon irradiation have restricted mobility in the crystalline phase and therefore radical-radical recombination reactions are unlikely. Both PFA and FEP are copolymers of TFE with co-monomers bearing a pendant group in the form of $-CF_3$ and $-OC_3F_7$, which imparts flexibility to the polymer backbone and yields comparatively lower crystallinity. Both PFA and FEP exhibit the tendency to side-chain cleavage. The higher radical yield, in particular at room temperature, in FEP, $G(R^\bullet) = 0.59\text{-}2.0$ [176], and PFA, $G(R^\bullet) = 0.93$ [225], is attributed to a higher chain mobility and lower crystallinity compared with PTFE, which limits the cage recombination.

Irradiation of fluoropolymers at elevated temperatures, typically above the glass transition point or even melting point of the polymer, promotes radiation-induced crosslinking of the chains as a result of the enhanced mobility of the molecular chains. Due to network formation, this leads to polymers with improved mechanical properties. If PTFE is irradiated in the absence of oxygen above its melting temperature of 327°C, crosslinking occurs, which results in a considerable decrease of the crystallinity, and a substantial improvement of its mechanical properties, radiation stability and optical properties [218]. This approach has been used by Yamaki et al. from the Japan Atomic Energy Agency (JAEA) to prepare base polymer films suitable for radiation grafting [226, 227].

FEP is a fluoropolymer similar to PTFE, yet it contains a fraction of hexafluoropropylene (HFP). The presence of the HFP units reduces the efficient packing of fluorocarbon chains, which leads to a significantly lower crystallinity compared to PTFE. The content of HFP is typically 8.5 mol-%. Being a perfluorinated polymer, the radiation chemistry bears resemblance to that of PTFE, there are a few distinct differences, though. FEP can undergo crosslinking when irradiated in inert atmosphere above its glass transition temperature (80°C), which is attributed to the disruptive effect of the fluoromethyl group on chain packing. The resulting higher chain mobility favors radical combination reactions and thus crosslinking. PFA is another type of perfluorinated TFE-copolymer, yet the comonomer (perfluoro(propylvinyl ether)) content is only around 1 %, as its disruptive effect is more pronounced compared to that of HFP [228]. Similar to the other perfluorinated polymers (PTFE, FEP), it undergoes degradation upon irradiation at room temperature.

Table 1-4. Typical properties of semi-crystalline fluoropolymers. T_g values determined via dynamic mechanical analysis are quoted when available.

Polymer	Crystallinity χ (%)		Glass transition temperature T_g (°C)		Melting point T_m (°C)		Typical molecular weight (MW) (g/mol)	
PTFE	92–98[a]	[228]	131	[231]	327	[228]	>1M, up to 10M	[208]
	14–50	[206, 229, 230]						
PFA	65–75[a]	[218]	-5	[232]	310	[218]	200k–450k	[233]
	27	[230]						
FEP	50–75[a]	[204, 232]	80	[218]	274	[229]	250k–600k	[233]
	15–26	[229, 230, 234]					325k	[235]
ETFE	15–37	[229, 230, 234]	145[b]	[231]	270	[229]	400k–1.2M	[233, 235, 237]
			110	[236]				
PVDF	35–70	[229, 230, 232]	-40	[233]	165	[229]	110k	[237]
PVF	20–60	[229, 230, 232]	41	[233]	193	[229]	100k-500k[c]	[232]

[a] as prepared
[b] for theoretical, perfectly alternating copolymer
[c] assume polydispersity index (PDI) = 2

PVDF has been widely used as base polymer for radiation grafting, and its radiation chemistry has been extensively investigated. PVDF is the only fluoropolymer that can be dissolved in common solvents, such as DMSO or NMP, which is a consequence of the alternating CH_2 and CF_2 units creating a dipole. This opens the possibility for a wide range of follow-up reactions. Being partially fluorinated, it tends to undergo crosslinking rather than chain scission when irradiated in the absence of oxygen. The generation of HF upon irradiation is a well-known feature in PVDF, which leads to the creation of double bonds in the polymer chain. P(VDF-*co*-HFP) has a glass transition temperature below ambient. It crosslinks when irradiated, in vacuum as well as in air [238], yet no radicals are observed because it is above its T_g at room temperature. PVF readily crosslinks upon exposure to ionizing radiation, $G(X) = 3$-8 [212]. Also, HF is emitted with high yield, $G(HF) = 4.5$ [208].

ETFE is a copolymer of TFE and ethylene with high degree of alternation. In addition, commercial polymers typically contain a third monomer, e.g., a perfluorinated alkylvinyl ether [232]. As it is structurally similar to PVDF, it is not surprising that it is a crosslinking type polymer and is of fairly high resistance against radiation-induced degradation. ETFE can be produced at high molecular weight (**Table 1-4**), which is an important prerequisite for the retention of the mechanical properties when the polymer undergoes degradation in the fuel cell environment.
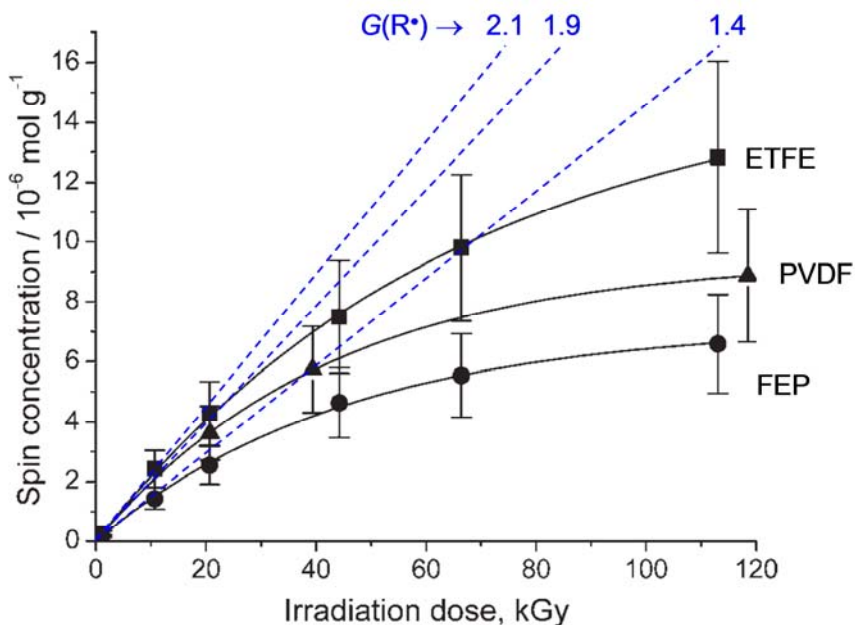
Figure 1-3. Radiation chemical yield for radical formation, determined from the spin concentration of e-beam irradiated films in inert (Ar) atmosphere at room temperature. ETFE: 100 μm, χ(crystallinity) = 30%, 400 kDa (Nowofol); PVDF: 50 μm, χ = 41%, 110 kDa (Nowofol); FEP: 75 μm, χ = 17%, 325 kDa (DuPont). Adapted from [239].

For the use of the polymers as substrate for radiation grafting, it is of interest to know the chemical yield for radical formation upon irradiation. The unpaired spins of radicals can be detected using electron spin resonance (ESR) / electron paramagnetic resonance (EPR) spectroscopy (**Table 1-2**). Evidently, the value of $G(R^{\bullet})$ depends on the conditions of irradiation and the environment. The number of radicals formed as a function of e-beam irradiation dose in inert atmosphere was measured for three types of film typically used for radiation grafting to prepare proton conducting membranes, FEP, PVDF, and ETFE (**Figure 1-3**). After an initial increase of spin concentration at low dose, corresponding to a $G(R^{\bullet})$ value of around 2, the values level off due to partial recombination of the radicals [239]. Irradiation in air leads to a lower extent of radical formation for ETFE and PVDF, possibly because some of the primary radical sites react with oxygen to eventually form (hydro)peroxides. In contrast, the irradiation of FEP in air led to a higher concentration of spins, probably owing to chain scission being more pronounced in the presence of oxygen. The difference in initial radical concentration was largely reflected in the final graft levels obtained [239].

In conclusion of this section, it is worthwhile noting that using a particular base polymer always implies that a specific technical product is used, with distinct associated properties. This is reflected, for instance, in the wide range of crystallinity values reported for a given polymer type (**Table 1-4**). Already the polymer resin used in the preparation of the film exhibits particular technical properties, such as its composition in terms of monomer type(s) and additives used, molecular weight and distribution thereof, extent of branching and imperfections, and nature of the chain ends. Furthermore, film formation and processing conditions yield product specific properties, for instance crystallinity, crystallite size and distribution, and degree of orientation. Moreover, some films are post-treated to modify the surface, for example by corona-treatment. Additives may affect the process of radiation grafting considerably. "Antirads", i.e., additives that render the polymer more stable against ionizing radiation, may reduce the yield for active site generation. Antioxidants, added to the polymer to inhibit oxidative degradation, are very likely to disturb the grafting reaction. It is therefore not unexpected that films of the same type but from different suppliers may behave differently in the process and yield membranes with different final properties. In the description of experimental procedures, it is therefore always advisable to provide as many base film properties as are available from the supplier or can be determined experimentally.

2.2 *Mechanical Properties*

The importance of the mechanical robustness of polymers when used as polymer electrolyte in fuel cells cannot be overemphasized. The membrane can only function as an electrolyte so long as

its mechanical integrity is maintained. Mechanical failure of the membrane through crack formation or tearing leads to catastrophic failure of the respective cell, even though the conductivity of the membrane may still be sufficient. Hence, the selection of a base polymer material for the preparation of radiation grafted membranes must include considerations of mechanical behavior and the changes thereof as a result of irradiation and chemical modification (grafting, sulfonation). The application in the fuel cell or electrolyzer calls for a polymer of high toughness, i.e., a combination of high yield strength and elongation at break. The membrane assembled into an electrochemical cell of the filter-press type can experience considerable levels of mechanical stress, which is a consequence not only of the compaction force of the cell, but also, and most importantly, a result of the changes in the hydration state of the membrane during cell operation [124]. The levels of stress can reach the yield stress of Nafion®, which drops quite significantly at elevated temperature and when the ionomer is hydrated [125], leading to viscoelastic creep. Accumulated damage will, eventually, lead to the failure of the membrane [240].
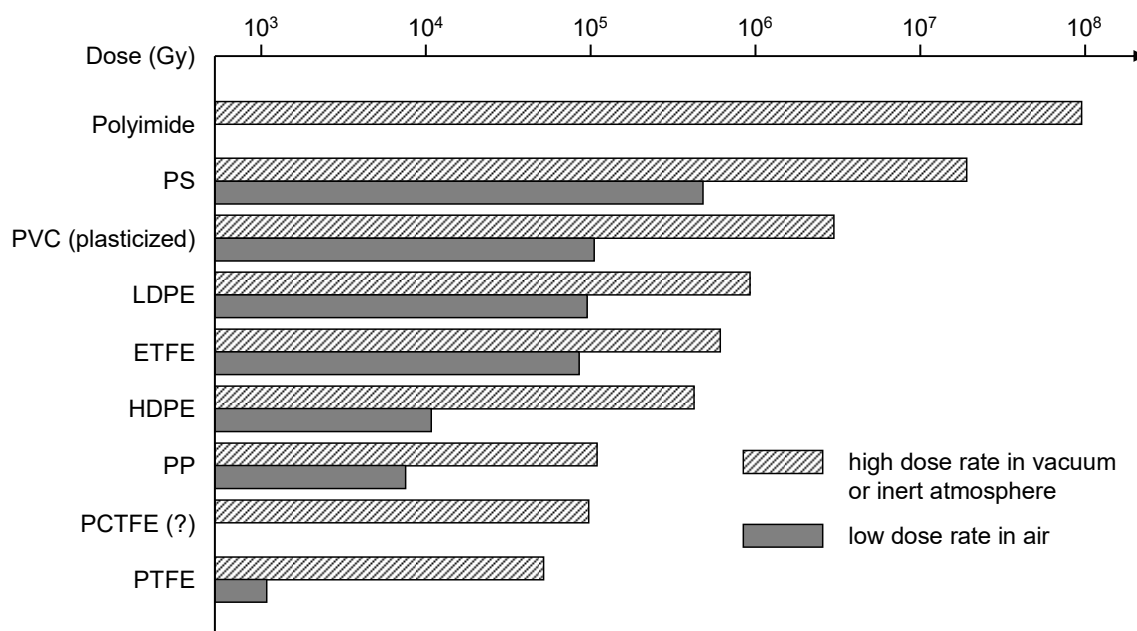
Figure 1-4. Resistance of polymers against ionizing radiation. The data represents the dose required to reduce mechanical properties to 50 % of their original value. Adapted from [202].

Considerations of a general nature concern the resistance of polymers towards ionizing radiation (**Figure 1-4**). It has been mentioned previously that polymers containing aromatic units display an intrinsic stability against radiation induced damage. Polyimides (e.g., Kapton®) are among the polymers with the highest stability. Also, polystyrene is considerably stable. Partially fluorinated, aliphatic polymers and polyolefins are in the intermediate range, wherease PTFE suffers heavily upon irradiation. All the polymers experience more severe damage when exposed to radiation and

oxygen at the same time, which results from the additional oxidative degradation triggered by the creation of radials.
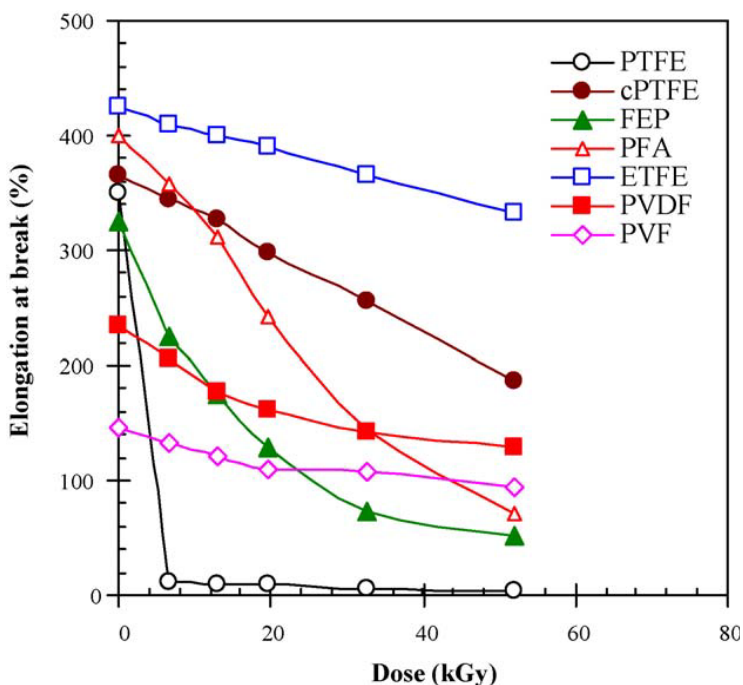
Figure 1-5. Mechanical properties of various fluoropolymers, expressed as elongation at break value, as a function of γ-irradiation dose at room temperature in air [230].

From the wide selection of polymeric materials, the polymers that have been considered by different research groups for the preparation of ion conducting membranes for fuel cells are semi-crystalline, aliphatic, perfluorinated or partially fluorinated polymers [31, 32, 65, 222]. These offer chemical and thermal stability, and their radiation chemistry has been sufficiently well studied to know that they can be modified by radiation grafting to introduce polar groups into their hydrophobic matrix. However, for a detailed investigation, the effect of radiation dose on the loss of mechanical toughness was investigated by Chen et al. from the JAEA (**Figure 1-5**). All the used base films except PVDF and PVF display an initial elongation at break above 300 %. The decrease with increasing dose is striking for the perfluorinated polymers, in particular PTFE, which is a consequence of their tendency to degrade upon irradiation. A notable exception is crosslinked PTFE (cPTFE) with its remarkable improvement of its radiation resistance. Its crystallinity, however, is only 5 % lower than that of the pristine PTFE [230]. All the partially fluorinated films show a better retention of their mechanical properties. The radiation induced degradation is compared to the graft level of styrene and divinylbenzene attained at 60°C after 8 h, which decreases along the following sequence: PVDF > PVF > ETFE > FEP > cPTFE > PFA> PTFE. This order is largely in agreement with what is expected from the radiation chemistry of these polymers. As initially mentioned, the polymers also need to withstand the sulfonation

reaction following the grafting reaction. Among the polymers tested, PVF deteriorated during treatment with chlorosulfonic acid. Hence, PVF cannot be used as substrate [230].

Similar findings were reported by Walsby et al. [229]. They carried out an extensive study on the grafting of styrene to a range of base polymers, namely PTFE, FEP, PVDF, P(VDF-HFP) with two different HFP concentrations (6 and 15%), ETFE, and PVF. Styrene was grafted in bulk into the electron pre-irradiated films at 70°C. With the exception of P(VDF-*co*-HFP), they found a correlation between the styrene uptake of the base polymer and the obtained graft level. In case of P(VDF-*co*-HFP), the polymer with higher HFP content showed a higher degree of swelling in styrene, yet the graft level was lower. This was explained by the lower crystallinity and the resulting more pronounced termination reactions in the amorphous phase of the polymer, since the grafting is carried out above the T_g. The highest graft levels were obtained with PVF, PVDF and ETFE. The grafted film based on PVF, however, turned black and brittle during the sulfonation reaction in 1.3 % chlorosulfonic acid solution in dichloroethane and therefore has to be discarded from the list of potential base polymer materials.
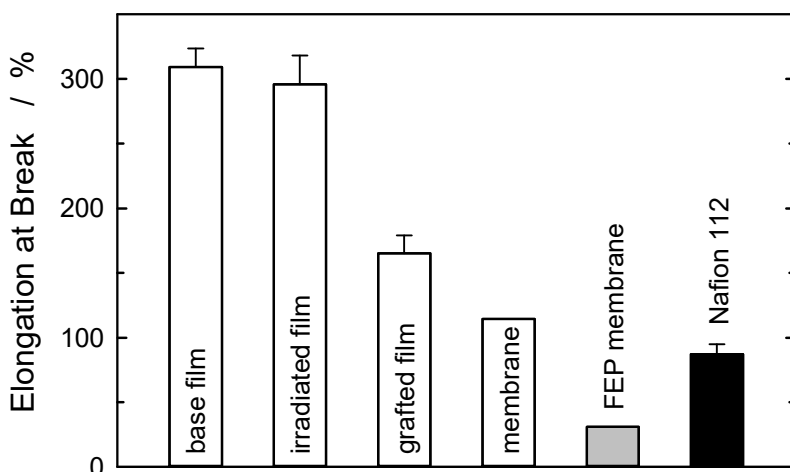
Figure 1-6. Elongation at break values for ETFE based membrane in different stages of processing (pristine, irradiated with 1.5 kGy, after grafting, and after sulfonation). Grafting monomer: styrene / 5 % divinylbenzene, graft level: ~25 %. Comparison against FEP based membrane (grafted styrene / 10 % divinylbenzene, graft level: ~20%) and Nafion® 112. Membranes were measured in K^+-echanged form and dry state in machining direction. Adapted from [241].

In the procedure used in our laboratory for the grafting of styrene and mixtures of styrene and divinylbenzene (DVB), an irradiation dose of ETFE of merely 1.5 kGy is required to reach graft levels of around 25 % in reasonable amounts of time, i.e. a few hours of reaction. Therefore, the radiation induced degradation of the base film is low (**Figure 1-6**). A considerable drop in the elongation at break is observed after grafting of styrene / DVB, yet the yield stress was found to increase by a factor of 2 for a grafted film with 44 % degree of grafting (not shown). This behavior is attributed to the presence of the polystyrene grafts, which render the material stiffer

and less ductile. Increase of the crosslinker concentration does not affect the yield stress considerably, but leads to enhanced strain hardening and reduced elongation at break, owing to the presence of the crosslinked network structure [241]. A further decrease in elongation at break is observed after sulfonation of the grafted film in the final membrane state (**Figure 1-6**). Despite the loss in mechanical toughness, the ETFE-based membrane shows much better mechanical properties than a comparable radiation grafted membrane based on FEP, and also compares favorably against commercial Nafion® 112. It is important to consider all the preparation steps and their impact on the mechanical properties of the polymer. In addition, the properties of the final membrane are a strong function of temperature and humidity. However, no detailed study has been reported yet on that topic in the context of radiation grafted membranes.

3 Choice of Grafting Monomer(s)

The grafting monomer that has been used in the vast majority of cases, up to the end of the 1990s, for the preparation of proton conducting radiation grafted membranes for fuel cell application has been styrene, owing to its being a readily available and low-cost chemical commodity, fast radical polymerization kinetics, and easy sulfonation [65]. In many cases, a crosslinker was employed as comonomer, typically divinylbenzene (DVB), to improve the chemical stability and prevent excessive swelling of the membranes. In this approach, the ionogenic constituent is identical to what has been used in the early days of the PEFC, when crosslinked polystyrene based ion exchange materials were formed into membranes and used, for instance, in the Gemini space missions of NASA (cf. Introduction). It was, however, already recognized at the time that polystyrene based membranes had limited durability under fuel cell operating conditions, and those materials were soon replaced by perfluoroalkylsulfonic acid (PFSA) membranes, such as Nafion®. The use of ion exchange polymers based on sulfonated polystyrene was found to be limited due to its poor stability against oxidative degradation [9]. The low bond strength of the α-H in poly(styrenesulfonic acid) (PSSA) was identified as a weakness [13]. Based on this insight, α,β,β-trifluorostyrene (TFS) based ion exchange materials were developed, which showed much improved oxidative stability [13, 15]. In the following sections, the choice of grafting monomers for the preparation of radiation grafted membranes for fuel cells applications will be reviewed. Emphasis is placed on systems for which characterization in the fuel cell has been reported.

3.1 Fluorinated Styrene Monomers

Styrene and TFS remained the monomers of choice in the preparation of radiation grafted membranes for electrolysis and fuel cell applications for a long time [4]. Despite the superior stability of TFS based membranes over styrene analogues, the use of TFS is associated with a number of shortcomings: TFS suffers from poor polymerization kinetics, and the reaction time required to obtain reasonable graft levels is therefore unacceptably long [60, 61, 63]. Furthermore, the sulfonation of poly-TFS was found to be difficult, which is a consequence of the electron withdrawing nature of the fluorinated chain [13]. Therefore, Ballard Power Systems (Burnaby, Canada) used substituted TFS derived monomers with electon-donating substituents in their BAM® Grafted PEM, such as *para*-methyl-, -methoxy- or -phenoxy-TFS [72, 73]. Furthermore, *para*-sulfonylfluoride-TFS was used as a grafting monomer, which eliminates the sulfonation process. The sulfonyl fluoride in the graft copolymer merely needs to be hydrolyzed to the sulfonic acid.

In an approach to improve the acid strength, styrene as well as TFS based monomers where the sulfonic acid group is attached to the aromatic ring via fluoroalkyl units ($-CF_2-$) were used [242, 243]. This imparts "superacid" character to the acid group and results in a much higher proton conductivity at reduced relative humidity compared to when the sulfonic acid is directly attached to the aromatic unit [243].

In general, however, fluorinated styrene derived monomers are expected to be of high cost. The development of a cost-efficient radiation grafted membrane calls for monomers that are of low cost and readily available.

3.2 Ring-Substituted Styrene Monomers

Substituted styrene monomers have been used in various laboratories with the aim of reducing the intrinsic chemical susceptibility of sulfonated polystyrene to graft chain degradation in the PEFC induced by radical species (HO•, HOO•) [244-246]. Chen et al. pre-irradiation grafted *p*-methylstyrene (MeSt) and *p-tert*-butylstyrene (tBuSt) (**Figure 1-7**) onto 50 μm ETFE film and characterized the sulfonated membranes for chemical stability using in an *ex situ* stability test in 3 % H_2O_2 at 60°C [244]. In other publications, the use of a mixture of *meta*- and *para*-MeSt is mentioned [245, 247]. The stability of both membranes, exhibiting a graft level of around 55 %, was superior to a comparable styrene grafted membrane. Among the two membranes, the tBuSt grafted membrane showed a higher stability compared to the one based on MeSt. As a reason for the improved stability against oxidative attack the favorable modification of the electronic structure of the aromatic unit was put forward, which leads to a stabilization of the α-hydrogen. However, the conductivity of the tBuSt grafted membrane was very low, which is probably the result of a poor degree of sulfonation. Introduction of crosslinking monomers, i.e., divinylbenzene (DVB), 1,2-bis(*p,p*-vinylphenyl)ethane (BVPE), and triallyl cyanurate (TAC), led to a further improvement in stability [245].
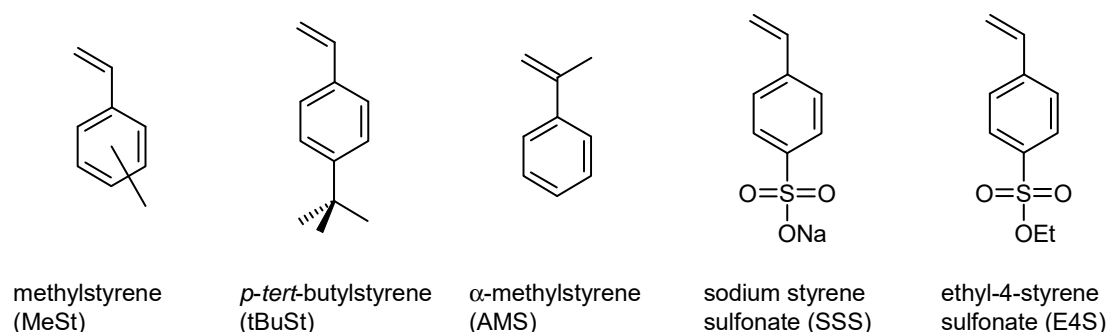
Figure 1-7. Various styrene-derived monomers used for the preparation of radiation grafted membranes.

Kim et al. grafted *o*-methylstyrene onto 125 µm thick FEP and found that the resulting sulfonated membranes exhibited a higher degree of sulfonation of around 1.5, compared to values of 0.9 to 1.3 for comparable styrene grafted membranes [248].

A concept that allows post-crosslinking of grafted monomers using alkoxysilane groups and sol-gel chemistry was introduced by the research group at the JAEA [249, 250]. They grafted *p*-styryltrimethoxysilane onto γ-ray pre-irradiated ETFE film of 50 µm thickness, followed by sulfonation, hydrolysis and condensation to form a siloxane-crosslinked proton conducting membrane (**Figure 1-8**). The hydrolysis-condensation step can be carried out either before or after the sulfonation step. The fuel cell relevant properties, such as proton conductivity and *ex situ* chemical stability in H_2O_2 solution, were found to be independent on the reaction sequence. Already crosslinked films, however, were found to be more difficult to sulfonate than uncrosslinked ones. The stability against oxidative degradation, measured *ex situ* in 3 % H_2O_2 solution at 60°C, of these siloxane-crosslinked membranes was found to be superior to that of conventional styrene-DVB grafted and sulfonated membranes. In addition, the water uptake and conductivity were higher at the same ion exchange capacity, which was ascribed to the presence of hydrophilic –Si–O–Si– and non-crosslinked –SiOH groups, which promote the formation of aqueous clusters.

Figure 1-8. Illustration of the use of a siloxane containing styrene derivative and sol-gel chemistry to obtain a crosslinked polymer structure. The sulfonation is preferably carried out before the crosslinking reaction, since an already crosslinked polymer is more difficult to sulfonate [163].

3.3 *α-Methylstyrene*

A concern regarding ring-substituted styrene derivatives is the potential lower degree of sulfonation, owing to steric hindrance. A promising monomer with protected α-position, unsubstituted aromatic ring, and ready availability is α-methylstyrene (AMS). Owing to the weak αC-H bond in styrene, α-methylstyrene (AMS) appears to be a promising monomer, because it carries a protective group at the critical position (**Figure 1-7**). In 1991, Assink et al. reported that

the chemical stability of AMS grafted and sulfonated membranes, using PTFE as base polymer, was superior to that of styrene-based membranes in an oxidative electrochemical environment [251]. Details on the preparation of the grafted membranes, however, were not provided. The major drawback of AMS is its poor radical polymerization kinetics. AMS by itself does not readily graft. AMS has a ceiling temperature of 60–65°C in bulk [252] (styrene: 310°C [253]). The dominant termination reaction is chain transfer to the monomer [254]. Consequently, free radical polymerization of AMS under conventional bulk or solution conditions gives low conversions and low molecular weights. It is possible, however, to co-graft AMS together with an appropriate comonomer, if AMS and the comonomer exhibit favorable copolymerzation kinetics. Li et al. reported to co-grafting of AMS with styrene and DVB into radiation-crosslinked and pre-irradiated PTFE base film [255]. The presence of AMS units in the grafts delayed the oxidative degradation of the resulting membranes, measured *ex situ* in H_2O_2 containing solution. The presence of styrene, however, still constitutes a shortcoming, since it cannot be entirely replaced by AMS. Other comonomers may be more suitable.

Becker and Schmidt-Naake have reported the co-grafting of AMS and acrylonitrile (AN) onto 50 µm thick FEP and ETFE films [191, 256, 257]. AN tends towards alternating copolymerization with AMS and greatly improves the effective rate of AMS grafting, although the grafting rate is not as high as that of styrene under the same conditions (60°C). In the *ex situ* stability analysis in H_2O_2 solution, the loss of ion exchange capacity of the AMS based membrane was less pronounced than that of a comparable styrene based membrane. At the Paul Scherrer Institut (PSI), methacrylonitrile (MAN) was chosen as a comonomer of AMS [258, 259]. The choice of MAN over AN was based on the notion that the presence of α-H should be avoided for stability reasons. Thus, with the choice of AMS and MAN, a fully α-methyl protected grafted chain can be obtained. Recently, it has been shown that grafted MAN units are much more stable against hydrolysis compared to AN units, during membrane preparation [260] as well as fuel cell operation [261]. The copolymerization of AMS and MAN in the pre-irradiation grafting into FEP, as well as ETFE, with a thickness of 25 µm yields a high degree of alternation, because the reactivity ratios of the two monomers are well below unity [262]. AMS / MAN co-grafted membranes have shown a stability in the fuel cell that is about an order of magnitude higher than styrene grafted membranes with comparable ion exchange capacity [258, 262]. The incorporation of a crosslinker further improves stability, and with an optimized design membranes based on 25 µm ETFE and grafted AMS, MAN and diisopropenylbenzene (DIPB, crosslinker) were obtained that outlasted Nafion® XL-100 membranes in the fuel cell under dynamic operating conditions [263] (cf. Section 4.3 below).

3.4 Sulfonated Monomers

In the approaches outlined thus far, the sulfonic acid group was introduced by sulfonation of the grafted polymer, which constitutes a second chemical step in the synthesis procedure. It would therefore be of interest to be able to directly graft monomers containing the sulfonate moiety. However, a direct single-step grafting of sulfonated monomers into a hydrophobic, dense base film has shown to be difficult to accomplish. This is a result of the chemical incompatibility of the highly polar monomer and the hydrophobic base polymer, which prevents the monomer and grafts from penetrating into the bulk of the film. Nevertheless, there have been a number of approaches to enable grafting of sulfonated monomers.

In the early eighties, Shkolnik and Behar reported attempts of grafting of sodium styrene sulfonate (SSS) (cf. **Figure 1-7**) and sodium vinyl sulfonate (SVS) onto e-beam pre-irradiated (100 kGy) 100 µm LDPE film [264]. Direct grafting of these monomers failed due to the above mentioned reasons. Using an alternative method, they hydrophilized the LDPE by radiation grafting of vinyl acetate (VAc), which was hydrolyzed to poly(vinyl alcohol) (PVA), and acrylic acid (AA). The "pre-grafted" films were then irradiated again and immersed in solutions of SSS and SVS. High yields of SSS grafting of up to 80 % could be prepared, in case of SVS, however, only a few percent graft level were obtained. A number of research groups were successful in radiation grafting SSS onto various dense polymer film substrates, such as LDPE, PP and FEP, with the assistance of AA as a suitable co-monomer and polymerization "promoter". Nasef et al. summarized this work recently [265]. Single-step grafting of SSS into dense polyamide film, which has a hydrophilic character, has been reported recently by Li et al. [266]. However, the grafting of SSS onto dense hydrophobic films has been elusive until recently. Nasef et al. evaluated various solvent mixtures for the grafting of SSS onto e-beam pre-irradiated (100 kGy, N_2 atmosphere) PVDF films of 50 µm thickness. With a 9:1 (v/v) mixture of DMF and 0.2 M sulfuric acid, high graft levels of SSS of over 50 % cold be obtained after 24 h, whereas with pure water, methanol and DMF as solvent, the obtained graft levels were below 1 % [267]. This was explained by a cumulative effect of swelling of the PVDF base polymer and a favorable modification of the partitioning coefficient of SSS between the film and the grafting solution. Other acids, i.e., hydrochloric, nitric and acetic acid, were also shown to promote grafting in a similar way, though they were not as effective as sulfuric acid [265].

Instead of directly grafting styrene sulfonate in the salt form, a non-ionic version of the monomer, i.e., a corresponding ester can be grafted. Researchers at the JAEA have reported the grafting of ethyl-4-styrene sulfonate (E4S) onto PEEK (25 µm) or DVB-modified PEEK following

γ-irradiation [203, 268]. The sulfonic acid was subsequently obtained by hydrolysis of the sulfonate ester. An accelerated fuel cell test at 95°C showed stable operation with this type of membrane, yet after 250 h membrane failure occurred due to crack formation. As a comparison, a cell with Nafion 212 membrane showed steady decrease in performance and degradation over time, evidenced by membrane thinning. Whether the grafting of E4S could be also accomplished on more hydrophobic base films is not known and has not been reported.
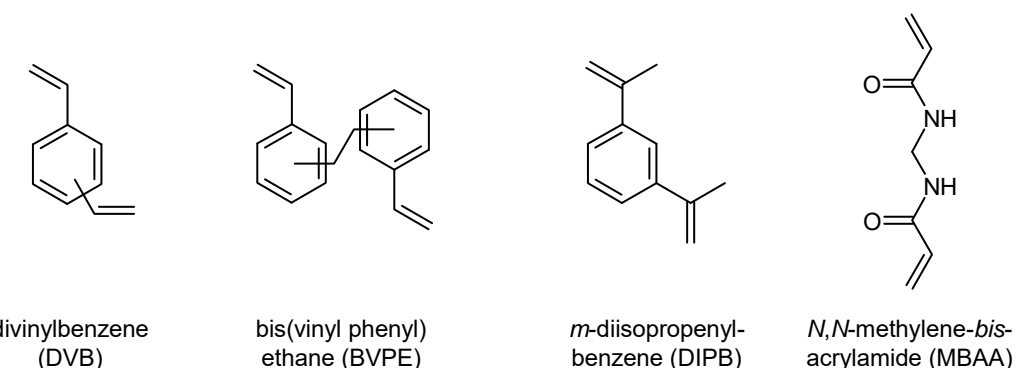
2-acrylamido-2-methyl-1-propanesulfonic acid (AMPSA) is a well-known and commercially available acrylic monomer. According to the author's knowledge, only Becker and Schmidt-Naake have reported its use as a monomer to prepare radiation grafted membranes. In their approach, AMPS was co-grafted together with *N*-vinylpyrrolidone (NVP), the reason for which, however, was not disclosed [256, 257]. Probably, AMPSA cannot be grafted by itself and requires the presence of a comonomer. AMPSA / NVP co-grafted membranes were found to be more stable against oxidative degradation, tested *ex situ* in H_2O_2 solution or in a small water electrolysis cell, compared to styrene / AN and even AMS / AN co-grafted membranes.

3.5 Crosslinkers

Since the early days of the synthesis of polystyrene based ion exchange resins, divinylbenzene (DVB) has been widely used as crosslinker at a concentration of a few percent. Also, DVB is used in a wide variety of styrene based radiation grafted polymers of porous and dense nature [51, 65]. However, the introduction of DVB at the level of a few percent in styrene based radiation grafted and sulfonated membranes leads to a significant decrease in the water uptake and conductivity of the material [269-271]. Since DVB is a relatively small and stiff molecule, an equally effective, yet more flexible crosslinker may be desireable. Becker and Schmidt-Naake reported the use of *N,N*,-methylene-*bis*-acrylamide (MBAA) together with styrene for the pre-irradiation grafting of styrene onto FEP and ETFE films [272]. 8% of MBAA in the grafting solution yielded a content of 2 % in the grafted film. MBAA crosslinked membranes showed an improved stability in an oxidative environment compared to uncrosslinked and DVB crosslinked membranes. It is expected, though, that the amide groups may undergo hydrolysis at some point, which will lead to the loss of the crosslinker functionality.

A styrenic crosslinker with a flexible, short alkyl chain between the aromatic units, bis(vinyl phenyl) ethane (BVPE), has been used by two groups in the preparation of styrene and methylstyrene based radiation grafted membranes [245, 273, 274]. Yamaki et al. grafted pure styrene, styrene/DVB and styrene/BVPE onto pre-irradiated 50 μm radiation-crosslinked PTFE film [274]. They reported that due to the lower reactivity of BVPE compared to DVB, a more

homogeneous distribution of the crosslinker over the thickness of the film is established. However, experimental evidence to support the hypothesis was not provided. In *ex situ* degradation tests at 50°C in 3 % H_2O_2 solution, BVPE crosslinked membranes showed improved stability over DVB crosslinked and uncrosslinked membranes. Chen et al. varied the concentrations of DVB and BVPE over a wide range of concentrations in their grafting experiments using methylstyrene as primary monomer onto pre-irradiated 50 μm ETFE film [245]. The oxidative stability test (**Figure 1-10**) showed a maximum in stability for membranes prepared with a few percent of DVB. The sudden decrease in stability for DVB crosslinked membranes is explained with the presence of unreacted double bonds, wich render the membrane more susceptible to oxidative attack. It should be kept in mind, though, that the crosslinker content given on the abscissa in **Figure 1-10** is the concentration in the grafting solution. The effective crosslinker content in the grafted film is not necessarily the same owing to the difference in reactivities of the monomer and the crosslinker and their diffusivities in the film. Another crosslinker, triallylcyanurate (TAC), was used by various groups [245, 275]. Yet the crosslinking effect appears to be negligible. It has been questioned, wheter TAC acts as a crosslinker at all [276].

| divinylbenzene (DVB) | bis(vinyl phenyl) ethane (BVPE) | *m*-diisopropenyl- benzene (DIPB) | *N,N*-methylene-*bis*- acrylamide (MBAA) |

Figure 1-9. Crosslinkers used as co-monomers with the primary monomer(s) during the grafting reaction.

Another styrene-derived crosslinker that has been used in the preparation of radiation grafted membranes is diisopropenylbenzene (DIPB). Ben youcef et al. compared the crosslinking behavior of DVB and DIPB in electron-beam pre-irradiation grafted films and membranes on the basis of 25 μm ETFE, using styrene as primary grafting monomer (**Figure 1-10**) [192]. The overall polymerization rate of DIPB is slower compared to that of DVB, which leads to a more homogenous distribution of the crosslinker over the thickness of the film. Furthermore, the second double bond appears to be more reactive in DIPB than in DVB, making it less probable to find pending double bonds at high crosslinker concentration, which were hypothesized to accelerate oxidative degradation [245].
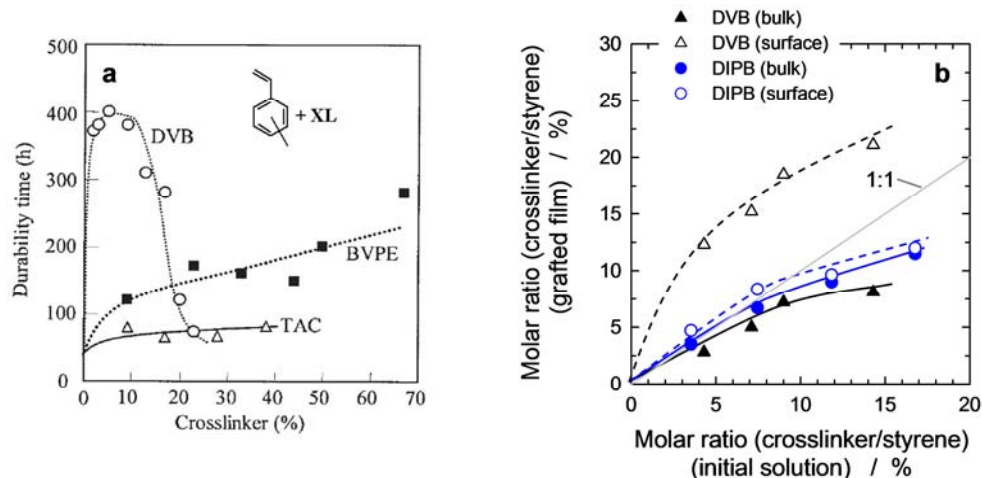
Figure 1-10. a) *Ex situ* chemical stability of grafted and sulfonated membranes in 3 % H_2O_2 solution at 50°C as a function of the crosslinker content (vol-%) in the grafting monomer mixture. 'Durability time' is associated with the onset of significant (more than ~10 %) membrane weight loss [245]. Reprinted with the permission. b) Molar ratio of crosslinker (DVB or DIPB) to styrene in ETFE (25 µm) grafted films in the surface (ATR) and in the bulk (trans) versus the molar ratio of crosslinker to styrene in the initial grafting solution. Adapted from [192].

A concept for crosslinking of radiation grafted membranes using alkoxysilane groups and sol-gel chemistry was introduced by the research group at the JAEA [249, 250]. They grafted *p*-styryltrimethoxysilane onto γ-ray pre-irradiated ETFE film of 50 µm thickness, followed by sulfonation, hydrolysis and condensation to form a siloxane-crosslinked proton conducting membrane. The hydrolysis-condensation step can be carried out either before or after the sulfonation step. The fuel cell relevant properties, such as proton conductivity and *ex situ* chemical stability in H_2O_2 solution, were found to be independent on the reaction sequence. Already crosslinked films, however, were found to be more difficult to sulfonate than uncrosslinked ones. The stability against oxidative degradation, measured *ex situ* in 3 % H_2O_2 solution at 60°C, of these siloxane-crosslinked membranes was found to be superior to that of conventional styrene-DVB grafted and sulfonated membranes. In addition, the water uptake and conductivity were higher at the same ion exchange capacity, which was ascribed to the presence of hydrophilic –Si–O–Si– and non-crosslinked –SiOH groups, which promote the formation of aqueous clusters.

3.6 Non-styrenic monomers

Styrene sulfonic acid based membranes have been known to be susceptible to oxidative attack since they were first used in fuel cells in the 1960s [9]. In the context of radiation grafted membranes, it has therefore been of interest to explore non-styrenic monomers with a potentially lower susceptibility to radical induced attack. Shkolnik and Behar carried out grafting of glycidyl acrylate onto electron beam irradiated 100 µm PE film and reported high graft levels of 100 % and more [264]. Grafted films were sulfonated in aqueous solution of $Na_2S_2O_5$ to obtain cation exchange membranes. However, it was observed that partial hydrolysis of the acrylate group took

place during the sulfonation reaction, yielding acrylic acid groups (**Figure 1-11**). In addition to sulfonation, sulfation was carried out in aqueous $Na_2S_2O_7$ solution. Hydrolysis was also observed in this case. Both types of membrane were furthermore reported to be susceptible to further hydrolysis upon immersion in dilute acid or base. This renders application in an aqueous electrochemical environment unsuitable.

glycidyl (meth)acrylate
(GMA / GA)
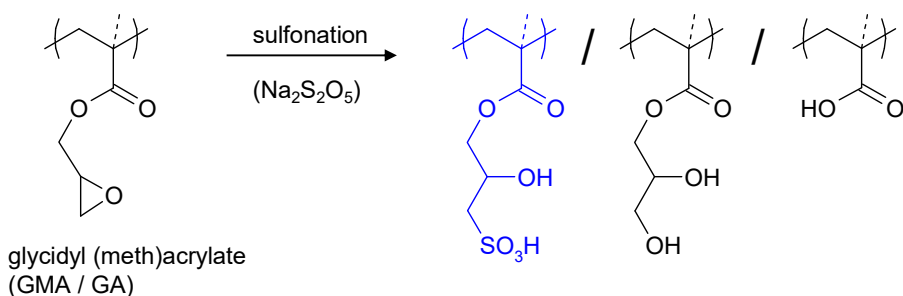
Figure 1-11. Sulfonation of grafted glycidyl acrylate (GA) or glycidyl methacrylate (GMA) leads not only to the sulfonated compound, a sizeable fraction hydrolyzes at the epoxy ring and the (meth)acrylate group to yield the diol and carboxylic acid, respectively. The hydrolytic stability of the methacrylate group is higher than that of the corresponding acrylate group.

Glycidylmethacrylate (GMA) grafted polymers are expected to be less susceptible to hydrolysis owing to the stabilizing effect of the α-methyl group. Many groups have investigated the use of GMA to introduce functional groups into polymer substrates, in many cases targeted at separation applications, because the epoxy group of GMA allows a wide variety of derivatization reactions [51]. With view to application in fuel cells much fewer studies are reported. Lee et al. pre-irradiation (e-beam, 100 kGy) grafted GMA onto ETFE, PE and PTFE, followed by sulfonation in a mixture of Na_2SO_3 and $NaHSO_3$ in isopropanol / water. PFTE and PE based membranes were reported to be brittle. The sulfonation reaction is rather slow, over 15 h reaction time at 80°C was necessary to obtain a degree of sulfonation exceeding 90 %. A problem found was that reasonable conductivity could only be obtained at graft levels above around 50 %, which was attributed to the presence of distinct areas of functionalization due to "front-like" grafting or sulfonation behavior. Choi and Nho reported the grafting of GMA onto gamma pre-irradiated PE films, followed by sulfonation and phosphonation [277]. Encouraging ion exchange capacities and conductivities were obtained, yet the membranes were also reported to be brittle at the high graft levels required when dried. Schmidt et al. therefore co-grafted mixtures of GMA / butylacrylate (BuA) and GMA / AN onto e-beam pre-irradiated ETFE films (50 kGy) [278]. The comonomers improved the flexibility of the grafted chain and thus the robustness of the grafted films. Sulfonation yielded proton conducting membranes. Evaluation of sulfonated GMA grafted membranes in the fuel cell has not been reported until recently [279]. In analogy to earlier reports, Buchmüller et al. found the grafting of GMA to proceed according to a distinct front mechanism.

Therefore, graft levels of around 100% have to be used for a reasonable conductivity of around 0.1 S/cm. Fuel cell tests showed, using the same electrodes and operating conditions, performance comparable to that of Nafion 212 and better than a pure styrene grafted membrane with similar conductivity. Moreover, the GMA based radiation grafted membrane exhibited higher durability in the fuel cell compared to the styrene grafted membrane. The application of GMA as grafting monomer, however, is associated with a number of shortcomings. Being an acrylic monomer, it is prone to hydrolysis under the operating conditions of the fuel cell. Furthermore, the high graft levels required to obtain attractive resistance values renders the membrane brittle and difficult to use.

Since the sulfonation of grafted GMA was found to be sluggish, Pacheco and Schmidt-Naake chose hydroxyethylmethacrylate (HEMA) as alternative monomer and grafted it onto e-beam pre-irradiated ETFE and PP films [280]. 2-Sulfobenzoic acid cyclic anhydride was used to sulfonate the HEMA grafted films, yet degree of sulfonation was only between 50 and 70 %. Membrane characterization in the fuel cell was not reported.

Acrlyates, but also methacrylates, have an intrinsic tendency to undergo hydrolysis, hence grafted acrylic acid (AA) may be a suitable basis for functionalization. Patri et al. prepared FEP-*g*-AA films by simultaneous irradiation grafting, followed by sulfonation with chlorosulfonic acid [281]. Low degree of sulfonation yielded poor conductivity (<1 mS/cm), which entailed poor performance (0.7 V @ 50 mA/cm^2) in the fuel cell.

An acrylamide with sulfonic acid terminal group (AMPSA) was used by Becker and Schmidt-Naake, using NVP as comonomer, to prepare radiation grafted membranes with sulfoalkyl protogenic groups [256, 257] (cf. also Section 3.4). The improved oxidative stability in *ex situ* tests compared to styrene and AMS based membranes was not explained, though.

A number of approaches for the preparation of alkyl sulfonic acid membranes by radiation grafting were reported from the group at the Japan Atomic Energy Agency (JAEA, Takasaki). Chen et al. used n-propyl vinyl ether (nPVE) and isopropyl vinyl ether (iPVE) as monomers to be grafted onto crosslinked PTFE base film [282]. Due to the low activity of alkyl vinyl ether monomers for radical induced polymerization, simultaneous irradiation grafting was performed in the presence of AlCl$_3$ as catalyst to promote cationic polymerization (radiation catalytic polymerization). Sulfonation with chlorosulfonic acid showed a poor yield, yet conductivities similar to those of Nafion® 112 could be obtained at IEC values as low as 0.8 mmol/g. The membranes assumed a deep brown color during sulfonation, indicating severe degradation.

Takahashi et al. grafted three acrylic monomers, i.e., methyl acrylate (MA), acrylic acid (AA), and *N,N,*-dimethylacrylamide (DMAAm), onto gamma pre-irradiated ETFE film of 50 µm thickness (20 kGy) [283]. Sulfonation was attempted using an equimolar (0.2 M) complex of chlorosufonic acid and 1,4-dioxane as a Lewis base, which was only successful in case of the MA grafted film. At the same time, the MA unit hydrolyzed to the carboxylic acid (**Figure 1-12**).

methylmeth-
acrylate (MMA)
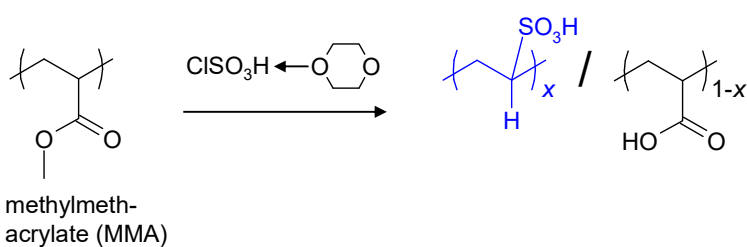
Figure 1-12. Preparation of alkyl sulfonic acid grafted membranes through grafting of methyl acrylate (MA), followed by sulfonation using a $ClSO_3H$-complex, yielding sulfonated, decarboxylated units ($x \approx 25$ %) and hydrolyzed units. Adapted from [283].

Chemical stability tests were carried out ex situ in water (85°C) and 3 % H_2O_2 solution (60°C). Degradation of the sulfoalkyl membranes was similar to those of PSSA grafted membranes, but much higher than for Nafion® membranes. In a subsequent study, MA was co-grafted with methyl methacrylate (MMA) and sulfonated with the same $ClSO_3H$-complex [284]. MMA units did not undergo sulfonation due to the presence of the methyl group. Membranes with higher MMA content exhibited higher durability in water and H_2O_2 solution.

Alternative proton conducting membranes typically show a more pronounced loss in conductivity upon reduction of the relative humidity compared to PFSA membranes. This is also the case for radiation grafted membranes. Based on the premise that incorporation of hydrophilic groups may improve proton conductivity at low relative humidity, Enomoto et al. prepared grafted membranes containing vinyl alcohol and sulfoalkyl groups [285]. To start with, vinyl acetate (VAc) was grafted onto gamma pre-irradiated ETFE film of 50 µm thickness, followed by hydrolysis in methanolic NaOH solution to yield polyvinyl alcohol (PVA) grafts. Sulfonation was performed using 1,3-propanesultone in toluene in the presence of triethylamine (**Figure 1-13**). However, the yield of this sulfonation reaction was low, a maximum of 40 % of vinyl alcohol units was converted to alkylsulfonic acid units.

A key asset exhibited by these hydrophilic sulfoalkyl membranes is their significantly improved conductivity at reduced relative humidities. Below 50 % r.h., the conductivity is around one order of magnitude higher compared to PSSA based grafted membranes of comparable ion exchange capacity. Also, membranes of the type sketched in **Figure 1-12** showed similar improvements in

low r.h. conductivity, which as attributed to enhanced proton mobility, owing to the presence of hydrophilic groups promoting hydrogen bond network formation, rather than increased water uptake. Fuel cell performance and, in particular, durability has not been reported for these types of membrane, yet in preliminary experiments it has been observed that the chemical stability is poor, in fact even inferior to that of PSSA based grafted membranes [286].
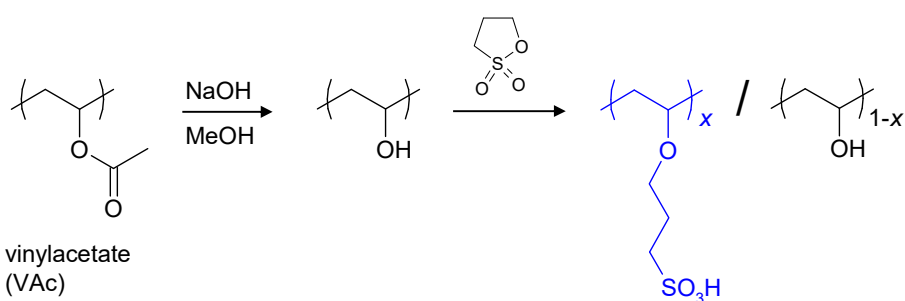
Figure 1-13. Preparation scheme of grafted sulfoalkyl membranes with vinyl alcohol units, wich are partially sulfonated using 1,3-propanesultone ($x_{max} \approx 0.4$). Adapted from [285].

3.7 Non-Crosslinking Comonomers

There has been some interest to incorporate comonomers to the primary monomer that do not act as a crosslinker for various reasons. Becker et al. co-grafted styrene and AN onto e-beam irradiated FEP and ETFE (150 kGy) of 50 µm thickness, highlighting that such membranes exhibit improved oxidative stability [191, 256, 257]. The rate of styrene incorporation was found to be enhanced in the presence of AN. Also, they mentioned the use of AN as a comonomer of AMS, which cannot be grafted on its own (cf. Section 3.3). AN tends towards alternating copolymerization with AMS and greatly improves the effective rate of AMS grafting. However, yet the grafting kinetics of the AMS / AN system was considerably lower than that of the styrene / AN system [191]. In the *ex situ* stability analysis in H_2O_2 solution, the loss of ion exchange capacity of the AMS based membrane was less pronounced than that of a comparable styrene based membrane.

A number of studies on the use of non-crosslinking co-monomers have been reported from the group at the Paul Scherrer Institut (PSI). Initially, AN and MAN were used as a comonomers to enable the grafting of AMS onto FEP [65, 258, 262] (cf. Section 3.3). Later, MAN was also co-grafted with styrene onto ETFE. Surprisingly, the resulting membranes exhibited an improved durability in the fuel cell compared to a pure styrene grafted membrane, which was attributed to the lower gas crossover in case of the MAN containing membranes [287]. Hence, the co-monomer appears to improve the gas barrier properties of the polymer. Compared to the AMS / MAN
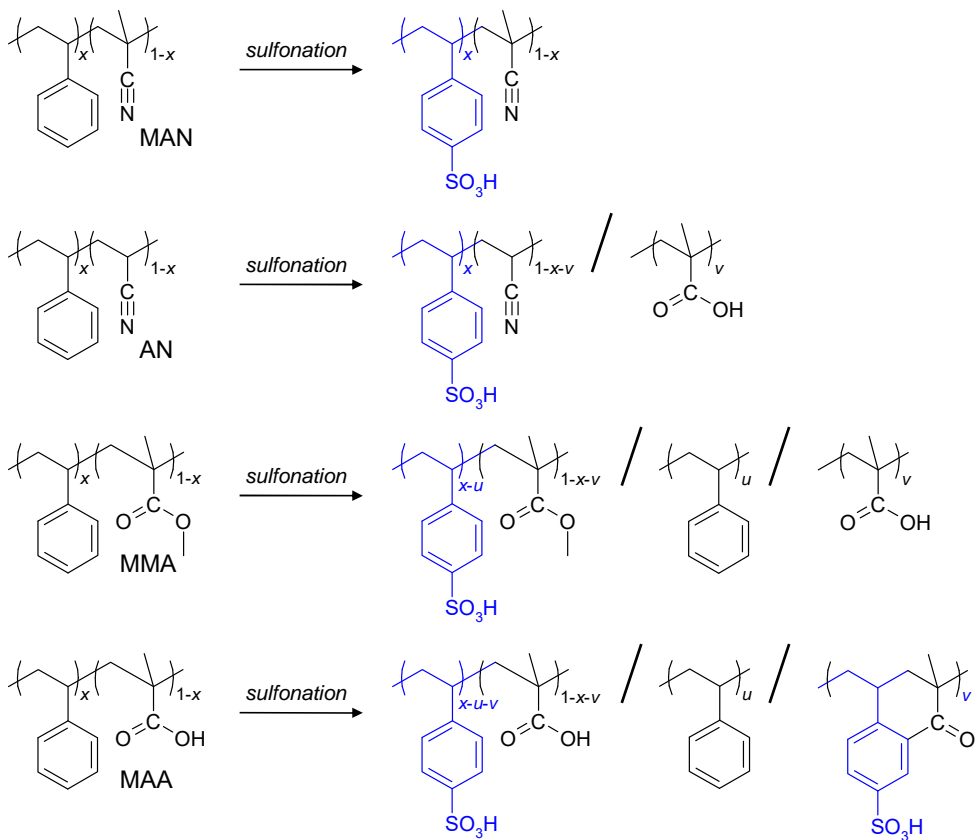
Figure 1-14. Molecular structures of co-grafted films, prepared using styrene and various comonomers, and corresponding membranes after sulfonation. MAN = methacrylonitrile, AN = acrylonitrile, MMA = methyl methacrylate, MAA = methacrylic acid. x and $1-x$ indicate the content of initial styrene and comonomer, respectively, and corresponding units in the sulfonated membrane; u represents the fraction of unsulfonated styrene units; v indicates the fraction of hydrolyzed comonomer, in case of MAA as comonomer it is the fraction of comonomer units that have undergone cyclization. (Adapted from [288])

system, the combination of styrene with MAN yields much higher grafting rates and allows the preparation of copolymers over the entire compositional range. A detailed analysis of the co-grafting of styrene with AN and MAN, respectively, shows that both combinations of monomers display a tendency to grow an alternating copolymer [260]. Both styrene / AN and styrene / MAN co-grafted membranes show similar *ex situ* properties, in terms of water uptake and proton conductivity, and exhibit an improved stability under accelerated chemical degradation conditions in the fuel cell compared to pure styrene grafted membranes [261]. However, the AN containing membranes underwent significant hydrolysis during the membrane preparation as well as during fuel cell operation, which leads to the loss of the nitrile functionality and formation of amide and carboxylic acid functional groups. The experimental results suggest that once the nitrile group, in case of AN, is hydrolyzed during the fuel cell test, the stabilizing functionality of the co-monomer is lost and the degradation rate of the membrane increases. Based on these findings, a range of other co-monomers, i.e., methyl methacrylate (MMA) and methacrylic acid (MAA), were co-grafted with styrene to elucidate whether these may also exhibit a stabilizing effect [288]. This was not the case, based on which it was concluded that the presence of nitrile groups is necessary

to impart the polymer with improved gas barrier properties. Styrene / MMA co-grafted membranes showed a maximum degree of sulfonation of 70 %, the reason of which could not be identified. Moreover, the methyl-ester showed signs of hydrolysis after sulfonation. A peculiar process appears to occur in styrene / MAA co-grafted membranes. During sulfonation , an internal Friedel-Crafts acylation takes place followed by a cyclic dehydration, leading to the formation of a conjugated, cyclic ketone structure. **Figure 1-14** summarizes the findings with various co-monomers of styrene.

Above, in Sections 3.4 and 3.6, the grafting of AMPSA was mentioned using NVP as comonomer. In analogy to the findings on nitrile co-monomer effects in styrene based membranes, the presence of NVP in the graft component may also have a stabilizing effect on the AMPSA based membrane. In the studies on the grafting of GMA onto e-beam pre-irradiated ETFE films (50 kGy), Schmidt et al. found that with butylacrylate (BuA) and AN as comonomers the obtained grafted films showed improved flexibility and robustness [278]. It was concluded that the chosen comonomers improved the chain flexibility and thus the robustness of the grafted films.

3.8 *Monomers for H₃PO₄ doped membranes*

The use of radiation grafted membranes has also been suggested in the context of the high temperature polymer electrolyte fuel cell (HT-PEFC), in which phosphoric acid doped polymers are used as electrolyte membrane [108]. Schmidt and Schmidt-Naake reported the e-beam pre-irradiation grafting of 4-vinylpyridine (4VP), 1-vinylimidazole (VIm), and *N*-vinylformamide (NVF) onto ETFE and FEP base film [289, 290] (**Figure 1-15**). The grafting of VIm was carried out in the presence of ferrous sulfate, which greatly increased the grafting rate, supposedly because of an enhanced decomposition rate of peroxide groups formed during irradiation according to $POOH + Fe^{2+} \rightarrow PO^{\bullet} + OH^{-} + Fe^{3+}$ [291]. The NVF grafted films were subsequently hydrolyzed in 1 M NaOH solution at 80°C for at least 12 h to obtain polyvinylamine (PVAm) grafted chains, obtaining graft levels of 50 % and higher. The films were doped by immersing them in phosphoric acid solution of varying concentration at 20 or 100°C. The resulting acid content of the membranes depends on the density of the functional basic groups and reaches values of 50 wt-% and more, yielding proton conductivities between 20 and 100 mS/cm at 120°C and dry conditions. In addition, the membranes were reported to be flexible, robust and mechanically stable. Fuel cell performance tests of selected membranes were carried out at 120°C in dry conditions and yielded performance comparable to that of a commercial H_3PO_4 doped AB-PBI (fumapem®, FuMA-Tech) membrane. Şanlı and Alkan-Gürsel carried out an extensive study on the effect of the solvent on the grafting kinetics of 4VP, NVP, and 2-vinylpyridine

(2VP) [292]. Further studies of doping with phosphoric acid and functional characterization has, however, not been reported so far.
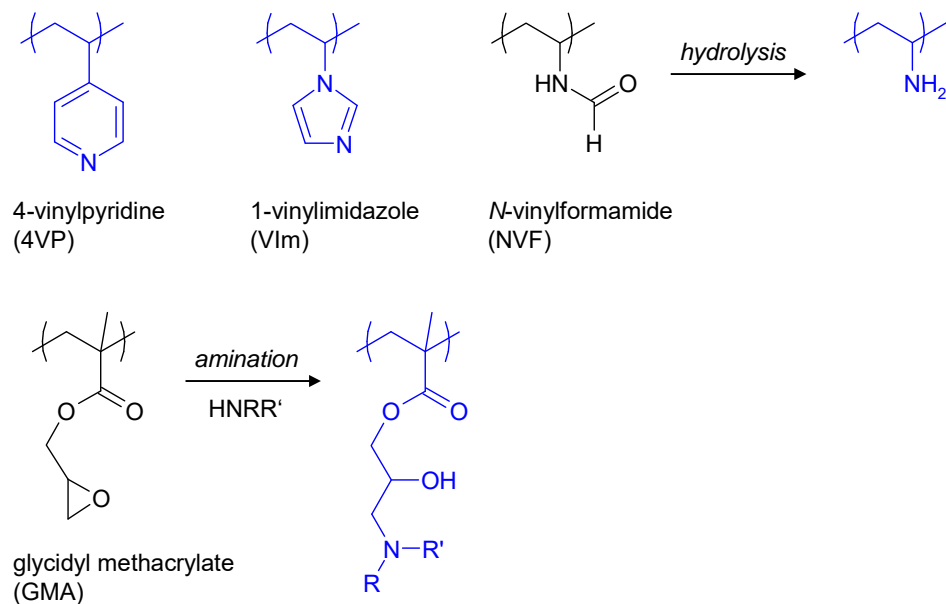
Figure 1-15. Synthesis of graft copolymers with basic character for the preparation of phosphoric acid doped proton conducting membranes. Amine functional groups are introduced into NVF and GMA grafted films in subsequent reaction steps.

Schmidt and Schmidt-Naake furthermore reported the co-grafting of GMA with BuA and AN onto pre-irradiated ETFE [290, 293]. Graft levels of up to 350 % were obtained. BuA and AN were used as comonomers to improve the mechanical robustness of the grafted films, as described above in Section 3.6. Subsequently, amination of the epoxy group was carried out with monoethylamine (EA), dimethylamine (DMA), diethylamine (DEA), or dibutylamine (DBA), followed by doping of the films with phosphoric acid to obtain ion conducting membranes. Conductivities of up to 120 mS/cm were obtained at 120°C under dry conditions. Fuel cell tests carried out at 120°C showed identical or slightly better performance than the commercial fumapem® membrane.

In analogy to sulfonic acid membranes, phosphonic acid membranes can be obtained by grafting precursor monomers onto a base polymer, followed by phosphonation. Schmidt-Naake grafted VBC and a mixture of VBC and AN onto e-beam pre-irradiated FEP and ETFE, obtaining graft levels between 24 and 190 % [294]. Phosphonation was carried out using triethyl phosphite in dichlorobenzene, using hydroquinone as catalyst, at temperatures up to 160°C, followed by hydrolysis in in concentrated hydrochloric acid. Conductivities or fuel cell tests have not been reported.

3.9 Anion exchange membranes

Hydroxide ion conducting membranes are of interest in the development of alkaline fuel cells, which offer the prospect of using non-noble metal catalysts [95, 96]. The preparation of anion exchange membranes by means of radiation grafting has been investigated extensively by Slade and Varcoe et al. [94, 295-301]. They used FEP, PVDF and ETFE films as base polymer, which were pre-irradiated using a gamma radiation source. VBC was used as a grafting monomer in these studies, as the benzyl chloride lends itself to derivatization via nucleophilic substitution reactions to introduce fixed cationic functional groups to serve as OH^- exchange sites. In most cases, VBC grafted films were reacted with trimethylamine (NMe_3) to introduce quaternary ammonium type anion exchange sites (**Figure 1-16**). The PVDF grafted films turned brown upon immersion in the NMe_3 solution and became brittle after exchange into the hydroxide form by immersion in KOH solution, which was explained by backbone degradation by dehydrofluorination according to $-(CH_2-CF_2)- \rightarrow -(CH=CF)- + HF$ [296]. For FEP and ETFE based membranes, a conductivity at 50°C in the OH^- form of around 20 to 30 mS/cm was obtained at a graft level around 25 % [297].
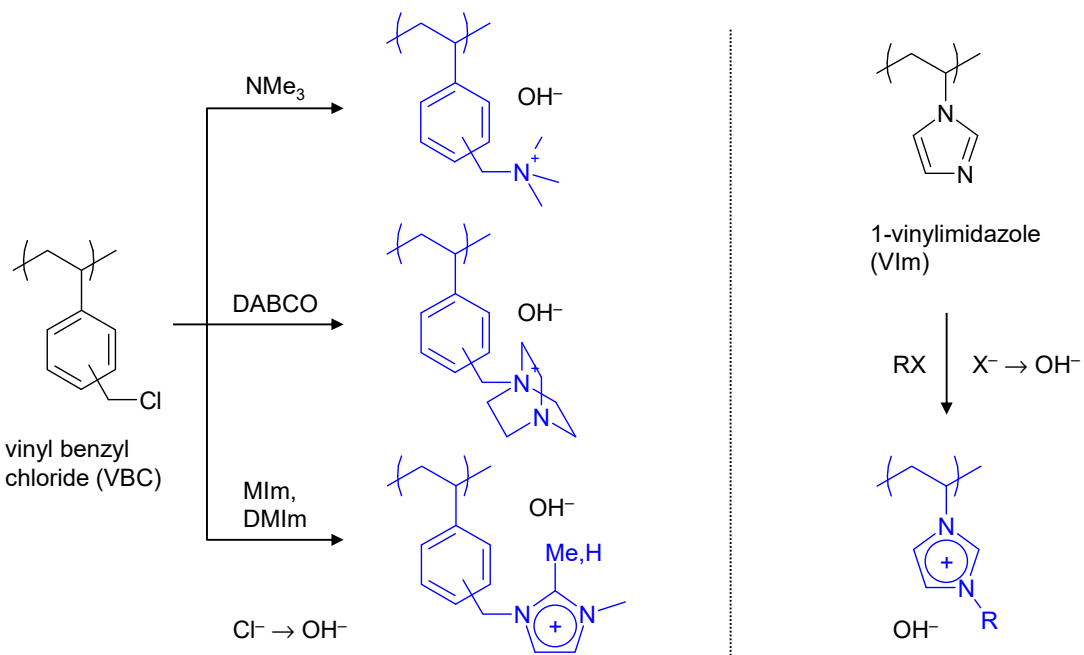
Figure 1-16. Preparation of ionomers with anion exchange functionality, based on grafted VBC and VIm. Subsequent functionalization introduces positively charged moieties, in this case ammonium and imidazolium groups. NMe_3 = trimethylamine, DABCO = 1,4-diazobicyclo[2,2,2]octane, MIm = 1-methylimidazole, DMIm = 1,2-dimethylimidazole, RX = alkyl halide.

In addition to quaternary ammonium exchange sites, other types of exchange site chemistries have been reported in conjunction with radiation grafted membranes. Ko et al. used VBC grafted ETFE film of 25 μm thickness, prepared by the simultaneous grafting method, as a basis for

quaternization reactions with trimethylamine (NMe$_3$) and 1,4-diazobicyclo[2,2,2]octane (DABCO) (**Figure 1-16**) [302]. The quaternization using DABCO was not complete, while with NMe$_3$ complete conversion was observed. The stability of the membrane functionalized with DABCO, measured by immersion in 10 M NaOH at 60°C, was found to be higher than that of the membrane quaternized with NMe$_3$. Yoshimura et al. introduced imidazolium anion exchange groups by reacting 1-methylimidazole with VBC grafted ETFE films (**Figure 1-16**) [303]. However, the resulting 1-benzyl-3-methylimidazolium (BMI) structures showed rapid degradation in 1 M KOH solution at 60°C, resulting from the nucleophilic attack of OH$^-$ at the benzyl carbon. Varcoe et al. also reported the derivatization of ETFE-g-PVBC using 1-methylimidazole [301]. The ionic conductivity was the same as that of a benzyltrimethylammonium (BTM) type membrane with same graft level and ion exchange capacity. However, its stability under alkaline conditions was inferior. Recently, the studies were extended to ETFE-*g*-PVBC films reacted with 1,2-dimethylimidazole to obtain 1-benzyl-2,3-dimethylimidazolium (BMMI) head groups (**Figure 1-16**). Although BMMI type membranes showed a superior alkali stability compared to BMI type membranes, it was still well below that of a BTM benchmark membrane [304]. It was therefore concluded that benzylimidazolium-type anion-exchange membranes have inadequate stability in anion-exchange membrane fuel cells.

In another approach, Yoshimura et al. grafted *N*-vinylimidazole (VIm) onto ETFE with subsequent *N*-alkylation in a iodopropane solution (**Figure 1-16**) [303, 305]. The conversion of the alkylation reaction was quantitative. The alkylated VIm groups were found to undergo β-elimination of imidazolium groups to reduce the electrostatic repulsion of neighboring imidazolium cations in the grafts. Therefore, VIm was co-grafted with styrene to increase the spacing of the resulting imidazolium units, which yielded improved stability in 1 M KOH solution at 80°C.

Unlike for fuel cells with cation exchange membranes, where soluble Nafion® ionomer is typically used to introduce ionic conductivity into the catalyst layer to form a spatially extended triple-phase boundary, anion exchange ionomers are not readily available for the preparation of MEAs using anion exchange membranes. In order to allow the characterization of their OH$^-$ conducting radiation grafted membranes based on the BTM head-group Varcoe, Slade and co-workers impregnated the (ionomer-free) catalyst layer of a gas diffusion electrode with poly(VBC) and subsequently immersed it in *N,N,N',N'*-tetramethylhexane-1,6-diamine to create a crosslinked ionomer network with quaternary ammonium anion exchange groups [298, 300, 306]. Fuel cell performance under H$_2$/O$_2$ was reported in several publications, showing power densities of around 30 to 60 mW/cm^2 at 0.6 V cell voltage and a cell temperature of 50 to 60°C with Pt loadings of

$0.5 \, mg/cm^2$ [300, 306]. Also, direct methanol fuel cell performance was reported with power densities on the order of a few mW/cm^2 using $4 \, mg/cm^2$ Pt and Pt-Ru electrodes, respectively [298, 306]. Since CO_2 is formed during electrooxidation of methanol, the associated formation of bicarbonate (HCO_3^-) leads to partial displacement of OH^- in the membrane, which significantly increases membrane resistance [307]. In alkaline fuel cells water is a reactant on the cathode side, therefore water management, the water transport properties of the membrane and the structure of the electrode are important aspects influencing the cell performance. Preconditioning the cell at high current density prior to recording of the polarization curve proved crucial to maximize fuel cell performance [299]. Using membranes prepared from ETFE base films of 12, 25 and 50 μm thickness, H_2/O_2 fuel cell performance of up to $130 \, mW/cm^2$ was reported using the conditions reported above. Furthermore, the potential to use Au and Ag as catalyst was demonstrated, yet the performance was significantly lower at the same loading as Pt. In a recent study, membranes based on the BMI head-group were tested in the fuel cell but showed much lower performance compared to a membrane with BTM head-group [301]. This was thought to be a result of, on the one hand, a rapid degradation of the BMI type membrane in the fuel cell and concomitant increase in membrane resistance, and, on the other hand, a poisoning of the catalyst by imidazolium or imidazolium-derived degradation products.

Mamlouk et al. reported a range of studies using radiation grafted alkaline anion exchange membranes of the BTM type [308-310]. They used LDPE (40 and 50 μm), HDPE (50 μm), and ETFE (25 μm) as base polymers and VBC as grafting monomer. The PE based membranes were prepared by simultaneous radiation grafting, using a ^{60}Co source, to achieve graft levels of up to 68 %, yielding an ion exchange capacity, after quaternization, of 2.13 mmol/g. The ETFE base film was pre-irradiation grafted (150 kGy), but the graft level obtained in the aqueous emulsion reaction mixture was only 24 %. While the articles from 2011 were mainly focused on the study of non-Pt catalyst, such as Co-based catalyst[309] and iron phtalocyanine catalyt[308] for the oxygen reduction reaction, the recent article reports detailed single cell studies using carbon supported Pt catalyst with a loading of $0.4 \, mg/cm^2$ on both sides [310]. The LDPE based grafted membranes yielded through-plane conductivities of up to 0.1 S/cm at 70°C. The peak power density of $820 \, mW/cm^2$ reported with O_2 at 60°C and atmospheric pressure is the highest value reported so far in the literature. With air at 2 bar absolute pressure, a power density of $470 \, mW/cm^2$ was attained.

Despite the superior stability of BTM compared to other head-groups, the chemical stability of quaternary ammonium containing anion exchange membranes has been considered to be somewhat problematic, especially at elevated temperatures above 60°C. Instability is mainly a

result of OH⁻ acting as nucleophile and attacking the ammonium group or adjacent carbon atoms [94]. Reports on durability in the fuel cell are limited. Varcoe et al. showed extended operation of a methanol / air cell over 230 h at 50°C without change in ohmic resistance, indicating no membrane degradation, which was confirmed by post test analysis of the ion exchange capacity [300].

4 Current Status

The characterization of a candidate membrane in the fuel cell is a key qualification step and ultimately provides information about the behavior of the material under the respective physico-chemical conditions. Unfortunately, though, in the open literature in the minority of cases in connection with studies focusing on the development of fuel cell membranes the set of experiments reported extends to tests in the fuel cell. In many cases perhaps, the expertise of the research group is rather in the area of polymer design and analysis and less on the engineering of membrane electrode assemblies and electrochemical characterization in single cells or stacks. In the few cases that fuel cell testing has been carried out and reported, the main findings have been outlined in the previous sections.

4.1 Balanced membrane properties

In the constellation of the author's laboratory, there has always been a strong belief that cell testing is a pivotal qualification experiment of any membrane (or any other material) developed for application in the fuel cell [311]. In many cases reported in the literature, an excessive focus is placed on the proton conductivity of the material alone, with other important aspects of fuel cell relevant properties being underrepresented. The function of the membrane is not only that of an electrolyte, but also it has to act as separator for electrons and reactants. This implies that mechanical properties of the material, its swelling behavior and, in particular for operating temperatures well above 80°C, the viscoelastic properties of the material can be decisive and limit its applicability in the fuel cell. In terms of the forming of a unitized membrane electrode assembly, bulk as well as surface properties of the membrane need to be taken into consideration and optimized [312]. An extensive review of performance and durability characteristics of radiation grafted membranes in fuel cells, using both hydrogen and methanol as fuel, has been published in 2005 [65]. The literature reviewed in this section concerns important insights gained during the past eight years, taken from studies carried out in the author's laboratory, owing to the various unique studies focused on the effect of membrane design and composition on fuel cell performance and durability characteristics.
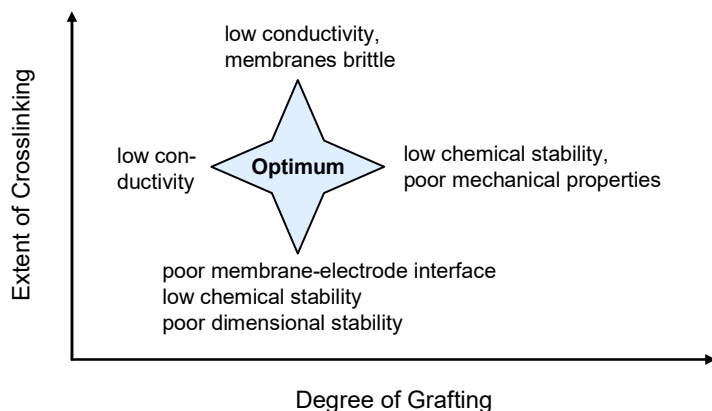
Figure 1-17. Optimum composition radiation grafted membranes with balanced properties is obtained at intermediate levels of grafting and cross-linking. Insufficient or excessive grafting and crosslinking, respectively, will lead to an unfavorable combination of properties. Adapted from [103].

In connection with the studies on radiation grafted membranes with fluoropolymer base film and styrenic graft component, an important lesson learned was that more ion exchange capacity and, thus, conductivity, is not necessarily advantageous from a fuel cell application point of view. High levels of grafting and high degrees of swelling entail poor chemical stability and render the membranes brittle. The mechanical integrity of the membrane is mainly given by the fluoropolymer base polymer, hence maximizing its volume fraction is required from a mechanical robustness point of view. On the other hand, the electrolyte properties are determined by the graft component and its ionic groups. The optimum composition, therefore, is at an intermediate graft level. Similar arguments can be put forward in connection with the optimization of the crosslinker content. Some degree of crosslinking is essential to stabilize the membrane mechanically and chemically, yet excessive crosslinking leads to poorly conducting and brittle membranes. The optimum therefore, again, is at an intermediate level of crosslinking (**Figure 1-17**). The exact optimum is a function of the target operating parameters and operation strategy. In a prospective application with frequent changes in power output and, consequently, fluctuations in hydration state and temperature of the cell, a membrane with slightly higher degree of crosslinking is probably a better choice, owing to its improved resilience against mechanical aging [313]. The possibility to fine-tune the composition and properties of membranes to a particular application profile is a key asset of the radiation grafting technology.

The importance of crosslinking has been mentioned above. In fact, this has already been found in the early days of the PEFC, yet at that time the need for crosslinking of PSSA was mainly to prevent the ionomer from dissolution. In radiation grafted membranes, the crosslinking has a dramatic impact on the rate of chemical degradation and, therefore, lifetime of the membrane in the fuel cell (**Figure 1-18**). A membrane based on 25 µm FEP with styrene graft level of around 18 %, corresponding to an ion exchange capacity of approximately 1.3 mmol/g, has a lifetime of

less than 100 h in a fuel cell operating at 80°C and constant operating conditions (**Figure 1-18**, sample 1a). With a membrane containing around 10 % DVB as crosslinker, a lifetime of several thousand hours can be reached under the same operating conditions (sample 1b). The significant improvement in chemical stability, evidenced by the rate of IEC loss being around two orders of magnitude lower, is thought to be a result of several factors. As crosslinked membranes exhibit a lower crossover rate for reactant gases (H_2, O_2), less radical species are expected to be formed at the catalyst [271]. In addition, the lower water uptake of the cross-linked membrane may reduce the diffusion of radical species formed at the catalyst into the bulk of the membrane. Furthermore, the polymer network formed via cross-linking is more resistant against loss of chain segments following bond scission, owing to the multiple connectivity of polymer chains [314].
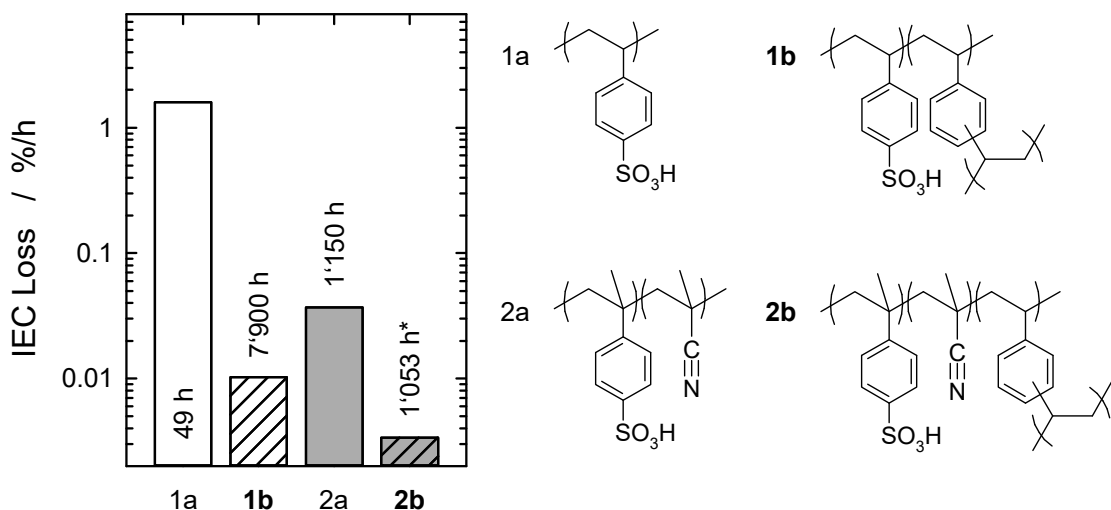
Figure 1-18. Chemical stability of styrene (1a, **1b**) and α-methylstyrene / methacrylonitrile (2a, **2b**) based radiation-grafted membranes (base film: 25μm FEP), with un-crosslinked (1a, 2a) and crosslinked (**1b**, **2b**) variations, expressed as IEC loss following single cell experiments at a temperature of 80°C and a constant current density of 0.5 A/cm^2. The indicated times represent the duration of the test (* = not failed). Adapted from [197].

4.2 *Beyond Traditional Styrene-Divinylbenzene Based Membranes*

The crosslinking, however, cannot banish the intrinsic susceptibility of styrene sulfonic acid to oxidative degradation, which mainly appears to be the consequence of the weak αC-H bond [315]. This has alredy been proposed in the 1960s [9]. Therefore, as outlined in Section 3.3 above, α-methylstyrene (AMS) was chosen as an alternative monomer. Since AMS could not be grafted by itself, a suitable co-monomer, methacrylonitrile (MAN), had to be chosen to enable co-polymerization [258, 262]. An AMS / MAN co-grafted membrane based on 25 μm FEP (**Figure 1-18**, sample 2a) with similar IEC, water uptake and conductivity compared to a pure styrene grafted membrane (sample 1a) showed a much improved lifetime of around 1'100 h and a concomitantly lower rate of chemical degradation. When DVB is introduced as crosslinker

(sample 2b) the chemical stability of AMS / MAN co-grafted membranes can yet be further improved. We refer to the new class of radiation grafted membranes based on AMS as "Generation 2" (Gen 2), whereas styrene based membranes are "Generation 1" (Gen 1) [197]. Taking the rate of IEC loss as an indicator of stability, the crosslinked Gen 2 membrane is around 500 times more stable than an uncrosslinked Gen 1 membrane of similar ion exchange capacity.
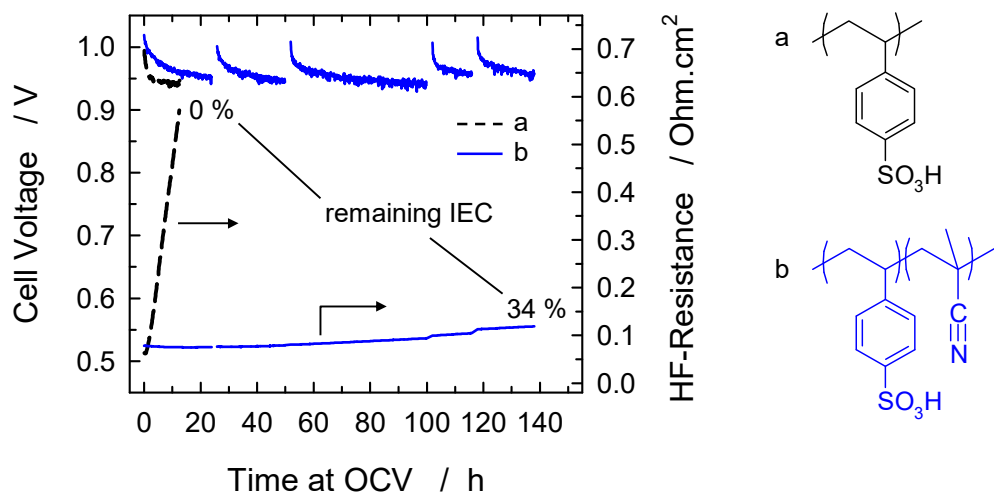
Figure 1-19. Accelerated stress test in the single cell at open circuit voltage (OCV) to promote chemical membrane degradation. Temperature: 80°C. The OCV and high frequency resistance (HFR) at 1 kHz are monitored. Samples, based on 25 μm ETFE: styrene grafted (a), styrene / methacrylonitrile grafted (b) (uncrosslinked) with IEC of around 1.5 mmol/g (cf. **Table 1-5**). The remaining ion exchange capacity (IEC) the end of test is determined using FTIR spectroscopy. Adapted from [261].

The improvement in durability with Gen 2 membranes was initially attributed to the replacement of styrene with AMS, which does not have a weak αC-H bond. Yet in order to graft AMS, a comonomer, in this case MAN, has to be used. This raised the question whether the presence of MAN could affect the properties of the membrane in some favorable (or unfavorable) way. Therefore, we studied the stability of membranes obtained by co-grafting of styrene and MAN, in this case using 25 μm ETFE as base polymer, in the fuel cell at 80°C and constant current density [287]. It turned out that MAN containing membranes showed an improved durability in the fuel cell. This was attributed to a lower gas crossover of the co-grafted membrane, which is thought to be an important cause for the formation of radical species at the electrodes [121]. Further analysis is reported in a recently published article [261]. In this case, a rapid aging test protocol in the fuel cell is used to accelerate membrane degradation. The test involves the operation of the cell at open circuit voltage (OCV), which as shown, for PFSA membranes, to accelerate the rate of ionomer decomposition due to increased gas crossover [316]. It was found that the pure styrene grafted membrane (**Figure 1-19**, sample a) shows a much steeper increase in resistance than the styrene / MAN co-grafted membrane. The increase in resistance is indicative of chemical degradation of the membrane through loss of the graft component. After a test duration

of 12 h, the styrene based membrane was disassembled from the cell and analyzed by FTIR. No signatures of the graft component could be found, suggesting that all of the styrene sulfonic acid was decomposed and removed from the membrane. It has to be pointed out that the membrane did not show mechanical failure at the end of test, the remaining ETFE base polymer still provided sufficient mechanical integrity. The base polymer does not appear to be chemically attacked by radical species in the fuel cell, at least not notably within the time period of the experiment.

In case of the styrene / MAN co-grafted membrane with similar IEC of 1.5 mmol/g, the increase in resistance was much slower. The test was discontinued after 138 h. The *post mortem* analysis revealed that still around 1/3 of the original IEC was retained. The gas crossover of the co-grafted membrane was lower than that of the pure styrene grafted membrane (**Table 1-5**), which can in first approach be explained by the higher thickness of the membrane. However, a similar improvement in chemical stability was not observed with a styrene / methacrylic acid (MAA) co-grafted membrane that has a thickness similar to that of the MAN containing membrane. In that case, a higher gas crossover rate and faster degradation under OCV conditions was observed [317]. Secondly, extraordinary gas barrier properties of copolymers of styrene and nitrile co-monomers were observed by Salame and Barnabeo et al. and attributed to the intrinsic high polarity of the nitrile group [318, 319]. It is therefore reasonable to assume that the presence of nitrile in the membrane improves the gas barrier properties of the membrane, which leads to a lower rate of radical formation at the noble metal catalyst and, as a result, a lower rate of chemical attack on the graft component.

The observed improvements in the chemical stability of the membrane in the presence of MAN raises the question whether the same or similar results can be found found for acrylonitrile (AN), a more common monomer (e.g., used for producing PAN fiber or impact-resistant polystyrene). Indeed, a styrene / AN co-grafted membrane shows very similar behavior and stability to a comparable styrene / MAN co-grafted membrane with similar IEC over 120 h of accelerated stress test identical to the one shown in **Figure 1-19** [261, 320]. However, AN is much more susceptible to hydrolysis and gradually hydrolyzes to the corresponding amide and carboxylic acid. MAN is more resistant, yet not entirely immune to hydrolysis, which is a consequence of the presence of an α-methyl group. The stabilizing effect of the α-methyl group is the result of a steric hindrance as well as an electronic inductive effect of the methyl group, which slows down the attack of a nucleophile, i.e., H_2O, on the carbon of the nitrile unit and stabilizes it due to its electron donating nature. The gradual loss of nitrile in case of the styrene / AN co-grafted membrane leads to an increase in the rate of degradation after around 120 h into the OCV hold test. It appears that once

the nitrile content drops below a certain value, its stabilization effect vanishes and chain degradation is accelerated [261].

4.3 Competing with Perfluoroalkylsulfonic Acid (PFSA) Membranes

Based on the insights gained on the improvement in stability with AMS and MAN containing membranes, an optimized crosslinked membrane was envisaged. As to the choice of crosslinker, DIPB (cf. Section 3.5) was selected over DVB, as it was found to result in a more homogeneous distribution of the crosslinker over the thickness of the grafted film [192]. Not knowing whether a more homogeneous crosslinking was advantageous or not in terms of durability, it was deemed reasonable to avoid gradients in crosslinking and, thus, in extent of swelling and, consequently, levels of internal stress development due to changes in hydration state. Furthermore, we reasoned that a crosslinker with methyl-protected α-positions would yield improvements in stability similar to that of AMS over styrene. The concentration of DIPB in the AMS / MAN co-grafted membrane based on 25 μm ETFE was optimized in similar manner as explained above (cf. **Figure 1-17**). An optimum was found at a concentration of 3.9 mol-% DIPB with respect to the total monomer content in the grafting solution [321]. An overview of key properties of radiation grafted membranes with increasingly complex composition of the graft component is given in **Table 1-5**. The introduction of MAN leads to an increase in water uptake owing to the overall higher graft level and increased hydrophilicity of the membrane. This is also reflected in the larger thickness of the membrane. The conductivity is comparable, though, to that of the pure styrene grafted membrane. Introduction of the crosslinker DIPB leads to a decrease in water uptake (and thickness) of the membrane, without dramatically affecting the conductivity. Both co-grafted membranes show a lower gas permeability in the fuel cell than the pure styrene grafted membrane. By contrast, the gas crossover in the Nafion® membranes is factors higher. The lower gas crossover in the grafted membranes is considered a key advantage over PFSA membranes, because the interaction of H_2 and O_2 on the surface of the noble metal catalyst is considered a key driver for the formation of reactive intermediates, which attack the membrane polymer and lead to chain scission [121].

Membranes of the type g-AMS.MAN:DIPB (**Table 1-5**) were selected for testing for extended periods of time. For this, 3 membranes of this type and 3 Nafion XL-100 membranes were assembled into a 6-cell stack optimized for operation on H_2 and O_2 with 60 cm^2 active area [263, 320]. The stack was operated using a dynamic load protocol with changes in current density approximately every 2 minutes ranging from 0.17 to 0.85 A/cm^2. Cell voltage values of individual cells were extracted at a current density of 1 A/cm^2 from polarization curves recorded intermittently (**Figure 1-20**). The test was carried out for a total of 2'470 h, after which 2 of the

radiation grafted membranes were still intact, whereas all the Nafion XL-100 membranes had failed due to excessive H_2 crossover (>10 mA/cm^2). The reason for the failure of the one radiation grafted membrane was the development of an internal short. It is worth noting that under the same operating conditions, Nafion 212 based MEAs have a lifetime of around 200 h only. The limitation is the formation of large crossover defects, which is probably a result of the repeated drying and swelling of the membranes [103]. The cell performance of MEAs with both types of membrane in (**Figure 1-20**) shows a similar decrease as a function of time. The increase in performance for the radiation grafted membranes in the latter part of the test is a result of i) the resolution of a test stand issue, which caused an undersupply of O_2, and ii) the removal of MEAs with high gas crossover or electrical short, which resulted in an effectively lower H_2 and O_2 flow stoichiometry in the cells with intact membrane.
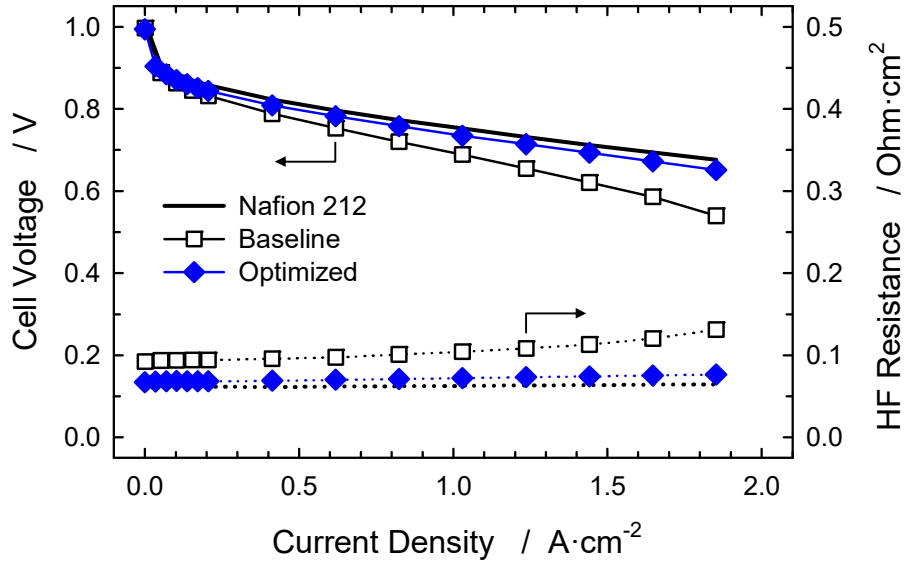
Table 1-5. *Ex situ* properties of radiation grafted (*g*-) membranes based on 25 μm ETFE with varying composition of the grafted polymer and a similar IEC of around 1.5 mmol/g. The ratio of styrene:MAN and AMS:MAN in the grafts is around 1, the content of DIPB cannot be determined experimentally, it corresponds to 3.9 mol-% DIPB with respect to the total monomer content in the grafting solution. Properties of Nafion® membranes are given for comparison. Hydration and conductivity are measured in liquid water equilibrated state at room temperature, the H_2 crossover current density was measured in the single cell at a temperature of 80 °C and a gas pressure of 2.5 bar$_a$ using fully humidified gases. Data compiled from [261] and unpublished results.

Membrane	IEC (mmol/g)	Thickness (μm)	Hydration (H_2O/SO_3^-)	Conductivity (mS/cm)	H_2 Crossover (mA/cm^2)
g-S	1.42 ± 0.08	37 ± 1	11 ± 1	79 ± 21	1.13 ± 0.10
g-S:MAN	1.54 ± 0.06	46 ± 1	18 ± 2	86 ± 6	0.84 ± 0.08
g-AMS:MAN:DIPB	1.59 ± 0.03	40 ± 2	9 ± 2	73 ± 12	0.82 ± 0.02
Nafion 212	1.10 ± 0.01	64 ± 1	17 ± 1	97 ± 15	2.54 ± 0.03
Nafion XL-100	0.90 ± 0.01	33 ± 2	19 ± 4	56 ± 5	4.09 ± 0.39

At the end of test (2'470 h), the crossover through the two intact radiation grafted membranes had only increased little from 0.82 to 1.0 mA/cm^2, which is still well below the value for Nafion XL-100 (4.1 mA/cm^2). After conclusion of the test, the remaining intact radiation grafted membranes were disassembled from the cell and MEA and *post test* analyzed using FTIR spectroscopy. The extent of degradation calculated based on the intensity of a vibrational band associated with aromatic units (764 cm^{-1}) was 8.3 and 6.1 %, respectively. This low degradation is encouraging regarding potential applications of the membrane. However, it was found that there was a significant degree of hydrolysis of the MAN units of 40 to 45 %. Although MAN is much more resistant to hydrolysis than AN, it is still subject to degradation during extended periods of operation. Whether a decrease of the nitrile content below a critical level will also lead to accelerated degradation is not known at present.
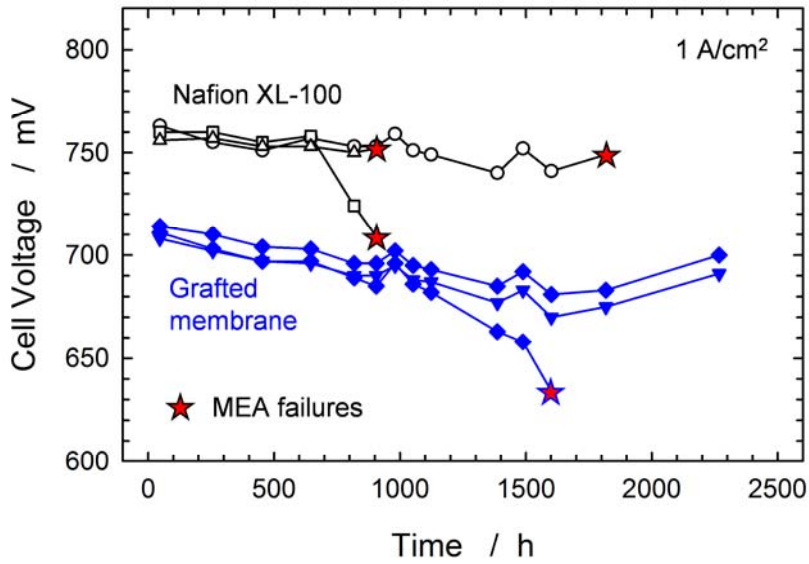
Figure 1-20. Durability test in a 6-cell stack (60 cm² active area) using the dynamic load protocol (cycling of current density: 0.34 → 0.17 → 0.85 A/cm², 2' each) shown on the top right. H₂/O₂, stack temperature: 80°C, gas dew points: 60°C, pressure: 2.5 barₐ. Empty black symbols: Nafion® XL-100, filled blue symbols: radiation grafted membranes. The data are cell voltage values extracted from polarization plots at 1 A/cm². Adapted from [320].

Figure 1-21. Improvement in performance through optimization of bulk and surface properties of radiation grafted membrane at constant graft level (cf. text for details). Adapted from [320].

The performance of the MEAs with radiation grafted membrane highlighted in **Figure 1-20** is about 60 mV short of that of Nafion XL-100 based MEAs. This was deemed insufficient and, hence, a study was initiated to identify the causes of the inferior performance. One of the critical aspects in the preparation of functionalized membranes via pre-irradiation grafting is the potential loss of surface-near active sites (radicals, peroxide groups) between the time of irradiation and the starting of the grafting reaction [322]. The following steps have been identified as key sources of deactivating active free surface radicals [323]:

i) *Irradiation and subsequent storage of films.* Antioxidants and stabilizers in storage bags used for irradiation can scavenge radicals at the surface of irradiated films that are in direct contact with the bag.

ii) *Film preparation prior to grafting process.* Irradiated films are exposed to environmental factors and foreign matter while handled and assembled into the grafting reactor, which can lead to radical decay at the film surface.

iii) *Grafting reaction.* Stabilizers and impurities in monomers and solvents can act as radical scavengers and chain transfer agents, limiting polymeric chain growth mostly during the initial phase of the graft copolymerization, which affects predominantly the membrane surface.

Membranes were prepared by addressing the above radical scavenging sources. Processing steps and the sequence of preparation have been modified to minimize losses of active surface radical. A detailed description of the implemented modifications of the process cannot be given, since the experiments were performed under a non-disclosure agreement with an industrial partner. With the implemented changes, the cell performance (cf. **Figure 1-21** for conditions) could be increased by 53 mV at a current density of 1 A/cm^2 with a corresponding decrease of the ohmic resistance from 104 down to 71 mOhm·cm^2, indicating that the performance improvement was predominantly of ohmic nature [323]. Another, rather surprising observation was made: membranes prepared using ETFE base films of 25 µm thickness from Saint-Gobain yielded, synthesized using the same procedure, a fuel cell performance that was 26 mV higher than that obtained with a membrane with similar graft level based on 25 µm ETFE from DuPont [323]. The exact reasons are not known at this stage and subject to ongoing investigations. The crystallinity of the two ETFE materials is in the range of 34 to 36 % and not significantly different from each other [324]. However, small-angle X-ray scattering (SAXS) experiments display a distinct difference in the scattering pattern, which indicates a difference in the crystalline arrangement [323]. These insights bring us back to the discussions at the beginning of the chapter, where it was highlighted that the base film materials used today for the preparation of ion conducting membranes through radiation grafting are not really optimized for this purpose, and probably there is room for improvement of base film properties. Putting all these findings together, i.e. using ETFE base film from Saint-Gobain and minimizing the loss of surface-near radicals during film handling and preparation, fuel cell performance using radiation grafted membranes based on AMS, MAN and DIPB can reach values comparable to those of Nafion® 212 and Nafion® XL-100 within 5 to 10 mV (**Figure 1-21**).

Chapter II

Experimental Methods

Some of the experimental descriptions in this chapter are taken from the various source articles listed on the table of contents pages of Chapters III and IV.

Experimental techniques for the preparation and characterization of radiation grafted membranes and important analytic methods used are outlined and discussed in this chapter. It is not intended to give a detailed account of the procedures used and methods employed, rather the distinctive features and key experimental and analytic tools are presented, mainly when the approaches chosen are of non-standard nature and when specific implementations and modifications of synthetic or analytic methods have been carried out. For a detailed description, the reader is referred to the original literature in the different sub-sections.

The main features of membrane synthesis and characterization are presented in Section 1. Section 2 focuses on the compositional analysis of multi-monomer grafted films and membranes to quantify the content of the individual grafted and possibly post-functionalized monomer units. In Section 3 the pulse radiolysis technique is outlined, which was used to create defined concentrations of radicals to study the radical induced attack and degradation of polyelectrolyte model compounds of the graft component.

1 Membrane Synthesis and Characterization

The preparation of ion conducting membranes via radiation grafting is described in this section, as well as the *ex situ* characterization of the samples to determine the primary fuel cell relevant properties of membranes. *In situ* testing in fuel cell hardware is outlined, also indicating the range of electrochemical methods used for cell characterization.

1.1 Synthesis Procedure

The ion-conducting membranes prepared in the framework of the studies reported in this thesis were cation exchange membranes with a sulfonic acid protogenic group, the same as the one used in perfluoroalkylsulfonic acid (PFSA) membranes, such as Nafion®. The membranes were prepared by pre-irradiation induced graft copolymerization ("radiation grafting") to obtain a polyelectrolyte constituent covalently attached to a thermally and chemically stable fluoropolymer backbone. Membrane preparation essentially involves the activation of the base film by electron beam irradiation, growth of a polymer by the radical polymerization mechanism onto the activated sites of the base polymer ('grafting'), followed by post-functionalization of the graft component to introduce sulfonic acid groups and potentially other motifs at the comonomer (**Figure 2-1**). Furthermore, a number of washing and intermediate steps are required, which are detailed further below.
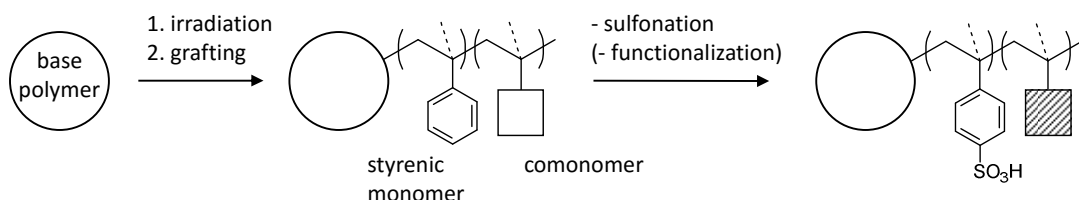
Figure 2-1. Schematic representation of the synthesis procedure of sulfonic acid based proton exchange membranes prepared by radiation grafting. A styrenic monomer was used, optionally in combination with a suitable comonomer. After the grafting step, the aromatic unit was sulfonated and, as needed, the comonomer unit functionalized.

The base polymer materials used were fluorinated ethylene propylene (FEP) and ethylene tetrafluoroethylene (ETFE) films of 25 μm thickness. The films of appropriate size were washed in ethanol, dried in the vacuum oven at 80°C and then placed in polyethylene zip-lock bags. Irradiation of the films was performed at LEONI Studer AG (Däniken, Switzerland) in air using an MeV class electron accelerator (**Figure 2-2**) with a dose of ranging from 1.5 up to 100 kGy. The residence time of the film in the accelerator was on the order of seconds. For doses above 25 kGy multiple passes were usually performed to avoid an excessive temperature rise in the sample and conveyor trays. The irradiated films were stored in dry ice during transit to the laboratory. There they were placed in a freezer at −80 ∘C until further use. Irradiated ETFE and PVDF films of 50 μm thickness irradiated with a dose of 30 kGy stored at -18°C have shown no change in grafting yield after more than a year [325].

Figure 2-2. Electron-beam irradiation of goods conveyed under the scan-horn of an electron accelerator. Typical electron energy is in the MeV range (photo: Leoni Studer AG, Däniken SO, Switzerland).

The grafting reaction was performed in a variety of reactors (**Figure 2-3**). A small glass reactor (60 mL) was used for kinetic studies and screening experiments. In this case, the size of the base film samples was around 8 cm × 8 cm. For larger batches, films of the size 14 cm × 16 cm were grafted in stacks of 6 in a flat 600 mL stainless steel reactor. For the preparation of membranes for technical size MEAs of a few hundred square centimeters, a 1.2 L glass reactor or a 6 L stainless steel reactor was used. In the latter, the largest prepared batch consisted of 24 films of 25 cm × 25 cm size, yielding a total membrane area of 1.5 m^2.

The reaction mixture was composed of the monomer(s) and solvents, typically a mixture of isopropanol and water, as this has been shown to be a favorable combination of solvents for the grafting of styrene type monomers. Polar solvents, such as isopropanol and isopropanol / water mixtures, yield substantially enhanced grafting kinetics compared to when non-polar solvents, such as benzene or toluene, are used. Polar non-solvents do not swell the polystyrene based grafts and thereby result in extended radical lifetimes [190]. In order to remove oxygen, the reactors were purged with nitrogen for at least 1 h. The reactors were subsequently sealed and heated, either by placing them in a water bath at a temperature between 50 and 60°C or by flowing heating fluid through the reactor jacket in case of the 6 L reactor. After a predefined reaction time, the grafting reaction was stopped by opening the reactor and removing the grafted film(s). The samples were subsequently soaked in toluene and / or acetone for at least 12 h, followed by drying in the vacuum oven at 80°C. The parameter of primary importance to characterize a grafted film is the graft level, degree of grafting or grafting yield *Y* given by

$$Y \quad = \quad \frac{m_g - m_0}{m_0} \qquad\qquad (2\text{-}1)$$

where m_0 and m_g are the mass of the film before and after grafting, respectively, obtained by weighing. A graft level of 100 % equals to a doubling of the weight of the sample.

The synthesis steps following the grafting reaction consist of post-functionalization of the graft component. This involves the sulfonation of the aromatic unit to introduce protogenic groups and possibly other modifications depending on the nature of the comonomer, which is performed before or after the sulfonation step. The sulfonating agent used is chlorosulfonic acid (ClSO$_3$H) at a concentration of 2 to 10 % in dichloromethane (DCM) as solvent. The reaction was performed at room temperature for 5 h. Sulfonyl chloride (-SO$_3$Cl) is mostly formed by the electrophilic aromatic substitution reaction. Quantitative conversion to the sulfonic acid (-SO$_3$H) was performed by hydrolysis overnight in 0.1 M NaOH solution, followed by re-acidification in 2 M

sulfuric acid for 5 h. Both of these reactions were carried out at room temperature. Finally, the membranes were rinsed and swollen in water at 80°C for at least 2 h. Alternatively, the hydrolysis can be performed by soaking the chlorosulfonated film in water at room temperature for 30 min, followed by treatment in water at 80°C for at least 12 h (overnight) [247]. As chlorosulfonic acid is a very powerful sulfonating agent, the resulting degree of sulfonation is close to 100 % [197]. The obtained membranes were stored in deionized water until further use.
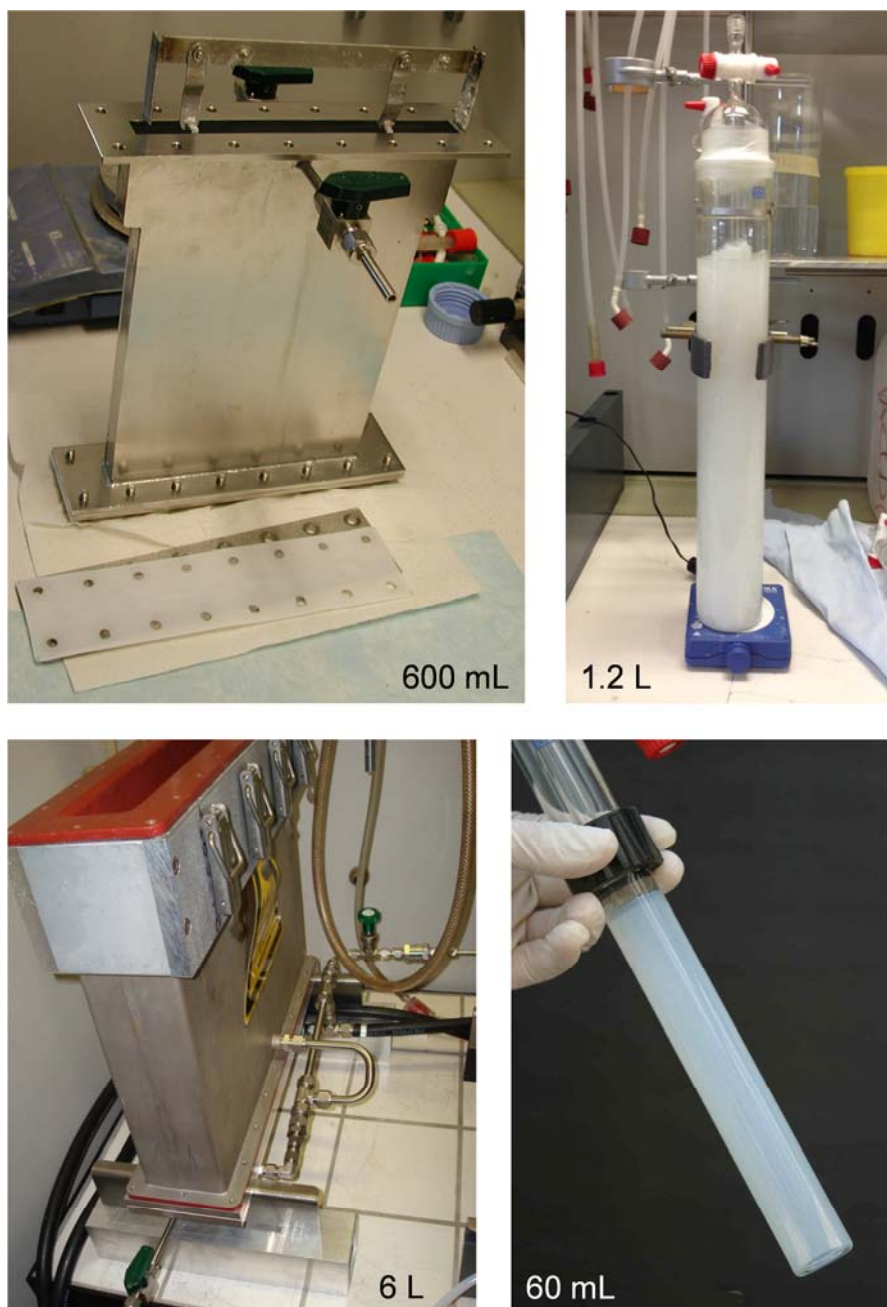
Figure 2-3.   Grafting reactors of various sizes. Film samples are rolled-up in the cylindrical glass shaped reactors. In the rectangular stainless steel reactors, stacks of film samples are inserted on a frame in flat configuration. The reactors comprise a means for purging the reactor with inert gas. The 6 L reactor is double-walled to circulate water as heating fluid, whereas the other reactors are placed in a water bath to control the reaction temperature.

1.2 Characterization

Initially, the membrane or the intermediates thereof in the various stages of preparation are analyzed for composition. The graft level gives but a crude measure indicating the overall amount of grafted component introduced. The individual constituents of the graft copolymer of membrane can be readily identified by Fourier transform infrared spectroscopy (FTIR), provided that corresponding vibrational bands are present and discernible from each other. The introduced changes can be characterized in qualitative as well as in quantitative terms (cf. Section 2.1). FTIR spectroscopy in transmission mode yields an average over the thickness of the membrane. Analysis of surface-near layers with information depth on the order of around 1 μm can be obtained from attenuated total reflectance (ATR) configuration of IR spectroscopic analysis. For example, with this approach it was found that the concentration of the crosslinker divinylbenzene (DVB) is much higher near the surface than in the bulk of a styrene : DVB co-grafted ETFE based film [192]. With an alternative crosslinker, diisopropenylbenzene (DIPB), the distribution of the crosslinker was found to be much more uniform.

In principle, solid-state nuclear magnetic resonance (NMR) spectroscopy can be used for compositional analysis, yet the technique is elaborate and cumbersome, but of high value if FTIR spectroscopy is inconclusive [288].

A true depth profile can be obtained for example from confocal Raman micro-spectroscopy using proper experimental configuration and data analysis [326]. An often used approach to measure graft profiles is to perform energy-dispersive X-ray (EDX) spectroscopy on the cross-section of a film or membrane in the scanning electron microscope (SEM) [327]. This technique can confirm a homogeneous distribution of grafts in a favorable system or the presence of distinct grafting fronts in case where monomer diffusion into the film is slow [279].

X-ray photoelectron spectroscopy (XPS) is an extremely surface-sensitive ultra-high vacuum (UHV) technique with information depth of around 5 nm to probe the composition and chemical environment of the identified elements at the surface of the sample. It has been shown, for example, for FEP based styrene : DVB grafted films that at increasing crosslinker content the concentration of grafts at the surface diminishes and the surface becomes increasingly hydrophobic [328].

Thermal analysis of materials is used to study phase transitions and temperature induced changes. Notably, crystallinity is readily obtained from differential scanning calorimetry (DSC). Thermogravimetric analysis (TGA) shows thermal stability features of the material, yet the

relevance of the findings for operation of a membrane in a cell at, say, 80°C has to be carefully considered. DSC can also be used to study the state of water in the membrane [329, 330], where commonly three types of water are identified: non-freezing, freezing bound, and free water [331].

The microstructure of ion-containing membranes has been known to be of a nano-phase separated nature for a long time [332]. The techniques of small-angle neutron scattering (SANS) and small-angle X-ray scattering (SAXS) are useful and powerful tools to study these features, as they allow the resolution of morphological characteristics on the length scale of nanometers to hundreds of nanometers [333, 334].

The investigation of the physico-chemical and functional characteristics of the film and membrane is essential to understand correlations between structure, composition and properties of the material. The distinction is made between *ex situ* and *in situ* characterization, the latter implying testing of the membrane in the fuel cell. *Ex situ* characterization consists of measuring film or membrane properties using dedicated methods aiming at measuring key characteristics under controlled conditions, for instance carrying out stress-strain tests on membrane strips to determine the tensile strength, Young's modulus, and strain to failure. The essential fuel cell relevant properties of a membrane are considered to be the ion exchange capacity (IEC), swelling in water and conductivity, outlined in the following sub-sections.

1.2.1 Ion Exchange Capacity (IEC)

The concentration of ionic sites is a key property of an ion exchange membrane and characterized by the ion exchange capacity (IEC), which is the number of ion exchange sites (in moles) per mass of dry polymer. The inverse value, the equivalent weight (EW), characterizing the mass of (dry) polymer per mole of exchange unit, is often used in the context of ion exchange membranes, in particular PFSA type membranes, such as Nafion®. Typical EW values of membranes used for fuel cell application are 800 to 1'000 g/mol [104]. In graft copolymer membranes, the ion exchange sites are introduced with the graft component. The IEC is measured by titration of the sulfonic acid units. For this, the membrane in its proton form is immersed in a salt solution, e.g. 0.5 M KCl solution, to exchange the H^+ by K^+ cations. It has to be ensured that there is a large excess of K^+ over H^+ to ensure complete ion exchange. The released H^+ lead to a decrease in the pH of the solution, typically around pH 3, depending on the number of exchange sites and the volume of the solution. The solution, with or without the immersed exchanged membrane, is then titrated to pH 7. From the volume V_t and concentration c_t of the added titrant, such as M/20 KOH solution, the number of protons $n(H^+)$ can be determined, $n(H^+) = V_t \cdot c_t$. The membrane is then removed, thoroughly washed with deionized water and dried at 80°C under vacuum. The dry

weight of the K^+-exchanged membrane is then measured, from which the dry weight of the membrane in the H^+-form can be calculated according to $m_0 = m_{H+} = m_{K+} - (M_K - M_H) \cdot n(H^+)$, where M is the molar mass. The IEC is then obtained from $IEC = n(H^+) / m_0$ [335].

It is of interest to estimate the IEC based on the graft level of a given grafting system. For exchange sites that are directly introduced with the grafted monomer, for example acrylic acid (AA), the calculation of the theoretical IEC is straightforward:

$$IEC_{th} \quad = \quad \frac{Y}{1+Y} \cdot \frac{1}{M_M} \tag{2-2}$$

Y is the mass-based graft level (cf. Eq. 2-1) and M_M is the molar mass of the monomer. In case that the ion exchange groups are introduced by functionalization of the graft component in a subsequent reaction step, such as in the case of the sulfonation of polystyrene grafts, the theoretical IEC is calculated, assuming a 100 % degree of sulfonation, according to

$$IEC_{th} \quad = \quad \frac{Y}{M_M + Y \cdot M_{M\text{-SA}}} \tag{2-3}$$

where $M_{M\text{-SA}}$ is the molar mass of the sulfonated monomer unit. Comparing this theoretical value with the actually measured IEC allows one to determine the degree of sulfonation. In the case of grafted and sulfonated styrene, this value is typically close to 100 % [197]. The situation becomes a bit more complicated if the monomer unit to be sulfonated, e.g., styrene, is co-grafted with a comonomer that does not undergo further reaction during sulfonation and post-processing. In that case, the theoretical IEC can be calculated if the composition of the grafts is known, for instance by knowing the mass fraction w_m of the monomer to be sulfonated with respect to the total mass of the graft component, which may have been determined using a suitable analytical method, such as elemental analysis or quantitative FTIR spectroscopy (see below):

$$IEC_{th} \quad = \quad \frac{w_M \cdot Y}{M_M \cdot (1+Y) + w_M \cdot Y \cdot (M_{M\text{-SA}} - M_M)} \tag{2-4}$$

In most cases, one is interested in the composition of the grafts on a molar basis. The mole fraction of monomer to be sulfonated in the grafts X_M is calculated from the mass ratio w_M according to

$$X_{\mathrm{M}} \quad = \quad \frac{w_{\mathrm{M}} \cdot M_{\mathrm{C}}}{M_{\mathrm{M}} - w_{\mathrm{M}} \cdot (M_{\mathrm{M}} - M_{\mathrm{C}})} \tag{2-5}$$

where M_{C} is the molar mass of the comonomer. This yields following expression:

$$IEC_{\mathrm{th}} \quad = \quad \frac{Y}{(M_{\mathrm{M}} + \dfrac{1 - X_{\mathrm{M}}}{X_{\mathrm{M}}} \cdot M_{\mathrm{C}})(1 + Y) + Y \cdot (M_{\mathrm{M\text{-}SA}} - M_{\mathrm{M}})} \tag{2-6}$$

In **Figure 2-4** examples of theoretical IEC are shown for various grafted membranes based on different monomers and one binary monomer system. The curves indicate that the higher the molar mass of the repetitive units of the grafts, the higher the required graft level to obtain a certain IEC. For acrylic acid (AA), the graft level for a given IEC is about half of that of styrene sulfonic acid (SSA) grafts. However, the strength of a carboxylic acid is much lower than that of a sulfonic acid, hence poly-AA grafts are not practical for fuel cell application [336]. Sulfonated glycidyl methacrylate (GMA) grafts have a somewhat lower IEC at a given graft level compared to SSA grafts, yet the main issue of GMA is that the degree of sulfonation is significantly lower (< 80 %) for graft levels below 50 % [279]. If one chooses a grafting system with a comonomer (for whatever reason) that will not contribute to the IEC, such as methacrylonitrile (MAN), the IEC for a given graft level is considerably lower, in particular if the comonomer is of high molar mass or the grafted comonomer units are post-functionalized with bulky pendant groups [337].
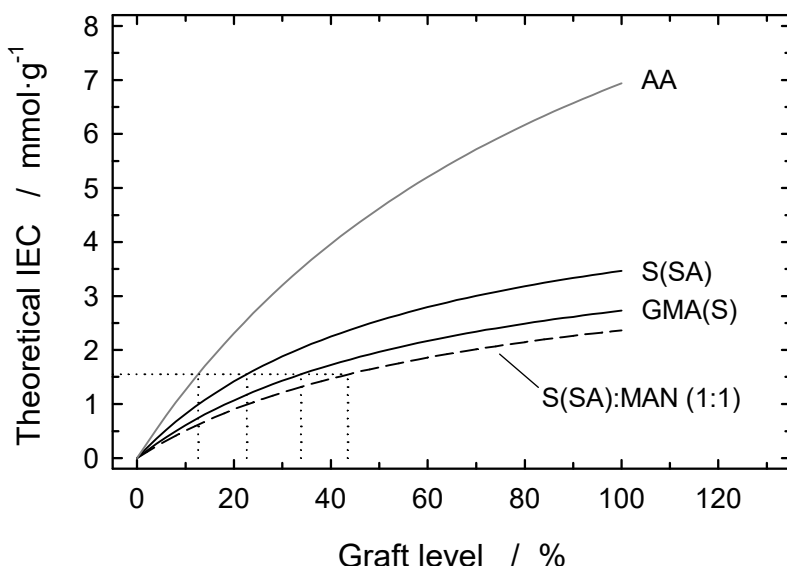
Figure 2-4. Theoretical IEC of membranes prepared with various grafting monomers on a given base polymer. AA = acrylic acid, S(SA) = styrene (sulfonic acid), GMA(S) = (sulfonated) glycidyl methacrylate, S(SA):MAN = co-grafts of styrene (sulfonic acid) and methacrylonitrile with a molar ratio of 1:1. The letters in parantheses indicate that the grafted units were post-sulfonated.

The examples shown in **Figure 2-4** are further characterized in **Table 2-1**, giving the theoretical graft level $Y_{1.55}$ to obtain an IEC of 1.55 mmol/g, a practical IEC for fuel cell application. For instance, for a styrene : MAN co-grafted membrane the required graft level is twice that of a styrene only grafted membrane. In addition, the theoretical IEC at infinite graft level is calculated, which corresponds to the IEC of the pure grafts, given by $IEC_\infty = 1 / (M_{\text{M-SA}} + M_C/F)$, where F is the molar ratio of sulfonated monomer and comonomer units in the grafts ($F = X_M / X_C = X_M / (1 - X_M)$).

Table 2-1. Molar mass of selected grafting monomers (cf. **Figure 2-4**) and their sulfonated analogues (where appropriate), the theoretical graft level $Y_{1.55}$ to obtain an IEC of 1.55 mmol·g^{-1}, and the theoretical IEC of the grafts (IEC_∞, limit of $Y \to \infty$).

Monomer	M_M (g·mol^{-1})	$M_{\text{M-SA}}$ (g·mol^{-1})	M_C (g·mol^{-1})	$Y_{1.55}$ (m-%)	IEC_∞ (mmol·g^{-1})
AA	72.1	-	-	12.6	13.9
S(SA)	104	184	-	22.6	5.43
GMA(S)	142	224	-	33.8	4.46
S(SA):MAN (1:1)	104	184	67.1	43.5	3.98

Often, one aims at synthesizing a membrane with a given IEC or various membranes of different composition at a fixed common IEC. The expressions given in Equations 2-2 to 2-6 can thus be rearranged to estimate the graft level Y of which the films need to be. In case of a monomer: comonomer system, one obtains:

$$Y = \frac{X_M \cdot M_M + (1 - X_M) \cdot M_C}{X_M \cdot (\dfrac{1}{IEC} - M_{\text{M-SA}}) - (1 - X_M) \cdot M_C} \tag{2-7}$$

If one plans an experimental series with varying monomer to comonomer ratio in the grafts at a fixed IEC, the required graft level increases dramatically towards low contents of the precursor monomer to be sulfonated (e.g., styrene) (**Figure 2-5**). In fact, an inspection of Eq. 2-7 reveals that there is a critical molar fraction $X_{\text{M,crit}}$ at and below which a given IEC cannot be reached, no matter how high the graft level Y. This critical value is given by

$$X_{\text{M,crit}} = \frac{IEC \cdot M_C}{1 - IEC \cdot (M_{\text{M-SA}} - M_C)} \tag{2-8}$$
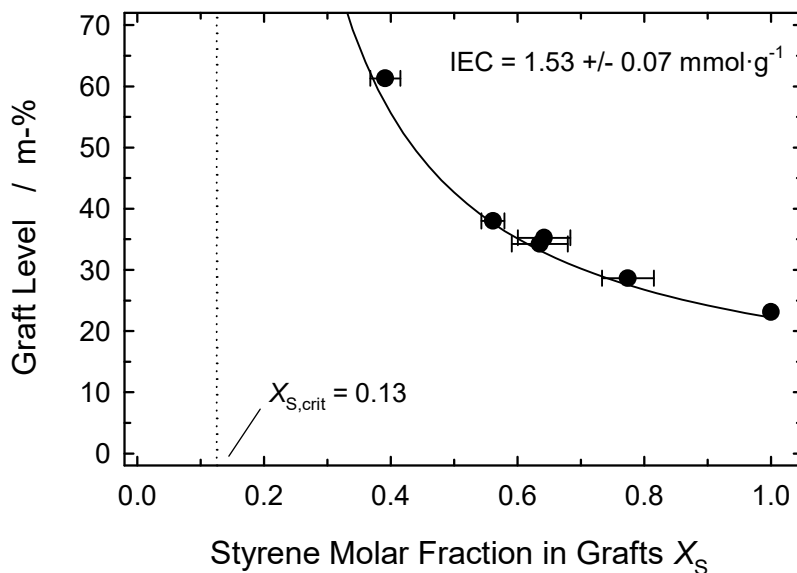
Figure 2-5. Example of a series of styrene : MAN co-grafted membranes of a fixed IEC or ~1.55 mmol/g with varying composition of grafts, characterized by $X_S = 1 - X_{MAN}$ [317]. The data points are well-described by the calculated values (Eq. 2-7). For this IEC, the critical composition $X_{S,crit}$ is indicated (cf. text).

1.2.2 Water Uptake

Ion exchange membranes swell when immersed in water. This leads to the dissociation of the ion exchange sites through the creation of mobile and fixed ionic species. The hydration of the mobile ion governs its mobility. Hence, the conductivity of the membrane depends on the charge of the mobile ions (mostly $+1$ or -1), its concentration, which is related to the IEC of the membrane, and mobility. A higher water uptake typically leads to an increase in conductivity up to a certain level of hydration, above which the conductivity drops again due to excessive dilution of the charge carriers. Therefore, the water uptake s ('swelling') of the membrane is an important property:

$$s_w \quad = \quad \frac{m_{wet}}{m_{wet} - m_0} \tag{2-9}$$

where m_{wet} is the mass of the wet, water-swollen membrane, and m_0 is the mass of the dry membrane in H$^+$-form. The mass of the wet membrane is difficult to measure and often operator dependent, because water droplets at the surface have to be carefully and completely removed, while extended exposure of the wet membrane to ambient conditions will lead to evaporation of some of the sorbed water. A quantity often used to characterize the water content in ion-exchange membranes in the fuel cell community is the hydration number λ , which describes the number of absorbed water molecures per exchange site [338]:

$$\lambda \;\; = \;\; \frac{s_{\mathrm{w}}}{IEC} \cdot \frac{1}{M(\mathrm{H_2O})} \tag{2-10}$$

Where $M(\mathrm{H_2O})$ is the molar mass of water (18.02 g/mol). A typical value for a water-swollen Nafion® membrane of equivalent weight 1'100 g/mol is a hydration number of around 20 $\mathrm{H_2O}$ / -$\mathrm{SO_3^-}$. At a given temperature, the conductivity of the membrane is found to show a linear dependence on the hydration number λ [338].

1.2.3 Conductivity

The one property of an ion conducting membrane that, in most cases, governs the ohmic loss in the fuel cell and thus influences the cell performance under given operating conditions is the conductivity. For a given membrane material, the conductivity is largely determined by the temperature and water content of the ionomer. A desirable design target for fuel cell membranes is to maximize conductivity at a minimum water content, as hydration of the ionomer leads to expansion and softening of the material, which impairs the mechanical integrity and durability of the material. From a morphological point of view, the presence of a phase separated microstructure comprising polymer-rich and water-rich domains, respectively, appears to be a distinctive feature of ion conducing membranes [118]. PFSA ionomers, such as Nafion®, have a particularly pronounced phase separated structure with domain sizes on the order of nanometers, which, together with the superacid property of the fluorocarbon sulfonic acid head-group, allows practical conductivity even at low levels of hydration, such as 5 $\mathrm{H_2O}$ / -$\mathrm{SO_3^-}$.

There are several experimental configurations to determine the conductivity of a membrane material. One distinguishes 2-point probe and 4-point probe setups on the one hand, in-plane and through-plane geometries on the other hand. The 2-point probe configuration is often used for through-plane conductivity measurements, owing to the straightforward experimental setup. The membrane sample, in most cases equilibrated in liquid water, is sandwiched between two metal electrodes. It is also possible to equilibrate the membrane in an atmosphere with defined relative humidity (r.h.), such as over a saturated solution of a given salt (e.g., 75 % r.h. for NaCl(sat) at 25°C), yet one has to ensure that the level of hydration is maintained when the sample is transferred to the measurement cell. This is best accomplished when the entire measurement is performed in a glove-box with uniform temperature and relative humidity [339]. An AC impedance spectrum of the measurement cell is then recorded, typically with an amplitude of 10 mV, from which the ohmic resistance is extracted at high-frequency at the intercept of the curve in the Nyqvist diagram with the real axis. The shortcoming of the 2-point probe method is

that the obtained ohmic resistance contains not only the membrane resistance, but also contributions of contact resistance between electrodes and the membrane. Therefore, in the procedure used in the experiments reported here (**Figure 2-6**, left), several measurements are performed with a different number of membrane discs (typically up to 6) stacked on top of each other [340]. From the slope of the linear regression line of the measured ohmic resistance as a function of the number of membrane samples and the known area and thickness of the discs, the conductivity of the material can be determined. The measurement cell can also be heated to study temperature dependence. For a more detailed description of the experimental procedure, the reader is referred to the literature [340, 341].
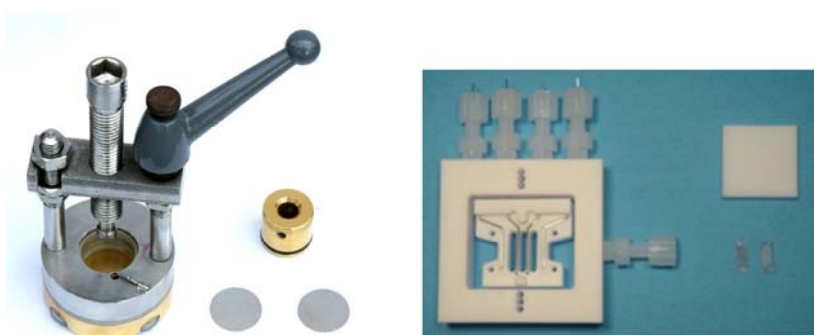
Figure 2-6. Experimental configurations to measure the conductivity of membrane samples. Left: 2-point probe through-plane conductivity cell, where stacks of membrane discs are sandwiched between two Pt-discs (ø2 cm). Right: 4-point probe in-plane conductivity cell (BT-112, Bekktech, Colorado, USA, now Scribner Associates, North Carolina, USA) for measurements under defined temperature and humidity conditions.

Since this experimental setup is somewhat impractical and the procedure to determine the conductivity as a function of temperature and relative humidity rather cumbersome, a 4-point probe in-plane configuration was used for this purpose (**Figure 2-6**, right). Here, a rectangular strip of membrane is contacted by four parallel Pt-wires. The outer wires serve as current source / sink, whereas the inner wires are for used as voltage probe. Hence, the measurement yields, taking into account the width and thickness of the membrane and separation distance of the voltage probes, directly the conductivity of the membrane. The PTFE frame with the inserted membrane sample can be immersed in liquid water at a defined temperature. Alternatively, the frame can be assembled into a fuel cell hardware and equilibrated at a given temperature, while gas with a defined relative humidity is supplied to the cell. In this way, membrane conductivity as a function of temperature and humidity can be recorded [288]. If the material is isotropic, the obtained values can be assumed to be representative of through-plane conductivity.

1.3 Fuel Cell Testing

The testing and evaluation of components in the fuel cell (*in situ*) is considered a pivotal element of materials research and development. Concerning the membrane, whereas the measurement of relevant properties in *ex situ* experiments yields intrinsic and fundamental materials data, such as conductivity, water uptake, and mechanical properties, only *in situ* testing ultimately allows one to assess the performance characteristics of a membrane, and its durability, under operating conditions representative of an application. Furthermore, the membrane and electrodes may interact in a non-straightforward manner. In particular for non-perfluorinated membranes and electrodes containing PFSA ionomer, it is well-known that typically higher membrane-electrode interfacial losses are observed, owing to the mismatch in the chemistry between the ionomer in the catalyst layer and the membrane polymer [195, 342]. Another important aspect regarding fuel cell operation is the water management properties of the membrane, i.e., water uptake and transport through hydraulic permeation, diffusion and electroosmosis. A delicate balance of water is to be established within the membrane-electrode assembly (MEA) to maintain the membrane and ionomer in the catalyst layers in a state of maximum hydration, while accumulation of liquid water in the gas diffusion layer is to be avoided to minimize reactant transport losses.

The study of the durability of components is even more crucial in a fuel cell configuration, as triggers for degradation are generated within the cell, such as radical intermediates through the interaction of hydrogen, oxygen and the Pt catalyst [121], or oscillatory changes in membrane hydration state caused by relative humidity cycling [343]. A typical and well-known case where *ex situ* membrane properties may be misleading is the comparison of chemical stability of hydrocarbon and PFSA membranes. Whereas a hydrocarbon membrane typically undergoes a much faster degradation and decomposition than a PFSA membrane in a Fenton test solution containing H_2O_2 and Fe^{2+} ions, which leads to the formation of $HO^{\bullet}$ radicals [5], the PFSA membrane fails much earlier in an accelerated fuel cell test, because the chemical degradation is caused by radical intermediates created as a result of H_2 and O_2 crossover through the membrane, and the hydrocarbon membrane has much better gas barrier properties than the PFSA membrane [141]. The various prevalent degradation phenomena can only be identified and examined though testing of components in on the device level, i.e., in the cell. The notion of accelerated stress test is yet another important topic in this context. Maximizing sample throughput and minimizing development cycles calls for testing methods where aging is accelerated and time to failure is shortened. The implementation of accelerated testing methods comes with the requirement of a detailed understanding of the underlying degradation mechanism, because only then the particular mode can be activated, while other degradation mechanisms are ideally "switched off", by choosing appropriate test conditions. Examples are the accelerated test

protocols defined by the US Department of Energy, for instance the test for membrane chemical stability, where the cell is held at open circuit voltage (OCV), which promotes radical induced attack of the polymer [344].

1.3.1 Cell Hardware

Characterization of membranes in the fuel cell also constitutes a central element in the studies reported in this work. While it is not the intention to provide a comprehensive account of cell and test configurations chosen in all of the various experiments reported in the results chapters, a condensed overview and outline of cell hardware, test conditions and experimental techniques are given in the following to highlight key features and aspects of cell testing and procedures. Most fuel cell tests were carried out in single cell hardware of 16 or 29 cm^2 active area (**Figure 2-7**). For some experiments, a fuel cell stack configuration was used with 6 cells, when high sample throughput was required or parallel tests of different membrane types ("rainbow stack") was to be done. The flow field plates consist of graphite plates (Diabon® NS2, SGL Carbon, Meitingen, Germany), into which the flow field was machined. Different sealing concepts are employed in the different cell designs, yet in all cases a compression of the the gas diffusion electrodes by about 20 % is targeted to ensure good electric contact between the gas diffusion medium and the flow field plate, while maintaining the porous structure to allow reactant access and product water removal. More details about the different cell designs used can be found elsewhere [271, 320, 345].
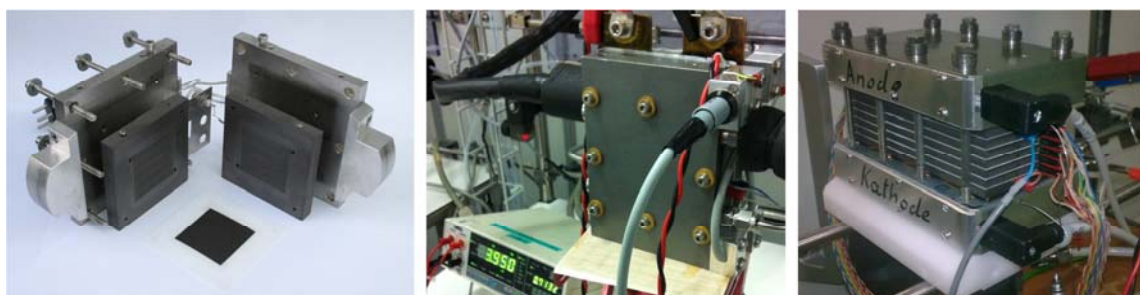
Figure 2-7.   Images of fuel cell hardware typically used in experiments for the *in situ* characterization of membrane electrode assemblies as well as durability experiments and accelerated stress tests. The flow field and bipolar plate material is graphite impregnated with phenolic resin in all cases. Left: Q30 single cell with 29 cm^2 active area and triple serpentine flow field. Center: N1D single cell hardware with 16 cm^2 active area and parallel flow field with vertical channels (low Δp) for operation under differential flow conditions. Right: Stack hardware (photo showing 6-cell stack) with liquid cooling / heating. Two flow field versions exist, one with a parallel flow field (active area: 30 cm^2) for differential operating conditions, and one with a serpentine flow field for H$_2$ / O$_2$ and H$_2$ / air operation (active area: 58 cm^2).

The membrane electrode assemblies (MEAs) were made by laminating gas diffusion electrodes and the membrane by hotpressing at elevated pressure, for instance 120°C, for up to 3 minutes. Gas diffusion electrodes were either of the carbon cloth type (E-TEK / BASF Fuel Cell, now De

Nora, USA) or carbon paper type (Johnson Matthey Fuel Cells, UK) with a typical Pt-loading of 0.4 mg·cm^{-2}. For the Q30 cell (**Figure 2-7**, left), the MEAs contained no subgaskets. In the N1D and stack design, membranes, electrodes and subgaskets (polyethylene naphtalate PEN, 25 µm) were hotpressed in one step. This allows the use of membranes of a smaller area, extending only about 0.5 cm beyond the active area, which allows a thrifty use of membrane material.

In some cases, in particular with FEP based membranes, the adhesion of the membrane and electrode and the interfacial properties were improved by impregnating the membrane with Nafion® prior to laminating the MEA. For this, the membrane was dried at 120°C for 2 h and then immersed in Nafion® solution, prepared from a 5 wt% solution of Nafion® with an equivalent weight of 1'100 g/mol (Solution Technologies, Mendenhall PA, USA, now available from Ion-Power, New Castle DE, USA) diluted with ethanol at a volumetric ratio of 1:9. After 1 h, the membrane was removed, the solution on the surface was shaken off. After leaving the membranes to dry at room temperature in the fume hood for about 1 h, the Nafion® coating was cured in a vacuum oven at 120°C for 2 h [195, 346].

The cells were normally conditioned at a constant current density of 0.5 A·cm^{-2} overnight before the measurement procedure was started. The test bench allowed the control of the electronic load, temperature of the cell, gas flows, gas humidity, and back-pressure. Mostly cells were operated at a constant stoichiometry (normally 1.5 for both H_2 and O_2, and 2.0 for air) with a minimum flow. Two methods to humidify the gas streams were used, depending on the type of teststand used: in one type, bubbler type humidifiers were used, and direct liquid water injection mixers in the other type. In both cases, the gas lines leading to the cell were heated to avoid condensation.

Test protocols and procedures varied according to the purpose of the experiment. Often, a test consisted of conditioning followed by electrochemical characterization of the cell using a range of techniques (see below) to characterize the performance characteristics of the MEA and shutdown of the cell after less than 100 h on test. An important accelerated test protocol used was the OCV hold test to study the chemical degradation of the membrane. In durability tests, the cell was operated either under constant current mode or with a dynamic protocol to simulate a load profile.

1.3.2 Electrochemical Techniques

The primary method to characterize the performance of an MEA and cell is the recording of a polarization curve. Thereby, the current I is increased in steps from OCV with a hold time of 30 s to 5 minutes per point up to the maximum current allowed by the electronic load or until the cell voltage U dropped below a minimum value. At the same time, the ohmic resistance of the cell R_Ω

was measured, either via the auxiliary current-pulse technique developed at PSI [347], or a high-frequency (1 kHz) resistance measurement using an AC milliohm meter (Tsuruga model 3566, Japan). The measuring of the ohmic resistance of the cell, which is mainly determined by the resistance of the membrane, is essential to deconvolute the voltage losses. When operating on O_2, or air at low current densities where mass transport losses can be neglected, the loss terms are assumed to be kinetic losses on the cathode due to the slugging oxygen reduction reaction (ORR) and ohmic losses of the cell. For analysis of the kinetic losses, the *iR*-corrected cell voltage $U_{iR\text{-free}}$ = $U + i \cdot R_\Omega$ is determined [348]. When polarization curves are used for the analysis of MEA degradation following a particular testing procedure, the ohmic resistance R_Ω is a good indicator of membrane degradation in case of radiation grafted membranes [261]. One caveat in the determination of R_Ω via an ac impedance measurement at 1 kHz is that the measured resistance value may not be entirely free of non-ohmic contributions, because analysis of an electrochemical impedance spectrum recorded under the same conditions shows that the intersection of the spectrum with the real axis at the high frequency end yields somewhat lower values than what is measured at 1 kHz [349]. In addition, the impedance value at high frequencies may be affected by cable inductance. All in all, the error associated with the measurement of the ohmic resistance of the cell by a fixed-frequency ac impedance measurement at 1 kHz is estimated to be 10 to 20 %.

Complete electrochemical impedance spectra were recorded over a frequency range from 100 mHz to 25 kHz, typically at a current density of 0.5 A·cm^{-2}, to break down loss terms to contributions due to ohmic and polarization resistance. It has been found for radiation grafted membranes that in MEAs using these non-PFSA membranes in combination with catalyst layers comprising PFSA ionomer also the loss term associated with the membrane-electrode interfacial properties, expressed by the polarization resistance R_p, is affected compared to all-PFSA MEAs [195, 350]. Electrochemical impedance spectra were recorded in H_2 / O_2 operating mode to largely neglect effects of limited O_2 transport on the cathode when operated with air. The resulting spectra show a somewhat distorted, depressed semi-circle, intercepting the real axis at the low and high-frequency end, respectively. The high-frequency intercept was interpreted as ohmic resistance R_Ω of the MEA, which is governed by the resistance of the membrane. The diameter of the semi-circle was interpreted as polarization resistance R_p. The analysis of various MEAs based on radiation grafted membranes showed that the polarization resistance is a measure for the quality of the membrane-electrode interface [195, 341, 351].

Reactant (H_2, O_2) permeability of an MEA is an important property in the context of the chemical stability of a membrane material (cf. Chapter IV). In the configuration of a single cell (or a stack), the hydrogen crossover through the membrane at a given temperature, humidity and pressure can

be determined electrochemically [352]. For this, N_2 was fed to the cathode compartment of the fuel cell and H_2 to the anode compartment with load cables detached (OCV condition). After equilibration a cell voltage of around 0.1 V is measured. The potential of the cell is then stepped from 0.2 to 0.8 V in steps of 0.1 V with a hold time of 60 s, while the current is measured. In principle, the current is generated due to the electrochemical oxidation reaction of H_2 that is diffusing from the H_2 to the N_2 electrode. The corresponding reaction on the H_2 side is the hydrogen evolution reaction. Theoretically, the measured current is independent of the cell potential and given by the limiting current corresponding to the rate of diffusion of hydrogen to the N_2 side, yet practically an ohmic behavior can generally be observed, where the cell current increases proportionally to the cell potential, which is a result of the finite electronic resistance of the MEA [352]. To distinguish the current originating from hydrogen crossover from the electric short of the MEA, the H_2 crossover current density is obtained from the intercept of the linear regression line at 0 V[1].

In the context of the assessment of membrane durability, various test protocols were employed. In all cases, the cells were operated on pure O_2 to minimize in-plane non-uniformities. In one approach, the cell was operated at a constant current density, for example for a duration of 1'000 h or until the MEA failed, with intermittent characterization of the cell to assess the state-of-health of the membrane [195, 262, 287, 341, 353]. For accelerated degradation, a protocol with dynamic load was implemented [197, 320]. Dedicated accelerated stress tests to probe the chemical stability of membranes were carried out at open circuit voltage (OCV) [196, 261, 320, 337, 354-356], which is known to accelerate the radical induced attack on the membrane (cf. Chapter IV). Furthermore, pure O_2 was chosen as oxidant, a reactant gas humidity of 100 %, and an elevated pressure of 2.5 bar_a to maximize chemical stress. For the investigation of the susceptibility of the membrane towards hydrolysis, a novel test protocol was designed, whereby the cell containing the membrane to be tested and electrodes was supplied with humidified nitrogen on both sides at a temperature of 90°C [260]. In the absence of hydrogen and oxygen the oxidative degradation of the membrane is "switched off".

---

[1] Strictly speaking, the extrapolation should be done to the OCV of the cell in H_2 / N_2 mode, not to 0 V. However, the associated error is comparatively small, since the OCV is typically below 0.1 V and thus close to 0 V.

2 Composition Analysis of Co-grafted Membranes

The analysis of the composition of a graft copolymer membrane obtained from a single monomer grafted into the base polymer is straightforward, provided the monomer or base polymer does not deteriorate during the reaction: the weight change upon grafting indicates the amount of graft polymer added to the base polymer. In case of styrene grafted and sulfonated membranes, the degree of sulfonation is close to 100 % and the obtained ion exchange capacity shows good agreement with the theoretical IEC calculated according to Eq. 2-3 [186, 227]. The analysis becomes more complex if a mixture of monomers is co-grafted. The situation is particularly challenging if the two (or more) comonomers have similar chemical structure, such as styrene and the crosslinker divinylbenzene. In the case of copolymers prepared in solution, NMR spectroscopy is a powerful method to analyze copolymer composition [357]. In case of graft copolymers, the solid state NMR technique can be used, yet quantitative analysis is cumbersome and resource-intensive. Alternatively, elemental analysis can be performed, which is particularly effective when distinctive elements are present in the base polymer and grafted comonomers. In the work reported here, elemental analysis was used to quantify the composition of FEP films grafted with α-methylstyrene (AMS) and methacrylonitrile (MAN) (see below). A versatile and simple method for the composition analysis of co-grafted films can be Fourier transform infrared spectroscopy (FTIR). Typically, FTIR is used for qualitative analysis, yet quantitative analysis is possible if distinct vibrational bands are available and suitable methods for calibration are implemented. Furthermore, FTIR spectroscopy is non-destructive and the analyzed sample can be further used. Moreover, locally resolved characterization is possible, depending on the size of the region analyzed or the experimental configuration (e.g., micro-FTIR). In the studies reported here, FTIR spectroscopy was the main analytic tool to quantify the composition of the grafted copolymer, in as prepared films and membranes as well as in membranes (artificially) aged in the fuel cell.

2.1 *Quantitative FTIR-Analysis*

The use of FTIR spectroscopy for the composition analysis of radiation co-grafted films was already reported in the 1960s by Odian et al. [358, 359]. In their first article, mixtures of styrene (S) with methyl acrylate (MA), 4-vinylpyridine (4VP), and acrylonitrile (AN) were graft copolymerized into LDPE [358]. The composition of the grafted copolymers was determined by IR analysis using the 14.3 μm (700 cm^{-1}) vibrational band of polystyrene. UV spectroscopy and elemental analysis were mentioned as complementary methods for composition analysis, yet further details were unfortunately not given. In a subsequent study, Odian et al. grafted styrene (S) / methyl acrylate (MA) and styrene (S) / acrylonitrile (AN) onto PTFE film [359]. For calibration, the absorbance of the vibrational band at 6.7 μm (1'493 cm^{-1}), corresponding to the aromatic C-C

stretch vibration in the aromatic ring, was plotted against the graft level of styrene-only grafted films, which yielded a linear relationship. However, the maximum graft level of styrene was merely 7 %, and it was recognized that higher graft levels would lead to errors using this technique due to the increase in the dimensions of the samples. The composition of co-grafted samples could thus be estimated by calculating the graft level of styrene using the calibration curve and the graft level of the comonomer as weight difference to the gravimetrically measured graft level.

In the methodology adopted for the studies reported here, FTIR spectroscopy was used for quantitative compositional analysis of co-grafted membranes using two calibration methods. In the first case, the co-grafting of AMS and MAN, elemental analysis of co-grafted films as well as of copolymers of AMS and MAN was performed to determine the actual content of the two monomers in the copolymer. In the second case, exemplified for co-grafting of styrene and MAN, calibration curves are established based on films grafted with each of the two monomers separately. Using appropriate normalization, the effect of expansion of the sample upon grafting is taken into consideration. This method can be used whenever "homo"-grafting of the two monomers is possible, which, for instance, is not the case for AMS. In Chapter III, this approach is also used for the analysis of styrene co-grafted with acrylonitrile, vinylbenzyl chloride and glycidyl methacrylate. The method can also be used if only one of the monomers can be readily grafted on its own, yet at the expense of the accuracy of the analysis. In principle, grafted films containing more than two monomer units can be analyzed in this manner, it may, however, become difficult to identify sufficiently independent vibrational bands assignable to each of the monomer units.

2.1.1 Calibration via Elemental Analysis of Copolymers

For the calibration of the FTIR method using elemental analysis, copolymers of AMS and MAN and co-grafted films of AMS and MAN on FEP base polymer (25 µm thickness, DuPont Teflon® FEP 100A) were prepared. Poly(AMS-*co*-MAN) copolymers of various compositions (molar fraction of AMS in the feed x_{AMS} ranged from 0.05 to 0.50) were prepared in bulk at 60-70°C in a reaction flask under N_2 using azo-bis-(isobutyronitrile) (AIBN) as initiator. The nitrogen content w_N of the resulting copolymers, determined via elemental analysis (LECO CHN-900, ETH Zürich), varied between 8 and 16 mass-% (**Table 2-2**), based on which the weight fraction of AMS in the copolymer w_{AMS} was calculated according to

Table 2-2. Determination of the molar fractions of AMS and MAN ($X_{AMS} + X_{,MAN} = 1$) in copolymers (1a-d) and co-grafted polymers (2a-e) on 25 µm FEP base film by elemental analysis for calibration of the composition using FTIR spectroscopic analysis.

No.	Sample	x_{AMS}[a] (feed)	Y (graft level) (m-%)	w_N (nitrogen content) (m-%)	X_{AMS}[b] (copolymer)	X_{AMS} / X_{MAN} (copolymer)	A_{1600} / A_{2230}[c]
1a	Copolymer	0.05	-	16.43 ± 0.08	0.133 ± 0.003	0.154 ± 0.003	0.137 ± 0.003
1b	Copolymer	0.10	-	13.84 ± 0.02	0.224 ± 0.001	0.289 ± 0.001	0.202 ± 0.004
1c	Copolymer	0.30	-	9.82 ± 0.10	0.390 ± 0.005	0.639 ± 0.012	0.484 ± 0.010
1d	Copolymer	0.50	-	8.28 ± 0.01	0.464 ± 0.000	0.865 ± 0.001	0.633 ± 0.003
2a	Graft copolymer	0.50	20.8	1.79 ± 0.11	0.364 ± 0.029	0.573 ± 0.072	0.365
2b	Graft copolymer	0.56	22.5	1.86 ± 0.09	0.377 ± 0.023	0.606 ± 0.058	0.443
2c	Graft copolymer	0.56	36.7	2.17 ± 0.01	0.474 ± 0.001	0.903 ± 0.005	0.725
2d	Graft copolymer	0.60	34.5	2.01 ± 0.06	0.486 ± 0.013	0.947 ± 0.048	0.734
2e	Graft copolymer	0.60	36.0	2.01 ± 0.01	0.499 ± 0.001	0.996 ± 0.006	0.798

[a]   molar fraction of AMS with respect to total monomer content (AMS + MAN)

[b]   determined from the nitrogen content

[c]   ratio of the FTIR intensities (peak areas) for AMS (1'600 cm^{-1}) and MAN (2'230 cm^{-1}) relevant vibrational bands; only single measurements are available for co-grafted samples (2a-e)

$$w_{AMS} = 1 - w_N \frac{M_{MAN}}{M_N} \tag{2-11}$$

where M_{MAN} and M_N are the molar masses of MAN (67.9 g mol^{-1}) and nitrogen (14.0 g mol^{-1}), respectively. Co-grafted films of AMS and MAN on FEP base film (e-beam dose: 25 kGy) were prepared at 50 or 60°C with x_{AMS} of 0.50, 0.56 and 0.60. The obtained graft levels ranged from 21 to 36 % (**Table 2-2**). Elemental analysis was performed in similar manner, which yielded the nitrogen content w_N of the grafted films. For the calculation of the AMS weight fraction in the grafts w_{AMS}, the graft level Y has to be taken into account:

$$w_{AMS} = 1 - w_N \frac{M_{MAN}}{M_N} \cdot \frac{1+Y}{Y} \tag{2-12}$$

The molar fraction of AMS X_{AMS} (and that of MAN, $X_{MAN} = 1 - X_{AMS}$) can then be determined using Eq. 2-5. FTIR spectra of the copolymer powders and co-grafted films were recorded and the intensity of the vibrational bands (peak area) pertinent to AMS (1'600 cm^{-1}) and MAN (2'230 cm^{-1}) analyzed by peak fitting. The basis for using FTIR spectroscopic analysis to determine the content of AMS and MAN in the (grafted) copolymer is the expectation that the ratio of the intensities of the vibrational bands accociated with AMS and MAN is proportional to the molar ratio $F = X_{AMS} / X_{MAN}$ of the comonomer units determined via elemental analysis (**Figure 2-8**). In case of the poly(AMS-*co*-MAN) copolymer samples linear regression through the origin yielded a satisfactory correlation coefficient of 0.998 and the calibration factor k_{calib}:

$$\left.\frac{X_{AMS}}{X_{MAN}}\right|_{copolymer} = k_{calib} \cdot \frac{A_{1600}}{A_{2230}} \tag{2-13}$$

The value determined was $k_{calib} = 1.34 \pm 0.03$. Since the standard deviation of the composition is considerably higher in case of the co-grafted samples, owing to the overall lower nitrogen content measured (**Table 2-2**), only the copolymer data is used in the regression analysis. The molar ratio of AMS and MAN in the graft component of the co-grafted films and the corresponding FTIR band ratio are shown in **Figure 2-8** to check how these data compare with the calibration curve. Evidently, the nitrogen content of the co-grafted films is lower than that of the copolymers (**Table 2-2**), owing to the 'dilution' of the AMS:MAN copolymer in the matrix of the base polymer. Consequently, the calculated ratio of monomer units is associated with a higher error of 6 % compared to that of the copolymer samples. Overall, the result shows that the composition of co-

grafted films of AMS and MAN can be determined via FTIR spectroscopic analysis with reasonable accuracy. Thus, the FTIR method based on the calibration curve shown here was used for this graft copolymer system (AMS:MAN) throughout the studies reported in this thesis.
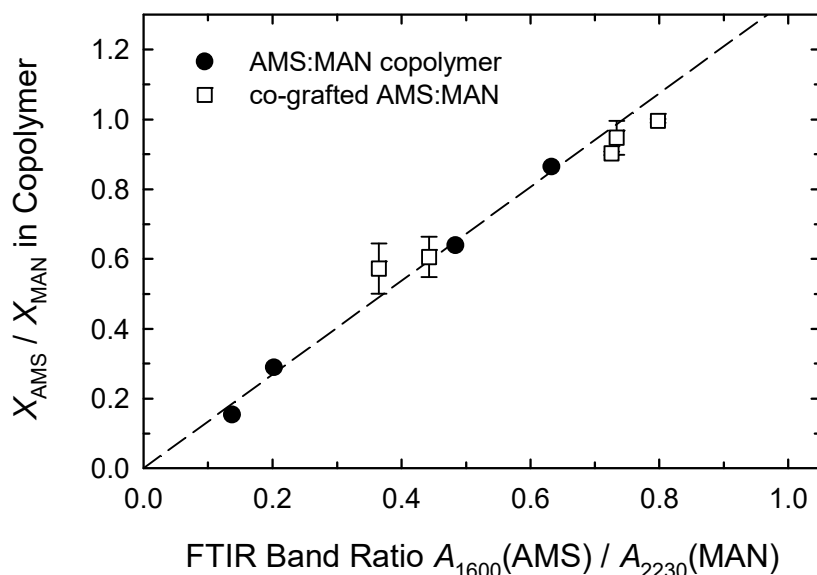
Figure 2-8. Calibration curve for determining the AMS:MAN content via FTIR spectroscopic analysis of AMS (1'600 cm^{-1}, aromatic C-C vibration) and MAN (2'230 cm^{-1}, C≡N stretch vibration) relevant vibrational bands. The composition of AMS and MAN in copolymers and co-grafted samples is determined via elemental analysis. The slope of the calibration curve is determined based on the copolymer samples only.

2.1.2 Calibration based on Single Monomer Grafted Films

Besides the calibration of the FTIR analytic method using standards with 'known' composition determined via, e.g., elemental analysis, it is furthermore possible to use a calibration method based on FTIR spectra of grafted films prepared with each of the monomers separately. In this case, however, the effect of 'dilution' as a result of sample expansion upon grafting needs to be taken into consideration. The introduction of the graft component leads to an area expansion and an increase in the thickness of the film undergoing grafting (**Figure 2-9**). Since the transmission
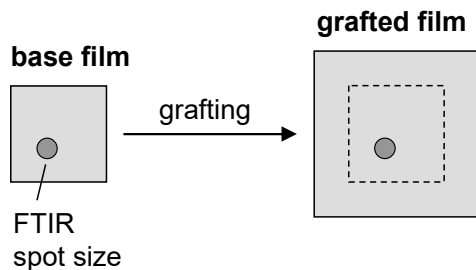
Figure 2-1. Schematic representation of the expansion of the film upon grafting. Since the spot size of the IR beam does not change, the dimensional change of the grafted film leads to a 'dilution' of the base polymer.

FTIR analysis of the polymer film probes an area of given size (spot size), the expansion of the film leads effectively to a 'dilution' of the base polymer in the probed volume. Therefore, the intensity of vibrational bands associated with the base polymer decreases with increasing graft level (**Figure 2-10**, upper diagram). The factor by which the intensity decreases is given by the area expansion of the film as a result of grafting, i.e., the ratio of the area of the grafted film and the area of the base film. For the same reason, the intensity of vibrational bands associated with the graft component will not increase in proportion to the graft level, but will be lower by the same factor related to the film expansion. Since the graft level represents the ratio of the amount of grafted polymer with respect to the amount of base polymer, the ratio of the intensity of vibrational bands associated with the graft polymer and base polymer is expected to be proportional to the graft level. Therefore, the intensity of the vibrational band associated with the graft component or one of the graft components A_g normalized by the intensity of the vibrational band associated with the base polymer A_{ETFE} :

$$\widetilde{A}_g \quad = \quad \frac{A_g}{A_{ETFE}} \tag{2-14}$$

ought to show a linear dependence on the graft level. The symbol $\widetilde{A}_g$ represents the normalized intensity. The lower diagram in **Figure 2-10**, which shows the results of two series of grafting experiments onto ETFE using styrene and MAN, respectively, shows that this is indeed the case. The slope m_g ($= m_S$, m_{MAN}) of the best-fit straight lines going through the origin can therefore be used as a calibration to determine the partial graft levels Y_g of styrene (Y_S) and MAN (Y_{MAN}) in co-grafted samples according to $Y_g = \widetilde{A}_g / m_g$. The basis for the compositional analysis of co-grafted films now is that the relationship 2-14 still holds, because the presence of a second graft

Table 2-1. Graft levels for styrene and MAN determined via FTIR analysis and the calibration curve in **Figure 2-2** for a range of co-grafted membranes, prepared using a styrene molar fraction in the monomer mixture of $x_S = 0.6$ (hence, $x_{MAN} = 0.4$). Calculated overall and measured graft level, and calculated molar fraction of styrene in grafts X_S ($X_{MAN} = 1 - X_S$) are given.

Styrene graft level Y_S (m-%)	MAN graft level Y_{MAN} (m-%)	Combined graft level $Y = Y_S + Y_{MAN}$ (m-%)	Measured graft level Y_{exp} (m-%)	Styrene molar fraction in grafts X_S[a]
11.4 ± 0.7	2.5 ± 0.8	13.9 ± 1.1	10.9	0.74 ± 0.06
23.3 ± 5.7	7.1 ± 1.6	30.5 ± 7.5	28.5	0.68 ± 0.07
37.4 ± 8.0	13.8 ± 2.5	51.2 ± 8.4	50.9	0.64 ± 0.06

[a] $$X_S = \frac{m_S / M_S}{m_S / M_S + m_{MAN} / M_{MAN}} = \frac{Y_S / M_S}{Y_S / M_S + Y_{MAN} / M_{MAN}}$$

where Y_S and Y_{MAN} are the fractional graft levels of S and MAN, respectively, and M_S and M_{MAN} are the corresponding molar masses ($M_S = 104$ g·mol^{-1}, $M_{MAN} = 67$ g·mol^{-1})
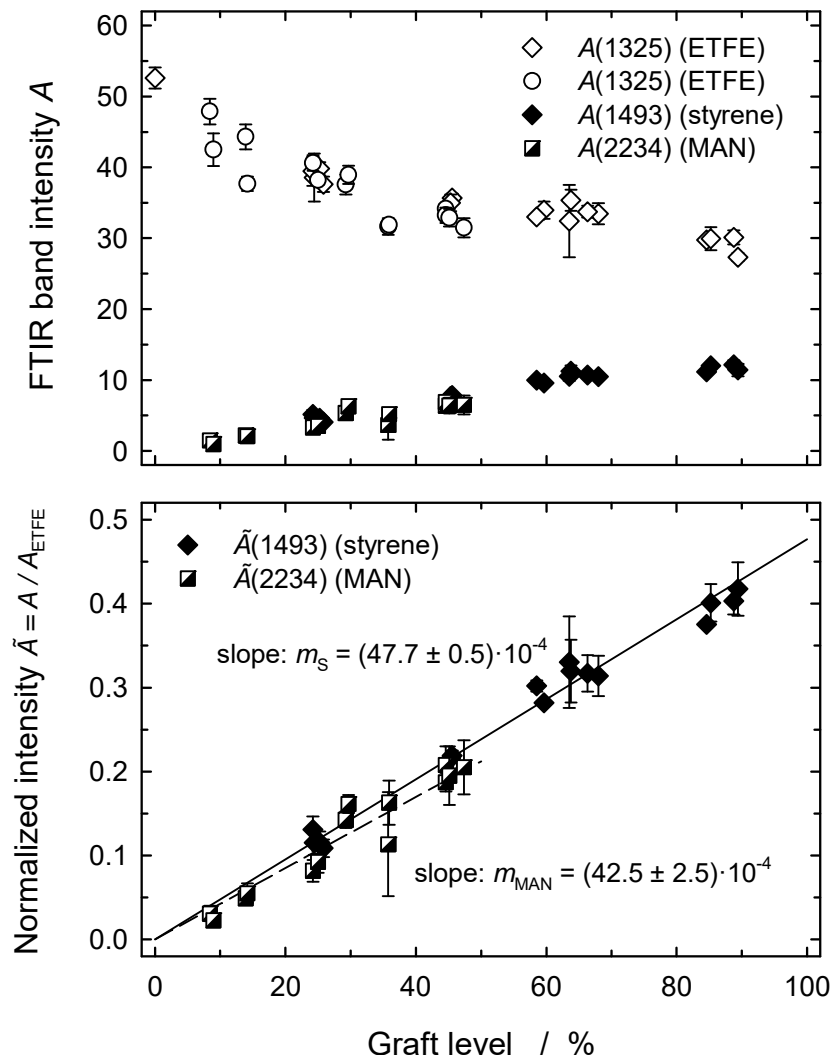
Figure 2-2. Above: intensity of vibrational bands assigned to the base film and co-grafted monomers. As illustrated in Figure 2-1 the expansion of the film upon grafting leads to a dilution of the base polymer, which causes a decrease in vibrational band intensity for ETFE. Below: normalization of the intensity of vibrational bands assigned to the graft component A to the intensity of a base film relevant vibrational band A_{ETFE} yields a linear relationship between the normalized intensity $\tilde{A}$ and the graft level.

component B leads to a dilution of the base polymer and graft component A by the same factor, thus the normalized intensity $\tilde{A}_A$ remains the same. The same holds for $\tilde{A}_B$.

The calibration method was validated using a series of styrene : MAN co-grafted films of different graft level. The partial graft levels of styrene and MAN were calculated from the normalized intensities of the vibrational bands, $\tilde{A}_S$ and $\tilde{A}_{MAN}$, and calibration factors, m_S and m_{MAN}. The combined graft level $Y = Y_S + Y_{MAN}$ showed reasonably good agreement with the experimentally determined graft level Y_{exp} (**Table 2-3**).

2.2 Determining Reactivity Ratios

The FTIR method outlined in the previous section allows the determination of the partial graft levels of the different graft components and, therefore, the compositional analysis of the grafts. This can serve as a basis for the estimation of the reactivity ratios for the two monomers, such as styrene, r_S, and MAN, r_{MAN} (cf. Chapter III). An example for a series of S:MAN co-grafted samples prepared with different ratios of styrene and MAN in the reaction mixture is shown in **Figure 2-11**. With today's office computer power, reactivity ratios can be determined in straightforward manner within seconds via non-linear least squares (NLLS) fitting using an appropriate software package (e.g. Origin). It was already shown in the 1960s that this approach is superior to the long-used Finneman-Ross and Kelen-Tüdős linearization methods in that the error structure is not distorted [360, 361].
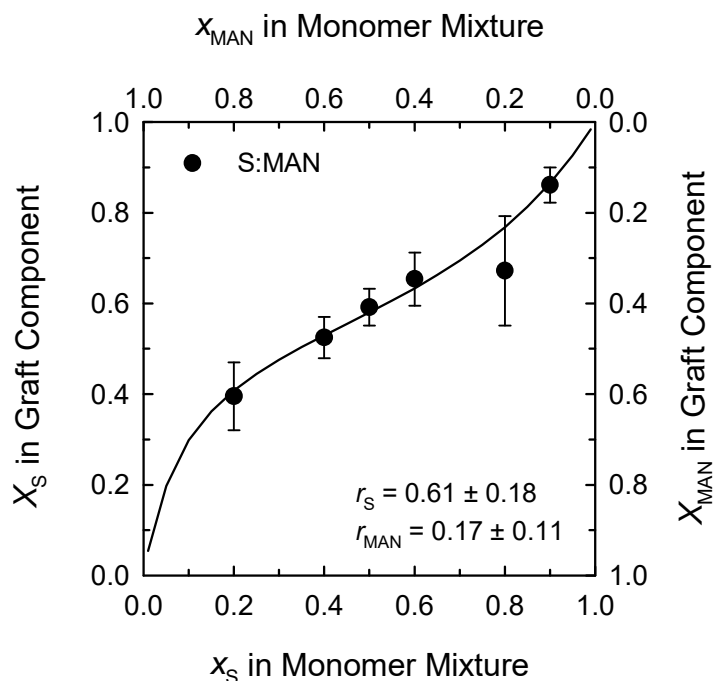

Figure 2-11. Copolymerization diagram for the co-grafting of S and MAN. x_S ($x_{MAN} = 1 - x_S$) and X_S ($X_{MAN} = 1 - X_S$) are the molar fraction of styrene (MAN) in the monomer feed and the grafted copolymer, respectively. Films with a graft level of approximately 40 % were selected. Reactivity ratios r_S and r_{MAN} are determined from the weighted non-linear least squares (NLLS) fit of the copolymerization equation (cf. Chapter III).

The algorithm finds the best-fit values of r_S and r_{MAN} corresponding to the minimum in the sum of squares of residuals, $S(r_S, r_{MAN})$, space [362]:

$$S(r_S, r_{MAN}) \quad = \quad \sum_{i=1}^{n} \left(\frac{F_i - F(f_i, r_S, r_{MAN})}{\Delta F_i} \right)^2 \tag{2-15}$$

where $F(f_i, r_S, r_{MAN})$ is the copolymer equation (Chapter III, Eq. 3-10), which relates the composition of the feed mixture f_i (dependent variable) to the composition of the grafts F (dependent variable) and ΔF_i is the error of F_i. F and f are the molar ratios of styrene and MAN in the copolymer ($F = X_S / X_{MAN}$) and feed ($f = x_S / x_{MAN}$), respectively. A typical NLLS fitting routing yields the best-fit values of the reactivity ratios and a corresponding estimate of uncertainty, typically the standard deviation. When the estimated parameters are correlated, i.e., not independent of each other, the standard deviations of the individual parameters give an incomplete account of the reliability of the estimates. In this case, the covariance of the two parameters is non-zero. The confidence interval of the parameters can then be visualized in the diagram of the parameter space by drawing the error ellipse corresponding to a given confidence level (**Figure 2-12**). The standard error ellipse corresponds to a confidence level of 39 % [363]. A non-zero covariance leads to a tilted error ellipse, which indicates that the parameters show some degree of correlation. The standard deviations of the two parameters correspond to the bounding rectangle of the standard error ellipse. Strictly speaking, the error ellipse is merely an estimate of the joint confidence region based on the approximation of a parabolic shape of the sum of squares function $S(r_S, r_{MAN})$ around its minimum. Since the relationship between the dependent variable F and independent variable f is nonlinear, the true, unbiased joint confidence region is given by contours of the $S(r_S, r_{MAN})$ function, which does not necessarily yield an elliptic shape (**Figure 2-12**). In the example reported here, however, the unbiased joint confidence region is fairly well-approximated by the error ellipse.
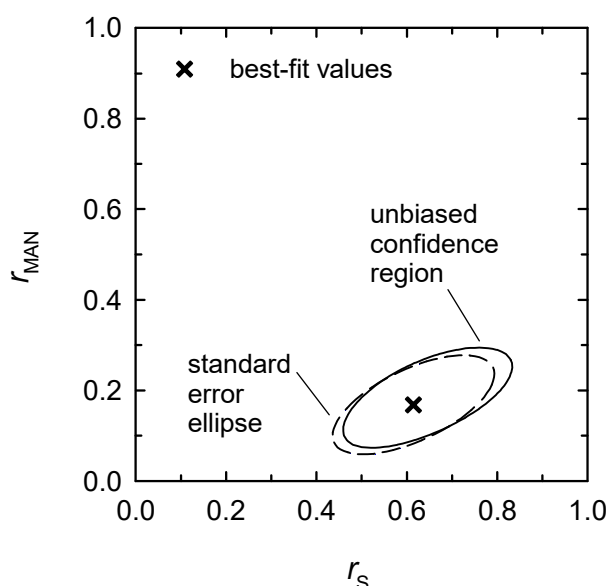
Figure 2-12.   Least-squares estimates of the reactivity ratios of styrene and MAN, obtained from the data in **Figure 2-11**, and 39 % confidence limits based on the contour of the sum of squares space $S(r_S, r_{MAN})$ (solid line), and corresponding estimate (standard error ellipse) obtained from the covariance matrix.

These considerations show that for a rigorous statistical analysis, the covariance needs to be taken into account to estimate the uncertainty of the reactivity ratios, also the unbiased joint confidence region may be useful to judge the validity of the simplified analysis. For an estimate of the reactivity ratios to obtain a ballpark number it is considered sufficient in the framework of the studies reported in this thesis (cf. Chapter III) to simply use the standard deviations to quantify the uncertainty of the obtained best-fit values.

2.3 Degradation Analysis

The quantitative FTIR spectroscopic analysis of the sample composition can also be used to calculate the extent of degradation of a membrane caused by an *ex situ* or *in situ* test protocol. In the same way that the content of a graft component can be determined based on the normalized intensity of a suitable vibrational band, the loss thereof can be calculated. The degree of degradation *D* of the graft component can thus be obtained according to

$$D \quad = \quad 1 - \frac{\widetilde{A}_g}{\widetilde{A}_g^0} \tag{2-16}$$

where $\tilde{A}_g$ and $\tilde{A}^0_g$ are the normalized intensities of the FTIR band in the tested and pristine membrane, respectively. To obtain the extent of degradation of the grafted chain, a vibrational band has to be chosen that constitutes an integral part of the graft component, such as the aromatic unit of styrene sulfonic acid (SSA). Since the degradation of SSA yields mainly fragments of aromatic units with attached sulfonic acid group [269], also vibrational bands associated with the sulfonic acid can be used to quantify the degradation of the graft component. For a series of controlled accelerated degradation experiments at different temperatures using model radiation grafted membranes, a good correlation between the loss of IR intensity of the sulfonic acid and the IEC was found (**Figure 2-13**).

In the event that a constituent of the grafted polymer chain undergoes a reaction that does not lead to chain scission, an analysis of the fate of that group of functionality may be possible depending on the availability of suitable IR vibrational bands to analyze. This is, for instance, a situation one encounters when a comonomer is undergoing hydrolysis, such as in the case of co-grafted acrylonitrile (AN) or methacrylonitrile (MAN) (cf. Chapter III). Hydrolysis of the nitrile units leads to a decrease in the intensity of the C≡N vibrational band around 2'235 cm^{-1} and an increase in intensity around 1'700 cm^{-1}, indicative of the C=O stretch vibration, owing to the formation of amide and carboxylic acid groups [260]. In comparing IR spectra of the membrane before and

after artificial aging experiments, be it *in situ* or *ex situ*, an assessment of the fate of the grafted monomer units with a nitrile group is possible [261]. For that, the normalized intensity of the C≡N vibrational band around 2'235 cm^{-1} is assessed before ($\tilde{A}^0_{CN}$) and after ($\tilde{A}_{CN}$) the test. The loss of nitrile groups can then be calculated as for SSA units via Eq. 2-15, which however does not necessarily mean that the corresponding comonomer units are lost due to chain scission. The nitrile can be lost to chain degradation *or* hydrolysis (**Figure 2-14**).
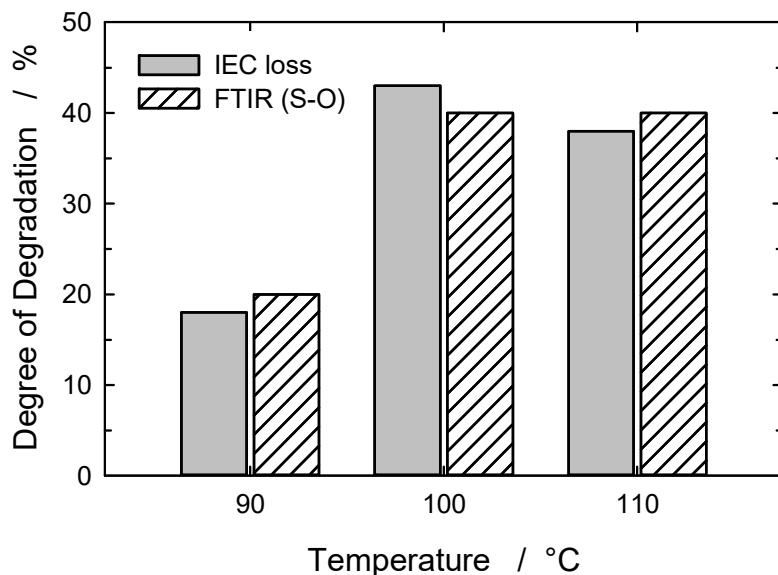
Figure 2-13. Degree of degradation of the PSSA graft component after OCV hold tests at different temperatures of ETFE (25 μm) based pure styrene grafted membranes with graft level of ~25 %, calculated based on the change of the intensity of the IR absorption band at 831 cm^{-1} (S-O stretch vibration) and IEC data [364].
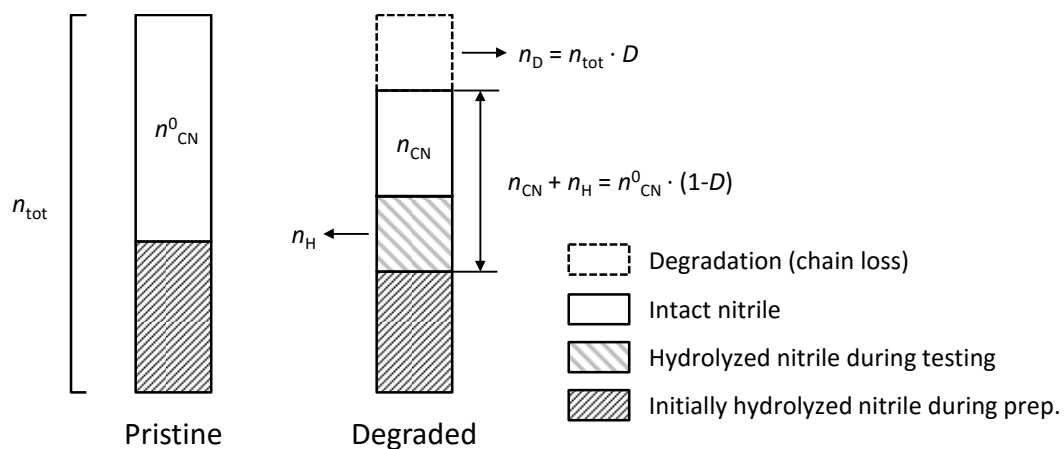
Figure 2-14. Illustration of the fate of nitrile units of (co-)grafted acrylonitrile (AN) or methacrylonitrile (MAN) due to degradation in the fuel cell or in an *ex situ* test. Initially n_{tot} comonomer units are grafted, of which only n^0_{CN} remain after sulfonation, because the balance is already hydrolyzed during the sulfonation procedure. In the degraded membrane, some of the nitrile units are lost due to chain degradation (n_D), and some underwent hydrolysis during the test (n_H). Of the remaining comonomer units, only a fraction of the nitrile stays intact (n_{CN}).

Based on the known extent of chain degradation D, for instance through analysis of vibrational bands associated with the SSA units, and the intensity ratio of the C≡N vibration before and after the test ($\tilde{A}^0_{CN} / \tilde{A}^0_{CN}$), the fraction of hydrolyzed units H, caused by the test, of the initially present nitrile groups (n^0_{CN}) can be calculated:

$$H \;=\; \frac{n_H}{n_H + n_{CN}} = 1 - \frac{n_{CN}}{n_H + n_{CN}} = 1 - \frac{n_{CN}}{n^0_{CN} \cdot (1-D)} = 1 - \frac{\tilde{A}_{CN}}{\tilde{A}^0_{CN}} \cdot \frac{1}{1-D} \qquad (2\text{-}17)$$

It may also be that a fraction of the nitrile $H_0 = 1 - n^0_{CN} / n_{tot}$ already underwent hydrolysis during membrane preparation, typically during the sulfonation procedure. H_0 cannot be determined from FTIR analysis of the membrane alone, and other approaches need to be invoked, such as elemental analysis or estimation on the basis of IR spectral analysis of grafted films and membranes using calibration standards [317]. The fate of the grafted nitrile in the comonomer units can thus be calculated (**Table 2-4**): nitrile units may have undergone hydrolysis already during the sulfonation procedure, $X(H_i)$, or during the test procedure, $X(H_t)$. The fraction of nitrile lost to chain degradation, $X(D)$, is equal to the fraction of lost SSA units, since the loss of the comonomer units is proportionate [261]. Finally, there is the fraction of intact nitrile units, $X(CN)$, unharmed by degradation or hydrolysis.

Table 2-4. Calculation of the fate of nitrile comonomer units, expressed as molar fraction X of the initially grafted nitrile, in co-grafted membranes that underwent degradation.

Fraction of nitrile groups	Calculation	Equation
Intact	$X(CN) \;=\; \dfrac{\tilde{A}_{CN}}{\tilde{A}^0_{CN}} \cdot (1-H_0)$	2-18
Lost due to chain degradation	$X(D) \;=\; \dfrac{n_D}{n_{tot}} = D$	2-19
Hydrolyzed during test	$X(H_t) \;=\; \dfrac{\tilde{A}_{CN}}{\tilde{A}^0_{CN}} \cdot \dfrac{H}{1-H} \cdot (1-H_0)$	2-20
Remaining initially hydrolysed	$X(H_i) \;=\; H_0 \cdot (1-D)$	2-21

3 Pulse Radiolysis

Pulse radiolysis experiments were performed at room temperature with a 2 MeV Febetron 705 accelerator (**Figure 2-15**) manufactured by Titan Systems Corporation, presently L-3 Communications (San Leandro, CA), which produces 50 ns electron pulses [365]. Upon irradiation of an aqueous sample solution with a high energy electron beam, these primary electrons loose their kinetic energy primarily through Coulombic interactions with the solvent molecules. As a result, excitation and ionization of the water molecules takes place until primary and secondary electrons are thermalized, a process that takes place within 10 fs (10^{-14} s) in water. Pulse radiolysis of water results in the formation of primary species according to

$$H_2O \quad \rightarrow \quad HO^\bullet, H^\bullet, e_{aq}^-, H_3O^+, HO^-, H_2, H_2O_2 \qquad \qquad (2\text{-}22)$$

Most of the excited and ionized species remain in close vicinity to the trajectory of the fast electrons, thereby forming so-called spurs with a typical diameter of 20 Å. Diffusion of species out of the spurs finally results in the homogeneous distribution of radicals and molecular products [366].

Figure 2-15.   2 MeV Febetron 705 accelerator at ETH Zürich, with detection equipment.

The absorbed dose D, which is expressed in Gy (Gray)[1], represents the energy effectively absorbed by the sample system, while the radiation chemical yield G indicates the number of events of a given kind per 100 eV of absorbed dose. For reactions, $G = 1$ corresponds to

---

[1] 1 Gy (Gray) = 1 J / kg energy deposition by the radiation

0.1036 µmol generated or changed species per 1 J absorbed energy. $HO^{\bullet}$, e_{aq}^{-} and $H^{\bullet}$ are formed with known yields $G(HO^{\bullet})$, $G(e_{aq}^{-})$ and $G(H^{\bullet})$ of 2.75, 2.65 and 0.55, respectively [367, 368], which allows to calculate their concentration, knowing the dose D and the density of the medium (~1 kg/dm^3 for dilute aqueous solutions). The Febetron can deliver doses of 2-20 Gy per pulse. The effectively absorbed energy by the sample solution was quantified by thiocyanate dosimetry [369].

Detection of intermediates was carried out by optical absorption measurements in the UV/Vis region of the spectrum, using a 75 W Xe arc lamp as light source, which was passed through a 1 cm quartz irradiation-cell containing the sample solution. The transmitted light was passed through a monochromator onto a photomultiplier and amplifier. The final signal was recorded with a digital storage oscilloscope.

In many of the experiments, the yield of hydroxyl radicals was increased by converting the hydrated electrons to additional $HO^{\bullet}$ in N_2O saturated solution:

$$N_2O + e_{aq}^{-} + H_2O \quad \rightarrow \quad N_2 + HO^{\bullet} + HO^{-} \tag{2-23}$$

This reaction has a rate constant of $9.1 \cdot 10^9$ M^{-1}·s^{-1} [370]. Thus, $G_{N2O}(HO^{\bullet}) = 5.4$. The radiation chemical yield of a compound formed upon the reaction with $HO^{\bullet}$ radicals from an N_2O-saturated solution depends on the substrate concentration [S] and the rate constant k_S for the reaction of $HO^{\bullet}$ with that substrate, where the track recombination frequency $\lambda = 4.7 \cdot 10^8$ M^{-1}·s^{-1} [371]:

$$G^{N_2O}(HO^{\bullet} - product) \quad = \quad 5.2 + 3.0 \cdot \frac{\sqrt{k_S \cdot [S]/\lambda}}{1 + \sqrt{k_S \cdot [S]/\lambda}} \tag{2-24}$$

$H^{\bullet}$ reacts with O_2 to yield $HOO^{\bullet}$, which has a pK_a of 4.8 [372], with $k = 1.2 \cdot 10^{10}$ M^{-1}·s^{-1} [370]. As $G(H^{\bullet})$ is about one tenth of $G_{N2O}(HO^{\bullet})$, the $O_2^{\bullet-}$ formed around neutral pH is at an equally low level. Furthermore, in the presence of O_2, e_{aq}^{-} also reacts with O_2 to give $O_2^{\bullet-}$ with $k = 1.9 \cdot 10^{10}$ M^{-1}·s^{-1} [370] at the expense of the reaction with N_2O (Reaction 2-23). Therefore, to minimize $O_2^{\bullet-}$ formation in solutions saturated with N_2O/O_2 mixtures, [O_2] was kept below 400 µM.

Formation of $O_2^{\bullet-}$ was followed by measuring the absorbance of the trinitromethanide anion, $k = 2 \cdot 10^9$ M^{-1}·s^{-1} [372], in solutions that contained 0.5-$1 \cdot 10^{-4}$ M tetranitromethane and 0.1 mM phosphate buffer:

$$O_2^{\bullet-} + C(NO_2)_4 \quad \rightarrow \quad O_2 + C(NO_2)_3^- + NO_2^{\bullet} \tag{2-25}$$
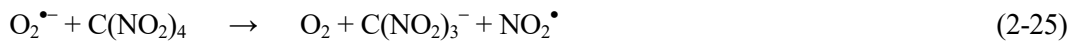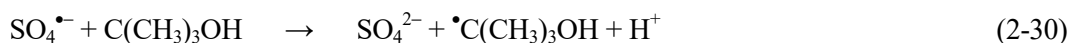
The formation of the trinitromethanide anion was followed at 350 nm or 360 nm to avoid spectral interference with the HO-adduct.

At low pH, hydrated electrons react with protons to yield additional hydrogen radicals with $k = 2.3 \cdot 10^{10}$ M^{-1}·s^{-1} [373]:

$$e_{aq}^- + H^+ \quad \rightarrow \quad H^{\bullet} \tag{2-26}$$

In Ar-saturated solutions that contain $S_2O_8^{2-}$, hydrated electrons are converted to $SO_4^{\bullet-}$, $k = 1.2 \cdot 10^{10}$ M^{-1}s^{-1} [370] (Reaction 2-27). The principal reactions in such a solution in the absence of a substrate, with t-butanol as HO$^{\bullet}$-scavenger, are Reactions 2-28 to 2-31, with respective rate constants $k = 1.4 \cdot 10^7$ M^{-1}s^{-1} [374], $6 \cdot 10^8$ M^{-1}s^{-1} [370], $8.4 \cdot 10^5$ M^{-1}s^{-1} [375] and $6.1 \cdot 10^5$ M^{-1}s^{-1} [376]. Experimentally, a yield $G(SO_4^{\bullet-})$ of (4.0 ± 0.2) in irradiated argon-saturated 0.05 M $K_2S_2O_8$ solutions at pH 2.4 with doses of 10 to 70 Gy was determined [377].

$$e_{aq}^- + S_2O_8^{2-} \quad \rightarrow \quad SO_4^{\bullet-} + SO_4^{2-} \tag{2-27}$$

$$H^{\bullet} + S_2O_8^{2-} \quad \rightarrow \quad SO_4^{\bullet-} + SO_4^{2-} + H^+ \tag{2-28}$$

$$HO^{\bullet} + C(CH_3)_3OH \quad \rightarrow \quad H_2O + {}^{\bullet}CH_2C(CH_3)_2OH \tag{2-29}$$

$$SO_4^{\bullet-} + C(CH_3)_3OH \quad \rightarrow \quad SO_4^{2-} + {}^{\bullet}C(CH_3)_3OH + H^+ \tag{2-30}$$

$$SO_4^{\bullet-} + S_2O_8^{2-} \quad \rightarrow \quad S_2O_8^{\bullet-} + SO_4^{2-} \tag{2-31}$$

Chapter III

Multi-Monomer Grafted Membranes

1 Introduction

Ion exchange membranes based on sulfonated polystyrene were among the early classes of polymer electrolytes used in fuel cell application (cf. Introduction). It was realized early on that the stability of these materials under the operating condition of a fuel cell, although sufficient for a space mission for a few days, was limited to a few hundred hours. The majority of proton exchange membranes prepared by radiation grafting are based on post-sulfonated polystyrene embedded in a fluoropolymer matrix [65, 378]. Therefore, the chemical stability of the obtained membranes has always been a concern and a large share of the studies reported has been on approaches to improve the oxidative stability of poly(styrene sulfonic acid) (PSSA) based membranes.

The reasons of the poor oxidative stability of PSSA have been put forward already in the 1960s based on the work performed in the GE laboratories [9]. It was suspected that the degradation of PSSA involved the attack by HO•, followed by chain scission owing to the weakness of the benzylic α-hydrogen (**Figure 3-1**). This mechanism was corroborated by later studies, notably by Hübner and Roduner [315].
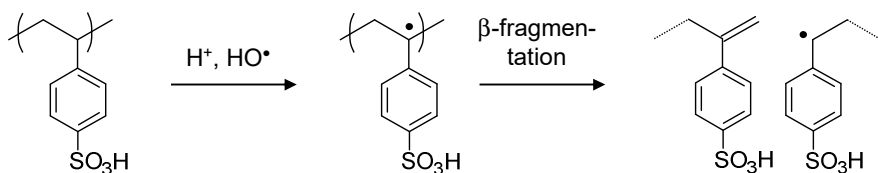
Figure 3-1. Simplified representation of the radical-induced degradation mechanism of poly(styrene sulfonic acid) (PSSA), involving loss of the weak α-H and formation of a benzyl radical.

In the early work at GE, the ion exchange resins and membranes prepared for the Gemini space missions contained, in addition to styrene, a crosslinker, divinylbenzene (DVB), to prevent dissolution of the resin and enable the formation of a crosslinked network of Aclar, a copolymer of vinylidene fluoride (VDF) and chlorotrifluoroethylene (CTFE), and polyelectrolyte. Crosslinking actually improves the chemical stability of PSSA against oxidative degradation. Therefore, it is the primary approach to improve the stability of PSSA based radiation grafted membranes and was therefore implemented already in early studies [186]. The improvement in membrane stability with a crosslinked graft copolymer over an uncrosslinked membrane is dramatic: in direct comparison under identical operating conditions, a styrene grafted and sulfonated membrane based on FEP base film (25 μm thickness) with a graft level of 18 % had a lifetime in the fuel cell of only about 50 h, whereas a comparable membrane prepared with 10 % DVB monomer in the grafting solution exhibited a lifetime of over 4'000 h [195]. The improved

stability is a combined result of different phenomena. Firstly, the lower water uptake of the cross-linked membrane reduces the diffusion of radical species formed at the catalyst into the bulk of the membrane. Secondly, owing to the lower gas crossover rate in cross-linked membranes, fewer radical species are expected to be formed at the catalyst in the first place. Last but not least, the polymer network formed through crosslinking is more robust against loss of chain segments following bond scission, owing to the multiple connectivity of polymer chains [197]. However, crosslinking inevitably entails a loss in conductivity of the membrane because of the reduced water uptake. Therefore, it is reasonable to identify further approaches to improve the oxidative stability of the styrenic graft component.
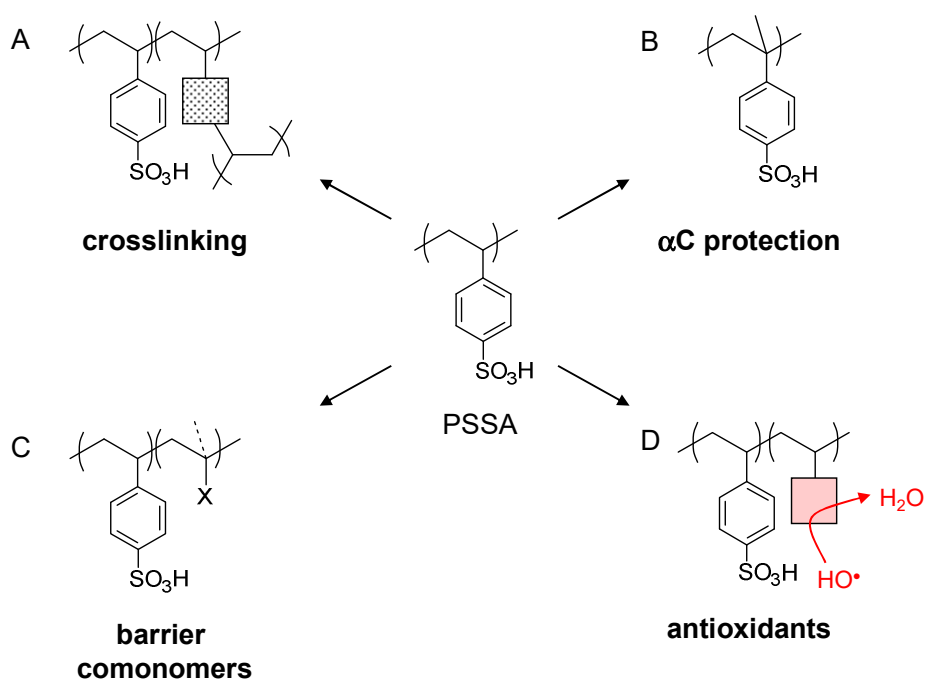
Figure 3-2. Synthetic approaches to improve the chemical stability of styrene based radiation grafted fuel cell membranes.

The options identified at the Electrochemistry Laboratory at PSI to improve the chemical stability of styrenic radiation grafted membranes are outlined in **Figure 3-2**. The effect of crosslinking, highlighted above, has been summarized in in recent book chapters [196, 197]. Option B consists of replacing styrene with an intrinsically more stable styrene derivative. Since it has been recognized that the weak αC-H bond (348 kJ·mol^{-1} [379]) is the reason for the poor oxidative stability of PSSA, it appears reasonable to substitute the hydrogen at this position. One approach is the use of α,β,β- trifluorostyrene (TFS) [57], which had already been used in the 1960s to prepare homopolymers with higher stability than SSA [13]. Yet besides the rather moderate polymerization kinetics of TFS and the difficult sulfonation process of the resulting polymer, an

evident drawback of TFS is its high cost. A straightworward approach appears to be to use α-methylstyrene (AMS) [251]. This monomer, however, shows poor radical polymerization kinetics (cf. Section 1.1 below), and it needs to be copolymerized with a suitable comonomer to obtain practical graft levels. The (co)polymerization of AMS will be discussed in the following sub-section and Section 2 of this chapter. Option C addresses one of the root causes of chemical degradation, the interdiffusion of H_2 and O_2 across the membrane and subsequent formation of reactive intermediates, for example $HO^•$, which attacks the polymer and causes membrane degradation. The incorporation of suitable comonomers that improve the gas barrier properties of radiation grafted membranes can reduce the crossover of the reactants, which leads to a lower rate of radical formation. For instance, polyvinyl alcohol (PVA) is a polymer with excellent oxygen barrier properties [318]. It is obtained from polyvinyl acetate (PVAc) through hydrolysis. In principle, VAc could be co-grafted with styrene, followed by sulfonation and hydrolysis. Unfortunately, the copolymerization behavior of styrene and VAc is unsuitable ($r_S = 55$, $r_{VAc} = 0.01$). Therefore, other, more suitable comonomers have to be found. Although the "weak link" in the sulfonated styrene units is still the same, the lower concentration of radicals effectively reduces the degradation of the graft component. This approach will be discussed in detail in Section 3, using nitrile comonomers. Option C is aimed at incorporating antioxidant functionalities into the graft component of the membrane. In technical polymers, lubricating oils, fats, etc., antioxidants are widely used to for protection against oxidative degradation [380]. Therefore it appears reasonable to develop antioxidant strategies for fuel cell membranes, knowing that under the prevailing conditions, the materials are constantly bombarded with various types of reactive intermediates [381]. The study of incorporating antioxidant functionality into the graft component of fuel cell membranes is discussed in Section 4.

1.1 Polymerization of α-Methylstyrene (AMS)

Unlike styrene, α-methylstyrene (AMS) does not undergo spontaneous polymerization upon heating [382]. In conventional polymerization reactions using free radical initiators, only low molecular weight poly(AMS) (PAMS) is obtained [383]. This is associated with the fact that the polymerization of AMS has a ceiling temperature of 60-65°C in bulk [252]. Consider the following polymerization reaction with forward reaction (propagation) and backward reaction (depolymerization) with respective rate constants k_p and k_d:

$$\sim M_n^• + M \quad \underset{k_p}{\overset{k_p}{\rightleftarrows}} \quad \sim M_{n+1}^• \qquad (3\text{-}1)$$

The ceiling temperature T_c represents the temperature above which the rate of depolymerization is greater than the rate of propagation. The existence of a ceiling temperature is a result of the thermodynamics of radical polymerization reactions. All addition polymerizations are exothermic ($\Delta H < 0$) and involve a decrease in entropy ($\Delta S < 0$) [384]. The system is in thermodynamic equilibrium if $\Delta G = 0 = \Delta H - T_c \cdot \Delta S$. Therefore,

$$T_c = \frac{\Delta H}{\Delta S} = \frac{\Delta H}{\Delta S^\circ - R \cdot \ln([M])} \tag{3-2}$$

Where ΔS° is the reaction entropy referred to a standard state of unit monomer concentration and [M] is the concentration of the monomer at the equilibrium with high molecular weight polymer. Although polymerization is thermodynamically favored below T_c, the rate of polymerization decreases when the temperature approaches T_c. For comparison, the polymerization of styrene has a ceiling temperature of 310°C [253]. The low ceiling temperature of PAMS is a result of the steric hindrance in the polymer, brought about by the presence of the aromatic ring and the methyl group at the α-carbon. This results in a much lower heat of polymerization compared to styrene. The dominant termination reaction in the polymerization of AMS is chain transfer to the monomer [254]. The chain transfer coefficient at 50 °C ($4.12 \cdot 10^{-3}$) is 80 times higher than that of styrene ($5.27 \cdot 10^{-5}$). Consequently, free radical polymerizations of AMS under conventional bulk or solution conditions give low conversions and low molecular weights.

There are, however, approaches to polymerize AMS, even to high molecular weights. Polymerization at low temperature, i.e. room temperature or even below 0°C, obviously favors the propagation reaction over the depropagation reaction. In addition, specific additives favor the formation of high molecular weight polymers, such as Friedel-Crafts catalysts [382], sodium [385], or surfactants [254]. Under such conditions, PAMS with moleculear weights of 60'000 to 80'000 g·mol^{-1} can be obtained.

In the context of radiation induced grafting, Assink et al. reported the preparation of electrolyte membranes for the zinc / ferricyanide battery based on PTFE grafted with styrene and AMS, respectively, followed by sulfonation [251]. Unfortunately, details of the membrane synthesis were not provided, it was merely mentioned that the membranes were prepared by RAI Research Corp. (Happauge, NY) via radiation grafting. It has been shown in the patent by Scherer et al. that AMS can indeed be radiation grafted [386]. FEP was used as substrate and the grafting reaction was carried out in 40% AMS in toluene at -20°C for 50 h to obtain a graft level of 19%.

Although AMS cannot be easily homopolymerized, it can be readily copolymerized by the radical mechanism with many suitable comonomers, such as styrene [387], maleic anhydride [388], acrylonitrile [389], methacrylonitrile [389], and methyl methacrylate [390]. Typically, the rate of polymerization decreases with the increase in the fraction of AMS in the binary monomer mixture, as shown, for instance, in the case of copolymerization with styrene [387]. In this concept, the comonomer serves as a polymerization promoter for AMS. Hence, it can be expected that a favorable combination of AMS with a comonomer can also be used for radiation induced graft copolymerization. The effective grafting of AMS is enabled by the presence of the comonomer.

1.2 Copolymeization

The first general mechanistic description of the copolymerization kinetics of two monomers was published by Alfrey and Goldfinger in 1944 [391], followed almost concurrently by Mayo and Lewis [392] and Wall [393]. In the case of "high" polymers, i.e., polymers with a large average degree of polymerization, the composition of the growing copolymer chain is determined by the propagation reactions, consisting of the four possibilities of chain growth, namely, addition of the two monomers to the two possible monomer units at the end of the growing chain. Alfrey and Goldfinger highlighted the dependence of the composition of the growing copolymer on the ratio of the monomers in the reaction mixture and their relative rates of propagation. Also, probabilities for the formation of the various diads and sequence lengths were calculated. Mayo and Lewis coined the today well-known term *monomer reactivity ratio* [392], which constitutes the ratio of the rate constant for the reaction of one type of radical with the corresponding monomer (*self-propagation*) and with the other monomer (*cross-propagation*). This mechanism of copolymerization, in which the chemical reactivity of the growing chain is dependent only on the type of the monomer unit at the chain end, is referred to as *first-order Markov* or *terminal model* of copolymerization [394]. Consider the two monomers, M_1 and M_2, the respective chain end units $\sim M_1^{\bullet}$ and $\sim M_2^{\bullet}$, and the associated four possible chain propagation reactions with rate constant k_{ij} ($i,j = 1,2$) for *self-propagation* reactions ($i = j$), with resulting chain end sequences $\sim M_1\text{-}M_1^{\bullet}$ or $\sim M_2\text{-}M_2^{\bullet}$, and *cross-propagation* reactions ($i \neq j$) with chain end sequences $\sim M_1\text{-}M_2^{\bullet}$ or $\sim M_2\text{-}M_1^{\bullet}$ [395]:

$$\sim M_1^{\bullet} + M_1 \xrightarrow{\;k_{11}\;} \sim M_1\text{--}M_1^{\bullet} \tag{3-3}$$

$$\sim M_1^{\bullet} + M_2 \xrightarrow{\;k_{12}\;} \sim M_1\text{--}M_2^{\bullet} \tag{3-4}$$

$$\sim M_2^{\bullet} + M_2 \xrightarrow{\;k_{22}\;} \sim M_2\text{--}M_2^{\bullet} \tag{3-5}$$

$$\sim M_2^{\bullet} + M_1 \xrightarrow{\;k_{21}\;} \sim M_2\text{--}M_1^{\bullet} \tag{3-6}$$

The ratio of the self- to the cross-propagation rate constant is defined as the *monomer reactivity ratio r*:

$$r_1 \quad = \quad \frac{k_{11}}{k_{12}} \tag{3-7}$$

$$r_2 \quad = \quad \frac{k_{22}}{k_{21}} \tag{3-8}$$

With $r > 1$, self-propagation is favored, for $r < 1$ cross-propagation. In general, the composition of the copolymer is different from the composition of the monomer feed solution, governed by the values of the reactivity ratios r_1 and r_2. Pairs of monomers in which the individual monomers show higher reactivity with chain ends featuring the respectively other monomer, which manifests in the form of both reactivity ratios being below unity, tend towards forming an alternating monomer sequence in the copolymer. The extent of alternation depends on the magnitude of the reactivity ratios and their product, $r_1 \cdot r_2$. For $r_1 \cdot r_2 \approx 0$ a perfectly alternating polymer is obtained. In **Figure 3-3** the composition of the instantaneously formed copolymer as a function of the composition of the monomer mixture is shown for three examples of reactivity ratio pairs. The case $r_1 = r_2 = 1$ represents ideal statistical copolymerization with no preference of self-propagation or cross-propagation. The composition of the copolymer is equal to the composition of the monomer mixture over the entire compositional range. In the general case $r_1 \neq 1$ and $r_2 \neq 1$ the composition of the copolymer will therefore be different from that of the monomer mixture. With $r_1 = 2$ and $r_2 = 0.1$, for example, monomer 1 is preferentially added over monomer 2 to the growing copolymer chain, regardless whether the chain end is an $M_1^\bullet$ or an $M_2^\bullet$ unit. Therefore, the copolymer will generally be rich in sequences of monomer 1, and the copolymer would have a low degree of monomer unit alternation. The case $r_1 = 0.10$ and $r_2 = 0.50$ shows some degree of alternation, in particular at high molar ratios of M_1 to M_2, because $r_1 < r_2$. If both reactivity ratios are significantly lower than 1, there is a strong tendency to form an alternating copolymer over a wide range of feed compositions, as exemplified by the example $r_1 = r_2 = 0.05$. The point where the curve intersects the diagonal indicates the azeotropic point. It represents a feed composition that yields a copolymer of identical composition [396]. On the other hand, there is no known case of a free-radical-propagated copolymerization for which both reactivity ratios are greater than unity. It is essential to point out that the reactivity ratios for a given binary monomer system may be a strong function of the type of polymerization reaction, i.e., radical, anionic, or cationic. In the case of styrene and methyl methacrylate (MMA), for instance, the radical polymerization is nearly ideally statistical, yet anionic polymerization yields a copolymer rich in MMA, whereas cationically grown polymers are rich in styrene [253].
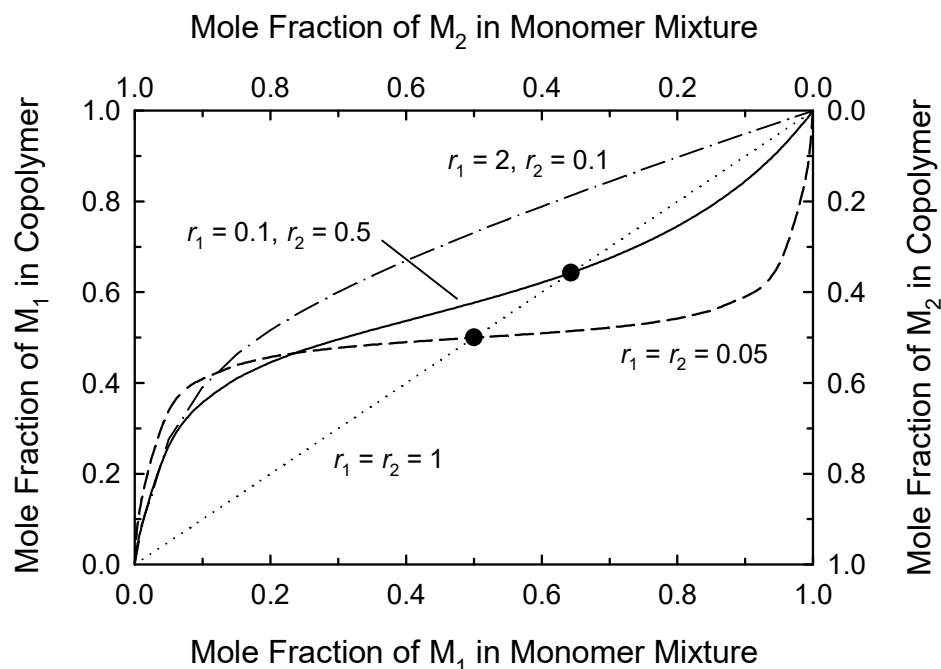
Figure 3-3. Variation of the composition of the instantaneously formed copolymer (vertical axis) with the composition of the monomer mixture (horizontal axis) for various pairs of monomer ratios r_1 and r_2. The filled circles represent azeotropic mixtures (cf. text).

The composition of the copolymer and other relevant copolymerization parameters can be calculated from the known composition of the monomer mixture and the reactivity ratios. In the steady state, the concentration of the chain end radicals $\sim M_1^\bullet$ and $\sim M_2^\bullet$ is constant, which leads to the condition

$$k_{21} \cdot [M_2^\bullet] \cdot [M_1] = k_{12} \cdot [M_1^\bullet] \cdot [M_2] \tag{3-9}$$

Based on the rate equations for the reaction of the two monomers M_1 and M_2 and the steady-state condition (Eq. 3-7), the composition of the growing copolymer chain can be calculated. The ratio of the monomer units being copolymerized is then given by:

$$\frac{d[M_1]}{d[M_2]} = \frac{1 + r_1 [M_1]/[M_2]}{1 + r_2 [M_2]/[M_1]} \tag{3-10}$$

This is known as the *copolymer equation*, also referred to as *Mayo-Lewis equation*, since it gives the composition of the copolymer being formed, at a given instant, as a function of the concentration of the two comonomers in the reaction mixture and their reactivity ratios [392]. We now introduce the variables x_1 and x_2 for the molar fraction of M_1 and M_2 in the reaction mixture, respectively:

$$x_1 = \frac{[M_1]}{[M_1]+[M_2]} \tag{3-11}$$

$$x_2 = \frac{[M_2]}{[M_1]+[M_2]} \tag{3-12}$$

where $x_1 + x_2 = 1$. In analogy, we define the molar fraction X_1 and X_2 of monomer units M_1 and M_2 entering the copolymer:

$$X_1 = \frac{d[M_1]}{d([M_1]+[M_2])} \tag{3-13}$$

$$X_2 = \frac{d[M_2]}{d([M_1]+[M_2])} \tag{3-14}$$

also with $X_1 + X_2 = 1$. In addition, the molar fraction of monomer units in the reaction mixture and the copolymer are formed:

$$f = \frac{x_1}{x_2} = \frac{x_1}{1-x_1} = \frac{[M_1]}{[M_2]} \tag{3-15}$$

$$F = \frac{X_1}{X_2} = \frac{X_1}{1-X_1} = \frac{d[M_1]}{d[M_2]} \tag{3-16}$$

With the definition of these variables, the copolymer equation can therefore be rewritten as follows:

$$F = \frac{1+r_1 \cdot f}{1+r_2 / f} \tag{3-17}$$

For the azeotropic reaction mixture the formed copolymer is of identical concentration as the monomer mixture, hence $F = f =: f_c$, which is given by

$$f_c = \frac{1-r_2}{1-r_1} \tag{3-18}$$

Considering a binary comonomer system in which the self-propagation of one of the comonomers is strongly hindered, such as in the case of AMS, and a suitable "promoting" comonomer is used,

one wishes to maximize the degree of alternation to minimize the content of the "promoting" comonomer having no functional task in the copolymer. The maximum degree of alternation is always reached at an equimolar copolymer composition, i.e., at $F = 1$ or $X_1 = X_2 = 0.5$. This composition is obtained, after insertion into Eq. 3-10, for a molar fraction of monomers f_a in the reaction mixture of:

$$f_a = \sqrt{\frac{r_2}{r_1}} \tag{3-19}$$

The fraction of alternating monomer sequences ~M_1–M_2~ and ~M_2–M_1~, and that of the diads ~M_1–M_1~ and ~M_2–M_2~ can be calculated based on the *run number* concept of Harwood and Ritchey [397], which is defined as the average number of uninterrupted monomer sequences (or "runs") in a copolymer chain per hundred monomer units. The run number R is predicted as follows [398]:

$$R = \frac{200}{2 + r_1 \cdot f + r_2 \cdot / f} \tag{3-20}$$

For an ideal random copolymer at equimolar composition R is 50, for a perfectly alternating copolymer R is 100. The fraction of diads in the copolymer is then obtained using following expressions:

$$\%(M_1 - M_1) = 100 \cdot X_1 - \frac{R}{2} \tag{3-21}$$

$$\%(M_2 - M_2) = 100 \cdot X_2 - \frac{R}{2} \tag{3-22}$$

$$\%(M_1 - M_2) + \%(M_2 - M_1) = R \tag{3-23}$$

The maximum fraction of alternating diads R_{max} is thus given by the number R at $f = f_a$, which is obtained by inserting Equation Equation 16 into Equation Equation 17:

$$R_{max} = \frac{100}{1 + \sqrt{r_1 \cdot r_2}} \tag{3-24}$$

This expression confirms the statement made earlier that the lower the reactivity ratios, the higher the degree of alternation of the copolymer.

1.3 Co-grafting

The design of polymers containing more than one type of monomer, obtained through copolymerization, has led to the creation of a plethora of new materials with improved properties, for instance acrylonitrile-butadiene-styrene (ABS), which is tougher than pure polystyrene. Another example, which is particularly important in the context of the studies reported in this monograph, is ethylene-tetrafluoroethylene (ETFE), which has a favorable combination of properties of the corresponding homopolymers, i.e., polyethylene (PE) and polytetrafluoroethylene (PTFE), such as chemical / thermal stability and radiation chemistry (cf. Chapter I). In addition, many technical polymers, although nominally homopolymers, contain a small amount of comonomer to improve specific properties, such as processability or stability [399]. It seems therefore reasonable to apply the concept to radiation grafted polymers to combine desirable properties of individual monomer constituents in the graft copolymer. The preparation of radiation co-grafted polymers has already been reported in the early 1960s. Odian et al. co-grafted styrene with different comonomers, i.e. methyl acrylate (MA), 4-vinylbenzene (4VP) and acrylonitrile (AN) [358, 359]. The copolymerization kinetics during co-grafting onto a polymer substrate (film, fabric) and composition of the formed copolymer need not be similar to the kinetics observed in solution copolymerization. Grafting is a combination of reaction and diffusion, hence in addition to polymerization and termination reactions, monomer solubility and partitioning between the solution and the polymer phase, as well as monomer and solvent transport into the base film can be influential phenomena. Furthermore, since the composition of the polymer undergoing grafting is constantly changing, these parameters are also expected to be affected by the degree of grafting. Odian reported differences in the composition of copolymerized grafts to the composition of the corresponding copolymer in solution. In the first study, LDPE film was swollen in mixtures of styrene and methyl acrylate (MA), 4-vinylpyridine (4VP) and acrylonitrile (AN) and exposed to gamma radiation for grafting [358]. In the second study, PTFE was used as a substrate, resulting merely in surface grafting [359]. In all instances, the composition of the grafts was richer in the polar monomer than predicted by the copolymer composition equation. The explanation put forward is a preferential solvation of the growing graft copolymer, the mobility of which is restricted by the polar monomers.

In more recent work, El-Naggar et al. have investigated the co-grafting of styrene (S) / acrylonitrile (AN) and styrene (S) / acrylamide (AAm) mixtures onto polyester fabrics and found that the reactivity ratios differed substantially compared to the values obtained in solution polymerization [400]. In particular, in case of the S / AAm binary mixture, the reactivity ratios were found to be almost reversed, with $r_S = 0.41$ / $r_{AAm} = 1.82$ for co-grafting, and $r_S = 1.65$ / $r_{AAm} = 0.32$ for solution copolymerization. In another co-grafting study using polyester and

cotton / polyester fabric as substrates, they found that the reactivity ratios for S / AN and S / AAm mixtures depend on the type of substrate used [401].

2 AMS-MAN Co-grafted Membranes

The aim of the topic described in this section is to graft AMS via copolymerization with a suitable comonomer into a fluoropolymer matrix. The comonomer should have a favorable copolymerization behavior with AMS, i.e., the two monomers should exhibit the tendency to form an alternating copolymer. At the same time, the comonomer should not excessively homo-graft. Furthermore, the comonomer should not be too "bulky" to prevent diffusion limitations during grafting on the one hand, and to avoid excessive dilution of the sulfonated AMS units in the final membrane on the other hand. Moreover, the comonomer unit should not represent a preferred locus of degradation under fuel cell operating conditions. Last but not least, the comonomer should be readily available and of low cost. Becker and Schmidt-Naake have reported the use of acrylonitrile (AN) as co-monomer of AMS in the graft copolymerization onto ETFE base film (50 µm thickness) [191]. An irradiation dose (e-beam) of 150 kGy was used. Grafting was performed at 60°C in bulk monomer, i.e., without the addition of solvent. Unfortunately, the ratio of the two monomers in the grafting solution was not given. The molar fraction of AMS in the grafts was found to increase with the graft level and approach a molar ratio of AMS:AN close to 1:1. This was explained with an initially higher rate of grafting of AN due to its faster diffusion compared to AMS. AN tends towards alternating copolymerization with AMS and greatly improves the effective rate of AMS polymerization [389]. *Ex situ* analysis of chemical stability in H_2O_2 solution containing ppm-level Fe(II) (Fenton's reagent) showed a lower degradation rate of the AMS:AN co-grafted membrane compared to a styrene-only grafted membrane [256, 257]. Unfortunately, no fuel cell tests have been reported to validate the concept. Also, the co-grafting kinetics of AMS and AN have not been established.

In the study reported here, the approach of using methacrylonitrile (MAN) as co-monomer of AMS is adopted. Preparation of such membranes via radiation grafting for application in the PEFC is a novel approach [259]. MAN offers potentially higher chemical stability because of the methyl-protected α-position. The monomer system AMS:MAN was found to exhibit the tendency towards alternation when copolymerized in solution [389]. The sequence distribution in AMS:MAN copolymers, prepared via emulsion copolymerization, was investigated by Kenney and Patel [402, 403]. They found that the copolymer, prepared at a temperature of 60 °C, has a high tendency to alternate. In view of the preparation steps involved to obtain proton exchange

membranes, it is important to note that unwanted side reactions of MAN in the further preparation steps, such as hydrolysis, is not observed [258].
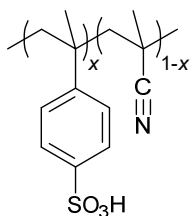
Figure 3-4. Molecular structure of an α-methylstyrene (AMS) and methacrylonitrile (MAN) co-grafted and sulfonated polymer. *x* and 1-*x* indicate the molar fraction of AMS and MAN in the grafts, respectively.

In the study reviewed here, the preparation and characterization of radiation grafted membranes using AMS and MAN as grafting monomers are investigated in detail (**Figure 3-4**). FEP film with a thickness of 25 μm was used as base polymer. In selected samples, the polymer structure was crosslinked by including a third, crosslinking monomer, divinylbenzene (DVB) or diisopropenylbenzene (DIPB), into the grafting solution. In case of DVB, the grafting solution contained a molar fraction of 1.7 % with respect to the total monomer content (AMS+MAN+DVB), in case of DIPB, the concentration in the grafting solution was slightly higher (3.3 %). The fuel cell durability is greatly enhanced for crosslinked radiation grafted membranes [404]. In addition to the analysis of the grafting kinetics, determination of composition and membrane properties, fuel cell performance and durability tests, including *post mortem* analysis, are reported.

2.1 Membrane Synthesis

Poly(tetrafluoroethylene-*co*-hexafluoropropylene) (FEP) film with a thickness of 25 μm (Teflon® FEP 100A, DuPont) was used as base polymer in this study. Films of appropriate size were washed in ethanol (technical grade), dried in vacuum at 80 °C and placed in polyethylene zip-lock bags. Irradiation of the films was carried out at Leoni Studer AG (Däniken, Switzerland), using an MeV class electron-beam, to a dose of 25 kGy. The residence time of the film in the accelerator was of the order of a few seconds. The irradiated films were stored in dry ice during transit to the laboratory, there stored at -80 °C until used. Irradiated films were loaded into glass tube reactors, subsequently 60 ml of the grafting solution were added. In order to remove oxygen, reactors were purged with nitrogen for 1 h. The reactors were subsequently sealed and placed in a heated water bath at 50 or 60 °C. After elapsing of the reaction time, the grafted film was removed, washed in acetone and dried in the vacuum oven at 80 °C for 3 h. The consumption of monomers during grafting was determined to be below 5 %. Changes in grafting solution concentration are therefore

neglected. Grafted films were sulfonated to convert them into a proton conducting membrane. Six films were sulfonated simultaneously in a mixture of 30 ml chlorosulfonic acid and 650 ml dichloromethane at room temperature for 6 h. The membranes were then removed, washed in water and immersed in a 0.4 % aqueous solution of sodium hydroxide for 6 h for hydrolysis of the sulfonyl chloride. Exchange of sodium with protons was carried out by immersion in 2 M sulfuric acid for 6 h. Final stage in membrane preparation was rinsing and treatment in water at 80 °C for at least 6 h. Water was replaced until the pH was above a value of 6.

2.2 Co-grafting of AMS and MAN

A set of grafting experiments with varying AMS : MAN feed ratio was carried out with a reaction time of 65 h. The grafting reaction can be carried out in undiluted mixtures of AMS and MAN. It is, however, preferable to use diluted monomer mixtures, on the one hand to improve monomer utilization and, on the other hand, because favorable solvent effects may be exploited. For the grafting reaction of mixtures of styrene and divinylbenzene (DVB) (crosslinker) onto FEP base film, it was found that the use of polar solvents, such as methanol, isopropanol or acetic acid, which are poor solvents for styrene and DVB, enhances the grafting kinetics substantially compared to good solvents (toluene, cyclohexane) [190]. For the series of grafting experiments as a function of the ratio of AMS and MAN reported here, neat isopropanol and a mixture of isopropanol and water were used as solvent, respectively, with a monomer concentration of 30 % (v/v) in the grafting solution. The graft level was found to generally decrease with increasing AMS content of the feed solution (**Figure 3-5**). This is a consequence of decreasing polymerization rate and increasing number of chain transfer events, and at the limit of $x_{AMS} = 1$, negligible grafting is observed, in accordance with the failure of AMS to polymerize by the radical mechanism at this temperature [402]. The difference in graft level obtained with and without water in the grafting solution at low ($x_{AMS} < 0.4$) and very high ($x_{AMS} > 0.8$) AMS feed contents is striking, whereas the graft level appears to be insensitive to the addition of water at $x_{AMS} \approx 0.6$. At low AMS contents and in the absence of water, the effective concentration of monomers in the polymer phase may be lower, thereby limiting the graft level. On the other hand, whereas the grafted chains are insolubilized in the presence of water, owing to the incompatibility of the polar solvent with the polymer, swelling of the polymer by the solvent may be higher in the absence of water, increasing thereby the mobility of the growing polymer chains, which leads to shorter radical lifetimes. At a high AMS feed ratio ($x_{AMS} > 0.8$) the grafting solvent is increasingly non-polar. Hence, the addition of water results in a shift of the partitioning equilibrium between the liquid and polymer phase, because it acts as a precipitant, which leads to an increase of the effective monomer concentration in the polymer [190].
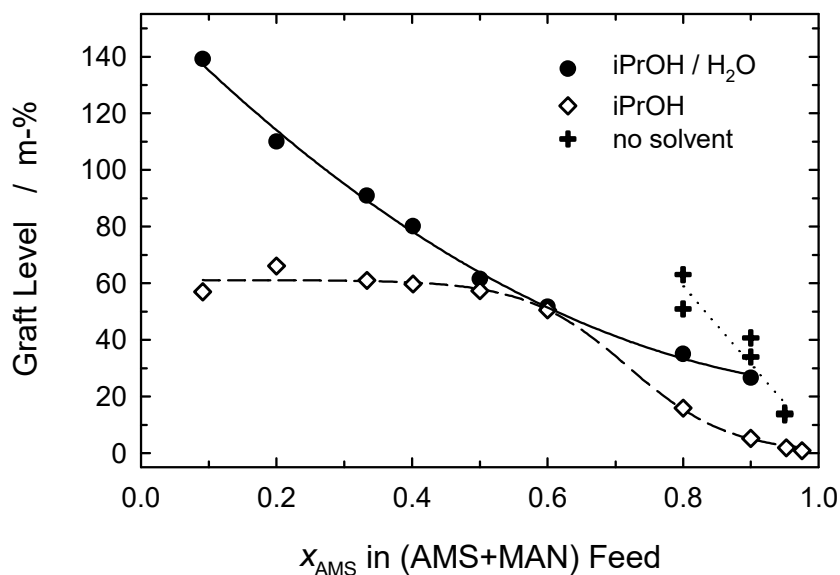
Figure 3-5. Graft level obtained in AMS-MAN co-grafted films at various comonomer ratios. Temperature: 50 °C; grafting time: 65 h; monomer concentration in diluted feeds ($\lozenge$ / $\bullet$): 30 v-%; isopropanol / water ratio for ($\bullet$): 5:2 v/v. Lines are guides to the eye.

Table 3-1. Determination of the composition of grafts in 25 μm FEP co-grafted films.

x_{AMS} feed	Graft level (m-%)	X_{AMS} copolymer [a]	X_{AMS} copolymer [b]
0.50	20.8	0.364 ± 0.029	0.329 ± 0.005
0.56	22.5	0.377 ± 0.023	0.373 ± 0.005
0.56	36.7	0.474 ± 0.001	0.494 ± 0.005
0.60	34.5	0.486 ± 0.013	0.496 ± 0.005
0.60	36.0	0.499 ± 0.001	0.517 ± 0.005

[a] determined via elemental analysis (cf. Chapter II)
[b] determined from FTIR intensities (peak areas) for AMS (1'600 cm^{-1}) and MAN (2'230 cm^{-1}) relevant vibrational bands and the calibration curve derived in Chapter II.

The content of AMS and MAN in the graft component is determined via elemental analysis and Fourier transform infrared spectroscopy (FTIR), as described in Chapter II. Based on the obtained molar fractions of AMS and MAN in the grafts, the effective reactivity ratios r_{AMS} and r_{MAN} can be obtained for comparison with bulk copolymerization of AMS and MAN. Vibrational bands associated with AMS and MAN in a background of FEP are readily available [405]. The FTIR spectra are recorded in transmission mode. Therefore, we obtain an average intensity over the film thickness, and neglect possible gradients in AMS:MAN composition ratio across the film thickness. Such a composition drift may arise as a consequence of changing monomer solubility and / or diffusivity in the polymer film undergoing grafting. The molar ratio F of AMS and MAN in the grafts is determined based on the ratio of the vibrational bands (peak area) associated with AMS (1'600 cm^{-1}) and MAN (2'230 cm^{-1}) and the calibration factor determined in Chapter II. The

molar fraction of AMS X_{AMS} is then obtained according to $X_{AMS} = F/(1+F)$. Evidently, $X_{MAN} = 1 - X_{AMS}$. The composition values obtained by elemental analysis and FTIR are listed in **Table 3-1**.

Owing to the satisfactory agreement between the FTIR and the elemental analysis method (deviation below 10%), the composition of the graft component is determined via FTIR in the following. Based on the compositional analysis of the samples prepared using different ratios of AMS and MAN in the monomer mixture (**Figure 3-5**), the copolymerization diagram can be established (**Figure 3-6**). It indicates that the degree of AMS incorporation into the graft copolymer is higher in the presence of water in the grafting solution. A possible explanation is a different partitioning of AMS and MAN between the solution phase and the polymer phase. Since AMS is less polar than MAN, the addition of water will force AMS out of the solution into the non-polar polymer, thereby increasing the effective AMS concentration at the grafting front. Hence, the addition of water results in a shift of the partitioning equilibrium of AMS and MAN between the liquid and polymer phase. Based on the data presented in **Figure 3-6**, the reactivity ratios for AMS and MAN can be determined using a non-linear least-squares (NLLS) fitting of the copolymerization equation to the experimental data points. It appears that the AMS / MAN co-grafting system is qualitatively well-described by the Mayo-Lewis model.

The deviation of the experimental data points from the fitted copolymer composition equation at high AMS contents, however, deserves some more in-depth consideration. It was not possible in any of the experiments to obtain an AMS content of more than 60 % in the grafted chain, even at very high AMS molar fractions of $x_{AMS} = 0.98$. Under these conditions, mainly AMS-AMS sequences are expected to be formed in the copolymer. Yet this is in line with the notion that AMS shows a poor tendedy to homopolymerize by the radical mechanism, and close to the ceiling temperature depropagation of extended sequences of AMS are likely to occur [406]. In the approach of Ham, deviations from the simple Mayo-Lewis terminal model (Eq. 3-10) can also be explained based on penultimate effects. The model put forward demonstrates the inability of AMS to form sequences longer than 3 units [407].

The reactivity ratios for AMS and MAN obtained by fitting are given in **Table 3-2** and compared against literature data, obtained in solution using different procedures and experimental conditions. The fact that both r_{AMS} and r_{MAN} are well below unity indicates that cross-propagation is favored and the formation of an alternating copolymer chain is highly likely. The influence of the solvent composition is also reflected in the reactivity ratios: r_{MAN} is lower in the presence of water and r_{AMS} is higher, meaning that AMS is preferentially incorporated. This leads to an overall higher content of AMS in the grafted chain over the entire compositional range. Evidently, the

literature values reported for copolimerizations in bulk or solution show some degree of variation, yet the general trend observed is similar, i.e. both reactivity ratios are well below unity and $r_{AMS} < r_{MAN}$. The feed composition, using the isopropanol / water solvent system, required to obtain a molar ratio of 1:1 in the graft component, thereby maximizing the degree of alternation in the copolymer chain, is indicated in **Figure 3-6** to be at an AMS molar fraction of around $x_{AMS} = 0.6$ in the reaction mixture.
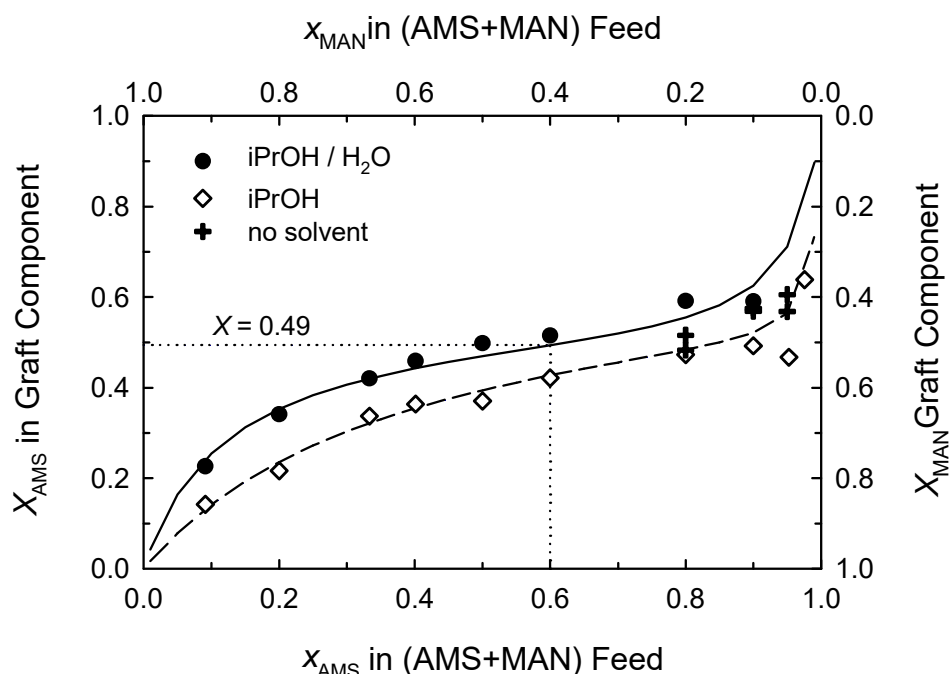
Figure 3-6. AMS fraction in the graft component of AMS : MAN co-grafted films as a function of monomer feed composition. Data from Figure 3-5. The Mayo-Lewis copolymerization equation (3-10) was fitted to the data points to determine the reactivity ratios for AMS and MAN (Table 3-2). Chosen standard feed composition of $X_{n,AMS} = 0.6$ and the corresponding value in the graft component (0.49) is highlighted for the isopropanol / water solvent system.

Table 3-2. Copolymerization ratios for AMS (r_{AMS}) and MAN (r_{MAN}) in different systems.

Series	r_{AMS}	r_{MAN}	Reference
copolymer	0.11 ± 0.02	0.28 ± 0.01	this work[a]
co-grafted in iPrOH / H_2O [b]	0.08 ± 0.02	0.22 ± 0.03	this work
co-grafted in bulk and in iPrOH [c]	0.018 ± 0.004	0.56 ± 0.06	this work
copolymer [d]	0.12	0.35	[389]
copolymer [e]	0.06	0.28	[402]
copolymer	0.15	0.28	[233]
copolymer [f]	0.54	0.38	[408]

[a] cf. Chapter II
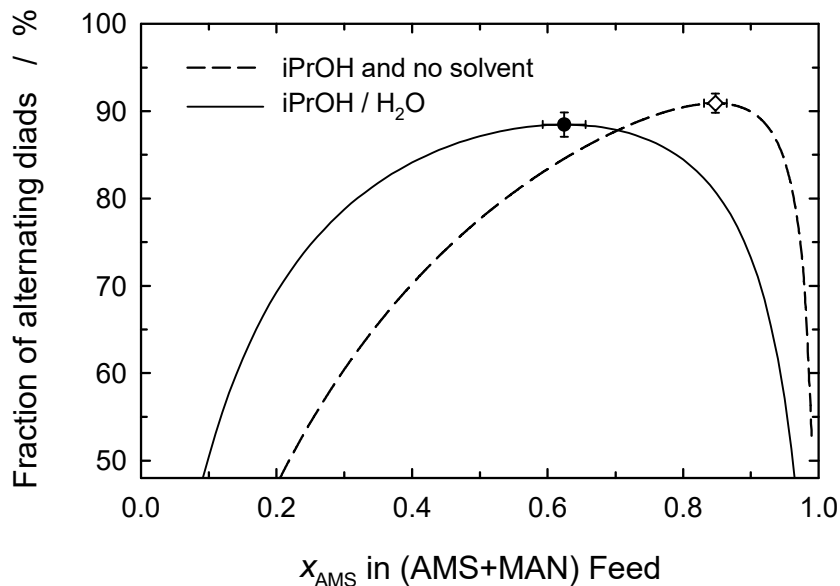[b] data points (●) in Figure 3-6
[c] data points (◊) and (+) in Figure 3-6
[d] 80°C, no solvent
[e] 60°C, emulsion copolymerization
[f] 60°C, toluene

The sequence distribution in AMS : MAN copolymers, prepared via emulsion copolymerization, was investigated by Kenney and Patel [402, 403]. They found that the copolymer, prepared at a temperature of 60 °C, has a high tendency to alternate. The fraction of alternating diads in a copolymer with a 1:1 molar ratio is 88 %, whereas only 7 % are MAN-MAN sequences, and 5 % AMS-AMS. The fact that both r_{AMS} and r_{MAN} are well below unity in our co-grafting system indicates that cross-propagation is favored and the formation of an alternating copolymer chain highly probable.

Figure 3-7. Estimated degree of alternation in the two experimental series co-grafted in different solvent systems, calculated based on the "run number" concept with reactivity ratios given in Table 3-2. The single data points indicate at which monomer feed concentration the maximum degree of alternation in the copolymer is expected.

Table 3-3. Composition of the monomer mixture ($x_{AMS,a}$) at which the maximum degree of alternation in the grafted component is expected, and fraction of alternating diads and diads of the same kind. Note that at the composition of maximum alternation, the ratio of monomer units in the copolymer is unity ($F = 1$ or $X_{AMS} = X_{MAN} = 0.5$).

Co-grafting series solvent system	$x_{AMS,a}$	AMS-MAN / MAN-AMS (%)	AMS-AMS & MAN-MAN (%)
iPrOH / H_2O	0.62 ± 0.03	88 ± 1	5.8 ± 0.7
iPrOH and bulk	0.85 ± 0.02	91 ± 1	4.6 ± 0.5

As outlined in Section 1.2, the degree of alternation can be calculated using the "run number" concept to estimate the fraction of alternating diads in a copolymer with given reactivity ratios (Eq. 3-23). For the co-grafting of AMS and MAN in bulk and in isopropanol on the one hand, and in isopropanol and water on the other hand (**Table 3-2**) the calculated fraction of alternating diads is displayed in **Figure 3-7**. With the mixed isopropanol / water solvent system, a high fraction of

alternating diads is expected over a wider range of monomer compositions. Again, this is explained by a favourable partitioning effect, whereby the presence of water in the solution "drives" the non-polar AMS into the polymer phase. The calculated fraction of diads at the composition of maxiumum alternation is given in **Table 3-3**. It happens that at this point the AMS-AMS and MAN-MAN diads occur with the same probability (cf. Eq. 3-21/22). In reality, however, deviations from the predicted values are probable, owing to the fact that significant fractions of AMS sequences are not likely to form. Taking into consideration the much higher rate of grafting in the mixed solvent system at $x_{AMS} = 0.6$ compared to the grafting in isopropanol at $x_{AMS} = 0.85$ (**Figure 3-5**), the former grafting system is certainly to be preferred in practice.

2.2.1 Effect of Solvent Type and Monomer Concentration

The type of solvent used in monomer mixtures for radiation grafting can have a dramatic effect on the resulting degree of grafting. In addition, it is of interest to minimize the monomer content in the grafting solution and maximize yield. It was found for the grafting of styrene / divinylbenzene (DVB) mixtures onto FEP base film that the maximum graft level was not obtained in the bulk monomer mixture, i.e., with no solvent present, but at diluted mixtures with lower monomer concentration in isopropanol and methanol (polar solvents), in particular if water is used as a co-solvent [190]. Yet, with toluene as (non-polar) solvent the graft level increased steadily with increasing monomer concentration with a maximum at 100 % monomer. A grafting series of AMS : MAN ($x_{AMS} = 0.6$) in different solvents and at various monomer concentrations yielded a qualitatively somewhat dissimilar picture, although some of the trends are the same (**Figure 3-8**).

The highest graft levels are obtained for monomer mixtures close to bulk AMS:MAN. In contrast to the styrene / DVB monomer mixture, which is highly non-polar, the mixture of AMS and MAN constitutes a combination of a non-polar and polar moiety, which may lead to a different partitioning characteristic between liquid and polymer phase. With toluene as solvent, the graft level shows more or less a linear increase with monomer concentration, which was also observed by Rager [190]. Yet, unlike the reults obtained with styrene / DVB, the lowest graft levels are obtained using methanol as solvent. This is attributed to a higher chain transfer rate from the radical from the chain end to methanol than in case of styrene / DVB. Grafting in isopropanol-water yielded the highest graft levels at low concentration of monomers (< 35 %). As already discussed, the addition of water increases the effective concentration of the monomers in the polymer phase. Consequently, a monomer concentration of 30 % was chosen as standard, yielding an optimum of high graft level and low monomer usage.
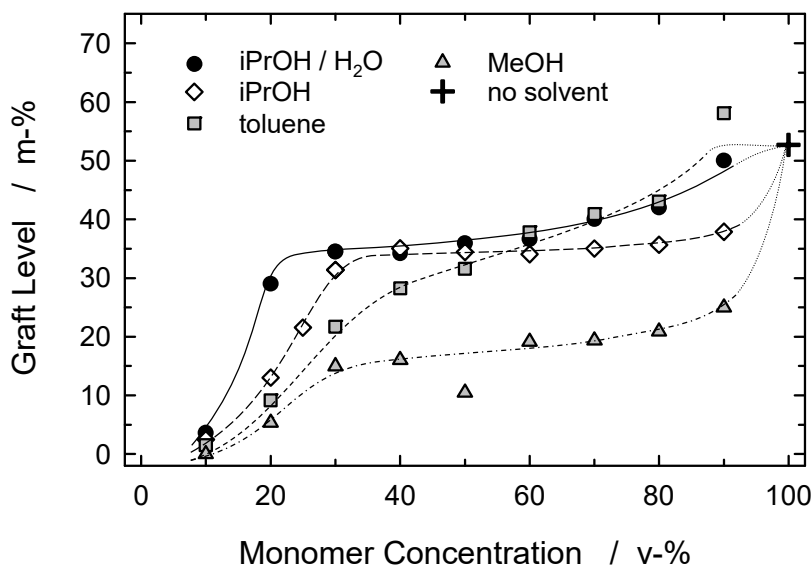
Figure 3-8. Influence of the composition of the grafting solution (monomer concentration, solvent) on the obtained graft level. Feed composition: $x_{AMS} = 0.6$; temperature: 60 °C; grafting time: 22 h; isopropanol / water ratio for (●): 5:2 v/v. Lines are guides to the eye.
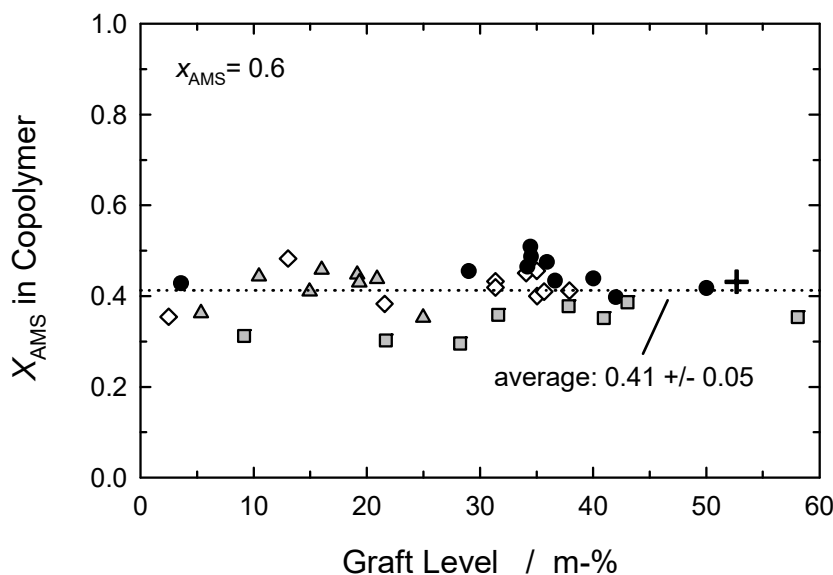
Figure 3-9. Molar fraction of AMS in the graft component (samples from Figure 3-8). The average composition is calculated based on all data points.

The content of AMS and MAN in the graft component was obtained from FTIR analysis (**Figure 3-9**), and the average molar fraction of AMS in the copolymer X_{AMS} was determined (**Table 3-4**). The different compositions are attributed to dissimilar extents of monomer partitioning between the liquid and polymer phase. The lowest AMS fraction was obtained in toluene as solvent. Being non-polar and therefore a good solvent for AMS, it results in a lower tendency for AMS to accumulate in the polymer phase. A polar solvent, such as isopropanol or methanol, increases the effective AMS concentration in the film undergoing grafting. The effect is even stronger in the presence of a non-solvent (water). The highest AMS fraction of 50 % is obtained in the isopropanol-water solvent system at a monomer concentration of 30 %.

Table 3-4. AMS molar fraction in the grafts (calculated based on data in **Figure 3-9**).

Solvent system	X_{AMS} in graft component	
	average	at 30 % monomer
iPrOH / H$_2$O [a]	0.45 ± 0.03	0.50 ± 0.02
iPrOH	0.42 ± 0.04	0.43 ± 0.01
toluene	0.34 ± 0.03	0.30 [b]
MeOH	0.42 ± 0.04	0.41 [b]
no solvent	0.43 [b]	-

[a] 5:2 v/v
[b] single measurements

A further argument worth considering is the partitioning of the inhibitor, since the monomers were used without purification. In the case of polar solvents, the inhibitor, being a polar phenol derivative, tends to accumulate in the liquid phase. The lower concentration in the polymer phase might allow higher graft levels to be reached.

2.2.2 Grafting Kinetics

Since the grafting reactions reported so far have been carried out with constant duration, the grafting kinetics, i.e., the increase of graft level with time, was investigated subsequently (**Figure 3-10**), using isopropanol and isopropanol-water as solvent. The shape of the grafting curve is characterized by a high initial grafting rate, followed by a decrease and levelling off tendency of the degree of grafting. The grafting rate is governed by the rate of polymerization, termination of radicals, and solubility / diffusivity of the monomers in the polymer [41]. The termination reaction during graft copolymerization is governed by the mobility of the growing chains, bearing terminal radicals, in the polymer matrix. Therefore, the use of solvents that are incompatible with the polymer phase, i.e., polar solvents in our case, leads to a lower extent of solubilization of the polymer chains and therefore, according to the *Trommsdorff-Norrish* or 'gel' effect, to extended radical lifetimes and a reduced termination rate [190]. In this context, the higher grafting rate

observed in the presence of of water can be explained by a more pronounced 'gel' effect, in addition to the already discussed favorable monomer partitioning, with the monomer preferentially accumulating in the polymer phase.

The composition of the graft component was analyzed using the calibrated FTIR method (**Figure 3-11**). The composition appears to be relatively constant over a wide range of graft levels, with higher average AMS content for the isopropanol-water solvent system, in agreement with the previously found results (**Figure 3-6**). In an early phase of the reaction (< 10 h), the AMS content seems to be lower than in the later phase. It is speculated that MAN grafts faster initially. A similar behavior was described by Becker and Schmidt-Naake for AMS and AN grafted onto ETFE [191]. It was found that in the course of the reaction the composition of the graft component drifts from lower to higher AMS fraction. It was suggested that AN reacts faster initially due to its higher diffusion rate, owing to its smaller size compared to AMS, until a quasi-steady state of AN and AMS concentration at the graft front propagating into the film is reached. Yet, we have to consider that the homo-polymerization rate constant for MAN is about 1'000 times lower than that of AN [233]. There are two possible phenomena governing the composition change in the early phase of grafting, a kinetic effect related to initiation, and a partitioning effect related to the effective monomer concentration in the grafting zone. Spatially resolved characterization of the graft component may be accomplished using confocal Raman spectroscopy [326, 409], confocal laser scanning microscopy [410], or cross-sectional analysis via scanning electron microscopy with energy dispersive X-ray spectroscopy (SEM/EDX) [327]. The isopropanol / water solvent system was adopted as a standard for the co-grafting of AMS and MAN.
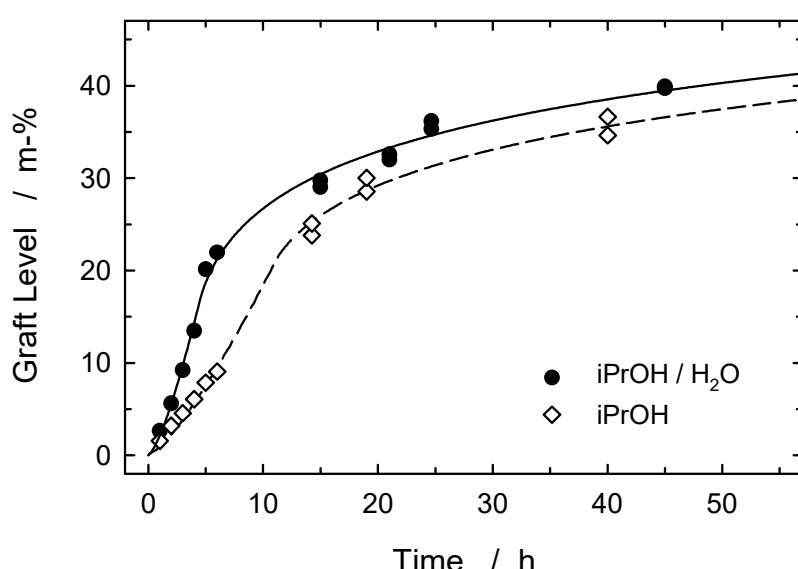
Figure 3-10. Influence of the addition of water to the grafting solution on the grafting kinetics. Feed composition: $x_{AMS} = 0.6$; monomer concentration: 30 %; temperature: 60 °C; isopropanol / water ratio for (●): 5:2 v/v.
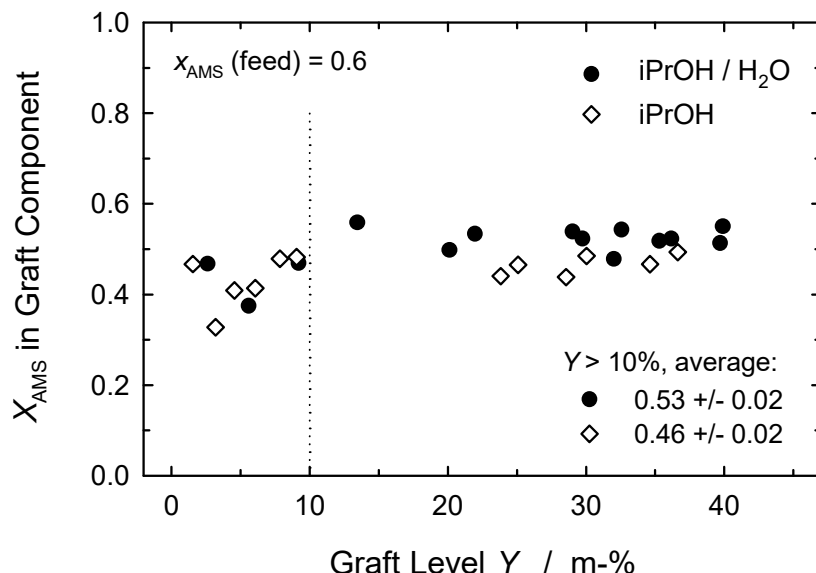
Figure 3-11. Molar fraction of AMS in the graft component (samples from Figure 3-10). Average compositions are calculated for graft levels higher than 10 %.

2.3 Characterization of AMS-MAN Co-grafted Films and Membranes

The co-grafting of AMS and MAN leads to the simultaneous incorporation of both monomers into the film. FTIR analysis of a sulfonated AMS:MAN membrane shows the presence of sulfonic acid on the aromatic ring of the AMS units (**Figure 3-2**). The band for the C≡N stretching vibration proves the inertness of the MAN component during the membrane preparation process. *Post mortem* FTIR analysis of tested membranes shows the same C≡N band, indicating that also during fuel cell operation the MAN units remain unaffected.

Ultimately, one of the key requirements for a polymer electrolyte membrane is to provide a maximum of conductivity without adversely impacting other target properties of the membrane (cf. **Figure 0-8**, Introduction). The ionic conductivity of an ionomer is largely determined by the density and mobility of the charge carriers, in this case protons. The density of the ionic sites, i.e., the ion exchange capacity (IEC), is therefore an essential property of a proton exchange membrane. In the case of radiation grafted membranes, the IEC increases with the graft level, as more ionic groups are introduced [186]. Typically, sulfonation degrees of around 100 % are obtained for styrene grafted membranes, corresponding to one sulfonic acid per styrene unit [197]. It is unlikely that there is more than one sulfonic acid group attached to the aromatic ring due to electronic and steric reasons. The IEC of a range of AMS:MAN co-grafted membranes with varying degree of grafting, along with two sets of data for crosslinked membranes using divinylbenzene (DVB) and diisopropenylbenzene (DIPB) as co-monomers, is reported in **Figure 3-13**.
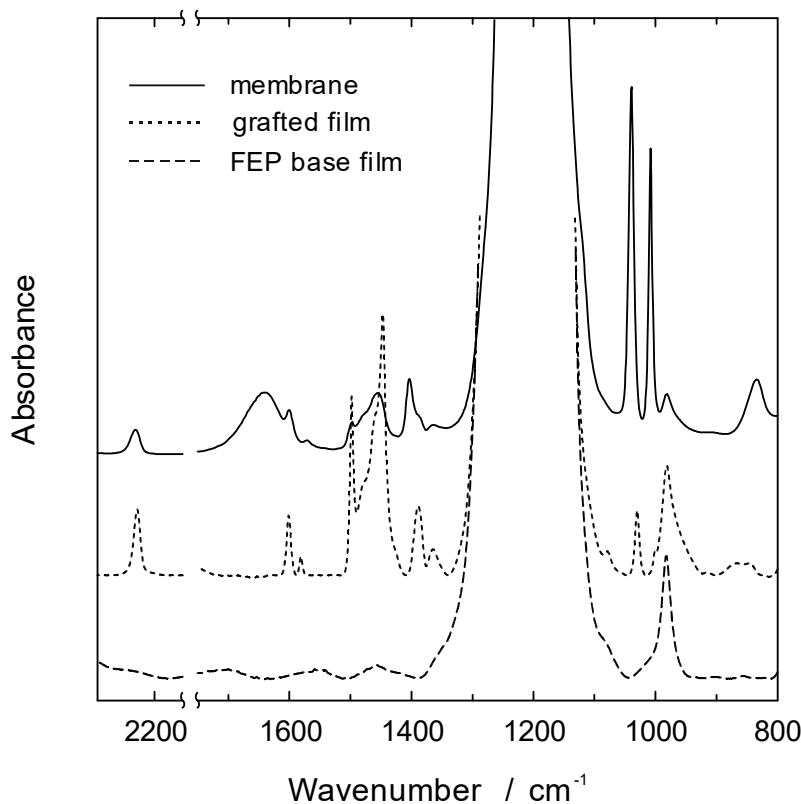
Figure 3-12. Transmission FTIR spectra of FEP base film (25 μm), AMS:MAN co-grafted film (graft level: 32 %), and sulfonated membrane (K$^+$ exchanged, dried).

Table 3-5. Relevant vibrational bands in FTIR spectra of base film, grafted film and membrane.

Wavenumber (cm^{-1})	Vibration	Group / compound	Strength*
831	ν(S-O)	sulfonated AMS	m
982	ν(CF) CF$_3$	FEP	s
1'010	aromatic in-plane	sulfonated AMS	s
1'028	aromatic in-plane	AMS	m
1'040	ν^s(SO$_3$)	sulfonated AMS	s
1'052 – 1'385	ν^{s,a}(CF$_2$)	FEP	vs
1'388	δ(CH$_3$)	α-CH$_3$ of MAN ("umbrella")	m
1'420-1'490	compound ar	AMS	s
1'498	ν(C-Car)	AMS	s
1'580	ν(C-Car)	AMS	w
1'600	ν(C-Car)	AMS	m
1'630	δ(HOH)	water	s
2'230	ν(C≡N)	nitrile in MAN	m
2'810-3'150	ν(C-H)	various	s
3'000-3'800	ν(O-H)	water, sulfonic acid	s

* w = weak, m = moderate, s = strong, vs = very strong
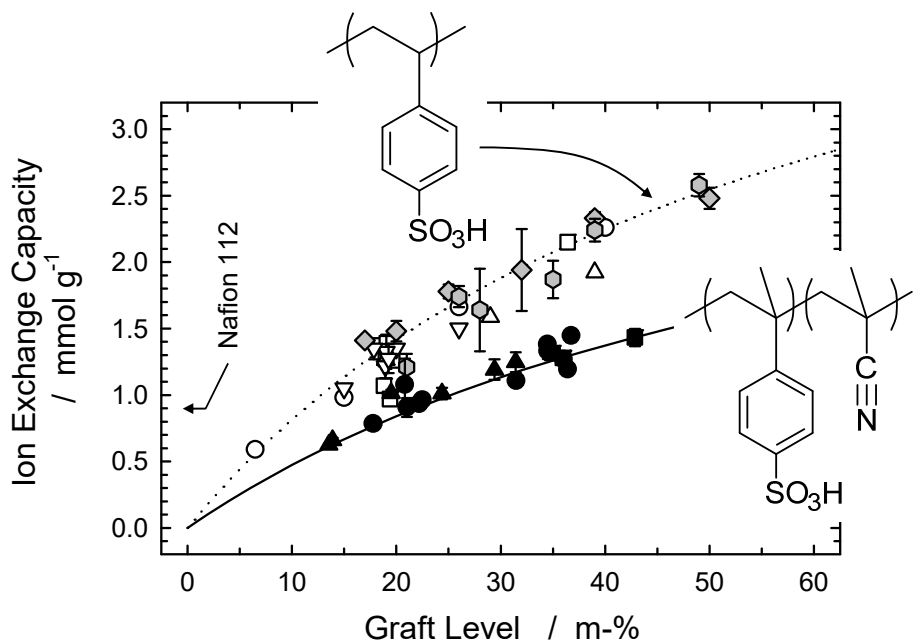
Figure 3-13. Ion exchange capacity (IEC) of various radiation grafted membranes based on styrene and AMS:MAN, respectively. Solid lines represent calculated values based on 100 % degree of sulfonation of the aromatic unit, and a 1:1 molar ratio of AMS:MAN in the graft copolymer.
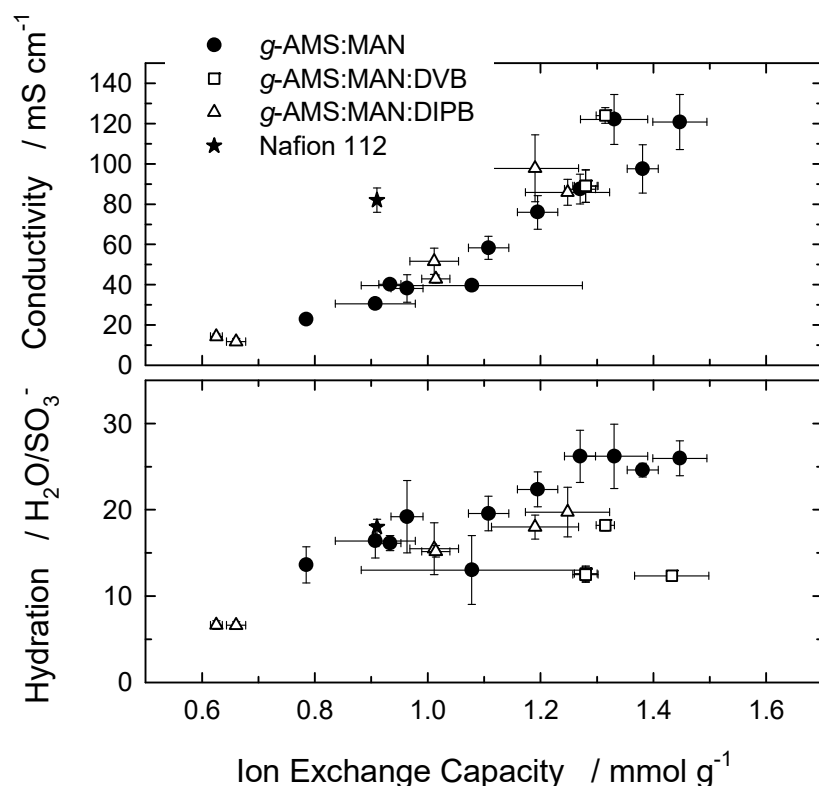
Figure 3-14. Conductivity and water uptake of membranes, measured at room temperature in water-swollen state, as a function of ion exchange capacity (IEC). The properties of Nafion® are shown for comparison.

Compared to the values obtained for styrene-only grafted membranes, represented by the calculated line corresponding to 100 % degree of sulfonation, the IEC of the AMS:MAN co-grafted membranes is markedly lower at a given graft level. A minor reason is the higher molar mass of AMS compared to styrene. The main reason is related to the fact that the MAN units do not contribute to the IEC. Assuming a perfectly alternating chain of AMS and MAN, justified by the compositional analysis (**Figure 3-11**), an excellent agreement between experiment and theoretical values is obtained. We can therefore conclude that in the co-grafted membranes a degree of sulfonation of the AMS units of close to 100 % is achieved.

The dependence of the conductivity on the IEC of the co-grafted membranes is displayed in **Figure 3-14**, including data for un-crosslinked samples as well as DVB- and DIPB-crosslinked samples. The conductivity increases with ion exchange capacity, as expected, as a result of the increasing proton density. The increase, however, is disproportionate rather than linear with IEC, which can be explained with the increasing level of hydration of the membranes, expressed as the number of water molecules per sulfonic acid site. The mobility of the proton increases with the hydration number, as it has been shown for perfluorinated membranes of the Nafion® type [338]. In comparison of the crosslinked with the uncrosslinked samples, one notices that the two types of membrane exhibit similar conductivity values, although the crosslinked membranes, in particular the DVB-crosslinked ones, display a lower level of hydration. This is a consequence of a higher structural density in the crosslinked material, yet it does not appear to adversely affect proton conductivity. DVB is the more effective crosslinker than DIPB, leading to a denser network, despite the fact that the concentration of DVB was only approximately half of that of DIPB in the grafting solution. However, owing to the high reactivity of DVB, an uneven distribution of crosslinker across the thickness of the grafted film is obtained. In experiments using styrene and DVB or DIPB as crosslinker, it was reported that the surface is enriched with crosslinker when DVB is used. On the other hand, when DIPB is used, the crosslinker is more evenly distributed across the thickness of the film [192]. This is deemed a more suitable configuration, since the development of gradients in internal stress is less likely when the crosslinking is uniform. It is interesting to note that Nafion® 112 has a water uptake similar to that of the radiation grafted membranes with identical IEC, yet the conductivity is higher. It has to be kept in mind, though, that the IEC, which is a mass based quantity, can be misleading. The volume based IEC, i.e., the volumetric density of protons, although not often used in the context of the characterization of fuel cell membranes, is a more suitable parameter to compare dissimilar membrane classes, in particular when the density of the material is very different.

The *ex situ* properties of suitable membranes selected for later fuel cell testing are collated in **Table 3-6**. For comparison, the properties of styrene based membranes for an uncrosslinked (membrane ID #1) and an adequately DVB-crosslinked (ID #2) membrane are shown. The membrane of type #2 has been optimized with respect to composition and extent of crosslinking and displayed a lifetime of over 4'000 h at a steady state current density of 0.5 A/cm^2 at a temperature of 80 °C [195, 351]. Note that for a similar IEC, AMS:MAN based membranes have to be grafted to higher levels, typically 35 %, to obtain membranes with IEC similar to that of styrene based ones with a degree of grafting of around 18 %. This is a result of a lower ion concentration in the graft component (**Figure 3-13**). The conductivity of the uncrosslinked co-grafted membrane (ID #3) is around 100 mS/cm, which is identical to that of the uncrosslinked styrene-only grafted membrane (ID #1). The conductivity of Nafion® 112 is in the same range, albeit a bit lower. The conductivity of the DVB crosslinked co-grafted sample (ID #3, 89 mS/cm) is only slightly inferior and not as low as the conductivity of the styrene:DVB grafted sample (ID #2, 41 mS/cm), suggesting lower effective crosslinking, which is confirmed by the intermediate water content of 12.6 molecules of water per sulfonic acid, whereas the styrene:DVB grafted membrane has a water uptake of only 6.7 H_2O/SO_3H. Note that for the latter sample, the content of crosslinker (DVB) in the grafting solution is the highest among all the samples investigated. The graft level of the DIPB crosslinked membrane (ID #5) was somewhat lower than that of the other AMS based membranes, which is also reflected in the lower IEC value. This is also a likely explanation for the somewhat lower conductivity of 52 mS/cm compared to the DVB crosslinked sample (ID #4), despite the slightly higher level of hydration.

For the uncrosslinked AMS:MAN co-grafted membrane (ID #3), the content of the two comonomers in the grafted film was determined via elemental analysis. The result highlights that the molar ratio of AMS and MAN is close to 1:1, supporting the notion of a grafted chain with high degree of alternation. In addition, based on the result the degree of sulfonation can be calculated, yielding a value of 113 %. Based on the unlikeliness of 'over-sulfonated' AMS units, a sulfonation degree clearly in excess of 100 % might indicate partial hydrolysis of the nitrile group and formation of a carboxylic acid functional group. Unfortunately, elemental analysis cannot be used for the crosslinked AMS based samples (IDs #4 and #5), because the incorporated ratio of AMS and crosslinker is unknown. The AMS content in the graft component was therefore estimated by back-calculating the AMS graft level from the measured IEC, assuming a degree of sulfonation of 100 % and neglecting the crosslinker content (which should be around or below 5 % anyway). As a result, an AMS to MAN molar ratio of close to 1:1 is found, indicating values similar to that of the uncrosslinked membrane.

Table 3-6. Comparison of *ex situ* properties of AMS-MAN co-grafted membranes and pure styrene grafted membranes based on 25 µm FEP base film. Divinylbenzene (DVB) and diisopropenylbenzene (DIPB) are used as crosslinkers in selected samples.

ID	Membrane	Crosslinker [c] (v-%)	Graft level (m-%)	AMS content in graft component (mol-%)	Ion exchange capacity (mmol g^{-1})	Water uptake [f] ([H$_2$O]/[SO$_3$H])	Conductivity [f] (mS cm^{-1})	Degree of sulfonation [g] (%)
#1	*g*-S [a]	-	18.0	-	1.33 ± 0.02	29.5 ± 0.7	72 ± 6	102 ± 4
#2	*g*-S [a]	10% DVB	18.2	-	1.36 ± 0.06	6.7 ± 0.7	41 ± 1	103 ± 6
#3	*g*-AMS:MAN [b]	-	34.5	48 ± 1.3 [d]	1.38 ± 0.03	24.6 ± 0.8	98 ± 12	113 ± 3
#4	*g*-AMS:MAN [b]	1.7% DVB	36.0	(50)[e]	1.28 ± 0.02	12.6 ± 0.9	89 ± 8	n/a
#5	*g*-AMS:MAN [b]	3.3% DIPB	24.4	(53)[e]	1.01 ± 0.04	15.5 ± 3.0	52 ± 6	n/a
#6	Nafion® 112	-	-	-	1.08 ± 0.01	21.6 ± 0.8	97 ± 15	-

[a] S = styrene
[b] molar ratio of AMS:MAN = 3:2 (x_{AMS} = 0.6) in the grafting solution
[c] with respect to the total volume of monomers in the grafting solution
[d] obtained from elemental analysis
[e] calculated based on ion exchange capacity, assuming 100% degree of sulfonation of AMS, crosslinker content neglected
[f] at room temperature in liquid water equilibrated state
[g] 100 % = 1 sulfonic acid per aromatic ring (styrene or AMS)

2.4 Ex Situ Chemical Stability

The improved chemical stability of AMS based membranes over styrene based membranes was initially thought to be verified in an *ex situ* chemical stability test in aqueous H_2O_2 solution. The oxidative degradation mechanism is believed to be similar to the mechanism of *in situ* chemical membrane aging [5, 247]. Although the test is somewhat crude and not suited for the determination of kinetic rate constants for membrane degradation, comparative trends between different membranes yield a qualitative measure for the susceptibility of the polymers towards oxidative degradation. The test involved the immersion of styrene and AMS based grafted membrane samples, both uncrosslinked, in 5 % H_2O_2 solution at a temperature of 68 °C. The release of aromatic species, originating from cleaved chains of the graft component, into the solution is monitored via UV spectroscopy. The styrene grafted membrane appears to release more aromatic species over time compared to the AMS:MAN co-grafted membrane, indicating a faster rate of chemical degradation. In addition, it appears that the rate of degradation increases for the styrene-only grafted membranes, whereas the increase in absorbance of the solution in case of the co-grafted membrane samples is slow and steady.
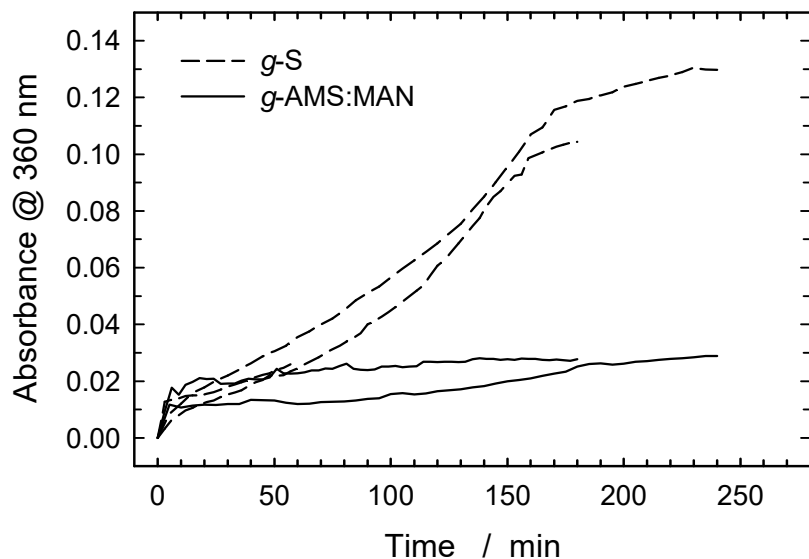
Figure 3-15. *Ex situ* chemical stability experiment. Release of aromatic species from a styrene (S) (DG ~20%) and an AMS : MAN (DG ~35 %) grafted and sulfonated membrane in a 5 % H_2O_2 solution at 68 °C. The relative increase of the absorbance at a wavelength associated with aromatic species, with the initial solution as reference, is recorded.

2.5 Fuel Cell Tests

Selected AMS based membranes with promising *ex situ* conductivities of 50 to 100 mS cm^{-1} (**Table 3-6**) were assembled together with commercial gas diffusion electrodes into membrane electrode assemblies (MEAs) and tested in single cells of 30 cm^2 active area. After start-up, the cells were conditioned, using humidified H_2 and O_2 as reactants, at a constant current density of

0.5 A cm^{-2} for around 100 to 300 h. The performance obtained in polarization experiments with the radiation grafted membranes was compared to that of an MEA comprising Nafion® 112 as a standard membrane (**Figure 3-16**). The ohmic resistance of the MEAs, which is mainly determined by the resistance of the membrane, was recorded simultaneously. The MEA comprising membrane #3 in **Table 3-6**, an uncrosslinked AMS:MAN co-grafted membrane, shows the same performance as the Nafion® 112 based MEA. The fact that the lower ohmic resistance of the AMS:MAN membrane (~55 mOhm·cm^2) compared to that of Nafion® 112 (~100 mOhm·cm^2) does not result in higher performance is attributed to more pronounced membrane-electrode interfacial losses associated with the radiation grafted membrane. This phenomenon was observed already using styrene based radiation grafted membranes [195, 271, 351]. The explanation put forward is a lower chemical compatibility between the ionomer in the grafted membranes and the Nafion® used as ionomer in the catalyst layer of the gas diffusion electrodes. This material mismatch entails higher interfacial losses compared to the Nafion® 112 MEA, where there is Nafion® ionomer in the membrane as well as the catalyst layer.
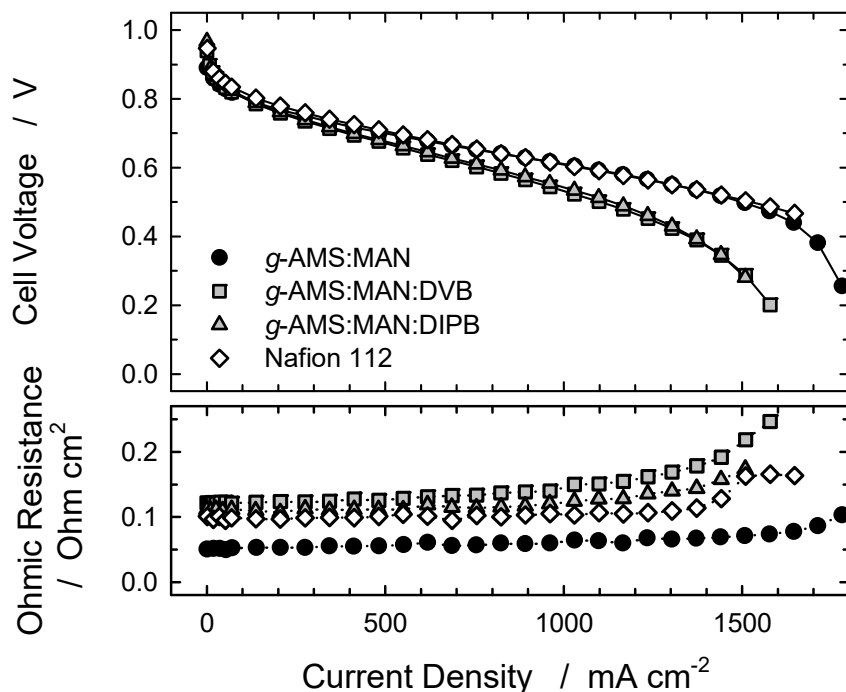
Figure 3-16. Fuel cell performance of AMS:MAN based membranes (Table 3-6, membrane IDs #3, #4, and #5) compared against Nafion$^®$ 112 (ID #6). Electrodes: carbon cloth (E-TEK) with 0.5 mgPt cm^{-2}; reactants: fully humidified H$_2$/O$_2$; cell temperature: 80 °C; pressure: 1 bar$_a$.

The MEAs comprising grafted membranes crosslinked with DVB and DIPB (membrane IDs #4 and #5 in **Table 3-6**), respectively, show somewhat lower performance compared to the uncrosslinked membrane. The additional losses are a consequence of the higher ohmic resistance

using the crosslinked membranes (130 and 110 mOhm·cm^2 below 0.8 A·cm^{-2}, respectively). Although crosslinking entails some loss in performance, it is important regarding the durability of the membranes, as will be shown in the following.
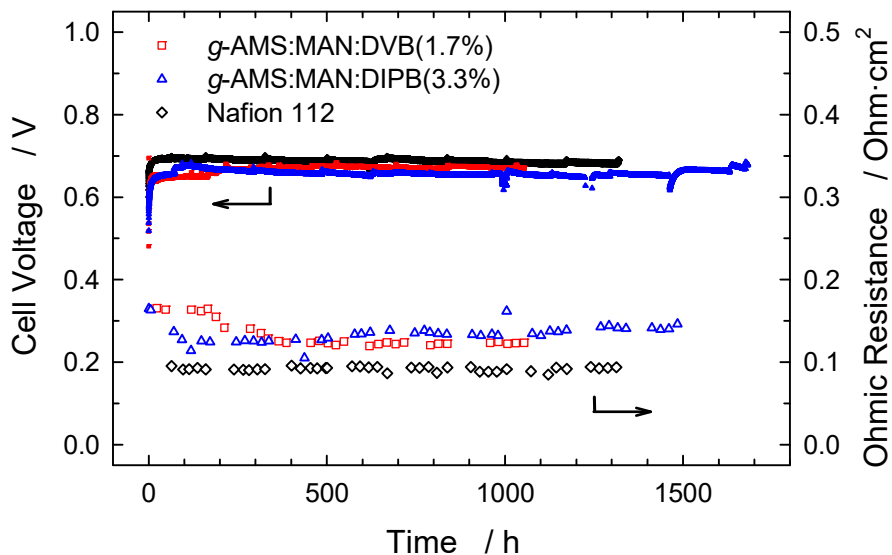
Figure 3-17. Long-term fuel cell experiments at a constant current density of 0.5 A cm^{-2} of AMS:MAN membranes with DVB and DIPB crosslinker, respectively, with a graft level of ~25 %, an IEC of ~1.0 mmol/g and an *ex situ* conductivity of ~50 mS/cm at room temperature. An experiment with Nafion® 112 is shown for comparison. Cell temperature was initially 60°C, then 80°C (cf. drop in ohmic resistance); other conditions cf. Figure 3-16. The experiments were stopped after different time on test (no failure).

The cells with the grafted membranes were operated at constant conditions (temperature: 80 °C; current density: 0.5 A cm^{-2}) until membrane failure occurred through crack or pinhole formation, or until 1'000 h of operating time were reached. Durability tests using crosslinked membranes are shown in **Figure 3-17**. The cell temperature was 60 °C initially, after conditioning of the cell it was ramped up to 80°C. The ohmic resistance shows a concurrent decrease, which is a consequence of membrane conductivity increasing with temperature. The cells with the grafted membranes exhibited stable performance and no indication of degradation. The tests were discontinued after around 1'050 and 1'500 h, respectively, without failure of the MEA having occurred.

2.6 Post Test Analysis

After conclusion of the fuel cell test, the MEAs were disassembled from the cell and delaminated to extract the membrane for *post test* analysis to determine the extent of degradation. The residual IEC of the membranes in the active area was determined via titration. The extent of degradation was calculated using the membrane outside of the active area as reference. The IEC loss divided by the testing time is subsequently calculated to determine the degradation rate. Although this is a crude estimate of the chemical stability of the membrane, it was used to characterize the different

classes of materials qualitatively and in general terms (**Figure 3-18**, **Table 3-7**). The fact that uncrosslinked styrene grafted membranes are highly instable in the fuel cell environment has been known for a long time [269]. In the present case, the MEA failed after approximately 50 h (**Table 3-6**, ID #1). The effect of introducing DVB as crosslinker (ID #2) on the resulting MEA lifetime is dramatic. The corresponding degradation rate is lower by a factor of 160 compared to the uncrosslinked membrane. On the one hand, crosslinking leads to a reduction in gas (H_2, O_2) transport across the membrane as a consequence of a higher compactness (lower swelling) of the crosslinked polystyrene domains [271]. Hence, the formation rate of $HO^\bullet$ / $HOO^\bullet$ radicals through interaction of H_2 and O_2 with the Pt catalyst is reduced. On the other hand, the polymer network formed via crosslinking is more resilient against loss of chain segments following bond scission, owing to the multiple connectivity of polymer chains. The MEA comprising the uncrosslinked AMS:MAN co-grafted membrane (ID #3) shows a 10-fold increase in lifetime (~550 h) over the styrene-only grafted membrane (ID #1), and a 30-fold decrease in degradation rate. This can be considered an improvement of the intrinsic chemical stability of the material. It appears that the concept originally conceived, i.e., the substitution of styrene with AMS:MAN and the concomitant avoidance of α-hydrogen, proves to be successful, resulting in higher stability in the fuel cell environment. The crosslinking introduced by DVB further improves durability. The different reaction rates of AMS, MAN, styrene and DVB require a re-assessment of the optimum DVB content in the grafting solution to obtain the desired extent of crosslinking in the grafted film. The higher hydration level of the crosslinked AMS:MAN based membrane (ID #4) compared to the styrene:DVB sample (ID #2) suggests a lower effective degree of crosslinking. It is likely that the stability of the AMS:MAN grafted membranes can be further enhanced by increasing the degree of crosslinking, aiming at hydration levels similar to those of the styrene:DVB grafted membrane.

The degradation rates calculated and presented in **Figure 3-18** and **Table 3-7** are of rather qualitative nature to characterize the stability of the membranes. It cannot be elucidated how the degradation rate changes over time, i.e., if the ionic site loss is accelerating or decreasing with progressing time on test. In addition, the titration method used provides merely an average over the active area. Therefore, transmission FTIR spectroscopy has been used to quantify the residual concentration of sulfonated aromatic species in 6 different sectors of the active area of tested membranes (**Figure 3-19**), taking the pristine membrane as reference. Visual inspection of the membrane already suggests inhomogeneities in the extent of degradation. In addition, hole formation near the oxygen inlet at the edge of the active area is observed, indicating high localized chemical stress.
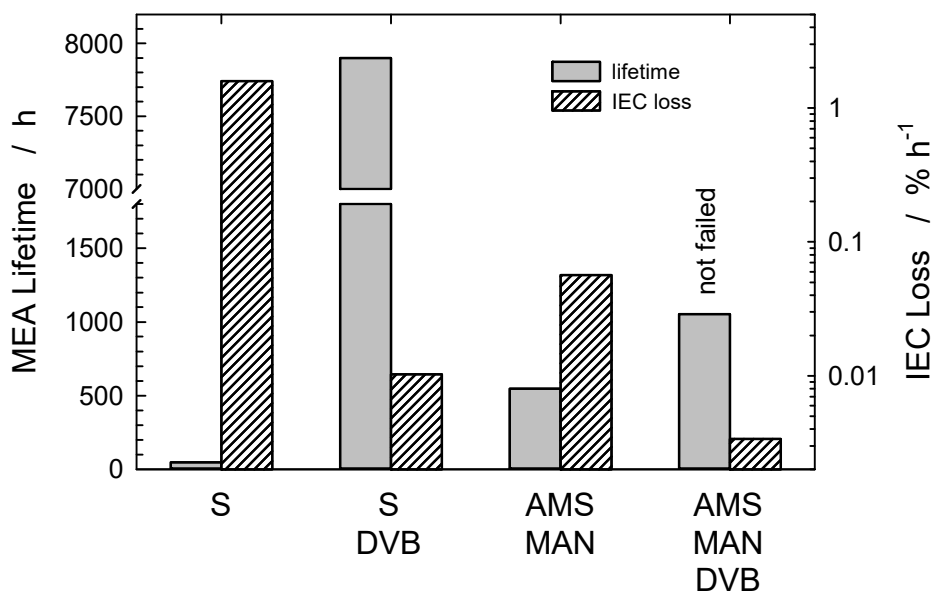
Figure 3-18. Comparison of single cell lifetime and rate of ion exchange capacity (IEC) loss for different radiation-grafted membranes. Cell temperature 80°C. Samples (Table 3-6): membrane IDs #1-4.

Table 3-7. Long-term test results in H_2/O_2 single cells at 80 °C, 1 bar_a and 0.5 A cm^{-2}. *Post mortem* analysis of degradation via titration.

Membrane	Table 3-6 ID	MEA lifetime (h)	Extent of degradation (%)	Degradation rate (% h^{-1})
g-S	#1	49	78	1.6
g-S:DVB [a]	#2	7'900	81	0.010
g-AMS:MAN	#3	547	31	0.057
g-AMS:MAN:DVB	#4	1'053 [b]	16	0.015

[a] Ref. [195]
[b] MEA not failed
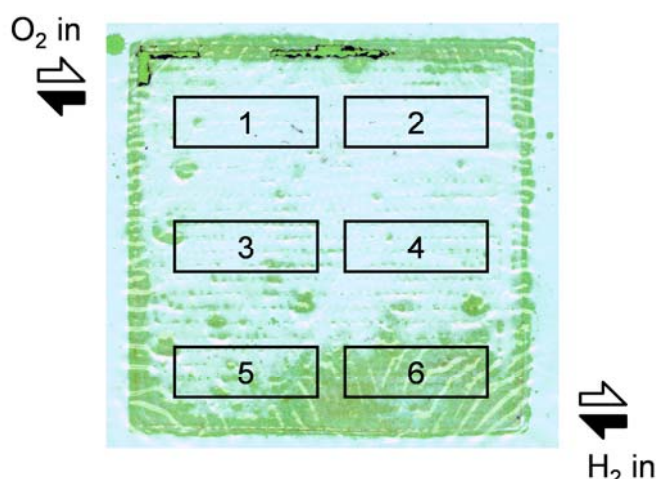
Figure 3-19. Sectors for *post mortem* analysis via FTIR of an uncrosslinked AMS:MAN co-grafted membrane with 21 % graft level and an MEA lifetime of 526 h. The cell was operated in counter-flow mode. Scan with dark background, the dark regions are transparent areas of the membrane. Note the holes near the O_2 inlet.

FTIR degradation analysis was carried out on 3 tested membranes in the same manner (**Figure 3-20**). Generally, it is found that the ionic site loss is subject to high local variations. More pronounced degradation is detected in membrane areas close to the hydrogen inlet. This is in disagreement with results obtained using styrene:DVB grafted membranes (**Table 3-6**, ID #2), where more notable degradation was observed in regions close to the oxygen inlet [411]. The resons for the dissimilar behaviour are unknown. The result could indicate that breakdown of the grafted chains may follow different pathways in AMS:MAN co-grafted membranes compared to poly(styrenesulfonic acid) containing materials.
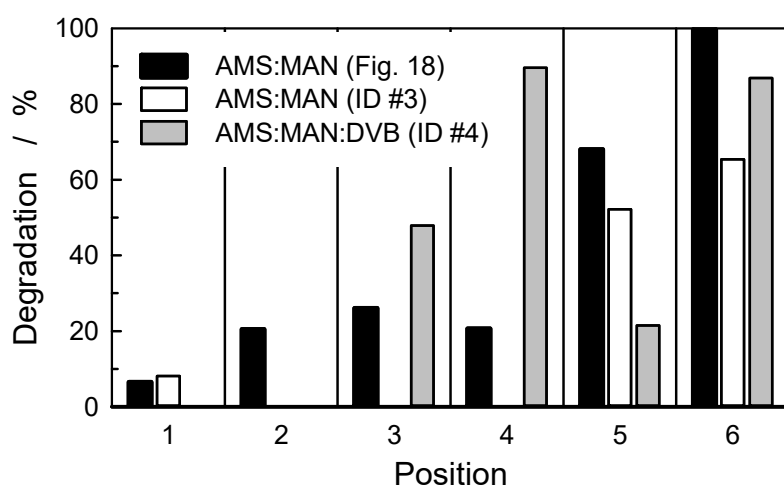

Figure 3-20. *Post mortem* study of the AMS:MAN co-grafted membrane (for membrane IDs cf. Table 3-6) in 6 sectors of the active area via FTIR spectroscopic analysis of the sulfonated aromatic unit at 1'009 cm^{-1}.

In summary, the results shown in this section demonstrate that AMS can be effectively grafted in the presence of a suitable comonomer, such as AMS, and membranes with practical IEC can be obtained. As expected from the copolymerization in solution, AMS and MAN tend towards alternating copolymerization. There is an influence of the composition of the grafts on the choice of solvent in the reaction mixture. Adding water to the isopropanol solvent lead to a higher content of AMS in the grafts, which is probably a result of a more favorable partitioning of the monomers between solution and polymer. In *ex situ* and *in situ* experiments, AMS:MAN co-grafted membranes were found to exhibit a significantly improved chemical stability compare to styrene-only grafted membranes. Crosslinking further stabilizes the membrane against degradation. Long term tests demonstrated, however, that the extent of degradation is not uniform over the active area of the cell, which is probably a result of gradients in operating conditions and local performance, such as dry inlet and wet outlet situations. This is a consequence of the type of single cell used in these experiments comprising a serpentine flow field. In the experiments reported in the subsequent sections, another cell was used, comprising a parallel flow field for differential operation of the cell (cf. also Chapter II).

3 S-MAN and S-AN Co-grafted Membranes

In the previous section it was demonstrate that AMS based membranes exhibit improved chemical stability under fuel cell operating condition. The implication of being able to graft AMS, however, is that a suitable comonomer, here MAN, has to be used, since AMS on its own does not readily graft. One may therefore object to the premature conclusion that the presence of AMS is responsible for the improved stability, since the effect of MAN has not been independently investigated. Hence, in the study reported in this section, MAN is co-grafted together with styrene to tackle this issue (**Figure 3-21**). The advantage of the styrene / MAN copolymerization system is that, other than in the case of AMS and MAN, the entire compositional range from pure styrene to pure MAN can be readily grafted. Therefore, the copolymerization kinetics and properties of the resulting membranes can be comprehensively studied.
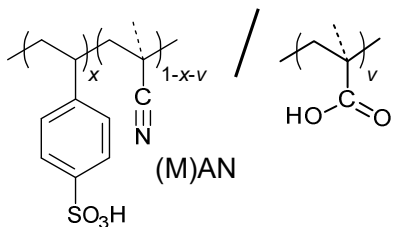
Figure 3-21. Molecular structure of co-grafted membranes using acrylonitrile (AN) and methacrylonitrile (MAN) as comonomers of styrene. x and $1-x-v$ indicate the content of styrene and (M)AN, respectively, in the grafts, v stands for the fraction of nitrile comonomer that has undergone hydrolysis during the sulfonation step.

In addition, acrylonitrile (AN) is chosen as a second comonomer to avoid potential effects of the presence of the α-methyl group in MAN on membrane stability. The hydrolysis of nitrile compounds is a concern regarding the operating conditions of the fuel cell, thus this aspect will also be studied with some detail.

3.1 Membrane Synthesis

Poly(ethylene-*alt*-tetrafluoroethylene) (ETFE) film of 25 μm thickness (Tefzel® 100LZ, DuPont) was used as base polymer for the synthesis of the membranes based on co-grafted styrene and (M)AN. The ETFE base films were electron beam irradiated in air at Leoni Studer AG (Däniken, Switzerland). For details see Section 2.1. The grafting solution consisted of a 20% (v/v) monomer mixture (styrene / AN or styrene / MAN), 70% (v/v) isopropanol and 10% water. The ratio of styrene and (M)AN in the grafting solution was varied over the entire composition range, i.e., $0 \leq x_S \leq 1$, and correspondingly for $x_{(M)AN} = 1 - x_S$. All grafting reactions were carried out at a temperature of 60ºC. The grafting kinetics study was carried out in a glass reactor (60 ml). For the preparation of larger batches of grafted films a stainless steel reactor (600 ml) was employed to

obtain sufficiently large samples for characterization and testing in in single fuel cells. The grafted films were extracted with toluene overnight and dried at 80ºC under vacuum. Proton conducting membranes were obtained by sulfonation of the grafted films in 2 % (v/v) chlorosulfonic acid in dichloromethane at room temperature for 5 hours, followed by hydrolysis and swelling in deionized water at 80ºC for 8 hours.

The composition of the co-grafted films was determined by FTIR based on calibration curves established for single-monomer grafted films in the case of styrene and MAN (cf. Chapter II). Owing to the poor grafting kinetics of AN (see below), a calibration curve could not be established for AN. Therefore, for S:AN co-grafted films the composition was calculated based on the overall graft level (measured gravimetrically) and the fractional graft level of styrene (determined spectroscopically using the FTIR calibration curve).

3.2 Co-grafting kinetics of styrene and (M)AN

In contrast to the co-grafting of AMS and MAN, styrene can be co-grafted with both MAN and AN over the entire compositional range, i.e., from pure styrene grafted films to pure co-monomer grafted films. This allows, on the one hand, an assessment of the copolymerization kinetics for an arbitrary ratio of styrene and comonomer in the grafting solution. On the other hand, one can use FTIR spectra of single-monomer grafted films to establish a calibration curve, based on which the
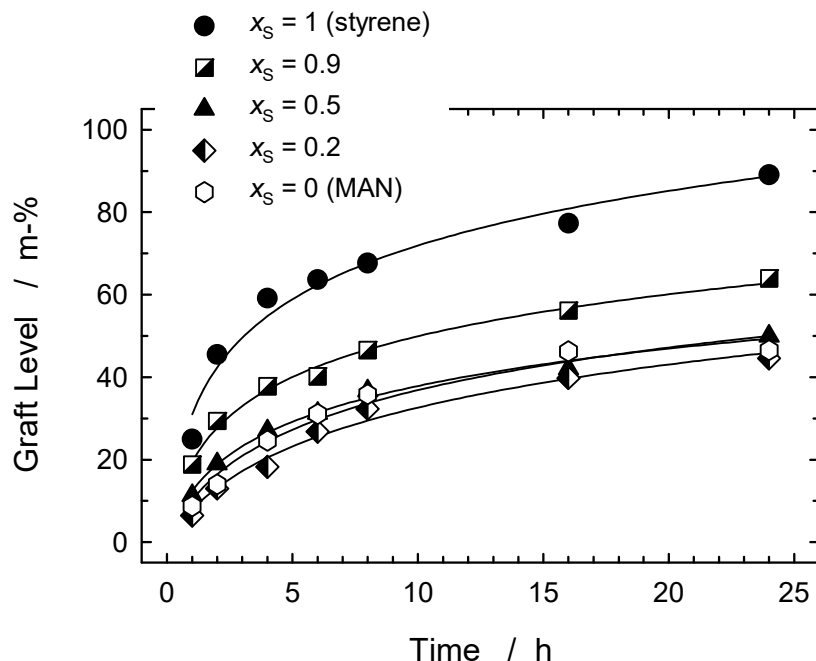
Figure 3-22. Grafting kinetics for the (co-)grafting of styrene and MAN into 25 μm ETFE base film. Pre-irradiation dose: 1.5 kGy. x_S: styrene molar fraction in the monomer mixture ($x_{MAN} = 1 - x_S$). Composition of grafting solution: 20 v-% monomer, 70 v-% isopropanol, 10 v-% H_2O.

content of styrene and comonomer in the grafts can be determined (cf. Chapter II). In practice, however, the grafting kinetics of AN are rather poor (see below).

A series of co-grafting experiments of styrene and MAN at different monomer ratios were performed for a range of reaction times to establish the grafting kinetics (**Figure 3-22**). The increase in graft level as a function of time follows a logarithmic dependence, which is typical for monomers that polymerize rapidly and without a pronounced "front mechanism" [190, 279]. The highest grafting rate is observed with styrene as the only monomer ($x_S = 1$). An increase in MAN molar fraction is associated with a decreasing grafting rate except for $x_S = 0$ (grafting of pure MAN), which showed a slightly higher grafting rate than the reaction mixture with $x_S = 0.2$.
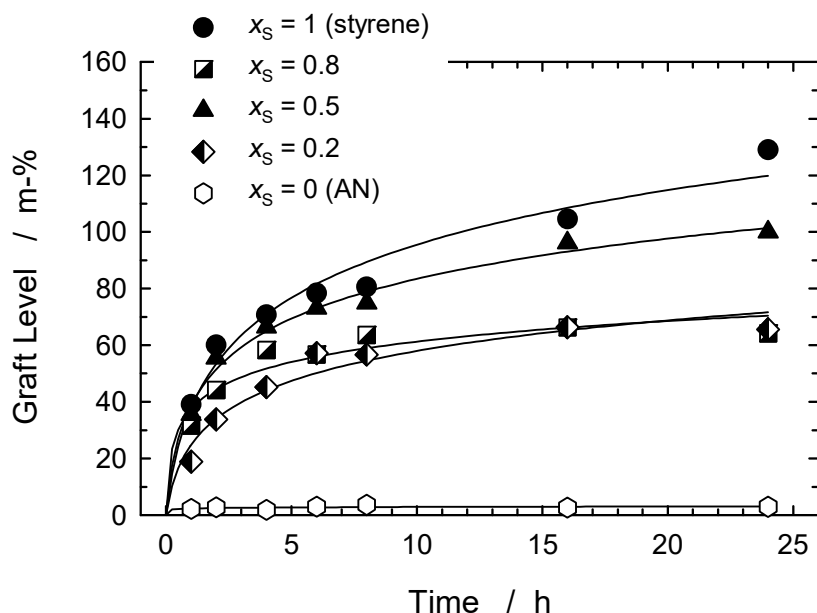
Figure 3-23. Grafting kinetics for the (co-)grafting of styrene and AN into 25 μm ETFE base film with a styrene molar fraction in the monomer mixture of x_S ($x_{AN} = 1 - x_S$). Pre-irradiation dose: 3 kGy. Composition of grafting solution: cf. Figure 3-22.

Significant differences in grafting rate can be observed for films grafted with $x_S = 1$ and 0.9. This may indicate that a small amount of MAN can create substantial difference in the diffusion of the monomers into the ETFE matrix being grafted. It has to be mentioned at this point that the mass based graft level is somewhat misleading for a system containing more than one monomer, since it neglects the fact that the incorporated monomers do not have the same molar mass. The difference between the mole based graft level of pure styrene and pure MAN is found to be less pronounced than in the case of the mass based graft level. This emphasizes that the grafting rate of styrene is indeed higher than that of MAN. Besides the compatibility of the monomer and the base film, the polymerization kinetics is also expected to play a role in the grafting procedure. The propagation rate constants for the polymerization of styrene and MAN in bulk at 60°C are 187 M^{-1}s^{-1} and

55 M^{-1}s^{-1}, respectively [412]. Therefore, it is not surprising that styrene shows a higher grafting rate than MAN. Furthermore, the solvent can also affect the grafting rate [190].

The co-grafting kinetics of styrene and AN are qualitatively similar (**Figure 3-23**), except that the grafting kinetics of pure AN is very poor, the maximum graft level obtained was only 3.6 %. This may appear a bit surprising considering the fact that the propagation rate constant for the polymerization of AN is 1'960 M^{-1}s^{-1} (60°C) [413], which is much higher than that of styrene. The low graft level of AN is a consequence of the incompatability between the monomer and its polymer. Since poly-AN (PAN) is insoluble in its monomer [36, 414], the diffusion of AN into the PAN grafted ETFE is limited. It has been shown, however, that AN can be grafted very well onto polypropylene fibers, where the AN does not need to diffuse into the polymer [49].
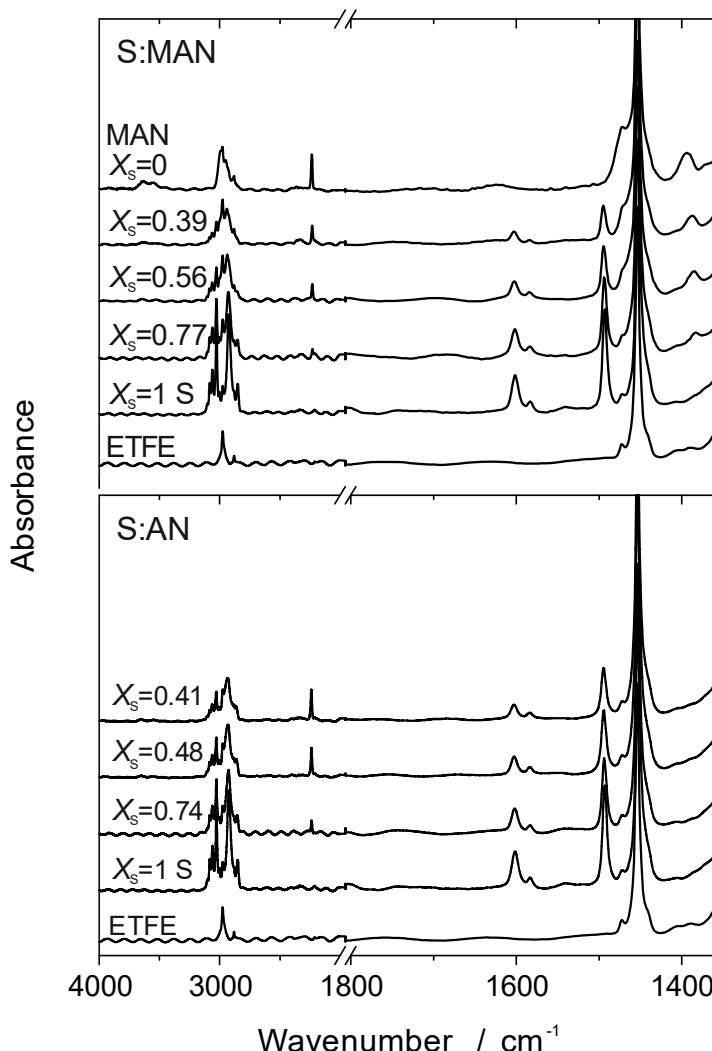
Figure 3-24. Transmission FTIR spectra of S:MAN and S:AN co-grafted films with a fixed graft level of ~40 %. X_S indicates the molar fraction of styrene in the graft component ($X_{(M)AN} = 1 - X_S$), determined based on the on the peak integration method and established calibration curves (cf. Chapter II).

FTIR spectroscopic analysis of the grafted films was performed to characterize the composition of the materials in qualitative and quantitative terms. Spectra of selected grafted films with a constant graft level of 40 % are shown in **Figure 3-24**. At this graft level, a styrene:(M)AN co-grafted and sulfonated membrane with a molar ratio of styrene and co-monomer of 1:1 in the grafts ($X_S = 0.5$) exhibits an ion exchange capacity (IEC) of around 1.5 mmol/g, which is a suitable and balanced IEC for a fuel cell membrane [197]. The spectra contain typical vibrational bands characteristic of ETFE in the 1480-1430 cm^{-1} region (cf. **Table 3-8**). One can see that that vibrational bands associated with styrene increase with the styrene molar fraction in the grafting solution, whereas those associated with the comonomer decrease, and vice-versa. For instance, the band at 1'493 cm^{-1} corresponds to the aromatic ring-stretching vibrations. The characteristic band for MAN and AN is the C≡N stretching vibration around 2234-2241 cm^{-1}, which is largely undisturbed by neighboring bands. These two vibrational bands are used for quantification of the composition of the grafted films (for details, cf. Chapter II). In the case of the presence of grafted MAN, an additional small peak around 1390 cm^{-1} is observed, which is associated with the symmetric CH$_3$ ("umbrella") deformation vibration of the α-methyl group.

Table 3-8. Relevant vibrational bands in FTIR spectra of base film, grafted film and membrane. Source: [415]

Wavenumber (cm^{-1})	Vibration	Group / compound	Strength*
1'388	δ(CH$_3$)	α-CH$_3$ of MAN ("umbrella")	m
1'412	ν(C-Car)[a]	sulfonated styrene	m
1'450	δ(CH$_2$)	ETFE	s
1'493	ν(C-Car)	styrene	s
1'580	ν(C-Car)	styrene	w
1'605	ν(C-Car)	styrene	m
1'637	δ(HOH)	water	s
1'671	ν(C=O) CONH$_2$	hydrolyzed nitrile	w-s[b]
1'700	ν(C=O) COOH dimer	hydrolyzed nitrile	w-s[b]
1'720	ν(C=O) COOH	hydrolyzed nitrile	w-s[b]
2'230	ν(C≡N)	nitrile in (M)AN	m
2'810-3'150	ν(C-H)	various	s
3'000-3'800	ν(O-H)	water, sulfonic acid	s

* w = weak, m = moderate, s = strong, vs = very strong
[a] *para*-disubstituted benzene
[b] depending on compound and extent of hydrolysis

Using the FTIR data and the calibration curves established based on single-monomer grafted films, the composition of all co-grafted films was determined. A possible concern is the creation of a composition drift with increasing reaction time, because the ratio of the monomers may change with time at the location of grafting, either as a result of a change in the monomer concentration in the bulk grafting solution due to depletion, or because the diffusion rates of the monomers may change with the advancing grafting front moving deeper into the base polymer, or

both. In the two grafting systems investigated here, however, a negligible change of composition was observed with increasing graft level [317], which suggests that the composition of the reaction mixture at the location where graft copolymerization takes place does not change significantly over time. The monomer excess in the grafting solution is at least a factor of several hundred, which minimizes monomer depletion effects.
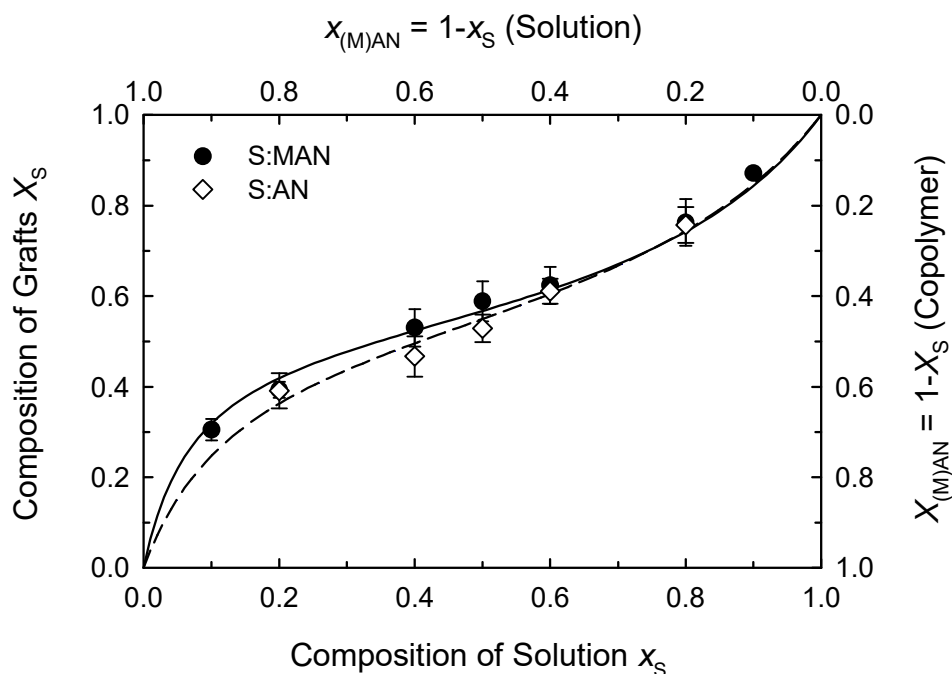
Figure 3-25. Copolymerization diagram for the co-grafting of S:MAN and S:AN. x_S and X_S are the molar fraction of styrene in the monomer feed and the grafted copolymer, respectively. Films with a graft level of approximately 40 % were selected. Reactivity ratios are determined (Table 3-9) from the non-linear least squares (NLLS) fit of the copolymerization equation.

The Mayo-Lewis copolymerization model [392] was subsequently applied to styrene:MAN and styrene:AN co-grafted films to determine the reactivity ratios for styrene and the comonomer for the two systems. For this analysis, the composition of grafted films with a graft level of around 40 % was plotted versus the composition of the reaction mixture in a copolymerization diagram (**Figure 3-25**). It can be seen that the grafting behavior of S:MAN and S:AN is rather similar. The reactivity ratios were calculated based on a non-linear least-squares (NLLS) fit of the copolymerization equation (Eq. 3-10) to the data points. The slight difference in the fitted curves is reflected in the reactivity ratios (**Table 3-9**). For both combinations of monomers, the reactivity ratios are lower than unity, indicating that the grafting of styrene:MAN and styrene:AN into ETFE shows a tendency of alternating chain formation, which is in agreement with data reported in literature. Under similar polymerization conditions, the reactivity ratios obtained from different research groups are largely in agreement. The most obvious difference in the reactivity ratios is

found between grafted S:AN copolymer and bulk S:AN copolymerization. This may be a result, as highlighted earlier, of the difficulty of AN to swell an AN-rich graft component.

Table 3-9. Comparison of reactivity ratios for styrene and (M)AN determined in this study with values reported in the literature.

System	Copolymerization conditions	r_S	$r_{(M)AN}$	Ref.
S:AN	grafting into ETFE (60ºC)	0.52 ± 0.06	0.25 ± 0.05	this study
	grafting into PET	0.05	0.04	[400]
	bulk (60ºC)	0.40 ± 0.05	0.04 ± 0.04	[416]
	bulk (60ºC)	0.41 ± 0.08	0.04 ± 0.04	[417]
	bulk (70ºC)	0.41	0.04	[418]
S:MAN	grafting into ETFE (60ºC)	0.50 ± 0.06	0.14 ± 0.03	this study
	bulk (80ºC)	0.25 ± 0.02	0.25 ± 0.02	[389]
	in benzene solution (60ºC)	0.30 ± 0.10	0.16 ± 0.06	[419]
	in toluene solution (60ºC)	0.39 ± 0.07	0.32 ± 0.05	[420]
	in benzyl alcohol solution (60ºC)	0.40 ± 0.02	0.32 ± 0.05	[421]
	bulk (60ºC)	0.3	0.27	[422]

3.3 Ex Situ Membrane Characterization

The introduction of the sulfonic acid group through sulfonation turns the film into an ion exchange membrane, which can absorb water and conduct protons within the aqueous domains in its structure. Although the membranes were exchanged into potassium form and analyzed in nominally dry state, water is still present in the membrane, especially in the first hydration shell, which is strongly bound to the sulfonate groups. The O-H stretching band of water (3'000-3'700 cm^{-1}) and H-O-H scissor vibration (around 1640 cm^{-1}) are clearly visible in the spectra of the membranes (**Figure 3-26**). The presence of the sulfonic acid group leads to the appearance of characteristic vibrational bands. Unfortunately, the vibrations around 1'010 cm^{-1} and 1'040 cm^{-1} (**Table 3-5**) are not visible due to overlap with the ETFE peak. The peak at 1'412 cm^{-1} can be associated with the C-C vibration of the *para*-disubstituted aromatic ring. For S:MAN co-grafted membranes with high MAN content and S:AN co-grafted membranes an increase in intensity around 1700 cm^{-1} is observed, which is attributed to the presence of carbonyl groups (**Table 3-8**). The nitrile groups undergo hydrolysis under the conditions of the sulfonation procedure. The extent of hydrolysis correlates with the intensity of the C=O vibration. Its intensity is most pronounced in case of the MAN-only grafted membrane. In fact, the broad peak can be deconvoluted into several peaks centered around 1'720, 1'700 and 1'670 cm^{-1} associated with the C=O stretch vibration of carboxylic acid, carboxylic acid dimer and amide, respectively, which are hydrolysis products of the nitrile:

(3-25)

nitrile   amide   carboxylic acid
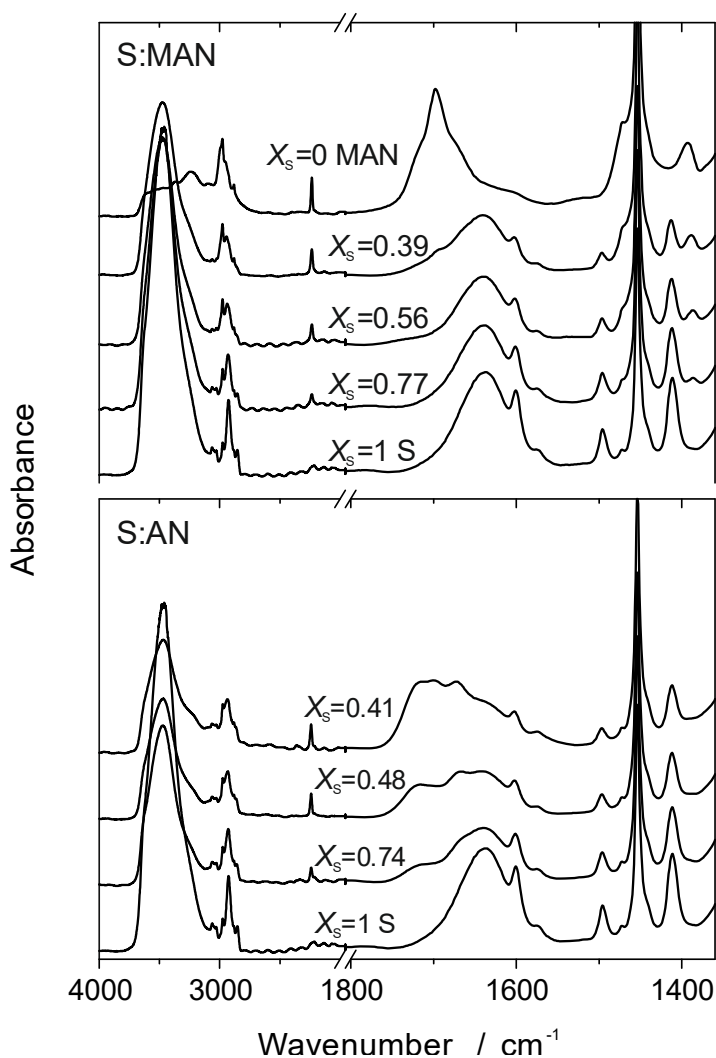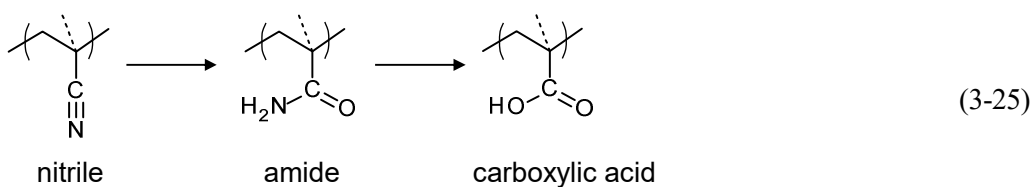
Figure 3-26. Transmission FTIR spectra of S:MAN and S:AN co-grafted membranes (graft level ~40 %). Nominally dry membranes in salt (K^+) form. X_S indicates the molar fraction of styrene in the graft component.

The peak of the $C \equiv N$ stretch vibration around 2'235 cm^{-1} is still visible in all membranes containing MAN or AN, indicating that the hydrolysis of the nitrile groups is only partial. The degree of hydrolysis in the MAN-only grafted film is estimated, based on an FTIR analysis method, to be 46 ± 11 % [423]. For S:MAN co-grafted membranes, a signature of hydrolysis is only visible for the membrane with the highest MAN content ($X_S = 0.39$). For this membrane, the estimated degree of hydrolysis is below 10 %. All membranes with higher styrene content show no signs of hydrolysis. In contrast, all S:AN co-grafted films appear to have undergone hydrolysis.

The extent of hydrolysis was calculated independently using FTIR and elemental analysis [317]. The estimate based on the quantification of the FTIR spectra is associated with rather high uncertainty of approximately 20%. With both methods an increase in the degree of hydrolysis with increase in the AN content in the grafts is obtained, ranging from 10-20 % ($X_S = 0.74$) to 30-45 % ($X_S = 0.41$).

Overall, S:AN co-grafted membranes showed a much higher degree of hydrolysis compared to S:MAN co-grafted membranes. This suggests that the presence of the α-methyl group in MAN significantly decreases the susceptibility to hydrolysis. The methyl substituent is more electron donating compared to a hydrogen, thereby making the carbon of the nitrile less reactive toward nucleophilic attack by the water molecule compared to that of AN. The inductive effect of the α-methyl group is also evidenced by the position of the nitrile peak in the FTIR spectra. The peak of the $\nu(C{\equiv}N)$ vibrational band of MAN and AN was observed at 2'234 cm^{-1} and 2'241 cm^{-1}, respectively. This implies that the C≡N bond of AN is stronger than that of MAN. The electron donating effect of the α-methyl group reduces the C≡N bond strength, resulting in a red-shift of 7 cm^{-1}.

The series of co-grafted membranes was characterized for their fuel cell relevant properties, namely ion exchange capacity (IEC), water uptake and conductivity. The latter two properties were measured on liquid water equilibrated samples at room temperature. The IEC values of S:MAN and S:AN co-grafted membranes with a constant graft level of around 40 % are plotted in **Figure 3-27**. It is observed that, for both membrane series, the IEC increases with the molar fraction of styrene in the grafts X_S. The values follow the calculated theoretical value, assuming that each styrene unit carries one sulfonic acid group. The average degree of sulfonation was above 95 % for both S:MAN and S:AN co-grafted membranes, indicating a nearly complete sulfonation.

The water uptake values of S:MAN and S:AN co-grafted membranes are plotted and compared in **Figure 3-28**. There is no significant difference in the swelling of the two membranes types. The same is found also for the conductivity data. The carboxylic acid in the hydrolyzed AN units apparently does not contribute to the proton conductivity, because the acid strength is too weak (pK$_a$ ~4) compared to the pH in the membrane (pH <1). For comparison, the water uptake of Nafion® 212 is around 40 % and the conductivity between 90 and 100 mS/cm.
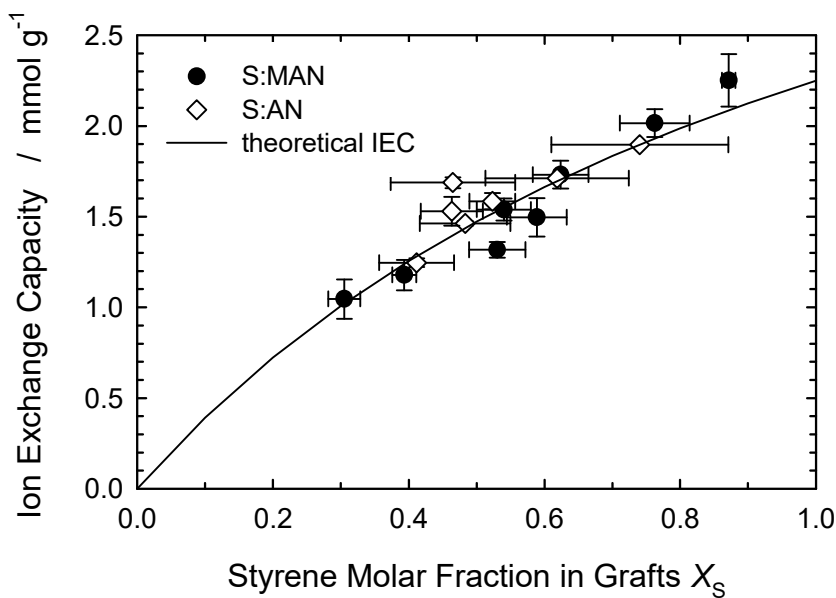
Figure 3-27. Ion exchange capacity (IEC) of the two types of co-grafted membrane with fixed graft level of ~40 %. The theoretical IEC is calculated assuming a graft level of 40 % and 100 % degree of sulfonation of the styrene unit (Chapter II, Eq. 2-6).
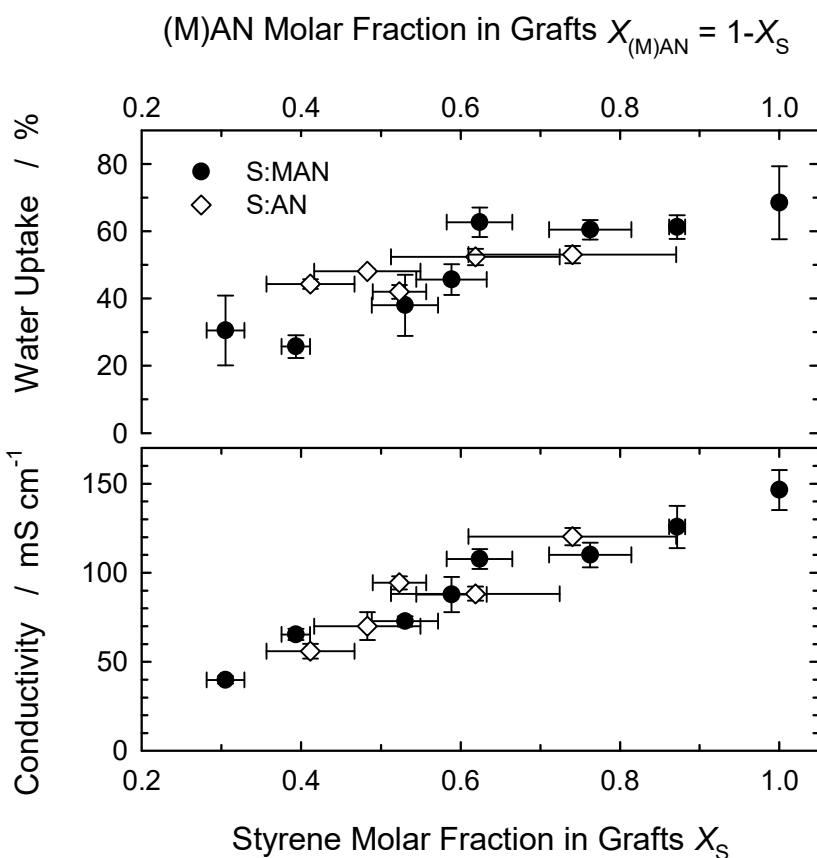
Figure 3-28. *Ex situ* fuel cell relevant properties of co-grafted membranes (graft level ~40 %) measured in liquid water equilibrated state at room temperature. Conductivity was measured through-plane (cf. Chapter II).
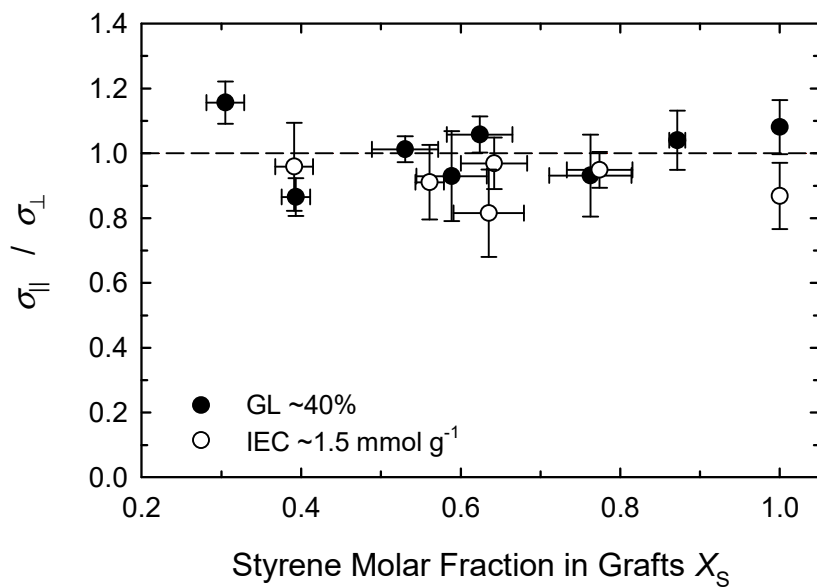
Figure 3-29. Ratio between in-plane ($\sigma_\parallel$) and through-plane ($\sigma_\perp$) conductivity for S:MAN co-grafted membranes of constant graft level of 40 % and constant IEC of ~1.5 mmol/g, respectively. Measurements performed with liquid water equilibrated samples at room temperature. The dashed line indicates isotropic conditions.

In radiation grafted membranes, there is always the concern that through-plane conductivity is different from in-plane conductivity, owing to the potential presence of a gradient in the degree of grafting across the thickness of the film, which could result from a pronounced "grafting front" mechanism [327]. Therefore, the through-plane conductivity was compared to the in-plane conductivity measured in the same membranes. The ratio of the two values (**Figure 3-29**) is close to one, indicating that the proton conductivity is isotropic. If anything, the through-plane conductivity would be expected to be lower than the in-plane conductivity. This is not the case, except maybe for the data point at 40 % graft level at low styrene molar fraction, which could indicate that in this case grafting fronts may exist to some extent in the membrane.

The conductivity values discussed so far were recorded at room temperature in the water swollen state. To mimic conditions in the fuel cell, experiments at elevated temperature (70°C) and varying relative humidity were carried out. In this case, only in-plane conductivity measurements could be carried out, because an equipment to measure through-plane conductivity at different relative humidities was not available in the laboratory. A series of S:MAN con-grafted membranes with a fixed IEC yet varying styrene molar fraction in the grafts was characterized in this manner (**Figure 3-30**). Therefore, the membranes had different graft levels ranging from 23 % ($X_S = 1$) to 61 % ($X_S = 0.39$). At high humidity, these membranes displayed a similar conductivity of around 0.1 S/cm, which is also similar to the conductivity of Nafion® 212. However, compared to Nafion® the grafted membranes displayed a more pronounced drop in conductivity towards lower relative humidities. Furthermore, it appears that the higher the MAN content the more pronounced

the drop is. This finding was surprising initially, since it was rather expected that the incorporation of the polar MAN comonomer could promote conductivity under dry conditions. The differences in the proton conductivity between Nafion® and grafted membranes may be rationalized in terms of the differences in the acid strength (pKa) [424]. Yet other factors have to be responsible for the difference among the grafted membranes. Incorporation of a comonomer may lead to differences in polymer conformation. It may speculated that the presence of MAN results in a greater separation between the protogenic (sulfonic acid) sites. Paddison provided theoretical evidence that the proton dissociation in PFSA ionomers also depends on chain conformation and the distance between neighboring sulfonic acid groups. A close proximity of the sulfonic acid groups allows stronger interaction by electrostatic forces, hence, larger and purer ionic aggregates can be formed [425]. According to Tsang et al., larger ionic aggregates favor proton conductivity and inhibit membrane swelling [426].
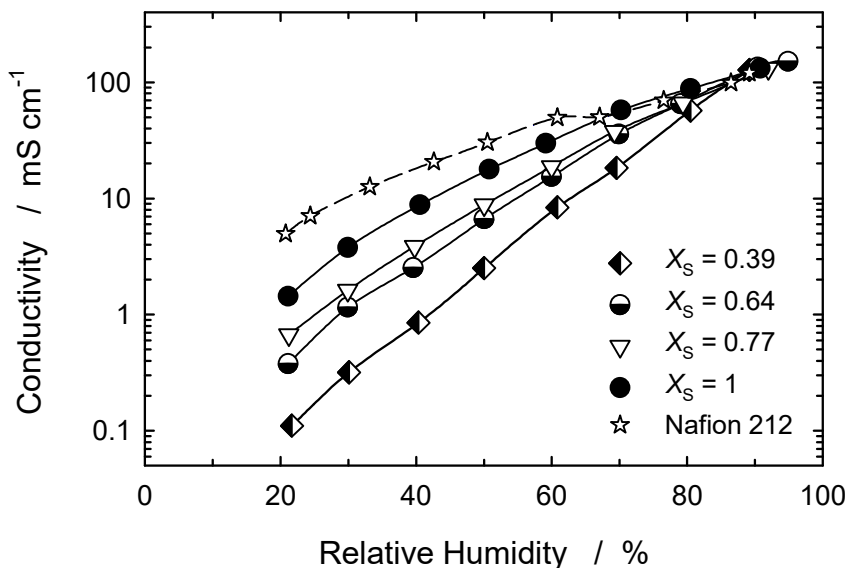
Figure 3-30. Conductivity as a function of relative humidity of S:MAN co-grafted membranes with constant IEC of ~1.5 mmol/g and varying composition of the grafts and Nafion 212 measured at 70°C (in-plane 4-point probe configuration).

In an attempt to correlate conductivity data to morphological features of the membranes on the sub-micron scale, which are a result of the semi-crystalline nature and the phase separated nature of the polymer, small-angle x-ray scattering (SAXS) experiments were carried out on Cs^+-exchanged, dry membranes. In this case the morphology of the polymer is representative of the morphology at low relative humidity, where there is little sorption of water [427]. A characteristic feature in the SAXS spectrum of ionomer membranes is the so-called ionomer peak. Its position and intensity are related to the membrane structure. The presence of a single scattering peak without higher-order interference peaks implies that the ion-rich clusters lack long range ordering and are randomly distributed within the volume of the membrane with a fluid-like arrangement.

Therefore, the use of a hard-sphere fluid structural model suggests itself to describe the morphology [427]. The ionic domains are of a certain size and have a characteristic distance. The analysis of the scattering spectra of the membranes with different composition of the grafts shows that i) the distance between neighboring ion-rich aggregates and ii) their size decreases with increasing styrene content in the grafts (**Figure 3-31**). This results in a more effective percolation, which entails a better connectivity between the ionic clusters and therefore higher proton conductivity [317].
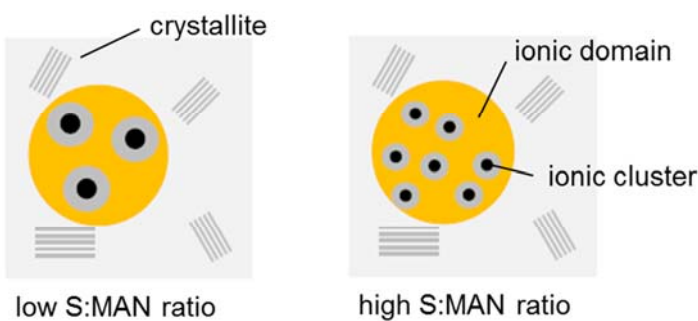
Figure 3-31. Schematic representation for the spatial arrangement of ionic aggregates in dry membranes prepared by radiation grafting based on a hard-sphere fluid structural model. The size and density of ionic aggregates is determined by the molar ratio of co-monomers (styrene and MAN) in the grafts rather than the IEC. Illustration adapted from [317].

3.4 Fuel Cell Tests

For the characterization of S:MAN co-grafted membranes in the single fuel cell, one is interested in probing the effect of different ratios of styrene and MAN in the graft component. It is therefore conceivable to prepare and test membranes with a constant graft level of, say, 40 %. This implies, however, that the membranes with different contents of styrene and MAN in the grafts, characterized by the molar fraction of styrene X_S, where $X_{MAN} = 1 - X_S$, have different IECs (**Figure 3-27**) and thus different conductivities (**Figure 3-28**). It was therefore deemed more appropriate for a fair comparison to prepare membranes with a constant IEC of around 1.5 mmol/g. Potential effects of the presence of MAN can thus be probed, in analogy to the conductivity measurements as a function of relative humidity reported in the previous section. Three co-grafted membranes with different styrene to MAN ratio and a styrene-only grafted membrane were tested in the single cell. Nafion® 212 served as a benchmark for comparison (**Figure 3-32**). It is found that all the cells show comparable performance, which can be understood based on the almost identical conductivity at high levels of hydration (**Figure 3-30**). The thickness of the membranes is not markedly different to cause large differences in area resistance. The membrane with a S:MAN molar ratio of around 1:1 ($X_S = 0.56$) shows the best

performance, which is slightly superior to that of Nafion® 212. On the whole, however, there is no recognizable trend regarding the grafted membranes. For a more detailed analysis, impedance spectra at a current density of 0.5 A·cm^{-2} were recorded and the ohmic and polarization resistance were extracted from the obtained spectra (**Table 3-10**). In the MEA configuration in these experiments, i.e. with commercial gas diffusion electrodes laminated (hot-pressed) with the membrane, the comparison of the polarization resistance yields insights into the quality of the membrane-electrode interface [195]. Again, there are no clear trends except maybe that the polarization resistance is somewhat higher for the membranes with higher styrene content.
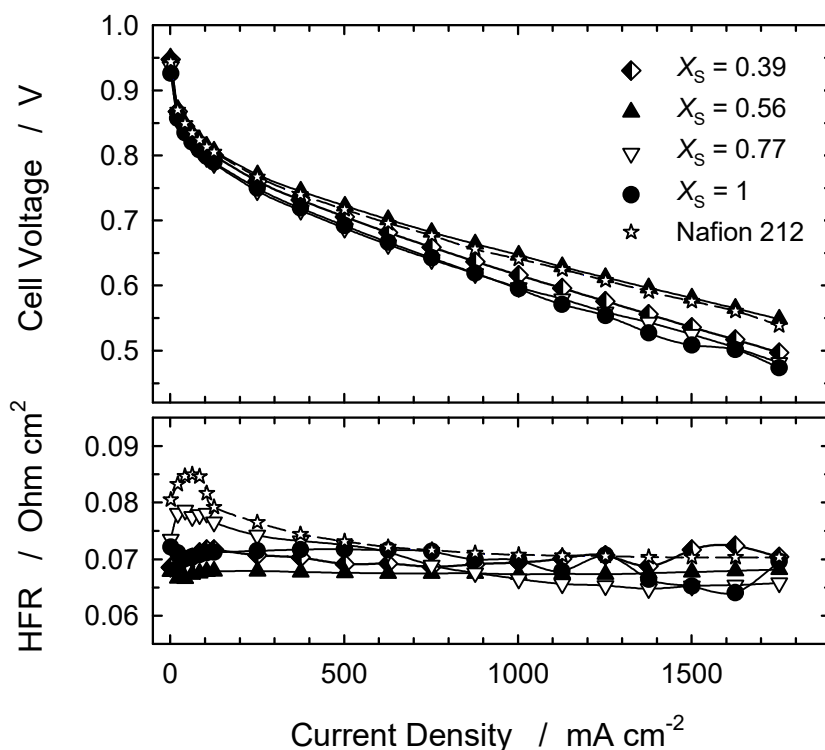
Figure 3-32. Polarization curves and high frequency resistance (HFR) at 1 kHz of MEAs based on S:MAN co-grafted membranes (IEC ~1.5 mmol/g, varying composition of grafts) and Nafion 212. Electrodes: carbon paper type (Johnson Matthey Fuel Cells ELE0162) with 0.4 mgPt cm^{-2}. Temperature: 80°C, H$_2$/O$_2$ stoichiometry: 1.5/2.0, humidifier temperature: 80°C, ambient pressure.

The experiments also involved the measurement of the hydrogen crossover, which was found to be notably lower for the grafted membranes compared to Nafion® 212, despite the lower thickness. It is known that PFSA type membranes have a rather high permeability for hydrogen and oxygen, which is a drawback of this type of polymer, since reactant crossover is linked to the formation of reactive intermediates, which attack the membrane and cause chemical degradation of the ionomer [428]. Hydrocarbon membranes of the polyaromatic type and radiation grafted membranes generally show better gas barrier properties. Therefore, even if the intrinsic chemical stability of these membranes may be lower than that of PFSA membranes, they may show an

enhanced lifetime in an accelerated chemical degradation test under open circuit voltage (OCV) conditions [141, 320].

Table 3-10. Parameters obtained from cell tests using various co-grafted membranes with constant IEC of ~1.5 mmol/g (cf. Figure 3-32) and Nafion 212. Cell voltage (U_{cell}), ohmic resistance (R_Ω), polarization resistance (R_p) measured at a current density of 0.5 A·cm^{-2}. The hydrogen crossover i_x is measured in H$_2$/N$_2$ configuration (cf. Chapter II).

Membrane	X_S	t (wet) (µm)	U_{cell} (mV)	R_Ω[a] (mΩ·cm^2)	R_p[a] (mΩ·cm^2)	i_x (mA·cm^{-2})
g-S:MAN	0.39 ± 0.02	45 ± 2	706	56	147	0.19
g-S:MAN	0.56 ± 0.02	41 ± 1	723	56	130	0.27
g-S:MAN	0.64 ± 0.04	40 ± 2	708	54	152	0.30
g-S:MAN	0.77 ± 0.04	39 ± 1	688	55	187	0.29
g-S	1	37 ± 1	692	56	185	0.37
Nafion 212	-	64 ± 1	717	59	146	0.64

[a] determined from AC impedance spectra.

The membrane type discussed in this section consists of ETFE with grafted styrene:MAN and styrene:AN moieties. It is therefore of interest to investigate whether there are differences in membrane properties and performance characteristics when tested in the single cell. Despite the notable difference in the extent of nitrile hydrolysis (**Figure 3-26**), the *ex situ* properties of the two types of membrane are quite similar (**Figure 3-27**, **Figure 3-28**). Fuel cell experiments using styrene: MAN and styrene:AN co-grafted membranes ($X_S \cong 0.6$, $Y \cong 40\%$) were performed for comparison. The MEA based on the styrene:MAN co-grafted membrane shows comparable performance to that of the Nafion® 212 membrane (**Figure 3-33**), which is in agreement with the results presented above (**Figure 3-32**). The polarization curves were recorded after 24 h of conditioning at a current density of 0.5 A·cm^{-2}. However, the MEA based on the styrene:AN co-grafted membrane showed markedly lower performance. The more pronounced increase in the HFR during cell conditioning compared to that of the styrene:MAN membrane suggests degradation of the styrene:AN membrane. One may speculate that the presence of hydrolyzed products affects fuel cell performance. What is striking is that the hydrogen crossover of the AN containing membranes is much higher than that of the MAN containing membrane. It will be shown later in Chapter IV that initially the two types of membrane show the same hydrogen crossover rate. It is therefore hypothesized that the gradual hydrolysis of the AN led to a loss of the barrier properties, which resulted in an increase in gas crossover and, therefore, a more pronounced chemical degradation of the membrane.
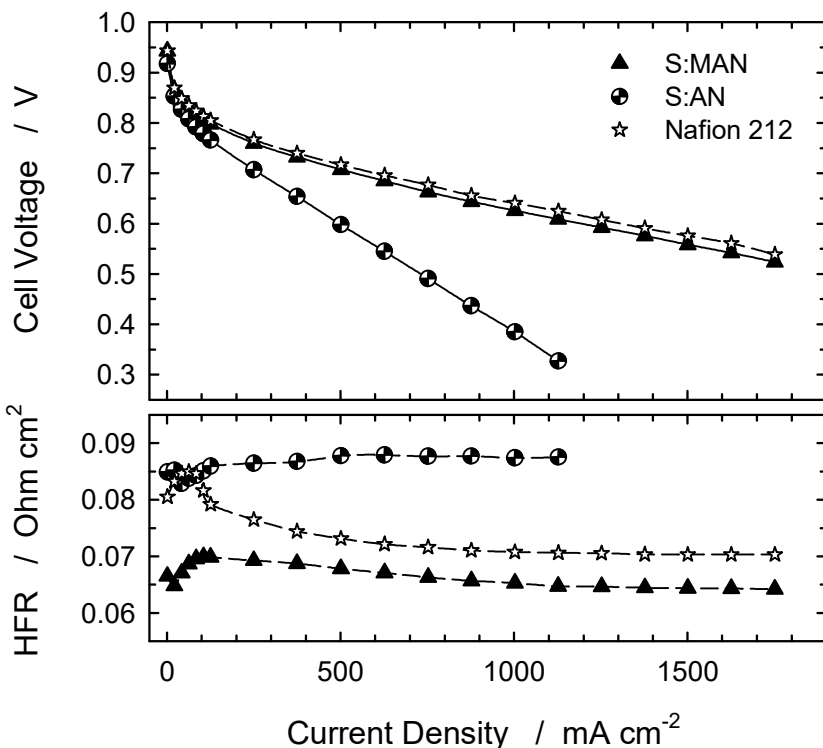
Figure 3-33. Fuel cell performance of MEAs based on S:MAN and S:AN co-grafted membranes (graft level ~40 %, X_S ~0.6) and Nafion 212. Cell temperature: 80°C, H_2/O_2 stoichiometry: 1.5/2.0, humidifier temperature: 80°C, ambient pressure.

For a more in-depth analysis of the performance loss, AC impedance spectroscopy was performed at 0.5 mA·cm^{-2} (**Table 3-11**). The interfacial resistances (polarization resistance, R_p) obtained from the impedance spectra were comparable for the MEAs based on styrene:MAN and Nafion® 212, whereas a much higher value was measured in case of the styrene:AN co-grafted membrane. In addition, the ohmic resistance (R_Ω) of the styrene:AN membrane is somewhat higher than that of the other two membranes. The increased ohmic polarization resistance may well be a consequence of a more pronounced membrane degradation, which is in qualitative agreement with earlier findings on long-term tests of grafted membranes [195].

Table 3-11. MEA performance characteristics of styrene:MAN and styrene:AN cografted membranes (for details see caption of Figure 3-33) and Nafion® 212 after conditioning for 24 h. The ohmic resistance (R_Ω) and polarization resistance (R_p) were obtained from AC impedance spectra recorded at 0.5 A·cm^{-2}. The hydrogen crossover i_x is measured in H_2/N_2 configuration (cf. Chapter II).

Membrane	X_S	U_{cell} (mV)	R_Ω (mΩ·cm^2)	R_p (mΩ·cm^2)	i_x (mA·cm^{-2})
g-S:MAN	0.62 ± 0.04	708	54	133	0.24
g-S:AN	0.62 ± 0.11	598	67	534	0.45
Nafion 212	-	717	59	146	0.64

It appears that the styrene:MAN co-grafted membranes hold some promise for improved stability under fuel cell operating conditions, owing to the improved gas barrier properties, knowing that gas crossover is a key driver for the chemical degradation of membranes (cf. Chapter IV). Therefore, long-term fuel cell testing using two types of styrene:MAN co-grafted membrane was performed. As a reference, a styrene-only grafted membrane was used. The cells were operated at a constant current density of 0.5 A·cm^{-2} (**Figure 3-34**).
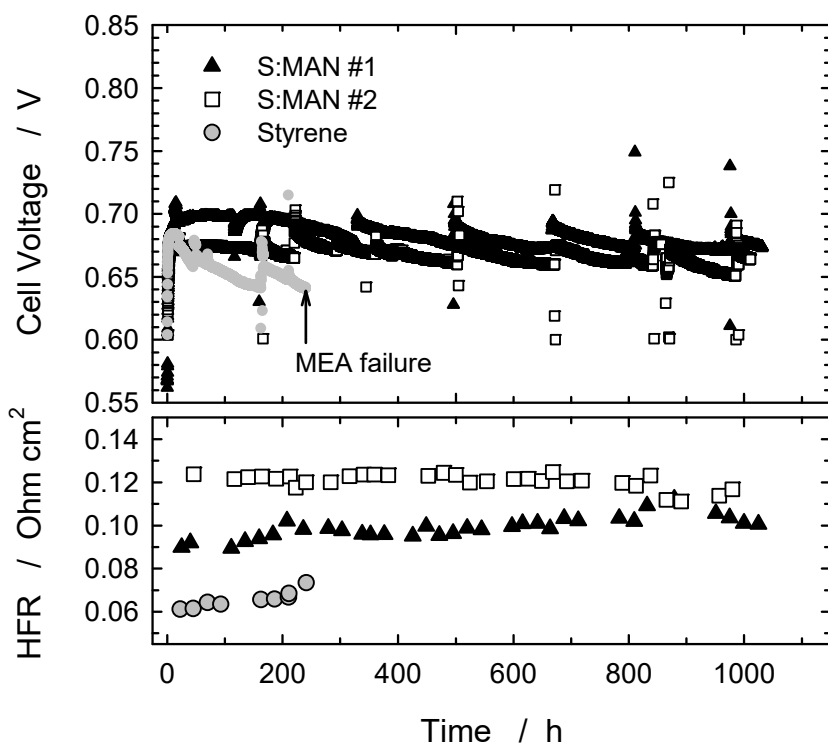
Figure 3-34. Single cell durability tests at a constant current density of 0.5 A·cm^{-2} using S:MAN co-grafted (graft level: 27 %) and styrene-only grafted (graft level: 21 %, IEC = 1.46 mmol/g) membranes. Membrane #1: IEC = 1.35 ± 0.07 mmol/g (x_S = 0.5); membrane #2: IEC = 1.14 ± 0.02 mmol/g (x_S = 0.2). Cell temperature: 80°C, H$_2$/O$_2$ stoichiometry: 1.5/1.5, humidifier temperature: 80°C, ambient pressure.

The two styrene:MAN cografted membranes had a graft level of around 27 %, yet somewhat different IEC owing to the different ratio of styrene and MAN in the grafts. The case of the styrene-only grafted membrane, the cell performance experienced a rapid decay after conditioning, and after 241 h time on test, the experiment was discontinued due to a high gas crossover leak of >10 ml·min^{-1}, indicating membrane failure. Both styrene:MAN co-grafted membranes showed rather steady performance over 1'000 h. The slightly higher performance / lower HFR of membrane #1 is most likely a result of the higher IEC. The cells were shut down after 1'032 h (membrane #1) and 1'009 h (membrane #2), respectively. The hydrogen crossover rates at the end of test were 5.9 and 0.47 mA·cm^{-2}, respectively. In comparison to the values at the beginning of test (0.31 and 0.35 mA·cm^{-2}, respectively), this suggests that membrane #1

experienced considerable chemical degradation, whereas membrane #2 did not. This may be a result of the slightly lower IEC of membrane #2 and / or the higher MAN content in the grafts, which renders the membrane more stable.

In summary, the findings of this section highlight that both MAN and AN can be copolymerized with styrene over a wide compositional range, yielding similar reactivity ratios. The resulting membranes have similar properties, despite the fact that AN undergoes partial hydrolysis during sulfonation, whereby the nitrile is converted to an amide and, eventually, carboxylic acid group. For styrene:MAN co-grafted membranes, the conductivity was measured as a function of relative humidity. Although conductivities were similar at high relative humidity, the membranes with higher MAN content exhibited a more pronounced conductivity loss towards lower relative humidity values. Small-angle x-ray scattering studies suggest that this could be related to a less favourable structure of the ionic domains in co-grafted membranes compared with styrene-only grafted membranes. Fuel cell tests with both styrene:MAN and styrene:AN cografted membranes were carried out. The cell with styrene:AN co-grafted membrane showed notably inferior performance, exhibiting a higher ohmic as well as polarization loss. This is explained by poor interfacial properties in the AN containing membrane, which could be a result of the hydrolysis of the nitrile group to carboxylic acid. Hence, for pratical applications MAN is preferred over AN as comonomer.

All in all, the results demonstrate that styrene:MAN co-grafted membranes have a great potential for membranes with high performance and durability. In comparison to AMS:MAN co-grafted membranes, the styrene:MAN membranes allow the adjustment of the comonomer ratio in the grafts over a wide range of values. Most importantly, though, the grafting kinetics with styrene as primary monomer is much superior to that using AMS as primary monomer. Hence, an improved compliance with an industrial reel-to-reel process can be expected.

4 Membranes with Polymer-Bound Antioxidants

The introduction of antioxidant functionalities represents a further approach to improve the chemical stability of radiation grafted membranes based on grafted styrene or its derivatives, as outlined in the introductory section of this chapter. Knowing that radicals are responsible for membrane degradation in the fuel cells, it appears reasonable to attempt breaking the oxidation chain reaction typically found in hydrocarbon polymers (cf. Chapter IV) using suitable antioxidant compounds embedded in the membrane.
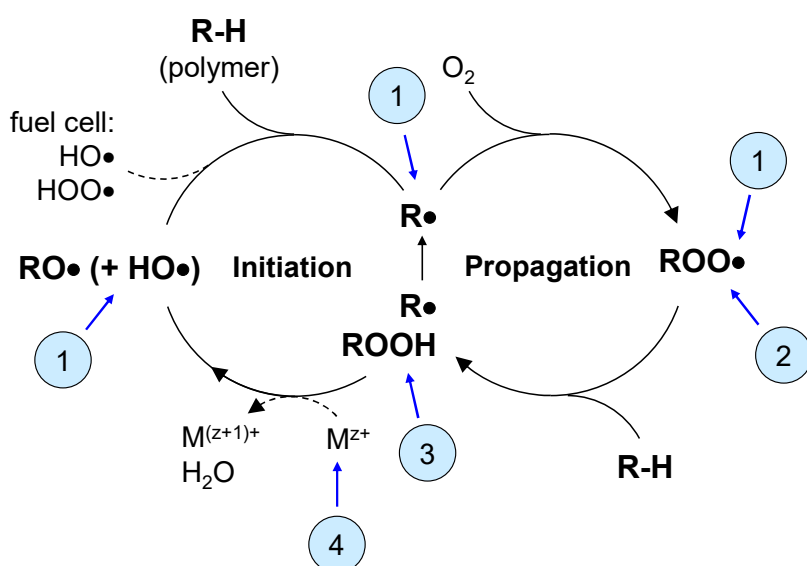
Figure 3-35. Site of action of antioxidants in the autooxidation chain reaction of hydrocarbon polymers (cf. also Chapter IV, Section 2). 1: radical scavengers, 2: hydrogen donors, 3: hydroperoxide decomposers, 4: metal chelating agents (adapted from Grassie & Scott [91] and www.specialchem4adhesives.com).

Successful mitigation of oxidative aging in polymers involves the inhibition of reactions in the autooxidation cycle (**Figure 3-35**). Technical polymer products typically contain additives to protect the material from temperature, oxygen, light, UV or radiation induced degradation. The different classes of antioxidants compounded into polymers exhibit different mechanisms of action [429]:

1. Radical scavengers are antioxidants capable of trapping radicals (e.g. lactones, hydroxylamines), thereby immediately inhibiting the autooxidation cycle.

2. Hydrogen donors react with peroxyl radicals to form hydroperoxides, and prevent the abstraction of hydrogen from the polymer backbone (e.g. phenols, hydroquinones).

3. Hydroperoxide (ROOH) decomposers (e.g. phosphites, sulfides) yield ROH and thereby prevent the formation of the extremely reactive $RO^{\bullet}$ and $HO^{\bullet}$ radicals.

4. Metal chelating agents (e.g. diamines) slow down the transition metal catalyzed hydroperoxide decomposition and concomitant generatation of alkoxyl radicals ($RO^{\bullet}$).

In technical polymers, several antioxidants may be combined (e.g. H-donor and hydroperoxide decomposer), yielding a synergistic effect. In most cases, the antioxidant is consumed during its action. Yet ideally, antioxidants undergo cyclic regeneration, such as compounds containing nitroxyl radical, which can react alternately with alkyl radicals ($R^\bullet$) and peroxyl radicals ($ROO^\bullet$) [429].

In the context of mitigating oxidative degradation of ionomers in fuel cells, a comprehensive antioxidant strategy has thus far not been adopted. One has to keep in mind that approaches successful in stabilizing technical plastic materials cannot be adapted in straightforward manner to proton conducting fuel cell membranes. As an example, the addition of a free radical scavenger (catechin) to sulfonated PEEK membranes even reduced the oxidative stability of the ionomer, because the scavenger underwent chemical interaction with pendant acid groups and shows notable radical-generating quality [430]. Quite often there is a delicate balance between a compound having antioxidant or pro-oxidant properties, which is a phenomenon well-known in biology and medicine [431]. It can be regarded as two sides of the same sword, and which of the two is dominant often depends on the environmental conditions, such as pH or oxygen content.

It is essential to realize that, on the one hand, the fuel cell represents an environment fundamentally different from that found in technical polymers, considering the aqueous constitution of the ionomer (~30% water uptake by weight), elevated temperature (~80°C), high ionic strength (~1 M), low pH (~0), and presence of H_2, O_2 and the Pt catalyst. On the other hand, the fuel cell membrane is constantly bombarded by radicals in the fuel cell [381], suggesting that the use of a regenerative radical deactivation additive is essential. It has been discovered that the incorporation of certain compounds, such as manganese oxide or ceria, or the corresponding transition metal ions, into the membrane leads to a substantial improvement of PFSA membrane chemical stability, measured as a reduction of fluoride emission, in some cases lower by an order of magnitude [168, 169, 432-436]. The presence of a multivalent transition metal ion, which can cycle between two oxidation states, is a key feature of this stabilization mechanism (cf. Chapter IV).

The incorporation of cerium into a styrene-only radiation grafted membrane was performed to examine whether this is also viable approach to stabilize non-PFSA membranes. It was found, however, that there was not a clear reduction of chemical degradation in Ce-doped radiation grafted membranes [437]. This can be understood based on the competition kinetics for the reaction of $HO^\bullet$ with the polymer. In PFSA ionomer, the lifetime of the $HO^\bullet$ radical is relatively high, i.e., around 2 µs, owing to the slow rate of reaction with the polymer [438]. Since the

reaction of HO$^\bullet$ with Ce^{3+} is fast ($3\cdot10^8$ M^{-1}s^{-1}), a concentration equivalent to only 1 % of cerium with respect to the total –SO$_3$H concentration is sufficient to scavenge 90 % of the HO$^\bullet$ radicals, thus providing effective stabilization against ionomer attack. However, in membranes containing aromatic units, such as PSSA, the lifetime of HO$^\bullet$ is expected to be much lower. HO$^\bullet$ reacts very rapidly with aromatic units, mainly by addition, with rate constants of 10^8 M^{-1}s^{-1} and higher (cf. also Chapter IV). In a styrene-only grafted and sulfonated membrane with an ion exchange capacity of 1.5 mmol/g, this leads to a lifetime of HO$^\bullet$ of around 1 ns. This precludes effective scavenging of significant fractions of HO$^\bullet$ by reasonable amounts of cerium in the membrane. In addition, Ce^{4+} may react with PSSA through abstraction of the hydrogen at the α-position, since $E°$(Ce^{4+}/Ce^{3+}) = 1.44 V [439], and $E°$(αC$^\bullet$/αC-H) = 1.1 V [379, 440]. It is conceivable to look for other, more suitable redox pairs with lower redox potential. However, the choice of transition metal redox pairs with suitable redox potential and chemistry is limited. All Fenton active metal ions, such as iron or copper, which catalyze the decomposition of H$_2$O$_2$ to HO$^\bullet$, are disqualified. In addition, the rate constant for the reaction with HO$^\bullet$ is expected to be rather low. Therefore, alternative, more reactive radical scavengers have to be used. Phenolic compounds suggest themselves in this context, as this type of antioxidant reacts very rapidly with HO$^\bullet$. In fact, phenol derivatives are widely used as antioxidants in plastics [441]. Furthermore, using non-ionic additives as antioxidants is not associated with a loss of proton exchange sites, which in the case of cerium has shown to lead to performance loss [169].

In a first attempt, the introduction of small organic molecules with potential antioxidant character into radiation grafted membranes by doping was investigated. For this, styrene-only grafted membranes were immersed in a DMF solution of selected compounds, such as tocopherol and butylated hydroxy toluene (BHT), a class of synthetic antioxidants of the hindered phenol type. After removal of the solvent (DMF), the membranes were tested in single cells using an accelerated stress test protocol. In some experiments, an improvement of stability was seen in the presence of these additives, yet reproducibility was limited [442]. A rather surprising observation was the considerable improvement of fuel cell performance in the presence of BHT or tocopherol compared to the undoped membrane. This performance "boost" is explained by an improved conductivity of the membrane, owing to a plasticizing effect of the small hydrophilic organic additive. Yet the effect faded over time, as the additive was gradually washed out from the membrane. This loss of the additive is also problematic regarding the antioxidant functionality: the stabilizing effect is thus eventually lost.

The approach proposed here is aimed at the incorporation of organic redox couples attached to the polymer. With this concept, it is expected that the stabilizing function can be maintained over time so long as the graft component remains intact. As mentioned previously, aromatic compounds exhibit high rate constants for the reaction with HO[•] [370]. Typical chain-breaking antioxidants of the H-donor type are phenolic compounds. Phenols act as antioxidants because the phenoxyl radical formed upon the reaction with oxygen radicals does not lead to adverse follow-up reactions. The abstraction of a hydrogen atom from the polymer is unlikely due to the low oxidative strength of the phenoxyl radical. A model for a phenol type antioxidant is hydroquinone (**Figure 3-36**). The reaction of hydroquinone with oxygen radicals yields the oxidized product, the quinone, water and hydrogen peroxide. It was stated by Halalay et al. that "if an electronically conducting path is available, the quinones can be converted back into hydroquinones electrochemically at the operating potential of the fuel cell" [443]. Therefore, the concept of using phenolic antioxidants also offers the prospect of a regenerative antioxidant. In addition, the redox potential of phenolic compounds can be modified and adjusted by the appropriate choice of substituents on the ring [444].
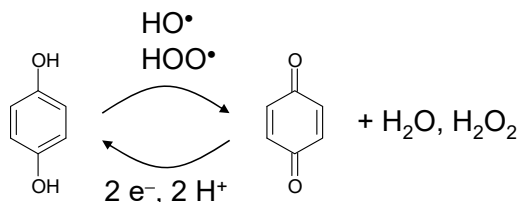
Figure 3-36. (H-donor type) model antioxidant (hydroquinone), mode of action (deactivation of radicals), and general concept for regeneration by reduction. Adapted from [443].

In the concept presented here, the phenol type antioxidant will be covalently attached to the polymer using the method of radiation grafting. Direct introduction of an antioxidant functionality via grafting, such as the co-grafting of styrene and vinylphenol, is unlikely to be successful since the antioxidant is expected to scavenge the radicals in the polymerization reaction. Therefore, the synthesis of polymer-bound antioxidants has to be accomplished via an intermediate step. Two methods have been identified for this (**Figure 3-37**). The first option (A) consists in the use of a precursor monomer, which is co-grafted with styrene to yield the corresponding grafted film. Evidently, the comonomer needs to exhibit favorable copolymerization kinetics with styrene to allow easy adjustment of the composition of the grafts. The styrene units are then sulfonated to introduce the protogenic group, and the comonomer is deprotected to "unveil" the antioxidant functionality. The appropriate sequence of these two reactions needs to be established to maximize yield. As an example, 4-vinylanisole (4-methoxystyrene) or *p-tert*-butoxycarbonyloxy(boc)styrene

could be used as a comonomer, and the protecting group in the co-grafted film subsequently removed to yield the phenol group.
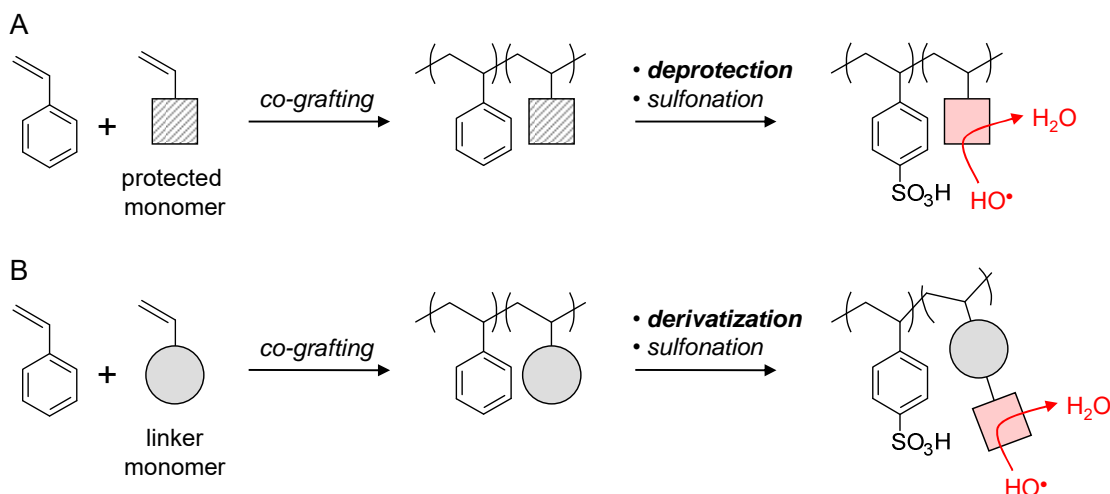
Figure 3-37. Synthetic approaches for the introduction of polymer-bound antioxidants to radiation grafted membranes. A: co-grafting of styrene and comonomer comprising a protected antioxidant functionality. During the final preparation stage, the antioxidant is unlocked by removal of the protective group. B: co-grafting of styrene and a linker comonomer, to which the antioxidant is subsequently attached.

In the second option (B) styrene is co-grafted together with a suitable linker monomer, to which the antioxidant is subsequently attached in a follow-up reaction. Again, the sequence of the post-functionalization reactions of the grafted film, consisting of the sulfonation to introduce proton exchange sites and the derivatization to link the antioxidant to the grafted chain, needs to be well chosen to maximize the yield of functionalization. The linker monomer is characterized in that it contains, in addition to the double bond, a reactive group to attach to it the antioxidant. From a conceptual point of view, the linker can be of a nucleophilic character and the antioxidant of an electrophilic character, or vice-versa. The latter approach appears to be more promising, as there are a number of radically polymerizable monomers with electrophilic groups, such as vinylbenzene chloride (VBC), glycidyl methacrylate (GMA), or acryloyl chloride. Formation of bonds that may undergo hydrolysis during fuel cell operation, such as esters or amides, are to be avoided. Both VBC and GMA are readily available and low-cost monomers that are widely used. In fact, chloromethylated polystyrene is typically used to synthesize anion exchange resins through reaction with amines [445]. Radiation grafted VBC has been used to synthesize anion exchange membranes and phosphonated cation exchange membranes (cf. Chapter I). The (co)polymers of GMA offer a wide range of possible post-polymerization reactions with nucleophilic agents [446]. This can also exploited in graft copolymers of GMA, for instance to produce metal-ion adsorbents [447]. The epoxy group in GMA can be used to perform a range of different derivatization of functionalization reactions, such as sulfonation, phosphonation,

amination, and reaction with H_2S. This can be used, as described in a recent review article by Nasef and Güven, to prepare porous materials for filtration and separation applications with a wide range of different functional groups based on post-treated grafted GMA [51].

4.1 Membrane Synthesis

The membranes prepared in the framework of the study reported here are based on styrene co-grafted with VBC or GMA. Subsequently, tyramine (4-hydroxyphenethylamine), a phenol linked to a C_2 alkyl chain with terminal –NH_2 unit. This amine, a nucleophile, can react with the electrophilic group, benzylchloride or epoxy group, of the linker. Thus the phenol type antioxidant is attached to the grafted chain. Sulfonation yields the final proton conducting membrane (**Figure 3-38**).
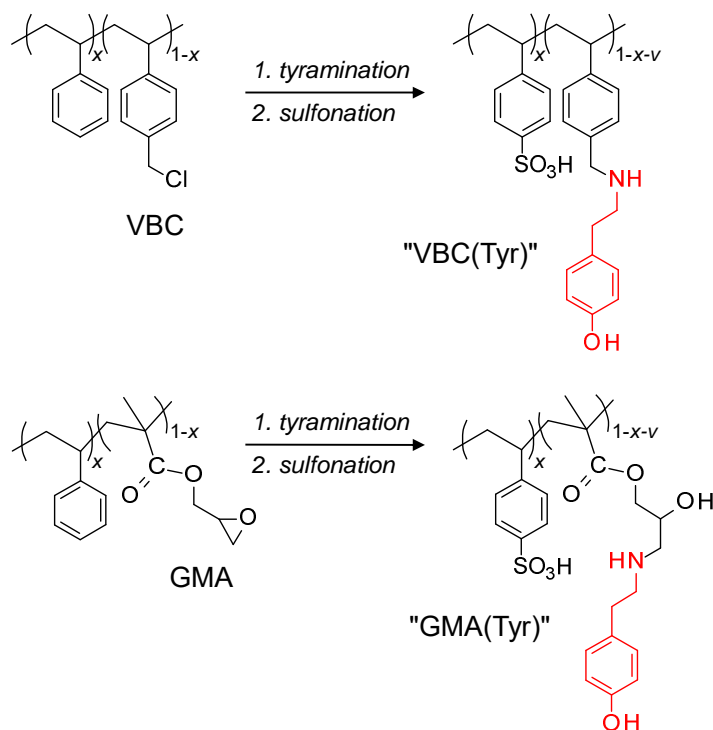
Figure 3-38. Schematic for the preparation of radiation grafted membranes with polymer-bound phenol moiety, which potentially acts as antioxidant. Styrene is co-grafted together with linker co-monomers, here vinylbenzyl chloride (VBC) and glycidyl methacrylate (GMA), where *x* and 1-*x*, respectively, indicate the molar fraction of styrene and comonomer in the grafts, and *v* is the fraction of hydrolysed GMA. Subsequently, tyramine (4-hydroxyphene-thylamine) is attached to the linker. In the last step, the polymer is sulfonated.

ETFE (Tefzel® 100LZ, DuPont) film with a thickness of 25 µm was used as base polymer and electron beam irradiated (Leoni Studer AG, Däniken, Switzerland) for activation with a dose of 1.5 kGy for styrene grafting, 15 kGy for styrene / GMA co-grafting, and 30 kGy for styrene / VBC co-grafting. After irradiation, the films were stored at -80°C before use. The grafting reactions were performed in 60 mL glass reactors under nitrogen at a temperature of 60°C.

Styrene (20 v-% monomer content) was diluted in a 7/1 (v/v) mixture of isopropanol and water. For the co-grafting of styrene and VBC, the two monomers were mixed with DMF at a volumetric ratio of 1/1/2. This monomer ratio corresponds to a molar fraction of styrene with respect to the total monomer content of $X_S = 0.55$. For the co-grafting of styrene and GMA, the two monomers were mixed with isopropanol at a volumetric ratio of 7/3/40 ($X_S = 0.73$). It was observed that the styrene / VBC system grafted much more slowly compared to the styrene / GMA system, despite the higher irradiation dose. Co-grafting of styene / GMA yields pratical graft levels of around 50 % within hours, whereas for styrene / VBC, the synthesis takes around 20 h. The content of the monomers in the grafts was determined using transmission FTIR spectroscopic analysis of the co-grafted films and previously established calibration curves for the pure monomers (cf. Chapter II). For the styrene / VBC co-grafted films, a molar fraction of styrene in the grafts of $x_S = (62 \pm 2)$ % was obtained. The VBC was suspected to undergo elimination of HCl, which could be confirmed based on elemental analysis of the grafted film. In the case of co-grafted styrene and GMA, the composition of the grafts ($x_S = (73 \pm 2)$ %) is identical to the one of the grafting mixture. In the final membranes a target IEC of 1.6-1.7 mmol/g was targeted to allow comparison to a benchmark styrene-only grafted membrane with a graft level of 25 % and an IEC of 1.7 mmol/g. An overview of the samples prepared in the study reported here is given in **Table 3-12**.

The functionalization of the grafted films to introduce the phenol-type antioxidant was performed in a 0.25 M solution of tyramine in a 9/1 v/v mixture of DMF and water. The glass reactors were purged with N_2 and then placed in a water bath at 80°C for 12 h. Afterwards, the functionalized films were washed in acetone overnight to remove residual tyramine and DMF. This reaction was performed before the sulfonation to preserve the reactive electrophilic group on the grafted linker as much as possible. The conversion of the amination reaction was determined gravimetrically. In case of VBC co-grafted with styrene, the conversion to the tyraminated compound is only (25 ± 1) %. In VBC-only grafted films, the conversion is around 50 %. It is suspected that di-functionalization of the tyramine, i.e., the reaction of the primary amine with two VBC units, takes place. This would be supported by FTIR spectra, which show the signature of both secondary and tertiary amines. In styrene / GMA co-grafted films, (59 ± 1) % of the GMA units are tyraminated, which is identical to the value obtained with GMA-only grafted films. The more polar nature of GMA compared to that of VBC could be an explanation for the different conversions found. In both grafting systems, an increase in reaction time from 12 to 24 h did not result in a higher conversion.

Table 3-12. Overview of membrane properties and cell test data. X_S is the molar fraction of styrene in the grafts, hence the content of the comonomer (VBC or GMA) is 1 - X_S. The high frequency (HF) resistance at 1 kHz is extracted from polarization curves measured (conditions cf. Figure 3-40) at the beginning of test (BOT) after conditioning and at the end of test (EOT) after 4 h at OCV. The same applies to the H_2 crossover data, which are masured electrochemically (cell in H_2 / N_2 mode).

ID	Membrane	Graft level (m-%)	X_S (mol-%)	Thickness (wet) (µm)	Ion exchange capacity (mmol·g^{-1})	Water uptake[a] (m-%)	Conductivity[a] (mS·cm^{-1})	HF Resistance[b] BOT (mΩ·cm^2)	EOT (mΩ·cm^2)	H_2 crossover BOT (mA·cm^{-2})	EOT (mA·cm^{-2})
#1	S	25	100	38.2 ± 1.1	1.73 ± 0.13	50 ± 4	58 ± 4	62	186	1.80 ± 0.03	2.38 ± 0.02
#2	S:VBC(Tyr)	66	62 ± 2	42.9 ± 1.2	1.63 ± 0.06	20 ± 6	21 ± 2	246	247	0.61 ± 0.10	0.65 ± 0.06
#3	S:GMA(Tyr)	35	73 ± 2	39.1 ± 1.1	1.62 ± 0.05	35 ± 3	41 ± 10	68	68	1.32 ± 0.05	1.19 ± 0.04
#4	S:GMA(Tyr)	55	72 ± 3	48.1 ± 0.8	1.99 ± 0.01	52 ± 3	100 ± 10	62	62	1.06 ± 0.04	0.92 ± 0.05
#5	S:GMA(diol)	35	73 ± 2	41.1 ± 1.2	1.62 ± 0.02	43 ± 2	66 ± 7	74	96	1.21 ± 0.04	1.55 ± 0.02
#6	S:GMA(diol)	55	73 ± 3	44.2 ± 1.3	2.09 ± 0.07	64 ± 11	91 ± 11	55	58	1.30 ± 0.02	2.00 ± 0.05
#7	Nafion® 212	-	-	64.0 ± 0.8	1.08 ± 0.01	42 ± 1	97 ± 15	63	-	2.59 ± 0.03	-

[a] measured at room temperature in water-swollen state
[b] @ 1 A·cm^{-2}

In the final step, the tyraminated films were sulfonated in 2 % (v/v) chlorosulfonic acid in dichloromethane at room temperature. Hydrolysis of the acid chloride was performed in water at 80°C overnight. The degree of sulfonation for the styrene / VBC grafted membrane was around 80 % and much lower than that of the styrene-only and styrene / GMA co-grafted membrane, for which a value close to 100 % is found. Elemental analysis performed on the styrene / VBC co-grafted membranes yielded a sulfur content corresponding to a degree of sulfonation of 200 %. This discrepancy could not be resolved.
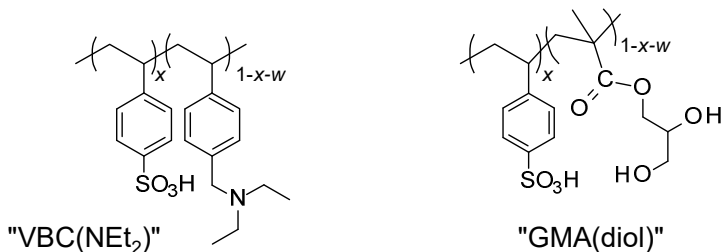
Figure 3-39. Structure of benchmark membranes without tyramine. In case of VBC, the benzylic chloride is reacted with diethylamine (NEt_2), and GMA is hydrolyzed to yield the diol.

In the comparison of fuel cell performance and, in particular, chemical stability of the co-grafted membranes using an accelerated stress test protocol, the use of a styrene-only grafted membrane as benchmark is questionable, since a potential stabilizing effect of the linker co-monomer is neglected. Therefore, a suitable benchmark for co-grafted membranes was prepared. In this case, the linker was not tyraminated but reacted to yield a moiety not expected to have a stabilizing effect. In case of the styrene / GMA co-grafted film, the tyramination step was simply omitted. The epoxy unit of the GMA was thus simply hydrolyzed to the diol during the sulfonation reaction (**Figure 3-39**). In case of the styrene / VBC co-grafted membrane, the benzylchloride was reacted with diethylamine ($HNEt_2$) in a 0.5 M solution of $HNEt_2$ in THF at a temperature of 50°C for 12h. The conversion of the amination reaction was 41%.

4.2 Membrane Properties & Fuel Cell Performance

An overview of the properties of the membranes prepared within the study reported here is given in **Table 3-12**. As mentioned previously, an IEC of 1.6-1.7 mmol/g was targeted for the (co-)grafted membranes. For the styrene-only grafted membrane (ID #1), a graft level of around 25 % yields the target IEC. In case of the co-grafted membranes, a higher graft level is required, because the grafted chain also contains the linker and, eventually, the tyramine. For the styrene / GMA co-grafted membrane, an IEC of 1.6 mmol/g was achieved with a graft level of 35 %. In addition, a second set of membranes was prepared with a graft level of 55 % and an IEC of around 2 mmol/g. For the styrene / VBC co-grafted membrane, a graft level of 66 % was required for an IEC of 1.6 mmol/g. This is a result, on the one hand, of the lower styrene content in the grafts (X_S

= 62 %) compared to the values obtained for GMA based membranes (X_S = 72-73 %). On the other hand, as mentioned above, the degree of sulfonation in VBC(tyr) type membranes was only about 80 %.

The membranes with similar ion exchange capacity may be expected to show similar water uptake values, since all samples were uncrosslinked. Yet it is observed that the VBC(tyr) membrane shows considerably lower water uptake compared to the other membranes, which translates into poor conducitivity. This confirms the strong correlation between water uptake and conductivity. Similarly, the findings for GMA containing membranes with and without linked tyramine, i.e., GMA(tyr) vs. GMA(diol), can be explained based on the different water uptake values. The lower water uptake in GMA(tyr) membranes may be a result of acid-base interactions in the graft component between the sulfonic acid groups and the amine links, leading to the formation of ionic crosslinks ($-SO_3^-\dots H_2N^+RR'$). In addition, the presence of the hydrophilic –OH groups in the diol compound, in particular at the low graft level, may improve proton mobility. Comparing the GMA based membranes at low and high graft level / IEC, evidently an increased water uptake and improved conductivity is observed at the higher graft level.
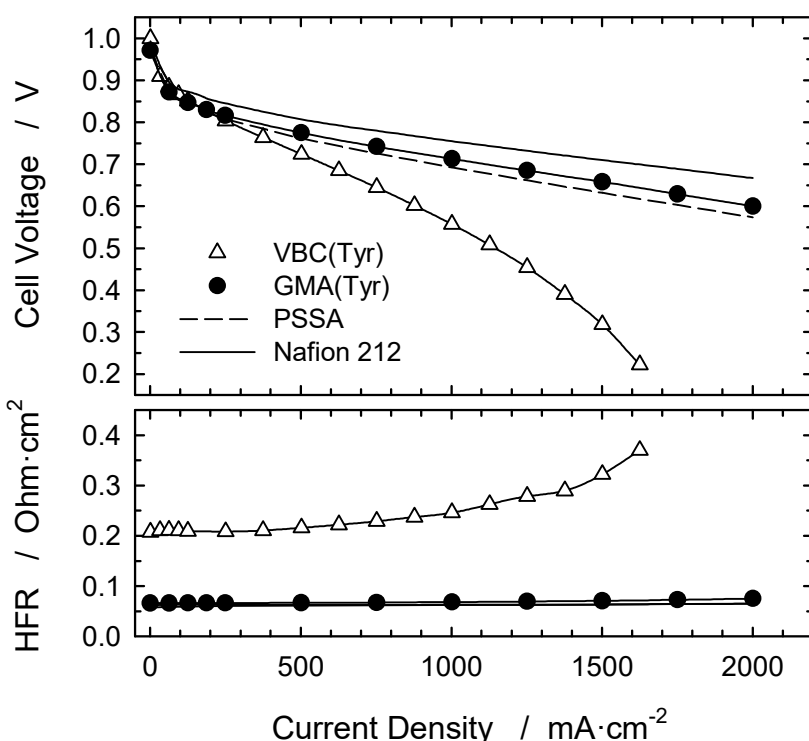
Figure 3-40. Polarization curves recorded after conditioning of cells comprising tyraminated membranes based on VBC and GMA as linker (Table 3-12, IDs #2 and #3), compared to a styrene-only grafted membrane (ID #1)) and Nafion® 212 (ID #7). Electrodes: carbon paper type (Johnson Matthey Fuel Cells ELE0162) with 0.4 mg$_{Pt}$ cm^{-2}. Temperature: 80°C, H$_2$/O$_2$ stoichiometry: 1.5/1.5, humidifier temperature: 85°C, pressure: 2.5 bar$_a$.

The performance of the various membranes was evaluated in the single cell. Selected polarization curves for tyraminated membranes are shown in **Figure 3-40**, including Nafion® 212 and the styrene-only grafted membrane as reference. The GMA(Tyr) membrane showed good performance, which is even superior to that of the styrene-only membrane. The VBC(Tyr) membrane, however, showed substantially inferior performance, which is also reflected in the much higher ohmic resistance of the cell of 200 mΩ·cm^2 compared to around 65 mΩ·cm^2 for the other membranes. This is in agreement with the conductivity measured *ex situ* (**Table 3-12**). Another reason for the inferior performance of this type of membrane may be the low mobility of the grafted chains due to π-stacking of the aromatic units of the grafts. Considering the low water uptake for this membrane, the π-stacking may be more of an issue compared to the styrene-only grafted membrane, which exhibits a higher level of hydration. Polarization curves of the other membranes are not shown to avoid a crowded graph. However, the high frequency resistance data, indicative of the ohmic resistance of the membrane, for all measured membranes are listed in **Table 3-12**. The GMA containing membranes all show similar HFR, the ones with higher graft level tend to have lower ohmic resistance, but the effect is not very pronounced. In any case, there are no unpleasant surprises, as all the membranes are "well-behaved". It is worth noting that the performance of the Nafion® based cell is superior to all grafted membranes. The grafted membranes used in the study reported here have to be considered model systems to investigate the effect of a polymer-bound antioxidant. In this sense, the membranes are not optimized for maxiumum performance by, for instance, implementing procedures during the synthesis of the membranes to minimize loss of surface radicals (cf. Chapter I). It is expected that with these additional measures, the performance could be significantly improved, possibly beyond the level of a Nafion® 212 based MEA.

4.3 Chemical Stability under Conditions of Accelerated Stress

The key experiment in the study is aimed at identifying the chemical stability of the prepared membranes to assess whether the introduction of the prospective antioxidant indeed does lead to more stable membranes. To this end, fuel cell tests were performed under conditions of accelerated stress at open circuit voltage (OCV). Holding the cell at OCV leads to accelerated chemical degradation of the membrane owing to an increased rate of radical formation [103]. The membranes investigated here are based on sulfonated styrene as protogenic unit and uncrosslinked, hence the stability of the membranes without tyramine is expected to be rather low. The OCV hold time used, therefore, is only 4 h, because this already leads to a significant degradation of the styrene-only grafted membrane. Potential effects in the co-grafted and stabilized membranes are therefore expected to be readily detectable. The fuel cell performance

before and after the 4 h OCV hold period for the various membranes is documented in **Figure 3-41**. As expected, the performance of the styrene-only grafted membrane drops considerably. The performance of the tyraminated membranes with GMA linker shows little change upon 4 h at OCV, whereas the membranes with hydrolyzed epoxy groups, GMA(diol), show a more pronounced loss in cell performance. This unequivocally confirms that the antioxidant concept in the form of polymer-bound tyramine successfully stabilizes the membrane against chemical degradation. The improved stability of the GMA(diol) membranes compared to the styrene-only grafted membrane could be explained by the higher H_2 crossover of the latter. It is known that gas crossover is an essential driver of chemical membrane degradation. It cannot be excluded, however, that there is also a potential, albeit small, stabilizing effect of the linker unit. As mentioned previously, the VBC based membrane had a much inferior performance, yet also this membrane showed only a small degradation after the accelerated stress test. Therefore, the antioxidant seems to be also effective in this kind of membrane. The data for the VBC(Et_2N) type membrane, i.e. the benchmark VBC based membrane without linked tyramine, is not shown here because the performance was appallingly low with a corresponding high-frequency resistance of around 3 $\Omega \cdot cm^2$. The reason for this is not known, yet it is suspected that a proper membrane-electrode interface formation during MEA assembly could not be established.
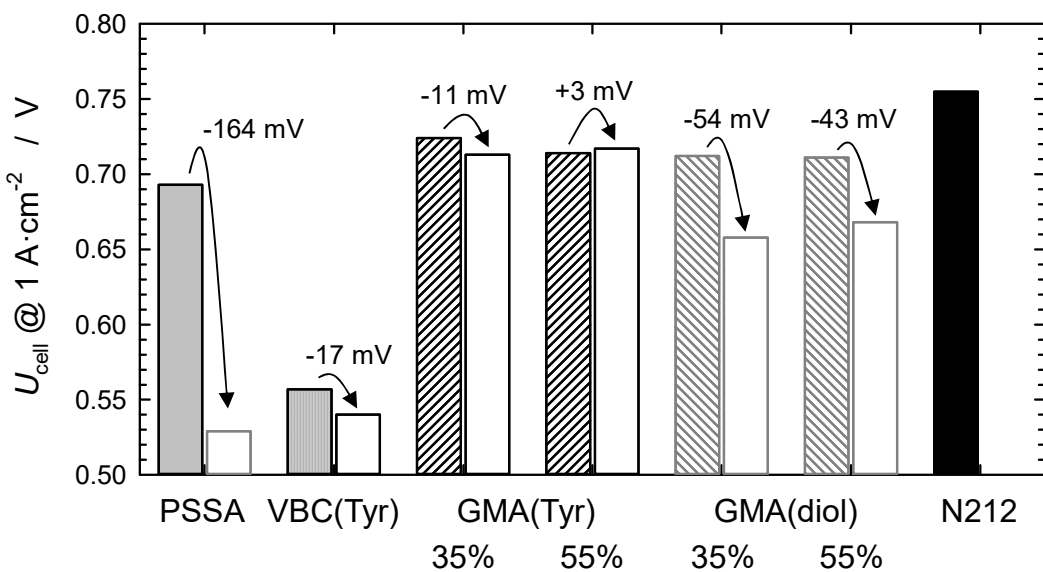
Figure 3-41. Cell performance data extracted from polarization curves (conditions cf. Figure 3-40) before (filled bars) and after (empty bars) the accelerated stress test (4 h at OCV). The percentage values indicate the graft level.

For a more detailed analysis of membrane stability, we consult the HFR and H_2 crossover data reported in **Table 3-12**. All tyraminated membranes show no change in HFR after the accelerated stress test, indicating that no or only little chemical degradation took place. All membranes without tyramine showed an increase in HFR, although the change was rather small in case of the

GMA(diol) membrane with high graft level. The hydrogen crossover of a membrane usually increases during an OCV hold test as a result of fragmentation of the graft component, loss of chain constituents and concomitant increase of the porosity of the membrane. An increase in H_2 crossover is measured for all membranes devoid of tyramine, whereas all chemically stabilized membranes show the opposite trend. This could be caused by crosslinking through recombination of phenoxyl radicals. For butylated phenol recombination of the phenoxyl radicals is well known and proved [448, 449]. In contrast, the GMA(diol) membranes show an increase in H_2 crossover.
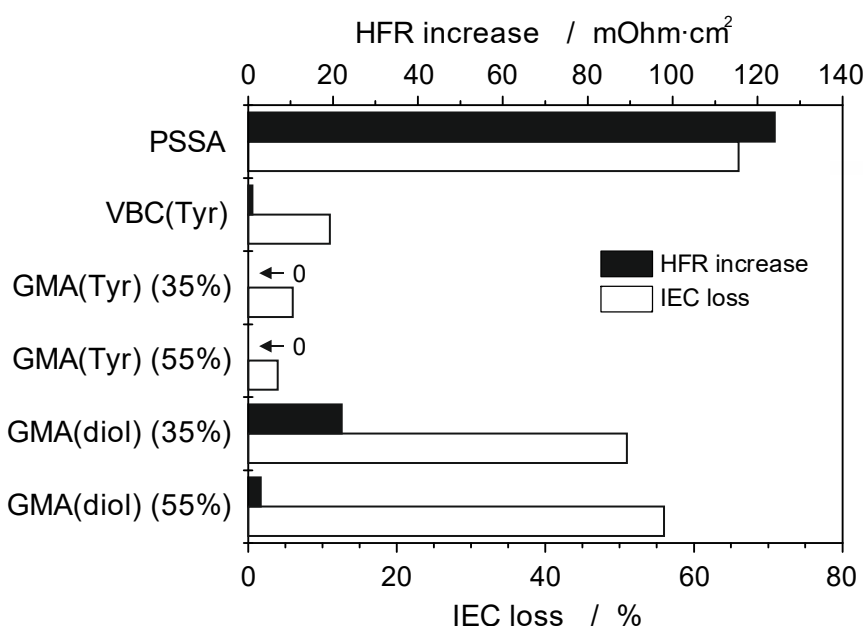
Figure 3-42. Increase in HFR at 1 A·cm^{-2} extracted from polarization curves before and after the 4 h OCV, and IEC loss determined by titration after disassembly of the membrane from the cell and comparison to the pristine value of the untested membrane (cf. Table 3-12).

After discontinuation of the fuel cell test, the MEAs were disassembled from the cells and delaminated to retrieve the membrane for *post mortem* characterization. This was done by measuring the residual IEC in the active area of the cell and comparing it with the value of the pristine membrane. Subsequently, the extent of degradation was calculated. The styrene-only grafted membrane and the GMA(diol) type membranes showed an IEC loss of 50 % or more, whereas the loss in case of the tyraminated membranes was 10 % or less (**Figure 3-42**). The increase in HFR is much smaller than would be expected from the loss in IEC. This could be related to the fact that during the process of removing the catalyst layer from the membrane after the test and preparation of the membrane for *post mortem* IEC measurement fragments of the graft component detached from the backbone during the cell test are washed out, leaving behind a membrane with much lower IEC. In the cell, cleaved fragments of the graft component may still contribute to proton conductivity.

4.4 Prospects and Limitations of Tyramine as Antioxidant

The results presented in the previous section highlight the potential of stabilizing the graft component against chemical degradation by including a phenol-type antioxidant. Yet, the short duration of the OCV hold test (4 h) does not provide a realistic picture of membrane behavior over extended periods of time. Therefore, two GMA(tyr) type membranes were prepared at the same time and tested one after the other in an extended OCV hold test over 144 h. The second membrane tested was stored for about a week under argon in a fridge. The development of cell voltage and HFR for the GMA(tyr) type membranes during the 144 h OCV test is documented in **Figure 3-43**. For comparison, an OCV hold test for a styrene-only grafted membrane over 12 h is shown. The "fresh" GMA(tyr) type membrane shows a lower OCV decay rate (0.83 mV·h^{-1}) than the "stored" GMA(Tyr) type membrane (0.98 mV·h^{-1}), which implies a lower membrane degradation rate for the "fresh" membrane. The sharp increase in HFR from 0.07 Ω·cm^2 to 0.45 Ω·cm^2 within 12 h of the cell with the styrene-only grafted membrane and the concomitant voltage decay rate of 4.16 mV·h^{-1} is a clear signal of severe membrane degradation. In contrast, both tyraminated membranes, which show a similar initial HFR, exhibit a much lower rate of HFR increase. The HFR of the "fresh" membrane only increased slightly from 75 to 77 mΩ·cm^2 over 144 h at OCV, whereas the "stored" membrane shows an accelerated HFR increase after 50 h,
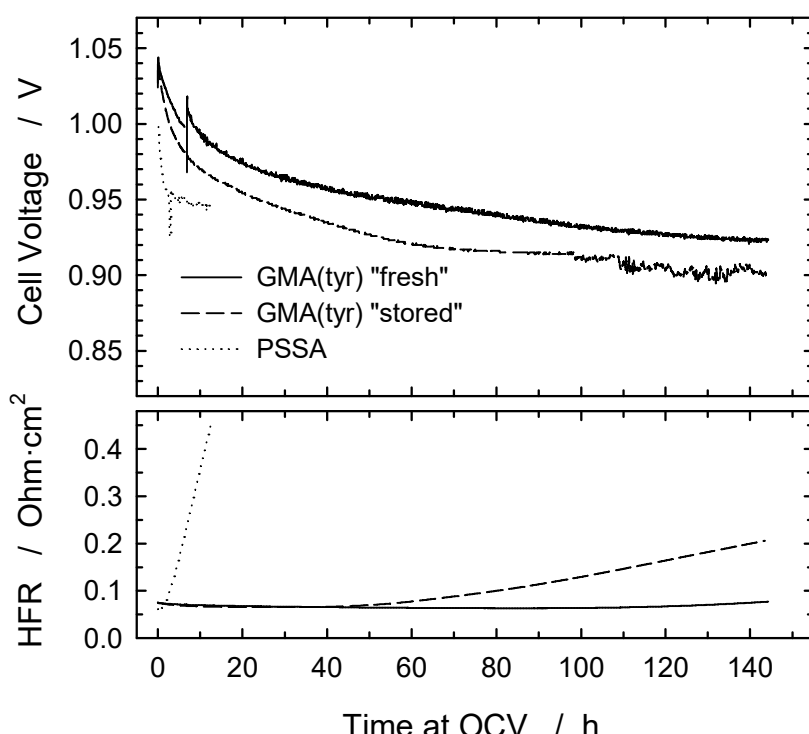
Figure 3-43. Evolution of cell data during extended OCV hold tests (conditions cf. Figure 3-40) using GMA based tyraminated membranes (graft level: 41 %, IEC: ~1.7 mmol/g) assembled immediately after membrane preparation ("fresh") and after the membrane had been exposed to ambient conditions for 1 week ("stored"). The PSSA membrane had a graft level of 21 % (IEC: 1.42 mmol/g).

which leads to a much higher HFR of 206 m$\Omega\cdot$cm^2 at the end of the test. The results suggest that the "stored" membrane is less stable than the "fresh" membrane, perhaps because of the loss in the antioxidant functionality during storage, although the stabilizing effect of the antioxidant is still notable in comparison with the unstablized styrene membrane.
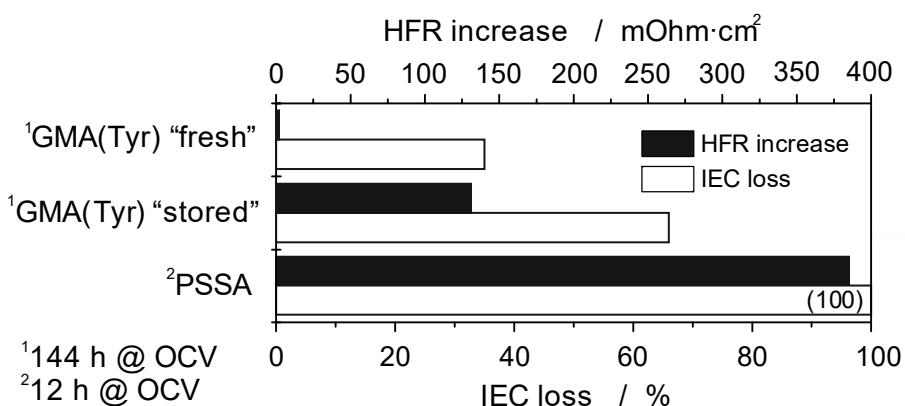
Figure 3-44. HFR increase and IEC loss upon OCV hold test (Figure 3-43). HFR values are extracted from polarization curves at 1 A$\cdot$cm^{-2} recorded before and after the OCV hold test, respectively.

The H$_2$ crossover of the styrene-only membrane increased from 1.14 to 2.58 mA$\cdot$cm^{-2} during the 12 h OCV hold test, indicating severe degradation. In fact, *post mortem* analysis of the membrane revealed that the graft component was completely decomposed. The H$_2$ crossover of the "fresh" GMA(tyr) membrane decreased from 0.89 to 0.76 mA$\cdot$cm^{-2}, while an increase from 0.97 to 1.26 mA$\cdot$cm^{-2} was observed in case of the "stored" GMA(tyr) membrane. As before, a decrease in H$_2$ crossover suggests an active stabilization of the membrane by the antioxidant, whereas an increase indicates deterioration of the membrane material. *Post mortem* analysis of the IEC by titration showed a difference in the extent of degradation between the two membranes (**Figure 3-44**). The loss in IEC follows the trend of HFR increase over the duration of the OCV hold test. Again, the increase in HFR may not be as dramatic as the IEC loss may imply, since cleaved fragments of the graft component can remain in the membrane until they are washed out during the preparation of the membrane after the test for the *post mortem* analysis. The results suggest that the storage of tyraminated membranes somehow reduces the antioxidant functionality of the membrane, which leads to a decreased number of antioxidant groups in the membrane and thus accelerated chemical degradation after 50 h at OCV. The approach adopted to store the membrane seems not adequate to retain the antioxidant functionality of the membrane.

4.5 Regeneration of Antioxidants

The extended OCV hold test of GMA(tyr) type membranes over 144 h shown in the previous section suggests that the antioxidants can be consumed or depleted over time. Since accelerated

tests over longer periods of time are not available, the author can only but speculate about the ultimate fate of a "fresh" tyraminated membrane. Whether the HFR will also start to show an increased rate of degradation at some point is not known. However, under the premise that phenol-type antioxidants are gradually consumed, one must assume that, when the tyramine is used up and thus the stabilizing effect is lost, the membrane will undergo rapid degradation. The advantage of the use of the Ce(III)/Ce(IV) redox couple in PFSA membranes to stabilize the ionomer against radical attack by scavenging $HO^{\bullet}$ is that the Ce(III) is restored very effectively through the reaction of the Ce(IV) with H_2O_2 [438]. The concentration of H_2O_2 in the fuel cell membrane is around 0.5 mM. Thus with a rate constant for the reaction of Ce(IV) with H_2O_2 of 10^6 $M^{-1}s^{-1}$ [372] the lifetime of Ce(IV), the "spent" state of the cerium antioxidant, is only on the order of 1 ms. Therefore, there is a very effective regeneration mechanism of the antioxidant, thanks to the presence of H_2O_2. For this reason, the stabilizing effect of the cerium can be sustained over hundreds of hours and more. With the phenol type antioxidants presented here, there does not seem to be a straightforward approach or mechanism to restore the phenol. In principle, the regeneration of the antioxidant could be accomplished as follows:

- *Chemical regeneration.* One could imagine introducing a suitable and reactive reducing agent, such as ascorbic acid, $E^{\circ\prime}(Asc\bullet^-,H^+/AscH^-) = 0.282$ V at pH 7 [450], into the reactant stream of the fuel cell. The compound would have to be of the H-donor type to restore the phenoxyl radical to the phenol. The practicality of this approach, however, is limited, as it would entail a more complex fuel cell system. In addition, to access the spent antioxidants buried within the bulk of the membrane, the reducing agent would have to diffuse across the electrode and catalyst layer and reach the phenoxyl radical before it undergoes follow-up reactions. This is unlikely to be a viable approach. Alternatively, one may argue that the H_2 used as fuel can act as reducing agent, yet the bond dissociation energy of H_2 is 436 kJ/mol and that of PhO-H 377 kJ/mol [451]. Yao et al. claim that vitamin E, also a phenol type antioxidant, is regenerated by H_2 in the fuel cell, yet solid proof is not given [452]. In fact, the regeneration through H_2 is thermodynamically or kinetically unfavorable. In the work carried out in the framework of this study, the drop in H_2 crossover seen for membranes with antioxidants exposed to periods of oxidative stress is attributed to follow-up reactions of the antioxidant, resulting in crosslinking of the polymer [337].

- In search for a suitable reducing agent, it may be argued that H_2O_2 can act as a reducing agent under the oxidatively stressed conditions in the fuel cell. The reaction $HOO^{\bullet} + H^+ + e^- \rightarrow H_2O_2$ has a standard electrode potential of $E^{\circ}(HOO^{\bullet},H^+/H_2O_2) = 1.46$ V at pH 0 [453]. In the presence of $HO^{\bullet}$, such as in the fuel cell or during a Fenton reaction, H_2O_2 can react with $HO^{\bullet}$ with a rate constant of $2.7 \cdot 10^7$ $M^{-1}s^{-1}$ [370]. The standard electrode

potential of the phenoxyl / phenol redox couple, however, is $E°(PhO^•,H^+/PhOH) =$ 1.31 V at pH 0 [454], and a phenol with electron donating substituent in the para position, such as in the case of tyramine, has an even lower electrode potential [444]. Therefore, the phenoxyl radical is not a sufficiently strong oxidant to oxidize H_2O_2, and this regeneration mechanism is thermodynamically not favored. It is conceivable to increase the redox potential of the phenol by introducing electron-withdrawing substituents, such as nitro-groups. Yet even if the electrode potential can be increased above that of the $HOO^• / H_2O_2$ couple, the resulting reaction is expected to be very slow. Even with $HO^•$ as a reaction partner, $E°(HO^•,H^+/H_2O) = 2.72$ V at pH 0 [455], the reaction rate constant is rather low, as mentioned above.

- Within the study reported here, the idea was developed to use the low electrochemical potential of the fuel cell anode to reduce the oxidized antioxidant functionalities in the membrane. Owing to the low electrochemical potential (0 – 0.1 V) there is theoretically sufficient driving force to restore the phenol-type antioxidant. Since the antioxidant is not only located at the surface of the membrane in contact with the anode but also within the bulk of the membrane, the electrochemical potential of the anode has to be extended into the membrane. This could be accomplished by embedding an electronically conductive polymer on the anode side of the membrane, which can shuttle electrons to the redox couples buried within the membrane (**Figure 3-45**). Obviously, the electronically conductive layer is not allowed to penetrate all the way to the cathode side to prevent shorting of the electrodes. In this way, an active radical scavenging layer near the anode could be realized, keeping in mind that membrane degradation is typically more pronounced on the anode side [428]. The electronically conductive polymer chosen is polypyrrole (PPy), which was introduced into the membrane via one-sided polymerization of pyrrole [456]. Thus the electrochemical 2D-interface between the anode and the membrane could be extended to a 3D-interphase to maximize access to the redox couples buried within the membrane. It could be shown that with the incorporated PPy layer, the electrochemical response of a model compound embedded in the membrane (hydroquinone) could be increased by around two orders of magnitude [456, 457]. The incorporated PPy, however, led to a considerable increase of the ohmic resistance of the membrane, owing to the fact that the PPy is located in the hydrophilic channels of the membrane, where proton transport is supposed to take place. Therefore, the performance of the cells with PPy-modified membrane was unacceptably low. In addition, the electronic conductivity of the PPy / ionomer composite appeared to be very low, leading to a substantial potential drop in the PPy pathway. Experimentally, using cyclic voltammetry the oxidation of the tyramine compound could be observed as an anodic peak at around

0.85 V vs. RHE. However, a corresponding clear reduction peak could not be observed. Probably, the lifetime of the phenoxyl radical, once formed, is too short for electrochemical reduction to be effective. Most phenoxyl radicals are short-lived intermediates, which react with each other and with other radicals relatively rapidly. Typical reactions are disproportionation and dimerization of phenoxyl radicals [448]. The latter leads, in the case of the membrane with polymer-bound tyramine reported here, to crosslinking of the grafted chains, which could be responsible for the observed decrease in H_2 crossover upon accelerated aging in tyraminated membranes (**Table 3-12**). In the presence of other, reasonably long-lived radicals, corresponding recombination reactions with phenoxyl radicals may occur [458], which may also lead to crosslinking. It always has to be kept in mind, though, that rate constants in a more or less hydrated ionomer can be considerably slower, and the lifetime of intermediates markedly higher, compared to the situation encountered in dilute aqueous solution, which are typically employed for studying kinetics [365].
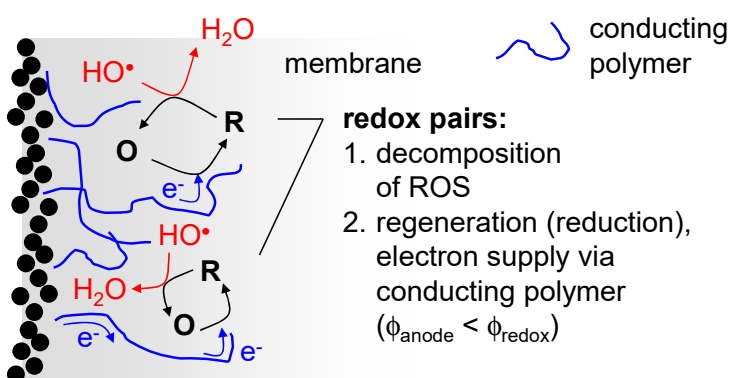
Figure 3-45. Conceptual approach for electrochemical regeneration of spent antioxidant functionalities (R: antioxidant, O: oxidized form) embedded in the membrane near the anode electrode. Regeneration of the antioxidant is accomplished by electrochemical reduction, with electrons provided via a conductive path from the fuel cell anode.

The regeneration of organic antioxidants appears to be more challenging than the one of cerium or manganese ions. In the study reported here, it was shown that, in principle, an electrochemical regeneration of the antioxidant may be possible, but from a practical point of view, the approach could not be shown to be viable. Considering further studies on phenol type antioxidants, it may be necessary to adjust the chemistry of the compound to facilitate regeneration. In the plastics industry, typically "hindered" phenols are used, such as compounds based on 2,6-di-*tert*-butylphenol [441], in which adverse follow-up reactions of the phenoxyl radical are hindered by the presence of the two adjacent *tert*-butyl groups. Use of such compounds may increase the lifetime of the phenoxyl radical and thereby increase the possibilities for reduction reactions. In

addition, it may be advisable to use dihydroxy compounds, e.g., derivatives of hydroquinone or catechol, which can undergo reversible oxidation / reduction reactions [454].
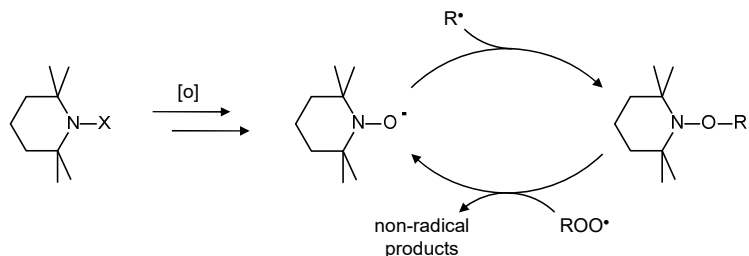
Figure 3-46. Simplified mechanism of the Denisov cycle, showing protection using a piperidine type hindered amine light stabilizer (HALS), where X is typically H or an alkyl chain. Reproduced from [459].

The regenerative character of phenol-type antioxidants is rather limited. Therefore, it may be useful to look for another, more favorable chemistry. In the plastics industry, derivatives of 2,2,6,6-tetramethyl piperidine are used to protect the polymer from light-induced degradation. These compounds, known as hindered amine light stabilizers (HALS), do not absorb UV light but act as radical scavengers. In particular, the HALS can undergo regenerative antioxidant action in a process referred to as Denisov cycle (**Figure 3-46**). In the first step, the hindered amine is oxidized to the corresponding nitroxide radical. The nitroxide then reacts with an alkyl polymeric radical to form an alkoxyamine. The alkoxyamine can react with a peroxyl radical to reform the nitroxide as well as yield nonradical products. Therefore, the Denisov cycle acts in a catalytic fashion to transform both R• and ROO• radicals to nonradical species [459]. Whether this mechanism can also work in the context of a partially fluorinated fuel cell membrane is not known. Clearly, the conditions are rather specific, such as the low pH, under which an (acidified) hindered amine may not be effective [460].

5   Conclusion

The rationale of the studies reported in this chapter was to improve the durability of styrene based radiation grafted membranes. Membranes grafted with styrene only show a very low lifetime under fuel cell operating conditions, which is a result of the poor oxidative stability of the PSSA grafts. One of the main weaknesses is the presence of the weak α-hydrogen. Strategies to mitigate degradation encompass various approaches. One of the options is to target the α-hydrogen and replace it with another group, such as –CH$_3$, as in the case of α-methylstyrene (AMS). AMS is a cheap and readily available monomer. However, it shows poor radical polymerization kinetics and has to be copolymerized with a suitable comonomer to enable grafting. In the study reported here (Section 2), AMS was co-grafted with methacrylonitrile (MAN). AMS and MAN tend towards alternating copolymerization. The membranes obtained showed a significantly improved durability in the fuel cell compared to styrene only grafted membranes. In case of uncrosslinked membranes, lifetime increased by around an order of magnitude from 50 to 500 h. The improvement in stability was thought to be mainly caused by replacement of styrene with AMS. However, since AMS based membranes always contain MAN, the influence of MAN needed to be understood. To this end, MAN was co-grafted with styrene. In the fuel cell test, S:MAN co-grafted membranes also showed a substantially improved stability compared to styrene-only grafted membranes. As a reason for this, the lower gas crossover in S:MAN co-grafted membranes was put forward. The presence of nitrile groups increases the gas barrier properties of the membrane. The reduced gas crossover leads to a lower rate of radical formation at the electrodes and concomitantly to a lower rate of membrane attack and degradation. To verify this hypothesis, membranes based on co-grafted styrene and acrylonitrile (AN) were prepared and tested. The AN unit was found to undergo significant hydrolysis during membrane preparation, leading to poor fuel cell performance. Comparison of the stability of S:MAN and S:AN co-grafted membranes is not reported here, but will be discussed in Chapter IV. An observation of a bit of a concern is the more pronounced conductivity loss of co-grafted membranes towards low relative humidities, which correlates with the content of the co-monomer. This could be explained based on the nano-scale morphology of the ionic phase using results of small angle x-ray scattering experiments. In the study reported in Section 4, yet another option to improve the stability of radiation grafted membranes was explored: antioxidants were introduced into the grafted polymer using a "linker" concept. Tyramine was used as a model compound for a phenol type chain-breaking antioxidant. All tyraminated membranes displayed superior chemical stability compared to tyramine-free membranes, demonstrating that the concept is successful. However, the antioxidant is consumed over time. Therefore, options to regenerate the antioxidant were

discussed. The electrochemical regeneration was attempted and was shown to work in principle, yet lacks practicality because the ionic conductivity of the membrane is strongly impaired.

In summary, the approaches implemented to stabilize the graft component consisted of i) improving the intrinsic stability of the styrenic monomer, ii) reducing the amount of radicals formed by creating membranes with improved gas barrier properties, and iii) introducing polymer-bound antioxidants to alleviate the radical induced degradation of the graft copolymer. In addition, as mentioned in the introductory section, crosslinking of the graft component is an effective means to boost lifetime of radiation grafted membranes. It may be surmised that the effects of the different approaches are additive, hence a grafted membrane with combined stabilization strategies can expected to provide a maximum in stability. In fact, the use of AMS and MAN as grafting monomers and diisopropenylbenzene (DIPB) as crosslinker has been shown to yield membranes with exceptional stability, which can even outlast Nafion® XL-100, a state-of-the-art mechanically reinforced and chemically stabilized, commercial membrane [320]. These recent achievements are reported in Detail in Chapter I. The concept of polymer-bound antioxidants has not been implemented to date in an overall optimized membrane. Based on the current understanding, there is further work required to identify a more suitable antioxidant, including a possibility for regeneration.

Chapter IV

Mechanisms of Chemical Degradation

1 Introduction

The polymer electrolyte fuel cell (PEFC) has reached a level of technological development where a number of commercial applications have emerged for near-term niche markets, for instance in back-up power solutions for telecommunication installations, materials handling vehicles (e.g., forklifts), and distributed power generation units operating on available low-cost by-product hydrogen [82]. In addition, PEFC based systems are deployed for stationary applications, in many cases with considerable government subsidies, for instance the ENE-FARM natural gas fed 1 kW class combined heat-and-power units in Japan [461], or for vehicle fleet programs, such as hydrogen fueled buses in the framework of zero-emission transit programs [462]. However, fuel cells have not yet found their way into applications for large volume markets, such as for distributed power generation or powering of electric vehicles. The 'Mirai' fuel cell vehicle, launched by Toyota in 2015, will only be produced in small numbers of 700 units per year initially [463]. The prospect of zero-emission mobility combined with attractive range has fueled research and development of fuel cells for automotive applications for over two decades now [464]. Although the battery electric vehicle is gaining considerable attention today, fuel cells continue to be a promising power source for automobiles for driving ranges over 200 km [465]. The power density in passenger cars has reached attractive levels [70, 466], yet a number of shortcomings prevent broad-scale technological breakthrough, such as insufficient cold-start capability, start-stop induced degradation, catastrophic membrane failure, as well as lack of H_2 infrastructure. Above all, however, the main challenges that remain to be tackled are durability, reliability and cost [467]. As for lifetime, a durability of 5'000 h is required for vehicle applications, and 80'000 h in case of stationary applications [468]. Although cost targets are less demanding in case of stationary applications, additional system components, e.g., reformer and gas clean-up stages, have to be included in lifetime and cost assessment.

The limited durability of PEFC systems is related to various balance-of-plant components, the stack hardware, but also the electrochemically active component, the membrane-electrode assembly (MEA) [469, 470]. The current generation of materials (membrane and catalyst) used in the PEFC is not durable enough under the 'real world' operating conditions prevailing in the stack. The shortcomings of current MEA technology with respect to durability have been identified as loss of membrane functionality (proton conductivity, mechanical integrity) and loss of catalyst activity through carbon corrosion, Pt sintering and dissolution [103, 471] The aging phenomena occurring in the PEFC are subject to a complex interaction of different mechanisms acting simultaneously, the understanding of which is still limited today. Observations indicate that carbon corrosion, Pt particle ripening and dissolution-reprecipitation contribute to catalyst

degradation [472, 473]. Concerning membrane aging and failure, degradation can be associated with three classes of mechanisms (**Figure 4-1**): temperature induced reactions, radical induced attack, and mechanical stress induced damage [5, 69, 79, 471, 474, 475].
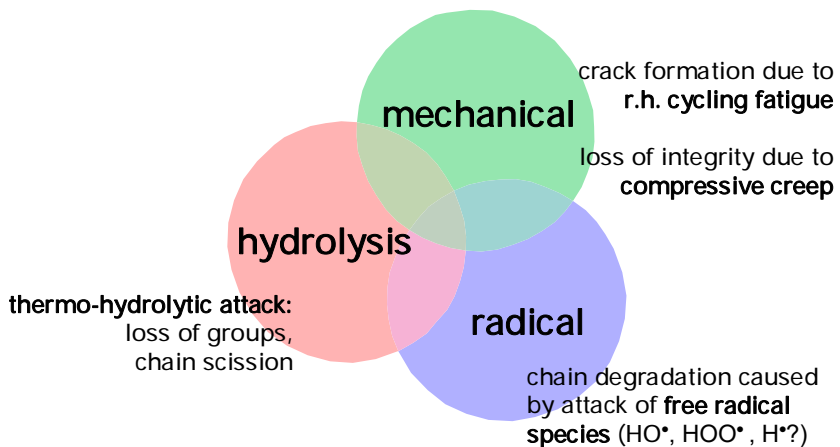
Figure 4-1. Membrane degradation mechanisms in the polymer electrolyte fuel cell (PEFC).

The mechanisms by which damage is inflicted on the membrane are a consequence of the operating environment and conditions of the PEFC:

i) With operating temperatures up to 100°C, possibly with intermittent excursion to 120°C, and the presence of water vapor or liquid water, hydrolysis is a likely mechanism of chemical deterioration of the ionomer. Hydrolysis is of particular importance for condensation polymers with respective susceptible functional groups, such as esters, urethanes, imides, etc. [139, 476]. Attack of the main chain leads to a decrease in molecular weight with ensuing eventual dissolution and leaching out of chain fragments and loss of mechanical robustness. Hydrolyis of pendant groups or side chain constituents without loss of the sulfonic acid functional group does not lead to chain scission or loss of ion exchange capacity, yet the chemical properties of the polymer change and thus, possibly, the functionality of the membrane. In some of the radiation grafted membranes prepared at PSI containing specific comonomers, hydrolysis of functional groups has been observed. This will be discussed in Sections 4.1.2 and 4.2 of this chapter. The more traditional styrene based radiation grafted membranes, however, appear to be resistant against hydrolysis [477]. Perfluorosulfonic acid (PFSA) membranes, such as Nafion®, are stable against hydrolytic attack. They have been used for several decades in industrial size chlor-alkali cells, where they are in contact with 30 wt-% caustic soda [478].

ii)   Membrane failure through pinhole formation and membrane rupture appears to be a matter of concern especially for thin membranes (< 35 μm) designed for automotive applications under dynamic operating conditions [69]. As to the mechanical failure of PEFC membranes, internal stress as a consequence of drying-swelling cycles of the polymer have been identified as a cause for degradation [79]. A "free standing" membrane will increase in size upon swelling in water and shrink when dried. A membrane constrained in a cell fixture experiences in-plane tension and compression upon changes in humidity and hydration state [479]. Cycling between dry and wet state leads to fatigue that will eventually cause fracture of the membrane. Water acts as a plasticizer of the polymer, and viscoelastic creep under the cell compaction force may lead to membrane thinning and, eventually, pinhole formation [126, 480]. Relative humidity (r.h.) cycling fatigue of an MEA in a single cell under inert gas conditions has been observed to lead to membrane failure after several thousand cycles [481]. Some membrane types, for instance polyaromatic membranes, have shown a substantially higher susceptibility towards r.h. cycling fatigue compared to PFSA membrane types (e.g. Nafion®) [482].

iii)   Proton exchange membranes in fuel cells undergo chemical degradation via polymer chain scission, loss of functional groups or constituents (blocks, side chains, blend component) caused by the chemical attack of radicals, which are created in the MEA in the presence of H_2, O_2 and the Pt electrocatalyst [121]. The study of the pathways of formation of these reactive intermediates and the reactions they undergo, in particular the reaction with the polymer electrolyte, is the main topic of this chapter and will be discussed in the forthcoming sections. The chemical attack of the polymer leads to a decrease in chain length and release of low molecular weight products or short chain segments from the MEA, which can then be detected in the effluent water of the cell [483]. The chemical changes, such as the loss of molecular weight, cause deterioration of the mechanical properties of the membrane. An essential and important consequence of the simultaneous presence of mechanical and chemical stress factors is an effect of accelerated degradation based on a positive feedback loop: chemical attack leads to thinning and mechanical weakening of the membrane, and mechanical deterioration via creep and crack formation in turn leads to increased gas crossover and, hence, a higher rate of radical formation and, therefore, more serious chemical attack. Hence, this combined mechanical-chemical attack substantially accelerates membrane degradation and failure [123, 484].

In addition to these main degradation mechanisms, further effects, more of a physical nature, have been found to affect membrane functionality and integrity. Metal-ion contaminants brought into

contact with the MEA cause partial ion-exchange and thus a blocking of the cationic sites, leading to a loss in conductivity, some of which is partially reversible, depending on the cation type [485].

In the context of radiation grafted membranes, a swelling-induced damage to the graft copolymer was proposed [486]. Membranes prepared by radiation grafting and sulfonation of styrene onto crosslinked PTFE and ETFE base film, with graft levels around 50%, were immersed in hot water at 85 and 95°C for several hundred hours. Detached grafted chains were found to accumulate in the water over time, such that after 500 h a significant fraction of the initial ionic content of the membrane was lost. The authors concluded that hydrophilic poly(styrenesulfonic acid) (PSSA) grafts detach from hydrophobic polymer due to swelling-induced stress at the interfacial boundary between crystallines of the base polymer and grafted domains within the amorphous region in the grafted membranes. Hence, the swelling-induced detachment supposedly takes place at the point where the grafted chain is attached to the base polymer chain. At PSI, aging experiments carried out in fuel cell configuration, yet under conditions where radical formation does not take place (H_2 / N_2 or N_2 / N_2 operation), using uncrosslinked styrene / acrylonitrile co-grafted membranes with around 40 % graft level, which exhibit a water uptake of approximately 50 wt-% (cf. Section 4.1.2), did not show any indication of degradation according to the proposed mechanism after 310 hours at 90°C (cf. Section 4.2). It is conceivable that the susceptibility of a membrane to swelling-induced degradation depends on whether the bare membrane is immersed in water or assembled into an MEA, which is clamped in a single cell fixture.

2 Radical-Induced Membrane Degradation

Oxidative degradation of polymer membranes in fuel cells was a challenge from the very beginning [5]. The membranes used in the Gemini space program consisted of styrene-divinylbenzene (DVB) copolymerized within the interstices of a rubbery fluoropolymer matrix, followed by sulfonation. The limited lifetime of around 500 h at 60°C of these membranes was attributed to a "weak link" in the styrene-DVB structure associated with the presence of αC-H bonds. The polyelectrolyte was found to break down into small, water-soluble fragments that were found in the product water. Early studies on the degradation mechanism of poly(styrenesulfonic acid) (PSSA) of a very thorough nature were therefore carried out at General Electric (GE), including fuel cell tests [9]. Key insights were as follows: PSSA was found to degrade under various experimental conditions. Potential hold using a platinized tantalum electrode of an aqueous PSSA solution at 1.2 V of up to 50 h led to degradation, observed as a lowering of the molecular weight and yellow discoloration of the solution as a result of the formation of metastable hydroperoxide. PSSA was found to be more easily oxidized than cumenesulfonic acid, toluenesulfonic acid, benzenesulfonic acid, and sulfuric acid. Furthermore, PSSA was found to undergo degradation when H_2 containing 5 % O_2 was bubbled through the solution in the presence of Pt catalyst in 3 M H_2SO_4 electrolyte. After 48 h, the molecular weight of the PSSA had decreased from 635 kDa to 42 kDa. In addition, the authors reported that PSSA in solution underwent *autoxidation* upon storage in air at room temperature. In a nitrogen atmosphere, no degradation was observed.
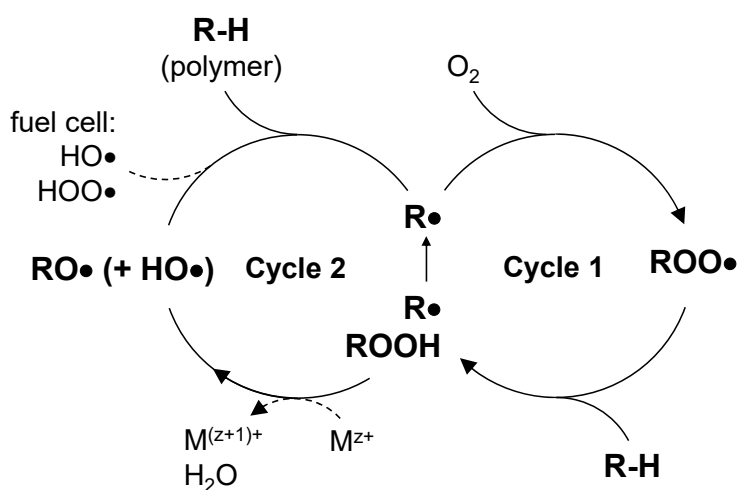
Figure 4-2. Mechanism of autoxidation of a hydrocarbon polymer. Polymer oxidation is initiated by radicals, for instance formed in the fuel cell at the electrodes. Cycle 1 is the chain propagation reaction, in cycle 2 new radicals are created and injected into the reaction sequence (adapted from [223]).

Autoxidation of hydrocarbon polymers was already known in the 1960s. It is the same mechanism by which fat becomes rancid. Autoxidation of organic compounds proceeds as a self-accelerated reaction, consisting of a chain reaction mechanism of oxidation and a slow rate of chain auto-initiation through the decomposition of intermediate hydroperoxides into free radicals (**Figure 4-2**). The reaction is initiated by abstraction of a hydrogen atom by a radical, creating a radical on the polymer chain (R$^\bullet$). The propagation reaction is the addition of O$_2$ to this radical, forming a peroxyl radical (ROO$^\bullet$), followed by the abstraction of another hydrogen from a nearby position on the chain (inter-chain or intra-chain), yielding a hydroperoxide (ROOH) and a new carbon centered radical (R$^\bullet$). The latter reaction is often rate determining, depending on the strength of R-H bonds in the polymer. The hydroperoxide can undergo homolytic cleavage, for instance in the presence of a transition metal ion catalyst, leading to an increase in the number of propagating radicals. Termination typically occurs through recombination of radicals. Gradually, thus, the polymer is oxidized ("peroxidized") and its physical properties deteriorate. Chain scission readily occurs in polymers containing alkoxy radicals (RO$^\bullet$), eventually rendering the polymer useless. Note that similar mechanisms are involved during the "activation" of the base polymer for the grafting reaction by irradiation in air (cf. Chapter I).

Polystyrene and PSSA are particularly susceptible to autoxidation, owing to the weakness of the αC-H bond (~350 kJ/mol [379]). Peroxide formation at the α-position of PSSA can therefore be readily expected to occur, which can directly lead to chain fragmentation [487]. Furthermore, according to Hodgdon et al., chain scission is likely to take place via hydroperoxide rearrangement to give an unstable polymeric peroxide, which can easily lead to fragmentation of the chain. It was deemed most probable that initiation reactions involving the oxidation of PSSA requires an initial weak bond in the polymer chain, such as an oxygenated group, a peroxide link in the chain, or a point of unsaturation ("weak link" theory). For the latter case, peroxide rearrangement was proposed to proceed as follows:

(4-1)
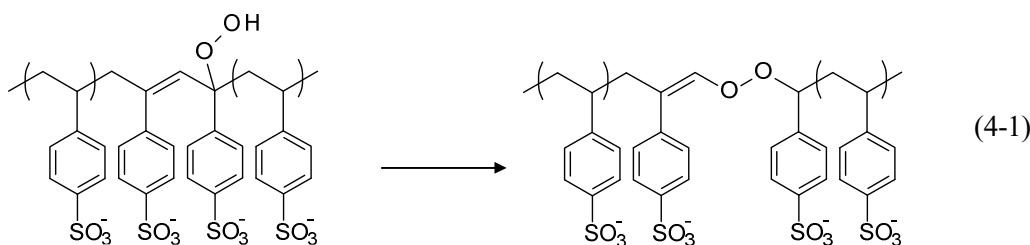
The "weak link" theory was particularly convincing to explain degradation of PSSA in solution exposed to oxygen, which requires initiating sites to trigger autoxidation. All the degradation experiments carried out at GE mentioned above appear to lead to similar products, i.e.,

benzaldehyde sulfonic acid, sulfobenzoic acid, formaldehyde, formic acid, and PSSA telomers. Therefore, it was presumed that the chain degradation mechanism is similar in all these cases.

In the context of fuel cells, polymer chain degradation is triggered by radical species produced in the fuel cell. This argument was already put forward in the 1960s [9]. It was known that PSSA undergoes degradation in the presence of H_2O_2 and traces of Fe^{2+}, which leads to the formation of the aggressive $HO^{\bullet}$ (Fenton reaction). It was observed that membranes tested in fuel cells showed more pronounced degradation on the anode, i.e., H_2 side. Based on these premises, the following mechanism of intermediate and radical formation was proposed:

$$H_2 \rightarrow 2\,H^{\bullet}\ (\text{on Pt}) \tag{4-2}$$

$$H^{\bullet} + O_2\ (\text{diffused through membrane}) \rightarrow HOO^{\bullet} \tag{4-3}$$

$$HOO^{\bullet} + H^{\bullet} \rightarrow H_2O_2 \tag{4-4}$$

$$H_2O_2 + M^{2+}\ (M = Fe, Cu) + H^+ \rightarrow M^{3+} + H_2O + HO^{\bullet} \tag{4-5}$$

$$HO^{\bullet} + H_2O_2 \rightarrow H_2O + HOO^{\bullet} \tag{4-6}$$
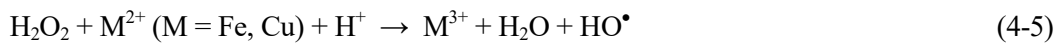
At the potential of the anode, which is in the range between 0 and 50 mV vs. RHE, dissociative adsorption of H_2 yields a monolayer of hydrogen on Pt (Reaction 4-2, the notation should rather be Pt-H, not $H^{\bullet}$). Crossover of oxygen from the cathode side to the anode side was deemed a key process, as O_2 reacts with adsorbed hydrogen to yield $HOO^{\bullet}$ (Reaction 4-3). The reaction of $HOO^{\bullet}$ with "$H^{\bullet}$", i.e. Pt-H, yields H_2O_2 (Reaction 4-4), which can diffuse into the membrane, where it undergoes the Fenton reaction to yield $HO^{\bullet}$ (Reaction 4-5). In Reaction 4-6, $HOO^{\bullet}$ reacts with H_2O_2 to yield $HOO^{\bullet}$. The hydroperoxyl radical ($HOO^{\bullet}$) was thought to be the main culprit for causing PSSA degradation, not $HO^{\bullet}$. This is clearly not the case, since $HO^{\bullet}$, ($E°(HO^{\bullet}/H_2O)$ = 2.72 V [455], is a much more potent oxidizing agent than $HOO^{\bullet}$, $E°(HOO•/H_2O_2)$ = 1.46 V [453]. Of all the intermediates, H_2O_2 had been found in the product water of fuel cells, while the radicals are too short-lived to be detected directly. Also, H_2O_2 was found when H_2 containing 5 % O_2 was bubbled through water in the presence of Pt catalyst. From today's point of view, some adjustment to this sequence of reactions is required. A current understanding of radical formation in the fuel cell is given in the next section. With the advent of Nafion$^{®}$ and other types of perfluoroalkylsulfonic acid (PFSA) membranes in the 1960s, attention shifted to this new class of ionomer with much superior chemical stability. PFSA ionomers underwent constant improving over the next decades by the various manufacturers to arrive at today's chemically stabilized, mechanically reinforced, thin (<20 μm) membranes used in automotive and other applications.

Considering the comparatively high crossover of H_2 and O_2 through these thin membranes, chemical stability and lifetime of PFSA membranes are still a focus of attention.

2.1 Radical Formation in the Fuel Cell

There has been some controversy regarding the origin of reactive intermediates, such as H_2O_2 and radicals ($HO^{\bullet}$/ $HOO^{\bullet}$), in the PEFC. H_2O_2 can, in principle, be formed directly at the cathode in the 2-electon oxygen reduction reaction (ORR) [488]:

$$O_2 + 2\,H^+ + 2\,e^- \;\rightarrow\; H_2O_2 \qquad\qquad (4\text{-}7)$$
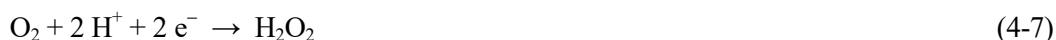
which has a standard electrode potential of $E° = 0.68$ V. The kinetics of H_2O_2 produced during ORR, however, will depend on the nature of the catalyst [489], the weight ratio of metal to carbon support [490] and the catalyst loading [491]. Also, the presence of specifically adsorbing anions, such as the sulfonic acid group in the ionomer, may promote the formation of H_2O_2 [492]. Yet, in OCV hold tests H_2O_2 production at the cathode can be neglected [122] because of , i) the absence of faradaic current, and ii) the high cathode potential of >0.9 V.

Hydrogen peroxide formation also takes place at the anode, via reaction of O_2 crossed-over from the cathode with hydrogen adsorbed on the Pt catalyst [5]. This is in agreement with the observation that H_2O_2 production during ORR increases dramatically at electrode potentials where hydrogen adsorption takes place [493]. The H_2O_2 formed within the catalyst layer may subsequently diffuse, together with water, into the gas diffusion layer (GDL) and out of the MEA into the product water, where it can be detected [494]. Alternatively, it may diffuse into the membrane. Owing to the presence of Pt in the catalyst layer, another possible fate of H_2O_2 is its decomposition on the surface of the platinum to oxygen and water, as it has been described in the 1950s by Gerischer and Gerischer [495]. They proposed that the reaction pathway involves hydroxyl and hydroperoxyl radicals, which are and remain adsorbed on the platinum surface, as intermediates.

The formation of $HO^{\bullet}$ and $HOO^{\bullet}$ from H_2O_2 via the Fenton reaction and related processes is well-known [5, 496, 497]. There has been some debate whether those oxygen centered radicals could also be formed directly at the anode or cathode catalyst. Release of $HO^{\bullet}$ and/or $HOO^{\bullet}$ from the cathode catalyst, for instance, during an intermediate step of ORR has been proposed based on density functional theory (DFT) studies [498, 499]. Since the platinum surface is covered with oxygenated species at the cathode side over most of the operating regime [500], the formation of

$HO^\bullet$ via the reaction of Pt-O with H_2O_2 has been proposed [501, 502]. Likewise, it is conceivable that radical intermediates generated at the anode are released into the bulk of the catalyst layer and membrane [503]. Furthermore, Vogel et al. have proposed that membrane-bound hydroxyl radicals can be formed from H_2O_2 via a dissociative Langmuir mechanism [504]. They used sulfonated polyarylene membranes in their experiments.

The operation of a fuel cell in an electron spin resonance (ESR) cavity has confirmed the presence of $HO^\bullet$ and $HOO^\bullet$ as well as $H^\bullet$ in the MEA via spin-trapping [381]. In particular, the presence of $H^\bullet$ may lead to different polymer attack mechanisms than the ones known in connection with $HO^\bullet$. Hydroxyl radicals were detected at the cathode only under load, not under OCV conditions, which is in support of H_2O_2 formation according to two-electron reduction of O_2, followed by decomposition to $HO^\bullet$. Hydrogen radicals were detected on both sides under OCV conditions as well as under load. Occurrence of $H^\bullet$ at the cathode is explained by the reaction of crossover H_2 with $HO^\bullet$. Hydroperoxyl radicals were found at both electrodes at OCV, and at the cathode after operation under load for ≥ 2 h, which was explained by electrochemical generation of $HOO^\bullet$ at the cathode and its chemical generation at the anode from hydrogen and crossover oxygen. The findings confirm that crossover of reactants is a decisive factor in the formation of reactive intermediates. At potentials near 0 V, mimicking conditions at the fuel cell anode, hydroxyl radicals were detected in the presence of O_2, but none under oxygen-free conditions [502]. Ghassemzadeh et al. exposed a catalyst coated PFSA membrane to mixtures of humidified H_2 and O_2 at a temperature of 80°C for 160 h [505]. They found, based on ^{19}F NMR analysis of the sample before and after the aging test, that the degradation rate was highest for H_2-rich mixtures of H_2 and O_2, which mimic the conditions on the anode side of the fuel cell. This finding supports the hypothesis that the formation of radicals via a chemical mechanism is important.

For the ranking of the oxidative strength of the various intermediates formed within the MEA, one can compare the bond dissociation energy (BDE) of the involved compounds and calculate the corresponding electrode potential for a one-electron reduction [365]. The hydroxyl radical is a very powerful oxidant, $E°(HO^\bullet/H_2O) = 2.72$ V. Because the H-O bond in water is very strong, abstraction of a hydrogen atom from another compound by $HO^\bullet$ is highly favorable. This can be particularly detrimental in hydrocarbon or partially fluorinated membranes, since the majority of bonds R-H have lower BDE than water. The kinetics of hydrogen abstraction by $HO^\bullet$ is usually very fast with rate constants of $10^8 - 10^{10}$ $M^{-1}s^{-1}$ [506]. In addition, $HO^\bullet$ reacts in many cases by addition to the reaction partner, in particular in case of aromatic compounds [507]. The OH-adduct then undergoes follow-up reactions, which can lead to the breakdown of the molecule.

Next in the oxidative strength pecking order is the hydrogen radical, $E°(H^•/H_2) = 2.32$ V, followed by the hydroperoxyl radical, $E°(HOO•/H_2O_2) = 1.46$ V. Thermodynamically, as a powerful oxidant, $H^•$ can potentially do harm to polymer constituents by hydrogen abstraction or addition with subsequent follow-up reactions. For instance, because of the lower bond strength in ROO-H and RO-OH, hydrogen abstraction can yield $ROO^•$ and $RO^•$, the latter again being a powerful oxidant. $H^•$ is also known to act as a reducing agent according to $H^• \rightarrow H^+ + e^-$ with $E°(H^+/H^•)$ = -2.32 V (IUPAC Task Group on Radical Standard Electrode Potentials, 2010, unpublished). For $HOO^•$, hydrogen abstraction reactions are generally several orders of magnitude slower than in the case of $HO^•$ [506]. For reactions in the gas phase, a linear correlation was found between the logarithm of hydrogen abstraction rate constants and R-H bond strengths [508]. A decrease in bond strength of 17 kJ/mol results in an increase in hydrogen abstraction rate of one order of magnitude. Therefore, based on the difference in hydrogen bond strength of water (497 kJ/mol) and hydrogen peroxide (366 kJ/mol), $\Delta H_{BDE} = 131$ kJ/mol, we estimate a difference in hydrogen abstraction rate by $HO^•$ and by $HOO^•$ of 7.7 orders of magnitude. According to Coms, it is very unlikely that the hydroperoxyl radical will participate in any kind of hydrogen abstraction reaction in PFSAs [169]. Concerning the role of H_2O_2, it is noteworthy that it does not tend to undergo reactions with the polymer directly, owing to its rather low oxidative strength. The concern associated with H_2O_2 is that it has to be regarded as a "carrier of disaster", as the much more aggressive $HO^•$ can be unleashed upon its decomposition.

2.2 PFSA Membrane Breakdown

PFSA membranes, such as Nafion®, were invented in the 1960s and showed excellent physical properties and oxidative stability compared to hydrocarbon based membranes, making them attractive for use in fuel cells and electrolysis cells [5]. This material represented the first durable and stable membrane for the PEFC, enabling lifetimes of many thousands of hours at a temperature of 80 to 90°C. However, studies at GE also showed that some fluoride ion as well as water-soluble, low-molecular-weight PFSA was found in the product water along with evolved CO_2. It was recognized early that the oxidative attack is caused by reactive oxygen species formed in the presence of H_2, O_2, and the Pt catalyst. According to the radical formation mechanism of LaConti et al. based on the crossover of O_2 through the membrane to the anode side (cf. Reactions 4-2 to 4-6), H_2O_2 is formed, which then decomposes in the presence of metal-ion impurities, such as Fe^{2+}, to form $HO^•$ (Fenton reaction). The $HO^•$ reacts with H_2O_2 to form $HOO^•$, which is thought to attack the polymer [9]. The mechanism is in agreement with the observation that membrane degradation is more pronounced on the H_2 side, for fuel cells as well as water electrolyzers [428]. The mechanism is flawed in the sense that $HO^•$ is much more likely to cause polymer degradation

compared to $HOO^{\bullet}$ owing to its higher oxidative power [440, 509]. The susceptibility to oxidative attack was attributed to the presence of traces of $-CHF_2$, originating from the synthesis procedure of the ionomer [5]. Those may undergo peroxo insertion to yield carboxyl groups, which could be easily detected in pristine and fuel cell tested membranes via IR spectroscopy.

Based on the notion of the presence of weak end-groups in fluoropolymers [510], the following often-cited mechanism of attack of $HO^{\bullet}$ on carboxylic end-groups in the main chain of PFSA ionomers has been put forward by DuPont [20]:

$$R_f - CF_2COOH + HO^{\bullet} \; \rightarrow \; R_f - CF_2^{\bullet} + CO_2 + H_2O \tag{4-8}$$

$$R_f - CF_2^{\bullet} + HO^{\bullet} \; \rightarrow \; R_f - CF_2OH \tag{4-9}$$

$$R_f - CF_2OH \; \rightarrow \; R_f - COF + HF \tag{4-10}$$

$$R_f - COF + H_2O \; \rightarrow \; R_f - COOH + HF \tag{4-11}$$

The attack by the hydroxyl radical leads to the formation of a perfluorocarbon radical, which undergoes further reaction to eventually yield again a carboxylic end-group. The overall reaction describes what has become known as an "unzipping" reaction, because after this sequence of reactions, the polymer chain end is again a carboxylic end-group, yet in the process one CF_2 unit has been removed in the form of two equivalents of HF and one equivalent of CO_2. Although this is in agreement with experimental results, some individual steps are questionable. The second reaction in the sequence, the reaction of the perfluorocarbon radical with another $HO^{\bullet}$, is highly unlikely due to the expected low concentration and short lifetime of these radicals. Coms proposed a refined, more realistic mechanism, according to which the fluorocarbon radical can react with H_2 or H_2O_2 to yield $-CF_2H$ (**Figure 4-3**). Hydrogen abstraction by $HO^{\bullet}$ again creates the fluorocarbon radical. Reaction with H_2O_2 can also yield the fluoroalcohol, which undergoes hydrolysis to complete the unzipping reaction [509].

The actual concentration of these groups in commercial PFSA materials has not been readily disclosed by the manufacturers. It has been estimated that the $-COOH$ end-group concentration is 2 to 3 orders of magnitude lower than the side chain concentration, i.e., around $2 - 20$ mM [511]. Experimentally, the concentration of end-groups can be determined via FTIR analysis, using the carbonyl vibrational band at 1'690 cm^{-1} [512]. Based on calibration measurements with PFSA membranes (Flemion®, Asahi Glass Co., Japan) in carboxylic acid form with known ion exchange capacity, a -COOH concentration in pristine sulfonic acid PFSA membranes of around 0.01 mmol/g was determined [513]. This corresponds to a concentration of 20 mM.
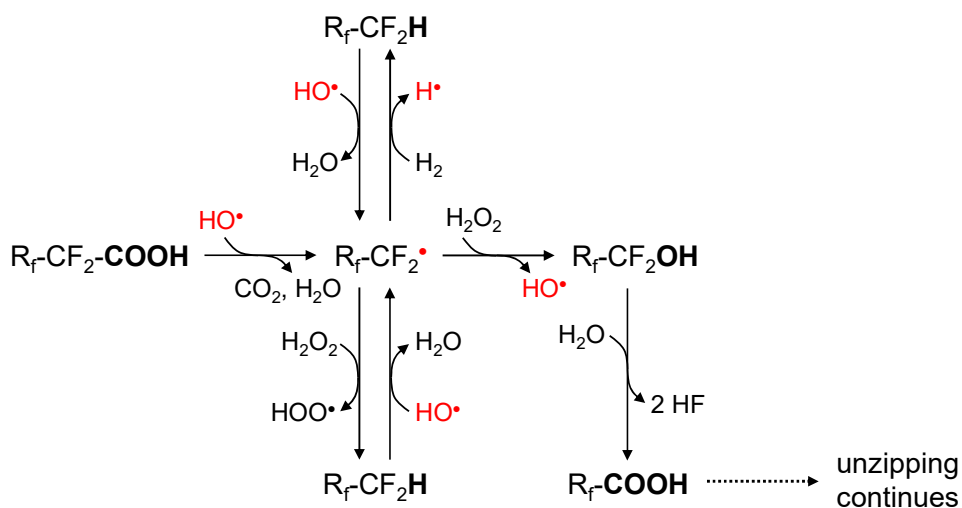
Figure 4-3. Mechanism of main chain unzipping in PFSA ionomers, initiated by the attack of HO$^\bullet$ on carboxylic acid end-groups. Adapted from Coms [509].

In view of the role of carboxyl end-groups triggering main chain unzipping in PFSA ionomers, PFSA manufacturers have successfully reduced the number of hydrogen bearing end groups through post-fluorination methods. In end-group stabilized PFSA membranes, no C=O vibration can be detected [514]. Thus chemically stabilized membranes showed a fluoride release rate that is more than an order of magnitude lower compared to that of unmodified membranes [20]. The observation that the rate of membrane degradation, as measured by the rate of fluoride release, increases with the –COOH concentration in the membrane is consistent with the proposed mechanism of the unzipping reaction [513]. A detailed analysis showed, however, that extrapolation of degradation rates to an end-group concentration of zero yielded a non-zero fluoride release rate. Indeed, stabilized membranes without measurable carboxylic end-group concentration showed a finite fluoride emission rate in accelerated fuel cell tests, in particular when sub-saturated reactant gas streams were used [514]. In the tested membranes, the signature of a carbonyl vibrational band appeared in the IR spectrum. This is attributed to side chain degradation mechanisms, which lead to the decomposition of the side chain and cleavage of the main chain at the branching point, creating two carboxylic end-groups [515]. In recent years, the notion of side chain attack has been gaining acceptance and is now considered an established fact. The mechanisms of side-chain attack, however, are not without controversy. A brief overview of the state of understanding is given in the following.

Side chain attack mechanisms have been discussed by various authors [509, 511, 516, 517]. According to Zhou et al., the ether linkages are weak points in the side chain of Nafion®, although they react around 500 times slower than –COOH end-groups [511]. Since, at least initially, the carboxylic end-group concentration is two to three orders of magnitude lower than that of the side

chains (based on one side chain every 15 -CF_2- main chain units in Nafion® with an equivalent weight of 1100 g/mol), the attack rate at the two locations could be similar. A recent DFT study confirmed that the C–O bond at the junction of the side chain and the main chain is the weakest bond (bond dissociation energy lower that 250 kJ/mol) in Nafion® [518]. Uegaki et al. exposed Nafion® 117 membrane selectively to $H^\bullet$, $HO^\bullet$ and $HOO^\bullet$ radicals using γ-irradiation under different conditions and observed side chain scission in all cases [517]. Both Cipollini and Coms propose $HO^\bullet$ attack at the sulfonic acid group [509, 516]. The mechanism involves hydrogen abstraction from the sulfonic acid group, yielding a sulfonyl radical (-$SO_3^\bullet$) according to Reaction 4-12 at low relative humidity, where sulfonic acid dissociation is less pronounced because of the lack of sufficient hydration energy [519]. This mode of hydrogen abstraction is supposedly facile [520].

$$R_f\text{-}CF_2\text{-}SO_3H + HO^\bullet \rightarrow R_f\text{-}CF_2\text{-}SO_3^\bullet + H_2O \tag{4-12}$$

$$R_f\text{-}CF_2\text{-}SO_3^\bullet \rightarrow R_f\text{-}CF_2^\bullet + SO_3 \tag{4-13}$$

Alternatively, a reaction of H_2O_2 with the sulfonic acid group is considered, leading to the formation of sulfonyl radicals via a bisulfonyl peroxide [509]. Subsequent fragmentation of the C-S bond and release of SO_3 leaves behind a -$CF_2^\bullet$ radical at the side chain end (Reaction 4-13), which will initiate side chain unzipping and, eventually, main chain cleavage. The presence of the chain end radical $ROCF_2CF_2^\bullet$ has been confirmed by EPR in Nafion exposed to Fe(II) and H_2O_2 [521]. This mechanism could explain the considerably higher fluoride release rates observed by most experimenters under sub-saturated conditions, e.g. Xu et al. [522]. Also, the finding that the fluoride release from a Nafion® 117 'cathode-only' MEA (90°C., H_2/O_2, 30 % r.h) was two orders of magnitude higher in the acid form compared to the alkali-ion exchanged form would be in agreement with this mechanism [121]. In a recent experimental study, PFSA membranes have been analyzed by ^{19}F NMR spectroscopy after having been exposed to a Fenton test solution for 12 h. Indeed, the side chain was found to have undergone stronger degradation than the main chain [523]. Predominant side-chain degradation was also found when a catalyst coated membrane was exposed to mixtures of humidified H_2 and O_2 in a chamber at 80°C for 160 h [505].

Regarding the reactivity of $HOO^\bullet$ with PFSA ionomer, there is only speculation. Cipollini suggested that $HOO^\bullet$ can react with the carboxylic end-groups [516], yet this mechanism does not appear plausible based on arguments of bond strength. Potentially, $HOO^\bullet$ can react with polymer-bound reactive intermediates after the attack by $HO^\bullet$. Fluorine atom abstraction by $H^\bullet$ from primary C-F bonds is unlikely to occur due to the high activation energy, yet F-abstraction from

secondary and tertiary C-F, thereby forming HF, is thermodynamically favorable [509]. The weakness of tertiary C-F bonds in Nafion® is confirmed in a DFT study [518]. Also, a Nafion® derived radical fragment in accordance with the mechanism of fluorine abstraction by H$^\bullet$ at the junction of the side chain with the main chain was detected by EPR [521]. This would lead to main chain scission and creation of additional -COOH end-groups [515], thereby accelerating the rate of degradation. Indeed, an increase in FER is observed in OCV hold tests, which, in addition to increased reactant crossover as a result of membrane thinning, can be explained by main chain scission and / or an enhanced radical formation rate due to Pt-band formation in the membrane as result of Pt dissolution from the cathode and redeposition in the membrane [473]. Danilczuk et al. carried out depth profiling on the cross-section of an accelerated stress tested Nafion® 115 membrane and detected vibrational bands consistent with the mechanism of abstraction of a fluorine atom by H$^\bullet$ from the tertiary carbon atoms at the junction of the side chain to the main chain and in the side chain. The reaction of H$^\bullet$ with the polymer is in strong competition with the reaction of H$^\bullet$ with O_2 to form HOO$^\bullet$ [370], which is very fast, but the concentration of tertiary fluorine in PFSA ionomer is rather high with around 1 M[1]. Despite the expected low concentration of hydrogen radicals [440], attack by H$^\bullet$ may account for substantial ionomer degradation and may be the reason for enhanced degradation on the anode side, which is observed by many experimenters, because the lifetime of H$^\bullet$ is longer near the anode owing to the lower O_2 concentration. It has even been argued that molecular hydrogen can react directly with the perfluoroalkyl chain (-CF_2-), replacing the fluorine by hydrogen and leading to the formation of HF [524, 525]. Although this reaction is favorable from an energetic point of view ($\Delta H_{BDE} \approx$ -67 kJ/mol), the activation energy is probably prohibitive.

2.3 Studying Radical-Induced Membrane Degradation

The understanding of radical induced degradation of the electrolyte membrane and ionomer in a PEFC is a challenging task. The membrane electrode assembly constitutes a complex combination of materials and components, where intermediates may be formed in various locations and the resulting radicals react according to a variety of mechanisms, which may or may not be harmful to the components of the cell. In addition, the pathways and kinetics of radical formation and reaction crucially depend on the operating conditions of the cell, such as temperature and humidity [526].

---

1   In a PFSA ionomer, there is at least on tertiary fluorine, at the carbon that links the side chain to the main chain. Depending on side chain chemistry, more tertiary fluorine is present.

In general, furthering the understanding of ionomer degradation can be tackled on various levels of complexity. In an integrated configuration, the membrane is assembled together with electrodes in a fuel cell hardware and its aging is assessed as a function of operating time of the cell or in post-test analysis. It is important to note, however, that, depending on the operating conditions, also the other components, such as catalyst and seals, undergo degradation, which may in turn affect the kinetics of radical formation and, consequently, the chemical stress the membrane is exposed to. In order to single out individual component degradation mechanisms, it has been common practice for more than a decade now to operate the MEA and cell under conditions of accelerated stress. An accelerated stress test (AST) is designed such that, at least ideally, only one single degradation mechanism is activated, such as radical induced membrane degradation or catalyst carbon support corrosion, while all other degradation mechanisms are minimized or deactivated. For this purpose, dedicated AST protocols for chemical membrane degradation, mechanical membrane degradation, electrocatalyst and catalyst support stability have been defined in the framework of the Hydrogen and Fuel Cells Program funded by the US Department of Energy (DOE) [522].

The AST for chemical degradation of the membrane involves operation of the cell at open circuit voltage (OCV). In the case of PFSA ionomer, chemical degradation of the membrane, measured by the fluoride emission rate (FER) from the cell, has been found to increase with decreasing current density, with the maximum rate obtained at OCV [316]. The decrease in H_2 and O_2 crossover rate has usually been put forward as the reason for the decrease in FER towards increasing cell current density [269, 527]. Yet an increase in current density also leads to a change in electrode and catalyst surface properties, activity of H^+ and H_2O. These changes may also influence the yield of membrane-degrading species [316]. The presence of transition metal ion impurities, such as iron, is believed to be an important factor regarding the formation of these reactive intermediates [440], because Fe^{2+} catalyzes the decomposition of H_2O_2 to form $HO^{\bullet}$ (Fenton reaction, Reaction 4-5). It has been recently suggested that the concentration ratio of Fe^{2+} to Fe^{3+} decreases with decreasing cell voltage / increasing current density [528]. Therefore, at OCV the concentration of Fe^{2+} would be at a maximum, which would explain the high rate of membrane degradation, since the Fenton reaction is maximized.

Another important factor for membrane degradation, besides temperature obviously, is the relative humidity of the reactants. For Nafion® membranes, it has been found that membrane degradation is promoted under sub-saturated conditions [428]. It has been suggested that lower humidity could lead to a higher local concentration of radical-generating Fenton reagents (e.g. H_2O_2) as a result of the reduced water content in the MEA, which can promote the formation of radicals and thus

chemical attack [529-531]. Accordingly, the FER shows an increasing trend with decreasing RH during OCV hold tests [531, 532]. Yet, the result of Xu et al. shows that at RH values well below 60% PFSA membrane degradation decreases again, which is attributed to two counteracting effects of RH on gas permeability and catalytic activity of the radical formation reaction on the platinum surface [522]. This trend of RH dependence may or may not be similar for non-perfluorinated membranes. The investigation of the effect of RH on the degradation of styrene based radiation grafted membranes will be presented in Section 4.1.1.

A test configuration with reduced level of complexity consists of the membrane being exposed to artificially generated reactive intermediates. A "Fenton test" is a widely used method to characterize the stability of a polymer against oxidative attack [440]. In an aqueous solution of H_2O_2 and Fe^{2+}, $HO^\bullet$ is generated. The shortcoming of these tests has repeatedly been highlighted, in that the outcome of the test may not be in agreement with stability data obtained in the fuel cell. Sethuraman et al. for example showed that although a polyaromatic membrane was much less stable than Nafion® in a Fenton test, the membrane outlasted Nafion® in an accelerated stress test at OCV in the single cell, which is a result of the much lower permeability of the polyaromatic membrane for H_2 and O_2 compared to Nafion® [141], yielding a lower concentration of membrane-degrading species. In other setups, the membrane or MEA is exposed to a H_2O_2 containing environment, either in a flow cell or a H_2O_2 / water vapor reactor [513, 515, 533, 534], where typically the amount of fluoride released from the membrane is quantified. In addition, more elaborate analysis methods of the condensate, such as HPLC [535] or NMR spectroscopy [534], can be employed.

In addition to measuring the concentration of decomposition products in the effluent water or cell characteristics, such as the OCV, to quantify membrane degradation of the membrane indirectly, a more direct method to assess the membrane state-of-health is desired, yet the approach is complicated by the fact that the interior of the cell and MEA has to be somehow probed. As already highlighted in Section 2.1, electron spin resonance (ESR) spectroscopy, also referred to as electron paramagnetic resonance (EPR) spectroscopy, can be used to detect radical species. However, due to the short lifetime of the radicals, spin-trapping is commonly used to obtain longer lived intermediates. In the work of Schlick et al., a miniature fuel cell was inserted into the resonator of an ESR spectrometer. In addition to the radicals $HO^\bullet$, $H^\bullet$ and $HOO^\bullet$ carbon centered radicals were identified, which are indicative of membrane attack and degradation [381]. A similar approach was used by Roduner et al. [536].

Ghassemzadeh et al. used solid-state ^{19}F-NMR spectroscopy to study chemical degradation of PFSA membranes exposed to Fenton solution [523, 537], HO$^{\bullet}$ and H$^{\bullet}$ radicals created by electron beam irradiation of water [538], a fuel cell test [539], and membranes as well as catalyst coated membranes exposed to mixtures of H_2 in O_2 and vice-versa [505]. The body of data confirms that side chain degradation is significant, in case of end-group stabilized membranes it is the predominant degradation mechanism.

Nosaka et al. introduced coumarin, a fluorescent probe, into the MEA, which reacts with HO$^{\bullet}$ formed during cell operation to form umbelliferone, which can be detected by fluorescence spectroscopy of the probe solution sampled from the MEA [503, 540]. The method does not allow the detection of the *concentration* of HO$^{\bullet}$ in an operating fuel cell but the *rate* of HO$^{\bullet}$ formation. Later, the method was refined to allow mapping of the umbelliferone over the crossection of the membrane disassembled from the cell after the test using an optical microscope modified for fluorescence measurements [526, 541].

A similar approach, yet using *in situ* fluorescence spectroscopy measurements, has been reported by Ramani et al. [542-545]. Fluorescin or 6-carboxy-fluorescin was used as fluorescent dye, which as incorporated into a Nafion® membrane. For the *in situ* fluorescence spectroscopy, a 200 μm thick optical probe was placed between two membranes that sandwiched it, which was then assembled into an MEA and a single cell. The optical probe provided a conduit for both the incident light used to excite the fluorescin dye and the resulting fluorescence response. The reaction of the fluorescin molecule with HO$^{\bullet}$ led to a loss of the fluorescence intensity, which could be continuously measured during cell operation. Also, the degradation mitigating effect of ceria particles incorporated into the membrane could be demonstrated in this manner.

With all the approaches and methods highlighted so far, although it is possible to detect the presence of radicals in the MEA in an operating fuel cell and measure, as reported in case of HO$^{\bullet}$, the rate of HO$^{\bullet}$ formation and the reactions it undergoes, it is not possible to determine kinetic rate constants for the reaction with radicals. This would be a prerequisite to allow the implementation of kinetics models to simulate membrane degradation. The determination of the mechanism and kinetics of radical attack on fuel cell membrane materials calls for methods where the reactive intermediates, such as HO$^{\bullet}$ and H$^{\bullet}$, can be created in a defined way and with known concentration and where the reaction of those species with the substrate can be accurately measured and quantified. In the literature, a number of methods have been reported to accomplish this. The approaches are typically based on the use of model compounds, i.e. low-molecular weight

constituents of the parent polymer, which are soluble in water and thus represent a homogeneous reaction medium, within which the radical intermediates are created. Hübner and Roduner studied the HO$^\bullet$ initiated degradation of sulfonated aromatic compounds, such as toluenesulfonic acid, as model compounds for polyaromatic and styrene based radiation grafted membranes [315]. Photolysis of H_2O_2 was used to generate HO$^\bullet$ radicals, and reaction products were identified by ESR. Based on the results, implications for fuel cell membranes containing aromatic units were discussed. Zhou et al. reported a similar approach for model compounds of PFSA membranes, which were exposed to Fenton's reagent and UV photolysis [511, 546]. Degradation products of model compounds as well as membranes were consistent with HO$^\bullet$ attack at the carboxylic groups and ether linkages, whereby the latter mechanism was 500 times slower than the former. Only Dreizler and Roduner reported kinetic rate constants for reactions of HO$^\bullet$ with various model compounds, such as trifluoroacetic acid and trifluoromethanesulfonic (triflic) acid, based on a competition kinetics approach [547]. They used photolysis of H_2O_2 to create HO$^\bullet$. The rate constants for the reaction between HO$^\bullet$ and the model compounds was determined by measuring the ESR signal intensities of the spin-trap/OH adduct first in the absence and then in the presence of a given model compound. The obtained rate constants showed reasonable agreement with literature values, mostly obtained in pulse radiolysis studies.

3 Studies of Radical Attack on Oligomer Model Systems

In the framework of the study reported here, model compounds of grafted membranes, consisting of poly(styrene sulfonate) (PSS) and poly(α-methylstyrene sulfonate) (PAMSS) oligomers in aqueous solution, were exposed to radicals created via the pulse radiolysis technique (cf. Chapter II). The ensuing reactions were followed via UV-VIS spectroscopy, which allows the determination of reaction rate constants. The oligomers represent the graft component, which is known to be susceptible to radical induced degradation [315]. They are polyelectrolytes and therefore soluble in water, which allows pulse radiolysis to be used. In general, the model compounds can be chosen from single monomer units to long chain polyelectrolytes representative of the grafted chain. Single unit model compounds have, for instance, been used by Assink et al. to study their stability in alkaline ferricyanide electrolyte [251].   Cumenesulfonic acid[1] represented the repetitive unit of poly(styrenesulfonic acid), whereas *tert*-butylbenzenesulfonic acid represented the repetitive unit of poly(α-methylstyrenesulfonic acid). The shortcoming of these compounds is that possible intramolecular reactions in the polyelectrolyte are neglected. On the other hand, long-chain polyelectrolytes are known to form coiled structures in aqueous solution [548]. Although this configuration mimics the situation in the water-swollen grafted membrane, it is not a representative constellation to study the intrinsic kinetics of radical attack on the polyelectrolyte. Therefore, in the study reported here, oligomers with a length of a few monomer units were chosen. Higher order coiled structures are not present when the molecular weight of the PSS is lower than ca. 4'500 g/mol [365]. The pulse radiolysis study is focused on studying the attack of HO$^\bullet$ on the PSS oligomer. The degradation caused by HO$^\bullet$ is considered the most important aging mechanisms, yet one has to keep in mind that H$^\bullet$ and HOO$^\bullet$ are also present and could also play a role in the degradation pathway.
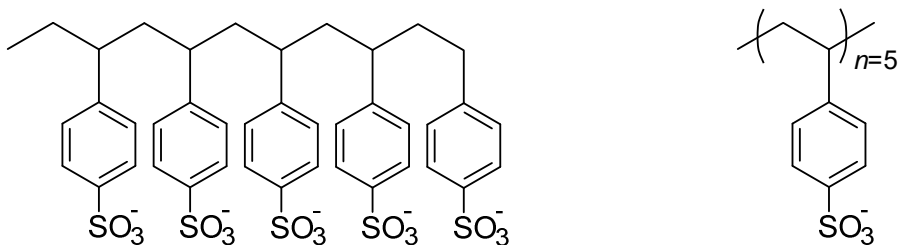
Figure 4-4. Model compound of poly(styrene sulfonate) (PSS) with an average molecular weight of 1'100 g/mol (PSS-1100) used in the pulse radiolysis study.

---

[1] cumene = isopropylbenzene

3.1 Poly(Styrene Sulfonate) Oligomer

In the study reported here, poly(styrene sulfonate) with an average molecular weight of 1'100 g/mol is used as substrate, corresponding to a degree of polymerization of $n = 5$ (**Figure 4-4**). HO$^\bullet$ radicals are created selectively via pulse radiolysis in N$_2$O saturated aqueous solution (cf. Chapter II). Follow-up reactions are studied in the presence and absence of O$_2$. Furthermore, decay of intermediates is studied at low pH, representative of the conditions in the fuel cell.

3.1.1 Reaction with HO$^\bullet$

The absorption spectrum of 100 μM PSS-1100 solution 3 μs after pulse irradiation at near-neutral pH indicates the formation of two types of intermediates (**Figure 4-5**): an OH-adduct and a benzyl radical, according to reactions 1 and 2 (Eq. 4-14 and 4-15). From the reported spectra in the literature of benzyl radicals and HO-adducts, it is possible to estimate the respective chemical yields of the two intermediates. The absorption maximum of benzyl radicals is at 280 nm, the maximum of HO-adducts at 340 nm. HO-adducts also contributes to the absorbance at 280 nm, which as to be taken into consideration. The analysis yields that around 90 % of the HO$^\bullet$ react via addition (reaction 1) and only 10 % abstract hydrogen from the α-carbon to create the benzyl radical (reaction 2) [365]. These values are consistent with those reported for the reaction of HO$^\bullet$ with monomeric alkylbenzene sulfonates (75-85 % HO$^\bullet$addition) [549] and toluene (97 %) [550].

$$(4\text{-}14)$$

$$(4\text{-}15)$$
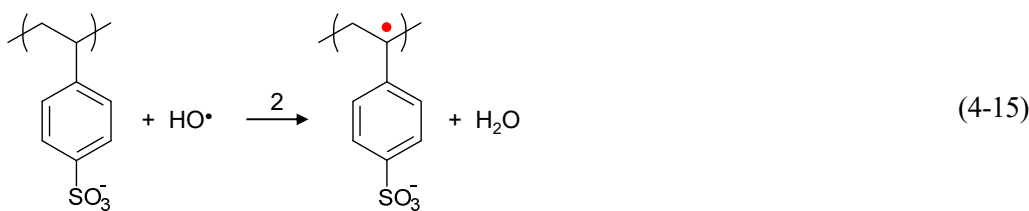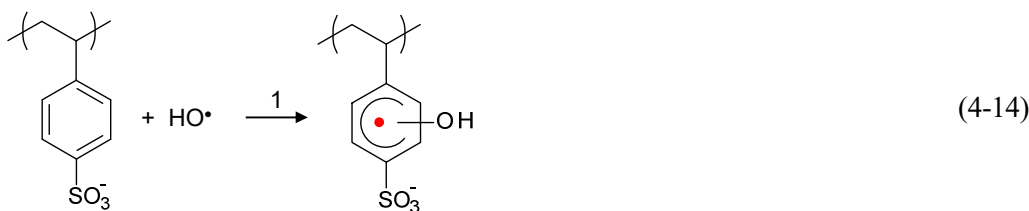
The kinetics of the attack of HO$^\bullet$ on the oligomer was studied by following the absorbance of the intermediates as a function of time after the pulse. Typically, the absorbance at a wavelength representative of an intermediate builds-up over a time frame of around 10 μs (**Figure 4-6**), from which the pseudo-first-order rate constant k_{obs} can be determined. A series of experiments with different concentration of the oligomer ranging from 30 to 300 μM was carried out in this manner. The observed rate constants follow a linear trend through the origin (**Figure 4-7**), from which the second-order rate constant for the reaction of HO$^\bullet$ with the oligomer can be obtained as a

combination of adduct and benzyl radical formation, $k_{tot} = k_1 + k_2 = (9.5 \pm 0.6) \cdot 10^9 \text{ M}^{-1}\text{s}^{-1}$. From the fraction of HO$^{\bullet}$ reacting to the HO-adduct (90 %) and benzyl radical (10 %), the reaction rate constants $k_1 = (8.5 \pm 1.0) \cdot 10^9 \text{ M}^{-1} \text{ s}^{-1}$ and $k_2 = (1.0 \pm 0.1) \cdot 10^9 \text{ M}^{-1} \text{ s}^{-1}$ are obtained, respectively.
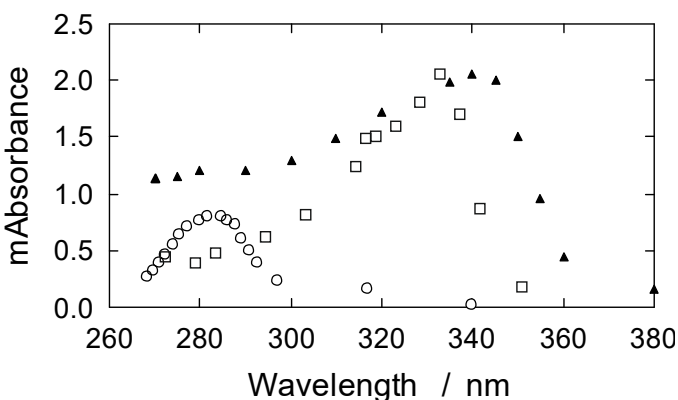
Figure 4-5. Absorption spectrum (▲) constructed from absorbance measurements, 3 μs after pulse irradiation (8 Gy) of 100 μM PSS-1100 N$_2$O-saturated solutions near neutral pH. The absorbance readings are normalized to 1 Gy and reflect the sum of the HO-adduct and benzyl radical products. Scaled spectra of the HO-adduct of 1,3,5-trimethylbenzene(□) (Ref. [551]) and benzyl radicals (O) (Ref. [549]) are shown for comparison.
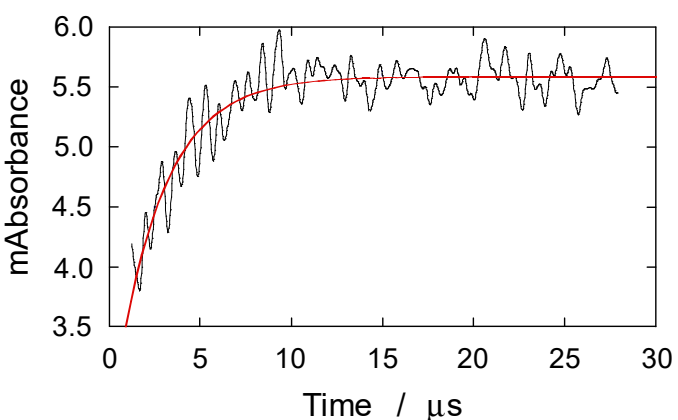
Figure 4-6. Change of optical density at 340 nm for a solution of 30 μM PSS-1100, N$_2$O saturated, at pH 6.5 and 9 Gy dose, indicating the formation of HO-adduct (cyclohexadienyl radical). The red line indicates a 2nd order fit.

Similar experiments were performed with PSS of a higher molecular weight of 77'000 g/mol, yielding a rate constant of $k_{tot} = (5.2 \pm 0.8) \cdot 10^8 \text{ M}^{-1}\text{s}^{-1}$. The values of k_{tot} for the reaction with monomeric compounds and PSS of different molecular weight, based on own measurements or literature data, are collected for comparison in **Table 4-1**. The coiled structure of higher molecular weight polymers of PSS minimizes the effective surface area for reaction. The second-order rate constants are consistent with correlations of molecular weight and surface area, as k_{tot} increases as a function of molecular weight up to PSS-1100, but decreases as a function of effective surface area for PSS-70k, PSSS-77k and PSSS-1M.
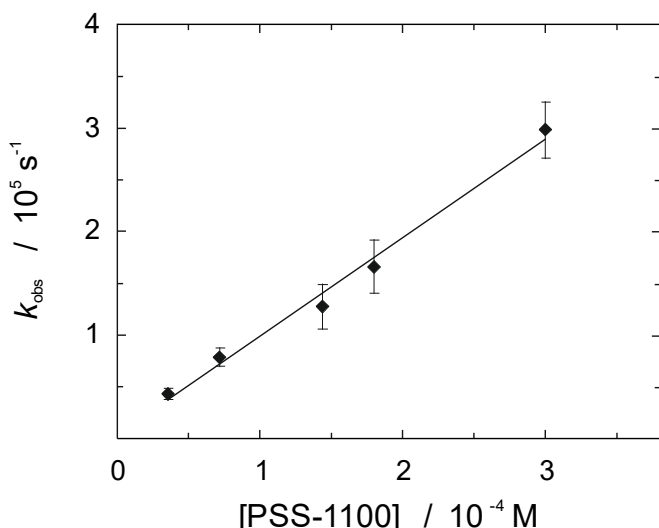
Figure 4-7. Pseudo-first-order rate constants for the reaction of HO$^\bullet$ with PSS-1100 as a function of PSS-1100 concentration; N$_2$O-saturated solutions, irradiated (dose 8 Gy) near neutral pH.

Table 4-1. Second-order rate constants for the reaction of HO$^\bullet$ with different sulfonated aromatic compounds near neutral pH. For PSS, the numbers indicate different molecular weights in Da.

Substrate	k(HO$^\bullet$) (M^{-1}s^{-1})	Ref.
benzenesulfonate	$(4\text{-}6)\cdot10^9$	this work
4-cumenesulfonate	$(8.0 \pm 0.8)\cdot10^9$	[549]
PSS-1100	$(9.5 \pm 0.6)\cdot10^9$	this work
PSS-1100[a]	$(1.9 \pm 0.1)\cdot10^9$	this work
PSS-70k[a]	$(7.5 \pm 1)\cdot10^8$	[552]
	$1.1\cdot10^9$	[548]
PSS-77k[a]	$(5.2 \pm 0.8)\cdot10^8$	this work
PSS-1M[a]	$5.5\cdot10^8$	[548]

[a] rate constant related to the concentration of monomer units

3.1.2 Follow-up reactions in the presence of O$_2$

The kinetic trace in **Figure 4-6** shows the change of absorbance within the first tens of microseconds. The intermediates formed, however, are radical species and expected to undergo follow-up reactions. Therefore, the optical properties of the irradiated solutions are investigated over longer periods of time, under inert conditions as well as in the presence of O$_2$, which is relevant for the conditions in the fuel cell. In fact, also the effect of the presence of H$_2$ ought to be investigated, yet this was beyond the scope of the study reported here. **Figure 4-8** shows the increase of absorbance at 340 nm during the first 5 µs, indicative of HO-adduct formation. The subsequent decay in absorbance appears to depend on the presence of oxygen. The presence of 100 µM oxygen accelerates the decay of the HO-adduct compared to the rate of decay in O$_2$-free solution, which suggests that the HO-adduct reacts with O$_2$ according to reaction 3 (Eq. 4-16).
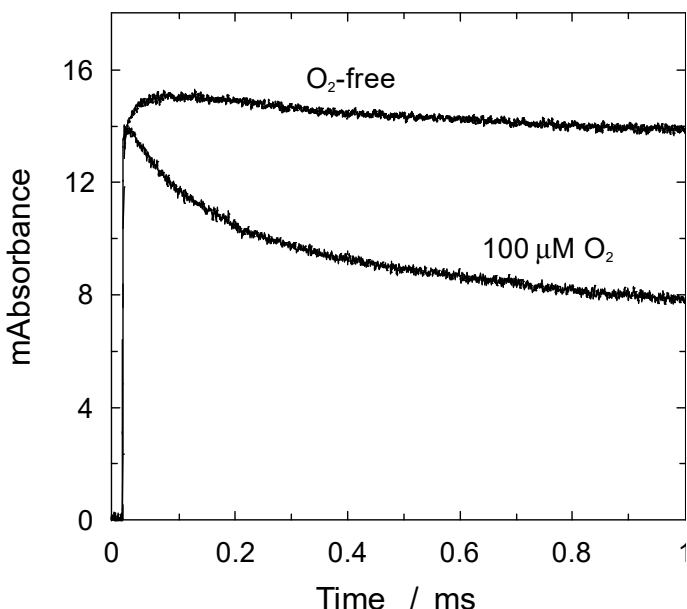
Figure 4-8. Pulse radiolysis (dose 7 Gy) of 120 µM PSS-1100 solutions purged with N_2O and O_2/N_2O, near neural pH, in the presence and absence of 100 µM O_2, indicating the formation and initial-phase decay (millisecond range) of HO- and H-adducts followed at 340 nm.

$$(4\text{-}16)$$
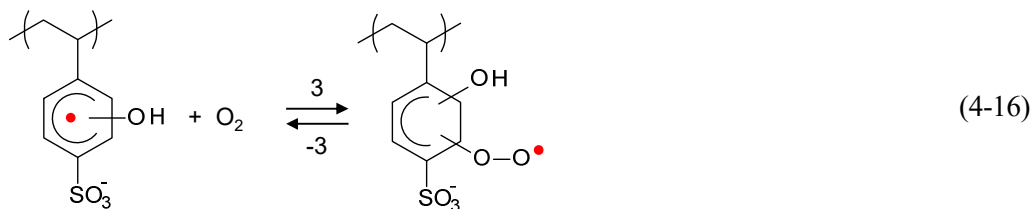
Based on a series of pulse radiolysis experiments with different O_2 concentrations ranging from 50 to 300 µM, the resulting kinetic traces could be fitted accurately up to at least 1 ms with a double-exponential function, describing HO-adduct formation according to reaction 1 (Eq. 4-14) and decay of this intermediate. The reaction of a C-centered radical with O_2 to form the corresponding peroxyl radical generally proceeds with a rate constant on the order of 10^9 $M^{-1}s^{-1}$ [553]. However, because of electron delocalization in allylic and dienylic C-centered radicals, oxygen binds relatively weakly [554-557], which results in slower and reversible O_2 addition. In analogy for the reversible addition of O_2 to pentadienyl radicals, in which the decay of the oxygen adduct is relatively slow, $k = (0.34 - 1.1) \cdot 10^3$ s^{-1} [558], the initial phase of the decay of absorbance up to (**Figure 4-8**) is treated as reaching equilibrium of reactions 3 and -3 (Eq. 4-16) with $k_{3obs} = k_3 \cdot [O_2]$ + k_{-3}. From a plot of k_{3obs} as a function of $[O_2]$ (**Figure 4-9**), we obtain a forward rate constant of $k_3 = (3.0 \pm 0.5) \cdot 10^7$ $M^{-1}s^{-1}$ and a reverse rate constant of $k_{-3} = (4.5 \pm 0.9) \cdot 10^3$ s^{-1}. The obtained rate constant k_3 is between the values reported for aromatics with electron-withdrawing substituents (10^6 $M^{-1}s^{-1}$) and aromatics with electron-donating substituents (10^8 $M^{-1}s^{-1}$), and ca. twice that reported for terephthalate ($1.6 \cdot 10^7$ $M^{-1}s^{-1}$) [558]. The resulting equilibrium constant for reactions 3 and -3 is $K_3 = k_3 / k_{-3} = (7 \pm 2) \cdot 10^3$ M^{-1}.
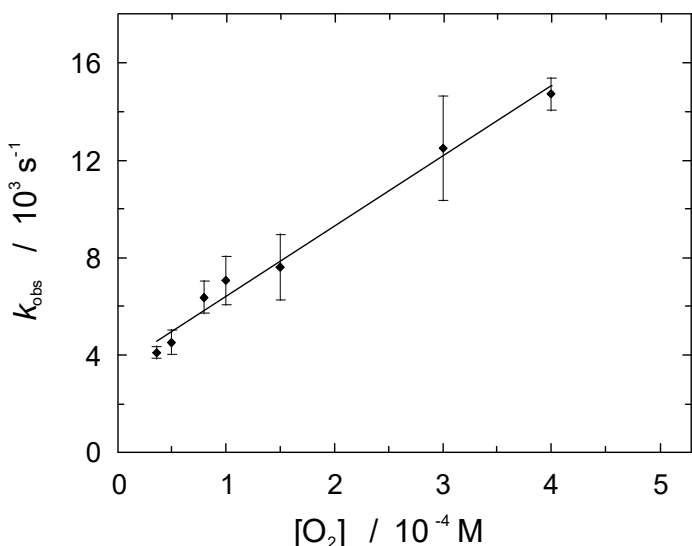
Figure 4-9. Observed rate constant for the pseudo-first-order decay of the OH-adduct, obtained from pulse radiolysis of 100 μM solutions of PSS-1100, at different O_2 concentrations (cf. Figure 4-8).
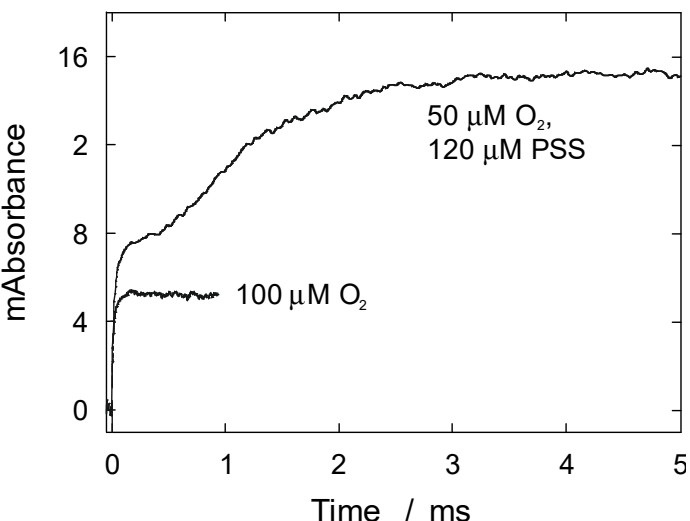
Figure 4-10. Change of optical density at 360 nm in the presence of 30 μM $C(NO_2)_4$, indicating the reaction with $O_2^{\bullet-}$ and formation of $C(NO_2)_3^-$ in the presence (upper trace) and absence (lower trace) of PSS-1100; N_2O/O_2-saturated, near neutral pH, dose 5 Gy.

In the later phase beyond 1 ms the absorbance at 340 nm does actually not stabilize at the equilibrium between reaction 3 and -3 but shows a continued slow decay (not shown). It is assumed that the reaction taking place is the elimination of HOO$^\bullet$ from the peroxyl adduct according to reaction 4 (Eq. 4-17). This reaction can be followed via trapping of the $O_2^{\bullet-}$ radical (pK$_a$ of HOO$^\bullet$ is 4.8 [372]) with tetranitromethane (TNM), forming the trinitromethanide anion, which absorbs at 360 nm: $O_2^{\bullet-} + C(NO_2)_4 \rightarrow O_2 + C(NO_2)_3^- + NO_2^\bullet$ ($k = 2 \cdot 10^9$ M^{-1}s^{-1} [372]).

$$(4\text{-}17)$$
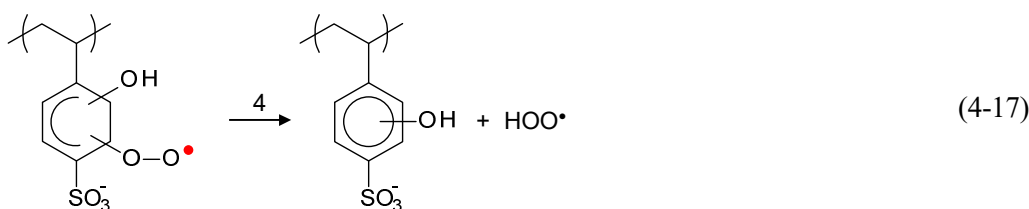
Kinetic traces of this reaction are shown in **Figure 4-10**. In the absence of the PSS oligomer, the reaction in the presence of 100 µM O_2 indicates the reaction of TNM with $HOO^\bullet$, formed via the reaction of primary $H^\bullet$ with O_2. In the presence of PSS-1100 the additional absorbance is due to additional $HOO^\bullet$ produced via reaction 4. The observed rate constant for this reaction is $k_{obs4} = k_4 \cdot K_3[O_2] / (1 + K_3[O_2])$, which is plotted in **Figure 4-11** as a function of the oxygen concentration. Fitting yields $k_4 = (2.7 \pm 0.3) \cdot 10^3$ s^{-1}, which agrees well with literature values [558].
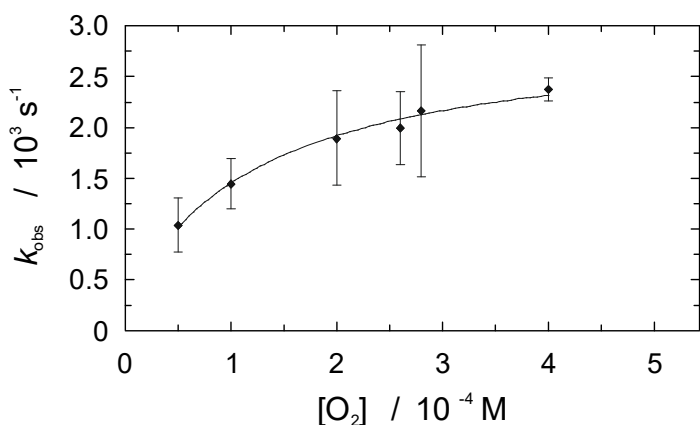
Figure 4-11. Observed rate constant for the elimination of $HOO^\bullet$ from the peroxyl-radical adduct (reaction 4), from which the first order rate constant k_4 can be estimated.

3.1.3 Reactions at low pH

The pulse radiolysis experiments discussed thus far have all been carried out at near-neutral pH. In the fuel cell, however, low pH conditions prevail. During pulse radiolysis at low pH, hydrated electrons react with H^+ to form additional $H^\bullet$ radicals (cf. Chapter II). Both $H^\bullet$ and $HO^\bullet$ react with the PSS-1100 oligomer to form the corresponding adduct, both of which show a maximum of absorption at 340 nm (in addition, both radicals react via α-H abstraction) [559]. To exclude the reaction with $HO^\bullet$, pulse radiolysis was carried out in the presence of 0.01 M *t*-BuOH, which serves as a $HO^\bullet$-scavenger. In this case, the decay of the H-adduct occurs with a first-order rate constant on the order of 10^4 s^{-1}. By subtracting the rate of decay of the H-adducts from the overall decay of HO- and H-adducts (**Figure 4-12**), a first-order rate constant for the decay of HO-adducts of $(6 \pm 1) \cdot 10^3$ s^{-1} is found at pH 1.
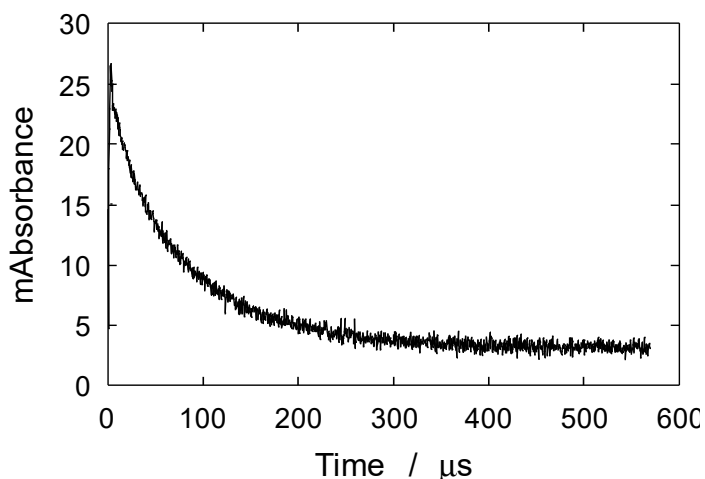
Figure 4-12. Formation and decay of H- and OH-adducts observed at 340 nm from pulse radiolysis of 90 μM PSS-1100 solutions (Ar saturated) at pH 1 (0.1 M HClO$_4$); dose 4 Gy, 0.01 M *t*-BuOH.

Protonation of the HO-adduct (Eq. 4-18) proceeds with $k_5 = 1.9 \cdot 10^9$ M^{-1} s^{-1} [560], which results in a pseudo-first order rate constant k_{obs5} of $1.9 \cdot 10^6$ s^{-1} and $1.9 \cdot 10^8$ s^{-1} at pH 3 and pH 1, respectively.
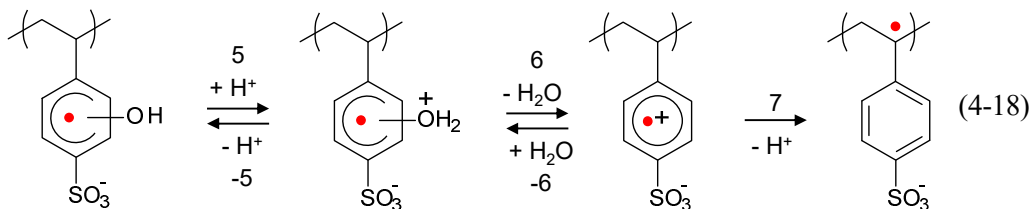
Water elimination from the protonated HO-adduct of aromatic compounds with electron-donating substituents results in the formation of a radical cation [560, 561]. To investigate the reaction mechanism at low pH in more detail, SO$_4^{\bullet-}$ radicals, $E°(SO_4^{\bullet-}/SO_4^{2-}) = 2.4$ V [562], were created by pulse radiolysis of solutions containing potassium persulfate (K$_2$S$_2$O$_8$). These react with aromatic compounds via electron-transfer to yield an intermediate radical cation:
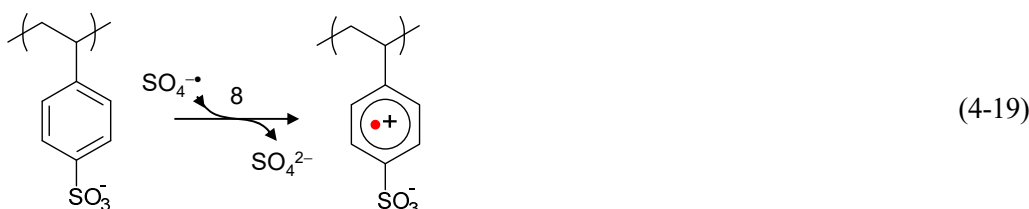
Figure 4-13 shows the formation and decay of SO$_4^{\bullet-}$, followed at 450 nm, in the presence of the PSS-1100. SO$_4^{\bullet-}$ reacts with the oligomer with $k_8 = (5.5 \pm 1) \cdot 10^8$ M^{-1} s^{-1}. **Figure 4-13** illustrates the simultaneous formation of a transient species that absorbs strongly at 280 nm. A spectrum recorded 6 μs after pulse irradiation of an aqueous solution that contained 1 mM PSS-1100, 0.1 M *t*-BuOH and 0.02 M K$_2$S$_2$O$_8$ at pH 3 is shown in **Figure 4-14** and is characteristic of the benzyl radical. We observed complete conversion of SO$_4^{\bullet-}$ to benzyl radicals.
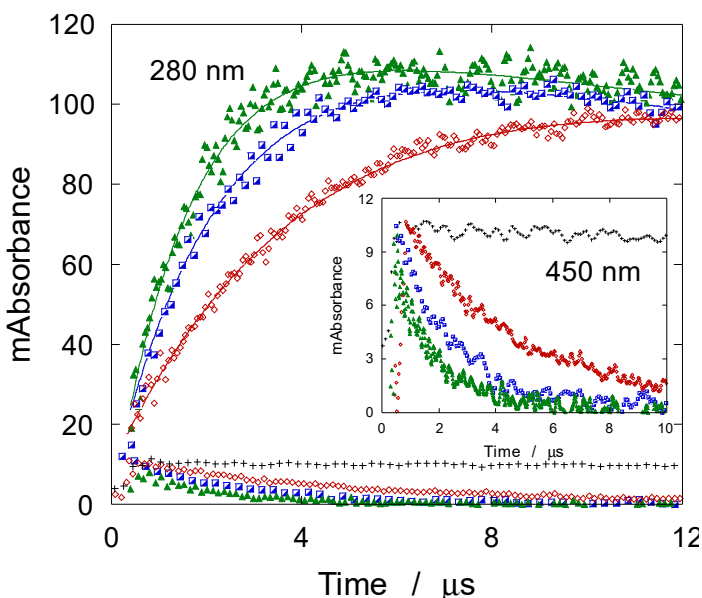
Figure 4-13. Formation and decay of $SO_4^{\bullet-}$ followed at 450 nm and corresponding increase of absorbance at 280 nm, which is mainly due to the formation of benzyl radicals, from pulse irradiated (dose 25-35 Gy) 0.05 M $K_2S_2O_8$ Ar purged solutions at pH 3.4, in the absence of PSS-1100 (+) and in the presence of 0.5 mM (red), 1 mM (blue) and 1.5 mM (green) PSS-1100. The points were fitted by simulation (solid lines) to an exponential curve with $k_{obs} = 2.7 \cdot 10^5$ s^{-1} (red), $5.2 \cdot 10^5$ s^{-1} (blue) and $7.6 \cdot 10^5$ s^{-1} (green) and a second-order decay with the rate constants k of $1.1 \cdot 10^9$ M^{-1}s^{-1}(red), $1.7 \cdot 10^9$ M^{-1}s^{-1} (blue), and $1.2 \cdot 10^9$ M^{-1}s^{-1} (green).
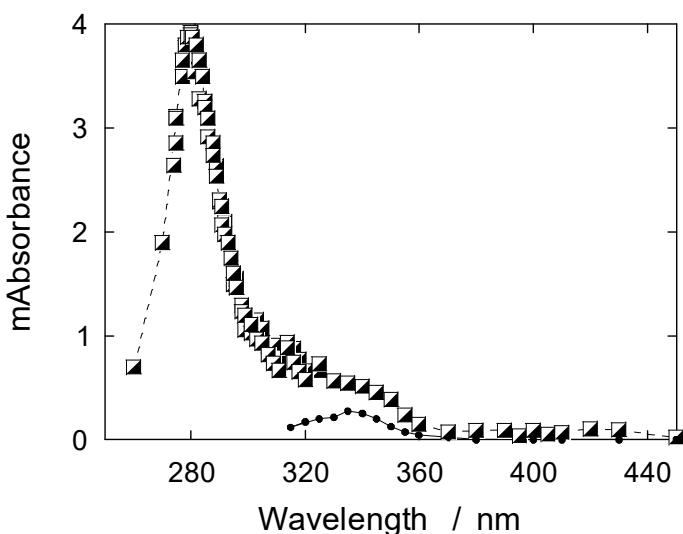
Figure 4-14. Normalized absorption spectrum recorded 6 μs after pulse irradiation (8 Gy) of a 1 mM PSS-1100 solution; 0.1 M *t*-BuOH, 0.05 M $K_2S_2O_8$, Ar-saturated, pH 3. In addition, the normalized spectrum of the H-adduct (●), which is formed in low yield ($G = 0.57$) due to the reaction of hydrogen radicals with the oligomer, is shown.

The time dependence of the formation of the benzyl radicals corresponds to the one of the decay of $SO_4^{\bullet-}$. This can be rationalized with the formation of the radical cation, which is too short lived to be observed, owing to electron-withdrawing sulfonate group. It deprotonates with a rate constant of $k_7 > 8 \cdot 10^5$ s^{-1} [559]. Therefore, in the Reaction sequence 4-18 from the HO-adduct to the protonated form, followed by water elimination and subsequent formation of the benzyl

radical, our derived rate constant, based on the kinetic trace shown in **Figure 4-12** of $(6 \pm 1) \cdot 10^3 \, s^{-1}$, is 2 to 3 orders of magnitude lower than the protonation of the HO-adduct (reaction 5) and the deprotonation of the radical cation (reaction 7). Therefore, the water elimination step (reaction 6) proceeds with a first-order rate constant k_6 of $(6 \pm 1) \cdot 10^3 \, s^{-1}$.

3.1.4 Reactions of benzyl radical in aerobic solution

To study the reaction of the benzyl radical with oxygen, pulse radiolysis experiments at pH 3.4 were performed by generating radical cations from PSS-1100 via the reaction with $SO_4^{\bullet-}$. $HO^{\bullet}$ radicals were scavenged by *t*-BuOH. The absorbance was followed at 280 nm, which is mainly attributed to the benzyl radical (**Figure 4-15**). The absorbance initially increases (benzyl radical formation) and then decays. The rate of decay depends on the oxygen concentration, which indicates the reaction of the benzyl radical with oxygen according to reaction 9 (Eq. 4-20). Analysis of the kinetic traces at different oxygen concentrations, taking into consideration the rate of formation of benzyl radicals and the observed pseudo-first order rate constant k_{9obs} for the reaction with O_2 [365], a rate constant of $k_9 = (2 - 5) \cdot 10^8 \, M^{-1} \, s^{-1}$ is obtained.

$$(4-20)$$
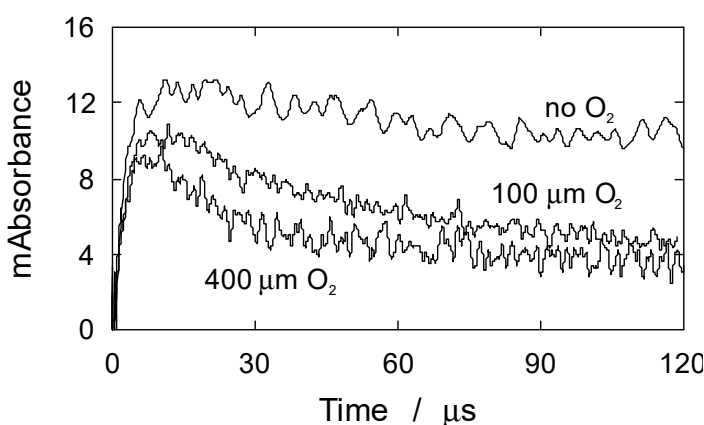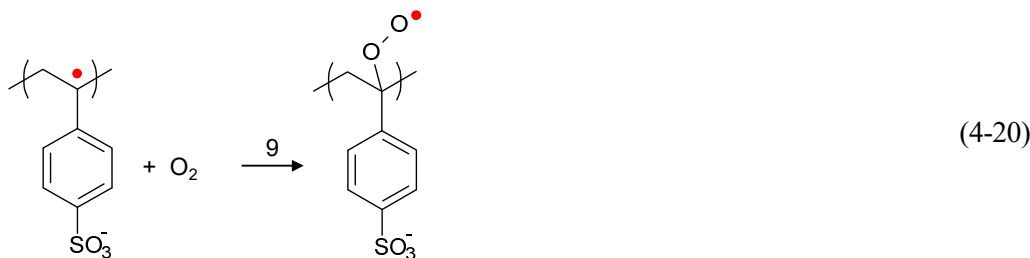
Figure 4-15. Absorbance changes at 280 nm observed for 0.7 mM PSS-1100, 0.02 M $K_2S_2O_8$, and 0.07 M *t*-BuOH in Ar-saturated solution at pH 3.4 and doses of 2–4 Gy in the absence of O_2 and presence of 100 µM and 400 µM O_2. The initial increase results from the formation of benzyl radicals.

3.1.5 Reaction scheme

Based on the set of pulse radiolysis results reported in the previous sections, a somewhat clearer picture now emerges as to the mechanisms of $HO^{\bullet}$ attack on PSS and the ensuing follow-up reactions, at least under the idealized conditions of the pulse radiolysis experiment. **Figure 4-16** provides an overview of the reaction scheme identified and shows the possible reaction pathways of the PSS oligomer. The $HO^{\bullet}$ radical reacts predominantly via addition to the aromatic ring (reaction 1), only 10 % of the $HO^{\bullet}$ directly abstract an α-H (reaction 2) to yield the benzyl radical (compound C). The OH-adduct (compound B) can undergo different follow-up reactions. In the presence of oxygen, which is the case in the fuel cell, in particular near the cathode, it can reversibly add O_2 (reactions 3 and -3), forming a peroxyl radical (compound D), which can decay (reaction 4) to a stable, hydroxylated product (compound E) and a hydroperoxyl radical ($HOO^{\bullet}$). At an estimated O_2 concentration in the fuel cell membrane of 7.5 mM, the lifetime of compound D would be on the order of 100 μs.
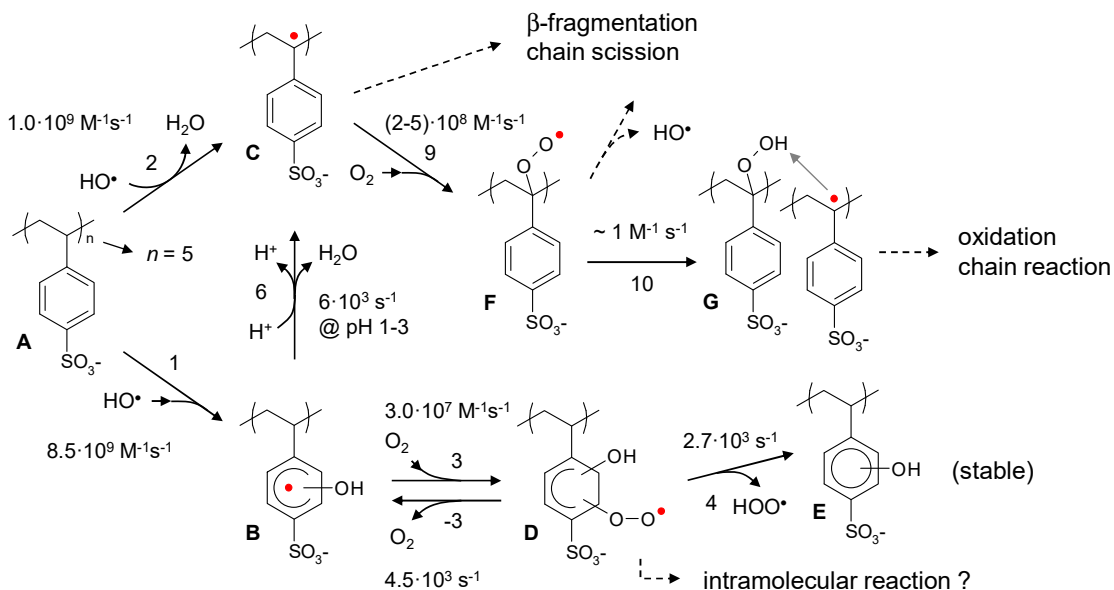
Figure 4-16. Mechanism and kinetics of the attack of $HO^{\bullet}$ on the poly(styrene sulfonate) oligomer and follow-up reactions at low pH with respective rate constants, ultimately leading to chain degradation or the formation of a stable hydroxylated product (E).

The reaction of PSS along the sequence 1, 3 and 4 leads to a stable product (compound E). In this case, the attack of the PSS chain by $HO^{\bullet}$ does eventually not lead to degradation of the grafted chain. This hydroxylated styrene sulfonate unit could, in fact, even enhance the stability of the polymer against radical induced degradation, since it could act as a phenol-type antioxidant. The incorporation of phenolic antioxidants by radiation grafting has shown to be successful in reducing the rate of degradation of grafted membranes in the fuel cells [337, 356] (cf. also

Chapter III). Over extended periods of time, the appearance of the hydroxylated product may be detected using suitable spectroscopic methods. In an accelerated chemical degradation study of styrene grafted and sulfonated membranes based on ETFE there is a vibration band in the FTIR spectrum measured post-test, which is not visible in the spectrum of the pristine membrane, that could be associated with such a product [364]. The emission of HOO$^\bullet$ in reaction 4 could be problematic, though, because it could participate in further degradation reactions.

All in all, the reaction sequence leading to the hydroxylated product constitutes a favorable pathway, because it does not lead to chain scission and thus polymer degradation. The extent to which this happens depends on the local concentration of O_2. Therefore, this mechanism may be prevalent in the fuel cell membrane near the cathode. On the other hand, at low oxygen content, such as in the fuel cell membrane near the anode, and at low pH, reaction 6 is predominant. The acid-catalyzed elimination of water, which takes place with a half-life time of $\tau_{1/2,6} = \ln2/k_6$ of $100\,\mu s$, leads to the formation of the benzyl radical (compound C), from which chain scission is likely to take place via β-fragmentation, either directly or via a peroxyl radical intermediate, which is formed as a result of the reaction of the benzyl radical with O_2 (reaction 9). The nature of these chain breakdown reactions have not been investigated in detail in the pulse radiolysis study. It is clear, however, that the chain degradation pathways and kinetics play an important role in the breakdown of styrene sulfonated based fuel cell membrane polymers.

(4-21)
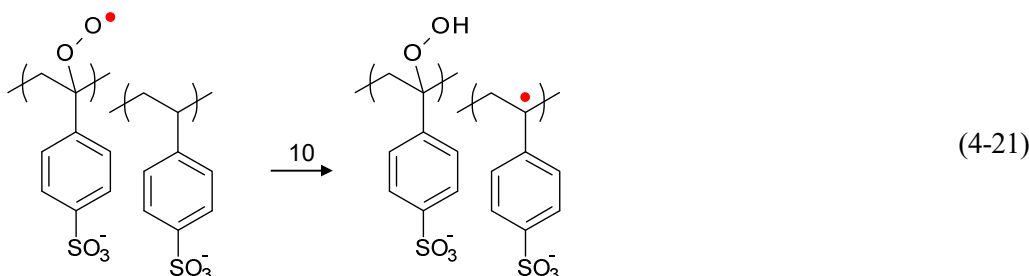
The benzyl radical may be the starting point of an autooxidation reaction, known for example from lipid peroxidation [223]. Because the binding energy of the peroxide ROO-H (360-370 kJ/mol) is higher than that of the relatively weak αC-H bond in PSS (~350 kJ/mol) [379], the peroxyl radical is able to abstract such weakly bound hydrogen (H-transfer reaction) according to reaction 10 (Eq. 4-21), leading to the formation of a hydroperoxide and a benzyl radical. The benzyl radical then again adds O_2 to form a peroxyl radical, which then again can undergo a hydrogen abstraction reaction. This oxidation chain reaction leads to the formation of a peroxidized chain (cf. also **Figure 4-2** in Section 2 of this Chapter). The difference in bond strength is the most important factor that determines the rate of reaction 10, yet steric factors also play a role: tertiary peroxyl radicals are 3 to 5 times less reactive than primary and secondary

ones. The rate constant for hydrogen abstraction from cumene by the peroxyl radical of cumene, a mechanism generally reported for a radical chain process in a polymer such as PSS, is $k_{10} = 1$ M^{-1}s^{-1} at 65°C [563]. The formed hydroperoxides may fragment directly or react with transition metal impurities to form an intermediate oxyl radical RO$^{\bullet}$. Oxyl radicals are more reactive than peroxyl radicals and, thus, undergo a variety of reactions, such as rapid β-fragmentation [564]. In summary, the benzyl radical is a key intermediate in the context of PSS chain degradation.

In view of the proposed reaction mechanism, based on the results of the pulse radiolysis study (**Figure 4-16**), the HO-adduct (compound B) is an important intermediate. Promoting O$_2$ addition according to reaction 3 and formation of the hydroxylated product (reaction 4) seems an effective means to avoid formation of benzyl radicals. The fraction of HO-adducts reacting along the two different pathways was crudely estimated for an oxygen concentration of 7.5 mM, which is a concentration representative of that in the membrane of a fuel cell [440]. Under these assumptions, around 15 % of HO-adducts react to the benzyl radical, and 85 % to the hydroxylated product. All the reactions evidently show a more or less strong dependence on the temperature. From the forward and backward reactions 3 and -3 and the associated equilibrium constant $K_3 \cong 7 \cdot 10^3$ M^{-1}, a Gibbs free energy of reaction of $\Delta G_3 \cong -22$ kJ·mol^{-1} is obtained. With an estimated reaction entropy of $\Delta S = 160$ Jmol^{-1}K^{-1} [565] a reaction enthalpy of $\Delta H \cong -69$ kJ·mol^{-1} is calculated. With this the value of K_3 at a temperature of 80°C can be estimated using the Van't Hoff equation[1], which yields an equilibrium constant ten times lower than at room temperature. Therefore, the formation of hydroxylated products is less likely at elevated temperature and, consequently, the formation of benzyl radicals more likely.

The scheme shown in **Figure 4-16** is by no means an exhaustive representation of possible reactions. Due to the proximity of aromatic groups in the oligomer, intramolecular reactions are likely. In the polymer, such as the swollen domains of a membrane with PSS grafts, intramolecular reactions are very likely. The autoxidation reaction highlighted above is the most well-known oxidation chain reaction. Other mechanisms are possible, however. At high oxygen concentrations, intramolecular addition of the aromatic peroxyl radical (compound D) to another aromatic unit according to becomes possible [566]. The aromatic radical thus formed can itself react with oxygen, forming a new peroxyl radical, which can further react with styrene sulfonate units, propagating the chain. It has also been proposed that compound D can undergo a ring opening reaction [315], which however seems unlikely because it involves the destruction of the energetically favorable aromatic ring.

---

[1] $\ln(K'/K) = \Delta H/R(1/T - 1/T')$

(4-22)
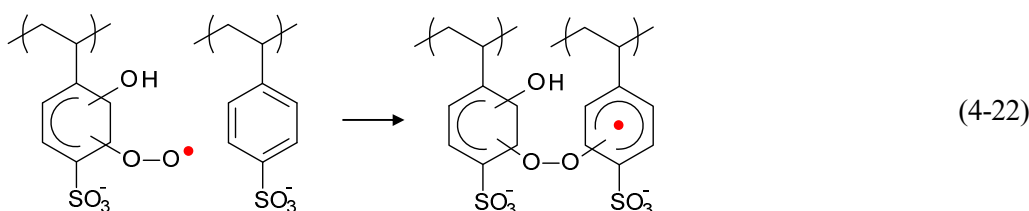
3.2 *Poly(α-Methylstyrene Sulfonate) Oligomer*

In view of the findings on the radical attack and oxidative degradation mechanism of PSS reported in the previous chapter, it is evident that a substitution of the α-H should improve the stability of the oligomer or polymer. Actually, since the susceptibility of PSS towards oxidative degradation had been recognized already in the early 1960s, the use of more stable polymers has been proposed. In the field of radiation grafted membranes, Assink et al. reported improved chemical stability (in an alkaline flow battery) of membranes based on grafted and sulfonated α-methylstyrene (AMS) compared to grafted and sulfonated styrene [251] (cf. also Chapter III). In the study reported here, the attack on HO• on oligomers of poly(α-methylstyrene sulfonate) (PAMSS) were studied in analogy to the study on PSS oligomers reported in the previous section. PAMS oligomers with a degree of polymerization of 12 (PAMSS-2640) and 30 (PAMSS-6400) were chosen. Irradiation of N_2O saturated PAMSS solutions at pH 7 yielded an absorption spectrum within a few µs after the pulse with a maximum near 340 nm, consisting of 90 % HO-adducts and 10 % H-adducts [377]. From a series of pulse radiolysis experiments with different concentration of PAMSS, the rate constant for the reaction of HO• with PAMSS can be obtained from a plot of pseudo-first order rate constants as a function of [PAMSS] (**Table 4-2**). The rate constant normalized to the concentration of monomer units is slightly lower in case of the longer chain PAMSS oligomer compared to the shorter PAMSS oligomer and the PSS oligomer, which could indicate that chain coiling becomes influential.

Table 4-2. Rate constants for the reaction of HO• with styrene and α-methylstyrene derived oligomers PSS and PAMSS, respectively. The number indicates the molecular weight of the compound in Da.

Substrate	Degree of polymerization n	k(HO•) (M^{-1}s^{-1})
PSS-1100	5	$(9.5 \pm 0.6)\cdot10^9$
PSS-1100[a]		$(1.9 \pm 0.1)\cdot10^9$
PAMSS-2640	12	$(2.0 \pm 0.5)\cdot10^{10}$
PAMSS-2640[a]		$(1.7 \pm 0.1)\cdot10^9$
PAMSS-6400	30	$(2\text{-}3)\cdot10^{10}$
PAMSS-6400[a]		$(0.7\text{-}1)\cdot10^9$

[a] rate constant related to the concentration of monomer units
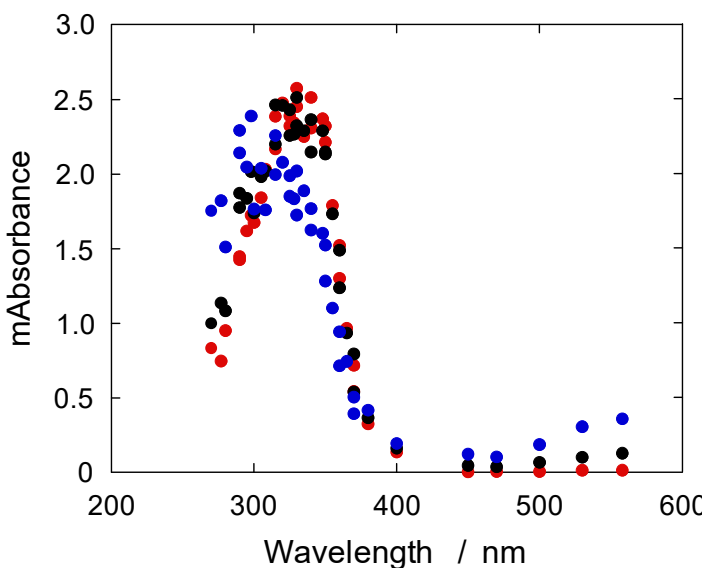
Figure 4-17. Transient absorption spectra showing the formation and decay of HO- and H-adducts of PAMSS-2640 at pH 2.4, constructed from time-resolved absorbance readings normalized to 1 Gy, 4 (●), 30 (●) and 130 (●) μs after irradiation (8-12 Gy) of 0.08 M PAMSS-2640 solutions saturated with N_2O.
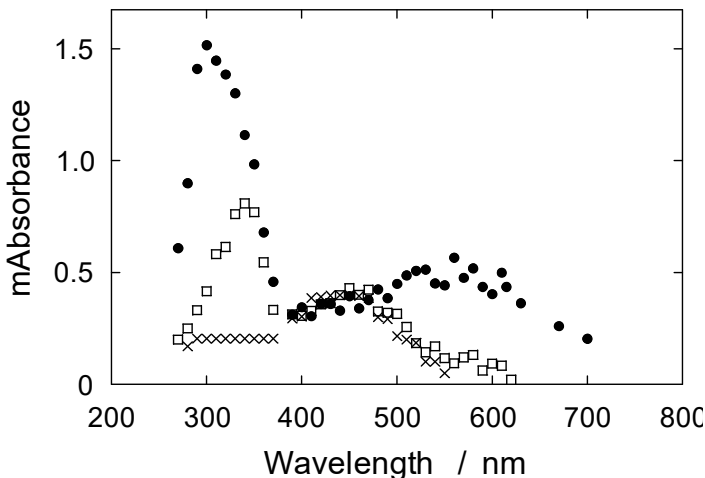
Figure 4-18. Transient absorption spectra 1 (□) and 10 (●) μs after the pulse (dose 10–15 Gy), obtained from time-resolved absorbance readings, normalized to 1 Gy, measured in Ar-saturated solutions containing 1 mM PAMSS-2640, 0.05 M $K_2S_2O_8$ and 0.1 M t-BuOH at pH 2.4. A scaled spectrum of $SO_4^{\bullet-}$ (×) from ref. [567] and based on $G = 4$ shows the contribution of $SO_4^{\bullet-}$ 1 μs after the pulse.

The absorption spectra at pH 2.4, obtained 4, 30 and 130 μs after the pulse indicate the initial formation of HO- and H-adducts of PAMS-2640, which subsequently decay (**Figure 4-17**). The decay of the adduct is faster at pH 2.4 than at pH 7 (not shown). In addition, the low pH brings about the appearance of an absorbance in the visible range of the spectrum around 550 nm. This absorbance does not develop when HO$^\bullet$ radicals are scavenged in the presence of 0.2 M t-BuOH. Transient species that exhibit broad absorptions in this wavelength region include radical cations [560, 561, 568-570], benzyl cations [571-573], phenyl-peroxyl radicals [556, 574-577], and cumyloxyl type radicals [578]. As in the case of the PSS oligomer, $SO_4^{\bullet-}$ radicals were created

by pulse radiolysis of solutions containing potassium persulfate ($K_2S_2O_8$) to investigate the reaction mechanism using PAMSS-2640 at low pH in more detail in the presence of *t*-BuOH to scavenge $HO^\bullet$ (**Figure 4-18**). In analogous experiments with PSS or benzenesulfonate, there is almost no increase in absorbance in the visible range of the spectrum. The rate of decay of the absorption of the intermediate in the visible region of the spectrum depends on the dose (20 - 50 kGy), which indicates a second-order component in the decay. The formation and decay of the intermediate does not depend on the oxygen concentration (not shown), hence the cumyloxyl type radical can be excluded as a candidate for the intermediate. Moreover, the intermediate of the longer chain PAMSS oligomer decays significantly slower (**Figure 4-19**). Furthermore, the absence of a characteristic signature at around 400 nm confirms the absence of a phenoxyl type radical.
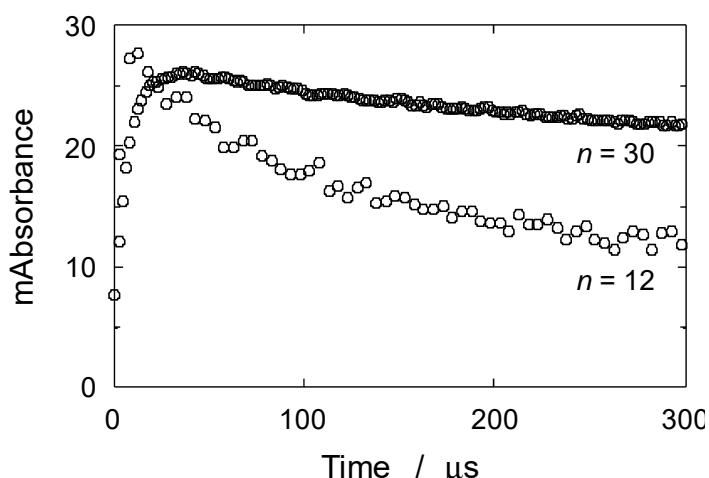
Figure 4-19. Course of absorbance followed at 560 nm within the first 300 μs after the pulse, observed in aerated 0.05 M $K_2S_2O_8$ solutions that contained 0.5 mM PAMS-2640 (*n*=12) and 0.2 mM PAMS-6440 (*n*=30) at pH 2.4, irradiated with a dose of 50-55 Gy.

This points to the acid-catalyzed reaction of the HO-adduct to the radical cation (cf. Reactions 5 and 6 in Section 3.1.3 for the PSS analogue). Both aromatic radical cations and benzyl cations exhibit absorptions in the visible region of the spectrum. The latter may be formed via a fast heterolytic cleavage of the β-C-C bond of the radical cation according to

$$(4\text{-}23)$$
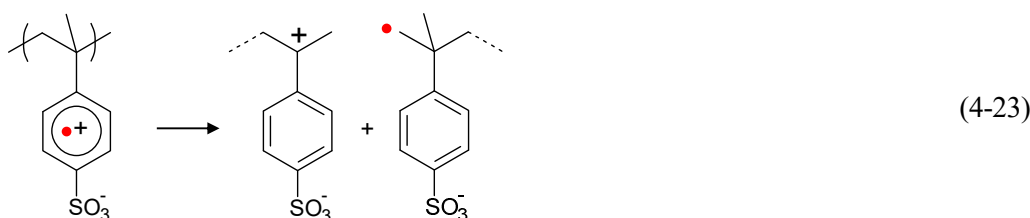
However, the radical cation may be expected to be too short-lived to be observed in aqueous solution due to the reaction with water:

(4-24)
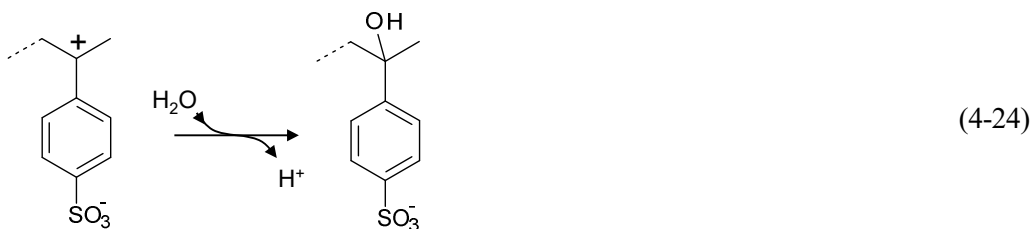
Based on the findings of pulse radiolysis, product analysis, and available literature, it is proposed that the appearance of the absorption in the visible region of the spectrum is caused by the formation of the radical cation via acid catalyzed water elimination from the HO-adduct of PAMSS. Thus, the radical cation of PAMSS appears to be longer-lived than the radical cation of PSS. The decay of the absorption is of mixed second- and first-order kinetics. As seen in **Figure 4-19**, the decay of the transient absorption is slower for the longer-chain PAMSS oligomer, which may be rationalized with the lower mobility of the higher MW polymer and with the corresponding higher probability of intramolecular reactions. In addition, charge resonance and formation of dimer radical cations are thought to stabilize radical cations or aromatic systems [568, 569, 579], whereby an intramolecular addition of a radical cation takes place to another vicinal aromatic ring in the coiled structure of the polymer (**Figure 4-20**).
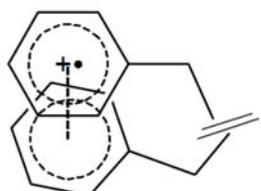
Figure 4-20. A radical cation may be stabilized by forming an adduct to another, neighboring aromatic ring.

As it was beyond the scope of the project, not the same range of follow-up reactions could be studied in case of PAMSS as it was the case for PSS. It is expected, however, that the HO-adduct of PAMSS reacts with O_2 in a similar manner, which can eventually yield a hydroxylated product. Owing to the slower decay of the HO-adduct via the radical cation route, the non-detrimental reaction path may actually be more likely in case of PAMSS.

3.3 Relevance of Findings for Fuel Cell Membrane Degradation

The results obtained in the pulse radiolysis study, the corresponding reaction rate constants determined and reaction pathways identified have been obtained with a model system consisting of short-chain oligomers at dilute concentration in water. The significance of the findings for the situation of a membrane in a fuel cell has to be carefully discussed. First and foremost, the substrate material in the membrane is less dilute, i.e., there is a high concentration of polymer,

consisting of the backbone material and the graft component, with relatively little water. The rate of initial attack of HO$^\bullet$ on PSSA is somewhat influenced by its molecular weight (cf. **Table 4-1**). Some of the follow-up reactions are expected to be more strongly affected by coiling, consider for instance the influence of the chain length of PAMSS on the decay of the radical cation (**Figure 4-19**). Consequently, in the coiled polymer or membrane, the lifetime of the intermediates is considerably higher. In particular, the limited chain mobility affects those reactions where a rearrangement of bond angles is required. For instance, during the deprotonation reaction of the radical cation derived from PSS the hybridization of the benzylic carbon changes from sp^3 to sp^2 [580]. Thus, the rearrangement of the bond angles may be slower in the polymer compared to the dilute aqueous solution. Hence, the lifetime of the radical cation in the polymer is expected to be (much) higher than 1 µs and influenced by the state of hydration of the membrane. All in all, reactions leading to chain fragmentation and membrane degradation are therefore slower in the polymer.

Another key finding of the analysis of the reaction pathways is that not all reactions necessarily lead to chain fragmentation. As outlined in **Figure 4-16**, there is a reaction sequence leading to a stable hydroxylated product. One may argue that with a clever choice of graft component, substituents or comonomers, such reactions may be favored over chain scission reactions. Certainly, the substitution of styrene by α-methylstyrene is a key improvement in this respect, because the benzyl radical is less likely to be formed in this case.

The radicals responsible for polymer degradation in the fuel cell, namely HO$^\bullet$ and, possibly, also H$^\bullet$, react rapidly with aromatic compounds, such as the constituents of fuel cell membranes based on grafted styrene or α-methylstyrene. This is in strong contrast to the situation in perfluorosulfonic acid ionomers or membranes, where the reaction of these intermediates with the polymer is much slower, in particular in case of end-group stabilized ionomers. The lifetime of HO$^\bullet$ in a water swollen PFSA membrane is estimated to be in the range of 1 µs, whereas in a radiation grafted membrane based on grafted and sulfonated styrene, the HO$^\bullet$ lifetime is on the order of 1 ns [440]. This has a number of implications on the considerations of radical induced attack on membranes and strategies to mitigate the corresponding degradation. In case of PFSA membranes, the lifetime of HO$^\bullet$ is sufficiently long to allow capturing a significant fraction of the radical through the addition of a suitable HO$^\bullet$ scavenger [168, 169, 436, 581-590]. It has been found that the addition of CeO_2 or MnO_2 particles, or the respective metal ions, leads to a substantially lower rate of membrane degradation [168, 169, 436, 581-583]. The reaction of HO$^\bullet$ with Ce^{3+} ($3 \cdot 10^8$ M^{-1}s^{-1} [370]) and Mn^{2+} ($3 \cdot 10^7$ M^{-1}s^{-1} [591]) is fast enough to efficiently scavenge

$HO^\bullet$ at cerium and manganese concentrations in the membrane that do not considerably impact the performance of the membrane electrode assembly due to blocking of the ion exchange sites. In addition, the great charm of using these metal ions is that they are regenerative radical scavengers, since the oxidized species (Ce^{4+} and Mn^{3+}) readily reacts with H_2O_2 and $HOO^\bullet$ present in the membrane, whereby the radical scavenger (Ce^{3+} and Mn^{2+}) is restored within milliseconds ($Ce^{4+} \rightarrow Ce^{3+}$) or a couple of hundred milliseconds ($Mn^{3+} \rightarrow Mn^{2+}$) [169, 438]. Therefore, those transition metal ions act as $HO^\bullet$ scavenging catalysts, which means that the corresponding doped PFSA membrane is effectively and sustainably stabilized over long periods of time.

In alternative membranes containing sulfonated aromatic moieties, cerium or manganese cannot provide notable stabilization against radical attack, because $HO^\bullet$ reacts much too quickly with the aromatic units [438, 442, 592]. In addition, the oxidized form or the transition metal ion may have a sufficiently high redox potential to attack weak points in the polymer, such as the α-position in poly(styrenesulfonic acid) (PSSA) [440]. An estimate based on a kinetic framework developed for understanding the regenerative scavenging mechanism of Ce and Mn shows that in case of a PSSA type membrane even a doping level of 10 % Ce with respect to the total concentration of sulfonate the attack on PSSA by $HO^\bullet$ is not notably mitigated [438]. Therefore, alternative antioxidant strategies have to be adopted for these types of membrane. One approach that has been pursued is the incorporation of a phenol type antioxidant into the grafted chain. The corresponding membranes showed a substantially improved chemical stability compared to non-stabilized membranes. However, devising a regenerative mode of antioxidant action seems to be difficult (cf. Section 4 of Chapter III).

Considering the fast reaction of $HO^\bullet$ with PSS or PAMSS, it may be a more effective approach to target the intermediates of radical attack. One could try to steer the reaction sequence in a non-detrimental direction, such as towards the formation of the hydroxylated product (compound E in **Figure 4-16**). This would be the case, as already outlined, for high O_2 concentration. In case of PSS, the estimated lifetime of the HO-adduct is 3 µs and that of the peroxyl adduct 100 µs. This may leave sufficient time for a suitable "repair mechanism" to take effect. Yet the author is unable to identify a possible reactant that could be added or approach that could be devised to accomplish this. Another intermediate that might be worth targeting is the radical cation, in particular as it is a precursor for the formation of the benzyl radical or a chain scission event. In case of the PSS oligomer, the lifetime of the radical cation ($\tau_{R^{\bullet+}} = \ln 2 / k_7$) is below 1 µs, whereas the radical cation derived from the PAMSS oligomer has an estimated lifetime of over 100 µs (**Figure 4-19**). This may leave sufficient time for "repair" of the radical cation. A conceivable reaction could

obviously be the reaction with H_2O, i.e., the reverse of the acid catalyzed water elimination reaction (Reaction sequence 4-18), yet these reactions are evidently not favored at low pH [593]. In analogy to the regeneration reaction in case of cerium and manganese, H_2O_2 could react with the radical cation, yielding the original compound, $HOO^\bullet$ and an H^+. Thermodynamically, this reaction would be favorable, as the standard electrode potential of the radical cation is estimated to be between 2.0 and 2.2 V [594], while $E°(HOO^\bullet,H^+/H_2O_2) = 1.46$ V [453]. This reaction, however, is probably slow, because H_2O_2 already reacts slowly with $HO^\bullet$, $E°(HO^\bullet,H^+/H_2O)$ = 2.72 V [455], with a rate constant of $2.7 \cdot 10^7$ $M^{-1}s^{-1}$ [370]. Therefore, the reaction with the radical cation is expected to be more than two orders of magnitude slower. At a representative concentration of H_2O_2 in the MEA of 0.5 mM [595], this would yield a pseudo-first order reaction with the radical cation with $\tau_{1/2}$ of >5 ms, which is too slow considering the lifetime of the radical cation. However, if the lifetime of the radical cation is significantly higher in the polymer due to restricted mobility, this could possibly be a reaction of relevance.

4 Accelerated Aging Tests of Fuel Cell Membranes

As outlined in the introductory sections of this chapter, the testing of fuel cells under conditions of accelerated stress is a valuable tool to characterize cell components with high throughput with respect to specific degradation phenomena. In general terms, regarding the membrane of a PEFC one can identify three main degradation mechanisms: oxidative aging due to radical attack, mechanical deterioration, and thermal degradation, such as hydrolysis. In this section, topics of oxidative degradation of various types of radiation grafted membranes, model systems as well as "product-type" membranes, are discussed with a focus on aspects that differ from those encountered in PFSA membranes, for instance the effect of relative humidity on the rate of membrane degradation. The presence of nitrile groups in the case of S:MAN and S:AN co-grafted membranes represents a specific constellation, which is worth investigating, also in combination with the hydrolysis of the nitrile. The hydrolysis of nitrile in the absence of oxidative stress is investigated in the last section.

4.1 Oxidative Stress

It has been widely accepted that hydrogen peroxide (H_2O_2) and radical intermediates, such as $HO^{\bullet}$, $HOO^{\bullet}$, and $H^{\bullet}$, are generated in the fuel cell as a result of the interaction of H_2, O_2 and the Pt catalyst. This results in oxidative degradation of both PFSA and PSSA based membranes [596-599]. Therefore, the gas crossover rate is critical for the chemical degradation mechanism of a polymer electrolyte membrane in the PEFC. The chemical stability of radiation grafted membranes in the results reported here were examined in the single cell via accelerated stress tests in the presence of H_2 and O_2 at OCV [600]. The cell characteristics measured during the OCV hold test are the cell voltage and the high frequency (HF) resistance at 1 kHz, which is a good measure for the ohmic resistance of the cell, which is mainly determined by the membrane. In some cases, the hydrogen crossover was measured intermittently to check the mechanical integrity of the membrane. FTIR spectroscopy is the main analytical technique employed to characterize the composition of the membrane qualitatively and quantitatively, in particular to compare the membrane after disassembly from the cell that underwent the accelerated stress test with the pristine membrane. Based on the approach outlined in Chapter II, the extent of degradation of the membrane can be determined from the FTIR analysis as well as the degree of hydrolysis of the nitrile groups.

4.1.1 Influence of relative humidity

In the case of PFSA membranes, low relative humidity (RH) promotes membrane degradation [428]. Previous research suggests that reduced RH could lead to a higher local concentration of H_2O_2 as a result of the reduced water content in the MEA, which can promote the formation of radicals and thus chemical attack [141, 529, 531]. Accordingly, the fluoride emission rate (FER) shows an increasing trend with decreasing RH during OCV tests, indicating an accelerating effect of low RH on the degradation rate of PFSA membranes [531, 601]. Yet, the result of Xu et al. shows that at RH values well below 60% PFSA membrane degradation decreases again, which is attributed to two counteracting effects of RH on gas permeability and catalytic activity of the radical formation reaction on the platinum surface [522]. In the experiments reported here, styrene only grafted membranes based on 25 µm ETFE were used as a model system to study the effect of RH on membrane degradation, knowing that ETFE-*g*-PSSA membranes are known to exhibit poor stability in the fuel cell [602]. It is expected that the main findings may be applicable to more complex sulfonated styrene or α-methylstyrene based membranes.

The ETFE-g-PSSA membranes had a graft level of around 23 %, corresponding to an IEC of 1.5 mmol/g, and a thickness in the wet state of around 40 µm. MEAs with an active area of 16 cm^2 were prepared by hot-pressing the membrane with carbon paper based gas diffusion electrodes (ELE0162, Johnson Matthey Fuel Cells). The single cells were operated on H_2 and O_2 at a temperature of 80°C and a gas pressure of 2.5 bar$_a$. The cells were conditioned at 100 % RH of the reactants and a current density of 0.5 A/cm^2. The H_2 crossover rate through the membrane was evaluated at the specified RH before switching to the OCV hold test.

The OCV hold tests were conducted for 24 h for the experiments at reduced RH (30, 50 and 70 %) and 18 h in case of full humidification (100 % RH). The cell voltages showed a decreasing trend over time (not shown), which has to do with the formation of surface oxides on the Pt catalyst on the cathode side [603]. The mechanical integrity was maintained during the test in all cases, which was checked by electrochemical H_2 crossover measurement, and no membrane rupture was observed. The disassembled MEAs were artificially delaminated, the membranes exchanged in K^+ form and then analyzed by FTIR spectroscopy. The intensity of the vibrational bands assigned to aromatic C-C stretch vibration at 1494 cm^{-1} and 1600 cm^{-1} significantly diminish in case of the membrane tested at 100% RH for 18 h (**Figure 4-21**), indicating a notable loss of grafted SSA units. The loss of intensity appears less pronounced in case of the membranes tested under sub-saturated conditions.
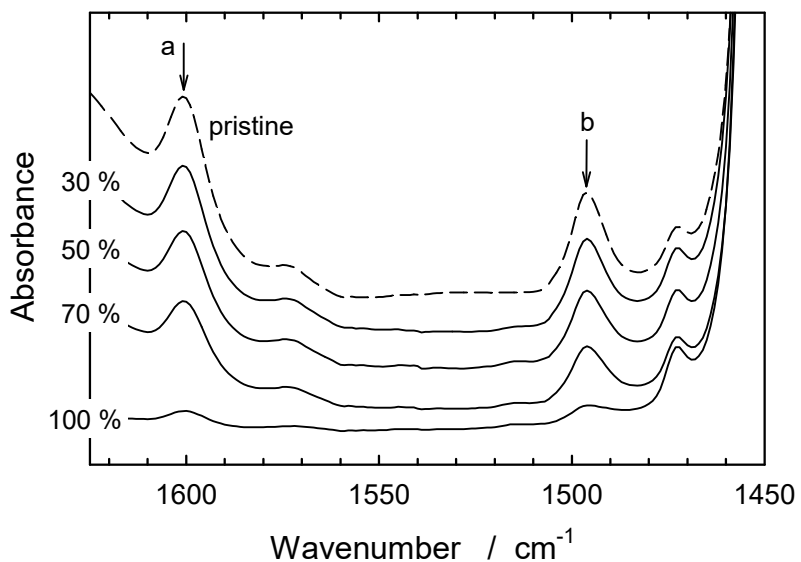
Figure 4-21. FTIR spectra, shown with offset for better readability, of a pristine ETFE-*g*-PSSA membrane and membranes after OCV tests at various RH conditions. The characteristic vibrational bands for PSSA (aromatic C-C vibration) are indicated with a and b.
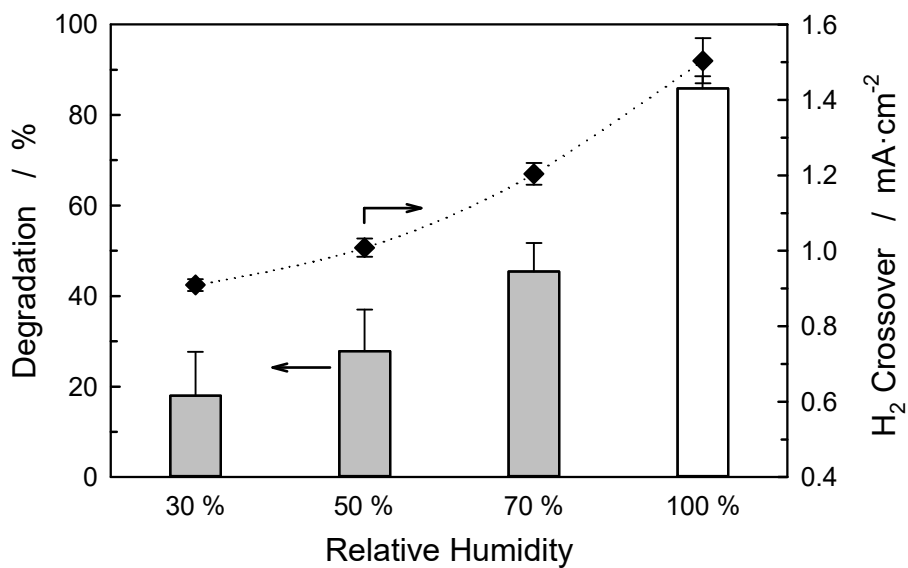
Figure 4-22. Calculated degree of membrane degradation (left axis) after the OCV hold test at various RH, determined from the loss of grafted SSA units based on pre- and post-test FTIR analysis of the membranes. Right axis: H_2 crossover rates of membranes measured electrochemically at the respective RH after cell conditioning. The duration of the OCV hold was 18 h in case of the test at 100 % RH and 24 h in all other cases.

The degradation of the grafted membranes mainly consists of the decomposition of the PSSA grafts. To quantitatively analyze the extent of membrane degradation, the loss of SSA units is calculated based on the intensity ratio of the vibrational band at 1'494 cm^{-1} in the tested and pristine membrane according to the method described in Chapter II. The degree of SSA loss in the membrane increases with increasing RH, with almost 90% of the grafts lost from the backbone after the OCV hold test at full humidification, which is in sharp contrast to the 24 h OCV hold test at 30 % RH, where only around 20 % of the original SSA units were decomposed (**Figure 4-22**). The results reveal a decreasing trend of membrane degradation with reduced RH. This observation is in stark contrast to the degradation behavior generally observed for PFSA membranes at different RH, where lower RH leads to a higher rate of membrane degradation [316, 525, 531, 601]. As a result of the detachment of grafts from the base polymer, membrane thinning is observed: 100 % RH → 29 μm, 70 % RH → 35 μm, 50 % RH → 38 μm, 30 % RH → 39 μm (wet state). For the membrane with the lowest extent of degradation, observed at 30% RH, the thickness after the test is very close that of the pristine membrane (~40 μm), whereas the membrane tested at 100% RH showed considerable thinning to ~29 μm. Along with the extent of degradation of the ETFE-*g*-PSSA membranes, the hydrogen crossover rates of the pristine membranes as a function of RH are shown in **Figure 4-22**. A notable decrease in the hydrogen crossover rate with decreasing RH is observed. This result is consistent with the RH dependency of reactant gas crossover found in PFSA membranes [522, 601]. This seems to be in contradiction to the fact that the chemical degradation of PFSA membranes is accelerated under dry conditions, as highlighted above.

In the case of PSSA based membranes, the attack of HO$^{\bullet}$ can lead to the formation of benzyl radicals, which are likely to undergo subsequent chain scission [365]. For PFSA membranes, it has been noted that ionomer degradation under dry conditions involves the initiation mechanism by the sulfonyl radical (R-SO$_3{}^{\bullet}$) on the side chain [509], in addition to the well-known main chain unzipping process as proposed by Curtin et. Al [20]. According to Coms, in case of R being a fluorocarbon alkyl chain, the extremely weak C-S bond of the sulfonyl radical is prone to form a fluorocarbon radical, which eventually leads to scission of the main chain, while an aryl sulfonyl radical, as it is expected to form in the PSSA grafted chain under dry conditions, is much more stable. Under high RH conditions, formation of the sulfonyl radical is unlikely due to the high degree of acid dissociation, rendering side-chain attack in PFSA unlikely. Therefore, the different trends found in the chemical stability of PFSA and PSSA based membranes between high and low RH may be a consequence of the dissimilar C-S bond strengths.

4.1.2 Methacrylonitrile and acrylonitrile co-grafted membranes

This section aims at probing effects of the presence of nitrile comonomers, methacrylonitrile (MAN) and acrylonitrile (AN), in styrene based grafted membranes on the chemical stability based on OCV hold tests carried out in single cells. Initially, AN and MAN co-monomers had been chosen to enable the grafting of α-methylstyrene (AMS) through copolymerization with (M)AN, because AMS shows poor homopolymerization kinetics [65, 258]. To study in more detail the effect of the nitrile comonomer, styrene and MAN were co-grafted and the resulting membranes were found to exhibit longer lifetimes compared to styrene-only grafted membranes (cf. also Chapter III) [287]. Despite the similar membrane properties, the S:AN co-grafted membrane resulted in inferior performance in the fuel cell compared to a S:MAN co-grafted membrane. The objective of the study reported here is to gain a more profound understanding of the chemical degradation behavior of S:MAN and S:AN co-grafted membranes, also with a view of the susceptibility to undergo hydrolysis and how this affects membrane stability.

As in the previous section, OCV hold tests are complemented by post-test FTIR spectroscopy to determine the extent of degradation of the membranes. In addition to chain loss, through analysis of the differences in styrene and nitrile loss, the extent of hydrolysis of the nitrile groups can be estimated, based on a formalism explained in Chapter II. The membranes tested in the series of experiments reported here are listed in **Table 4-3** along with their *ex situ* fuel cell relevant properties. For the grafted membranes, an IEC of around 1.5 mmol/g was targeted. In case of the co-grafted membranes, this means that a higher graft level of around 40 % had to be chosen, since the molar ratio of styrene to (M)AN in the grafts is around 1:1. The membranes were grafted using the procedure described in Chapter III. MEAs were prepared by hot-pressing using carbon paper type gas diffusion electrodes (ELE0162, Johnson Matthey Fuel Cells). The single cells of 16 cm^2 active area were conditioned for 20 h at a temperature of 80°C under H$_2$ and O$_2$ and a current density of 0.5 A/cm^2. Gas pressure was 2.5 bar$_a$, the humidity of the reactant gases 100 %.

Table 4-3. Properties of membranes tested in this section. Molar fraction of styrene in grafts (X_S), graft level (Y), thickness (t), ion exchange capacity (IEC), conductivity (σ) and hydration number (λ).

Membrane	X_S	Y (%)	t (wet) (μm)	IEC (mmol·g^{-1})	σ^a (mS·cm^{-1})	λ^a (H$_2$O/SO$_3^-$)
g-S	1	~21	37 ± 1	1.42 ± 0.08	79 ± 21	11 ± 1
g-S:MAN	0.53 ± 0.05	~40	46 ± 1	1.54 ± 0.06	86 ± 8	18 ± 2
g-S:AN	0.46 ± 0.09	~42	45 ± 2	1.69 ± 0.03	79 ± 8	20 ± 1
Nafion 212	-	-	68 ± 1	1.10 ± 0.02	105 ± 5	17 ± 1

^{a} determined at room temperature in water-swollen state.

The results of the OCV hold tests over 12 h in case of styrene-only grafted membranes and 24 h in case of co-grafted membranes are shown in **Figure 4-23**. For radiation grafted membranes, the ohmic resistance of the cell is a suitable metric to probe the chemical state of health of the membrane [269]. At the initial phase of the test, the OCV shows a somewhat steeper drop, in particular in case of the styrene-only grafted membrane. As explained in the previous section, this drop in OCV is most likely a result of Pt oxidation at the cathode [603]. The slower decrease in OCV in case of the co-grafted membranes could be related to the lower gas permeability of these membranes. In any case, a sudden drop of the OCV was not observed, indicating that the membranes remained mechanically intact over the course of the experiment. The most striking observation is the different response of the HFR. The HFR of the pure styrene grafted membrane increased about 6-fold after 12 h at OCV, which indicates a significant degradation of the membrane. Interestingly, the HFR decreases in the first hour of the OCV hold test. This phenomenon has been repeatedly observed for grafted membranes in OCV hold experiments [313, 354-356]. A tentative explanation is that cleaved fragments of the graft component, constituting a polyelectrolyte, could temporarily improve the interface between electrode and membranes while these compounds are leached out from the membrane and are eventually removed from the MEA with the reactant gas stream and liquid water droplets. Both S:MAN and S:AN co-grafted membranes were tested under OCV conditions for 24 h. Compared to the styrene-only grafted membrane, the HFR of the co-grafted membranes remains largely unchanged, which indicates a much superior stability of these nitrile-containing membranes. This confirms the finding reported in Chapter III, Section 3.4.
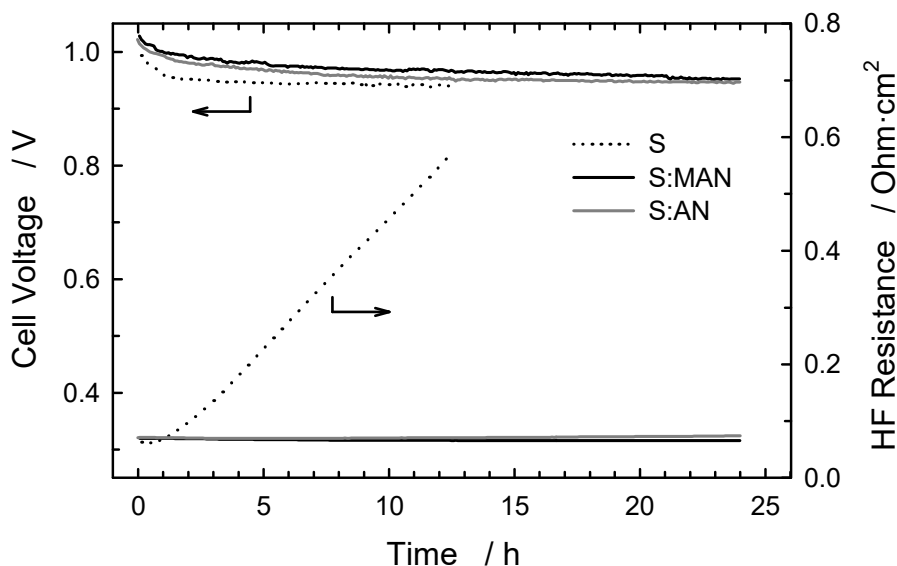
Figure 4-23. Cell voltage and membrane resistance (measured by HFR) as a function of time at OCV for three types of membrane. Temperature: 80°C, H_2/O_2 gas pressure: 2.5 bar$_a$.

After conclusion of the OCV hold test, the membranes were disassembled from the cells, exchanged to K^+ form and analyzed using FTIR spectroscopy. The IR spectra of the tested membranes are plotted in **Figure 4-24** together with the spectra of the pristine membranes. The vibrational bands at 1494 cm^{-1} and 1600 cm^{-1} (assigned to aromatic C-C vibration) completely vanished in case of the pure styrene grafted membrane after the test, while a change of those bands is hardly seen in the spectra of the nitrile-containing co-grafted membranes. This result is in agreement with the dramatic increase in HFR measured for the styrene-only grafted membrane and rather steady HFR of the co-grafted membranes over the duration of the test. The spectra of the S:AN co-grafted membrane reveal that the nitrile groups are partially hydrolyzed. It seems that already in the pristine membrane, the nitrile groups have suffered some degree of hydrolysis to the amide (1670 cm^{-1}) and, to a small extent, also to the carboxylic acid (1720 cm^{-1}). In the tested membrane, more hydrolysis to the carboxylic acid is observed. In contrast, the hydrolysis of the nitrile in the S:MAN co-grafted membrane is marginal, because there is merely a tiny change in absorbance in the region near 1700 cm^{-1}. Accordingly, the change of the absorption band at 2234 cm^{-1} (assigned to the C≡N vibration) is less pronounced for the S:MAN co-grafted membrane than for the S:AN co-grafted membrane. Note that the signature of H-O-H bending vibration of water is also observed in the range of 1630-1600 cm^{-1}.
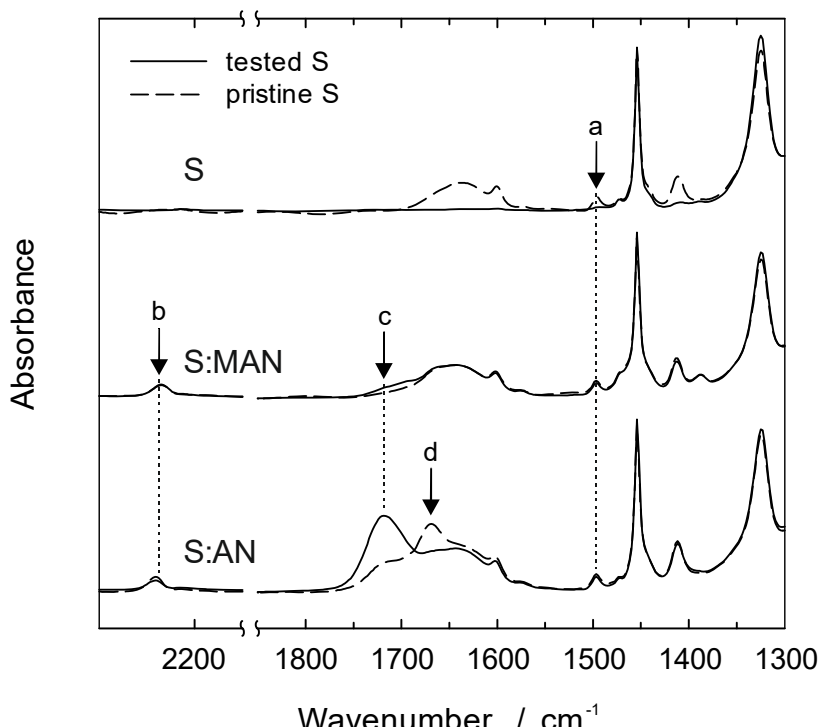
Figure 4-24. FTIR spectra of the pristine and tested membranes. Important vibrational bands are indicated: aromatic C-C at 1'494 cm^{-1} (a), C≡N stretch at 2'234 cm^{-1} (b), carbonyl stretch in carboxylic acid around 1'720 cm^{-1} (c), and carbonyl stretch in amide at 1'670 cm^{-1} (d).

The key finding of this experimental series is that the nitrile-containing radiation grafted membranes have considerably enhanced durability compared to the pure styrene grafted membrane during the OCV hold test. This is clearly a result of the presence of nitrile groups in the co-grafted membranes. Since the crossover of reactant gases is a critical factor regarding the chemical degradation of membranes, the hydrogen crossover in the different membranes, measured after cell conditioning before the OCV hold test, was compared. The styrene-only grafted membrane exhibited a H_2 crossover of 1.13 ± 0.10 mA/cm^2. For the S:MAN and S:AN co-grafted membrane, a value of 0.84 ± 0.08 and 0.88 ± 0.10 mA/cm^2 was measured, respectively. Note that for Nafion® 212 a H_2 crossover of 1.52 ± 0.13 was measured, which is higher than that of the grafted membranes, despite the larger thickness of the membrane (**Table 4-3**). It is clear that hydrogen crossover rates are the lowest for the nitrile containing grafted membranes. This is likely to have a notable effect on membrane degradation under OCV conditions. In the experiments reported in the previous section, using styrene-only grafted membranes, performed at different RH, a reduction of the relative humidity from 70 to 30 % was found to lead to a reduction in H_2 crossover by one third, yet the rate of membrane degradation decreased by a factor of more than two [355].

The lower gas crossover of the nitrile-containing co-grafted membranes can be explained by the following two aspects. Firstly, the higher thickness (cf. **Table 4-3**), which is a consequence of the higher grafting level, may be responsible for a lower gas permeation compared to the pure styrene grafted membrane. However, this does not seem to be the case for a styrene : methacrylic acid (MAA) co-grafted membrane, which has a similar thickness than the nitrile-containing membranes used here, because we observe a higher H_2 crossover rate and rapid degradation under OCV conditions for the S:MAA co-grafted membrane [317]. Secondly, extraordinary gas barrier properties of copolymers of styrene and nitrile co-monomers were observed by Salame and Barnabeo et al. and attributed to the intrinsic high polarity of the nitrile group [318, 319]. Possibly, the nitrile groups in the grafted chains increase the interaction between polymer chains due to the high polarity and enhance the stiffness of chains and the chain-to-chain binding, which results in a decrease in gas permeability. The high chain-to-chain binding and stiffness cannot only restrict the transport of reactant gases across the membrane but also the transport of membrane-degrading species, which are usually formed on the catalyst surface [121], into the bulk of the membrane.

Post test analysis by FTIR spectroscopy cannot only be used to characterize membrane degradation qualitatively but also quantitatively. The loss of functional groups can be quantified by integrating the areas of the corresponding vibrational bands, such as aromatic ring and nitrile (cf. Chapter II). For the nitrile-containing membranes used in the study reported here, the

loss of aromatic (i.e., SSA) and nitrile functional groups was quantified based on a set of continuous OCV hold experiments with increasing duration (24 h, 48 h, 96 h and 130 h) using membranes prepared in the same batch, respectively (**Figure 4-25**). In both S:MAN and S:AN co-grafted membranes a gradual loss of aromatic and nitrile groups is observed. However, the S:AN co-grafted membrane shows consistently more loss in nitrile units than the S:MAN co-grafted membrane. The more pronounced loss of nitrile in the S:AN co-grafted membranes is a consequence of the combination of the chemical attack of radical intermediates on the grafted chains and the hydrolysis of nitrile groups to amide and carboxylic acid. For the S:MAN co-grafted membrane the loss of aromatic and nitrile groups appears to be congruent whitin the limits of the accuracy of the method. This suggests that, in the S:MAN co-grafted membrane, the SSA and nitrile units are decomposed in equal proportions. This is not the case in the S:AN co-grafted membrane, where hydrolysis leads to additional loss of nitrile groups.
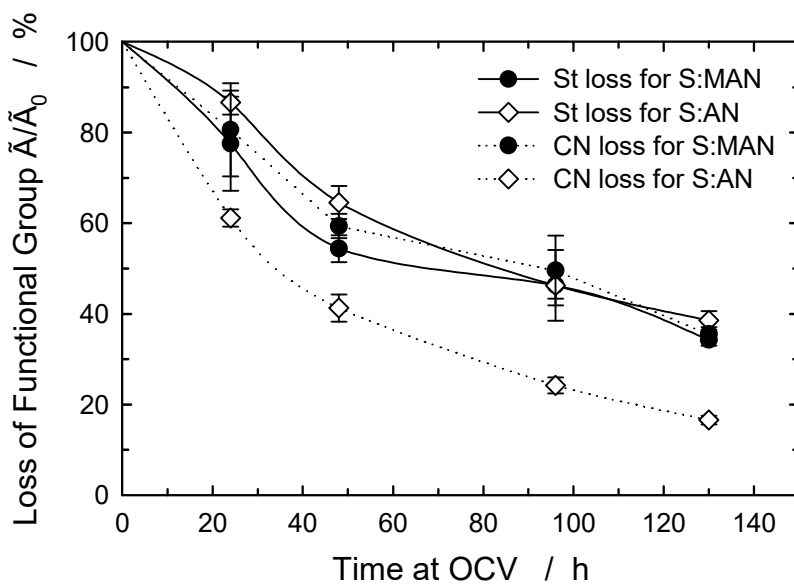
Figure 4-25. Decrease of normalized intensity of vibrational band for styrene (1'494 cm^{-1}) and nitrile (2'234 cm^{-1}) after OCV hold tests of different duration with respect to the intensity of the band in the pristine membrane.

Table 4-4. Normalized intensity of vibrational band for styrene (1'494 cm^{-1}) and nitrile (2'234 cm^{-1}) after OCV hold tests of different duration with respect to the intensity of the band in the pristine membrane. For S:AN membranes, the degree of hydrolysis of nitrile groups was calculated.

Time	S:MAN		S:AN		
(h)	St loss	CN loss	St loss	CN loss	Hydrolysis
24	78 ± 10	81 ± 10	87 ± 3	61 ± 2	29 ± 6
48	54 ± 3	59 ± 3	65 ± 4	41 ± 3	36 ± 8
96	46 ± 8	50 ± 8	46 ± 3	24 ± 2	48 ± 6
130	34 ± 1	36 ± 2	39 ± 2	17 ± 1	57 ± 5
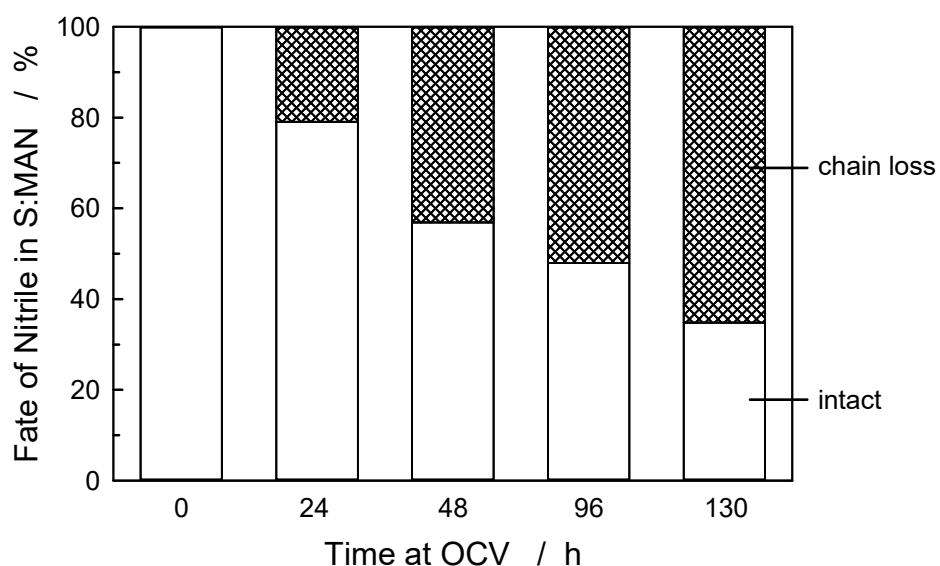
Figure 4-26. Analysis of the fate of the nitrile groups in S:MAN co-grafted membranes exposed to OCV hold tests of different duration.
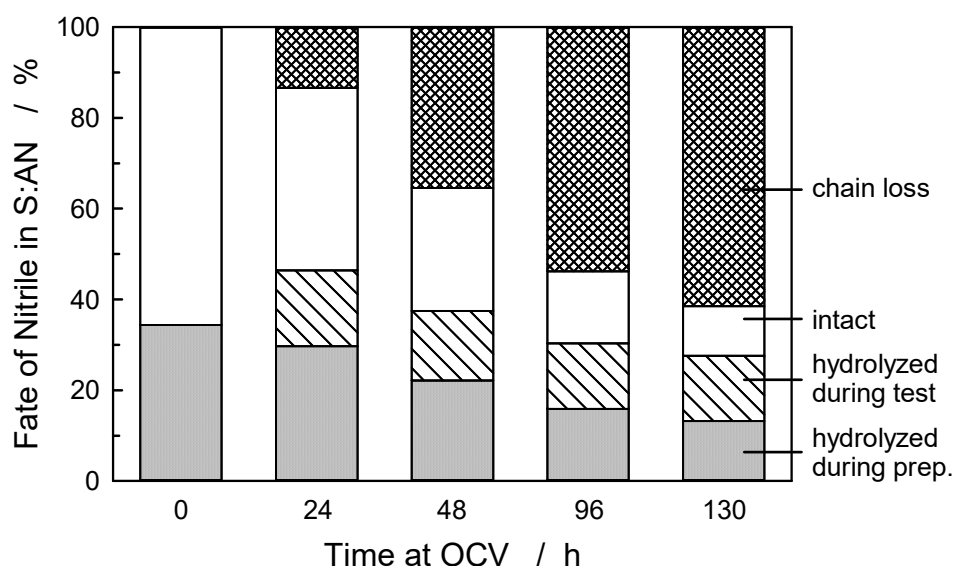
Figure 4-27. Analysis of the fate of the nitrile groups in S:AN co-grafted membranes exposed to OCV hold tests of different duration.
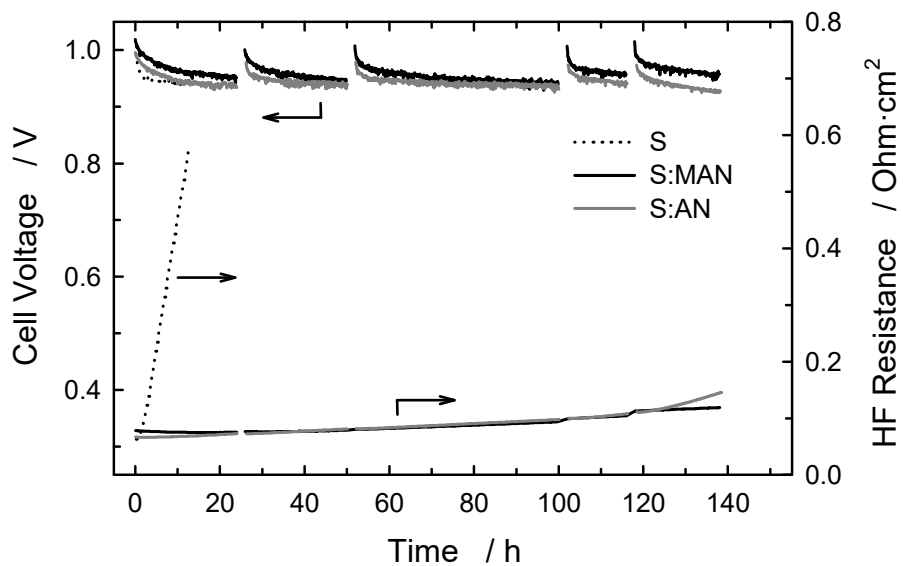
Figure 4-28. Evolution of cell voltage and high frequency (HF) resistance during OCV hold test. For S:(M)AN co-grafted membranes the H_2 crossover was measured intermittently (cf. spikes in cell voltage data).
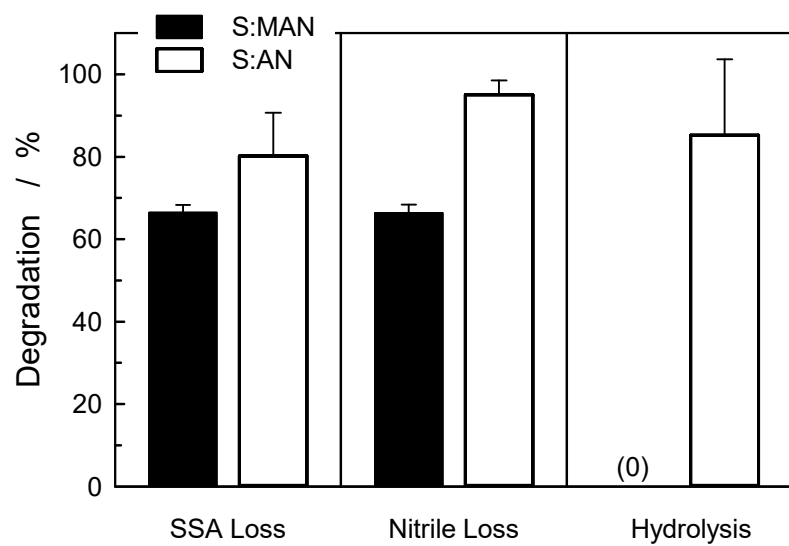
Figure 4-29. Calculated extent of SSA and nitrile loss for S:(M)AN and degree of hydrolysis of nitrile groups for co-grafted membranes after the 130 h OCV hold test.

Based on the difference in the loss of SSA and nitrile in case of the S:AN co-grafted membrane, the degree of hydrolysis of the comonomer units initially present as nitrile can be estimated, using the formalism presented in Chapter II. The hydrolysis is defined as the fraction of hydrolyzed co-monomer units with respect to the total number of comonomer units present (hydrolyzed and incact nitrile). It is found that, as could be expected, hydrolysis gradually increases over time (**Table 4-4**). After the OCV hold test over 130 h, around half of the comonomer units remaining in the graft component are hydrolyzed. Note, however, that a fraction of the AN units is already hydrolyzed in the pristine membrane as a result of the sulfonation procedure during the preparation of the membrane. For a membrane with an approximately 1:1 molar ratio of styrene to AN the initial degree of hydrolysis has been estimated to be, based on a combination of FTIR and elemental analysis, around 35 % [317].

The breakdown of contributions of SSA and nitrile loss allows the determination of the fate of the comonomer units in the co-grafted membranes. Again, the reader is referred to Chapter II for a detailed explanation of the formalism. The main assumption in this analysis is that during the loss of grafted chains, or rather fragments thereof, the two comonomers are lost in equal proportions. This can be justified with the similar content of styrene and (M)AN in the grafts (~50%) and the absence of long sequences of styrene and (M)AN in the grafts, based on the largely alternating nature of the copolymer (cf. Chapter III). In S:MAN co-grafted membranes, hydrolysis of the nitrile is negligible, hence the comonomer units either remain in the graft component as intact nitrile or are lost as a result of chain degradation along with the SSA units (**Figure 4-26**). The situation looks somewhat different for S:AN co-grafted membranes, as in this case the hydrolysis during the synthesis of the membrane has to be taken into account on the one hand, and the hydrolysis as a result of the fuel cell testing on the other hand (**Figure 4-27**). The chain degradation is about the same for both MAN and AN containing membranes, ca. 60 % after the 130 h OCV hold test. However, only about 11 % of the initial nitrile groups remain intact in case of the S:AN co-grafted membrane, because of significant hydrolysis, both during membrane preparation as well as cell testing.

In addition to the series of OCV hold tests with different duration reported in the above paragraphs, experiments with one cell, respectively, were carried out over 140 h, whereby the hydrogen crossover and cell performance were measured intermittently (**Figure 4-28**). The intermittent characterization can be seen in the diagram as spikes in the cell voltage. Since the Pt-oxide was reduced to metallic Pt during the measurement of the H_2 crossover, the cell voltage after switching to back to OCV was higher initially and then gradually decreased as the oxide started to grow on the Pt surface at the cathode. For comparison, the results of the styrene-only grafted

membrane shown already above were redrawn. The much more stable HFR in case of the nitrile-containing membranes indicates the higher chemical stability of these membranes. It can be argued, however, that the HFR increase becomes more significant in the later stages of the test, after, say, 100 h. In particular, the HFR increases in more pronounced manner in case of the S:AN co-grafted membrane and the two HFR curves start to diverge after around 120 h. The H_2 crossover measured intermittently showed an increasing trend, with initial values of around 0.95 mA/cm^2. Towards the end of the test, the H_2 crossover of the S:AN co-grafted membrane increased more notably, with an end-of-test value of 1.4 mA/cm^2 for the S:MAN co-grafted membrane and 1.8 mA/cm^2 for the S:AN co-grafted membrane, which indicates that the latter membrane suffered more degradation. This is confirmed by the lower thickness of the tested S:AN co-grafted membrane (28 µm) compared to the tested S:MAN co-grafted membrane (41 µm).

To quantify chain loss and extent of hydrolysis, again analysis of FTIR intensity for aromatic and nitrile vibrational bands in tested and pristine membranes was performed. As was found in the previous experiments, the SSA and nitrile loss are similar in case of the S:MAN co-grafted membrane, and hydrolysis of the nitrile is negligible (**Figure 4-29**). The SSA loss and, thus, chain degradation is, as expected, higher for the S:AN co-grafted membrane, and the degree of hydrolysis of the nitrile is around 85 %. This value is higher than the one reported previously for the 130 h OCV durability test of ~60 % (**Table 4-4**), because in the test reported here with intermittent cell characterization, the total time on test is more than 130 h, and since hydrolysis continues to take place during those intermittent periods, eventually a higher degree of hydrolysis is experienced. Considering the experimental findings reported in this section, it seems reasonable to assume that the extent of hydrolysis of the nitrile comonomer, or rather the concentration of remaining intact nitrile, influences the rate of degradation of the co-grafted membranes. This aspect will be revisited in Section 4.2.

4.1.3 Crosslinked membranes

In the experiments reported thus far in this section, uncrosslinked model-type radiation grafted membranes were used. In fuel cell application, it is likely that crosslinked membranes will be used, owing to the significantly higher chemical stability [195, 258, 351]. Therefore, in this sub-section, OCV hold experiments with crosslinked membranes will be reported. The membranes used include, one the hand, a "Generation 1" (Gen1) type membranes comprising sulfonated styrene and divinylbenzene (DVB) as crosslinker in the graft component. The base polymer in all cases is 25 µm ETFE film (Tefzel® 100LZ, DuPont). Membranes of this type, yet using 25 µm FEP as base film, have shown a lifetime of 7'900 h in the single cell at 80°C and a current density of 0.5 A/cm^2 [195]. The Gen1 membrane used here was prepared with a DVB content with respect

to the total monomer content in the grafting solution of 5 vol-% and had a graft level of around 25 % [271]. On the other hand, a "Generation 2" (Gen2) type membrane was used, which was prepared using α-methylstyrene (AMS) and MAN as co-monomers at a molar ratio in the grafting solution of 1.5, which yields an approximately 1:1 molar ratio in the grafts [262] (cf. also Chapter III). DVB crosslinker was added to the reaction mixture at a concentration of 1.7 vol-% with respect to the total momomer content. The membrane had a graft level of 41 %. The membranes were assembled into single cells using cloth type gas diffusion electrodes. A Nafion® 112 based MEA was used for comparison.
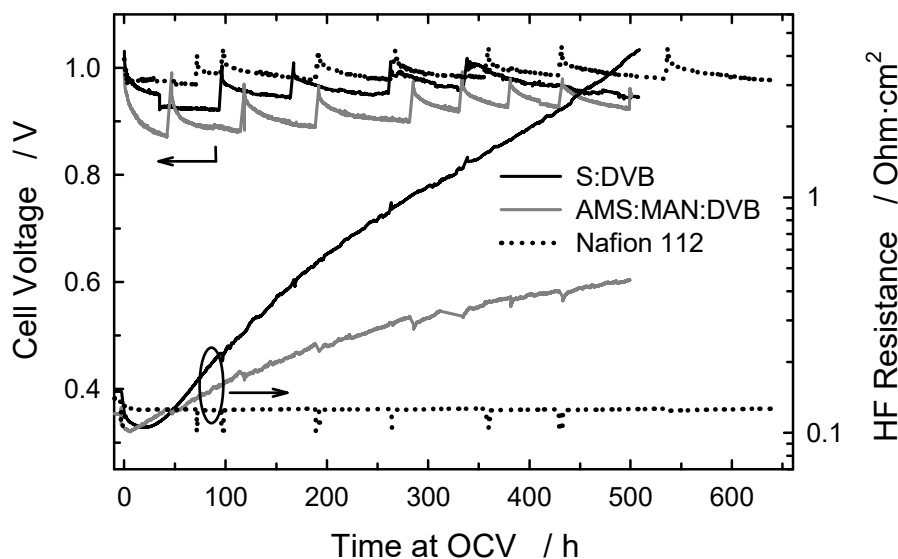
Figure 4-30. OCV hold test of a styrene and an AMS:MAN based radiation grafted membrane (both crosslinked with DVB), compared against Nafion® 112. Electrodes: ELAT® LT140EWSI (E-TEK). Temperature: 80°C, H_2 / O_2 with 100 % RH, pressure: 3 bar$_a$.

After conditioning, the cells were switched to OCV (**Figure 4-30**). The response of the HFR during the OCV hold is qualitatively similar to the one found for uncrosslinked membranes (**Figure 4-28**), in that an initial decrease in HFR is observed, followed by a steady increase. As highlighted above, the increase in HFR is associated with the loss of the graft component and, thus, ionic sites. The response of the Nafion® 112 membrane is noteworthy in this context: there is no change in HFR observed, which may be interpreted as absence of degradation. This, however, is not the case, as it is known that Nafion®, in particular the 11X family of membranes, which do not have end-group stabilization [20], are susceptible to chemical degradation under the conditions of an OCV hold test [428]. Yet Nafion® membranes typically do not show an increase in HFR upon chemical degradation, because they undergo homogeneous thinning of the material. Therefore, the HFR of the cell is not a good measure to characterize the state-of-health of Nafion® membranes. Rather, the fluoride emission rate (FER) from the cell is measured, which directly indicates the decomposition of the fluoropolymer. Under the conditions of the experiment reported

in **Figure 4-30**, the FER of a Nafion® 112 membrane is around $10 \, \mu g(F^-)/(h \cdot cm^2)$ [316]. Comparing the Gen1 with the Gen2 membrane, it appears that the latter is much more stable (note the logarithmic axis). *Post test* analysis by FTIR indicated that the Gen1 retained only 2.4 % of its initial IEC, whereas the IEC at the end of test in case of the Gen2 membrane was 17 %. It is important to note that for both membranes the mechanical integrity was maintained throughout the course of the experiment and no mechanical membrane failure was observed.

So far, OCV hold tests in single cells have been reported, which allows a detailed monitoring of the cell characteristics, such as performance, HF resistance, H_2 crossover, catalyst surface area, etc., as a function of time. However, if membranes with increasingly favorable chemical stability attributes are tested, the duration of an OCV hold test can, as shown in the previous paragraph, last for a couple of hundred hours or more. The sample throughput is therefore not very high and, in addition, series of tests including comparison and repeat experiments become very resource intensive. Furthermore, the comparability of results obtained in different cells or teststands is often limited. Therefore, it is of interest to test a number of MEAs simultaneously in a stack. Thus, tests on one test bench can be performed with multiple samples of the same kind or with MEAs of different design ("rainbow stack"). Moreover, benchmark MEAs can be included in the same stack. In case of unplanned events, the response of all MEAs to the same excursion of test parameters can be assessed.

In the experiment reported here, a 6-cell stack with small active area of $30 \, cm^2$ was used. The bipolar plates are composed of two half-plates, which allows the incorporation of a liquid coolant flow field. The reactant flow field is a parallel channel type configuration with low pressure drop, such that high gas flows can be used and the cells operated in differential flow mode. Gen2 type membranes were used in 4 cells, again based on 25 μm ETFE base film, grafted with AMS, MAN and diisopropenylbenzene (DIPB) as crosslinker (4.4 vol-% with respect to the total monomer content). DIPB was used as a crosslinker instead of DVB because it yields a more homogeneous distribution of the crosslinker through the thickness of the film [192]. The membranes had a graft level of 41 %. In addition, 2 Nafion® 212 based MEAs were used in the stack. Carbon paper type gas diffusion electrodes (ELE0162, Johnson Matthey Fuel Cells) were used.

After conditioning of the stack, the OCV hold test was started. Compared to the previous tests, the reactants were fed at a reduced relative humidity of 50 %, because this was known to accelerate the degradation of PFSA type membranes [532]. The polarization behavior, HF resistance and H_2 crossover of the cells were measured intermittently (**Figure 4-31**). In case of the Gen2 radiation grafted membranes an increase in HFR, indicative of the chemical state-of-health of the

membrane, from around 0.11 Ohm·cm^2 on average to 0.15 Ohm·cm^2 was observed, owing to a loss of a fraction of the graft component. For the Nafion® 212 based MEAs, a slight decrease in HFR was measured, which would be in agreement with a gradual thinning of the membrane (the last set of points at 288 h are probably erroneous due to poor signal quality, as the Nafion® membranes had already developed significant crossover). The OCV and H$_2$ crossover measurements show that the mechanical integrity of the Nafion® membranes deteriorated substantially during the test. After 290 h significant H$_2$ crossover was measured, indicating mechanical failure of the membranes, which also explains the drop in OCV.
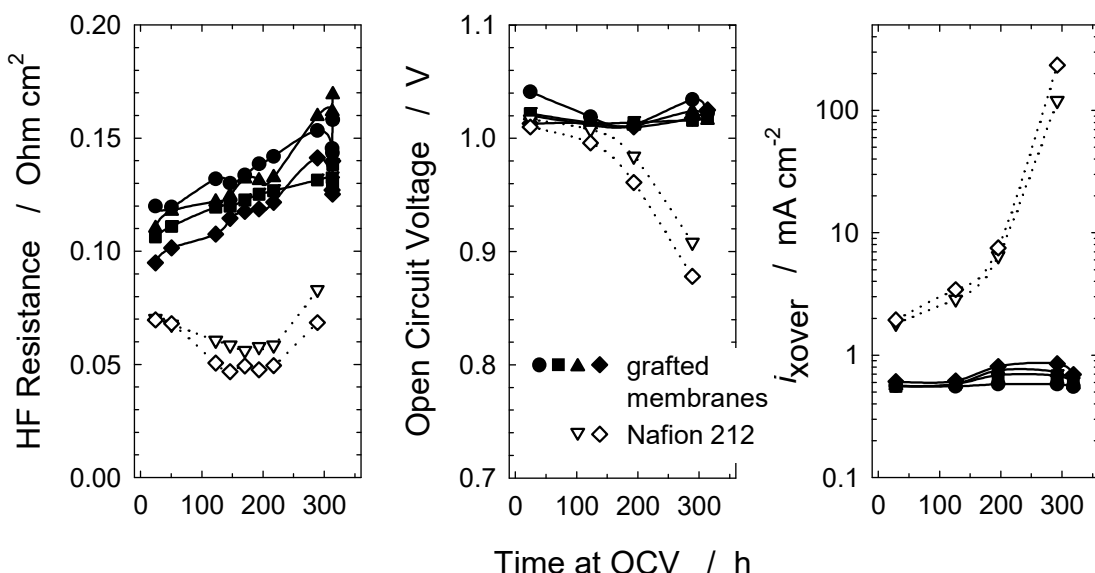
Figure 4-31. OCV hold test of a 6-cell stack (30 cm^2 active area) with radiation grafted membranes and Nafion 212, showing high frequency (1 kHz) resistance (HFR), open circuit voltage, and H$_2$ crossover current density (i_{xover}). H$_2$ / O$_2$, temperature: 80°C, pressure: 2.5 bara, reactant humidity: 50 % RH The HFR was measured intermittently at a current density of 0.5 A/cm^2, the OCV values were extracted from polarization curves.

The Gen2 membranes retained their mechanical integrity over the duration of the OCV hold test. These results support the notion of a different chemical degradation mechanism in radiation grafted membranes from that of PFSA membranes, where ionomer attack leads to the loss of polymer fragments and low molecular weight products (e.g., HF), membrane thinning and, eventually, failure of the cell due to pinhole formation. In radiation grafted membranes, mechanical failure as a result of chemical degradation is seldom observed, the base polymer (here: ETFE) continues to provide barrier properties and mechanical support even when the graft component is completely decomposed.

The test shown here demonstrates that Gen2 grafted membranes compare favorably with Nafion® membranes in terms of the chemical stability under accelerated stress conditions. Further tests

performed to compare the performance and durability with state-of-the-art Nafion® membranes are reported in Chapter I, Section 4.3.

4.2 Hydrolysis

The hydrolysis of the nitrile comonomer in S:AN an S:MAN co-grafted membranes has been highlighted in Section 4.1.2. This is likely also to be of relevance for AMS containing co-grafted membranes. Based on the results of OCV hold tests and *post test* analysis using FTIR spectroscopy it appears that AN containing membranes show a more pronounced degradation compared to MAN containing membranes after some time on test, although initially, both types of membrane show similar HFR evolution characteristics. This divergence is thought to be caused by the more pronounced hydrolysis of the nitrile in S:AN co-grafted membranes. In order to study the effect of hydrolysis in detail and separately, in the experiments reported in this section two membranes of similar composition (graft level of ~40%, ~1:1 molar ratio of styrene and nitrile comonomer), one with MAN and one with AN as comonomer, were assembled into MEAs and a single cell fixture. To promote hydrolysis of the nitrile groups, the single cell was heated to 90°C and fed with fully humidified (100 % RH) N_2 on both sides. The cell was operated under these conditions for 310 h with intermittent recording of HFR and H_2 crossover. No observable changes in HFR and H_2 crossover were measured during the course of the experiment.
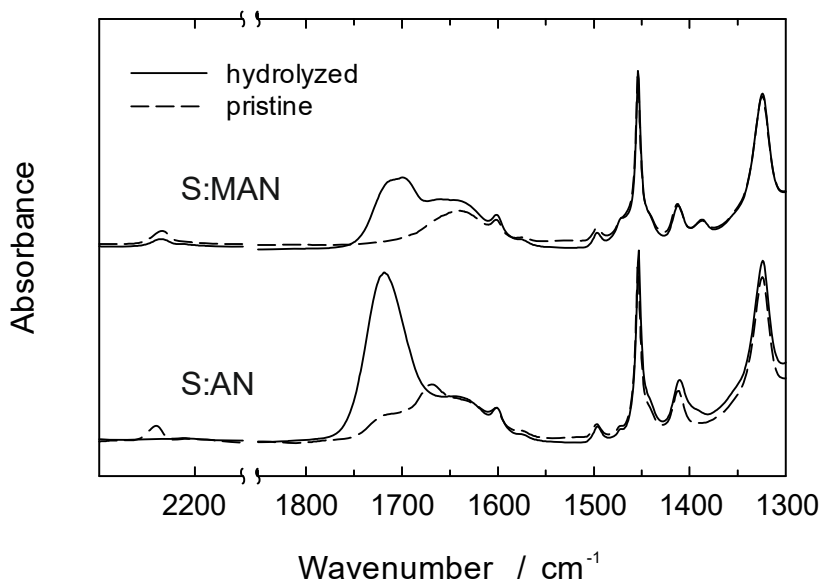
Figure 4-32. FTIR spectra of S:MAN and S:AN co-grafted membranes with graft level of ~40 % and a ~1:1 molar ratio of styrene and nitrile comonomer in the grafts before and after hydrolysis (310 h) in a single cell under N_2 conditions at 90 °C and 1 bar$_a$.

After the test, the MEAs were disassembled and the membranes retrieved for FTIR analysis (**Figure 4-32**). The obtained spectra clearly show an increased intensity in the region of the carbonyl stretch vibration around 1'700 cm^{-1} for both membrane types, yet with higher intensity in case of the S:AN co-grafted membrane, indicating a higher extent of hydrolysis. Note also that, as already highlighted above, that the S:AN co-grafted membrane also shows signatures of hydrolysis already in the as-prepared membrane. The styrene based peak at 1'493 cm^{-1}, normalized to the intensity of the ETFE base film peak at 1'325 cm^{-1}, was used to identify a possible loss of grafted chains. For both types of membrane, the styrene concentration at the end test did not differ significantly from the concentration in the pristine membrane, indicating that decomposition of grafted chains during the hydrolysis test was negligible. From the disappearance of the C≡N vibrational band at 2'234 cm^{-1} in the AN containing membrane it can be concluded that the nitrile was completely hydrolyzed, while in the case of the MAN containing membrane 36 ± 13 % of the nitrile groups were hydrolyzed. This underlines the much inferior stability of AN units against hydrolysis, be it during the preparation of the membrane, or, as shown here, during exposure of the acidic membrane to hot and humid conditions, which represents an accelerated test mimicking long-term operation in the fuel cell.
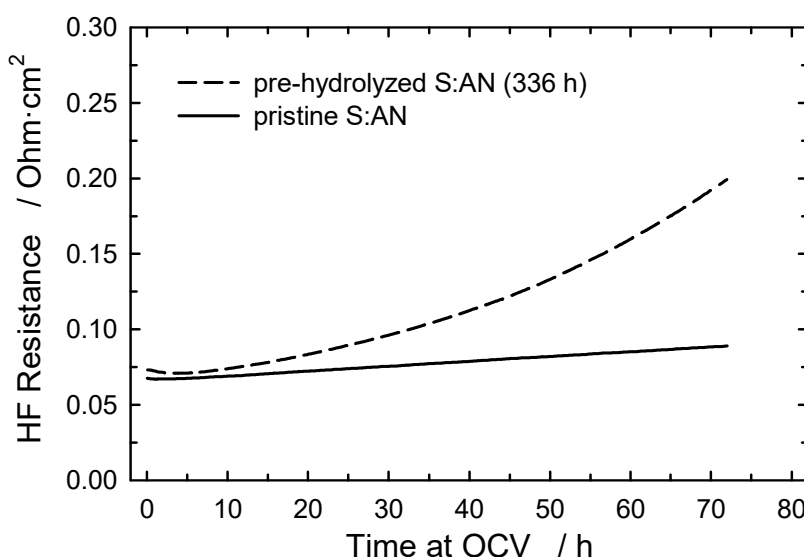
Figure 4-33. Effect of nitrile hydrolysis in S:AN co-grafted membrane on the increase in the HFR during an OCV hold test. Temperature: 80°C, humidity: 100 %, gas pressure: 2.5 bar$_a$.

In order to investigate the influence of the nitrile hydrolysis on the rate of degradation of a S:AN co-grafted membrane under the conditions of an accelerated chemical stress test at OCV, a membrane was artificially hydrolyzed in a single cell at a temperature of 80°C with H_2 fed to the anode and N_2 fed to the cathode [261]. Both gases were fully humidified. The membrane employed had a graft level of 42 % and a styrene to AN molar ratio in the grafts close to 1:1. The

cell was operated under hydrolysis conditions for 336 h (14 days). Subsequently, the membrane was disassembled from the cell and characterized with FTIR spectroscopy. A 75 % loss of nitrile groups was measured, and a decomposition of SSA units could not be detected within the limit of accuracy of the method (10%), which indicates that most of the nitrile groups in the tested S:AN co-grafted membrane were hydrolyzed during the test. Following that, a new S:AN co-grafted membrane was assembled into a single cell, hydrolyzed under identical conditions for 336 h and then exposed to an H_2 / O_2 OCV hold test for 72 h. The evolution of the HFR (**Figure 4-33**) shows that, in comparison to that of an identical membrane that had not been pre-hydrolyzed before the OCV test, the pre-hydrolyzed membrane underwent much faster degradation, indicated by the more pronounced increase in HFR.

It is therefore evident that the pre-hydrolyzed membrane ages much faster than the pristine S:AN co-grafted membrane, and the rate of degradation increases with the time at OCV. This behavior is similar to that observed for this type of membrane in the later stages of the 130 h OCV hold test reported in **Figure 4-28**. This confirms that the presence of nitrile can lower the degradation rate of the styrene-based radiation grafted membrane. When the fraction of intact nitrile drops below a critical level, membrane deterioration is accelerated.

In conclusion, the results show that the loss in the protecting effect of the nitrile group in the styrene based radiation grafted membranes leads to an accelerated degradation of the S:AN co-grafted membrane under OCV hold conditions and most likely also under regular conditions.

5 Conclusion

Low temperature fuel cells represent a challenging environment for a polymeric material that is water-swollen. Not only is there mechanical stress as a result of cell compression and changes in the hydration state of the membrane during cell operation, leading to material creep and fatigue, but also there is a considerably aggressive chemical environment: high temperature and acidic conditions favor hydrolytic reactions, and, in particular, the presence of hydrogen, oxygen and the noble metal catalyst leads to the formation of reactive intermediates, such as $HO^\bullet$, $H^\bullet$, and $HOO^\bullet$ radicals, which can attack the membrane. Radical induced chemical degradation is a serious issue, also in the case of PFSA ionomers. Although various approaches have been taken to improve the stability of PFSA membranes, such as by removing weak end-groups, reinforcing the membrane mechanically, and incorporating regenerative antioxidants, chemical aging under fuel cell operating conditions is still critical, in particular under hot (>90°C) and sub-saturated (<75 % RH) conditions.

Oxidative stability is even more of a challenge for partially fluorinated or hydrocarbon membranes, since the polymer constituents are more easily attached by radicals, in particular $HO^\bullet$, which is the most aggressive of the intermediates. Hydrogen abstraction by $HO^\bullet$ from a hydrocarbon polymer chain or other susceptible groups readily takes place. In addition, $HO^\bullet$ has a high affinity to form adducts with aromatic units, such as styrene sulfonate groups, which can trigger degradation reactions. The study of radical attack reactions is therefore of utmost importance to estimate the chemical stability of membranes. Various approaches have been taken in this respect, such as the application of accelerated test protocols on the single cell level. However, an in-depth understanding of the underlying mechanisms and kinetics is only possible if the radical attack reactions are studied under well-defined and controllable conditions. In the approach presented here, oligomers of poly(styrenesulfonic acid) (PSS) and poly(α-methylstyrenesulfonic acid) (PAMSS) were exposed to defined concentrations of $HO^\bullet$ in pulse radiolysis experiments. This allowed the determination of kinetic rate constants and identification of attack mechanisms. One key finding is that radical attack is but the first step in a sequence of reactions, which may or may not lead to chain degradation. One critical intermediate in the case of PSS is the benzyl radical, which is a precursor to chain fragmentation. In the case of PAMSS, the weak α-H is absent, yet other chain cleavage reactions are possible, albeit with slower kinetics.

For the development of hydrocarbon or partially fluorinated membranes for fuel cell application it is inevitable to devise strategies for chemical stabilization of the polymer to compete with PFSA

membranes. The incorporation of regenerative radical scavengers, such as cerium or manganese ions or oxides, as in the case of PFSA membranes, is not a viable option because the scavenging reaction is too slow compared to the rate of attack on the aromatic units of the polymer. So far, a sustainable antioxidant strategy for non-perfluorinated membranes remains to be found. Therefore, other strategies need to be pursued. In the studies presented here, the effect of nitrile comonomers, acrylonitrile (AN) and methacrylonitrile (MAN) is elaborated. Both monomers lead to an increase in the chemical stability of model styrene based uncrosslinked radiation grafted membranes, as measured in accelerated stress tests at open circuit voltage (OCV), which is a result of reduced reactant (H_2, O_2) crossover (cf. also Chapter III). However, the nitrile groups are susceptible to hydrolysis under the operating conditions of the fuel cell, in particular AN units are found to readily hydrolyze at 80°C over 140 h at OCV. MAN is more stable yet not immune to hydrolysis, as the results in Chapter I, Section 4.3, show.

Accelerated chemical stress tests using radiation grafted membranes based on AMS, MAN and DIPB (crosslinker) as monomers evidently display much superior stability compared to uncrosslinked styrene based membranes. In comparison with Nafion® 212 in a back-to-back accelerated test in a sub-scale stack showed failure of the Nafion® membranes after around 200 h due to excessive gas crossover, whereas the grafted membranes were perfectly intact and showed an increase in ohmic resistance of about 30-40 %. This observation highlights the different response to chemical stress and degradation of PFSA membranes and radiation grafted membranes: there is a strong coupling of chemical and mechanical degradation in the former, which results in an accelerating rate of degradation. In radiation grafted membranes, chemical and mechanical degradation are more independent, hence a loss of mechanical integrity as a result of chemical degradation is rarely observed.

The different response of PFSA and radiation grafted membranes to fuel cell operating conditions is also highlighted in the study on the effect of relative humidity (RH) on membrane degradation. Whereas Nafion® membranes tend to loose stability towards reduced RH, radiation grafted membranes show an increase in stability. This is explained with the activation of additional chain degradation mechanisms in case of PFSA ionomers at low RH, which appears not to be the case for radiation grafted membranes. This shows that the mechanisms of the degradation of membranes (or other components) are decisive in the choice of accelerated testing protocols and the respective experimental conditions. It may be that the comparison of different materials on the basis of a particular accelerated test protocol may not be "fair", because the correlation to regular operating conditions lacks consistency.

Conclusions & Prospects[1]

The challenges associated with the development of radiation grafted electrolyte membranes for fuel cell application can be categorized into functionality, processing, and economy related issues. Regarding the functionality, i.e., performance, durability and reliability during operation, the development has come a long way. Since it has been recognized early that styrene based membranes exhibit poor durability under fuel cell operating conditions, various routes have been pursued to improve the stability of radiation grafted membranes. Fluorinated monomers, such as α,β,β-trifluorostyrene (TFS) and its derivatives, have shown some success, yet at the price of high monomer cost and limited grafting kinetics. The choice of adequate (non-fluorinated) and commercially readily available styrene derivatives and suitable co-monomers, i.e. crosslinkers and non-crosslinking ones, has shown to be a promising approach. With optimized membrane architecture and composition, performance and durability attributes similar to those of current state-of-the-art perfluoroalkylsulfonic acid (PFSA) membranes can be attained. In addition to proton conducting membranes, the versatility of the radiation grafting method also allows the design of anion exchange membranes and membranes for doping with phosphoric acid for the high-temperature PEFC. The one challenge common to all design approaches, however, is the required careful balance of composition between backbone polymer and grafted polymer. The base polymer is the chemically and mechanically stable constituent, hence maximizing its content improves the robustness of the membrane. The grafted component provides the ion-containing functional groups and, ultimately, governs the performance of the cell. In addition to addressing the bulk composition and morphology, emphasis has to be placed on the optimization of surface and membrane-electrode interface properties. Therefore, the focus of development ought to be more on the membrane-electrode assembly (MEA) rather than on the membrane alone. Proton transport losses and water management properties are influenced in critical manner by the particular combination of membrane, catalyst layer and gas diffusion medium. In this regard, it is also worth contemplating to introduce alternative ionomer materials in the catalyst layer to improve the chemical compatibility to the membrane material.

From a product development point of view, it is probably insufficient to aim at matching the properties and characteristics of PFSA membranes. It is advisable and advantageous, in addition to the argument of cost efficiency, to identify functionality attributes that provide an added value compared to the established technology. One such key asset is the designability of the graft copolymer. The degrees of freedom associated with the synthesis of radiation grafted membranes

---

[1] Excerpt from L. Gubler, *Adv. Energy Mater.* 4 (2014), 1300827

with respect to the choice of base polymer, grafting monomer(s), degree of grafting, options for post-processing, etc., allow the adjustment of polymer composition and properties in a wide range to create tailor-made membranes for specific target applications and operating strategies. For instance, in applications with frequent changes in load or start/stop operation, it is essential to minimize the swelling of the membrane in water to avoid damage induced by repeated uptake and loss of water, which can eventually lead to hydration-cycling induced failure of the membrane and MEA. Another unique selling proposition (USP) of radiation grafted membranes could be the lower coupling of chemical and mechanical degradation mechanisms and failure modes compared to PFSA membranes. In fact, mechanical failure through pinhole or crack formation as a result of chemical degradation is rarely observed in radiation grafted membranes, unlike in PFSA membranes, even in mechanically reinforced types. Last but not least, the lower gas permeability is worth mentioning, which is an important parameter in the context of H_2 and O_2 crossover induced formation of reactive intermediates (H_2O_2, radicals), which trigger chemical degradation of the ionomer.

In the many articles and book chapters focusing on the influence of the type of base polymer, commercial film materials have been used. Many film properties that can strongly influence the irradiation and grafting process, however, are unknown or difficult to establish. For instance, the type and concentration of additives in the polymer, e.g., radical scavengers or UV-stabilizers, can influence the formation and distribution of radicals in critical manner. Also, molecular weight (distribution), crystallinity, size and distribution of crystallites, extent of orientation of the film and its thermal history can affect the processing and final properties of the membrane. The polymers currently chosen as base films for the preparation of radiation grafted membranes are not designed for this purpose, and in all likelihood there is considerable room for improvement of the base film to enhance its compatibility with the process. Yet there is currently limited understanding of which attributes exactly an "ideal" base polymer would need to have.

Related to the base polymer is the question to which extent and in which manner the film properties influence the morphology of the grafted film and final membrane at various length scales. Since the grafting only takes place in the amorphous regions of the polymer, the volume fraction, size and distribution of crystallites undoubtedly influence the final properties. To date, the understanding what the relevant structure-property relationships are is rather limited. The membrane "inherits" many of the (favorable or unfavorable) morphological features of the base polymer. With the possibility to influence the processing and properties of the base polymer another set of parameters would be available to tune the material to its best use. Currently, however, the experimenter has to use what the film manufacturer offers as a commercial product.

The scale-up of the membrane preparation from a batch type laboratory process to a reel-to-reel pilot line represents a major challenge, which may involve a complete reconfiguration of the process. The time between irradiation and grafting is no longer several weeks or months, but the activated film is contacted with the monomer to commence grafting a few minutes to less than an hour after irradiation. Furthermore, the irradiation may be carried out in inert atmosphere or in the presence of oxygen, which will have a large impact on the grafting kinetics and properties of the final product. Key cost drivers in the reel-to-reel process are the monomer utilization and line speed. Monomer utilization largely depends on how the monomer is brought into contact with the activated film and how efficiently the monomer is being used. A large monomer bath is uneconomic and more clever methods of monomer application need to be devised. The line speed is closely related to the grafting rate. Therefore, the grafting system (irradiation dose, monomer content, type and concentration of solvents and additives) has to be optimized in such a way that the target graft level can be reached in the shortest time possible, ideally within 1 h, evidently without deleterious gradients in graft level across the thickness of the film. For the sulfonation reaction, it is conceivable to use gas phase sulfonation with SO_3, which does not require subsequent hydrolysis. Obviously, adequate safety precautions need to be taken when implementing such a process. In any case, scale-up to small manufacturing volumes with possibilities of further increasing throughput is only justified if there are tangible prospects for business development. Therefore, product and process development not only of the membrane material but also of membrane electrode assemblies or even more highly integrated unitized components have to go hand-in-hand with a development of relationship to an end-user. Fuel cell stack and system builders have to be convinced of the assets of radiation grafted membranes and the products made therefrom.

The method of radiation grafting is a versatile method and lends itself to the preparation of functionalized polymer structures (films, fibers, non-wovens) for a range of different purposes. In the context of electrochemical energy storage and conversion, designed polymer electrolytes could be developed for a number of cell types other than fuel cells. The use in electrolysis cells is perhaps straightforward, and the requirements are largely similar to the ones pertinent to fuel cell application. Furthermore, membranes with transport properties for specific ions are required in redox flow cells, for which interest has greatly increased in recent years in connection with the need to deploy installations and systems for grid-scale storage of electricity to balance an increasing share of renewable electricity. Last but not least, polymers with selective transport of Li-ions and barrier properties for unwanted species are of interest for next generation lithium batteries, i.e. lithium-sulfur and lithium-oxygen(air) cells, which are expected to have energy

densities several times higher than current lithium-ion battery cells based on graphite and oxide intercalation compounds at the negative and positive electrode, respectively.

References

1. W.T. Grubb, "Fuel Cell", *US Patent 2,913,511*, General Electric Company, USA, Aug 18, 1959

2. W. Juda, W.A. McRae, "Coherent Ion-Exchange Gels and Membranes", *J. Am. Chem. Soc.* **72** (1950), 1044-1044

3. E.W. Justi, "Seventy Years Fuel Cell Research", *Brit. J. Appl. Phys.* **14** (1963), 840-853

4. G.G. Scherer, "Polymer Membranes for Fuel Cells", *Ber. Bunsenges. Phys. Chem.* **94** (1990), 1008-1014

5. A.B. LaConti, H. Hamdan, R.C. McDonald, "Mechanisms of Membrane Degradation", in *Handbook of Fuel Cells - Fundamentals, Technology and Applications*, Volume 3, W. Vielstich, H.A. Gasteiger, A. Lamm, John Wiley & Sons, Chichester, 2003, 647-662

6. F.G. Helfferich, *Ion Exchange*, McGraw-Hill, New York, 1962

7. W.T. Grubb, L.W. Niederach, "Batteries with Solid Ion-Exchange Membrane Electrolytes", *J. Electrochem. Soc.* **107** (1960), 2, 131-135

8. E.M. Cohn, "NASA's Fuel Cell Program", in *Fuel Cell Systems*, Volume 47, G.J. Young, H.R. Linden, American Chemical Society, 1969, 1-8

9. R.B. Hodgdon, J.R. Boyack, A.B. LaConti, "The Degradation of Polystyrene Sulfonic Acid", *TIS Report 65DE 5*, General Electric Company, Lynn MA, USA, 1966

10. G. Smets, M. Claesen, "Copolymères Greffés", *J. Polym. Sci.* **8** (1952), 3, 289-311

11. B.C. Hacker, J.M. Grimwood, "On the Shoulders of Titans: A History of Project Gemini", NASA, Published as NASA Special Publication 4203 in the NASA History Series, http://www.hq.nasa.gov/office/pao/History/SP-4203/ch8-4.htm.

12. G.N. Richards, "Ion-Exchange Membranes by Sulfonation of Poly(vinylidene Fluoride) Films", *J. Appl. Polym. Sci* **8** (1964), 2269-2280

13. R.B. Hodgdon, "Polyelectrolytes Prepared from Perfluoroalkylaryl Macromolecules", *J. Polym. Sci. Part A: Polym. Chem.* **6** (1968), 171-191

14. A.B. LaConti, "Application of Perfluoro Carbon Solid Polymer Electrolytes in Fuel Cells and Electrolyzers", *Paper Presented at the Topical Workshop on Perfluorinated Ionomer Membranes, American Chemical Society - Polymer Division*, General Electric Company, Lake Buena Vista, Florida, Feb 23-26, 1982

15. R.B. Hodgdon, J.F. Enos, E.J. Aiken, "Sulfonated Polymers of α,β,β-Trifluorostyrene, with Applications to Structures and Cells", *US Patent 3,341,366*, General Electric Company, USA, 1967

16. J. Wei, C. Stone, A. Steck, "Trifluorostyrene and Substituted Trifluorostyrene Copolymeric Compositions and Ion-exchange Membranes Formed Therefrom", *US Patent 5,422,411*, Ballard Power Systems Inc., 1995

17. A.E. Steck, C. Stone, "Development of the BAM Membrane for Fuel Cell Applications", *Proc. Second International Symposium on New Materials for Fuel Cell and Modern Battery Systems*, O. Savadogo, P.R. Roberge, Montreal, Canada, 1997, 792-807

18. M. Doyle, G. Rajendran, "Perfluorinated Membranes", in *Handbook of Fuel Cells - Fundamentals, Technology and Applications*, Volume 3, W. Vielstich, H.A. Gasteiger, A. Lamm, John Wiley & Sons, Chichester, 2003, 351-395

19. M. Yoshitake, A. Watakabe, "Perfluorinated Ionic Polymers for PEFCs (Including Supported PFSA)", *Adv. Polym. Sci.* **216** (2008), 127-155

20. D.E. Curtin, R.D. Lousenberg, T.J. Henry, P.C. Tangeman, M.E. Tisack, "Advanced Materials for Improved PEMFC Performance and Life", *J. Power Sources* **131** (2004), 41-48

21. M. Gebert, A. Ghielmi, L. Merlo, M. Corasaniti, V. Arcella, "AQUIVION^{TM} - The Short-Side-Chain and Low-EW PFSA for Next-Generation PEFCs Expands Production and Utilization", *ECS Trans.* **26** (2010), 1, 279-283

22. W.G. Grot, "Perfluorinated Ion Exchange Polymers and their use in Research and Industry", *Macromol. Symp.* **82** (1994), 161-172

23. W. Grot, "Perfluorierte Ionenaustauscher-Membrane von hoher chemischer und thermischer Stabilität", *Chem. Ing. Tech.* **44** (1972), 4, 167-169

24. W. Grot, "Perfluorierte Kationenaustauscher-Polymere", *Chem. Ing. Tech.* **47** (1975), 14, 617

25. W.G. Grot, "$CF_2=CFCF_2CF_2SO_2F$ and Derivatives and Polymers thereof", *US Patent 3,718,627*, E. I. du Pont de Nemours and Company (DuPont), 1973

26. M.L. Perry, T.F. Fuller, "A Historical Perspective of Fuel Cell Technology in the 20th Century", *J. Electrochem. Soc.* **149** (2002), 7, S59-S67

27. S.J.C. Cleghorn, D.K. Mayfield, D.A. Moore, J.C. Moore, G. Rusch, T.W. Sherman, N.T. Sisofo, U. Beuscher, "A Polymer Electrolyte Fuel Cell Life Test: 3 Years of Continuous Operation", *J. Power Sources* **158** (2006), 446-454

28. M. Nakao, M. Yoshitake, "Composite Perfluorinate Membranes", in *Handbook of Fuel Cells - Fundamentals, Technology and Applications*, Volume 3, W. Vielstich, H.A. Gasteiger, A. Lamm, John Wiley & Sons, Chichester, 2003, 412-419

29. K.E. Schwiebert, K.G. Raiford, G. Escobedo, G. Nagarajan, "Strategies for Mitigation of PFSA Polymer Degradation in PEM Fuel Cells", *ECS Trans.* **1** (2006), 8, 303-311

30. H. Zhang, P.K. Shen, "Recent Development of Polymer Electrolyte membranes for Fuel Cells", *Chem. Rev.* **112** (2012), 2780-2832

31. M.M. Nasef, E.S.A. Hegazy, "Preparation and Applications of Ion Exchange Membranes by Radiation-Induced Graft Copolymerization of Polar Monomers onto Non-Polar Films", *Prog. Polym. Sci.* **29** (2004), 499-561

32. T.R. Dargaville, G.A. George, D.J.T. Hill, A.K. Whittaker, "High Energy Radiation Grafting of Fluoropolymers", *Progr. Polym. Sci.* **28** (2003), 1355-1376

33. M. Magat, *J. Chim. Phys.* **52** (1955), 709

34. J. Behr, R.B. Mesrobian, A.J. Restaino, D.S. Ballantine, A. Glines, D.J. Metz, "*G* Values of Gamma-Ray Initiation of Vinyl Polymerization and their Relation to Graft Copolymer Formation", *J. Polym. Sci.* **19** (1956), 219-224

35. W.K.W. Chen, R.B. Mesrobian, D.S. Ballantine, D.J. Metz, A. Glines, "Studies on Graft Copolymers derived by Ionizing Radiation", *J. Polym. Sci.* **23** (1957), 903-913

36. A. Chapiró, *Radiation Chemistry of Polymeric Systems*, Interscience Publishers, New York, London, 1962

37. A. Chapiró, "Préparation des Copolymères Greffés du Polytetrafluoroethylène (Teflon) par Voie Radiochimique", *J. Polym. Sci.* **34** (1959), 481-501

38. A. Bozzi, A. Chapiró, "Synthesis of Perm-selective Membranes by Grafting Acrylic Acid into Air-irradiated Teflon-FEP Films", *Radiat. Phys. Chem.* **32** (1988), 193

39. B. Gupta, A. Chapiró, "Preparation of Ion-Exchange Membranes by Grafting Acrylic Acid into Pre-Irradiated Polymer Films — 1. Grafting into Polyethylene", *Eur. Polym. J.* **25** (1989), 1137-1143

40. B. Gupta, A. Chapiró, "Preparation of Ion-Exchange Membranes by Grafting Acrylic Acid into Pre-Irradiated Polymer Films — 2. Grafting into Teflon-FEP ", *Eur. Polym. J.* **25** (1989), 1145

41. G. Odian, R.L. Kruse, "Diffusion Effects in Radiation-Induced Graft Polymerization", *J. Polym. Sci. Part C* **22** (1969), 691-712

42. G. Odian, D.-H. Lee, V. Patel, A. Rabie, A.Z. Zahran, "Diffusion-Controlled Reaction. VI. Radiation Graft Polymerization of Styrene to Polyethylene", *J. Polym. Sci. Polym. Chem.* **22** (1984), 769-779

43. G. Odian, A. Derman, K. Imre, "Diffusion-Controlled Reaction. VI. Radiation Graft Polymerization of 4-Vinylpyridine to Polyethylene", *J. Polym. Sci. Polym. Chem.* **18** (1980), 737-748

44. H.Z. Friedlander, "Battery Separators Containing Sulfonamide Groups", *US Patent 3,240,723*, American Machine and Foundry Co., 1966

45. W.K.W. Chen, "Method of Forming Graft Copolymer Ion Exchange Membranes", US Patent 3,247,133, American Machine and Foundry Co., 1966

46. V.F. D'Agostino, J.Y. Lee, E.H. Cook, "Trifluorostyrene Sulfonic Acid Membranes", *US Patent 4,012,303*, Hooker Chemicals & Plastics Corp., RAI Research Corporation, 1978

47. G. Ellinghorst, A. Niemöller, D. Vierkotten, "Radiation Initiated Grafting of Polymer Films - An Alternative Technique to Prepare Membranes for Various Separation Problems", *Radiat. Phys. Chem.* **22** (1983), 3-5, 635-642

48. J. Dobó, A. Somogyi, T. Czvikovszky, "Grafting of Styrene onto Teflon and Polyethylene by Preirradiation", *J. Polym. Sci.: Part C* **4** (1963), 1173-1193

49. K. Makuuchi, S. Cheng, *Radiation Processing of Polymer Materials and its Industrial Applications*, John Wiley & Sons, Hoboken NJ, USA, 2012

50. G.-H. Hsiue, W.-K. Huang, "Preirradiation Grafting of Acrylic and Methacrylic Acid onto Polyethylene Films: Preparation and Properties", *J. Appl. Polym. Sci.* **30** (1985), 1023-1033

51. M.M. Nasef, O. Güven, "Radiation-grafted Copolymers for Separation and Purification Purposes: Status, Challenges and Future Directions", *Prog. Polym. Sci.* **37** (2012), 1597-1656

52. V.S. Ivanov, *Radiation Chemistry of Polymers*, VSP, Utrecht, 1992

53. K. Fujiwara, "Separation Functional Fibers by Radiation Induced Graft Polymerization and Application", *Nucl. Instr. Meth. Phys. Res. B* **265** (2007), 150-155

54. N. Seko, M. Tamada, F. Yoshii, "Current Status of Adsorbent for Metal Ions with Radiation Grafting and Crosslinking Techniques", *Nucl. Instr. Meth. Phys. Res. B* **236** (2005), 21-29

55. G.G. Scherer, "Membrane Evaluation for the Membrel® Water Electrolysis Process", *Proceedings of the 6th World Hydrogen Energy Conference*, T.N. Veziroglu, N. Getoff, P. Weinzierl, Pergamon Press, Vienna, Austria, July 20-24, 1986, 382-389

56. G.G. Scherer, T. Momose, K. Tomiie, "Membrel-Water Electrolysis Cells with a Fluorinated Cation Exchange Membrane", *J. Electrochem. Soc.* **135** (1988), 12, 3071-3073

57. V.F. D'Agostino, J.Y. Lee, E.H. Cook, "Trifluorostyrene Sulfonic Acid Membranes", US Patent 4,113,922, Hooker Chemicals & Plastics Corp., RAI Research Corporation, 1978

58. V.F. D'Agostino, J.Y. Lee, E.H. Cook, "Process for Electrolysing Sodium Chloride or Hydrochloric Acid, an and Electrolytic Cell, Employing Trifluorostyrene Sulfonic Acid Membrane", US Patent 4,107,005, Hooker Chemicals & Plastics Corp., RAI Research Corporation, 1978

59. T. Momose, K. Tomiie, H. Harada, M. Miyachi, H. Kato, "Method for Preparation of Graft Polymeric Membranes", *US Patent 4,605,685*, Chlorine Engineers Corp., 1986

60. T. Momose, H. Yoshioka, I. Ishigaki, J. Okamoto, "Radiation Grafting of Alpha,Beta,Beta-Trifluorostryrene onto Poly(Ethylene-Tetrafluoroethylene) Film by Preirradiation Method. I. Effects of Preirradiation Dose, Monomer Concentration, Reaction Temperature, and Film Thickness", *J. Appl. Polym. Sci.* **37** (1989), 10, 2817-2826

61. T. Momose, K. Tomiie, I. Ishigaki, J. Okamoto, "Radiation Grafting of Alpha,Beta,Beta-Trifluorostryrene onto Various Polymer Films by Preirradiation Method", *J. Appl. Polym. Sci.* **37** (1989), 2165-2168

62. T. Momose, T. Kitazumi, I. Ishigaki, J. Okamoto, "Radiation Grafting of Alpha,Beta,Beta-Trifluorostryrene onto Poly(Ethylene-Tetrafluoroethylene) Film by Preirradiation Method. III. Properties of Anion-Exchange Membrane Obtained by Chloromethylation and Quaternization of the Grafted Film", *J. Appl. Polym. Sci.* **39** (1990), 1221-1230

63. T. Momose, H. Yoshioka, I. Ishigaki, J. Okamoto, "Radiation Grafting of Alpha,Beta,Beta-Trifluorostryrene onto Poly(Ethylene-Tetrafluoroethylene) Film by Preirradiation Method. II.

Properties of Cation-Exchange Membrane Obtained by Sulfonation and Hydrolysis of the Grafted Film", *J. Appl. Polym. Sci.* **38** (1989), 2091-2101

64. Z.-l. Xu, G.-h. Wang, H.-i. Wang, G. Cian, M.-h. Ni, "Radiation Induced Grafting of Styrene and its Mixture with Divinylbenzene onto F46 Film", *Radiat. Phys. Chem.* **22** (1983), 3-5, 939-945

65. L. Gubler, S. Alkan-Gürsel, G.G. Scherer, "Radiation Grafted Membranes for Polymer Electrolyte Fuel Cells", *Fuel Cells* **5** (2005), 3, 317-335

66. K. Fujiwara, Y. Okamura, R. Ishihara, T. Sugo, T. Kojima, D. Umeno, K. Saito, "Cesium Adsorptive Fibers Containing Potassium Cobalt-hexacyanoferrate Prepared by Radiation-induced Graft Polymerization", *Proc. 10th Meeting of the Ionizing Radiation and Polymers Symposium (IRaP)*, A.G. Chmielewski, J.M. Rosiak, Cracow, Poland, Oct 14-19, 2012, 70

67. C. Stone, A.E. Morrison, "From Curiosity to "Power to Change the World"", *Solid State Ionics* **152-153** (2002), 1-13

68. T.R. Ralph, G.A. Hards, J.E. Keating, S.A. Campbell, D.P. Wilkinson, M. Davis, J. St-Pierre, M.C. Johnson, "Low Cost Electrodes for Proton Exchange Membrane Fuel Cells: Performance in Single Cells and Ballard Stacks", *J. Electrochem. Soc.* **144** (1997), 11, 3845-3857

69. W. Liu, K. Ruth, G. Rusch, "Membrane Durability in PEM Fuel Cells", *J. New Mater. Electrochem. Syst.* **4** (2001), 227-231

70. M. Matsunaga, T. Fukushima, K. Ojima, "Advances in the Power Train System of Honda FCX Clarity Fuel Cell Vehicle", *SAE World Congress, Fuel Cell Vehicle Application Session, SP-2236*, Society of Automotive Engineers (SAE), Detroit (USA), April 20-23, 2009, 2009-01-1012

71. W. Schmittinger, A. Vahidi, "A Review of the Main Parameters Influencing Long-Term Performance and Durability of PEM Fuel Cells", *J. Power Sources* **180** (2008), 1-14

72. C. Stone, A.E. Steck, "Graft Polymeric Membranes and Ion-Exchange Membranes Formed Therefrom", *US Patent 6,359,019*, Ballard Power Systems, 2002

73. C. Stone, A.E. Steck, B. Choudhury, "Graft Polymeric Membranes and Ion-Exchange Membranes Formed Therefrom", *US Patent 6,723,758*, Ballard Power Systems, 2004

74. C. Stone, A.E. Steck, "Graft Polymeric Membranes and Ion-Exchange Membranes Formed Therefrom", *WO 01/58576A1*, Ballard Power Systems, 2001

75. C. Stone, L.M. Bonorand, "Process for Preparing Graft Copolymer Membranes", *WO 2003/018654A1,* Ballard Power Systems, 2003

76. C. Stone, "Process for Preparing Graft Copolymer Membranes", *WO 03/018655A1*, Ballard Power Systems Inc., 2003

77. N. Chouhan, R.-S. Liu, "Electrochemical Technologies for Energy Storage and Conversion", in *Electrochemical Technologies for Energy Storage and Conversion*, Volume 1, R.-S. Liu, L. Zhang, X. Sun, H. Liu, J. Zhang, Wiley-VCH, 2012, Chapter 1, 1-43

78. W. Vielstich, H.A. Gasteiger, A. Lamm, H. Yokokawa, "Handbook of Fuel Cells - Fundamentals, Technology and Applications", Wiley, Chichester, United Kingdom, 2010

79. M.F. Mathias, R. Makharia, H.A. Gasteiger, J.H. Conley, T.J. Fuller, C.J. Gittleman, S.S. Kocha, D.P. Miller, C.K. Mittelstaedt, T. Xie, S.G. Yan, P.T. Yu, "Two Fuel Cell Cars in Every Garage ?", *Electrochem. Soc. Interface* **14** (2005), 3, 24-35

80. U. Eberle, B. Müller, R.von Helmolt, "Fuel Cell Electric Vehicles and Hydrogen Infrastructure: Status 2012", *Energy Environ. Sci.* **5** (2012), 8780-8798

81. J.P. Meyers, "Getting Back into Gear: Fuel Cell Development after the Hype", *Electrochem. Soc. Interface* **17** (2008), 4, 36-39

82. S. Knights, R. Bashyam, P. He, M. Lauritzen, C. Startek, V. Colbow, T.T.H. Cheng, J. Kolodziej, S. Wessel, "PEMFC MEA and System Design Considerations", *ECS Trans.* **41** (2011), 1, 39-53

83. "Toyota Mirai - The Turning Point", www.toyota.com/mirai/fcv.html, Toyota Motor Corporation, accessed May 2015

84. I. Staffel, M. Matian, D.J.L. Brett, N.P. Brandon, A.D. Hawkes, "Fuel Cell Micro-CHP", in *Domestic Microgeneration – Renewable and Distributed Energy Technologies, Policies and Economics*, I. Staffel, D.J.L. Brett, N.P. Brandon, A.D. Hawkes, Routledge, 2015, 219-251

85. Y. Wang, K.S. Chen, J. Mishler, S.C. Cho, X.C. Adroher, "A Review of Polymer Electrolyte Membrane Fuel Cells: Technology, Applications, and Needs on Fundamental Research", *Applied Energy* **88** (2011), 981-1007

86. R. O'Hayre, S.-W. Cha, W. Colella, F.B. Prinz, *Fuel Cell Fundamentals*, John Wiley & Sons, Hoboken NJ, 2009

87. A.J. Appleby, A.C. Lloyd, C.K. Dyer, "The Future of Fuel Cells", *Sci. Am.* **7** (1999), 72-93

88. T.R. Ralph, G.A. Hards, "Fuel Cells: Clean Energy Production for the New Millennium", *Chem. Ind.* **9** (1998), 334-335

89. T.R. Ralph, G.A. Hards, "Powering the Cars and Homes of Tomorrow", *Chem. Ind.* **9** (1998), 337-342

90. K.C. Neyerlin, W. Gu, J. Jorne, H.A. Gasteiger, "Study of the Exchange Current Density for the Hydrogen Oxidation and Evolution Reactions", *J. Electrochem. Soc.* **154** (2007), 7, B631-B635

91. S.R. Narayanan, T.I. Valdez, N. Rohatgi, "DMFC System Design for Portable Applications", in *Handbook of Fuel Cells - Fundamentals, Technology and Applications*, Volume 4, Chapter 65, W. Vielstich, H.A. Gasteiger, A. Lamm, John Wiley & Sons, Chichester, 2003, 894-904

92. X. Ren, P. Zelenay, S. Thomas, J. Davey, S. Gottesfeld, "Recent Advances in Direct Methanol Fuel Cells at Los Alamos National Laboratory", *J. Power Sources* **86** (2000), 111-116

93. R.M. Moore, S. Gottesfeld, P. Zelenay, "Comparison of the Conversion Efficiency of a Direct-Methanol vs. A Hydrogen Fuel Cell", *Proc. Second International Symposium on Proton Conducting Membrane Fuel Cells II, PV 98-27*, S. Gottesfeld, T.F. Fuller, The Electrochemical Society, 1998, 365-379

94. J.R. Varcoe, R.C.T. Slade, "Prospects for Alkaline Anion-Exchange Membranes in Low Temperature Fuel Cells", *Fuel Cells* **5** (2005), 2, 187-200

95. G. Merle, M. Wessling, K. Nijmeijer, "Anion Exchange Membranes for Alkaline Fuel Cells: A Review", *J. Membr. Sci.* **377** (2011), 1-35

96. G. Couture, A. Alaaeddine, F. Boschet, B. Ameduri, "Polymeric Materials as Anion-Exchange Membranes for Alkaline Fuel Cells", *Prog. Polym. Sci.* **36** (2011), 1521– 1557

97. M.G. Marino, K.D. Kreuer, "Alkaline stability of quaternary ammonium cations for alkaline fuel cell membranes and ionic liquids", *ChemSusChem* **8** (2015), 3, 513-23

98. T. Gilchrist, "Fuel Cells to the Fore", *IEEE Spectrum* **11** (1998), 35-40

99. J. Meusinger, B. Höhlein, R. Menzer, E. Riensche, U. Stimming, "Fuel Processing in Fuel Cell Systems", *Proc. Second International Symposium on New Materials for Fuel Cell and Modern Battery Systems*, O. Savadogo, P.R. Roberge, Montreal, Canada, July 6-10, 1997, 522-535

100. H.A. Gasteiger, N.M. Markovic, P.N. Ross, "H_2 and CO Electrooxidation on Well-Characterized Pt, Ru, and Pt-Ru. 2. Rotating Disk Electrode Studies of CO/H_2 Mixtures at 62 °C", *J. Phys. Chem.* **99** (1995), 16757-16767

101. J.M. Larson, S.J. Hamrock, G.M. Haugen, P. Pham, W.M. Lamanna, A.B. Moss, "Membranes Based on Basic Polymers and Perfluorinated Acids for Hotter and Drier Fuel Cell Operating Conditions", *J. Power Sources* **172** (2007), 108-114

102. K.D. Kreuer, M. Schuster, B. Obliers, O. Diat, U. Traub, A. Fuchs, U. Klock, S.J. Paddison, J. Maier, "Short-Side-Chain Proton Conducting Perfluorosulfonic Acid Ionomers: Why they Perform Better in PEM Fuel Cells", *J. Power Sources* **178** (2008), 499-509

103. R. Borup, J. Meyers, B. Pivovar, Y.S. Kim, R. Mukundan, N. Garland, D. Myers, M. Wilson, F. Garzon, D. Wook, P. Zelenay, K. More, K. Stroh, T. Zawodzinski, J. Boncella, J.E. McGrath, M. Inaba, K. Miyatake, M. Hori, K. Ota, Z. Ogumi, S. Miyata, A. Nishikata, Z. Siroma, Y. Uchimoto,

K. Yasuda, K.-i. Kimijima, N. Iwashita, "Scientific Aspects of Polymer Electrolyte Fuel Cell Durability and Degradation", *Chem. Rev.* **107** (2007), 3904-3951

104. A. Ghielmi, P. Vaccarono, C. Troglia, V. Arcella, "Proton Exchange Membranes based on the Short-Side-Chain Perfluorinated Ionomer", *J. Power Sources* **145** (2005), 108-115

105. Q. Li, D. Aili, H.A. Hjuler, J.O. Jensen, "High Temperature Polymer Electrolyte Membrane Fuel Cells", Springer, 2016

106. J.S. Wainright, M.H. Litt, R.F. Savinell, "High-temperature Membranes", in *Handbook of Fuel Cells - Fundamentals, Technology and Applications*, Volume 3, W. Vielstich, H.A. Gasteiger, A. Lamm, John Wiley & Sons, Chichester, 2003, 436-446

107. T.J. Schmidt, J. Baurmeister, "Development Status of High-Temperature PBI-based Membrane Electrode Assemblies", *ECS Trans.* **16** (2008), 2, 263-270

108. D.C. Seel, B.C. Benicewicz, L. Xiao, T.J. Schmidt, "High-Temperature Polybenzimidazole-Based Membranes", in *Handbook of Fuel Cells: Advances in Electrocatalysis, Materials, Diagnostics and Durability, Volume 5*, W. Vielstich, H.A. Gasteiger, H. Yokokawa, John Wiley & Sons, Chichester, United Kingdom, 2009, Chapter 19, 300-312

109. T. Norby, "The Promise of Protonics", *Nature* **410** (2001), 877-878

110. S.M. Haile, D.A. Boysen, C.R.I. Chisholm, R.B. Merle, "Solid Acids as Fuel Cell Electrolytes", *Nature* **410** (2001), 910-913

111. C.R.I. Chisholm, D.A. Boysen, A.B. Papandrew, S. Zecevic, S. Cha, K.A. Sasaki, Á. Varga, K.P. Giapis, S.M. Haile, "From Laboratory Breakthrough to Technological Realization: The Development Path for Solid Acid Fuel Cells", *Electrochem. Soc. Interface* **18** (2009), 53-59

112. D.A. Boysen, S.M. Haile, H. Liu, R.A. Secco, "High-Temperature Behavior of CsH_2PO_4 under Both Ambient and High Pressure Conditions", *Chem. Mater.* **15** (2003), 727-736

113. Y. Jin, Y. Shen, T. Hibino, "Proton Conduction in Metal Pyrophosphates (MP_2O_7) at Intermediate Temperatures", *J. Mater. Chem.* **20** (2010), 6214-6217

114. M. Nagao, T. Kamiya, P. Heo, A. Tomita, T. Hibino, M. Sano, "Proton Conduction in In^{3+}-Doped SnP_2O_7 at Intermediate Temperatures", *J. Electrochem. Soc.* **153** (2006), 8, A1604-A1609

115. X. Chen, C. Wang, E.A. Payzant, C. Xia, D. Chu, "An Oxide Ion and Proton Co-Ion Conducting $Sn_{0.9}In_{0.1}P_2O_7$ Electrolyte for Intermediate-Temperature Fuel Cells", *J. Electrochem. Soc.* **155** (2008), 12, B1264-B1269

116. L. Gubler, S. Alkan-Gürsel, F. Hajbolouri, D. Kramer, N. Beck, A. Reiner, B. Steiger, G.G. Scherer, A. Wokaun, B. Rajesh, K.R. Thampi, "Materials for Polymer Electrolyte Fuel Cells", *Chimia* **58** (2004), 12, 826-836

117. T.A. Zawodzinski, M. Neeman, L.O. Sillerud, S. Gottesfeld, "Determination of Water Diffusion Coefficients in Perfluorosulfonic Ionomeric Membranes", *J. Phys. Chem.* **95** (1991), 6040-6044

118. K.-D. Kreuer, S.J. Paddison, E. Spohr, M. Schuster, "Transport in Proton Conductors for Fuel-Cell Applications: Simulations, Elementary Reactions, and Phenomenology", *Chem. Rev.* **104** (2004), 4637-4678

119. P. Choi, N.H. Jalani, R. Datta, "Thermodynamics and Proton Transport in Nafion I. Membrane Swelling, Sorption, and Ion-Exchange Equilibrium", *J. Electrochem. Soc.* **152** (2005), 3, E84-E89

120. M.A. Yandrasits, S.J. Hamrock, "Membranes for PEM Fuel Cells", in *Fuel Cell Chemistry and Operation*, ACS Symposium Series, Volume 1040, A.M. Herring, T.A. Zawodzinski Jr., S.J. Hamrock, American Chemical Society, Washington, DC, 2010, 15-29

121. V.O. Mittal, H.R. Kunz, J.M. Fenton, "Membrane Degradation Mechanisms in PEMFCs", *J. Electrochem. Soc.* **154** (2007), 7, B652-B656

122. C. Chen, T.F. Fuller, "Modeling of H_2O_2 Formation in PEMFCs", *Electrochim. Acta* **54** (2009), 3984-3995

123. S. Kreitmeier, G.A. Schuler, A. Wokaun, F.N. Büchi, "Investigation of Membrane Degradation in Polymer Electrolyte Fuel Cells using Local Gas Permeation Analysis", *J. Power Sources* **212** (2012), 139-147

124. A. Kusoglu, A.M. Karlsson, M.H. Santare, S. Cleghorn, W.B. Johnson, "Mechanical Response of Fuel Cell Membranes Subjected to a Hygro-Thermal Cycle", *J. Power Sources* **161** (2006), 987-996

125. Y. Tang, A.M. Karlsson, M.H. Santare, M. Gilbert, S. Cleghorn, W.B. Johnson, "An Experimental Investigation of Humidity and Temperature Effects on the Mechanical Properties of Perlfuorosulfonic Acid Membrane", *Mater. Sci. Eng. A* **425** (2006), 297-304

126. P.W. Majsztrik, A.B. Bocarsly, J.B. Benziger, "Viscoelastic Response of Nafion. Effects of Temperature and Hydration on Tensile Creep", *Macromolecules* **41** (2008), 9849-9862

127. L. Gubler, G.G. Scherer, "Trends for Fuel Cell Membrane Development", *Desalination* **50** (2009), 1037-1037

128. B. Smitha, S. Sridhar, A.A. Khan, "Solid Polymer Electrolyte Membranes for Fuel Cells - A Review", *J. Membr. Sci.* **259** (2005), 10-26

129. M. Doyle, G. Rajendran, "Perfluorinated Membranes", in *Handbook of Fuel Cells - Fundamentals, Technology and Applications*, Volume 3, Chapter 30, W. Vielstich, H.A. Gasteiger, A. Lamm, John Wiley & Sons, Chichester, 2003, 351-395

130. G. Maier, J. Meier-Haack, "Sulfonated Aromatic Polymers for Fuel Cell Membranes", *Adv. Polym. Sci.* **216** (2008), 1-62

131. M. Gross, G. Maier, T. Fuller, S. MacKinnon, C. Gittleman, "Design rules for the improvement of the performance of hydrocarbon-based membranes for proton exchange membrane fuel cells (PEMFC)", in *Handbook of Fuel Cells*, Volume 5, W. Vielstich, H.A. Gasteiger, H. Yokokawa, Wiley-VCH, Chichester, United Kingdom, 2009, 283-299

132. M.A. Hickner, B.S. Pivovar, "The Chemical and Structural Nature of Proton Exchange Membrane Fuel Cell Properties", *Fuel Cells* **5** (2005), 2, 213-229

133. K.D. Kreuer, "On the Development of Proton Conducting Polymer Membranes for Hydrogen and Methanol Fuel Cells", *J. Membr. Sci.* **185** (2001), 29-39

134. Y. Li, A. Roy, A.S. Badami, M. Hill, J. Yang, S. Dunn, J.E. McGrath, "Synthesis and Characterization of Partially Fluorinated Hydrophobic–Hydrophilic Multiblock Copolymers Containing Sulfonate Groups for Proton Exchange Membrane", *J. Power Sources* **172** (2007), 30-38

135. S. Takamuku, P. Jannasch, "Fully Aromatic Block Copolymers for Fuel Cell Membranes with Densely Sulfonated Nanophase Domains", *Macromol. Rapid Commun.* **32** (2010), 474-480

136. Y.A. Elabd, M.A. Hickner, "Block Copolymers for Fuel Cells", *Marcomolecules* **44** (2011), 1-11

137. M.L. Einsla, Y.S. Kim, M. Hawley, H.-S. Lee, J.E. McGrath, B. Liu, M.D. Guiver, B.S. Pivovar, "Toward Improved Conductivity of Sulfonated Aromatic Proton Exchange Membranes at Low Relative Humidity", *Chem. Mater.* **20** (2008), 5636-5642

138. H. Hou, M.L. Di Vona, P. Knauth, "Durability of Sulfonated Aromatic Polymers for Proton-Exchange-Membrane Fuel Cells", *ChemSusChem* **4** (2011), 1526-1536

139. A. Kabasawa, J. Saito, H. Yano, K. Miyatake, H. Uchida, M. Watanabe, "Durability of a Novel Sulfonated Polyimide Membrane in Polymer Electrolyte Fuel Cell Operation", *Electrochim. Acta* **54** (2009), 1076-1082

140. B. Bae, K. Miyatake, M. Uchida, H. Uchida, Y. Sakiyama, T. Okanishi, M. Watanabe, "Sulfonated Poly(Arylene Ether Sulfone Ketone) Multiblock Copolymers with Highly Sulfonated Blocks. Long-Term Fuel Cell Operation and Post-Test Analysis", *ACS Appl. Mater. Interfaces* **3** (2011), 2786-2793

141. V.A. Sethuraman, J.W. Weidner, A.T. Haug, L.V. Protsailo, "Durability of Perfluorosulfonic Acid and Hydrocarbon Membranes: Effect of Humidity and Temperature", *J. Electrochem. Soc.* **155** (2008), 2, B119-B124

142. J. Goldbach, S. Gaboury, R. Umpleby, J. Parvole, D. Mountz, "Blend of Ionic (Co)polymer Resins and Matrix (Co)polymers ", *US Patent 7,396,880*, Arkema Inc., 2008

143. T. Zhang, W. He, J. Goldbach, D. Mountz, J. Yi, "In Situ Proton Exchange Membrane Fuel Cell Durability of Poly(vinylidene fluoride) / Polyelectrolyte Blend Arkema M43 Membrane", *J. Power Sources* **196** (2011), 1687-1693

144. L. Chikh, V. Delhorbe, O. Fichet, "(Semi-)Interpenetrating Polymer Networks as Fuel Cell Membranes", *J. Membr. Sci.* **368** (2011), 1-17

145. J. Qiao, T. Hamaya, T. Okada, "Chemically Modified Poly(vinyl alcohol) - Poly(2-acrylamido-2-methy-1-propanesulfonic acid) as a Novel Proton-Conducting Fuel Cell Membrane", *Chem. Mater.* **17** (2005), 2413-2421

146. J. Qiao, T. Okada, H. Ono, "High Molecular Weight PVA-Modified PVA/PAMPS Proton-Conducting Membranes with Increased Stability and their Application in DMFCs", *Solid State Ionics* **180** (2009), 1318-1323

147. A. Bhattacharya, B.N. Misra, "Grafting: A Versatile Means to Modify Polymers. Techniques, Factors and Applications", *Prog. Polym. Sci* **29** (2004), 767-814

148. K.E. Ayers, E.B. Anderson, C.B. Capuano, B.D. Carter, L.T. Dalton, G. Hanlon, J. Manco, M. Niedzwiecki, "Research Advances Towards Low Cost, High Efficiency PEM Electrolysis", *ECS Trans.* **33** (2010), 1, 3-15

149. K.A. Lewinski, D.F.v.d. Vliet, S.M. Luopa, "NSTF Advances for PEM Electrolysis – The Effect of Alloying on Activity of NSTF Electrolyzer Catalysts and Performance of NSTF Based PEM Electrolyzers.", *ECS Trans.* **69** (2015), 17, 893-917

150. M. Schalenbach, T. Hoefner, P. Paciok, M. Carmo, W. Lueke, D. Stolten, "Gas Permeation through Nafion. Part 1: Measurements", *J. Phys. Chem. C* **119** (2015), 45, 25145-25155

151. B. Dunn, H. Kamath, J.-M. Tarascon, "Electrical Energy Storage for the Grid: A Battery of Choices", *Science* **334** (2011), 928-935

152. M. Skyllas-Kazacos, M.H. Chakrabarti, S.A. Hajimolana, F.S. Mjalli, M. Saleem, "Progress in Flow Battery Research and Development", *J. Electrochem. Soc.* **158** (2011), 8, R55-R79

153. V. Viswanathan, A. Crawford, D. Stephenson, S. Kim, W. Wang, B. Li, G. Coffey, E. Thomsen, G. Graff, P. Balducci, M. Kintner-Meyer, V. Sprenkle, "Cost and performance model for redox flow batteries", *J. Power Sources* **247** (2014), 1040-1051

154. A.Z. Weber, M.M. Mench, J.P. Meyers, P.N. Ross, J.T. Gostick, Q. Liu, "Redox Flow Batteries: A Review", *J. Appl. Electrochem.* **41** (2011), 1137-1164

155. E.J. Berg, C. Villevieille, D. Streich, S. Trabesinger, P. Novák, "Rechargeable Batteries: Grasping for the Limits of Chemistry", *J. Electrochem. Soc.* **162** (2015), 14, A2468-A2475

156. P.G. Bruce, S.A. Freunberger, L.J. Hardwick, J.-M. Tarascon, "Li-O_2 and Li-S Batteries with High Energy Storage", *Nature Materials* **11** (2012), 19-29

157. S. Urbonaite, T. Poux, P. Novák, "Progress Towards Commercially Viable Li–S Battery Cells", *Adv. Energy Mater.* **5** (2015), 16, 1500118

158. A. Albert, A.O. Barnett, M.S. Thomassen, T.J. Schmidt, L. Gubler, "Radiation-Grafted Polymer Electrolyte Membranes for Water Electrolysis Cells: Evaluation of Key Membrane Properties", *ACS Appl. Mater. Interfaces* **7** (2015), 40, 22203-22212

159. A. Albert, T.J. Schmidt, L. Gubler, Paul Scherrer Institut, unpublished work.

160. F. Oldenburg, L. Bonorand, L. Gubler, Paul Scherrer Institut, unpublished work.

161. M.G. Marino, J.P. Melchior, A. Wohlfarth, K.D. Kreuer, "Hydroxide, Halide and Water Transport in a model Anion Exchange Membrane", *J. Membr. Sci.* **464** (2014), 61-71

162. L. Gubler, O. Nibel, L. Bonorand, "Electrolyte membrane with Selective Ion Transport Properties and a Redox Flow Battery comprising an Electrolyte Membrane", *European Patent Application EP15154151*, Paul Scherrer Institut, 2015

163. O. Nibel, T.J. Schmidt, L. Gubler, Paul Scherrer Institut, unpublished work.

164. J. Conder, S. Urbonaite, D. Streich, P. Novák, L. Gubler, "Taming the polysulphide shuttle in Li–S batteries by plasma-induced asymmetric functionalisation of the separator", *RSC Adv.* **5** (2015), 97, 79654-79660

165. J.M. Conder, L. Gubler, P. Novák, S. Trabesinger, "Polysulfides Confined ! New Design of the Separator for Enhanced Lithium Sulfur Cell Performance", *PSI Electrochemistry Laboratory – Annual Report 2015* (DOI: 10.3929/ethz-a-007047464)

166. A. Forner-Cuenca, J. Biesdorf, L. Gubler, P.M. Kristiansen, T.J. Schmidt, P. Boillat, "Engineered Water Highways in Fuel Cells: Radiation Grafting of Gas Diffusion Layers", *Adv. Mater.* **27** (2015), 6317-6322

167. R. Devanathan, "Recent Developments in Proton Exchange Membranes for Fuel Cells", *Energy Environ. Sci.* **1** (2008), 101-119

168. P. Trogadas, J. Parrondo, V. Ramani, "Degradation Mitigation in Polymer Electrolyte Membranes Using Cerium Oxide as a Regenerative Free-Radical Scavenger", *Electrochem. Solid-State Lett.* **11** (2008), 7, B113-B116

169. F.D. Coms, H. Liu, J.E. Owejan, "Mitigation of Perfluorosulfonic Acid Membrane Chemical Degradation Using Cerium and Manganese Ions", *ECS Trans.* **16** (2008), 2, 1735-1747

170. A. Charlesby, *Atomic Radiation and Polymers*, Pergamon Press, Oxford, UK, 1960

171. D.W. Clegg, A.A. Collyer, "Irradiation Effects on Polymers", Elsevier, London and New York, 1991

172. K. Dawes, L.C. Glover, D.A. Vroom, "The Effects of Electron Beam and γ-Irradiation on Polymeric Materials", 2nd edition, in *Physical Properties of Polymers Handbook*, J.E. Mark, Springer Science + Business Media, New York, 2007, 867-887

173. P. Apel, "Tracketching Technique in Membrane Technology", *Radiat. Meas.* **34** (2001), 559–566

174. N. Betz, "Ion Track Grafting", *Nucl. Instr. Meth. Phys. Res. B* **105** (1995), 55-62

175. T. Yamaki, "Quantum-Beam Technology: A Versatile Tool For Developing Polymer Electrolyte Fuel-Cell Membranes", *J. Power Sources* **195** (2010), 5848-5855

176. Z.X. Zhen, "Long Llived Fluoropolymeric Radicals in Irradiated Fluoropolymer Powders at Room Temperature", *Radiat. Phys. Chem.* **35** (1990), 194-198

177. S.J. Zhen, "The Effect of Chain Flexibility and Chain Mobility on Radiation Crosslinking of Polymers", *Radiat. Phys. Chem.* **60** (2001), 445-451

178. A. Bozzi, A. Chapiró, "The Nature of the Initiation Centres for Grafting in Air-Irradiated Perfluoro Polymers", *Eur. Polym. J.* **23** (1987), 3, 255-257

179. A. Bozzi, A. Chapiró, "Synthesis of Perm-Selective Membranes by Grafting Acrylic Acid into Air-Irradiated Teflon-FEP FIlms", *Radiat. Phys. Chem.* **32** (1988), 2, 193-196

180. J.F. Rabek, "Oxidative Degradation of Polymers", in *Degradation of Polymers*, Volume 14, C.H. Bamford, C.F.H. Tipper, Elsevier, Amsterdam a.o., 1975, 425-538

181. A. Chapiró, "Radiation-Induced Grafting", *Radiat. Phys. Chem.* **9** (1977), 1-3, 55-67

182. H.A. Battaerd, G.W. Tregear, *Graft Copolymers*, Interscience Publishers, New York, 1967

183. J.E. Wilson, *Radiation Chemistry of Monomers, Polymers, and Plastics*, Marcel Dekker, New York, 1974

184. A. Heger, *Technologie der Strahlenchemie von Polymeren*, Hanser, München, 1990

185. P.A. Dworjanyn, J.L. Garnett, "Radiation Grafting of Monomers on Plastics and Fibers", in *Radiation Processing of Polymers*, A. Singh, J. Silverman, Hanser, Munich, 1991, 93-120

186. S. Alkan-Gürsel, L. Gubler, B. Gupta, G.G. Scherer, "Radiation Grafted Membranes", *Adv. Polym. Sci.* **215** (2008), 157-218

187. G. Odian, T. Acker, M. Sobel, "Accelerative Effects in Radiation-induced Graft Polymerization", *J. Appl. Polym. Sci* **7** (1963), 245-250

188. G.G. Odian, A. Rossi, E.N. Trachtenberg, "The Accelerating Effect of Methanol on the Gamma Radiation-induced Graft Copolymerization of Styrene to Polyethylene", *J. Polym. Sci.* **42** (1960), 140, 575–578

189. G. Odian, M. Sobel, A. Rossi, R. Klein, "Radiation-Induced Graft Polymerization: The Trommsdorff Effect of Methanol", *J. Polym. Sci.* **55** (1961), 663-673

190. T. Rager, "Pre-Irradiation Grafting of Styrene/Divinylbenzene onto Poly(tetrafluoroethylene-*co*-hexafluoropropylene) from Non-Solvents", *Helv. Chim. Acta* **86** (2003), 1966-1980

191. W. Becker, M. Bothe, G. Schmidt-Naake, "Grafting of Poly(Styrene-*co*-Acrylonitrile) onto Pre-Irradiated FEP and ETFE Films", *Angew. Makromol. Chem.* **273** (1999), 57-62

192. H. Ben youcef, L. Gubler, A. Foelske-Schmitz, G.G. Scherer, "Improvement of Homogeneity and Interfacial Properties of Radiation Grafted Membranes for Fuel Cells using Diisopropenylbenzene Crosslinker", *J. Membr. Sci.* **381** (2011), 102-109

193. J. Ding, C. Chuy, S. Holdcroft, "A Self-Organized Network of Nanochannels Enhances Ion Conductivity through Polymer Films", *Chem. Mater.* **13** (2001), 7, 2231-2233

194. E.M.W. Tsang, Z. Zhang, A.C.C. Yang, Z. Shi, T.J. Peckham, R. Narimani, B.J. Frisken, S. Holdcroft, "Nanostructure, Morphology, and Properties of Fluorous Copolymers Bearing Ionic Grafts", *Macromolecules* **42** (2009), 9467-9480

195. L. Gubler, H. Kuhn, T.J. Schmidt, G.G. Scherer, H.P. Brack, K. Simbeck, "Performance and Durability of Membrane Electrode Assemblies Based on Radiation-Grafted FEP-*g*-Polystyrene Membranes", *Fuel Cells* **4** (2004), 3, 196-207

196. L. Gubler, G.G. Scherer, "Durability of Radiation Grafted Fuel Cell Membranes", in *Polymer Electrolyte Fuel Cell Durability*, M. Inaba, T.J. Schmidt, F.N. Büchi, Springer Science+Business Media, New York, 2009, 133-155

197. L. Gubler, G.G. Scherer, "Radiation-Grafted Proton Conducting Membranes", in *Handbook of Fuel Cells: Advances in Electrocatalysis, Materials, Diagnostics and Durability, Volume 5*, W. Vielstich, H.A. Gasteiger, H. Yokokawa, John Wiley & Sons, Chichester, United Kingdom, 2009, Chapter 20, 313-321

198. S. Nezu, H. Seko, M. Gondo, N. Ito, "High Performance Radiation-Grafted Membranes and Electrodes for Polymer Electrolyte Fuel Cells", *1996 Fuel Cell Seminar*, Orlando, Nov 17 - 20, 1996, 620-623

199. L. Bonorand, personal communication,

200. C. David, "High Energy Degradation of Polymers", in *Degradation of Polymers*, Volume 14, C.H. Bamford, C.F.H. Tipper, Elsevier, Amsterdam a.o., 1975, 175-332

201. A. Chapiró, "Chemical Modifications in Irradiated Polymers", *Nucl. Instrum. Methods Phys. Res., Sect. B* **32** (1988), 111-114

202. R.L. Clough, K.T. Gillen, M. Dole, "Radiation Resistance of Polymers and Composites", in *Irradiation Effects on Polymers*, D.W. Clegg, A.A. Collyer, Elsevier, Barking, Essex, UK, 1991, 79-156

203. S. Hasegawa, S. Takahashi, H. Iwase, S. Koizumi, N. Morishita, K. Sato, T. Narita, M. Ohnuma, Y. Maekawa, "Radiation-induced Graft Polymerization of Functional Monomer into Poly(ether ether ketone) Film and Structure-Property Analysis of the Grafted Membrane", *Polymer* **52** (2011), 98-106

204. A. Oshima, T. Seguchi, Y. Tabata, "ESR Study on Free Radicals Trapped in Crosslinked Polytetrafluoroethylene (PTFE). II Radical Formation and Reactivity", *Radiat. Phys. Chem.* **55** (1999), 61-71

205. A. Oshima, T. Seguchi, Y. Tabata, "ESR Study on Free Radicals Trapped in Crosslinked Polytetrafluoroethylene (PTFE)", *Radiat. Phys. Chem.* **50** (1997), 601

206. A. Oshima, T. Seguchi, Y. Tabata, "Radiation-Induced Free Radicals and their Behaviour in Crosslinked Polytetrafluoroethylene (PTFE)", *Polym. Int.* **48** (1999), 996-1003

207. M.R. Cleland, *Presented at the CERN Accelerator School, Small Accelerator Course*, Zeegse, Netherlands, May 24 – June 2, 2005.

208. R.E. Florin, "Radiation Chemistry of Flurocarbon Polymers", in *Fluoropolymers*, L.A. Wall, Wiley, New York, 1972, 317-380

209. D. Evans, M.A. Crook, "Irradiation of Plastics: Damage and Gas Evolution", *MRS Bulletin* **22** (1997), 4, 36-40

210. T. Seguchi, K. Makuuchi, T. Suwa, N. Tamura, T. Abe, M.J. Takehisa, "Radiation Effects on Poly(vinylidene fluoride). III. Electron Spin Resonance Study on Irradiated Poly(vinylidene fluoride)", *Chem. Soc. Jpn. Chem. Ind. Chem.* **7** (1974), 1309-1315

211. T. Yoshida, R.E. Florin, L.A. Wall, *J. Polym. Sci. Part A* **3** (1965), 1685-1712

212. L.A. Wall, S. Straus, R.E. Florin, *J. Polym. Sci. Part A-1* **4** (1966), 349-365

213. B.J. Lyons, "Radiation Crosslinking of Fluoropolymers - A Review", *Radiat. Phys. Chem.* **45** (1995), 2, 159-174

214. D.J. Carlsson, S. Chmela, J. Lacoste, "On the Structures and Yields of the First Peroxyl Radicals in g-Irradiated Polyolefins", *Macromolecules* **23** (1990), 4934-4938

215. Y. Feng, Z. Ma, "Crosslinking of Wire and Cable Insulation using Electron Accelerators", in *Radiation Processing of Polymers*, A. Singh, J. Silverman, Hanser, 1991, 71-92

216. V.D. McGinnise, in *Encyclopedia of Polymer Science and Engineering*, J.I. Kroschwitz, Wiley, New York, 1986, 418

217. M. Dole, in *Crystalline Olefin Polymers*, R.A.V. Raff, K.W. Doak, Wiley, New York, 1965, 870

218. J.S. Forsythe, D.J.T. Hill, "The Radiation Chemistry of Fluoropolymers", *Prog. Polym. Sci.* **25** (2000), 101-136

219. L.A. Wall, "Factors Influencing the Behavior of Polymers Exposed to High-Energy Radiation", *J. Polym. Sci.* **17** (1955), 141

220. A. Chapiró, "Synthèse des Copolymeres Greffés à partir des Polymères ayant subi l'Action des Radiation Ionisantes. III. Etude Comparée du Greffage sur le Polyéthylène et sur le Polypropylène", *J. Polym. Sci.* **48** (1960), 109-120

221. S. Ebnesajjad, P.R. Khaladkar, *Fluoropolymers Applications in the Chemical Processing Industries*, William Andrew Inc., Norwich, NY, USA, 2004

222. M.M. Nasef, "Fuel Cell Membranes by Radiation-Induced Graft Copolymerization: Current Status, Challenges, and Future Directions", in *Polymer Membranes for Fuel Cells*, S.M.J. Zaidi, T. Matsuura, Springer Science+Business Media, New York, 2009, 87-114

223. N. Grassie, G. Scott, *Polymer Degradation and Stabilization*, Cambridge University Press, 1985

224. E. Giannetti, "Thermal Stability and Bond Dissociation Energy of Fluorinated Polymers: A Critical Evaluation", *J. Fluorine Chem.* **126** (2005), 625-632

225. T.R. Dargaville, D.J.T. Hill, A.K. Whittaker, "An ESR Study of Irradiated Poly(tetrafluoroethylene-co-perfluoropropy-vinyl-ether) (PFA)", *Radiat. Phys. Chem.* **62** (2001), 25-31

226. T. Yamaki, M. Asano, Y. Maekawa, Y. Morita, T. Suwa, J. Chen, N. Tsubokawa, K. Kobayashi, H. Kubota, M. Yoshida, "Radiation Grafting of Styrene into Crosslinked PTFE Films and Subsequent Sulfonation for Fuel Cell Applications", *Radiat. Phys. Chem.* **67** (2003), 403-407

227. T. Yamaki, K. Kobayashi, M. Asano, H. Kubota, M. Maekawa, "Preparation of Proton Exchange Membranes based on Crosslinked Polytetrafluoroethylene for Fuel Cell Applications", *Polymer* **45** (2004), 6569-6573

228. D.P. Carlson, W. Schmiegel, "Fluoropolymers, Organic", in *Ullmann's Encyclopedia of Industrial Chemistry*, W. Gerhartz, VCH, Weinheim, 1988, 393-429

229. N. Walsby, F. Sundholm, T. Kallio, G. Sundholm, "Radiation-Grafted Ion-Exchange Membranes: Influence of the Initial Matrix on the Synthesis and Structure", *J. Polym. Sci. Part A: Polym. Chem.* **39** (2001), 18, 3008-3017

230. J. Chen, M. Asano, Y. Maekawa, M. Yoshida, "Suitability of Some Fluoropolymers used as Base Films for Preparation of Polymer Electrolyte Fuel Cell Membranes", *J. Membr. Sci.* **277** (2006), 1-2, 249-257

231. K. Arai, A. Funaki, S. Phongtamrug, K. Tashiro, "Influence of Alternating Sequential Fraction on the Melting and Glass Transition Temperatures of Ethylene-Tetrafluoroethylene Copolymer", *Polymer* **51** (2010), 4831-4835

232. S. Ebnesajjad, "Introduction to Fluoropolymers", in *Applied Plastics Engineering Handbook: Processing and Materials*, M. Kutz, Elsevier, 2011, Chapter 4, 49-60

233. J. Bandrup, E.H. Immergut, *Polymer Handbook*, 4th ed., Wiley, New York, 1999

234. S. Alkan-Gürsel, J. Schneider, H. Ben youcef, A. Wokaun, G.G. Scherer, "Thermal Properties of Proton-Conducting Radiation-Grafted Membranes", *J. Appl. Polym. Sci.* **108** (2008), 3577-3585

235. H.P. Brack, F.N. Büchi, J. Huslage, M. Rota, G.G. Scherer, "Development of Radiation-Grafted Membranes for Fuel Cell Applications Based on Poly(ethylene-*alt*-tetrafluorethylene)", *ACS Symposium Series 744*, I. Pinnau, B.D. Freeman, American Chemical Society, 2000, 174-188

236. Y. Leterrier, L. Gubler, unpublished results

237. H.P. Brack, H.G. Bührer, L. Bonorand, G.G. Scherer, "Grafting of Pre-Irradiated Poly(ethylene-*alt*-tetrafluoroethylene) Films with Styrene: Influence of Base Polymer Film Properties and Processing Parameters", *J. Mater. Chem.* **10** (2000), 1795-1803

238. R.E. Florin, L.A. Wall, *J. Res. Natl. Bur. Stand. - A* **65** (1961), 375-387

239. S. Mitov, G. Hübner, H.-P. Brack, G. Scherer, E. Roduner, "*In Situ* Electron Spin Resonance Study of Styrene Grafting of Electron Irradiated Fluoropolymer Films for Fuel Cell Membranes", *J. Polym. Sci. Part B: Polym. Phys.* **44** (2006), 3323-3336

240. A. Kusoglu, A.M. Karlsson, M.H. Santare, S. Cleghorn, W.B. Johnson, "Mechanical Behavior of Fuel Cell Membranes under Humidity Cycles and Effect of Swelling Anisotropy on the Fatigue Stresses", *J. Power Sources* **170** (2007), 345-358

241. H. Ben youcef, S. Alkan-Gürsel, A. Buisson, L. Gubler, A. Wokaun, G.G. Scherer, "Influence of Radiation-Induced Grafting Process on Mechanical Properties of ETFE Based Membranes for Fuel Cells", *Fuel Cells* **10** (2010), 3, 401-410

242. S. Alkan-Gürsel, Z. Yang, B. Choudhury, M.G. Roelofs, G.G. Scherer, "Radiation Grafted Membranes using a Trifluorostyrene Derivative", *J. Electrochem. Soc.* **153** (2006), 10, A1964-A1970

243. M. Kawakado, T. Morimoto, N. Hasegawa, A. Kamiya, C. Yamada, M. Kato, M. Akakabe, "Highly Proton-Conductive Electrolyte", *JP2001302721A2*, Toyota Central Research & Development Laboratory Inc., Aisin Seiki Co. Ltd., 2001

244. J. Chen, M. Asano, T. Yamaki, M. Yoshida, "Improvement of Chemical Stability of Polymer Electrolyte Fuel Cell Membranes by Grafting of New Substituted Styrene Monomers into ETFE Films", *J. Mater. Sci.* **41** (2006), 1289-1292

245. J. Chen, M. Asano, T. Yamaki, M. Yoshida, "Effect of Crosslinkers on the Preparation and Properties of ETFE-Based Radiation-Grafted Polymer Electrolyte Membranes", *J. Appl. Polym. Sci.* **100** (2006), 4565-4574

246. M.J. Larsen, Y. Ma, P.B. Lund, E.M. Skou, "Crosslinking and Alkyl Substitution in Nano-Structured Grafted Fluoropolymer for use as Proton-Exchange Membranes in Fuel Cells", *Appl. Phys. A* **96** (2009), 569–573

247. J. Chen, M. Asano, T. Yamaki, M. Yoshida, "Preparation and Characterization of Chemically Stable Polymer Electrolyte Membranes by Radiation-Induced Graft Copolymerization of Four Monomers into ETFE Films", *J. Membr. Sci.* **269** (2006), 194-204

248. B.N. Kim, D.H. Lee, D.H. Han, "Characteristics of Fuel Cell Membranes Prepared by EB Radiation Grafting onto FEP with Styrene Derivatives, Styrene and 2-Methylstyrene", *J. Electrochem. Soc.* **155** (2008), 7, B680-B685

249. J. Chen, M. Asano, Y. Maekawa, M. Yoshida, "Polymer Electrolyte Hybrid Membranes Prepared by Radiation Grafting of p-Styryltrimethoxysilane into Poly(Ethylene-*co*-Tetrafluoroethylene) Films", *J. Membr. Sci.* **296** (2007), 77-82

250. J. Chen, M. Asano, Y. Maekawa, M. Yoshida, "Chemically Stable Hybrid Polymer Electrolyte Membranes Prepared by Radiation Grafting, Sulfonation, and Silane-Crosslinking Techniques", *J. Polym. Sci. Part A: Polym. Chem.* **46** (2008), 5559-5567

251. R.A. Assink, C. Arnold, R.P. Hollandsworth, "Preparation of Oxidatively Stable Cation-Exchange Membranes by the Elimination of Tertiary Hydrogen", *J. Membr. Sci.* **56** (1991), 143-151

252. J. Fleischhauer, G. Schmidt-Naake, D. Scheller, "Untersuchungen zum Reaktionsverhalten beim Vorliegen von Depolymerisationsreaktionen. Untersuchung von Copolymerisationen des α-Methylstyrols", *Angew. Makromol. Chem.* **243** (1996), 11-37

253. J.M.G. Cowie, *Polymers: Chemistry and Physics of Modern Materials*, Second Edition, Chapman & Hall, 1991

254. S.C. Pilcher, W.T. Ford, "High Molecular Weight Poly(α-methylstyrene) Formed by Free Radical Polymerization in Emulsions", *J. Polym. Sci. Part A: Polym. Chem.* **39** (2001), 525-529

255. L. Li, F. Muto, T. Miura, A. Oshima, M. Washio, S. Ikeda, M. Iida, Y. Tabata, C. Matsuura, Y. Katsumura, "Improving the Properties of the Proton Exchange Membranes by Introducing α-Methylstyrene in the Pre-Irradiation Induced Graft Polymerization", *Eur. Polym. J.* (2006), 1222-1228

256. W. Becker, G. Schmidt-Naake, "Eigenschaften polymerer Protonenaustauschermembranen aus strahlungsinduzierter Pfropfpolymerisation", *Chem. Eng. Technol.* **72** (2000), 12, 1541-1545

257. W. Becker, G. Schmidt-Naake, "Properties of Polymer Exchange Membranes from Irradiation Introduced Graft Polymerization", *Chem. Eng. Technol.* **24** (2001), 11, 1128-1132

258. L. Gubler, M. Slaski, A. Wokaun, G.G. Scherer, "Advanced Monomer Combinations for Radiation Grafted Fuel Cell Membranes", *Electrochem. Commun.* **8** (2006), 1215-1219

259. L. Gubler, M. Slaski, G.G. Scherer, "A method for preparing a radiation grafted fuel cell membrane with enhanced chemical stability and a membrane electrode assembly", *WO2006084591*, Paul Scherrer Institut, 2005

260. K. Jetsrisuparb, H. Ben youcef, A. Wokaun, L. Gubler, "Radiation Grafted Membranes for Fuel Cells containing Styrene Sulfonic Acid and Nitrile Comonomers", *J. Membr. Sci.* **450** (2014), 28-37

261. Z. Zhang, K. Jetsrisuparb, A. Wokaun, L. Gubler, "Study of Nitrile-Containing Proton Exchange Membranes Prepared by Radiation Grafting: Performance and Degradation in the Polymer Electrolyte Fuel Cell", *J. Power Sources* **243** (2013), 306-316

262. L. Gubler, M. Slaski, F. Wallasch, A. Wokaun, G.G. Scherer, "Radiation Grafted Fuel Cell Membranes based on Co-Grafting of α-Methylstyrene and Methacrylonitrile into a Fluoropolymer Base Film", *J. Membr. Sci.* **339** (2009), 68-77

263. L. Gubler, L. Bonorand, J. Thut, G.G. Scherer, "Durability of Radiation Grafted Membranes under Dynamic Operating Fuel Cell Conditions in Comparison to Nafion 212 and Nafion XL-100 Membranes", *PSI Electrochemistry Laboratory – Annual Report 2011* (DOI: 10.3929/ethz-a-007047464) (2012), 17-18

264. S. Shkolnik, D. Behar, "Radiation-Induced Grafting of Sulfonates on Polyethylene", *J. Appl. Polym. Sci.* **27** (1982), 2189-2196

265. M.M. Nasef, H. Saidi, K. Zaman, M. Dahlan, "Acid-Synergized Grafting of Sodium Styrene Sulfonate onto Electron Beam Irradiated-Poly(vinylidene fluoride) Films for Preparation of Fuel Cell Membranes", *J. Appl. Polym. Sci* **118** (2010), 2801-2809

266. D. Li, J. Chen, M. Zhai, M. Asano, Y. Maekawa, H. Oku, M. Yoshida, "Hydrocarbon Proton-Conductive Membranes Prepared by Radiation-Grafting of Styrenesulfonate onto Aromatic Polyamide Films", *Nucl. Instr. Meth. Phys. Res. B* **267** (2009), 103-107

267. M.M. Nasef, H. Saidi, K.Z.M. Dahlan, "Single-Step Radiation Induced Grafting for Preparation of Proton Exchange Membranes for Fuel Cell", *J. Membr. Sci.* **339** (2009), 115-119

268. J. Chen, M. Asano, Y. Maekawa, M. Yoshida, "Fuel Cell Performance of Polyetheretherketone-Based Polymer Electrolyte Membranes Prepared by a Two-Step Grafting Method", *J. Membr. Sci.* **319** (2008), 1-4

269. F.N. Büchi, B. Gupta, O. Haas, G.G. Scherer, "Study of Radiation-Grafted FEP-*g*-Polystyrene Membranes as Polymer Electrolytes in Fuel Cells", *Electrochim. Acta* **40** (1995), 3, 345-353

270. M.M. Nasef, H. Saidi, "Preparation of Crosslinked Cation Exchange Membranes by Radiation Grafting of Styrene/Divinylbenzene Mixtures onto PFA Films", *J. Membr. Sci.* **216** (2003), 27-38

271. L. Gubler, H. Ben youcef, S. Alkan-Gürsel, A. Wokaun, G.G. Scherer, "Crosslinker Effect in ETFE Based Radiation Grafted Proton Conducting Membranes. I. Properties and Fuel Cell Performance Characteristics", *J. Electrochem. Soc.* **155** (2008), 9, B921-B928

272. W. Becker, G. Schmidt-Naake, "Proton Exchange Membranes by Irradiation Induced Grafting of Styrene Onto FEP and ETFE: Influences of the Crosslinker N,N,-Methylene-bis-acrylamide", *Chem. Eng. Technol.* **25** (2002), 4, 373-377

273. T. Lehtinen, G. Sundholm, F. Sundholm, "Effect of Crosslinking on the Physicochemical Properties of Proton Conducting PVDF-g-PSSA Membranes", *J. Appl. Electrochem.* **29** (1999), 677-683

274. T. Yamaki, J. Tsukada, M. Asano, R. Katakai, M. Yoshida, "Preparation of Highly Stable Ion Exchange Membranes by Radiation-Induced Graft Copolymerization of Styrene and Bis(Vinyl Phenyl)Ethane into Crosslinked Polytetrafluoroethylene Films", *J. Fuel Cell Sci. Technol.* **4** (2007), 56-64

275. B. Gupta, F.N. Büchi, G.G. Scherer, "Cation Exchange Membranes by Pre-Irradiation Grafting of Styrene into FEP Films. I. Influence of Synthesis Conditions", *J. Polym. Sci., Polym. Chem.* **32** (1994), 1931-1938

276. L. Steuernagel, S. Reich, D.E. Kaufmann, A. Wokaun, G.G. Scherer, H.P. Brack, "Influence of Nitrogen-Containing Additives on the Radiation-Grafting Process", *PSI Scientific Report / Volume V - General Energy*, ISSN 1423-7342 (2002), 79-80

277. S.-H. Choi, Y.C. Nho, "Electrochemical Properties of Polyethylene Membrane Modified with Sulfonic and Phosphonic Acid Groups", *Korean J. Chem. Eng.* **16** (1999), 6, 725-730

278. C. Schmidt, T. Glück, G. Schmidt-Naake, "Protonenaustauschermembranen durch strahlungsinduzierte Pfropfpolymerisation von Glycidylmethacrylat auf ETFE - Modifizierung mit Butylacrylat und Acrylnitril", *Chem. Ing. Tech.* **79** (2007), 1-2, 137-145

279. Y. Buchmüller, A. Wokaun, L. Gubler, "Fuel Cell Membranes based on Grafted and Post-sulfonated Glycidyl Methacrylate (GMA)", *Fuel Cells* **13** (2013), 6, 1177-1185

280. M. Pacheco, G. Schmidt-Naake, "Protonenaustauschmembranen durch strahlungsinduzierte Pfropfpolymerisation von Polyhydroxyethylmethacrylat aus ETFE- und PP-Folien für den Einsatz in Brennstoffzellen", *Chem. Eng. Technol.* **76** (2004), 1-2, 122-126

281. M. Patri, V.R. Hande, S. Phadnis, B. Somaiah, S. Roychoudhuri, P.C. Deb, "Synthesis and Characterization of SPE Membrane based on Sulfonated FEP-g-Acrylic Acid by Radiation Induced Graft Copolymerization for PEM Fuel Cell", *Polym. Adv. Technol.* **15** (2004), 270-274

282. J. Chen, M. Asano, T. Yamaki, M. Yoshida, "Preparation of Sulfonated Crosslinked PTFE-*graft*-poly(alkyl vinyl ether) Membranes for Polymer Electrolyte Membrane Fuel Cells by Radiation Processing", *J. Membr. Sci.* **256** (2005), 38-45

283. S. Takahashi, H. Okonogi, T. Hagiwara, Y. Maekawa, "Preparation of Polymer Electrolyte Membranes Consisting of Alkyl Sulfonic Acid for a Fuel Cell using Radiation Grafting and Subsequent Substitution / Elimination Reactions", *J. Membr. Sci.* **324** (2008), 173-180

284. T.T. Hanh, S. Takahashi, J. Chen, S.-i. Sawada, Y. Maekawa, "Polymer Electrolyte Membranes Having Sulfoalkyl Grafts into ETFE Film prepared by Radiation-induced Copolymerization of Methyl Acrylate and Methyl Methacrylate", *J. Appl. Polym. Sci* **114** (2009), 231-237

285. K. Enomoto, S. Takahashi, R. Rohani, Y. Maekawa, "Synthesis of Copolymer Grafts Containing Sulfoakyl and Hydrophilic Groups in Polymer Electrolyte Membranes", *J. Membr. Sci.* **415-416** (2012), 36-41

286. Y. Maekawa, personal communication, 2012

287. H. Ben youcef, L. Gubler, S. Alkan-Gürsel, D. Henkensmeier, A. Wokaun, G.G. Scherer, "Novel ETFE Based Radiation Grafted Poly(Styrene Sulfonic Acid-*co*-Methacrylonitrile) Proton Conducting Membranes with Increased Stability", *Electrochem. Comm.* **11** (2009), 941-944

288. K. Jetsrisuparb, S. Balog, C. Bas, L. Perrin, A. Wokaun, L. Gubler, "Proton Conducting Membranes Prepared by Radiation Grafting of Styrene and Various Co-monomers", *Eur. Polym. J.* **53** (2014), 75-89

289. C. Schmidt, G. Schmidt-Naake, "Proton Conducting Membranes Obtained by Doping Radiation-Grafted Basic Membrane Matrices with Phosphoric Acid", *Marcomol. Mater. Eng.* **291** (2007), 1164-1175

290. G. Schmidt-Naake, "Polymer-Säure-Komposite auf Basis strahlungsinduzierter Pfropfpolymersation für Hochtemperatur-PEM-Brennstoffzellen", *Chem. Ing. Tech.* **81** (2009), 5, 599-609

291. C. Schmidt, G. Schmidt-Naake, "Fe^{2+} Catalyzed Synthesis of Radiation Grafted Functional Membranes and Application in Fuel Cells and Ion Recovery", *Macromol. Symp.* **259** (2007), 181-187

292. L.I. Şanlı, S. Alkan-Gürsel, "Synthesis and Characterization of Novel Graft Copolymers by Radiation-Induced Grafting", *J. Appl. Polym. Sci* **120** (2011), 2313-2323

293. C. Schmidt, G. Schmidt-Naake, "Phosphorsäuredotierte Protonenleiter auf Basis von aminierten Membranen aus ETFE-graft-poly(glycidylmethacralyat)-Derivaten", *Chem. Ing. Tech.* **80** (2008), 3, 317-325

294. G. Schmidt-Naake, M. Böhme, A. Cabrera, "Synthesis of Proton Exchange Membranes with Pendent Phosphonic Acid Groups by Irradiation Grafting of VBC", *Chem. Eng. Technol.* **28** (2005), 6, 720-724

295. H. Herman, R.C.T. Slade, J.R. Varcoe, "The Radiation-Grafting of Vinylbenzyl Chloride onto Poly(Hexafluoropropylene-co-tetrafluoroethylene) Films with Subsequent Conversion to Alkaline Anion-Exchange Membranes: Optimisation of the Experimental Conditions and Characterisation", *J. Membr. Sci.* **218** (2003), 147-164

296. T.N. Danks, R.C.T. Slade, J.R. Varcoe, "Alkaline Anion-Exchange Radiation-Grafted Membranes for Possible Electrochemical Application in Fuel Cells", *J. Mater. Chem.* **13** (2003), 712-721

297. R.C.T. Slade, J.R. Varcoe, "Investigations of Conductivity in FEP-Based Radiation-Grafted Alkaline Anion-Exchange Membranes", *Solid State Ionics* **176** (2005), 585-597

298. J.R. Varcoe, R.C.T. Slade, E.L.H. Yee, S.D. Poynton, D.J. Driscoll, D.C. Apperley, "Poly(ethylene-*co*-tetrafluoroethylene)-Derived Radiation-Grafted Anion-Exchange membrane with Properties Specifically Tailored for Application in Metal-Cation-Free Alkaline Polymer Electrolyte Fuel Cells", *Chem. Mater.* **19** (2007), 2686-2693

299. S.D. Poynton, J.P. Kizewski, R.C.T. Slade, J.R. Varcoe, "Novel Electrolyte Membranes and Non-Pt Catalysts for Low Temperature Fuel Cells", *Solid State Ionics* **181** (2010), 219-222

300. J.R. Varcoe, R.C.T. Slade, E.L.H. Yee, "An Alkaline Polymer Electrochemical Interface: A Breakthrough in Application of Alkaline Anion-Exchange Membranes in Fuel Cells", *Chem. Commun.* (2006), 1428-1429

301. O.I. Deavin, S. Murphy, A.L. Ong, S.D. Poynton, R. Zeng, H. Herman, J.R. Varcoe, "Anion-Exchange Membranes for Alkaline Polymer Electrolyte Fuel Cells: Comparison of Pendent Benzyltrimethylammonium- and Benzylmethylimidazolium-Head-Groups", *Energy Environ. Sci.* **5** (2012), 8584

302. B.-S. Ko, J.-Y. Sohn, J. Shin, "Radiation-Induced Synthesis of Solid Alkaline Exchange Membranes with Quaternized 1,4-diazobicyclo[2,2,2] Octane Pendant Groups for Fuel Cell Application", *Polymer* **53** (2012), 4652-4661

303. K. Yoshimura, H. Koshikawa, T. Yamaki, Y. Maekawa, K. Yamamoto, H. Shishitani, K. Asazawa, S. Yamaguchi, H. Tanaka, "Alkaline Durable Anion Exchange Membranes Based on Graft-type Fluoropolymer Films for Hydrazine Hydrate Fuel Cell", *ECS Trans.* **50** (2012), 2, 2075-2081

304. O.M.M. Page, S.D. Poynton, S. Murphy, A.L. Ong, D.M. Hillman, C.A. Hancock, M.G. Hale, D.C. Apperley, J.R. Varcoe, "The alkali stability of radiation-grafted anion-exchange membranes containing pendent 1-benzyl-2,3-dimethylimidazolium head-groups", *RSC Advances* **3** (2013), 2, 579-587

305. K. Yoshimura, H. Koshikawa, T. Yamaki, H. Shishitani, K. Yamamoto, S. Yamaguchi, H. Tanaka, Y. Maekawa, "Imidazolium Cation Based Anion-Conducting Electrolyte Membranes Prepared by Radiation Induced Grafting for Direct Hydrazine Hydrate Fuel Cells", *J. Electrochem. Soc.* **161** (2014), 9, F889-F893

306. J.R. Varcoe, R.C.T. Slade, "An Electron-Beam-Grafted ETFE Alkaline Anion-Exchange Membrane in Metal-Cation-Free Solid-State Alkaline Fuel Cells", *Electrochem. Commun.* **8** (2006), 839-843

307. H. Sarode, M.A. Vandiver, A.M. Maes, B. Caire, J.L. Horan, Y. Yang, Y. Li, G.E. Lindberg, J.F. Dama, C. Knight, R. Jorn, M.E. Lenz, R. Kaspar, S. Gu, B. Zhang, S. Seifert, T.-h. Tsai, W. Zhang, E.B. Coughlin, D.M. Knauss, Y. Yan, G.A. Voth, T.A. Witten, M.W. Liberatore, A.M. Herring, "Designing Alkaline Exchange Membranes from Scratch", *ECS Trans.* **41** (2011), 1, 1761-1774

308. M. Mamlouk, X. Wang, K. Scott, J.A. Horsfall, C. Williams, "Characterization and Application of Anion Exchange Polymer Membranes with Non-Platinum Group Metals for Fuel Cells", *P. I. Mech. Eng. A - J. Pow.* **225** (2011), 152-160

309. M. Mamlouk, S.M.S. Kumar, P. Gouerec, K. Scott, "Electrochemical and Fuel Cell Evaluation of Co based Catalyst for Oxygen Reduction in Anion Exchange Polymer Membrane Fuel Cells", *J. Power Sources* **196** (2011), 7594-7600

310. M. Mamlouk, J.A. Horsfall, C. Williams, K. Scott, "Radiation grafted membranes for superior anion exchange polymer membrane fuel cells performance", *Int. J. Hydrogen Energy* **37** (2012), 16, 11912-11920

311. B. Gupta, F.N. Büchi, G.G. Scherer, A. Chapiró, "Materials Research Aspects of Organic Solid Proton Conductors", *Solid State Ionics* **61** (1993), 213-218

312. L. Gubler, G.G. Scherer, "A Proton-conducting Polymer Membrane as Solid Electrolyte - Function and Required Properties", *Adv. Polym. Sci.* **215** (2008), 1-14

313. L. Gubler, S. Alkan-Gürsel, H. Ben youcef, F. Wallasch, A. Wokaun, "Recent Advances in Radiation Grafted Fuel Cell Membranes", *Fundamentals and Developments of Fuel Cell Conference (FDFC)*, Nancy, France, Dec 10-12, 2008

314. H. Galina, J.B. Lechowicz, "Monte-Carlo Modeling of Degradation of Polymer Networks: 3. Lattice Networks", *Polymer* **41** (2000), 615-619

315. G. Hübner, E. Roduner, "EPR Investigations of HO$^\bullet$ Radical Initiated Degradation Reactions of Sulfonated Aromatics as Model Compounds for Fuel Cell Proton Conducting Membranes", *J. Mater. Chem.* **9** (1999), 409-418

316. V.O. Mittal, H.R. Kunz, J.M. Fenton, "Effect of Catalyst Properties on Membrane Degradation Rate and the Underlying Degradation Mechanisms in PEMFCs", *J. Electrochem. Soc.* **153** (2006), 9, A1755-A1759

317. K. Jetsrisuparb, "Comonomer Effects in Radiation Grafted Membranes for Polymer Electrolyte Fuel Cells", *Diss. ETH Nr. 21257*, DOI: 10.3929/ethz-a-009973173, ETH Zürich, 2013

318. M. Salame, "Transport Properties of Nitrile Polymers", *J. Polym. Sci. Symp.* **41** (1973), 1-15

319. A.E. Barnabeo, W.S. Creasy, L.M. Robeson, "Gas Permeability Characteristics of Nitrile-Containing Block and Random Copolymers", *J. Polym. Sci. Polym. Chem.* **13** (1975), 1979-1986

320. L. Gubler, L. Bonorand, "Radiation Grafted Membranes for Fuel Cells: Strategies to Compete with PFSA Membranes", *ECS Trans.* **58** (2013), 1, 149-162

321. L. Gubler, H. Ben youcef, D. Henkensmeier, G.G. Scherer, unpublished results

322. L. Bonorand, P. Reichel, J. Thut, L. Gubler, "Performance Enhancements of the PSI Gen2 Radiation Grafted Membrane", *PSI Electrochemistry Laboratory – Annual Report 2012* (DOI: 10.3929/ethz-a-007047464) (2013), 9-10

323. L. Bonorand, P. Reichel, J. Thut, L. Gubler, "Radiation Grafted Membranes providing Low Cost, High Performance and Durability", *Proc. 4th European PEFC & H2 Forum*, paper no. A0403, Lucerne, Switzerland, July 2-5, 2013.

324. D.S.A. De Focatiis, L. Gubler, "Uniaxial Deformation and Orientation of Ethylene-Tetrafluoroethylene Films", *Polym. Test.* **32** (2013), 1423–1435

325. J.A. Horsfall, K.V. Lovell, "Synthesis and Characterisation of Sulfonic Acid-Containing Ion Exchange Membranes Based on Hydrocarbon and Fluorocarbon Polymers", *Eur. Polym. J.* **38** (2002), 1671-1682

326. F. Wallasch, M. Abele, L. Gubler, A. Wokaun, K. Müller, G.G. Scherer, "Characterization of Radiation-Grafted Polymer Films using CP/MAS NMR Spectroscopy and Confocal Raman Microscopy", *J. Appl. Polym. Sci* **125** (2012), 3500-3508

327. Y. Kimura, M. Asano, J. Chen, Y. Maekawa, R. Katakai, M. Yoshida, "Influence of Grafting Solvents on the Properties of Polymer Electrolyte Membranes prepared by γ-Ray Preirradiation Method", *Radiat. Phys. Chem.* **77** (2008), 864-870

328. B. Schnyder, T. Rager, "Surface Modification of Radiation-Grafted Polymer Films and Membranes by Crosslinking", *J. Appl. Polym. Sci.* **104** (2007), 1973-1978

329. N. Walsby, S. Hietala, S.L. Maunu, F. Sundholm, T. Kallio, G. Sundholm, "Water in Different Poly(Styrene Sulfonic Acid)-Grafted Fluoropolymers", *J. Appl. Polym. Sci.* **86** (2002), 1, 33-42

330. M. Elomaa, S. Hietala, M. Paronen, N. Walsby, K. Jokela, R. Serimaa, M. Torkkeli, T. Lehtinen, G. Sundholm, F. Sundholm, "The State of Water and the Nature of Ion Clusters in Crosslinked Proton Conducting membranes of Styrene Grafted and Sulfonated Poly(Vinylidene Fluoride)", *J. Mater. Chem.* **10** (2000), 2678-2684

331. H. Yoshida, Y. Miura, "Behavior of Water in Perfluorinated Ionomer Membranes Containing Various Monovalent Cations", *J. Membr. Sci.* **68** (1992), 1-2, 1-10

332. A. Eisenberg, M. King, *Ion-Containing Polymers: Physical Properties and Structure*, Academic Press, New York a.o., 1977

333. K. Mortensen, U. Gasser, S. Alkan-Gürsel, G.G. Scherer, "Structural Characterization of Radiation Grafted Block Copolymer Films, using SANS technique", *J. Polym. Sci. Part B: Polym. Phys.* **46** (2008), 1660-1668

334. S. Balog, U. Gasser, K. Mortensen, H. Ben youcef, L. Gubler, G.G. Scherer, "Structure of the Ion-rich Phase in DVB Crossl-linked Graft-copolymer Proton-exchange Membranes", *Polymer* **53** (2012), 175-182

335. H.P. Brack, M. Wyler, G. Peter, G.G. Scherer, "A Contact Angle Investigation of the Surface Properties of Selected Proton-Conducting Radiation-Grafted Membranes", *J. Membr. Sci.* **214** (2003), 1-19

336. J.A. Horsfall, K.V. Lovell, "Comparison of Fuel Cell Performance of Selected Fluoropolymer and Hydrocarbon Based Grafted Copolymers Incorporating Acrylic Acid and Styrene Sulfonic Acid", *Polym. Adv. Technol.* **13** (2002), 381-390

337. Y. Buchmüller, A. Wokaun, L. Gubler, "Polymer-bound Antioxidants in Grafted Membranes for Fuel Cells", *J. Mater. Chem. A* **2** (2014), 16, 5870-5882

338. T.A. Zawodzinski, C. Derouin, S. Radzinski, R.J. Sherman, V.T. Smith, T.E. Springer, S. Gottesfeld, "Water Uptake by and Transport through Nafion 117 Membranes", *J. Electrochem. Soc.* **140** (1993), 4, 1041-1047

339. L. Gubler, T. Finsterwald, G.G. Scherer, "Investigations on the Conductivity of Various Proton Exchange Membranes", *PSI Electrochemistry Laboratory – Annual Report 2004* (2004), 111

340. J. Halim, F.N. Büchi, O. Haas, M. Stamm, G.G. Scherer, "Characterization of Perfluorosulfonic Acid Membranes by Conductivity Measurements and Small-Angle X-Ray Scattering", *Electrochim. Acta* **39** (1994), 8/9, 1303-1307

341. L. Gubler, N. Prost, S. Alkan-Gürsel, G.G. Scherer, "Proton Exchange Membranes Prepared by Radiation Grafting of Styrene / Divinylbenzene onto Poly(Ethylene-*Alt*-Tetrafluoroethylene) for Low Temperature Fuel Cells", *Solid State Ionics* **176** (2005), 2849-2860

342. Y.S. Kim, B.S. Pivovar, "The Membrane-Electrode Interface in PEFCs. IV. The Origin and Implications of Interfacial Resistance", *J. Electrochem. Soc.* **157** (2010), 11, B1616-B1623

343. B.P. Pearman, N. Mohajeri, R.P. Brooker, M.P. Rodgers, D.K. Slattery, M.D. Hampton, D.A. Cullen, S. Seal, "The Degradation Mitigation Effect of Cerium Oxide in Poylmer Electrolyte Membranes in Extended Fuel Cell Durability Tests", *J. Power Sources* **225** (2013), 75-83

344. M.P. Rodgers, L.J. Bonville, H.R. Kunz, D.K. Slattery, J.M. Fenton, "Fuel Cell Perfluorinated Sulfonic Acid Membrane Degradation Correlating Accelerated Stress Testing and Lifetime", *Chem. Rev.* **112** (2012), 6075-6103

345. N. Linse, G.G. Scherer, A. Wokaun, L. Gubler, "Quantitative Analysis of Carbon Corrosion during Fuel Cell Start-up and Shut-down by Anode Purging", *J. Power Sources* **219** (2012), 240-248

346. J. Huslage, T. Rager, B. Schnyder, A. Tsukada, "Radiation-Grafted Membrane Electrode Assemblies with Improved Interface", *Electrochim. Acta* **48** (2002), 247-254

347. F.N. Büchi, A. Marek, G.G. Scherer, "*In Situ* Membrane Resistance Measurements in Polymer Electrolyte Fuel Cells by Fast Auxiliary Current Pulses", *J. Electrochem. Soc.* **142** (1995), 6, 1895-1901

348. H.A. Gasteiger, W. Gu, R. Makharia, M.F. Mathias, B. Sompalli, "Beginning-of-Life MEA Performance - Efficiency Loss Contributions", in *Handbook of Fuel Cells - Fundamentals, Technology and Applications*, Volume 3, W. Vielstich, H.A. Gasteiger, A. Lamm, John Wiley & Sons, Chichester, 2003, 593-610

349. B. Andreaus, G.G. Scherer, "Proton Conducting Polymer Membranes in Fuel Cells - Humidification Aspects", *Solid State Ionics* **168** (2004), 311-320

350. J. Huslage, T. Rager, J. Kiefer, L. Steuernagel, G.G. Scherer, "Improved Membrane Electrode Assemblies for Polymer Electrolyte Fuel Cells based on Radiation-Grafted Membranes", *Proc. 197th Electrochemical Society Meeting*, Toronto, Canada, May 14-18, 2000

351. T.J. Schmidt, K. Simbeck, G.G. Scherer, "Influence of Cross-Linking on the Performance of Radiation Grafted and Sulfonated FEP 25 Membranes in H_2-O_2 PEFC", *J. Electrochem. Soc.* **152** (2005), 1, A93-A97

352. S.S. Kocha, J.D. Yang, J.S. Yi, "Characterization of Gas Crossover and its Implications in PEM Fuel Cells", *AIChE Journal* **52** (2006), 5, 1916-1925

353. H. Ben youcef, L. Gubler, T. Yamaki, S. Sawada, A. Wokaun, G.G. Scherer, "Crosslinker Effect in ETFE Based Radiation Grafted Proton Conducting Membranes. II. Extended Fuel Cell Operation and Degradation Analysis", *J. Electrochem. Soc.* **156** (2009), 4, B532-B539

354. M.M. Menamparambath, G.G. Scherer, A. Wokaun, L. Gubler, "Insights into the Local Degradation of Chemically Aged Radiation Grafted Membranes", *European Fuel Cell Forum 2009*, Lucerne, Switzerland, June 29 - July 2, 2009, Session A0505 – Manuscript 062

355. Z. Zhang, Y. Buchmüller, A. Wokaun, L. Gubler, "Degradation Study of Radiation Grafted Membranes under Low Humidity Conditions in the PEFC", *ECS Electrochem. Lett.* **2** (2013), 10, F69-F72

356. Y. Buchmüller, Z. Zhang, A. Wokaun, L. Gubler, "Antioxidants in Non-Perfluorinated Fuel Cell Membranes: Prospects and Limitations", *RSC Adv.* **4** (2014), 51911–51915

357. T. Kitayama, K. Hatada, *NMR Spectroscopy of Polymers*, Springer, 2004

358. G. Odian, A. Rossi, E. Ratchik, T. Acker, "Monomer Reactivities in Radiation-Induced Graft Copolymerization", *J. Polym. Sci.* **54** (1961), 159, S11-S13

359. G. Odian, T. Acker, A. Rossi, E. Ratchik, "Monomer Reactivities in Radiation-Induced Graft Copolymerization. Part II. Graft Copolymerization to Teflon", *J. Polym. Sci.* **57** (1962), 661-667

360. D.W. Behnken, "Estimation of Copolymer Reactivity Ratios: An Example of Nonlinear Estimation", *J. Polym. Sci. Part A* **2** (1964), 645-668

361. P.W. Tidwell, G.A. Mortimer, "An Improved Method of Calculating Copolymerization Reactivity Ratios", *J. Polym. Sci. Part A* **3** (1965), 369-387

362. A.M. van Herk, T. Dröge, "Nonlinear Least Squares Fitting Applied to Copolymerization Modeling", *Macromol. Theory Simul.* **6** (1997), 1263-1276

363. S.L. Meyer, *Data Analysis for Scientists and Engineers*, Wiley, 1975

364. Z. Zhang, Y. Buchmüller, L. Bonorand, A. Wokaun, T.J. Schmidt, L. Gubler, "Effects of Temperature and Catalyst Type on Chemical Degradation of Radiation Grafted Membranes in PEFCs", *Fuel Cells*, accepted

365. S.M. Dockheer, L. Gubler, P.L. Bounds, A.S. Domazou, G.G. Scherer, A. Wokaun, W.H. Koppenol, "Damage to Fuel Cell Membranes. Reaction of HO• with an Oligomer of Poly(Sodium Styrene Sulfonate) and Subsequent Reaction with O_2 ", *Phys. Chem. Chem. Phys.* **12** (2010), 11609-11616

366. A. Henglein, W. Schnabel, J. Wendenburg, *Einführung in die Strahlenchemie*, Verlag Chemie GmbH, Weinheim, Germany, 1969

367. R.H. Schuler, T.I. Balkas, J.H. Fendler, "Radiolysis of Aqueous Solutions of Methyl Chloride. The Concentration Dependence for Scavenging Electrons within Spurs", *J. Phys. Chem.* **74** (1970), 4497-4505

368. C. von Sonntag, *The Chemical Basis of Radiation Biology*, Taylor & Francis, London, 1987

369. R.H. Schuler, L.K. Patterson, E. Janata, "Yield for the Scavenging of Hydroxyl Radicals in the Radiolysis of Nitrous Oxide-saturated Aqueous Solutions", *J. Phys. Chem.* **84** (1980), 2088-2089

370. G.V. Buxton, C.L. Greenstock, W.P. Helman, A.B. Ross, "Critical Review of rate constants for reactions of hydrated electrons, hydrogen atoms and hydroxyl radicals (•OH/•O⁻) in Aqueous Solution", *J. Phys. Chem. Ref. Data* **17** (1988), 513-886

371. R.H. Schuler, A.L. Hartzell, B. Behar, "Track Effects in Radiation Chemistry. Concentration Dependence for the Scavenging of ˙OH by Ferrocyanide in N_2O-saturated Aqueous Solutions", *J. Phys. Chem.* **85** (1981), 192-199

372. B.H.J. Bielski, D.E. Cabelli, R.L. Arudi, A.B. Ross, "Reactivity of HO_2/O_2^- Radicals in Aqueous Solution", *J. Phys. Chem. Ref. Data* **14** (1985), 4, 1041-1100

373. A.J. Elliot, D.R. McCracken, G.V. Buxton, N.D. Wood, "Estimation of Rate Constants for Near-Diffusion-Controlled Reactions in Water at High Temperature", *J. Chem. Soc. Faraday Trans.* **86** (1990), 1539-1547

374. R.W. Matthews, H.A. Mahlmann, T.J. Sworski, "Kinetics of the Oxidation of Cerium(III) by Peroxysulfuric Acids induced by Cobalt-60 γ-Radiation.", *J. Phys. Chem.* **74** (1970), 2475-2479

375. C.L. Clifton, R.E. Huie, "Rate Constants for Hydrogen Abstraction Reactions of the Sulfate Radical, $SO_4^{•-}$ ", *Int. J. Chem. Kinet.* **21** (1989), 677-687

376. W.J. McElroy, S.J. Waygood, "Kinetics of the reactions of the SO_4^- radical with $SO_4^{•-}$, $S_2O_8^{2-}$, H_2O and Fe(II)", *J. Chem. Soc. Faraday Trans.* **86** (1990), 2557-4505

377. S.M. Dockheer, L. Gubler, W.H. Koppenol, "Reactions of the Tetraoxidosulfate(•–) and Hydroxyl Radicals with Poly(Sodium α-Methylstyrene Sulfonate)", *Phys. Chem. Chem. Phys.* **15** (2013), 4975-4983

378. L. Gubler, "Polymer Design Strategies for Radiation Grafted Fuel Cell Membranes", *Adv. Energy Mater.* **4** (2014), 1300827

379. Y.R. Luo, *Comprehensive Handbook of Chemical Bond Energies*, CRC Press, Boca Raton, Florida, 2007

380. R. Pitteloud, P. Dubs, "Antioxidants for Industrial Applications", *Chimia* **48** (1994), 417-419

381. M. Danilczuk, F.D. Coms, S. Schlick, "Visualizing Chemical Reactions and Crossover Processes in a Fuel Cell Inserted in the ESR Resonator: Detection by Spin Trapping of Oxygen Radicals, Nafion-Derived Fragments, and Hydrogen and Deuterium Atoms", *J. Phys. Chem. B* **113** (2009), 8031-8042

382. A.B. Hersberger, J.C. Reid, R.G. Heiligmann, "Polymerization of Alpha-methylstyrene", *Ind. Eng. Chem.* **37** (1945), 11, 1073-1078

383. G.D. Jones, R.E. Friedrich, T.E. Werkema, R.L. Zimmerman, "Poly-alpha-methylstyrene", *Ind. Eng. Chem.* **48** (1956), 12, 2123-2131

384. F.S. Dainton, K.J. Ivin, "Reversibility of the Propagation Reaction in Polymerization Processes and its Manifestation in the Phenomenon of a 'Ceiling Temperature'", *Nature* **162** (1948), 705-707

385. G.D. Jones, R.E. Friedrich, "Polymerization of Poly-alpha-methylstyrene", *Ind. Eng. Chem.* **51** (1959), 6, 745-748

386. G.G. Scherer, F.N. Büchi, B. Gupta, "Electrochemical Cell with a Polymer Electrolyte and Process for Producing these Polymer Electrolytes", *US Patent 5,656,386*, Paul Scherrer Institut, 1997

387. A. Rudin, S.S.M. Chiang, "Kinetics of Free-Radical Copolymerization of α-Methylstyrene and Styrene", *J. Polym. Sci. Part A* **12** (1974), 2235-2254

388. R.B. Seymour, F.F. Harris Jr., I. Branum Jr., "Copolymers of Vinyl Compounds and Maleic Anhydride", *Ind. Eng. Chem.* **41** (1949), 7, 1509-1513

389. R.G. Fordyce, E.C. Chapin, G.E. Ham, "Copolymerization. V. Relative Monomer Addition Rates in Vinyl Copolymerization", *J. Am. Chem. Soc.* **70** (1948), 2489-2492

390. C. Walling, E.R. Briggs, K.B. Wolfstirn, "Copolymerization XI. Copolymerizations Involving α-Vinylpyridine, α-Vinylthiophene, o-Chlorostyrene and α-Methylstyrene", *J. Am. Chem. Soc.* **70** (1948), 1543-1544

391. T. Alfrey, G. Goldfinger, "The Mechanism of Copolymerization", *J. Chem. Phys.* **12** (1944), 6, 205-209

392. F.R. Mayo, F.M. Lewis, "Copolymerization. I. A Basis for Comparing the Behavior of Monomers in Copolymerization; The Copolymerization of Styrene and Methyl Methacrylate ", *J. Am. Chem. Soc.* **66** (1944), 1594-1601

393. F.T. Wall, "The Structure of Copolymers. II", *J. Am. Chem. Soc.* **66** (1944), 2050-2057

394. G. Odian, *Principles of Polymerization*, McGraw-Hill, New York, 1970

395. T. Alfrey, F.R. Mayo, F.T. Wall, "Symbols for Copolymerization", *J. Polym. Sci. Polym. Chem.* **1** (1946), 6, 581

396. P.J. Flory, *Principles of Polymer Chemistry*, Cornell University Press, Ithaca, 1953

397. H.J. Harwood, W.M. Ritchey, "The Characterization of Sequence Distribution in Copolymers", *Polym. Lett.* **2** (1964), 6, 601-607

398. H.J. Harwood, "Sequence Distribution in Copolymers", *Angew. Chem. Int. Ed.* **4** (1965), 394-401

399. S. Al-Malaika, "Reactive Modifiers for Polymers", in *Chemical Reactions on Polymers*, J.L. Benham, J.F. Kinstle, American Chemical Society, 1988, 409-425

400. A.M. El-Naggar, M.H. Zohdy, S.M. Sahar, E.A. Allam, "Reactivity Ratios During Radiation-Induced Grafting of Comonomer Mixtures onto Polyester Fabrics", *Polym. Int.* **50** (2001), 1082-1088

401. M.H. Zohdy, S.M. Sahar, M.S. Hassan, E.M. Khalil, M. El-Hossamy, A.M. El-Naggar, "Selective Properties of Polyester and Cotton / Polyester Fabrics Gamma Irradation Grafted with Different Binary Mixtures of Vinyl Monomers", *Polym. Int.* **48** (1999), 515-525

402. J.F. Kenney, P.J. Patel, "Emulsion Copolymerization Behavior of α-Methylstyrene with Methacrylonitrile", *J. Polym. Sci.* **14** (1976), 105-111

403. J.F. Kenney, "Monomer Sequence Distribution in α-Methylstyrene-Methacrylonitrile Copolymer", *J. Polym. Sci.* **14** (1976), 113-121

404. L. Gubler, G.G. Scherer, "Durability of Radiation Grafted Fuel Cell Membranes", in *Proton Exchange Fuel Cells Durability*, M. Inaba, T.J. Schmidt, F.N. Büchi, Springer Science+Business Media, New York, 2008

405. M. Slaski, "Radiation Grafted Fuel Cell Membranes with Improved Oxidative Stability", *Diss. ETH Nr. 16995*, ETH Zürich, 2007

406. G.G. Lowry, "The Effect of Depropagation on Copolymer Composition. I. General Theory for One Depropagating Monomer", *J. Polym. Sci.* **42** (1960), 463-477

407. G.E. Ham, "Application of an Expanded Copoloymerization Theory to Systems Involving α-Methylstyrene", *J. Polym. Sci.* **45** (1960), 183-187

408. H.K. Johnston, A. Rudin, "Free-Radical Copolymerization of Methacrylonitrile and α-Methylstyrene", *Macromol.* **4** (1971), 6, 661-667

409. B. Mattsson, H. Ericson, L.M. Torel, F. Sundholm, "Micro-Raman Investigations of PVDF-Based Proton-Conducting Membranes", *J. Polym. Sci. Part A: Polym. Chem.* **37** (1999), 3317-3327

410. C. Schmidt, O. Töpfer, A. Langhoff, W. Oppermann, G. Schmidt-Naake, "Depth Profiling of Graft Polymer Membranes via Confocal Laser Scanning Microscopy", *Chem. Mater.* **19** (2007), 4277-4282

411. L. Gubler, M. Slaski, A. Wokaun, G.G. Scherer, "Aging Tests of Radiation Grafted Fuel Cell Membranes", *ECS Trans.* **3** (2006), 1, 569-577

412. J. Bandrup, E.H. Immergut, E.A. Grulke, A. Abe, D.R. Bloch, *Polymer Handbook*, 4th Edition, John Wiley & Sons, New York, 1999

413. G. Odian, *Principles of Polymerization*, 4th edition, John Wiley & Sons, New Jersey, 2004

414. H.M.M.N. El-Din, S.M. Badawy, A.M. Dessouki, "Chelating Polymer Granules Prepared by Radiation-induced Homopolymerization. I. Kinetic Study of Radiation Polymerization Process", *J. Appl. Polym. Sci.* **77** (2000), 1405-1412

415. G. Socrates, *Infrared and Raman Characteristic Group Frequencies. Tables and Charts*, 3rd edition, John Wiley & Sons, Chichester, UK, 2004

416. K.W. Doak, "Copolymerization. XV.1 Copolymerization of Acetylene Derivatives with Olefins. Retardation by Radicals from Acetylenes ", *J. Am. Chem. Soc.* **72** (1950), 4681-4686

417. F.M. Lewis, F.R. Mayo, W.F. Hulse, "Copolymerization. II. The Copolymerization of Acrylonitrile, Methyl Methacrylate, Styrene and Vinylidene Chloride", *J. Am. Chem. Soc.* **67** (1945), 1701-1705

418. K. Arita, T. Ohtomo, Y. Tsurumi, "Analysis of the Monomer Sequence Distribution in Alternating Acrylonitrile-Styrene Copolymers by ^{13}C-NMR", *Polym. Lett. Ed.* **19** (1981), 211-216

419. F.M. Lewis, C. Walling, W. Cummings, E.R. Briggs, F.R. Mayo, "Copolymerization. IV. Effects of Temperature and Solvents on Monoemr Reactiviy Ratios", *J. Am. Chem. Soc.* **70** (1948), 1519-1523

420. A. Rudin, R.G. Yule, "Effects of Temperature on Styrene-Methacrylonitrile Copolymerization", *J. Polym. Sci.: Part A-1* **9** (1971), 3009-3025

421. G. Cameron, G. Esslemont, "Solvent Effects in Free Radical Copolymerization of Styrene and Methacrylonitrile", *Polymer* **13** (1972), 435-438

422. D.J.T. Hill, L. Dong, J.H. O'Donnell, "Microstructural Analysis of Methacrylonitrile-Styrene Copolymers to Obtain Reactivity Ratios", *J. Polym. Sci. Part A: Polym. Chem.* **31** (1993), 2951-2957

423. K. Jetsrisuparb, personal communication, 2009

424. S.J. Paddison, "Proton Conduction Mechanisms at Low Degrees of Hydration in Sulfonic Acid-Based Polymer Electrolyte Membranes", *Annu. Rev. Mater. Res.* **33** (2003), 289–319

425. A. Eisenberg, B. Hird, R.B. Moore, "A New Multiplet-Cluster Model for the Morphology of Random Ionomers", *Macromolecules* **23** (1990), 4098-4107

426. E.M.W. Tsang, Z. Zhang, A.C.C. Yang, Z. Shi, T.J. Peckham, R. Narimani, B.J. Frisken, S. Holdcroft, "Nanostructure, Morphology, and Properties of Fluorous Copolymers Bearing Ionic Grafts", *Macromolecules* **42** (2009), 9467–9480

427. S. Balog, U. Gasser, K. Jetsrisuparb, L. Gubler, "Structure of the Hydrophilic Phase and its Impact on the Conductivity of Graft Copolymer Ionomers at Low Hydration Level", *Polymer* **54** (2013), 4266-4275

428. H. Liu, F.D. Coms, J. Zhang, H.A. Gasteiger, A.B. LaConti, "Chemical Degradation: Correlations Between Electrolyzer and Fuel Cell Findings", in *Polymer Electrolyte Fuel Cell Durability*, M. Inaba, T.J. Schmidt, F.N. Büchi, Springer Science+Business Media, New York, 2009, 71-118

429. E.T. Denisov, I.G. Afanas'ev, *Oxidation and Antioxidants in Organic Chemistry and Biology*, CRC Press, Boca Raton FL (USA), 2005

430. S.D. Mikhailenko, F. Celso, S. Kaliaguine, "Properties of SPEEK Based Membranes Modified with a Free Radical Scavenger", *J. Membr. Sci.* **345** (2009), 315-322

431. B. Halliwell, J.M.C. Gutteridge, *Free Rradicals in Biology and Medicine*, Clarendon Press, 1989

432. M.H. Frey, D.M. Pierpoint, S. Hamrock, "High Durability Fuel Cell Components with Cerium Salt Additives", *WO 2007/120189*, 3M Innovative Propterties Company, 2007

433. T.J. Fuller, M.R. Schoeneweiss, T. Xie, F.D. Coms, S.M. MacKinnon, G.W. Fly, "Additives for Fuel Cell Layers", *US Patent 2008/0166620*, General Motors Corporation, 2008

434. A.R. Neil, S.D. Knights, K.A. Murray, S.J. McDermid, S.M. MacKinnon, S. Ye, "Reduced Degradation of Ion-Exchange Membranes in Electrochemical Fuel Cells ", *US Patent 7,537,857*, Ballard Power Systems, 2009

435. P. Trogadas, J. Parrondo, V. Ramani, "Degradation Mitigation in Polymer Electrolyte Membranes using Free-Radical Scavengers", *ECS Trans.* **16** (2008), 2, 1725-1733

436. D. Zhao, B.L. Yi, H.M. Zhang, H.M. Yu, L. Wang, Y.W. Ma, D.M. Xing, "Cesium Substituted 12-Tungstophosphoric ($Cs_3H_{3-x}PW_{12}O_{40}$) Loaded on Ceria-Degradation Mitigation in Polymer Electrolyte Membranes", *J. Power Sources* **190** (2009), 301-306

437. Y. Buchmüller, personal communication, 2013

438. L. Gubler, W.H. Koppenol, "Kinetic Simulation of the Chemical Stabiliation Mechanism in Fuel Cell Membranes using Cerium and Manganese Redox Couples", *J. Electrochem. Soc.* **159** (2012), 2, B211-B218

439. L. Morss, in *Standard Potentials in Aqueous Solution*, A.J. Bard, R. Parsons, J. Jordan, Marcel Dekker, New York, 1985, 587 – 629

440. L. Gubler, S.M. Dockheer, W.H. Koppenol, "Radical (HO•, H• and HOO•) Formation and Ionomer Degradation in Polymer Electrolyte Fuel Cells", *J. Electrochem. Soc.* **158** (2011), 7, B755-B769

441. S. Al-Malaika, "Reactive Antioxidants for Polymers", in *Reactive Modifiers for Polymers*, S. Al-Malaika, Chapman & Hall, London, 1997, 266-302

442. Y. Buchmüller, "Antioxidants in Radiation Grafted Membranes for Fuel Cells", *Diss. ETH Nr. 22075*, ETH Zürich, 2014

443. I.C. Halalay, B.A. Merzougui, A.M. Mancea, "Three Mechanisms for Protecting the PEM Fuel Cell Membrane, Plates and Catalyst", *ECS Trans.* **16** (2008), 2, 969-981

444. J. Lind, X. Shen, T.E. Eriksen, G. Merényi, "The One-Electron Reduction Potential of 4-Substituted Phenoxyl Radicals in Water", *J. Am. Chem. Soc.* **112** (1990), 479-482

445. C.E. Harland, *Ion Exchange: Theory and Practice*, 2nd edition, The Royal Society of Chemistry, Cambridge, UK, 1994

446. M. Benaglia, A. Alberti, L. Giorgini, F. Magnoni, S. Tozzi, "Poly(Glycidyl Methacrylate): A Highly Versatile Polymeric Building Block for Post-Polymerization Modifications", *Polym. Chem.* **4** (2013), 124-132

447. K. Saito, T. Kaga, H. Yamagishi, S. Furusaki, T. Sugo, J. Okamoto, "Phosphorylated Hollow Fibers Synthesized by Radiation Grafting and Cross-linking", *J. Membr. Sci.* **43** (1989), 131-141

448. S. Steenken, "Transient Phenoxy Radicals: Formation and Properties in Aqueous Solutions", in *The Chemistry of Phenols*, Part 2, Z. Rappoport, John Wiley & Sons., Chichester, 2003, 1107-1152

449. K. Omura, "On the Structures of the Intermediates from Reversible Coupling between Hindered Phenoxy Radicals", *Tetrahedron* **51** (1995), 6901-6910

450. G.R. Buettner, "The Pecking Order of Free Radicals and Antioxidants: Lipid Peroxidation, α-Tocopherol, and Ascorbate", *Arch. Biochem. Biophys.* **300** (1993), 2, 535-543

451. S.J. Blanksby, G.B. Ellison, "Bond Dissociation Energies of Organic Molecules", *Acc. Chem. Res.* **36** (2003), 255-263

452. Y. Yao, J. Liu, W. Liu, M. Zhao, B. Wu, J. Gu, Z. Zou, "Vitamin E assisted polymer electrolyte fuel cells", *Energy Environ. Sci.* **7** (2014), 3362-3370

453. W.H. Koppenol, D.M. Stanbury, P.L. Bounds, "Electrode Potentials of Partially Reduced Oxygen Species, from Dioxygen to Water", *Free Radical Biol. Med.* **49** (2010), 317-322

454. T.A. Enache, A.M. Oliveira-Brett, "Phenol and *Para*-substituted Phenols Electrochemical Oxidation Pathways", *J. Electroanal. Chem.* **655** (2011), 9-16

455. H.A. Schwarz, R.W. Dodson, "Equilibrium between Hydroxyl Radicals and Thallium(II) and the Oxidation Potential of OH(aq)", *J. Phys. Chem.* **88** (1984), 3643-3647

456. R. Hafner, "Fuel Cell Membranes Containing an Electronically Conductive Polymer", Master Thesis, PSI / ETH Zürich, 2012

457. Y. Buchmüller, R. Hafner, A. Wokaun, T.J. Schmidt, L. Gubler, "From Electrochemical Interface to Interphase (2D → 3D) on Ionomer Membranes", *ChemElectroChem* **2** (2015), 338 – 342

458. L.R.C. Barclay, M.R. Vinqvist, "Phenolos as Antioxidants", in *The Chemistry of Phenols*, Part 2, Z. Rappoport, John Wiley & Sons Ltd., Chichester, 2003, 839-908

459. J.L. Hodgson, M.L. Coote, "Clarifying the Mechanism of the Denisov Cycle: How do Hindered Amine Light Stabilizers Protect Polymer Coatings from Photo-oxidative Degradation?", *Macromolecules* **43** (2010), 4573-4583

460. "Hindered Amine Stabilizers", http://www.specialchem4adhesives.com/tc/uv-light-stabilizers/?id=hals, SpecialChem, accessed May 2015

461. T. Elmer, M. Worall, S. Wu, S.B. Riffat, "Fuel Cell Technology for Domestic Built Environment Applications: State of-the-Art Review", *Renewable Sustainable Energy Rev.* **42** (2015), 913-931

462. T. Hua, R. Ahluwalia, L. Eudy, G. Singer, B. Jermer, N. Asselin-Miller, S. Wessel, T. Patterson, J. Marcinkoski, "Status of Hydrogen Fuel Cell Electric Buses Worldwide", *J. Power Sources* **269** (2014), 975-993

463. J. Voelcker, "2016 Toyota Mirai Priced At $57,500, With $499 Monthly Lease", in *Green Car Reports (17-11-2014)*. 2014.

464. R.A. Lemons, "Fuel Cells for Transportation", *J. Power Sources* **29** (1990), 251-264

465. F.T. Wagner, B. Lakshmanan, W. Gu, T.A. Greszler, M.F. Mathias, "Electrons to Go: Electrochemistry and the Future of the Automobile", *ECS Trans.* **41** (2011), 1, 13-26

466. T. Yoshida, K. Kojima, T. Yokoyama, S. Sekine, "Development Trends and Popularization Scenario for Fuel Cell Vehicle", *ECS Trans.* **41** (2011), 1, 3-12

467. "Fuel Cell Technology Challenges", http://www1.eere.energy.gov/hydrogenandfuelcells/fuelcells/fc_challenges.html, US Department of Energy, accessed March 2015

468. N. Garland, J. Kopasz, T. Benjamin, "Advanced Polymers in the DOE Hydrogen and Fuel Cells Program", in *Advances in Polymers for Fuel Cells and Energy Devices*, Pacific Grove CA, USA, 2015

469. H. Wang, H. Li, X.-Z. Yuan, *PEM Fuel Cell Failure Mode Analysis*, CRC Press, Boca Raton FL (USA), 2012

470. L. Dubau, L. Castanheira, F. Maillard, M. Chatenet, O. Lottin, G. Maranzana, J. Dillet, A. Lamibrac, J.-C. Perrin, E. Moukheiber, A. ElKaddouri, G. De Moor, C. Bas, L. Flandin, N. Caqué, "A Review of PEM Fuel Cell Durability: Materials Degradation, Local Heterogeneities of Aging and Possible Mitigation Strategies", *WIREs Energy Environ.* 3 (2014), 540-560G. Hinds, "Performance and Durability of PEM Fuel Cells: A Review", *NPL Report DEPC-MPE 002*, ISSN 1744-0262, National Physical Laboratory, Teddington (UK), 2004

471. C.A. Reiser, L. Bregoli, T.W. Patterson, J.S. Yi, J.D. Yang, M.L. Perry, T.D. Jarvi, "A Reverse-Current Decay Mechanism for Fuel Cells", *Electrochem. Solid-State Lett.* **8** (2005), 6, A273-A276

472. P.J. Ferreira, G.J.l. O', Y. Shao-Horn, D. Morgan, R. Makharia, S. Kocha, H.A. Gasteiger, "Instability of Pt/C Electrocatalysts in Proton Exchange Membrane Fuel Cells. A Mechanistic Investigation", *J. Electrochem. Soc.* **152** (2005), 11, A2256-A2271

473. D.A. Schiraldi, "Perfluorinated Polymer Electrolyte Membrane Durability", *J. Macromol. Sci. Polym. Rev.* **46** (2006), 315-327

474. J. Xie, D.L.W. III, D.M. Wayne, T.A. Zawodzinski, P. Atanassov, R.L. Borup, "Durability of PEFCs at High Humiditiy Conditions", *J. Electrochem. Soc.* **152** (2005), 1, A104-A113

475. G. Meyer, C. Perrot, G. Gebel, L. Gonon, S. Morlat, J.-L. Gardette, "Ex Situ Hydrolytic Degradation of Sulfonated Polyimide Membranes for Fuel Cells", *Polymer* **47** (2006), 5003-5011

476. H. Ericson, T.Kallio, T. Lehtinen, B. Mattsson, G. Sundholm, F. Sundholm, P. Jacobsson, "Confocal Raman Spectroscopic Investiagtions of Fuel Cell Tested Sulfonated Styrene Grafted Poly(vinylidene fluoride) Membranes", *J. Electrochem. Soc.* **149** (2002), 2, A206-A211

477. K.H. Simmrock, E. Griesenbeck, J. Jörissen, R. Rodermund, "Einsatz perfluorierter Kationenaustauscher-Membranen in Elektrolyseverfahren, insbesondere bei der Chloralkali-Elektrolyse", *Chem. Ing. Tech.* **1** (1981), 10-25

478. N.S. Khattra, A.M. Karlsson, M.H. Santare, P. Walsh, F.C. Busby, "Effect of Time-Dependent Material Properties on the Mechanical Behavior of PFSA Membranes Subjected to Humidity Cycling", *J. Power Sources* **214** (2012), 365-376

479. S.F. Burlatsky, M. Gummalla, J. O'Neill, V.V. Atrazhev, A.N. Varyukhin, D.V. Dimitriev, N.S. Erikhman, "A Mathematical Model for Predicting the Life of Polymer Electrolyte Fuel Cell Membranes Subjected to Hydration Cycling", *J. Power Sources* **215** (2012), 135-144

480. M. Crum, W. Liu, "Effective Testing Matrix for Studying Membrane Durability in PEM Fuel Cells: Part II. Mechanical Durability and Combined Mechanical and Chemical Durability", *ECS Trans.* **3** (2006), 1, 541-550

481. Y.-H. Lai, C.K. Mittelsteadt, C.S. Gittleman, D.A. Dillard, "Viscoelastic Stress Analysis of Constrained Proton Exchange Membranes under Humidity Cycling", *J. Fuel Cell Sci. Technol.* **6** (2009), 021002-1

482. J. Healy, C. Hayden, T. Xie, K. Olson, R. Waldo, M. Brundage, H. Gasteiger, J. Abbott, "Aspects of the Chemical Degradation of PFSA Ionomers used in PEM Fuel Cells", *Fuel Cells* **5** (2005), 2, 302-308

483. C. Lim, L. Ghassemzadeh, F.V. Hove, M. Laritzen, J. Kolodziej, G.G. Wang, S. Holdcroft, E. Kjeang, "Membrane Degradation during Combined Chemical and Mechanical Accelerated Stress Testing of Polymer Electrolyte Fuel Cells", *J. Power Sources* **257** (2014), 102-110

484. J. Qi, X. Wang, M.O. Ozdemir, M.A. Uddin, L. Bonville, U. Pasaogullari, T. Molter, "Effect of cationic contaminants on polymer Electrolyte Fuel cell performance ", *ECS Trans.* **58** (2013), 1, 537-542

485. K. Enomoto, S. Takahashi, T. Iwase, T. Yamashita, Y. Maekawa, "Degradation Manner of Polymer Grafts Chemically Attached on Thermally Stable Polymer Films: Swelling-induced Detachment of Hydrophilic Grafts from Hydrophobic Polymer Substrates in Aqueous Media.", *J. Mater. Chem.* **21** (2011), 9343

486. C.H. Bamford, C.F.H. Tipper, "Degradation of Polymers", *Chemical Kinetics*, Volume 14, Elsevier, Amsterdam a.o., 1975

487. J.P. Hoare, *The Electrochemistry of Oxygen*, John Wiley & Sons, New York a.o., 1968

488. U.A. Paulus, A. Wokaun, G.G. Scherer, T.J. Schmidt, V. Stamenkovic, V. Radmilovic, N.M. Markovic, P.N. Ross, "Oxygen Reduction on Carbon-Supported Pt-Ni and Pt-Co Alloy Catalysts", *J. Phys. Chem. B* **106** (2002), 4181-4191

489. M. Inaba, "Degradation Mechanism of Polymer Electrolyte Fuel Cells", *Proc. 14th International Conference on the Properties of Water and Steam* M. Nakahara, N. Matubayasi, M. Ueno, K. Yasuoka, K. Watanabe, International Association for the Properties of Water and Steam (IAPWS), Kyoto, Japan, Aug 29 - Sept 3, 2004, 395-402

490. M. Inaba, H. Yamada, J. Tokunaga, A. Tasaka, "Effect of Agglomeration of Pt/C Catalyst on Hydrogen Peroxide Formation", *Electrochem. Solid-State Lett.* **7** (2004), 12, A474-A476

491. H. Yano, E. Higuchi, H. Uchida, M. Watanabe, "Temperature Dependence of Oxygen Reduction Activity at Nafion-Coated Bulk Pt and Pt/Carbon Black Catalysts", *J. Phys. Chem. B* **110** (2006), 16544-16549

492. U.A. Paulus, T.J. Schmidt, H.A. Gasteiger, R.J. Behm, "Oxygen Reduction on a High-Surface Area Pt/Vulcan Carbon Catalyst: a Thin-Film Rotating Ring-Disk Electrode Study", *J. Electroanal. Chem.* **495** (2001), 134

493. G.G. Scherer, *Ber. Bunsenges. Phys. Chem.* **94** (1990), 145

494. R. Gerischer, H. Gerischer, "Über die katalytische Zersetzung von Wasserstoffsuperoxyd an metallischem Platin", *Z. Physik. Chem.* **6** (1956), 178-200

495. W.H. Koppenol, "The Centennial of the Fenton Reaction", *Free Radical Biol. Med.* **15** (1993), 645-651

496. E. Neyens, J. Baeyens, "A Review of Classic Fenton's Peroxidation as an Advanced Oxidation Technique", *J. Hazard. Mater.* **B98** (2003), 33-50

497. S.F. Burlatsky, V. Atrazhev, N.E. Cipollini, D.A. Condit, N. Erikhman, "Aspects of PEMFC Degradation", *ECS Trans.* **1** (2006), 8, 239-246

498. D. Zhao, B.L. Yi, H.M. Zhang, M. Liu, "The Effect of Platinum in a Nafion membrane on the Durability of the Membrane under Fuel Cell Conditions", *J. Power Sources* **195** (2010), 4606-4612

499. Y. Liu, M. Mathias, J. Zhang, "Measurement of Platinum Oxide Coverage in a Proton Exchange Membrane Fuel Cell", *Electrochem. Solid-State Lett.* **13** (2010), 1, B1-B3

500. M. Kitazawa, A.Y. Nosaka, Y. Nosaka, "Radical Formation in Polymer Electrolyte Fuel Cell Components as Studied by ESR Spectroscopy", *J. Appl. Electrochem.* **38** (2008), 491-496

501. Y. Nosaka, K. Ohtaka, M. Kitazawa, S.-y. Kishioka, A.Y. Nosaka, "Spin-Trapping ESR Detection of OH Radicals Generated in the Electrode Reactions for PEFCs", *Electrochem. Solid-State Lett.* **12** (2009), 2, B14-B17

502. N. Ohguri, A.Y. Nosaka, Y. Nosaka, "Detection of OH Radicals Formed at PEFC Electrodes by Means of a Fluorescent Probe", *Electrochem. Solid-State Lett.* **12** (2009), 6, B94-B96

503. B. Vogel, H. Dilger, E. Roduner, "Rapid Radical Degradation Test of Polyaromatic Fuel Cell Membranes by Electron Paramagnetic Resonance", *Macromolecules* **43** (2010), 4688-4697

504. L. Ghassemzadeh, K.-D. Kreuer, J. Maier, K. Müller, "Chemical Degradation of Nafion Membranes under Mimic Fuel Cell Conditions as Investigated by Solid-State NMR Spectroscopy", *J. Phys. Chem. C* **114** (2010), 14635-14645

505. NDRL/NIST Solution Kinetics Database on the Web, National Institute of Standards and Technology, http://kinetics.nist.gov/solution/, accessed June 2010

506. A. Quintanilha, "Reactive oxygen species in chemistry, biology, and medicine", *Life Sciences*, Volume 146, Plenum Press, New York, 1988

507. M. Danilczuk, F.D. Coms, S. Schlick, "Fragmentation of Fluorinated Model Compounds Exposed to Oxygen Radicals: Spin Trapping ESR Experiments and Implications for the Behaviour of Proton Exchange Membranes Used in Fuel Cells", *Fuel Cells* **8** (2008), 6, 436-452

508. F.D. Coms, "The Chemistry of Fuel Cell Membrane Chemical Degradation", *ECS Trans.* **16** (2008), 2, 235-255

509. M. Pianca, E. Barchiesi, G. Esposto, S. Radice, "End Groups in Fluoropolymers", *J. Fluorine Chem.* **95** (1999), 71-84

510. C. Zhou, M.A. Guerra, Z.-M. Qiu, T.A.Zawodzinsi Jr., D.A. Schiraldi, "Chemical Durability Studies of Perfluorosulfonic Acid Polymers and Model Compounds under Mimic Fuel Cell Conditions", *Macromolecules* **40** (2007), 8695-8707

511. T. Xie, C.A. Hayden, "A Kinetic Model for the Chemical Degradation of Perfluorinated Sulfonic Acid Ionomers: Weak End Groups versus Side Chain Cleavage", *Polymer* **48** (2007), 5497-5506

512. S. Hommura, K. Kawahara, T. Shimohira, Y. Teraoka, "Development of a Method for Clarifying the Perfluorosulfonated Membrane Degradation Mechanism in a Fuel Cell Environment", *J. Electrochem. Soc.* **155** (2008), 1, A29-A33

513. F.D. Coms, H. Xu, T. McCallum, C. Mittelsteadt, "Mechanism of Perfluorosulfonic Acid Membrane Chemical Degradation under Low RH Conditions", *ECS Trans.* **50** (2012), 2, 907-918

514. E. Endoh, S. Hommura, S. Terazono, H. Widjaja, J. Anzai, "Degradation Mechanisms of the PFSA Membrane and Influence of Deposited Pt in the Membrane", *ECS Trans.* **11** (2007), 1, 1083-1091

515. N.E. Cipollini, "Chemical Aspects of Membrane Degradation", *ECS Trans.* **11** (2007), 1, 1071-1082

516. R. Uegaki, Y. Akiyama, S. Tojo, Y. Honda, S. Nishijama, "Radical-induced Degradation Mechanism of Perfluorinated Polymer Electrolyte Membrane", *J. Power Sources* **196** (2011), 9856-9861

517. T. Tokumasu, I. Ogawa, M. Koyama, T. Ishimoto, A. Miyamoto, "A DFT Study of Bond Dissociation Trends in Perfluorosulfonic Acid Membrane", *J. Electrochem. Soc.* **158** (2011), 2, B175-B179

518. K.N. Grew, D. Chu, W.K.S. Chiu, "Ionic Equilibrium and Transport in the Alkaline Anion Exchange Membrane", *J. Electrochem. Soc.* **157** (2010), 7, B1024-B1032

519. T. Ishimoto, R. Nagumo, T. Ogura, T. Ishihara, B. Kim, A. Miyamoto, M. Koyama, "Chemical Degradation Mechanism of Model Compound, $CF_3(CF_2)_3O(CF_2)_2OCF_2SO_3H$, of PFSA Polymer by Attack of Hydroxyl Radical in PEMFCs", *J. Electrochem. Soc.* **157** (2010), 9, B1305-B1309

520. M.K. Kadirov, A. Bosnjakovic, S. Schlick, "Membrane-Derived Fluorinated Radicals Detected by Electron Spin Resonance in UV-Irradiated Nafion and Dow Ionomers: Effect of Counterions and H_2O_2", *J. Phys. Chem. B* **109** (2005), 7664-7670

521. H. Xu, R. Borup, E. Brosha, F. Garzon, B. Pivovar, "The Effect of Relative Humidity on Membrane Degradation Rates and Mechanisms in Proton Exchange Membrane Fuel Cells", *ECS Trans.* **6** (2007), 13, 51-62

522. L. Ghassemzadeh, K.D. Kreuer, J. Maier, K. Müller, "Evaluating Chemical Degradation of Proton Conducting Perfluorosulfonic Acid Ionomers in a Fenton Test by Solid-state ^{19}F NMR Spectroscopy", *J. Power Sources* **196** (2011), 2490-2497

523. D.P. Wilkinson, J. St-Pierre, "Durability", in *Handbook of Fuel Cells - Fundamentals, Technology and Applications*, Volume 3, W. Vielstich, H.A. Gasteiger, A. Lamm, John Wiley & Sons, Chichester, 2003, 611-626

524. J. Yu, T. Matsuura, Y. Yoshikawa, M.N. Islam, M. Hori, "Lifetime Behavior of a PEM Fuel Cell with Low Humidification of Feed Stream", *Phys. Chem. Chem. Phys.* **7** (2005), 373-378

525. Y. Nosaka, K. Ohtaka, N. Ohguri, A.Y. Nosaka, "Detection of OH Radicals Generated in Polymer Electrolyte Membranes of Fuel Cells", *J. Electrochem. Soc.* **158** (2011), 4, B430-B433

526. H. Wang, G.A. Capuano, "Behaviour of Raipore Radiation-Grafted Polymer Membranes in H_2/O_2 Fuel Cells", *J. Electrochem. Soc.* **145** (1998), 3, 780-784

527. K.H. Wong, E. Kjeang, "Mitigation of Chemical Membrane Degradation in Fuel Cells: Understanding the Effect of Cell Voltage and Iron Ion Redox Cycle", *ChemSusChem* **8** (2015), 1072-1082

528. C. Chen, T.F. Fuller, "H_2O_2 Formation under Fuel-Cell Conditions", *ECS Trans.* **11** (2007), 1, 1127-1137

529. V.A. Sethuraman, J.W. Weidner, A.T. Haug, S. Motupally, L.V. Protsailo, "Hydrogen Peroxide Formation Rates in a PEMFC Anode and Cathode", *J. Electrochem. Soc.* **155** (2008), 1, B50-B57

530. T. Madden, D. Weiss, N. Cipollini, D. Condit, M. Gummalla, S. Burlatsky, V. Atrazhev, "Degradation of Polymer-Electrolyte Membranes in Fuel Cells. I. Experimental", *J. Electrochem. Soc.* **156** (2009), 5, B657-B662

531. M. Inaba, T. Kinumoto, M. Kiriake, R. Umebayashi, A. Tasaka, Z. Ogumi, "Gas Crossover and Membrane Degradation in Polymer Electrolyte Fuel Cells", *Electrochim. Acta* **51** (2006), 5746-5753

532. H. Liu, J. Zhang, F.D. Coms, W. Gu, B. Litteer, H.A. Gasteiger, "Impact of Gas Partial Pressure on PEMFC Chemical Degradation", *ECS Trans.* **3** (2006), 1, 493-505

533. M. Takasaki, Y. Nakagawa, Y. Sakiyama, K. Tanabe, K. Ookubo, N. Sato, T. Minamide, H. Nakayama, M. Hori, "Degradation Study of Perfluorosulfonic Acid Polymer Electrolytes: Approach from Decomposition Product Analysis", *J. Electrochem. Soc.* **160** (2013), 4, F413-F416

534. A. Carlsson, L. Jörissen, "Accelerated Degradation of Perfluorinated Sulfonic Acid Membranes", *ECS Trans.* **25** (2009), 1, 725-732

535. A. Panchenko, H. Dilger, E. Möller, T. Sixt, E. Roduner, "*In Situ* EPR Investigation of Polymer Electrolyte Membrane Degradation in Fuel Cell Applications", *J. Power Sources* **127** (2004), 1-2, 325-330

536. L. Ghassemzadeh, S. Holdcroft, "Quantifying the Structural Changes of Perfluorosulfonated Acid Ionomer upon Reaction with Hydroxyl Radicals", *J. Am. Chem. Soc.* **135** (2013), 8181−8184

537. L. Ghassemzadeh, T.J. Peckham, T. Weissbach, X. Luo, S. Holdcroft, "Selective Formation of Hydrogen and Hydroxyl Radicals by Electron Beam Irradiation and Their Reactivity with Perfluorosulfonated Acid Ionomer", *J. Am. Chem. Soc.* **135** (2013), 15923−15932

538. L. Ghassemzadeh, M. Marrony, R. Barrera, K.D. Kreuer, J. Maier, K. Müller, "Chemical Degradation of Proton Conducting Perflurosulfonic Acid Ionomer Membranes Studied by Solid-state Nuclear Magnetic Resonance Spectroscopy ", *J. Power Sources* **186** (2009), 334-338

539. N. Ohguri, A.Y. Nosaka, Y. Nosaka, "Detection of OH Radicals as the Effect of Pt Particles in the Membrane of Polymer Electrolyte Fuel Cells", *J. Power Sources* **195** (2010), 4647-4652

540. Y. Nosaka, K. Ohtaka, N. Ohguri, A.Y. Nosaka, "Detection of OH Radicals Generated in Polymer Membranes of PEFC", *ECS Trans.* **33** (2010), 1, 899-905

541. V. Prabhakaran, C.G. Arges, V. Ramani, "An *In-situ* Probe for Investigating PEM Degradation Kinetics and Degradation Mitigation", *ECS Trans.* **41** (2011), 1, 1347-1357

542. V. Prabhakaran, C.G. Arges, V. Ramani, "Investigation of Polymer Electrolyte Membrane Chemical Degradation and Degradation Mitigation using *In Situ* Fluorescence Spectgroscopy", *Proc. Natl. Acad. Sci. U.S.A.* **109** (2012), 1029-1034

543. V. Prabhakaran, C.G. Arges, V. Ramani, "Investigationof PEM Degradation Kinetics and Degradation Mitigation using In-situ Fluorescence Spectroscopy and Real-time Monitoring of Fluoride-ion Release", *ECS Trans.* **50** (2012), 2, 935-944

544. V. Prabhakaran, V. Ramani, "Structurally-Tuned Nitrogen-Doped Cerium Oxide Exhibits Exceptional Regenerative Free Radical Scavenging Activity in Polymer Electrolytes", *J. Electrochem. Soc.* **161** (2014), 1, F1-F9

545. D.A. Schiraldi, C. Zhou, D. Savant, T.A. Zawodzinski, "Chemical Durability Studies of PFSA and Nonfluorinated PEM Materials", in *Fuel Cell Chemistry and Operation*, ACS Symposium Series,

Volume 1040, A.M. Herring, T.A. Zawodzinski Jr., S.J. Hamrock, American Chemical Society, 2010, 125–136

546. A.M. Dreizler, E. Roduner, "Reaction Kinetics of Hydroxyl Radicals with Model Compounds of Fuel Cell Polymer Membranes", *Fuel Cells* **12** (2012), 1, 132-140

547. Y.K. Bhardwaj, H. Mohan, S. Sabharwal, T. Mukherjee, "Radiation Effect on Poly(p-Sodium Styrene Sulphonate) of Different Degrees of Polymerization in Aqueous Solution: Pulse Radiolysis and Steady State Study", *Radiat. Phys. Chem.* **62** (2001), 229-242

548. D. Behar, "Are Positive Ion Radicals Formed in Pulse Radiolysis of Alkylbenzenefulfonates ?", *J. Phys. Chem.* **95** (1991), 4342-4347

549. H.C. Christensen, J. Sehested, E.J. Hart, "Formation of Benzyl Radicals by Pulse Radiolysis of Toluene in Aqueous Solutions", *J. Phys. Chem.* **77** (1973), 983-987

550. K. Sehested, H. Corfitzen, H.C. Christensen, E.J. Hart, "Rates of Reaction of O$^-$, OH, and H with Methylated Benzenes in Aqueous Solution. Optical Spectra of Radicals", *J. Phys. Chem.* **79** (1975), 310-315

551. D. Behar, J. Rabani, "Pulsed Radiolysis of Poly(Styrenesulfonate) in Aqueous Solutions", *J. Phys. Chem.* **92** (1988), 18, 5288-5292

552. B. Maillard, K.U. Ingold, J.C. Scaiano, "Rate constants for the reactions of free radicals with oxygen in solution", *J. Am. Chem. Soc.* **105** (1983), 15, 5095-5099

553. D.A. Pratt, J.H. Mills, N.A. Porter, "Theoretical Calculations of Carbon−Oxygen Bond Dissociation Enthalpies of Peroxyl Radicals Formed in the Autoxidation of Lipids", *J. Am. Chem. Soc.* **125** (2003), 19, 5801-5810

554. M. Kranenburg, M.V. Ciriano, A. Cherkasov, P. Mulder, "Carbon−Oxygen Bond Dissociation Enthalpies in Peroxyl Radicals", *J. Phys. Chem. A* **104** (2000), 5, 915-921

555. S. Naumov, C. von Sonntag, "UV–visible absorption spectra of alkyl-, vinyl-, aryl- and thiylperoxyl radicals and some related radicals in aqueous solution: a quantum-chemical study", *J. Phys. Org. Chem.* **18** (2005), 7, 586-594

556. J.S. Wright, H. Shadnia, L.L. Chepelev, "Stability of carbon-centered radicals: Effect of functional groups on the energetics of addition of molecular oxygen", *J. Comput. Chem.* **30** (2009), 7, 1016-1026

557. X. Fang, X. Pan, A. Rahmann, H.-P. Schuchmann, C. von Sonntag, "Reversibility in the Reaction of Cyclohexadienyl Radicals with Oxygen in Aqueous Solution", *Chem. Eur. J.* **1** (1995), 7, 423-429

558. S.M. Dockheer, L. Gubler, W.H. Koppenol, "Reaction of SO$_4{}^{\bullet-}$ with an oligomer of poly(sodium styrene sulfonate). Probing the mechanism of damage to fuel cell membranes", *Phys. Chem. Chem. Phys.* **13** (2011), 12429–12434

559. P. O'Neill, S. Steenken, D. Schulte-Frohlinde, "Formation of Radical Cations of Methoxylated Benzenes by Reaction with Hydroxyl Radicals, Thallium^{2+}, Silver^{2+}, and Peroxysulfate (SO$_4{}^{\bullet-}$) in Aqueous Solution. Optical and Conductometric Pulse Radiolysis and In Situ Radiolysis Electron Spin Resonance Study", *J. Phys. Chem.* **79** (1975), 25, 2773–2779

560. K. Sehested, J. Holcman, E.J. Hart, "Conversion of Hydroxycyclohexadienyl Radicals of Methylated Benzenes to Cation Radicals in Acid Media", *J. Phys. Chem.* **81** (1977), 14, 1363-1367

561. R.E. Huie, C.L. Clifton, P. Neta, "Electron Transfer Reaction Rates and Equilibria of the Carbonate and Sulfate Radical Cations", *Radiat. Phys. Chem.* **38** (1991), 5, 477-481

562. B.S. Middleteon, K.U. Ingold, "Hydrogen Atom Abstraction by Peroxy Radicals", *Can. J. Chem.* **45** (1967), 191-194

563. P. Neta, M. Dizdaroglu, M.G. Simic, "Radiolytic Studies of the Cumyloxyl Radical in Aqueous Solutions", *Isr. J. Chem.* **24** (1984), 25-28

564. M. Kranenburg, M.V. Ciriano, A. Cherkasov, P. Mulder, "Carbon-Ooxygen Bond Dissociation Enthalpies in Peroxyl Radicals", *J. Phys. Chem. A* **104** (2000), 915-921

565. M. Al-Sheikhly, D.L. Poster, J.-C. An, P. Neta, J. Silverman, R.E. Huie, "Ionizing Radiation-Induced Destruction of Benzene and Dienes in Aqueous Media", *Environ. Sci. Technol.* **40** (2006), 3082-3088

566. E. Hayon, A. Treinin, J. Wilf, "Electronic Spectra, Photochemistry, and Autoxidation Mechanism of the Sulfite-Bisulfite-Pyrosulfite Systems. SO_2^-, SO_3^-, SO_4^-, and SO_5^- Radicals", *J. Am. Chem. Soc.* **94** (1972), 47-57

567. M.O. Delcourt, M.J. Rossi, "Photoionization of Unsaturated Hydrocarbons at 249 nm in Acetonitrile. Visible Absorption Spectra of Radical Cations", *J. Phys. Chem.* **86** (1982), 3233-3239

568. R.A. McClelland, N. Mathivanan, S. Steenken, "Laser Flash Photolysis of 9-Fluorenol. Production and Reactivities of the 9-Fluorenol Radical Cation and the 9-Fluorenyl Cation", *J. Am. Chem. Soc.* **112** (1990), 4857-4861

569. H. Mohan, J.P. Mittal, "Hydroxyl Radical induced Reactions with 1-Bromo-2-Fluorobenzene in Aqueous Solutions: Formation of Radical Cations", *Chem. Phys. Lett.* **263** (1996), 263-270

570. N. Fujisaki, P. Comte, T. Gäumann, "Pulse Radiolysis of Benzyl Chloride and -Bromide; The UV-Visible Absorption Spectrum of the Benzyl Cation ", *Ber. Bunsenges. Phys. Chem.* **98** (1994), 1256-1262

571. J.A. Grace, M.C.R. Symons, "Unstable Intermediates. Part VI. Spectra of Certain Aryl Carbinols and Olefins in Strongly Acidic and Weakly Acidic Media", *J. Chem. Soc.* (1959), 958-962

572. R.A. McClelland, V.M. Kanagasabapathy, S. Steenken, "Nanosecond Laser Flash Photolytic Generation and Lifetimes in Solvolytic Media of Diarylmethyl and p-Methoxyphenethyl Cations", *J. Am. Chem. Soc.* **110** (1988), 20, 6913-6914

573. Z.B. Alfassi, S. Marguet, P. Neta, "Formation and Reactivity of Phenylperoxyl Radicals in Aqueous Solutions", *J. Phys. Chem.* **98** (1994), 8019-8023

574. Z.B. Alfassi, G.I. Khaikin, P. Neta, "Arylperoxyl Radicals. Formation, Absorption Spectra, and Reactivity in Aqueous Alcohol Solutions", *J. Phys. Chem.* **99** (1995), 265-268

575. X. Fang, R. Mertens, C. von Sonntag, "Pulse Radiolysis of Aryl Bromides in Aqueous Solutions: Some Properties of Aryl and Arylperoxyl Radicals", *J. Chem. Soc. Perkin Trans.* **2** (1995), 1033-1036

576. G.I. Khaikin, Z.B. Alfassi, P. Neta, "Inter- and Intramolecular Redox Reactions of Substituted Phenylperoxyl Radicals in Aqueous Solutions", *J. Phys. Chem.* **99** (1995), 16722-16726

577. D.V. Avila, J. Lusztyk, K.U. Ingold, "Color Benzyloxyl, Cumyloxyl Orange, and 4-Methoxycumyloxyl Blue. Unexpected Discovery That Arylcarbinyloxyl Radicals Have Strong Absorptions in the Visible", *J. Am. Chem. Soc.* **114** (1992), 6576-6577

578. T.N. Das, "Monomer and Dimer Radical Cations of Benzene, Toluene, and Naphthalene", *J. Phys. Chem. A* **113** (2009), 6489-6493

579. E. Baciocchi, M. Bietti, O. Lanzalunga, "Mechanistic Aspects of β-Bond-Cleavage Reactions of Aromatic Radical Cations", *Acc. Chem. Res.* **33** (2000), 243-251

580. P. Trogadas, V. Ramani, "Pt/C/MnO_2 Hybrid Electrocatalysts for Degradation Mitigation in Polymer Electrolyte Fuel Cells", *J. Power Sources* **174** (2007), 159-163

581. E. Endoh, "Development of Highly Durable PFSA Membrane and MEA for PEMFC under High Temperature and Low Humidity Conditions", *ECS Trans.* **16** (2008), 2, 1229-1240

582. D. Zhao, B.L. Yi, H.M. Zhang, H.M. Yu, "MnO_2/SiO_2-SO_3H Nanocomposite as Hydrogen Peroxide Scavenger for Durability Improvement in Proton Exchange Membranes", *J. Membr. Sci.* **346** (2010), 143-151

583. E. Endoh, "Electrolyte Membrane for Polymer Electrolyte Fuel Cell, Process for its Production and Membrane-Electrode Assembly for Polymer Electrolyte Fuel Cell ", *US Patent 2007/0111076*, Asahi Glass Co., 2007

584. E. Endoh, S. Terazono, "Electrolyte Membrane for Polymer Electrolyte Fuel Cell, Process for its Production and Membrane-Electrode Assembly for Polymer Electrolyte Fuel Cell ", *US Patent 2007/104994*, Asahi Glass Co., 2007

585. M.H. Frey, D.M. Pierpoint, S.J. Hamrock, "High Durability Fuel Cell Components with Cerium Salt Additives", *WO 2007/120189*, 3M Innovative Properties Company, 2007

586. M.H. Frey, D.M. Pierpoint, S.J. Hamrock, "High Durability Fuel Cell Components with Cerium Oxide Additives", *WO 2007/120190*, 3M Innovative Properties Company, 2007

587. F.D. Coms, J.E. O´Hara, "Fuel Cell Substrate with an Overcoat", *WO 2008/0107945*, General Motors Corporation, 2008

588. N.R. Andrews, S.D. Knights, K.A. Murray, S.J. McDermid, S.M. MacKinnon, S. Ye, "Reduced Degradation of Ion-Exchange Membranes in Electrochemical Fuel Cells", *US Patent 7,537,857*, Ballard Power Systems, 2009

589. T.J. Fuller, M.R. Schoeneweiss, T. Xie, F.D. Coms, S.M. MacKinnon, G.W. Fly, "Fuel Cell Substrate with an Overcoat", *WO 2008/0166620*, General Motors Corporation, 2008

590. S. Baral, C. Lume-Pereira, E. Janata, A. Henglein, "Chemistry of Colloidal Manganese Oxides. 3. Formation in the Reaction of Hydroxyl Radicals with Mn^{2+} Ions", *J. Phys. Chem.* **90** (1986), 6025-6028

591. E. Roduner, personal communication, 2013

592. K. Sehested, J. Holcman, "Reactions of the Radical Cations of Methylated Benzene Derivatives in Aqueous Solution", *J. Phys. Chem.* **82** (1978), 6, 651-953

593. M. Jonsson, J. Lind, T. Reitberger, T.E. Eriksen, G. Merényi, "Redox Chemistry of Substituted Benzenes. The One-Electron Reduction Potentials of Methoxy-Substituted Benzene Radical Cations", *J. Phys. Chem.* **97** (1993), 11278-11282

594. W. Liu, D. Zuckerbrod, "*In Situ* Detection of Hydrogen Peroxide in PEM Fuel Cells", *J. Electrochem. Soc.* **152** (2005), 6, A1165-A1170

595. L. Gubler, S.M. Dockheer, W.H. Koppenol, "Radical (HO$^{\bullet}$, H$^{\bullet}$ and HOO$^{\bullet}$) Formation and Ionomer Degradation in Polymer Electrolyte Fuel Cells", *J. Electrochem. Soc.* **158** (2011), 7, B755-B769

596. H. Liu, F.D. Coms, J. Zhang, H.A. Gasteiger, A.B. LaConti, "Chemical Degradation: Correlations Between Electrolyzer and Fuel Cell Findings", in *Polymer Electrolyte Fuel Cell Durability*, F.N. Büchi, M. Inaba, T.J. Schmidt, Springer Science + Business Media, New York, 2009, 73

597. R. Borup, J. Meyers, B. Pivovar, Y.S. Kim, R. Mukundan, N. Garland, D. Myers, M. Wilson, F. Garzon, D. Wood, P. Zelenay, K. More, K. Stroh, T. Zawodzinski, J. Boncella, J.E. McGrath, M. Inaba, K. Miyatake, M. Hori, K. Ota, Z. Ogumi, S. Miyata, A. Nishikata, Z. Siroma, Y. Uchimoto, K. Yasuda, K.-i. Kimijima, N. Iwashita, "Scientific Aspects of Polymer Electrolyte Fuel Cell Durability and Degradation", *Chem. Rev.* **107** (2007), 10, 3904-3951

598. S. Kreitmeier, G.A. Schuler, A. Wokaun, F.N. Büchi, "Investigation of membrane degradation in polymer electrolyte fuel cells using local gas permeation analysis", *J. Power Sources* **212** (2012), 0, 139-147

599. X.-Z. Yuan, H. Li, S. Zhang, J. Martin, H. Wang, "A review of polymer electrolyte membrane fuel cell durability test protocols", *J. Power Sources* **196** (2011), 22, 9107-9116

600. T. Kinumoto, M. Inaba, Y. Nakayama, K. Ogata, R. Umebayashi, A. Tasaka, Y. Iriyama, T. Abe, Z. Ogumi, "Durability of Perfluorinated Ionomer Membrane Against Hydrogen Peroxide", *J. Power Sources* **158** (2006), 1222-1228

601. Z. Zhang, Y. Buchmüller, T.J. Schmidt, A. Wokaun, L. Gubler, "The Effect of Relative Humidity on Chemical Degradation of Styrene Based Radiation Grafted Membranes in the PEFC", *ECS Trans.* **58** (2013), 1, 955-968

602. N. Linse, L. Gubler, G.G. Scherer, A. Wokaun, "The effect of platinum on carbon corrosion behavior in polymer electrolyte fuel cells", *Electrochim. Acta* **56** (2011), 7541– 7549

Curriculum Vitae

Personal

Date of Birth:	August 14, 1971
Place of Birth:	Liestal, Switzerland
Marital Status:	Married, 2 children
Nationality:	Swiss

Education

1991-1997:	Student of Materials Science, ETH Zürich
1997:	Master thesis with Prof. L.J. Gauckler
	Chair of Nonmetallic Materials
	Department of Materials Science, ETH Zürich
1997-2000:	PhD thesis with Prof. A. Wokaun
	Paul Scherrer Institut (PSI), Villigen PSI

Professional Career

2001-2002:	Product Development Scientist
	Johnson Matthey Fuel Cells, Reading, United Kingdom
2003-2011:	Scientist / Project Leader
	Paul Scherrer Institut (PSI), Villigen PSI, Switzerland
2012-:	Research Group Leader
	Paul Scherrer Institut (PSI), Villigen PSI, Switzerland

Teaching

Since 2012:	Contributions (7 lessons per year) to Lecture "Renewable Energy Technologies II", Prof. Dr. T.J. Schmidt, ETH Zürich
Since 2015	Lecture (2 lessons) on "Power to Gas", Lucerne University of Applied Sciences and Arts